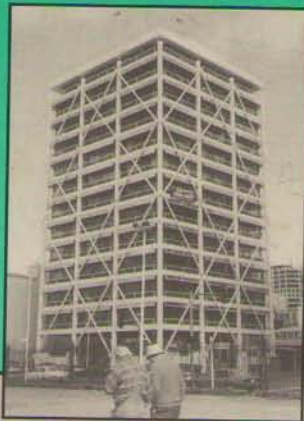


An Introduction to Seismic Isolation

R. I. Skinner
W. H. Robinson
G. H. McVerry



WILEY

Publishers Since 1807

Contents

An Introduction to Seismic Isolation

**R. Ivan Skinner¹, William H. Robinson²
and Graeme H. McVerry³**

*DSIR Physical Sciences, Wellington,
New Zealand*

¹**Current affiliation:**
*31 Blue Mountains Road, Silverstream,
Wellington, New Zealand*

²**Current affiliation:**
*New Zealand Institute for Industrial Research and Development
PO Box 31310, Lower Hutt, New Zealand*

³**Current affiliation:**
*Institute of Geological and Nuclear Sciences
PO Box 30368, Lower Hutt, New Zealand*

Copyright © 1993 by John Wiley & Sons Ltd,
Baffins Lane, Chichester,
West Sussex PO19 1UD, England

All rights reserved.

No part of this book may be reproduced by any means,
or transmitted, or translated into a machine language
without the written permission of the publisher.

Other Wiley Editorial Offices

John Wiley & Sons, Inc., 605 Third Avenue,
New York, NY 10158-0012, USA

Jacaranda Wiley Ltd, G.P.O. Box 859, Brisbane,
Queensland 4001, Australia

John Wiley & Sons (Canada) Ltd, 22 Worcester Road,
Rexdale, Ontario M9W 1L1, Canada

John Wiley & Sons (SEA) Pte Ltd, 37 Jalan Pemimpin #05-04,
Block B, Union Industrial Building, Singapore 2057

Library of Congress Cataloging-in-Publication Data

Skinner, R. Ivan (Robert Ivan)
An introduction to seismic isolation / R. Ivan Skinner, William H.
Robinson, and Graeme H. McVerry.
p. cm.
Includes bibliographical references and index.
ISBN 0 471 93433 X
1. Earthquake resistant design. 2. Seismic waves—Damping.
I. Robinson, William H. II. McVerry, G. H. III. Title.
TA658.44S55 1993
624.1'762—dc20 93-9128
CIP

British Library Cataloguing in Publication Data

A catalogue record for this book is available from the British Library

ISBN 0 471 93433 X

Typeset by Laser Words, Madras
Printed and bound in Great Britain by Biddles Ltd, Guildford, Surrey

Contents

Preface	xi
Acknowledgments	xiii
Frequently used Symbols and Abbreviations	xv
1 INTRODUCTION	1
1.1 Seismic Isolation in Context	1
1.2 Flexibility, Damping and Period Shift	4
1.3 Comparison of Conventional and Seismic Isolation Approaches	7
1.4 Components in an Isolation System	8
1.5 Practical Application of the Seismic Isolation Concept	10
1.6 Topics Covered in this Book	11
2 GENERAL FEATURES OF STRUCTURES WITH SEISMIC ISOLATION	15
2.1 Introduction	15
2.2 Role of Earthquake Response Spectra and Vibrational Modes in the Performance of Isolated Structures	16
2.2.1 Earthquake response spectra	16
2.2.2 General effects of isolation on the seismic responses of structures	20
2.2.3 Parameters of linear and bilinear isolation systems	22
2.2.4 Calculation of seismic responses	26
2.2.5 Contributions of higher modes to the seismic responses of isolated structures	27
2.3 Natural Periods and Mode Shapes of Linear Structures—Unisolated and Isolated	28
2.3.1 Introduction	28
2.3.2 Structural model and controlling equations	28
2.3.3 Natural periods and mode shapes	30
2.3.4 Example—modal periods and shapes	31
2.3.5 Natural periods and mode shapes with bilinear isolation	33

2.4	Modal and Total Seismic Responses	33
2.4.1	Seismic responses important for seismic design	33
2.4.2	Modal seismic responses	34
2.4.3	Structural responses from modal responses	37
2.4.4	Example—seismic displacements and forces	37
2.4.5	Seismic responses with bilinear isolators	38
2.5	Comparisons of Seismic Responses of Linear and Bilinear Isolation Systems	40
2.5.1	Comparative study of seven cases	40
2.6	Guide to Assist the Selection of Isolation Systems	48
3	ISOLATOR DEVICES AND SYSTEMS	55
3.1	Isolator Components and Isolator Parameters	55
3.1.1	Introduction	55
3.1.2	Combination of isolator components to form different isolation systems	56
3.2	Plasticity of Metals	59
3.3	Steel Hysteretic Dampers	63
3.3.1	Introduction	63
3.3.2	Types of steel damper	65
3.3.3	Approximate force-displacement loops for steel-beam dampers	68
3.3.4	Bilinear approximation to force-displacement loops	72
3.3.5	Fatigue life of steel-beam dampers	74
3.3.6	Summary of steel dampers	76
3.4	Lead-extrusion Dampers	76
3.4.1	General	76
3.4.2	Properties of the extrusion damper	81
3.4.3	Summary and discussion of lead-extrusion dampers	84
3.5	Laminated-Rubber Bearings for Seismic Isolators	85
3.5.1	Rubber bearings for bridges and isolators	85
3.5.2	Rubber bearing, weight capacity W_{max}	87
3.5.3	Rubber-bearing isolation: stiffness, period and damping	88
3.5.4	Allowable seismic displacement X_b	90
3.5.5	Allowable maximum rubber strains	93
3.5.6	Other factors in rubber bearing design	96
3.5.7	Summary of laminated-rubber bearings	96
3.6	Lead-Rubber Bearings	96
3.6.1	Introduction	96
3.6.2	Properties of the lead-rubber bearing	99
3.6.3	Summary of lead-rubber bearings	108
3.7	Further Isolator Components and Systems	108
3.7.1	Isolator damping proportional to velocity	110
3.7.2	PTFE sliding bearings	111
3.7.3	PTFE bearings mounted on rubber bearings	112

3.7.4	Tall slender structures rocking with uplift	112
3.7.5	Further components for isolator flexibility	114
3.7.6	Buffers to reduce the maximum isolator displacement	115
3.7.7	Active and tuned-mass systems for vibration control	116
4	STRUCTURES WITH SEISMIC ISOLATION: RESPONSES AND RESPONSE MECHANISMS	119
4.1	Introduction	119
4.2	Linear Structures with Linear Isolation	123
4.2.1	Introduction	123
4.2.2	Modal properties of a uniform linear 'shear beam' on a linear isolator	124
4.2.3	Non-uniform linear structure on a linear isolator	145
4.2.4	Base stiffness and damping for required isolated period and damping	148
4.2.5	Solution of equations of motion for forced response of isolated structures with non-classical damped modes	151
4.2.6	Studies using perturbations about fixed-base modes	159
4.3	Bilinear Isolation of Linear Structures	160
4.3.1	Introduction	160
4.3.2	Maximum bilinear responses	161
4.3.3	Equivalent linearisation of bilinear hysteretic isolation systems	165
4.3.4	Modes of linear structures with bilinear hysteretic isolation	169
4.3.5	Higher-mode acceleration responses of linear structures with bilinear isolation	186
4.4	Seismic Responses of Low-Mass Secondary Structures	199
4.4.1	Introduction	199
4.4.2	Seismic responses of two-degree-of-freedom secondary and primary structural systems	202
4.4.3	Seismic response of a multimode secondary structure on a multimode primary structure	206
4.4.4	Response of secondary systems in structures with linear isolation	214
4.4.5	Response of secondary systems in linear structures with non-linear isolation	217
4.5	Torsionally Unbalanced Structures	226
4.5.1	Introduction	226
4.5.2	Seismic responses of linear 2DOF structures with torsional unbalance	227
4.5.3	Seismic responses of structures with linear isolation and torsional unbalance	233
4.5.4	Seismic responses of structures with bilinear isolation and torsional unbalance	234
4.6	Summary	235

5 A BASIS FOR THE DESIGN OF SEISMICALLY ISOLATED STRUCTURES	239
5.1 General Approach to the Design of Structures with Seismic Isolation	239
5.1.1 Introduction	239
5.1.2 The seismic isolation option	240
5.1.3 Design earthquakes	242
5.1.4 "Trade-off" between reducing base shear and increasing displacement	246
5.1.5 Higher-mode effects	249
5.1.6 The locus of yield-points for a given N_L and K_B , for a bilinear isolator	251
5.2 Design Procedures	254
5.2.1 Selection of linear or non-linear isolation system	254
5.2.2 Design equations for linear isolation systems	255
5.2.3 Design procedure for bilinear isolation systems	257
5.3 Two Examples of the Application of the Design Procedure	261
5.3.1 Isolation of capacitor banks	261
5.3.2 Design of seismic isolation for a hypothetical eight-storey shear building	266
5.4 Aseismic Design of Bridges with Superstructure Isolation	270
5.4.1 Seismic features with superstructure isolation	270
5.4.2 Seismic responses modified by superstructure isolation	271
5.4.3 Discussion	275
5.5 Guidelines and Codes for the Design of Seismically Isolated Buildings and Bridges	276
6 APPLICATIONS OF SEISMIC ISOLATION	281
6.1 Introduction	281
6.2 Structures Isolated in New Zealand	283
6.2.1 Introduction	283
6.2.2 Road bridges	284
6.2.3 South Rangitikei Viaduct with stepping isolation	287
6.2.4 William Clayton Building	291
6.2.5 Union House	295
6.2.6 Wellington Central Police Station	297
6.3 Structures Isolated in Japan	299
6.3.1 Introduction	299
6.3.2 The C-1 Building, Fuchu City, Tokyo	302
6.3.3 The High-Tech R&D Centre, Obayashi Corporation	302
6.3.4 Comparison of three buildings with different seismic isolation systems	304
6.3.5 Oiles Technical Centre Building	306
6.3.6 Miyagawa Bridge	307

6.4 Structures Isolated in the USA	308
6.4.1 Introduction	308
6.4.2 Foothill Communities Law and Justice Centre, San Bernardino, California	308
6.4.3 Salt Lake City and County Building: retrofit	309
6.4.4 USC University Hospital, Los Angeles	313
6.4.5 Sierra Point Overhead Bridge, San Francisco	316
6.4.6 Sexton Creek Bridge, Illinois	319
6.5 Structures Isolated in Italy	320
6.5.1 Introduction	320
6.5.2 Seismically isolated buildings	321
6.5.3 The Mortaiolo Bridge	322
6.6 Isolation of Delicate or Potentially Hazardous Structures or Substructures	324
6.6.1 Introduction	324
6.6.2 Seismically isolated nuclear power stations	330
6.6.3 Protection of capacitor banks, Haywards, New Zealand	331
6.6.4 Seismic isolation of a printing press in Wellington, New Zealand	333
6.7 Notes added in proof (January 1993)	335
References	337
Index	349

Preface

Our interest in the field of seismic isolation began over 25 years ago in 1967, when a group at the (then) DSIR Physics and Engineering Laboratory, working in the field of earthquake engineering research, became involved in design studies for a 'stepping bridge' over the Rangitikei River. The system adopted included steel-beam dampers and laminated-rubber components. The utilisation of similar components was then considered as a means of providing seismic isolation for a proposed building in Wellington, namely the William Clayton Building.

Early in the seismic isolation programme, a fruitful interaction developed with a group engaged in materials science research at the same laboratory whose expertise included the behaviour of plastically deforming metals. They developed a range of isolator components based on the plastic deformation of lead, including lead extrusion dampers first used in the isolated Aurora Terrace and Bolton Street overbridges in Wellington and lead-rubber isolators which were the final choice for isolation of the William Clayton building.

Interaction between members of the two groups consolidated over the years and led to the further development, proving and application of isolation systems. At the same time, theoretical approaches necessary for the description and understanding of the seismic responses and performance of isolated structures were developed. Over the years the level of sophistication has increased but the general approach has not changed. This book is the product of our extensive involvement and experience in the seismic isolation field.

The book includes mathematical analysis of the seismic responses of isolated structures, which is oriented to give a clear understanding of the processes involved; discussion of various isolation systems, particularly those which have been developed in our laboratory; guidelines to provide initial isolator parameter values for engineers or architects wishing to incorporate seismic isolation into their designs; and a description of the application of the concept of seismic isolation worldwide.

Many of our devices have been installed in real structures, both in New Zealand and overseas. The remarkably rapid technology transfer has been in large part due to the close working relationships which have developed over the years between our researchers and design engineers in this field worldwide. We should like to thank these colleagues for their contribution to this book, both indirectly, through collaboration over the years, and directly, by supplying us with information and photographs, primarily for Chapter 6.

We dedicate this book to the memory of the late Otto Glogau, Chief Structural Engineer of the Ministry of Works and Development, whose active support led to the early application of seismic isolation in New Zealand.

We should also like to thank the support staff at DSIR Physical Sciences for the devoted effort which has made this book possible.

R. Ivan Skinner¹
William H. Robinson²
Graeme H. McVerry³

DSIR Physical Sciences, Wellington, New Zealand, 30 June 1992

¹**Current affiliation:**

*31 Blue Mountains Road, Silverstream,
 Wellington, New Zealand*

²**Current affiliation:**

*New Zealand Institute for Industrial Research and Development
 PO Box 31310, Lower Hutt, New Zealand*

³**Current affiliation:**

*Institute of Geological and Nuclear Sciences
 PO Box 30368, Lower Hutt, New Zealand*

Acknowledgments

The date of submission of this manuscript, 30 June 1992, is auspicious to us since it is the last day of existence of the DSIR, the New Zealand Department of Scientific and Industrial Research (1926–1992) which will now be restructured, together with other government-funded research organisations, into ten new Crown Research Institutes. This means that the three authors will be going in different directions from now on, with RIS finally moving to work in a private capacity, WHR going to the Institute for Industrial Research and Development and GHMcV, with other members of the engineering seismology section, moving into the Institute of Geological and Nuclear Sciences.

It seems very appropriate at this time to thank the DSIR, as an organisation, for having provided an environment in which our scientific endeavours could flourish. We also acknowledge the strong support of the various Directors of the DSIR Physics and Engineering Laboratory (PEL), later known as DSIR Physical Sciences, namely Dr M C Probine, Mr M A Collins, Dr W H Robinson and Dr G P Betteridge.

We also wish to thank the members of staff who have contributed to, and supported, our research and developments over the last 25 years. Many of our associates appear as co-authors of publications cited, except for Jiri Babor whom we should like to thank for the many calculations which underlie results given in the text. Excellent support has been provided over the years by the Mechanical Development Workshop of the Physics and Engineering Laboratory, with the manufacture of prototypes and testing equipment and the production of full-scale isolator components for installation in structures.

We should also like to thank the many support staff who have contributed to the production and quality of this book. In particular we should like to thank the illustrators and photographers for their contributions and Christine Keppel for typing the many drafts. We wish to say a special thanks to Dr Barbara Bibby for her editorial work during the last six months, which for much of the time was more akin to that of a fellow author than that of an editor.

Finally we should like to thank Pat Skinner, Barbara Robinson and the rest of our families for their support and encouragement during the time we have been working on the material covered here, and in particular during the final phases of our book.

Frequently used Symbols and Abbreviations

- β = tuning parameter for combined primary-secondary system, namely $(\omega_p - \omega_s)/\omega_s$.
- β_{ij} = analogue to β , for multimode primary-secondary systems.
- $\Gamma_{e,rn}$ = elastic-phase participation factor at position r in mode n .
- $\Gamma_n(z)$ = mode- n participation factor at position z .
- Γ_{Nn} = mode- n participation factor at top floor of structure (position N).
- Γ_n = weighting factor for the n th mode of vibration.
- Γ_n = participation factor vector.
- $\Gamma_n(I)$ = isolated mode weight factor.
- $\Gamma_n(U)$ = unisolated mode weight factor.
- Γ_{rn} = participation factor for response to ground excitation for a mass at level r of a structure vibrating in the n th mode.
- $\Gamma_{\gamma,rn}$ = yielding-phase participation factor at position r in mode n .
- γ_{sr} = shear strain of rubber disc.
- γ = interaction parameter of combined primary-secondary system, given by m_s/m_p .
- γ = 'engineering' shear strain.
- γ_{ij} = interaction parameter, analogue to γ , for multimode primary-secondary systems.
- γ_n = wave number of mode n , possibly complex.
- γ_y = shear-strain coordinate of yield point.
- Δ_n = difference between n th root of equation (4.17) and $(n-1)\pi$.
- δ_d = non-classical damping parameter in combined primary-secondary system.
- δ_{ij} = analogue to δ_d , for multimode primary-secondary systems.
- ϵ = ω_b/ω_{FBI} = ratio of frequencies of rigid-mass isolated structure and first-mode unisolated structure, used for expressing orders of perturbation.
- ϵ = strain = (increment in length)/(original length).
- ϵ_m = maximum amplitude of cyclic strain.
- ϵ_y = strain coordinate of yield point.
- θ_n = variation of spatial phase of mode- n displacement down shear beam.

ζ_s	= damping of secondary structure.
ζ_p	= damping of primary structure.
ζ_a	= average damping of combined primary–secondary system, given by $\zeta_a = (\zeta_p + \zeta_s)/2$.
ζ_d	= damping difference of combined primary–secondary system, given by $\zeta_d = \zeta_p - \zeta_s$.
ζ_{FBn}	= fraction of critical viscous damping of (unisolated) fixed-base mode n .
ζ	= velocity- (viscous-) ‘damping factor’ or ‘fraction of critical damping’ for single-mass oscillator.
ζ_b	= velocity-damping factor for isolator.
ζ_B	= ‘effective’ damping factor of bilinear isolator, given by sum of velocity- and hysteretic-damping factors.
ζ_{b1}	= velocity-damping factor in ‘elastic’ region of bilinear isolator.
ζ_{b2}	= velocity-damping factor in ‘plastic’ or ‘yielded-phase’ region of bilinear isolator.
ζ_h	= hysteretic damping factor of bilinear isolator.
ζ_n	= fraction of critical viscous damping of mode n ; also called mode- n damping factor.
μ_{j0}	= modal mass of free-free mode j . = $\mathbf{u}_{j0}^T [\mathbf{M}] \mathbf{u}_{j0}$.
μ_{sj}	= j th modal mass of secondary system = $\phi_{sj}^T [\mathbf{M}_s] \phi_{sj}$.
$\xi_n(t)$	= modal (relative displacement) coordinate for mode n at time t .
ρ	= uniform density of shear beam representing a uniform shear structure.
$\hat{\sigma}$	= nominal stress, as used in ‘scaled’ (σ - ϵ) curves for steel dampers in Chapter 3.
σ	= stress = force/area.
σ_y	= stress coordinate of yield point.
$\hat{\tau}$	= nominal shear stress, as used in ‘scaled’ (σ - ϵ) curves for steel dampers in Chapter 3.
τ	= shear stress = (shear force)/area.
τ_y	= shear-stress coordinate of yield point.
$[\Phi]$	= $[\phi_1, \dots, \phi_n, \dots, \phi_N]$, the mode shape matrix, a function of space, not time.
ϕ_n, ϕ_m	= mode shape in the n th or m th mode of vibration.
ϕ_{rn}	= mode shape at the r th level of the structure during the n th mode of vibration.
$\phi_{e, rn}$	= elastic-phase modal shape at position r in mode n .
$\phi_{y, rn}$	= yielding-phase modal shape at position r in mode n .
$\phi_n(z, t)$	= shape of mode n , used interchangeably with $\mathbf{u}_n(z, t)$; normalised to unity at the top level.
Ψ_{jn}	= phase angle of j th component of the n th mode participation factor vector Γ_n .
ω_s	= (circular) frequency of secondary structure.

ω_p	= (circular) frequency of primary structure.
ω_a	= average frequency of combined primary–secondary system, given by $\omega_a = (\omega_p + \omega_s)/2$.
ω_{pi}	= analogue to ω_p , for multimode primary–secondary systems.
ω_{sj}	= analogue to ω_s , for multimode primary–secondary systems.
$\omega_1(\text{U})$	= unisolated undamped first-mode natural (circular) frequency, the same as ω_{FB1} .
ω_{FBn}	= mode- n natural (circular) frequency with ‘free-free’ boundary conditions.
ω_b	= isolator frequency = $\sqrt{K_b/M}$ for a rigid mass M .
ω_{FB1}	= natural (circular) frequency of (unisolated) fixed-base mode 1, equivalent to $\omega_1(\text{U})$.
ω_{FBn}	= natural (circular) frequency of (unisolated) fixed-base mode n .
ω_n	= undamped natural (circular) frequency of mode n , related to frequency f_n by $\omega_n = 2\pi f_n$.
ω_d	= damped natural (circular) frequency of single-mass oscillator.
ω_n	= undamped natural (circular) frequency of single-mass oscillator, or n th-mode natural frequency of multi-degree-of-freedom linear oscillator.
A	= area of rubber bearing in Chapter 3.
A	= cross-sectional area of shear beam representing a uniform shear structure.
A_b	= area of bilinear hysteresis loop.
$\mathbf{a}_n(t)$	= absolute acceleration of mode n .
A'	= overlap area of rubber bearing in Chapter 3.
b	= subscript denoting base isolator.
$\dot{u}_b, \dot{u}_b(t)$	= relative velocity of base mass with respect to ground.
B	= subscript denoting bilinear isolator.
\underline{BF}	= ‘bulge factor’ describing the ratio $S_r/S_{r,1}$ of total shear to first-mode shear at level r in a structure, particularly at mid-height.
$c(r, s)$	= interlevel velocity-damping coefficient, defined only for $r \geq s$.
C_b	= coefficient of velocity-damping for a base isolator, with units such as $\text{N m}^{-1} \text{s} = \text{kg s}^{-1}$.
C_F	= ‘correction factor’ linking displacement of bilinear isolator to equivalent spectral displacement.
c_k	= stiffness-proportional damping coefficient of shear beam representing a uniform shear structure.
C_K	= overall stiffness-proportional damping coefficient $c_k A/L$ of uniform shear structure.
c_m	= mass-proportional damping coefficient of shear beam representing a uniform shear structure.
C_M	= overall mass-proportional damping coefficient $c_m AL$ of uniform shear structure.
c_{rs}	= element of damping coefficient matrix.
$[\mathbf{C}]$	= damping coefficient matrix, with elements c_{rs} related to $c(r, s)$.

e	= subscript used to denote 'elastic-phase'.
e	= subscript used to denote 'experimental model' in 'scaled' (σ - ϵ) or (τ - γ) curves for steel dampers in Chapter 3.
E	= Young's modulus = σ/ϵ in elastic region.
f	= force-scaling factor, as used in 'scaled' (σ - ϵ) or (τ - γ) curves for steel dampers in Chapter 3.
F	= force or shear-force, as obtained from 'scaled' (σ - ϵ) or (τ - γ) curves for steel dampers in Chapter 3.
$FA_r(T, \xi)$	= floor-acceleration spectrum at r th level of a structure.
F_b	= isolator force arising from bilinear resistance to displacement.
F'_e	= residual force in elastic phase of bilinear isolator.
FB	= subscript denoting 'fixed-base' boundary condition corresponding to no isolation.
FF	= subscript denoting 'free-free' boundary condition corresponding to perfect isolation.
FF $_n$	= subscript denoting mode- n 'free-free' vibration.
$F_n(z)$	= maximum seismic force per unit height, at height z of mode n .
F_r	= maximum inertia load on the mass m_r at level r .
F_{rn}	= maximum seismic force of mode n at the r th point of a structure.
F'_y	= residual force in yielding phase of bilinear isolator.
G	= shear modulus = τ/γ in elastic region.
G	= constant shear modulus of shear beam representing a uniform shear structure.
G_0	= white noise power spectrum level.
h_r	= height of r th level of a structure.
I	= 'degree of isolation' or 'isolation ratio' given by $\omega_{FB1}/\omega_b = T_b/T_{FB1} = T_b/T_1(U)$.
k	= stiffness of single-mass oscillator.
K	= overall stiffness GA/L of uniform shear structure.
$k(r, s)$	= interlevel stiffness, such that $k(r, r-1) = KN$ for a N -mass uniform structure and $k(1, 0) = K_b$ if it is isolated.
K_b	= stiffness of linear isolator.
K_B	= 'effective' or 'secant' stiffness of bilinear isolator.
$K_b(r)$	= stiffness of rubber component of lead-rubber bearing.
K_{b1}	= 'initial' or 'elastic' stiffness of bilinear isolator.
K_{b2}	= 'post-yield' or 'plastic' stiffness of bilinear isolator.
K_c	= stiffness of spring introduced to isolator to reduce higher-mode responses (Figure 2.2c).
K_n	= stiffness of n th 'spring' in discrete linear chain system.
k_{rs}	= element of stiffness matrix.
[K]	= stiffness matrix, with elements k_{rs} related to $k(r, s)$.
l	= length-scaling factor, as used in 'scaled' (σ - ϵ) or (τ - γ) curves for steel dampers in Chapter 3.

L	= length of shear beam representing a uniform shear structure.
m	= mass of single-mass oscillator.
M	= mass ρAL of uniform shear structure.
M	= total mass of structure; together with the mass of the isolator this gives M_T .
M_b	= isolator (base) mass.
m_p	= mass of primary structure.
m_r	= mass at r th level
	= M/N for a uniform structure with N levels.
m_s	= mass of secondary structure.
M_T	= total mass of structure plus isolator.
[M]	= mass matrix.
N	= number of masses in discrete linear system.
$\bar{X}_n(z)$	= maximum absolute seismic acceleration of mode n at position z .
n^*	= complex conjugate associated with mode n .
<u>NL</u>	= non-linearity factor.
<u>OM$_n$(z)</u>	= overturning moment at height z of mode n .
<u>OM$_{rn}$</u>	= maximum overturning moment at point r , and height h_r , of mode n of a structure.
p	= subscript used to denote 'primary' in primary-secondary systems.
p	= extrusion pressure in Chapter 3.
p	= subscript used to denote 'prototype' in 'scaled' ($\sigma - \epsilon$) or ($\tau - \gamma$) curves for steel dampers in Chapter 3.
P	= peak factor, namely ratio of peak response to RMS response.
P_a	= amplitude-scaling factor such that $\ddot{u}_g(t) = P_a \ddot{u}_{El\ Centro}(t/P_p)$.
p_n	= complex frequency of mode n , see equation (4.7).
p_{n0}	= zeroth-order term in the perturbation expression for the complex frequency.
p_{ni}	= i th term in perturbation expression for n th-mode complex frequency.
P_p	= frequency-scaling factor such that $\ddot{u}_g(t) = P_a \ddot{u}_{El\ Centro}(t/P_p)$.
P_{ps}	= peak factor for secondary structure when mounted on primary structure.
P_s	= peak factor for secondary structure when mounted on the ground.
Q	= force across Coulomb slider at which it yields.
Q_y	= yield force at which changeover from elastic to plastic behaviour occurs, at yield displacement X_y .
	= shear-force coordinate of yield point.
Q_y/W	= yield force-to-weight ratio of bilinear isolator.
S	= shape factor of elastomeric bearing = (loaded area)/(force-free area).
$S_A(T, \zeta)$	= spectral absolute acceleration for period T and damping ζ , as seen on response spectrum, Figure 2.1.
S_b	= maximum base-level shear.

- S_{bn} = maximum base shear in mode n .
 $S_D(T, \zeta)$ = spectral relative displacement for period T and damping ζ , as seen on response spectrum, Figure 2.1.
 $S_{n \max}$ = maximum shear at any position, in mode n .
 $S_n(z)$ = maximum seismic shear at height z of mode n .
 S_{rn} = maximum shear force at the r th point of a structure oscillating in mode n .
 $S_V(T, \zeta)$ = spectral relative velocity for period T and damping ζ .
 t = time.
 T = superscript indicating 'transpose'.
 T = natural period.
 $T_1(U)$ = unisolated undamped first-mode period, the same as T_{FB1} .
 T_b = natural period of linear base isolator = $2\pi/\omega_b$.
 T_B = 'effective' period for bilinear isolator.
 T_{b1} = period associated with K_{b1} , in 'elastic' region of bilinear isolator.
 T_{b2} = period associated with K_{b2} , in 'plastic' region of bilinear isolator.
 $T_n(I)$ = isolated n th period.
 $T_n(U)$ = unisolated n th period.
 \mathbf{u} = vector containing the displacements u_r .
 $u(z, t)$ = relative displacement, at position z in the structure, in the horizontal x direction, with respect to the ground at time t ; often written as u , without arguments, in the differential form of the equation of motion.
 $\ddot{u}(z, t)$ = relative acceleration with respect to ground of position z at time t .
 u_1 = displacement of bilinear isolator.
 $u_b, u_b(t)$ = relative displacement of base mass with respect to ground.
 $\ddot{u}_b, \ddot{u}_b(t)$ = acceleration of base mass with respect to ground.
 $u_{b/j0}$ = base displacement in free-free mode j .
 $u_{bn}(t)$ = n th-mode relative displacement, with respect to ground, at base of structure at time t .
 $u_{e,rn}$ = elastic-phase displacement at position r in mode n .
 $\ddot{u}_{e,rn}$ = elastic-phase relative acceleration at position r in mode n .
 $u_{FBn}(z, t)$ = fixed-base mode- n relative displacement with respect to ground at position z at time t .
 $u_{FFn}(z, t)$ = 'free-free' mode- n relative displacement with respect to ground, at position z and time t .
 $\ddot{u}_g, \ddot{u}_g(t)$ = ground acceleration.
 U_{Ln}, U_{Nn} = amplitude of n th-mode displacement at position $z = L$ (top of shear beam) (possibly complex); amplitude at top of discrete N -component structure.
 $u_n(z)$ = n th mode shape, used interchangeably with $\phi_n(z)$; usually normalisation is not defined.
 $u_n(z, t)$ = mode- n relative displacement, with respect to ground, of position z at time t .

- u_{n0} = zeroth-order term in the perturbation expression for the mode shape.
 u_{ps} = displacement of secondary structure mounted on the primary structure.
 \ddot{u}_{ps} = acceleration of secondary structure mounted on the primary structure.
 $u_{rn}(t)$ = $\phi_{rn}\xi_n(t)$ = displacement of mode n at r th level of the structure, where ϕ_{rn} is the spatial variation and ξ_n is the time variation.
 u_s = displacement of secondary structure mounted on the ground.
 \ddot{u}_s = acceleration of secondary structure mounted on the ground.
 $u_{y,rn}$ = yielding-phase displacement at position r in mode n .
 $\ddot{u}_{y,rn}$ = yielding-phase relative acceleration at position r in mode n .
 \mathbf{u}_n = displacement vector for discrete linear system in n th mode.
 \mathbf{v} = vector comprising the relative velocity and relative displacement vectors.
 \mathbf{v}_n = vector \mathbf{v} for mode n .
 W = total weight of structure.
 \bar{X} = displacement, as obtained from 'scaled' (σ - ϵ) or (τ - γ) curves for steel dampers in Chapter 3.
 X_b = maximum relative displacement of isolator or of base of isolated structure.
 X_{Nn} = maximum mode- n relative displacement at top floor of structure (position N).
 X_p = peak response of primary structure when mounted on the ground.
 $X_p(\text{RMS})$ = RMS response of primary structure when mounted on the ground.
 X_{ps} = peak response of secondary structure when mounted on primary structure.
 X_r = maximum relative displacement with respect to ground at any level r .
 X_{rn} = peak value of mode- n relative displacement at the r th point of a structure.
 X_s = peak response of secondary structure when mounted on the ground.
 $X_s(\text{RMS})$ = RMS response of secondary structure when mounted on the ground.
 X_y = yield displacement of bilinear isolator.
 X_y = displacement coordinate of yield point.
 \ddot{X}_{rn} = peak value of mode- n absolute acceleration at the r th point of a structure.
 \dot{X}_{rn} = peak value of mode- n relative velocity at the r th point of a structure.
 z = vertical coordinate; height of a point in a structure.
 $Z_n(t)$ = relative displacement response, of one-degree-of-freedom oscillator of undamped natural frequency ω_n and damping ζ_n , to ground acceleration $\ddot{u}_g(t)$.

COMMONLY USED ABBREVIATIONS

- CQC = abbreviation for 'Complete Quadratic Combination', a method of adding responses of several modes.
 DSIR = Department of Scientific and Industrial Research, New Zealand.

LRB	= lead-rubber bearing.
MDOF	= abbreviation for multiple-degree-of-freedom.
MWD	= Ministry of Works and Development, New Zealand, now Workscorp.
PEL	= Physics and Engineering Laboratory of the DSIR, later DSIR Physical Sciences.
PTFE	= polytetrafluoroethylene.
SRSS	= abbreviation for 'Square Root of the Sum of the Squares', a method of adding responses of several modes.
1DOF	= abbreviation for one degree of freedom.
2DOF	= abbreviation for two degrees of freedom.

1 Introduction

1.1 SEISMIC ISOLATION IN CONTEXT

A large proportion of the world's population lives in regions of seismic hazard, at risk from earthquakes of varying severity and varying frequency of occurrence. Earthquakes cause significant loss of life and damage to property every year.

Many aseismic construction designs and technologies have been developed over the years in attempts to mitigate the effects of earthquakes on buildings, bridges and potentially vulnerable contents. Seismic isolation is a relatively recent, and evolving, technology of this kind.

Seismic isolation consists essentially of the installation of mechanisms which decouple the structure, and/or its contents, from potentially damaging earthquake-induced ground, or support, motions. This decoupling is achieved by increasing the flexibility of the system, together with providing appropriate damping. In many, but not all, applications the seismic isolation system is mounted beneath the structure and is referred to as 'base isolation'.

Although it is a relatively recent technology, seismic isolation has been well evaluated and reviewed (e.g. Lee and Medland, 1978; Kelly, 1986; Anderson 1990); has been the subject of international workshops (e.g. NZ-Japan Workshop, 1987; US-Japan Workshop, 1990; Assisi Workshop, 1989; Tokyo Workshop, 1992); is included in the programmes of international, regional and national conferences on Earthquake Engineering (e.g. 9th and 10th WCEE World Conferences on Earthquake Engineering, Tokyo, 1988, Madrid, 1992; Pacific Conferences, 1987, 1991; Fourth US Conference, 1990); and has been proposed for specialised applications (e.g. SMiRT-11, Tokyo, 1991).

Seismic isolation may be used to provide effective solutions for a wide range of seismic design problems. For example, when a large multistorey structure has a critical Civil Defence role which calls for it to be operational immediately after a very severe earthquake, as in the case of the Wellington Central Police Station (see Chapter 6), the required low levels of structural and non-structural damage may be achieved by using an isolating system which limits structural deformations and ductility demands to low values. Again, when a structure or substructure is inherently non-ductile and has only moderate strength, as in the case of the newspaper printing press at Petone (see Chapter 6), isolation may provide a required level of earthquake resistance which cannot be provided practically by earlier aseismic techniques. Careful studies have been made of classes of structure for which

seismic isolation may find widespread application. This has been found to include common forms of highway bridges.

The increasing acceptance of seismic isolation as a technique is shown by the number of retrofitted seismic isolation systems which have been installed. Examples in New Zealand are the retrofitting of seismic isolation to existing bridges and to the electrical capacitor banks at Haywards (see Chapter 6), while the retrofitting of isolators under the old New Zealand Parliamentary Buildings is being considered at present (June 1992). Many old monumental structures of high cultural value have little earthquake resistance. The completed isolation retrofit of the Salt Lake City and County Building in Utah is described in some detail in Chapter 6.

Isolation may often reduce the cost of providing a given level of earthquake resistance. The New Zealand approach has been to design for some increase in earthquake resistance, together with some cost reduction, a typical target being a reduction by 5% of the structural cost. Reduced costs arise largely from reduced seismic loads, from reduced ductility demand and the consequent simplified load-resisting members, and from lower structural deformations which can be accommodated with lower-cost detailing of the external cladding and glazing.

Seismic isolation thus has a number of distinctive beneficial features not provided by other aseismic techniques. We believe that seismic isolation will increasingly become one of the many options routinely considered and utilised by engineers, architects and their clients. The increasing role of seismic isolation will be reflected, for example, in widespread further inclusion of the technique in the seismic provisions of structural design codes.

When seismic isolation is used, the overall structure is considerably more flexible and provision must be made for substantial horizontal displacement. It is of interest that, despite the widely varying methods of computation used by different designers, a consensus is beginning to emerge that a reasonable design displacement should be of the order of 50–400 mm, and possibly up to twice this amount if 'extreme' earthquake motions are considered. A 'seismic gap' must be provided for all seismically isolated structures, to allow this displacement during earthquakes.

It is imperative that present and future owners and occupiers of seismically isolated structures are aware of the functional importance of the seismic gap and the need for this space to be left clear. For example, when a road or approach to a bridge is resealed or resurfaced, extreme care must be taken to ensure that sealing material, stones etc. do not fall into the seismic gap. In a similar way, the seismic gap around buildings must be kept secure from rubbish, and never used as a convenient storage space.

All the systems presented in this book are passive, requiring no energy input or interaction with an outside source. Active seismic isolation is a different field, which confers different aseismic features in the face of a different set of problems. As it develops, it will occupy a niche among aseismic structures which will be different from that occupied by structures with passive isolation. In a typical case, a mass which is a fraction of a per cent of the structural mass is driven

with large accelerations so that the reaction to its inertia forces tends to cancel the effects of inertia forces arising in the structure as a result of earthquake accelerations. Such a system may be a practical, but expensive, means of reducing the effective seismic loads during moderate, and in some locations frequent, earthquakes. Practical limitations on the size and displacements of the active mass would normally render the system much less effective during major earthquakes. Moreover, it is difficult to ensure the provision of the increasing driving power required during earthquakes of increased severity. In principle, such an active isolation system might be used to complement a passive isolation system in certain special cases. For example, a structure with passive seismic isolation may be satisfactory in all respects, except that it may contain components which are particularly vulnerable to high-frequency floor-acceleration spectra. The active-mass power and displacement requirements for the substantial cancellation of these short-period low-acceleration floor spectra may be moderate, even when the earthquake is very severe. Moreover, such moderate power might be supplied by an in-house source, with its dependability increased by the reduced seismic attack resulting from isolation.

A number of factors need to be considered by an engineer, architect or client wishing to decide whether a proposed structure should incorporate seismic isolation. The first of these is the seismic hazard, which depends on local geology (proximity to faults, soil substructure), recorded history of earthquakes in the region, and any known factors about the probable characteristics of an earthquake (severity, period, etc). Various proposed solutions to the design problem can then be put forward, with a variety of possible structural forms and materials, and with some designs incorporating seismic isolation, some not. The probable level of seismic damage can then be evaluated for each design, where the degree of seismic damage can be broadly categorised as:

- (1) minor
- (2) repairable (up to about 30% of the construction cost)
- (3) not repairable, resulting in the building being condemned.

The whole thrust of seismic isolation is to shift the probable damage level from (3) or (2) towards (1) above, and thereby to reduce the damage costs, and probably also the insurance costs. Maintenance costs should be low for passive systems, though they may be higher for active seismic isolation. As discussed above, the construction costs including seismic isolation usually vary by ± 5 –10% from unisolated options.

The total 'costs' and 'benefits' of the various solutions can then be evaluated, where the analysis has to include the 'value' of having the structure or its contents in as good as possible a condition after an earthquake, and the reduced risk of casualties with reduced damage to the structure. In many cases such additional benefits may well follow the adoption of the seismic isolation option.

1.2 FLEXIBILITY, DAMPING AND PERIOD SHIFT

The 'design earthquake' is specified on the basis of the seismicity of a region, the site conditions, and the level of hazard accepted (for example, a '400-year return period' earthquake for a given location would be expected to be less severe than one which occurred on average once every 1000 years). Design earthquake motions for other seismic areas of the world are often similar to that experienced and recorded at El Centro, California, in 1940, or to scalings of this motion, such as '1.5 El Centro'. The spectrum of the El Centro accelerogram has large accelerations at periods of 0.1–1 s. Other earthquake records, such as that at Pacoima Dam in 1971 or 'artificial' earthquakes A1 or A2, are also used in specifying the design level.

It must also be recognised that occasionally earthquakes give their strongest excitation at long periods. The likelihood of these types of motions occurring at a particular site can sometimes be foreseen, such as with deep deposits of soft soil which may amplify low-frequency earthquake motions, the old lake bed zone of Mexico City being the best known example. With this type of motion, flexible mountings with moderate damping may increase rather than decrease the structural response. The provision of high damping as part of the isolation system gives an important defence against the unexpected occurrence of such motions.

Typical earthquake accelerations have dominant periods of about 0.1–1 s as shown in Figure 2.1, with maximum severity often in the range 0.2–0.6 s. Structures whose natural periods of vibration lie within the range 0.1–1 s are therefore particularly vulnerable to seismic attack because they may resonate. The most important feature of seismic isolation is that its increased flexibility increases the natural period of the structure. Because the period is increased beyond that of the earthquake, resonance and near-resonance are avoided and the seismic acceleration response is reduced.

This period shift is shown schematically in Figure 1.1(a) and in more detail in Figure 2.1. The 'isolation ratio' ('degree of isolation') I , which governs so many aspects of seismic response, is a measure of the period shift produced by isolation.

The increased period and consequent increased flexibility also affects the horizontal seismic displacement of the structure, as shown in Figure 1.1(b) for the simplest case of a single-mass rigid structure, and as shown in more detail in Figure 2.1. Figure 1.1(b) shows how excessive displacements are counteracted by the introduction of increased damping. Real values of the maximum undamped displacement for isolated structures could be as large as 1 m in typical strong earthquakes; damping typically reduces this to 50–400 mm, and this is the displacement which has to be accommodated by the 'seismic gap.' The actual motion of parts of the structure depends on the mass distribution, the parameters of the isolating system, and the 'participation' of various modes of vibration. This is discussed in detail in Chapters 2 and 4.

Seismic isolation is thus an innovative aseismic design approach aimed at protecting structures against damage from earthquakes by limiting the earthquake attack rather than resisting it. Conventional approaches to aseismic design provide a

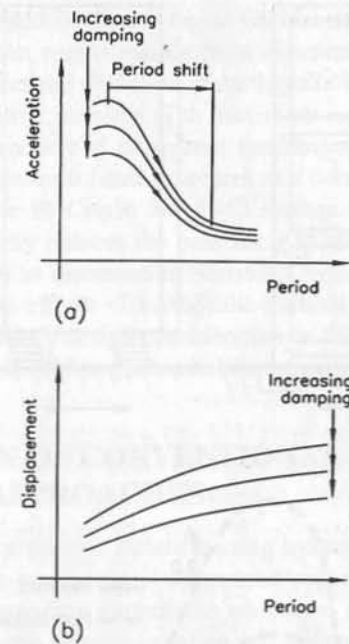


Figure 1.1 Effect of increasing the flexibility of a structure: (a) The increased period and damping lower the seismic acceleration response; (b) The increased period increases the total displacement of the isolated system, but this is offset to a large extent by the damping. (After Buckle and Mayes, 1990.)

structure with sufficient strength, deformability and energy-dissipating capacity to withstand the forces generated by an earthquake, and the peak acceleration response of the structure is often greater than the peak acceleration of the driving ground motion. On the other hand, seismic isolation limits the effects of the earthquake attack, since a flexible base largely decouples the structure from the horizontal motion of the ground, and the structural response accelerations are usually less than the ground accelerations. The forces transmitted to the isolated structure are further reduced by damping devices which dissipate the energy of the earthquake-induced motions.

Figure 1.2(a) illustrates the seismic isolation concept schematically. The building on the left is conventionally protected against seismic attack and that on the right has been mounted on a seismic isolation system. The performance of a pair of real test buildings of this kind, at Tohoku University, Sendai, Japan, is described in Chapter 6. Similar schematic diagrams can be drawn to illustrate the seismic isolation of bridges and of parts of buildings which contain delicate or potentially hazardous contents.

In Figure 1.2(a) it can be seen that large seismic forces act on the unisolated, conventional structure on the left, causing considerable deformation and cracking in the structure. In the isolated structure on the right, the forces are much reduced, and

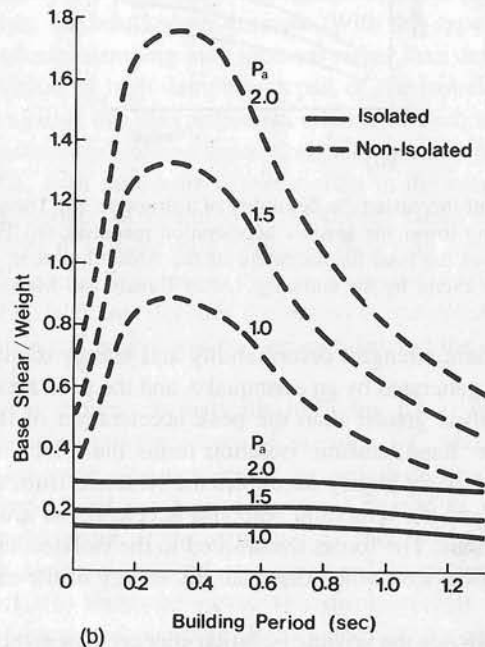
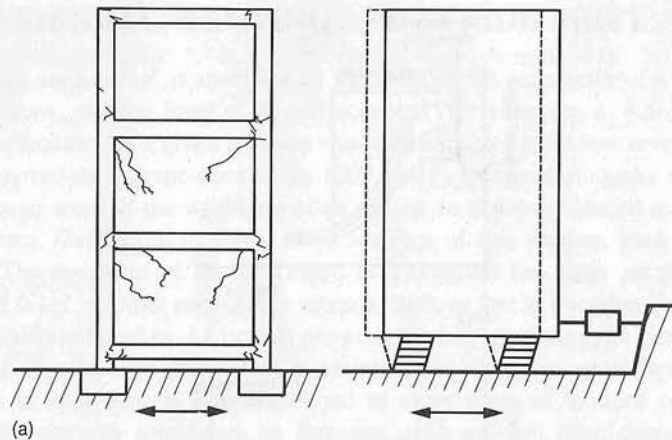


Figure 1.2 (a) Schematic seismic response of two buildings; that on the left is conventionally protected against earthquake, and that on the right has been mounted on a seismic isolation system. (b) Maximum base shear for a single-mass structure, represented as a linear resonator, with and without seismic isolation. The structure is subjected to P_a times the El Centro NS 1940 accelerogram (From Skinner and McVerry, 1975.)

most of the displacement occurs across the isolation system, with little deformation of the structure itself, which moves almost as a rigid unit. Energy dissipation in the

isolated system is provided by hysteretic or viscous damping. For the unisolated system, energy dissipation results mainly from structural damage.

Figure 1.2(b) illustrates the reduction of earthquake-induced shear forces which can be achieved by seismic isolation. The maximum responses of seismically isolated structures, as a function of unisolated fundamental period, are shown by a solid line and those of the unisolated structures as a dotted line, with results shown for three scalings of the El Centro NS 1940 earthquake motion. It is seen that seismic isolation markedly reduces the base shear in all cases.

It can also be shown, as discussed in Section 4.5, that seismic isolation is very effective in reducing the effects of earthquake-induced motion on torsionally unbalanced buildings. The key design consideration in this case is that the centre of stiffness of the isolator should be placed below the centre of mass of the structure.

1.3 COMPARISON OF CONVENTIONAL AND SEISMIC ISOLATION APPROACHES

Many of the concepts of seismic isolation using hysteretic isolators are similar to the conventional failure-mode-control approach ('capacity design') which is used in New Zealand for providing earthquake resistance in reinforced concrete and steel structures. In both the seismic isolation and failure-mode-control approaches, specially selected ductile components are designed to withstand several cycles well beyond yield under reversed loading, the yield levels being chosen so that the forces transmitted to other components of the structure are limited to their elastic, or low ductility, range. The yielding lengthens the fundamental period of the structure, detuning the response away from the energetic period range of most of the earthquake ground motion. The hysteretic behaviour of the ductile components provides energy dissipation to damp the response motions. The ductile behaviour of the selected components ensures sufficient deformation capacity, over a number of cycles of motion, for the structure as a whole to ride out the earthquake attack.

However, seismic isolation differs fundamentally from conventional seismic design approaches in the method by which the period lengthening (detuning) and hysteretic energy-dissipating mechanisms are provided, as well as in the philosophy of how the earthquake attack is withstood.

In well designed conventional structures, the yielding action is designed to occur within the structural members at specially selected locations ('plastic hinge zones'), e.g. mostly in the beams adjacent to beam-column joints in moment-resisting frame structures. Yielding of structural members is an inherently damaging mechanism, even though appropriate selection of the hinge locations and careful detailing can ensure structural integrity. Large deformations within the structure itself are required to withstand strong earthquake motions. These deformations cause problems for the design of components not intended to provide seismic resistance, because it is difficult to ensure that unintended loads are not transmitted to them when the structure is deformed considerably from its rest position. Further problems occur in the detailing of such items as windows and partitions, and for the seismic design

of building services. In the conventional approach, it is accepted that considerable earthquake forces and energy will be transmitted to the structure from the ground. The design problem is to provide the structure with the capacity to withstand these substantial forces.

In seismic isolation, the fundamental aim is to reduce substantially the transmission of the earthquake forces and energy into the structure. This is achieved by mounting the structure on an isolating layer (isolator) with considerable horizontal flexibility, so that during an earthquake, when the ground vibrates strongly under the structure, only moderate motions are induced within the structure itself. Practical isolation systems must trade off between the extent of force isolation and acceptable relative displacements across the isolation system during the earthquake motion. As the isolator flexibility increases, movements of the structure relative to the ground may become a problem under other vibrational loads applied above the level of the isolation system, particularly wind loads. Acceptable displacements in conjunction with a large degree of force isolation can be obtained by providing damping, as well as flexibility in the isolator. A seismic isolation system with hysteretic force-displacement characteristics can provide the desired properties of isolator flexibility, high damping and force-limitation under horizontal earthquake loads, together with high stiffness under smaller horizontal loads to limit wind-induced motions. A further trade-off is involved if it is necessary to provide a high level of seismic protection for potentially resonant contents and substructures, where increased isolator displacements and/or structural loads are incurred when providing this additional protection.

1.4 COMPONENTS IN AN ISOLATION SYSTEM

The components in a seismic isolation system are specially designed, distinct from the structural members, and installed generally at or near the base of the structure. However, in bridges, where the aim is to protect relatively low-mass piers and their foundations, they are more commonly between the top of the piers and the superstructure. The isolator's viscous damping and hysteretic properties can be selected to maintain all components of the superstructure within the elastic range, or at worst so as to require only limited ductile action. The bulk of the overall displacement of the structure can be concentrated in the isolator components, with relatively little deformation within the structure itself, which moves largely as a rigid body mounted on the isolation system. The performance can be further improved by bracing the structure to achieve high stiffness, which increases the detuning between the fundamental period of the superstructure and the effective period of the isolated system and also limits deformations within the structure itself. Both the forces transmitted to the structure and the deformation within the structure are reduced, and this simplifies considerably the seismic design of the superstructure, its contents and services, apart from the need for the service connections to accommodate the large displacements across the isolating layer.

Figure 1.3 is a schematic representation of the two major models encountered in

the practical design of seismic isolating systems. Figure 1.3(a) represents a linear damped isolator by means of a linear spring and 'viscous damper'. The resultant force-displacement loop has an effective slope (dashed line) which is the 'stiffness', or inverse flexibility, of the isolator. Figure 1.3(b) represents a 'bilinear' isolator as two linear springs, one of which has a 'Coulomb damper' in series with it. The resultant hysteresis loop is bilinear, characterised by two slopes which are the 'initial' and 'yielded' stiffnesses respectively, corresponding to the elastic and plastic deformation of the isolator. This is discussed in more detail in Chapters 2, 3 and 4.

A variety of seismic isolation and energy dissipation devices has been developed over the years, all over the world. The most successful of these devices also satisfy an additional criterion, namely they have a simplicity and effectiveness of design which makes them reliable and economic to produce and install, and which incorporates low maintenance, so that a passively isolated system will perform satisfactorily, without notice or forewarning, for 5-10 s of earthquake activity at any stage during the 30- to 100-year life of a typical structure. In order to ensure that the system is operative at all times, we suggest that zero or low maintenance be part of good design. Detailed discussion of the material and design parameters of seismic isolation devices is given in Chapter 3.

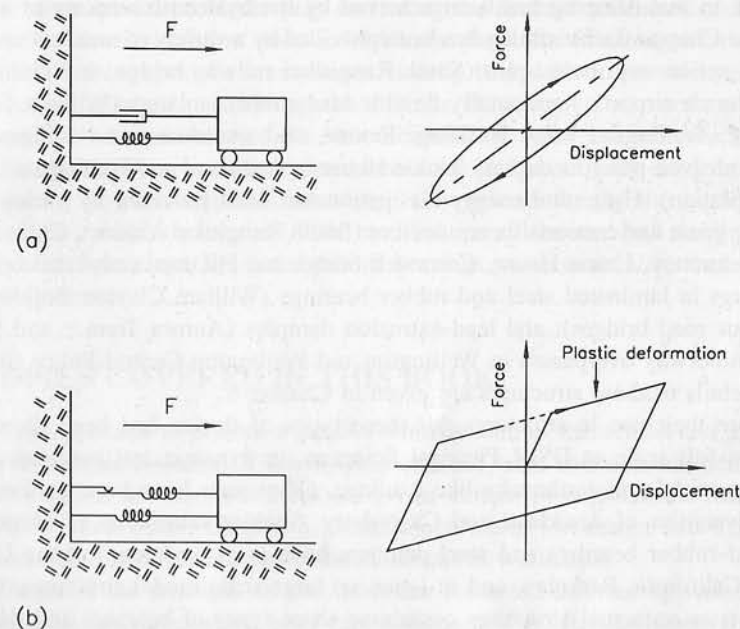


Figure 1.3 Schematic representation of the force-displacement hysteresis loops produced by (a) a linear damped isolator; (b) a bilinear isolator with a Coulomb damper

1.5 PRACTICAL APPLICATION OF THE SEISMIC ISOLATION CONCEPT

The seismic isolation concept for the protection of structures from earthquakes has been proposed in various forms at numerous times this century. Many systems have been put forward, involving features such as roller or rocker bearings, sliding on sand or talc, or compliant first-storey columns, but these have generally not been implemented.

The practical application of seismic isolation is a new development pioneered by a few organisations around the world in recent years. The efforts of these pioneers are now blossoming, with seismic isolation becoming increasingly recognised as a viable design alternative in the major seismic regions of the world.

The authors' group at DSIR Physical Sciences, previously the Physics and Engineering Laboratory of the Department of Scientific and Industrial Research (PEL, DSIR) in New Zealand, has pioneered seismic isolation, with research starting in 1967. Several practical techniques for achieving seismic isolation and a variety of energy-dissipating devices have been developed and implemented in over 40 structures in New Zealand, largely through the innovative approach and co-operation of engineers of the Ministry of Works and Development (MWD), as well as private structural engineering consultants in New Zealand.

All the techniques developed at DSIR Physical Sciences have had a common element, in that damping has been achieved by the hysteretic working of steel or lead (see Chapter 3). Flexibility has been provided by a variety of means: transverse rocking action with base uplift (South Rangitikei railway bridge, and chimney at Christchurch airport); horizontally flexible lead-rubber isolators (William Clayton Building; Wellington Press Building, Petone, and numerous road bridges); and flexible sleeved-pile foundations (Union House in Auckland and Wellington Central Police Station). Hysteretic energy dissipation has been provided by various steel bending-beam and torsional-beam devices (South Rangitikei Viaduct, Christchurch airport chimney, Union House, Cromwell bridge and Hikuwai retrofitted bridges); lead plugs in laminated steel and rubber bearings (William Clayton Building and numerous road bridges); and lead-extrusion dampers (Aurora Terrace and Bolton Street motorway overpasses in Wellington and Wellington Central Police Station). More details of these structures are given in Chapter 6.

Before their use in structures, all these types of device had been thoroughly tested at full scale at DSIR Physical Sciences, in dynamic test machines under both sinusoidal and earthquake-like loadings. Other tests have been performed at the Universities of Auckland and Canterbury. Shaking-table tests of elastomeric and lead-rubber bearings and steel dampers have been performed at the University of California, Berkeley, and in Japan on large-scale model structures. Quick-release tests on actual structures containing these types of bearings and damping devices have been performed in New Zealand and Japan. Some seismically isolated structures have now (1992) performed successfully during real, but so far minor, earthquake motions.

A number of organisations around the world have developed isolation systems different from those at DSIR Physical Sciences. Most have used means other than the hysteretic action of ductile metal components to obtain energy dissipation, force limitation and base flexibility. Various systems have used elastomeric bearings without lead plugs, damping being provided either by the use of high-loss rubber or neoprene materials in the construction of the bearings or by auxiliary viscous dampers. There have been a number of applications of frictional sliding systems, both with and without provision of elastic centring action. There has been substantial work recently on devices providing energy dissipation alone, without isolation, in systems not requiring period shifting, either because of the substantial force reduction from large damping or because the devices were applied in inherently long-period structures, such as suspension bridges or tall buildings, where isolation itself produces little benefit. There has also been work on very expensive mechanical linkage systems for obtaining three-dimensional isolation.

Seismic isolation has often been considered as a technique only for 'problem' structures or for equipment which requires a special seismic design approach. This may arise because of their function (sensitive or high-risk industrial or commercial facilities such as computer systems, semiconductor manufacturing plant, biotechnology facilities and nuclear power plants); their special importance after an earthquake (e.g. hospitals, disaster control centres such as police stations, bridges providing vital communication links); poor ground conditions; proximity to a major fault; or other special problems (e.g. increasing the seismic resistance of existing structures). Seismic isolation does indeed have particular advantages over other approaches in these special circumstances, usually being able to provide much better protection under extreme earthquake motions. However, its economic use is by no means limited to such cases. In New Zealand, the most common use of seismic isolation has been in ordinary two-lane road bridges of only moderate span, which are by no means special structures, although admittedly the implementation of seismic isolation required little modification of the standard design which already used vulcanised laminated-rubber bearings to accommodate thermal and other movements.

1.6 TOPICS COVERED IN THIS BOOK

In this book we seek to present a parallel development of theoretical and practical aspects of seismic isolation. Thus in Chapter 2 the main concepts are defined, in Chapter 3 details of various devices are given, Chapter 4 explores the theoretical concepts in more detail, Chapter 5 presents guidelines for design and Chapter 6 gives some details of seismically isolated structures worldwide.

In Chapter 2 the principal seismic response features conferred by isolation are outlined, with descriptions and brief explanations, which often anticipate the more extensive studies and discussions which appear in Chapter 4. Seismic response spectra are introduced as the maximum seismic displacements and accelerations of linear 1-mass damped vibrators. It is later shown that these spectra give good

approximations to the maximum displacements, accelerations and loads of structures mounted on linear isolation systems, which respond approximately as rigid masses with little deformation and little higher-mode response. The spectra vary depending on the accelerogram used to excite the seismic response, with El Centro NS 1940, or appropriately scaled versions of this design earthquake, being used most commonly throughout this book.

When the single mass is mounted on a bilinear isolation system, the maximum seismic displacement and acceleration responses can be represented in terms of 'effective' periods and dampings. This concept is an oversimplification but is valid for a wide range of bilinear parameters. It is convenient to introduce an 'isolator non-linearity factor' NL , which is defined in terms of the force-displacement hysteresis loop. However, unlike the case with linear isolation, many bilinear isolation systems result in large higher-mode effects which may make large or even dominant contributions to the maximum seismic loads throughout the isolated structure. They may also result in relatively severe appendage responses, as given by floor-acceleration spectra, for periods below 1.0 s.

The above and other features of the maximum seismic responses of isolated structures are illustrated at the end of Chapter 2 by seven case studies, as summarised in Table 2.1 and Figure 2.7 and further by Table 2.2. Features examined include the maximum seismic responses of a simple uniform shear structure and of 1-mass top-mounted appendages, when the structure is unisolated and when it is supported on each of six isolation systems. The responses given for individual 'modes' appropriate to the yielding phase have been evaluated using the mode-sweeping technique described later in Chapter 4.

Chapter 3 presents details of seismic isolation devices, with particular reference to those developed in our laboratory over the past 25 years, including steel-beam dampers, lead extrusion dampers and lead-rubber bearings. The treatment discusses the material properties on which the devices are based, and outlines the principal features which influence the design of these devices.

Chapter 4 comprises a more detailed analysis and expansion of ideas put forward in Chapter 2. It begins with a discussion of the modal features and seismic responses of linear structures mounted on linear isolators. Studies include the examination of non-classical higher modes which arise when the isolator damping is high and the structural damping is low. The concept of the 'degree of isolation' I , which controls the extent to which isolation changes the modal features, is introduced. The degree of isolation depends on the relative flexibilities of the isolator and the structure, and is conveniently expressed as the ratio of the isolator period (as given with a rigid structure) to the unisolated structural period (as obtained with a rigid isolator). If $I = 0$ then the structure is unisolated and if $I = \infty$ then it is completely isolated. In practice, a value of $I \geq 2$ gives 'well isolated' modal features.

The main thrust of Chapter 4 is to increase our knowledge and understanding of the consequences of seismic isolation. A preliminary database comprising 81 cases of different isolator and structural parameters is used to establish concepts and to simplify the evaluation of various features of isolated structures which may be

important for design. Considerable attention is given to the responses of substructures for unisolated and variously isolated structures. The extent to which isolators may reduce the seismic responses which torsional unbalance confers on unisolated structures is also examined.

Chapter 5 outlines an approach to the seismic design of isolated structures, using the results developed in previous chapters. The simple guidelines have the primary aim of enabling a designer to arrive at suitable starting parameters which can then be refined by computation.

Chapter 6 presents information on the world-wide use of seismic isolation in buildings, bridges and special structures which are particularly vulnerable to earthquakes. The information has been compiled with the help of colleagues around the world, who have enabled us to build up a picture of the isolation approaches which have been adopted in response to a wide range of seismic design problems; we should like to thank these colleagues for their contributions.

It is clear that engineers, architects and their clients all over the world are building up extensive experience in the development, design and potential uses of isolation systems. In time, these isolated structures will also provide a steadily increasing body of information on the performance of seismically isolated systems during actual earthquakes. In this way the evolving technology of seismic isolation may contribute to the mitigation of earthquake hazard worldwide.

2 *General Features of Structures with Seismic Isolation*

2.1 INTRODUCTION

For many structures the severity of an earthquake attack may be lowered dramatically by introducing a flexible isolator as indicated by Figure 1.1. The isolator increases the natural period of the overall structure and hence decreases its acceleration response to earthquake-generated vibrations. A further decrease in response occurs with the addition of damping. This increase in period, together with damping, can markedly reduce the effect of the earthquake, so that less-damaging loads and deformations are imposed on the structure and its contents.

This chapter examines the general changes in vibrational character which different types of seismic isolation confer on a structure, and the consequent changes in seismic loads and deformations. The study is greatly assisted by considering structural modes of vibration and earthquake response spectra, an approach which has proved very effective in the study and design of non-isolated aseismic structures (Newmark and Rosenblueth, 1971; Clough and Penzien, 1975).

The seismic responses of linear structures in general are introduced early to provide the concepts used throughout Chapters 2, 4 and 5. Attention is also given to seismic response mechanisms since they assist in understanding the seismic responses of isolated structures and how they are related to the responses of similar structures which are not isolated. The general consequences of seismic isolation are illustrated using six different isolation systems.

This chapter provides an introduction to the more systematic study in Chapters 4 and 5. It leads to some useful approaches for the study of seismic isolation, gives a greater understanding of the mechanisms involved, and indicates some useful design approaches. The discussions throughout this chapter assume simple torsionally balanced structures in which the structural masses at rest are centred on a vertical line, as illustrated in Figures 2.1-2.7.

2.2 ROLE OF EARTHQUAKE RESPONSE SPECTRA AND VIBRATIONAL MODES IN THE PERFORMANCE OF ISOLATED STRUCTURES

2.2.1 Earthquake response spectra

The horizontal forces generated by typical design-level earthquakes are greatest on structures with low flexibility and low vibration damping. The seismic forces on such structures can be reduced greatly by supporting the structure on mounts which provide high horizontal flexibility and high vibration damping. This is the essential basis of seismic isolation. It can be illustrated most clearly in terms of the response spectra of design earthquakes.

The main seismic attack on most structures is the set of horizontal inertia forces acting on the structural masses, these forces being generated as a result of horizontal ground accelerations. For most structures, vertical seismic loads are relatively unimportant in comparison with horizontal seismic loads. For typical design earthquakes, the horizontal accelerations of the masses of simple shorter-period structures are controlled primarily by the period and damping of the first vibrational mode, i.e. that form in which the system resonates at the lowest frequency. The dominance of the first mode occurs in isolated structures, and in unisolated structures with first-mode periods of up to about 1.0 s, a period range which includes most structures for which isolation may be appropriate. Neglecting the less important factors of mode shape and the contribution of higher modes of vibration, the seismic acceleration responses of the isolated and unisolated structures may be compared broadly by representing them as single-mass oscillators which have the periods and dampings of the first vibrational modes of the isolated and unisolated structures respectively.

The natural (fundamental) period T , natural frequency ω and damping factor ζ of such a single-mass oscillator, of mass m , are obtained by considering its equation of motion

$$m\ddot{u} + c\dot{u} + ku = -m\ddot{u}_g \quad (2.1)$$

where u is the displacement of the single-mass oscillator relative to the ground, u_g is the ground displacement, k is the 'spring stiffness' and c is the 'damping coefficient'.

The natural (fundamental) frequency of undamped, unforced oscillations ($c = 0$ and $\ddot{u}_g = 0$) is

$$\omega^2 = k/m \quad (2.2)$$

or

$$T = 2\pi\sqrt{(m/k)}. \quad (2.3)$$

The solution for damped, unforced oscillations is

$$u = Ae^{-(c/2m)t} \cos(\omega_d t + \delta)$$

where

$$\omega_d^2 = (k/m) - (c/2m)^2$$

and where A and δ are constants representing the initial displacement amplitude and initial phase of the motion.

The damped, unforced oscillation has thus a lower frequency ω_d than the natural frequency ω , and ω_d decreases as the value of the damping coefficient c is increased. If c is increased to a 'critical value' c_{cr} such that $\omega_d = 0$, the system will not oscillate. The critical damping is given by

$$c_{cr} = 2\sqrt{(mk)}.$$

A 'damping factor' ζ can then be defined which expresses the damping as a fraction of critical damping

$$\zeta = c/c_{cr} = c/[2\sqrt{(mk)}] = c/2m\omega = cT/4\pi m. \quad (2.4)$$

The equation of motion can then be divided by m to give

$$\ddot{u} + \frac{c}{m}\dot{u} + \frac{k}{m}u = -\ddot{u}_g$$

or

$$\ddot{u} + 2\zeta\omega\dot{u} + \omega^2u = -\ddot{u}_g. \quad (2.5)$$

For this (damped, forced) dynamic system, the displacement response to ground accelerations may be given in closed form as a Duhamel integral, obtained by expressing $\ddot{u}_g(t)$ as a series of impulses and summing the impulse responses of the system. When the system starts from rest at time $t = 0$, this gives the relative displacement response as

$$u(t) = -(1/\omega_d) \int_0^t \ddot{u}_g(\tau) \exp[-\zeta\omega(t-\tau)] \sin \omega_d(t-\tau) d\tau. \quad (2.6)$$

By successive differentiation, similar expressions may be obtained for the relative velocity response \dot{u} and the total acceleration response $\ddot{u} + \ddot{u}_g$. For particular values of ω and ζ , the responses to the ground accelerations of a given earthquake may be obtained from step-by-step evaluation of Equation (2.6) or from other evaluation procedures.

Since structural designs are normally based on maximum responses, a convenient summary of the seismic responses of single-mass oscillators is obtained by recording only the maximum responses for a set of values of the oscillator parameters ω (or T) and ζ . These maximum responses are the earthquake response

spectra. They may be defined as follows:

$$S_A(T, \zeta) = (\ddot{u} + \ddot{u}_g)(t)_{\max}; \quad S_V(T, \zeta) = \dot{u}(t)_{\max}; \quad S_D(T, \zeta) = u(t)_{\max}. \quad (2.7)$$

Such spectra are routinely calculated and published for important accelerograms e.g. EERL Reports (1972-5). Figure 2.1 shows response spectra for various damping factors (0, 2, 5, 10 and 20% of critical) for a range of earthquakes. Figure 2.1(a) shows acceleration response spectra for the accelerogram recorded in the S0°E direction at El Centro, California, during the 18 May 1940 earthquake (often referred to as 'El Centro NS 1940'). This accelerogram is typical of those to be expected on ground of moderate flexibility during a major earthquake. The El Centro accelerogram is used extensively in the following discussions because it is typical of a wide range of design accelerograms, and because it is used widely in the literature as a sample design accelerogram.

Seismic structural designs are frequently based on a set of weighted accelerograms, which are selected because they are typical of site accelerations to be expected during design-level earthquakes. The average acceleration response spectra for such a set of eight weighted horizontal acceleration components are given in Figure 2.1(b). Each of the eight accelerograms has been weighted to give the same area under the acceleration spectral curve, for 2% damping over the period range from 0.1-2.5 s, as the area for the El Centro NS 1940 accelerogram (Skinner, 1964).

Corresponding response spectra can be presented for maximum displacements relative to the ground, as given in Figure 2.1(c). These displacement spectra show that, for this type of earthquake, displacement responses increase steadily with period for values up to about 3.0 s. As in the case of acceleration spectra, the displacement spectral values decrease as the damping increases from zero. The spectra shown in Figure 2.1(b) and (c) are more exact presentations of the concept illustrated in Figure 1.1.

While the overall seismic responses of a structure can be described well in terms of ground response spectra, the seismic responses of a lightweight substructure can be described more easily in terms of the response spectra of its supporting floor. Floor-response spectra are derived from the accelerations of a point or 'floor' in the structure, in the same way that earthquake-response spectra are derived from ground accelerations. Thus they give the maximum response of lightweight single-degree-of-freedom oscillators located at a particular position in the structure, assuming that the presence of the oscillator does not change the floor motion. It is also possible to derive floor spectra which include interaction effects. Floor-response spectra tend to have peaks in the vicinity of the periods of modes which contribute substantial acceleration to that floor.

The response spectrum approach is used throughout this book to increase understanding of the factors which influence the seismic responses of isolated structures. The response spectrum approach also assists in the seismic design of isolated structures, as described in Chapter 5, since it allows separate consideration of the character of design earthquakes and of earthquake-resistant structures. A technique

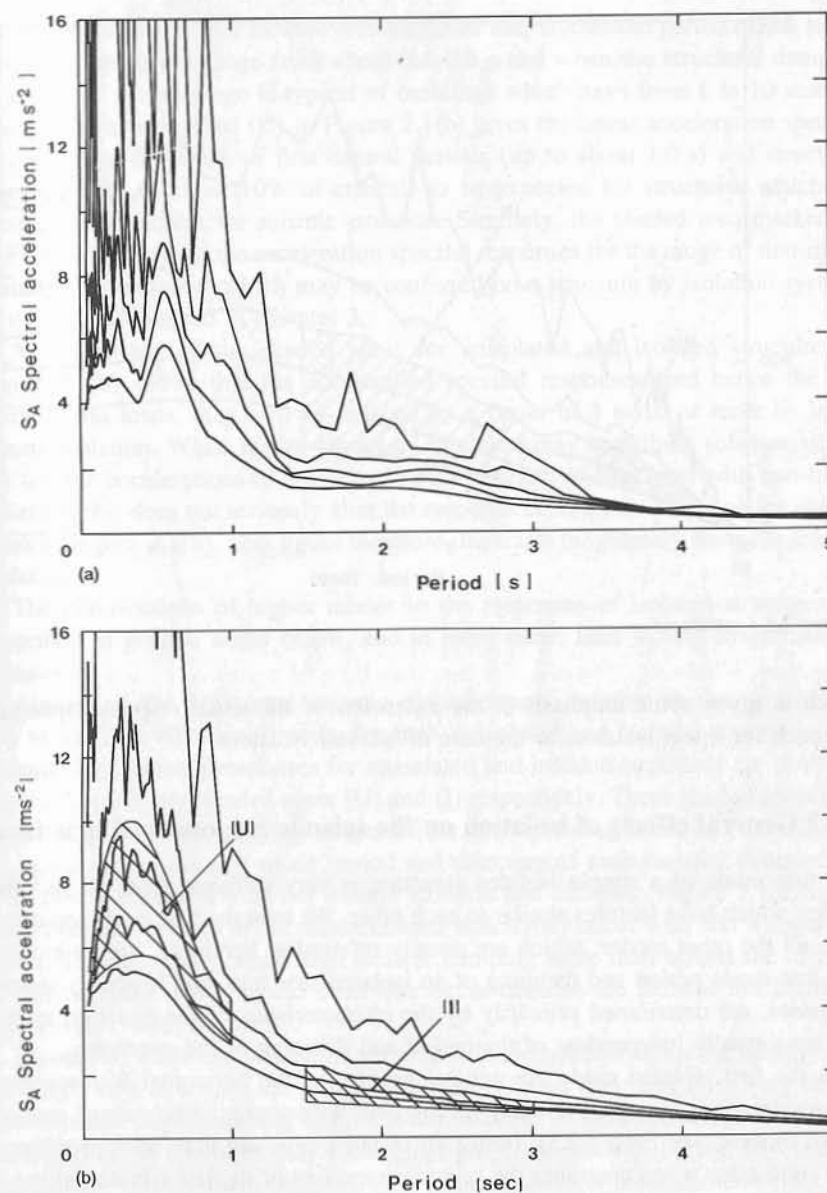


Figure 2.1 Response spectra for various damping factors. In each figure, the curve with the largest values has 0% damping and successively lower curves are for damping factors of 2, 5, 10 and 20% of critical. (a) Acceleration response spectrum for El Centro NS 1940. (b) Acceleration response spectrum for the weighted average of eight accelerograms (El Centro 1934, El Centro 1940, Olympia 1949, Taft 1952). The symbols U and I refer to unisolated and isolated structures respectively. (c) Displacement spectra corresponding to Figure 2.1(b)

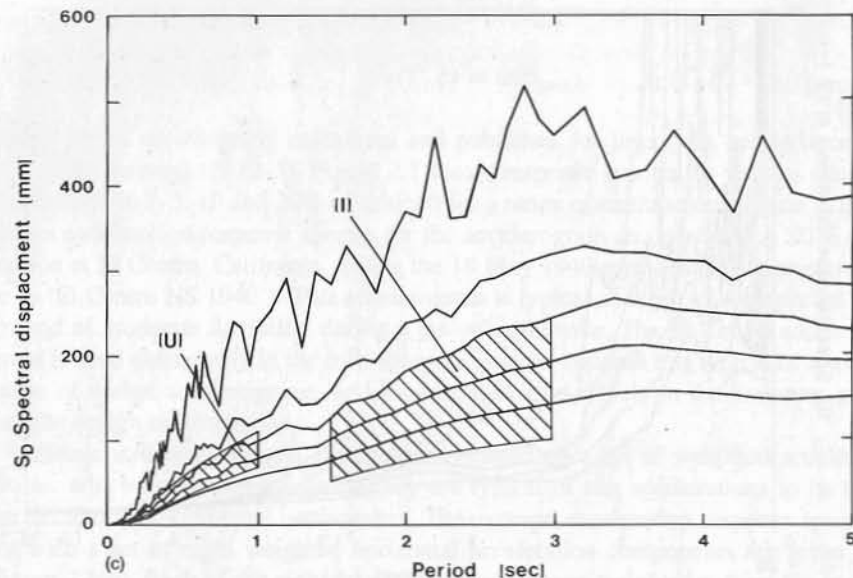


Figure 2.1 (continued)

which is given some emphasis is the extension of the usual response spectrum approach for linear isolators to the case of bilinear isolators.

2.2.2 General effects of isolation on the seismic responses of structures

The first mode of a simple isolated structure is very different from all its other modes, which have features similar to each other. We treat the first mode separately from all the other modes, which are usually referred to herein as 'higher modes'. The first-mode period and damping of an isolated structure, and hence its seismic responses, are determined primarily by the characteristics of the isolation system and are virtually independent of the period and damping of the structure.

In the first isolated mode the vertical profiles of the horizontal displacements and accelerations are approximately rectangular, with approximately equal motions for all masses (see Figure 2.5). Hence an isolated structure may be approximated by a rigid mass when assessing the seismic responses of its first vibrational mode.

Except for special applications, the seismic responses of structures with linear isolation can be described in terms of earthquake-response spectra, and the simple first mode of vibration. When the isolation is strongly non-linear, many important seismic responses can still be described in terms of mode 1, but higher modes can be of importance.

Figure 2.1(a) and (b) show acceleration response spectra for typical design earthquakes. It is seen that these maximum accelerations, and hence the general inertia

attacks on structures, are most severe when the first vibrational period of the structure is in the period range from about 0.1–0.6 s and when the structural damping is low. This period range is typical of buildings which have from 1 to 10 storeys. The shaded area marked (U) in Figure 2.1(b) gives the linear acceleration spectral responses for the range of first natural periods (up to about 1.0 s) and structural dampings (up to about 10% of critical) to be expected for structures which are promising candidates for seismic isolation. Similarly, the shaded area marked (I) in Figure 2.1(b) gives the acceleration spectral responses for the range of first-mode periods and dampings which may be conferred on a structure by isolation systems of the types described in Chapter 3.

A comparison of the shaded areas for unisolated and isolated structures in Figure 2.1(b) shows that the acceleration spectral responses, and hence the primary inertia loads, may well be reduced by a factor of 5 to 10 or more by introducing isolation. While higher modes of vibration may contribute substantially to the seismic accelerations of unisolated structures, and of structures with non-linear isolation, this does not seriously alter the response comparison based on the shaded areas of Figure 2.1(b). This figure therefore illustrates the primary basis for seismic isolation.

The contributions of higher modes to the responses of isolated structures are described in general terms below, and in more detail later in this chapter and in Chapter 4.

Almost all the horizontal seismic displacements, relative to the ground, are due to the first vibrational mode, for both unisolated and isolated structures. The seismic displacement responses for unisolated and isolated structures are shown in Figure 2.1(c) by the shaded areas (U) and (I) respectively. These shaded areas have the same period and damping ranges as the corresponding areas in Figure 2.1(b). As noted above, the first-mode period and damping of each isolated structure depend almost exclusively on the isolator stiffness and damping. Figure 2.1(c) shows a considerable overlap in the displacements which may occur with and without isolation. This may arise when high isolator damping more than offsets the increase in displacement which would otherwise occur because the isolator has increased the overall system flexibility.

Moreover, while displacements without isolation normally increase steadily over the height of a structure, the displacements of isolated structures arise very largely from isolator displacements, with little deformation of the structure above the isolator, giving the approximately rectangular profile of mode 1. Figure 2.1(c) shows that isolator displacements may be quite large. The larger displacements may contribute substantially to the costs of the isolators and to the costs of accommodating the displacements of the structures, and therefore isolator displacements are usually an important design consideration.

A convenient feature of the large isolator displacements is that the isolator location provides an effective and convenient location for dampers designed to confer high damping on the dominant first vibrational mode. Moreover, some dampers require large strokes to be effective. Such damping reduces both the accelerations

which attack the structure and the isolator displacements, for which provision must be made.

2.2.3 Parameters of linear and bilinear isolation systems

A typical isolated structure is supported on mounts which are considerably more flexible under horizontal loads than the structure itself. It is assumed here that the isolator is at the base of the structure and that it does not contribute to rocking motions. Other locations for isolators are discussed in Chapter 5. As a first approximation, the structure is assumed to be rigid, swaying sideways with approximately constant displacement along its height, corresponding to the first isolated mode of vibration.

Some isolation systems used in practice are 'damped linear' systems such as those presented in Equations (2.1) and (2.5). However, an alternative approach, for the provision of high isolator flexibility and damping, is to use non-linear hysteretic isolation systems, which also inhibit wind sway. Such non-linearity is frequently introduced by hysteretic dampers, or by the introduction of sliding components to increase horizontal flexibility, as discussed in Chapter 3. These isolation systems can usually be modelled approximately by including a component which slides with friction and gives a bilinear force-displacement loop when the model is cycled at constant amplitude. Models of linear and bilinear isolation systems, with the structure modelled by its total mass M , are shown in Figures 2.2(a) and 2.3(a).

The linear isolation system (Figure 2.2) has shear stiffness K_b and its coefficient of (viscous-) velocity-damping is C_b , where the subscript b is used to label parameters of the linear isolator. These parameters may be related to the mass M or the weight W of the isolated structure using Equations (2.3) and (2.4). This gives the natural period T_b and the velocity damping factor ζ_b

$$T_b = 2\pi\sqrt{(M/K_b)} \quad (2.8a)$$

and

$$\zeta_b = C_b T_b / (4\pi M). \quad (2.8b)$$

Figure 2.2(b) shows the 'shear force' versus 'displacement' hysteresis loop of such a damped linear isolator, which is traversed in the clockwise direction as the shear force and displacement cycle between maximum values $\pm S_b$ and $\pm X_b$ respectively. The 'effective stiffness' of the isolator is then defined as

$$K_b = S_b / X_b. \quad (2.9)$$

The design values chosen for T_b and ζ_b will usually be based on a compromise between seismic forces, isolator displacements, their effects on seismic resistance and the overall costs of the isolated structure.

When the isolator velocity-damping is quite high, say ζ_b greater than 20%, higher-mode acceleration responses may become important, especially regarding

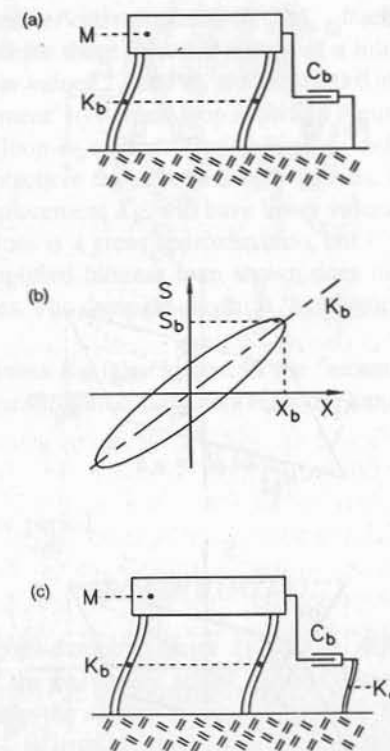


Figure 2.2 Schematic representation of a damped linear isolation system. (a) Structure of mass M supported by linear isolator of shear stiffness K_b , with velocity damper (viscous damper) of coefficient C_b . (b) Shear force S versus displacement X showing the hysteresis loop and defining the secant stiffness of the linear isolator: $K_b = S_b / X_b$. (c) Linear isolator with high damping coefficient and higher-mode attenuator K_c

floor-acceleration spectra. Such an increase in higher-mode responses may be largely avoided by anchoring the velocity dampers by means of components of appropriate stiffness K_c , as modelled in Figure 2.2(c).

The bilinear isolator model (Figure 2.3(a)) has a stiffness K_{b1} without sliding (the 'initial' or 'elastic-phase' stiffness), and a lower stiffness K_{b2} during sliding or yielding (the 'post-yield' or 'plastic-phase' stiffness). By analogy with the linear case, these stiffnesses can be related to corresponding periods of vibration of the system:

$$T_{b1}, T_{b2} = 2\pi\sqrt{(M/K_{b1})}, 2\pi\sqrt{(M/K_{b2})}. \quad (2.10a)$$

Corresponding damping factors can also be defined:

$$\zeta_{b1}, \zeta_{b2} = C_b T_{b1} / (4\pi M), C_b T_{b2} / (4\pi M). \quad (2.10b)$$

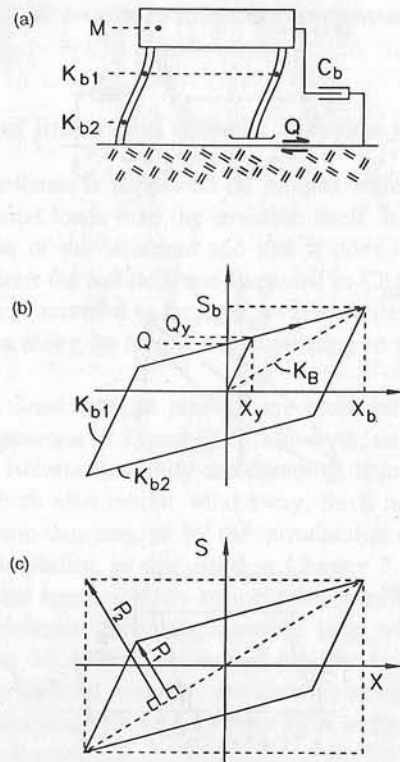


Figure 2.3 Schematic representation of a bilinear isolation system. (a) Structure of mass M supported by bilinear isolator which has linear 'spring' components of stiffnesses K_{b1} and K_{b2} , together with a sliding (Coulomb) damper component. (b) Shear force versus displacement showing the bilinear hysteresis loop and defining the secant stiffness of the bilinear isolator: $K_B = S_b/X_b$. The 'initial' or 'elastic-phase' and 'post-yield' or 'plastic-phase' stiffnesses K_{b1} and K_{b2} respectively are the slopes (gradients) of the hysteresis loop as shown, and (X_y, Q_y) is the yield point. (c) Comparison of linear hysteresis loop with a circumscribed rectangle, to enable definition of the non-linearity factor NL .

An additional parameter required to define a bilinear isolator is the yield ratio Q_y/W , relating the yield force Q_y of the isolator (Figure 2.3(b)) to the weight W of the structure. Yielding occurs at a displacement X_y given by Q_y/K_{b1} . When the design earthquake has the severity and character of the El Centro NS 1940 accelerogram it has been found that a yield ratio Q_y/W of approximately 5% usually gives suitable values for the isolator forces and displacements. In order to achieve corresponding results with a design accelerogram which is a scaled version of an El Centro like accelerogram, it is necessary to scale Q_y/W by the same factor, as described in Chapters 4 and 5.

It is found useful to describe the bilinear system using 'effective' values, namely

an appropriately defined 'effective' period T_B and 'effective' damping factor ζ_B . The subscript B is used for these effective values of a bilinear isolator.

The effective bilinear values T_B and ζ_B are obtained with reference to the 'shear force' versus 'displacement' hysteresis loop shown in Figure 2.3(b). This balanced-displacement bilinear loop is a simplification used to define these parameters of bilinear isolators. In practice, the reverse displacements, immediately before and after the maximum displacement X_b , will have lower values. In general, the concept of these 'effective' values is a gross approximation, but it works surprisingly well. Note also that the simplified bilinear loop shown does not include the effects of velocity-damping forces. The damping shown is 'hysteretic', depending on the area of the hysteresis loop.

The 'effective' stiffness K_B (also known as the 'secant' stiffness) is defined as the diagonal slope of the simplified maximum response loop shown in Figure 2.3(b):

$$K_B = S_b/X_b. \tag{2.11a}$$

This gives the effective period

$$T_B = 2\pi\sqrt{(M/K_B)}. \tag{2.11b}$$

An equivalent viscous-damping factor ζ_h can be defined to account for the hysteretic damping of the base. Any actual viscous damping ζ_b of the base must be added to ζ_h to obtain the effective viscous-damping factor ζ_B for the bilinear system. In practice ζ_h is usually larger than ζ_b , i.e. the damping of a bilinear hysteretic isolator is usually dominated by the hysteretic energy dissipation rather than by the viscous damping ζ_b . Thus

$$\zeta_B = \zeta_b + \zeta_h \tag{2.11c}$$

where, from Equation (2.4),

$$\zeta_b \approx C_b T_B / (4\pi M) \tag{2.12}$$

and where ζ_h is obtained by relating the maximum bilinear loop area to the loop area of a velocity-damped linear isolator vibrating at the period T_B with the same amplitude X_b , to give

$$\zeta_h = (2/\pi) A_h / (4S_b X_b) \tag{2.13}$$

where A_h = area of the hysteresis loop.

For non-linear isolators, it is convenient to have a quantitative definition of non-linearity. We have found it useful to define a non-linearity factor, NL , in terms of Figures 2.3(b) and 2.3(c), as the ratio of the maximum loop offset, from the secant line joining the points (X_b, S_b) and $(-X_b, -S_b)$, to the maximum offset of the axis-parallel rectangle through these points, i.e. P_1/P_2 . Hence the non-linearity factor increases from 0 to 1 as the loop changes from a zero-area shape to a rectangular

shape. For a bilinear isolator this is equivalent to the ratio of the loop area A_h to that of the rectangle. The non-linearity factor \underline{NL} is thus given by

$$\underline{NL} = A_h / (4S_b X_b) = Q_y / S_b - X_y / X_b. \quad (2.14)$$

From Equations (2.13) and (2.14) it is seen that the hysteretic damping factor ζ_h is proportional to the non-linearity factor \underline{NL} for bilinear hysteretic loops. However, re-entrant bilinear loops may have a much lower ratio of damping to non-linearity.

2.2.4 Calculation of seismic responses

When the isolator is linear and the base flexibility is sufficient for the first mode to dominate the response, the maximum seismic responses of the system may be approximated by design-earthquake spectral values, as given for example in Figure 2.1, for the isolator period T_b and damping ζ_b . For the approximately rigid-structure motions of the first isolated mode, the maximum displacement X_r at any level r in the structure is given by

$$X_r \approx S_D(T_b, \zeta_b). \quad (2.15a)$$

The maximum inertia load F_r , on the r th mass m_r , is given by

$$F_r \approx m_r S_A(T_b, \zeta_b). \quad (2.15b)$$

The inertia forces are approximately in phase and may be summed to give the shear at each level. In particular the base-level shear is given by

$$S_b \approx M S_A(T_b, \zeta_b). \quad (2.15c)$$

When the isolator is bilinear, seismic responses may still be obtained from design-earthquake spectral values, but the solutions are less exact than in the linear case, as discussed in Chapter 4. Some of the results of this later chapter are anticipated here so that the seismic responses of a range of isolators can be compared in Section 2.5. These results were obtained by calculating the responses of 81 different isolator-structure systems and analysing the patterns which emerged. It was found that the effective period T_B and effective damping ζ_B of Equations (2.11) to (2.13) may be used with earthquake spectra to obtain rough approximations for the seismic responses of the first mode. The maximum base displacement X_b and the maximum base shear S_b (neglecting velocity-damping forces) may be derived from the isolator parameters and 'bilinear' spectral displacement $S_D(T_B, \zeta_B)$ as follows:

$$X_b \approx C_F S_D(T_B, \zeta_B) \quad (2.16a)$$

$$S_b \approx Q_y + K_{b2}(X_b - X_y). \quad (2.16b)$$

Here C_F is a 'correction' factor which was found empirically. For the El Centro NS 1940 accelerogram, the correction factor C_F lies approximately in the range

0.85–1.15 for a wide range of the bilinear isolator parameters T_{b1} , T_{b2} and Q_y/W . This gives an idea of the uncertainties associated with this method. Note that the method is also iterative, as T_B and ζ_B are functions of X_b and S_b . Practical illustration of these concepts is given in Chapter 5 when discussing the design of isolation systems.

2.2.5 Contributions of higher modes to the seismic responses of isolated structures

The contributions of higher modes of vibration to the seismic responses of isolated structures can be described briefly in general terms. These contributions are examined systematically in Chapter 4.

A linear isolation system with a high degree of linear isolation and moderate isolator damping (i.e. $\zeta_b < 20\%$), or with high isolator damping which includes a higher-mode attenuator as in Figure 2.2(c), gives small higher-mode acceleration responses. Hence all the seismic responses of a structure with such linear isolation are approximated reasonably well by first-mode responses and by a rigid-structure model. Without higher-mode attenuation, high isolator damping may seriously distort mode shapes, and complicate their analysis, as described in Chapter 4. Also, higher-mode responses may increase as the damping increases, because greater base impedances caused by the base damping result in larger effective participation factors.

When a bilinear isolator has a high degree of non-linearity, there are usually relatively large higher-mode acceleration responses. These usually give substantial increases in the seismic inertia forces, compared with those produced by the first mode. Shear forces at various levels of the structure are typically increased by somewhat smaller amounts, the exception being near-base shears which remain close to their mode-1 values because shears arising from higher isolated modes have a near-zero value at the isolator level.

Increased floor-acceleration spectra may result from increased higher-mode acceleration responses and may be of concern when the seismic loads on lightweight substructures, or on the contents of the structure, are an important design consideration.

The higher-mode acceleration responses are generally reduced by reducing the non-linearity of the isolator, but other isolator parameters may modify the effects of non-linearity. When the isolator is bilinear the degree of non-linearity can usually be reduced by reducing the period ratio T_{b2}/T_{b1} and the yield ratio Q_y/W , since these changes usually give a less rectangular loop. However, the non-linearity should normally be left at the highest acceptable value, since the hysteretic damping of a bilinear isolator is proportional to the degree of non-linearity, and the first-mode response generally decreases as the damping increases.

For a given degree of non-linearity, the higher-mode acceleration responses can generally be reduced by making the elastic period T_{b1} considerably greater than the first unisolated period $T_1(U)$. This approach becomes more practical and effective

for structures whose period $T_1(U)$ is relatively low. The mechanisms underlying these higher-mode effects are discussed more fully in Chapter 4.

2.3 NATURAL PERIODS AND MODE SHAPES OF LINEAR STRUCTURES — UNISOLATED AND ISOLATED

2.3.1 Introduction

It has been stated above that most or all of the important seismic responses of a structure with linear isolation, and many of the seismic responses with non-linear isolation, can be approximated using a rigid-structure model. However, more detailed information is often sought, such as the effects of higher modes of vibration on floor spectra, especially for special-purpose structures for which seismic isolation is often the most appropriate design approach. Such higher-mode effects are conveniently studied by modelling the superstructure as a linear multi-mass system mounted on the isolation system.

Linear models and linear analysis can be used for unisolated structures and also when the structure is provided with linear isolation, except that high isolator damping may complicate responses. Simplified system models may be adopted to approximate the isolated natural periods and mode shapes when there is a high degree of modal isolation, namely when the effective isolator flexibility is high in comparison with the effective structural flexibility. This useful concept, the 'degree of isolation', is defined and discussed in Chapter 4.

When a structure is provided with a bilinear isolator, it is found that the distribution of the maximum seismic responses of higher modes can be interpreted conveniently in terms of the natural periods and mode shapes which prevail during plastic motions of the isolator. This approach is effective for the usual case in which the yield displacement is much less than the maximum displacement. These mode shapes and periods are given by a linear isolator model which has an elastic stiffness equal to the plastic stiffness K_{b2} of the bilinear isolator. These mode shapes explain the distribution of maximum responses through the structure, but in general the amplitudes of the responses will be different to those of a linear system with base stiffness K_{b2} . The elastic-phase isolation factor $I(K_{b1}) = T_{b1}/T_1(U)$ and the non-linearity factor NL are important parameters affecting the strengths of the higher-mode responses.

2.3.2 Structural model and controlling equations

The earthquake-generated motions and loads throughout non-yielding structures have been studied extensively (e.g. Newmark and Rosenblueth, 1971; Clough and Penzien, 1975). The structures are usually approximated by linear models with a moderate number N of point masses m_r , as illustrated in Figure 2.4(a) for a simple one-dimensional model.

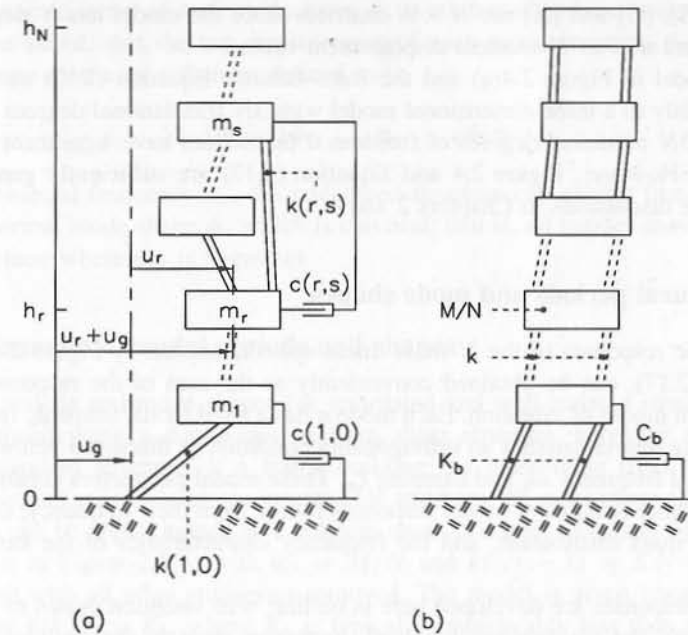


Figure 2.4 (a) Linear shear structure with concentrated masses. The seismic displacements of the ground and of the r th mass m_r are u_g and $(u_r + u_g)$ respectively. The relative displacement of the r th mass is u_r . Here $k(r, s)$ and $c(r, s)$ are, respectively, the stiffness and the velocity-damping coefficient of the connection between masses r and s . (b) Uniform shear structure with total mass M and overall unisolated shear stiffness K , such that the level mass $m_r = M/N$ and the intermass shear stiffness $k_r = KN$. If N tends to infinity, the overall height $l = h_N$, the mass per unit height $m = M/l$ and the stiffness per unit height $k = Kl$

In general, each pair of masses m_r, m_s is interconnected by a component with a stiffness $k(r, s)$ and a velocity damping coefficient $c(r, s)$. In Figure 2.4(a), each mass m_r has a single horizontal degree of freedom, u_r with respect to the supporting ground, or $u_r + u_g$ with respect to the pre-earthquake ground position, where the horizontal displacement of the ground is u_g .

At each point r , the mass exerts an inertia force $-(\ddot{u}_r + \ddot{u}_g)m_r$, while each interconnection exerts an elastic force $-(u_r - u_s)k(r, s)$ and a damping force $-(\dot{u}_r - \dot{u}_s)c(r, s)$. The N equations which give the balance of forces at each mass can be expressed in matrix form

$$[M]\ddot{u} + [C]\dot{u} + [K]u = -[M]l\ddot{u}_g \quad (2.17)$$

where $[M]$, $[C]$ and $[K]$ are the mass, damping and stiffness matrices, and where the matrix elements c_{rs} and k_{rs} are simply related to the damping coefficients and the stiffnesses, $c(r, s)$ and $k(r, s)$ respectively.

Here $[M]$, $[C]$ and $[K]$ are $N \times N$ matrices since the model has N degrees of freedom, and \mathbf{u} is an N -element displacement vector.

The model in Figure 2.4(a) and the force-balance Equation (2.17) can be extended readily to a three-dimensional model with $3N$ translational degrees of freedom (and $3N$ rotational degrees of freedom if the masses have significant angular momenta). However, Figure 2.4 and Equation (2.17) are sufficiently general for most of the discussions in Chapters 2 and 4.

2.3.3 Natural periods and mode shapes

The seismic responses of the N -mass linear system, defined by Figure 2.4(a) and Equation (2.17), can be obtained conveniently as the sum of the responses of N independent modes of vibration. Each mode n has a fixed modal shape ϕ_n (provided the damping matrix satisfies an orthogonality condition as discussed below), and a fixed natural frequency ω_n and damping ζ_n . These modal parameters depend on M , C and K . Other features of modal responses follow from their frequency, damping, shape and mass distribution, and the frequency characteristics of the earthquake excitation.

Modal responses are developed here in outline, with attention drawn to features which clarify the mechanisms involved. Important steps in the analysis parallel those for a simpler single-mass structure.

The natural frequencies of the undamped modes are obtained by assuming that there are free vibrations in which each mass moves sinusoidally with a frequency ω . Let

$$\mathbf{u} = \phi \sin(\omega t + \theta) \quad (2.18)$$

where the displaced shape ϕ varies with position in the structure and with ω , but is independent of t . Substitute Equation (2.18) in Equation (2.17), with the damping and ground acceleration terms removed

$$([K] - \omega^2[M])\phi \sin(\omega t + \theta) = \mathbf{0}. \quad (2.19)$$

Applying Cramer's rule it may be shown that non-trivial solutions are given by the roots of an N th-order equation in ω^2

$$\det([K] - \omega^2[M]) = 0. \quad (2.20)$$

For a general stable structure, Equation (2.20) is satisfied by N positive frequencies ω_n , termed the undamped natural or modal frequencies of the structure. The N natural frequencies are usually separate, although repeated natural frequencies can occur. The shape ϕ_n of mode n is now found by substituting ω_n in Equation (2.19) to give N linear homogeneous equations

$$([K] - \omega_n^2[M])\phi_n = \mathbf{0}. \quad (2.21)$$

Since the scale factor of each mode shape ϕ_n is arbitrary it is here assumed, unless otherwise stated, that the top displacement of each mode is unity: $\phi_{Nn} = 1$. A mode-shape matrix may then be defined as

$$[\Phi] = [\phi_1, \dots, \phi_n, \dots, \phi_N] \quad (2.22)$$

At each natural frequency ω_n , the undamped structure can exhibit free vibrations with a normal mode shape ϕ_n which is classical; that is, all masses move in phase (or antiphase where ϕ_{rn} is negative).

2.3.4 Example — modal periods and shapes

Natural periods and mode shapes for unisolated and well isolated structures may be illustrated using a continuous uniform shear structure, hereafter referred to as the standard structure. If a frame building has equal-mass rigid floors, and if the columns at each level are inextensible and have the same shear stiffness, the building can be approximated as a uniform shear structure. This may be modelled as shown in Figure 2.4(b) with $m_r = M/N$ and $k(r, r-1) = KN$ for $r = 1$ to N , and with all other stiffnesses removed. The model is given linear isolation by letting $k(1, 0) = K_b$, where K_b is typically considerably less than the overall shear stiffness K . It is given base velocity damping by letting $c(1, 0) = C_b$. The structural model is made continuous by letting $N \rightarrow \infty$.

From the partial differential form of Equations (2.17) which arises in the limit of $N \rightarrow \infty$, or otherwise, it may be shown that the mode shapes ϕ_n have a sinusoidal profile, and that the modal frequencies ω_n are proportional to the number of quarter-wavelengths in the modal profile. Unisolated modes have $(2n-1)$ quarter-wavelengths and isolated modes have just over $(2n-2)$ quarter-wavelengths, as shown in Figure 2.5. If the stiffnesses K and K_b are chosen to give first unisolated and isolated periods of 0.6 s and 2.0 s respectively, the periods of other modes follow from the number of quarter-wavelengths as shown in Figure 2.5. Moreover, there are 0.6/2.1 quarter-wavelengths in isolated mode 1, so that the first-mode shape value ϕ_{b1} at the base of the structure, above the isolator, is given by $\phi_{b1} = \cos(0.29 \times 90^\circ) = 0.90$, as shown. Higher isolated modes rapidly converge towards $(2n-2)$ quarter-wavelengths with increasing n , and corresponding periods occur.

Modal acceleration profiles have the same shapes as the corresponding displacement profiles but are of opposite sign, and hence, for a uniform mass distribution, the modal force profiles also have the same shapes as the displacement profiles. The shear at a given level may be obtained by summing the forces above that level, so it is evident from Figure 2.5 that the shear profiles for the higher modes ($n > 1$) of the isolated structures have small near-nodal values at the base level, because of the cancelling effects of the positive and negative half-cycles of the profile.

The unisolated and isolated natural periods and modal profiles of Figure 2.5

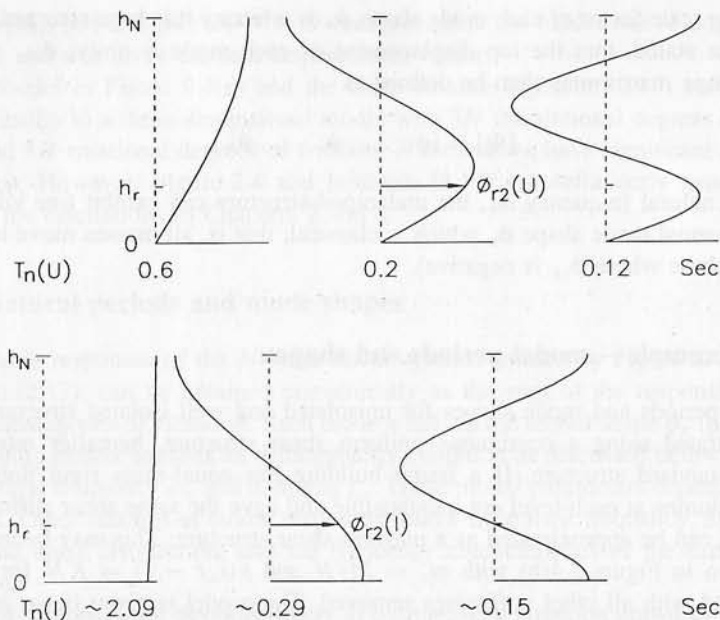


Figure 2.5 Variation, with height h_r , of ϕ_{rn} , which is the approximate shape of the n th mode at the r th level of the continuous uniform shear structure obtained by letting N tend to infinity in the structural model of Figure 2.4(b) shown for values of $T_1(U) = 0.6$ s and $T_b = 2.0$ s. The modal shapes and periods are shown when the structure is unisolated (U) and isolated (I). Note that the responses interleave, with periods $T_n(I)$ and $T_n(U)$ alternating between 2.09, 0.6, 0.29, 0.2, 0.15 and 0.12 s respectively

may be expressed as follows

$$T_n(U) = 0.6 / (2n - 1) \quad (s) \quad (2.23a)$$

$$T_1(I) = 2.1; \quad T_n(I) \approx 0.6 / (2n - 2), \quad \text{for } n > 1 \quad (s) \quad (2.23b)$$

$$\phi_{rn}(U) = \sin[(2n - 1)(\pi/2)(h_r/h_N)] \quad (2.23c)$$

$$\phi_{r1}(I) \approx \cos[(0.3(1 - h_r/h_N)(\pi/2))] \quad (2.23d)$$

$$\phi_{rn}(I) \approx \cos[(2n - 2)(\pi/2)(h_r/h_N)]. \quad (2.23e)$$

For structures which are non-shear and non-uniform, and have inter-mass stiffnesses in addition to $k(r, r - 1)$, period ratios are less simple but retain the general features given by Figure 2.5. For a well isolated structure, the first-mode period is controlled by the isolator stiffness. All other isolated and unisolated periods are controlled by the structure and are interleaved in the order given by Figure 2.5. The isolated mode-1 profile is still approximately rectangular. Higher-mode profiles are no longer sinusoidal but have the same sequences of nodes and antinodes.

Moreover, the shear profiles of higher isolated modes still have small near-nodal values at the isolator level.

For all well isolated structures, the damping of mode 1 is controlled by the isolator damping. The damping of all higher modes is controlled by structural damping, provided the velocity damping of the isolator is not much greater than that of the structure. It is commonly assumed that the structural damping is approximately equal for all significant modes.

2.3.5 Natural periods and mode shapes with bilinear isolation

When a structure is provided with a bilinear isolator there are two sets of natural periods and two corresponding sets of mode shapes; one set is given by a system model which includes a linear isolator which has the elastic stiffness K_{b1} of Figure 2.3, while the other set is given when the linear isolator has the plastic stiffness K_{b2} .

The yield level of a bilinear isolator is normally chosen to ensure that the maximum seismic displacement response, for a design-level excitation, is much larger than the isolator yield displacement. With such isolators the distribution of the maximum seismic motions and loads, and the floor spectra, can be expressed effectively in terms of the set of modes for which the shapes, and the higher-mode periods, are those of the normal modes which arise when the structure has a linear isolator of stiffness K_{b2} . An approximate effective period for mode 1 is derived from the secant stiffness K_B at maximum displacement, as given by Equation (2.11a) and illustrated in Figure 2.3(b). The relevance of the normal modes arising with a stiffness K_{b2} is to be expected, since maximum or near-maximum seismic responses should normally occur when the isolator is moving in its plastic phase, with an incremental stiffness K_{b2} . The relevance of this set of modes is discussed in the systematic studies in Chapter 4.

2.4 MODAL AND TOTAL SEISMIC RESPONSES

2.4.1 Seismic responses important for seismic design

This section considers the seismic response quantities which are commonly important for the design of non-isolated or isolated structures. Important seismic responses normally include structural loads and deformations and may include appendage loads and deformations. Appendage responses indicate the level of seismic attack on lightweight substructures, and on plant and facilities within the structures. For an isolator, seismic displacement is likely to be the most important and limiting design factor.

The contributions of structural modes and response spectra to the important seismic responses are indicated on the left of Figure 2.6. The earthquake accelerations give acceleration response spectra which combine with structural modes

to give mass accelerations and hence structural seismic forces. Similarly floor- (or structural-mass-) acceleration response spectra give the appendage seismic forces.

2.4.2 Modal seismic responses

The modal seismic responses of linear multi-mass structures can be expressed in a simple form when the shapes of all pairs of modes are orthogonal with respect to the stiffness, mass and damping matrices. It may be shown that undamped free-vibration mode shapes are orthogonal with respect to the mass and stiffness matrices. Moreover structural damping can usually be represented well by a matrix

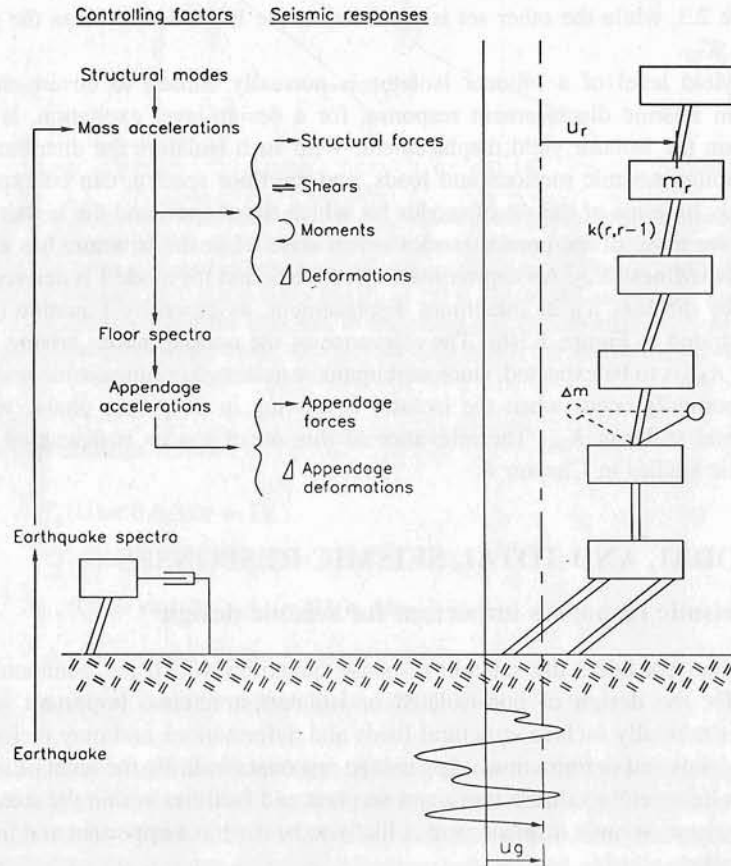


Figure 2.6 Schematic representation of the responses which dominate seismic design. The floor spectra have the same role in the response of the appendage as the earthquake spectra have in the response of the structure

which gives classical in-phase mode shapes. Such a damping matrix does not couple or change the shape of the undamped modes. Particular exceptions to orthogonal damping may arise with highly damped isolators or with damped appendages, as discussed in Chapter 4.

The orthogonality of the mode shapes, with respect to the mass and stiffness matrices, may be obtained from Equation (2.21) by noting that the mass and stiffness matrices are unaltered by transposition: the mass matrix because it is diagonal, and the stiffness matrix because it is symmetric.

If Equation (2.21), for mode n , is pre-multiplied by ϕ_m^T , and again the transpose of Equation (2.21), for mode m , is post-multiplied by ϕ_n , this gives

$$\omega_n^2 \phi_m^T [\mathbf{M}] \phi_n = \phi_m^T [\mathbf{K}] \phi_n \tag{2.24a}$$

$$\omega_m^2 \phi_m^T [\mathbf{M}]^T \phi_n = \phi_m^T [\mathbf{K}]^T \phi_n. \tag{2.24b}$$

Since $[\mathbf{M}]^T = [\mathbf{M}]$ and $[\mathbf{K}]^T = [\mathbf{K}]$, subtraction of Equation (2.24b) from Equation (2.24a) gives, for the usual case when $\omega_m^2 \neq \omega_n^2$, the orthogonality condition:

$$\phi_m^T [\mathbf{M}] \phi_n = 0, \quad \text{when } n \neq m \tag{2.25a}$$

Similarly

$$\phi_m^T [\mathbf{K}] \phi_n = 0, \quad \text{when } n \neq m. \tag{2.25b}$$

For the special case where two or more modes share the same frequency ω_m , the mode shapes for modes m and n with the common frequency can be chosen such that Equations (2.25a) and (2.25b) hold.

It is found that the responses of damped linear structures can also be described in terms of the same classical (in-phase) normal modes if the damping coefficients are also constrained by a similar orthogonality condition. That is, provided

$$\phi_m^T [\mathbf{C}] \phi_n = 0, \quad \text{when } n \neq m. \tag{2.25c}$$

It can be shown that Equations (2.25) imply that the inertia forces, the spring forces and the damping forces of any mode (n) do no work on the motions of any other mode (m).

The displacements $\mathbf{u}(t)$ of Equation (2.17) may be expressed as the sum of factored mode shapes:

$$\mathbf{u}(t) = \sum_1^N \phi_n \xi_n(t) \tag{2.26}$$

Substituting from Equation (2.26) into Equation (2.17), then pre-multiplying each term by ϕ_n^T and eliminating all terms given as zero by Equations (2.25) produces

$$\ddot{\xi}_n + \frac{\phi_n^T [\mathbf{C}] \phi_n}{\phi_n^T [\mathbf{M}] \phi_n} \dot{\xi}_n + \frac{\phi_n^T [\mathbf{K}] \phi_n}{\phi_n^T [\mathbf{M}] \phi_n} \xi_n = - \frac{\phi_n^T [\mathbf{M}] \mathbf{1}}{\phi_n^T [\mathbf{M}] \phi_n} \ddot{u}_g. \tag{2.27a}$$

When compared with Equation (2.5), Equation (2.27a) is seen to describe a single-degree-of-freedom damped oscillator with damping factor ζ_n and frequency ω_n given by

$$2\zeta_n\omega_n = \frac{\phi_n^T[\mathbf{C}]\phi_n}{\phi_n^T[\mathbf{M}]\phi_n} \quad (2.27b)$$

$$\omega_n^2 = \frac{\phi_n^T[\mathbf{K}]\phi_n}{\phi_n^T[\mathbf{M}]\phi_n} \quad (2.27c)$$

Here Equations (2.27) are the N -degree-of-freedom counterparts of Equations (2.2), (2.4) and (2.5).

Since $\mathbf{u} = \sum_{n=1}^N \mathbf{u}_n$ it follows from Equation (2.26) that the displacement at level r of the n th mode is given by

$$u_{rn} = \phi_{rn}\zeta_n \quad (2.28)$$

Substituting from Equation (2.28) into Equation (2.27) gives:

$$\ddot{u}_{rn} + 2\zeta_n\omega_n\dot{u}_{rn} + \omega_n^2u_{rn} = -\Gamma_{rn}\ddot{u}_g \quad (2.29)$$

where

$$\Gamma_{rn} = \phi_{rn} \frac{\phi_n^T[\mathbf{M}]\mathbf{1}}{\phi_n^T[\mathbf{M}]\phi_n} \quad (2.30a)$$

Hence, since $[\mathbf{M}]$ is a diagonal matrix,

$$\Gamma_{rn} = \phi_{rn} \frac{\sum_{i=1}^N m_i \phi_{in}}{\sum_{i=1}^N m_i \phi_{in}^2} \quad (2.30b)$$

$$= \phi_{rn} \Gamma_n \quad (2.30c)$$

The factor Γ_{rn} may be called a participation factor since it is the degree to which point r of mode n is coupled to the ground accelerations. Equation (2.30c) defines a mode weight factor Γ_n . It is here convenient to define $|\phi_{Nn}|$ as unity. For simple tower-like structures, when $\phi_{Nn} = (-1)^{n-1}$ then Γ_n is positive.

When Equations (2.5) and (2.7) are compared with Equation (2.29) and (2.30c) it is seen that

$$X_{rn} = \phi_{rn} \Gamma_n S_D(T_n, \zeta_n) \quad (2.31a)$$

$$\dot{X}_{rn} = \phi_{rn} \Gamma_n S_V(T_n, \zeta_n) \quad (2.31b)$$

$$\ddot{X}_{rn} = \phi_{rn} \Gamma_n S_A(T_n, \zeta_n) \quad (2.31c)$$

where the peak values X_{rn} , \dot{X}_{rn} and \ddot{X}_{rn} are defined as $u_{rn \max}$, $\dot{u}_{rn \max}$, and $(\ddot{u}_{rn} + \Gamma_{rn}\ddot{u}_g)_{\max}$ respectively. Note that these maximum seismic responses do not occur simultaneously, so, for instance the maximum acceleration \ddot{X} is NOT the derivative of the maximum velocity \dot{X} .

The maximum seismic displacements of mode n are given by Equation (2.31a). The maximum seismic forces F_{rn} follow directly from Equation (2.31c). Moreover, since all the mass accelerations for these classical normal modes are in phase, and therefore reach maximum values simultaneously, maximum shear forces S_{rn} and overturning moments \underline{OM}_{rn} , at level r , may be obtained by successive summation of maximum forces. This gives

$$F_{rn} = m_r \ddot{X}_{rn} \quad (2.32a)$$

$$S_{rn} = \sum_{i=r}^N F_{in} \quad (2.32b)$$

$$\underline{OM}_{rn} = \sum_{i=r+1}^N [(h_i - h_{i-1})S_{in}] \quad (2.32c)$$

where h_r = height to mass m_r .

2.4.3 Structural responses from modal responses

Usually the maximum structural responses cannot be obtained from the maximum responses of a set of modes by direct addition, since modal maxima occur at different times. The response levels of a mode, when plotted against time, vary in a somewhat noise-like way and the probable maximum combined response of several modes may usually be approximated by the square root of the sum of squares (SRSS) method (Wilson *et al*, 1981). For example, the probable force at level r , may be expressed as:

$$F_r = \sqrt{(\sum_i F_{ri}^2)} \quad (2.33)$$

where the mode i ranges over the significant modes.

However, if near-maximum responses of two or more modes are correlated in time by close modal periods (often arising with torsional unbalance or with near-resonant appendages), or by very short periods or very long periods, then the complete quadratic combination (CQC) method may need to be used. Strongly non-linear isolators may well provide a further mechanism which correlates modal responses, so that the SRSS combination is not accurate.

2.4.4 Example — seismic displacements and forces

Important features of Equations (2.30), (2.31) and (2.32) can be illustrated for the unisolated and the linearly isolated continuous uniform shear structure, but with more accurate profiles for higher isolated modes as given in Chapter 4. Top-mass

participation factors for successive modes are

$$\Gamma_{Nn}(U) = 1.27, 0.42, 0.25, \dots, 4/[\pi(2n - 1)]$$

$$\Gamma_{Nn}(I) \approx 1.0, 0.045, 0.011, \dots, 2/[(2n - 2)/0.3]^2$$

where $T_1(U)/T_b = 0.3$.

Higher isolated modes are seen to have much lower participation factors than corresponding unisolated modes.

The above mode-participation factors, together with the periods from Equation (2.23) and the spectra of Figure 2.1(b) and (c), can now be used to find important seismic motions and loads for modes 1 and 2 from Equations (2.31) and (2.32). For simplicity, a low damping factor of 5% is assumed for all modes. With practical isolated structures a higher damping would normally be provided for mode 1.

Since modal displacements may be represented by top displacements, consider $X_{Nn} = \Gamma_{Nn} S_D(T_n, 5)$:

$$X_{N1}(U) = 0.085; \quad X_{N2}(U) = 0.0037 \text{ (m)}$$

$$X_{N1}(I) \approx 0.18; \quad X_{N2}(I) \approx 0.0009 \text{ (m)}.$$

Notice that displacements are completely dominated by mode 1 for both unisolated and isolated structures. Moreover, for any well isolated structure, the base displacement is almost as large as the top displacement

$$X_b \approx X_{N1}(I).$$

Since modal loads may be represented by the force per unit height at the top of the structure F_{Nn} , consider $F_{Nn}/\rho = \Gamma_{Nn} S_A(T_n, 5)$, where $\rho = M/h_N$

$$F_{N1}(U)/\rho = 9.31; \quad F_{N2}(U)/\rho = 3.60 \text{ (ms}^{-2}\text{)}$$

$$F_{N1}(I)/\rho \approx 1.80; \quad F_{N2}(I)/\rho \approx 0.37 \text{ (ms}^{-2}\text{)}.$$

Note that the force for isolated mode 1 is relatively small because it has a low response spectrum factor, while the forces for higher isolated modes are relatively small because they have small participation factors.

2.4.5 Seismic responses with bilinear isolators

When the isolator is bilinear, there are a number of possible ways of defining the modes, as is discussed in Section 4.3.4. For any of the definitions we consider, the total response of a linear structure with bilinear isolation can be expressed exactly as the sum of the modal responses, as for a linear system. However, the modal equations of motion will be coupled, unlike those for classically damped linear systems.

Several of the possible definitions of the mode shapes with bilinear isolation are useful for interpreting the response or estimating the maximum response quantities.

In Section 2.2.3, we discussed the responses of a first mode defined by a rigid structure mounted on an 'equivalent' linear isolator with 'effective stiffness' K_B , 'effective period' T_B and 'effective damping' ζ_B . This model gives good approximations to the displacements and base shear of a structure on a bilinear isolator.

A useful set of modes for systems with bilinear isolation are those obtained by using the post-yield stiffness of the isolator. Then the higher-mode periods and all mode shapes are given by Equations (2.20) and (2.21) for a linear system with $K_b = K_{b2}$. Hence, as with moderately damped linear isolators, the bilinear modes are classical and normal. These modes are relevant for the maximum responses because they relate to the post-yield phase, when the maximum displacements and shears occur.

When the bilinear isolator has a high degree of non-linearity, the seismic responses of higher modes are often much greater than the responses which occur with the above 'equivalent' linear modes. Bilinearity usually gives greater higher-mode accelerations and loads, and particularly it usually gives greater values for floor-acceleration spectra over the period range covered by significant higher modes. The reasons for the larger seismic responses of the higher modes are discussed in Chapter 4 and are summarised briefly here.

With bilinear isolation, the input of seismic energy and the energy level of the overall system are given roughly by a rigid-structure model with a linear isolator of effective period T_B and effective damping factor ξ_B . When the structure is sufficiently flexible to give a substantial contrast between the mode-1 shapes for the first and second isolator stiffnesses, then there is usually significant energy in the higher modes, where relatively small fractions of the structural energy can result in relatively high modal accelerations and forces.

In terms of the modes for the plastic-phase stiffness K_{b2} , each isolator transition through the elastic phase redistributes the energy between the modes. This should result in a net transfer of energy from the large-energy mode 1 to the small-energy higher modes. The effects of the relatively large seismic responses of higher modes, with many bilinear isolators, are seen in the case studies below and in the more systematic studies of Chapter 4. The excitation mechanism for higher modes is also described more fully there.

The mode shapes corresponding to the post-yield stiffness K_{b2} are usually very similar in shape to the free-free mode shapes, obtained when the isolator stiffness is zero. It is sometimes more convenient to interpret the responses in terms of the free-free modes rather than those based on K_{b2} , because of the symmetry of the free-free modes and because there is no need to calculate new mode shapes for different values of K_{b2} . Decomposition of the response in terms of the free-free mode shapes also has the useful properties that the base shear is contributed entirely by the first mode, and that the first-mode displacements are uniform within the structure. Also, the base shear scaled by appropriate participation factors provides the driving forces for the higher modes.

The seismic responses of isolated structures can be decomposed into the contributions from suitably defined modes by a mode-sweeping technique described in Chapter 4. Either the modes based on base stiffness K_{b2} or the free-free modes can be used with this technique. The free-free mode shapes have been used to obtain the results given in Section 2.5.

2.5 COMPARISONS OF SEISMIC RESPONSES OF LINEAR AND BILINEAR ISOLATION SYSTEMS

2.5.1 Comparative study of seven cases

This section demonstrates many of the key features of seismic isolation, through seven examples which show the seismic responses of structures and appendages for various ranges of isolation system parameter values and structural flexibility. The examples are summarised in Table 2.1 in terms of the physical parameters of the systems, the maximum overall and modal response quantities, and the values of the non-linearity factor and elastic-phase isolation factor which are important parameters governing the isolated response.

Figure 2.7 shows the maximum values of the displacements, accelerations and shears and the 2% damped top-floor spectra calculated for an unisolated structure and six isolated structures in response to the El Centro 1940 NS ground acceleration. The solid lines represent maximum total responses, with the maximum values obtained from response history analysis. The dashed lines, and chain-dashed lines where given, represent respectively the maximum first- and second-mode responses at the various levels. In some cases the first-mode responses dominate to the extent that dashed and solid lines coincide (e.g. parts of the floor spectra, particularly at longer periods). In other cases, the difference between the solid and dashed lines indicates the higher-mode contribution to the response. The modal responses were obtained from the overall response histories at all masses in the structures by sweeping with the free-free mode shapes, as discussed in Section 4.3.4, except for the unisolated structure, where the modal responses are in terms of the true unisolated modes.

The 'unisolated' structure (case (i)) is a uniform linear chain system, with four equal masses and four springs of equal stiffness, the lowest being anchored to the ground. It has a first-mode undamped natural period of 0.5 s, and 5% damping in all its modes. Most of the 'isolated' cases represent systems obtained simply by adding below this structure an isolation system modelled as a base mass, a linear or bilinear-hysteretic base spring and a linear viscous base damper. However, two of the 'isolated' cases involve stiffer structures, with unisolated periods of 0.25 s, in order to show the effects of high elastic-phase isolation factors. In all the isolated cases, the added base mass is of the same value as the other masses, comprising 0.2 of the total isolated mass.

The viscous damping of the isolated structures is 5% of critical for all the free-free modes, with the non-linear isolation systems having linear viscous base

dampings ζ_{b2} which are 5% of critical in the post-yield phases, as well as hysteretic damping. The table shows values of ζ_b for the linear isolators, and values of ζ_b , ζ_{b1} and ζ_{b2} for the bilinear isolators, where $\zeta_b = \zeta_{b2} T_B / T_{b2}$.

The cases were chosen to represent a wide variety of isolation systems, with various degrees of non-linearity and pre- and post-yield isolation ratios. In calculating the isolation factors, $I = T_b / T_1(U)$ and $I(K_{b1}) = T_{b1} / T_1(U)$, the unisolated period $T_1(U)$ corresponds to that of the structure when the isolator is rigid, while the isolator periods T_b and T_{b1} are calculated for the five masses from the structure and the isolator with all their interconnecting springs treated as rigid, mounted on the isolator spring.

Cases (ii) and (iii) represent medium-period structures with a high degree of linear isolation ($T_1(U) = 0.5$ s, $T_b = 2.0$ s, $I = 4$), and with low ($\zeta_b = 5\%$) and high ($\zeta_b = 20\%$) values for the viscous damping of the isolator, respectively.

Case (iv) is a bilinear hysteretic system with similar characteristics to that of the William Clayton Building (Section 6.2.4), which was the first building isolated on lead-rubber bearings. The parameter values are typical for structures with this type of isolation system. The unisolated period of the structure is 0.25 s (the William Clayton Building has a nominal unisolated period of 0.3 s), with a pre-yield isolator period T_{b1} of 0.8 s and a post-yield isolator period $T_{b2} = 2.0$ s. The yield force ratio Q_y/W is 0.05, less than the William Clayton Building's value of 0.07. However, the latter value was chosen to give a near-optimal base shear response (see Section 4.3.2) in 1.5 El Centro, so scaling down the yield-force/weight ratio by approximately 2/3 is appropriate for a system with El Centro as the design motion. The post-yield isolator period is equal to the isolator period of the linear systems of cases (ii) and (iii). The equivalent viscous damping from the combined hysteretic and viscous base damping at the amplitude of its maximum response to El Centro is 24% (Table 2.1), comparable with the viscous damping of 20% for the linear system (iii).

Case (v) represents bilinear systems with elastic- and yielding-phase isolation factors towards the low ends of their practical ranges. The unisolated period is 0.5 s, with the isolator periods $T_{b1} = 0.3$ s and $T_{b2} = 1.5$ s, giving isolation factors of 0.6 and 3 in the two phases. The yield force ratio Q_y/W is 0.05, as for all the non-linear cases. This system has a moderate non-linearity factor which is virtually identical to that of case (iv) (0.33 compared with 0.32), but considerably reduced isolation factors, most importantly in the elastic phase where it is 0.6. The low elastic-phase isolation gives response characteristics similar to those for a system with an isolator which is rigid before it yields.

In case (vi), the post-yield period of the isolator has been doubled from that of case (v), to $T_{b2} = 3.0$ s, but the other parameter values are the same. This change produces a considerably higher non-linearity factor of 0.60, but still a low elastic-phase isolation factor of only 0.6. The response characteristics are similar to those for what is sometimes referred to as a 'resilient-friction base isolator' (Fan and Ahmadi, 1990, 1992; Mostaghel and Khodaverdian, 1987).

The final example, case (vii), is a strongly non-linear system, with a non-linearity

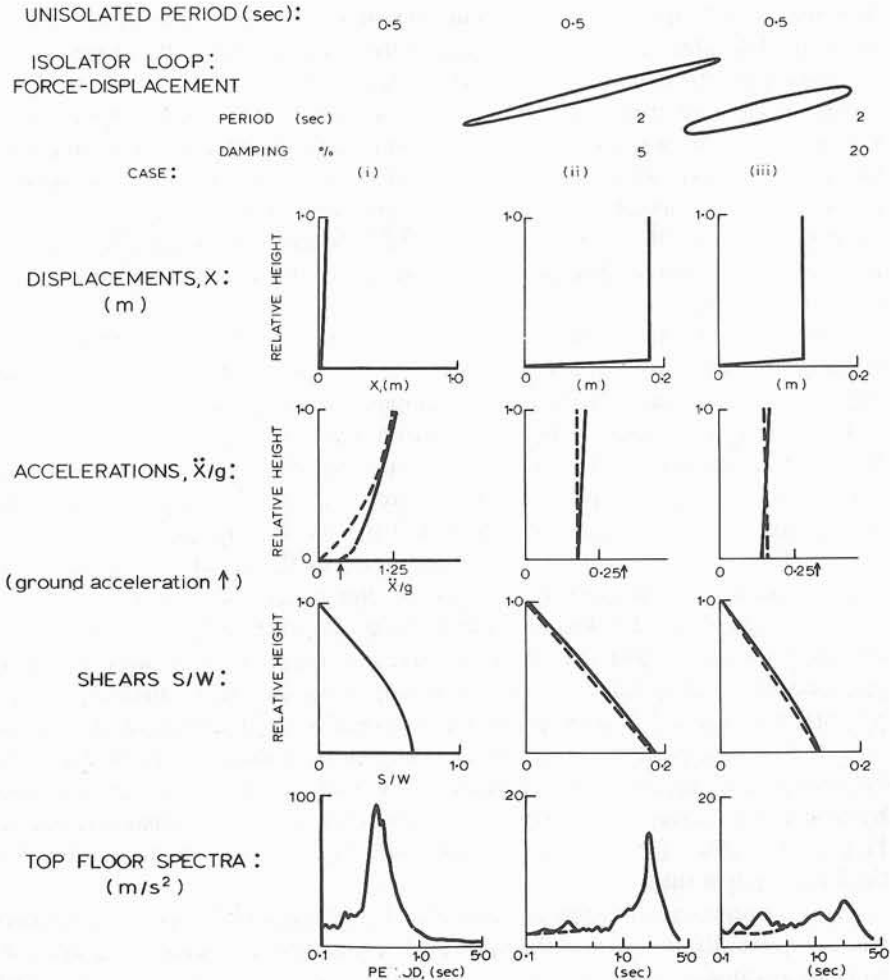
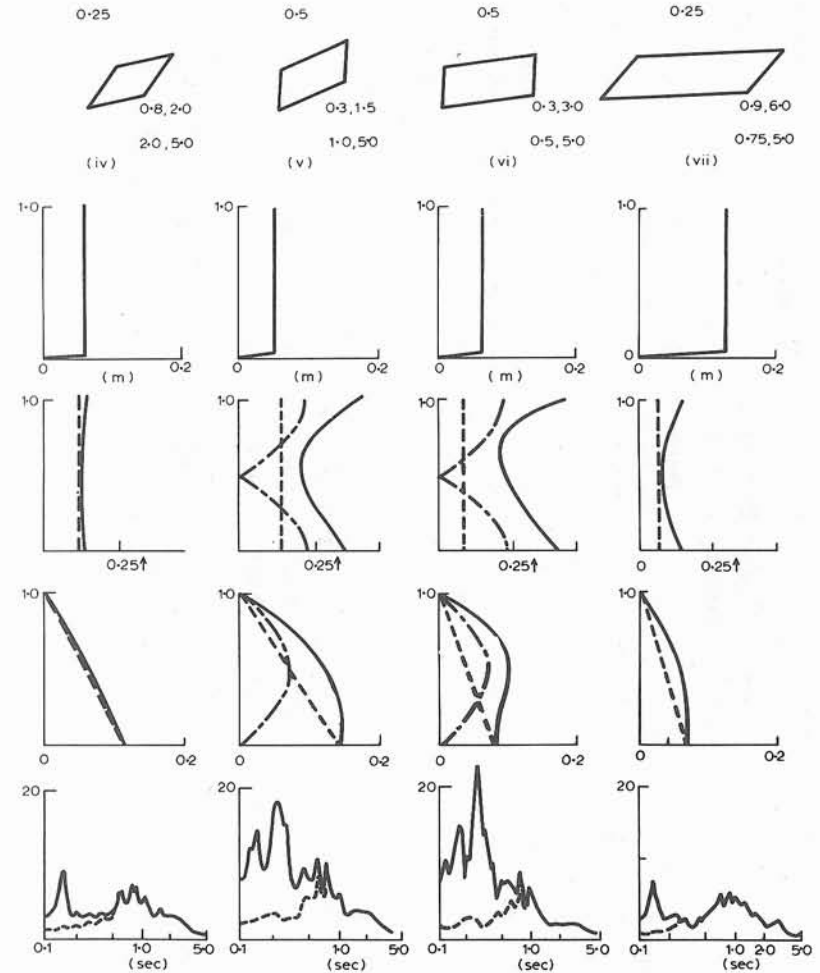


Figure 2.7 Responses to the El Centro NS 1940 accelerogram of a uniform shear structure when unisolated (case i), when linearly isolated (cases ii and iii) and when bilinearly isolated (cases iv to vii). The information in this figure complements that in Table 2.1. The floor spectra are for the low-damping case of 2%. The solid lines are the total response, while dashed and chain-dashed lines are the seismic responses of modes 1 and 2 respectively. Note the

factor of 0.71, but unlike case (vi) it has high isolation factors in both phases of the response. The force-displacement characteristics of the isolator are almost elasto-plastic, with a post-yield period of 6.0 s. The unisolated period of the structure ($T_1(U) = 0.25$ s) and the yield-force ratio ($Q_y/W = 0.05$) are identical to case (iv), and the pre-yield isolator period ($T_{b1} = 0.8$ s) and hence the elastic-phase isolation factor are very similar to those in case (iv). This represents a system with high



five-fold differences in scale of the unisolated and isolated cases. The scale changes are along the abscissae for X , \ddot{X}/g and S/W , and along the ordinate for the floor spectra. Note also that the shear-force/displacement hysteresis loops have been drawn for cyclic displacements of $\pm 0.4X_b$ in order to show the various stiffnesses clearly

hysteretic damping, high isolation in both phases of the response, and a maximum base shear closely controlled by the isolator yield force because of the nearly perfectly plastic characteristic in the yielding phase.

The response characteristics of this wide range of examples are illustrated in Figure 2.7, and demonstrate many of the key features of the response characteristics of base-isolated structures. Comparisons can be made between features of

Table 2.1 Responses to the El Centro NS 1940 accelerogram of an unisolated uniform shear structure, and of six isolated structures

Case →	Units	UNISOLATED			ISOLATED			
		(i)	Linear		(iv)	Bilinear		
			Low damping	High damping		High elastic and high plastic flexibility	Low elastic and low plastic flexibility	Low elastic and high plastic flexibility
(ii)	(iii)	(v)	(vi)	(vii)				
System parameters								
Unisolated mode-1 period, $T_1(U)$	s	0.5	0.5	0.5	0.25	0.5	0.5	0.25
Isolator periods, $T_b; T_{b1}, T_{b2}$	s		2.0	2.0	0.8, 2.0	0.3, 1.5	0.3, 3.0	0.9, 6.0
Structural dampings, $\zeta_n(U), \zeta_n(I)$	%	5	5	5	5	5	5	5
Isolator velocity damping $\zeta_b, \zeta_{b1}, \zeta_{b2}$	%		5	20	4, 2, 5	4, 1, 5	3, 0.5, 5	2, 0.8, 5
Isolator yield/weight, Q_y/W	%				5	5	5	5
Maximum responses								
Base shear/mass, S_b/M	ms^{-2}	8.18	1.78	1.36	1.08	1.38	0.79	0.627
Base displacement, X_b	m	($X_4 = 0.07$)	0.180	0.124	0.058	0.050	0.067	0.127
Top acceleration, \ddot{X}_5	ms^{-2}	12.4	1.914	1.603	1.33	3.346	3.405	1.278
Mode 1, top acceleration $\ddot{X}_{5,1}$	ms^{-2}	10.8	1.785	1.358	1.082	1.377	0.793	0.627
Mode 2, top acceleration $\ddot{X}_{5,2}$	ms^{-2}	4.28	0.308	0.658	0.919	2.11	2.01	0.793
Top-floor resonant appendage accn:								
at (yielding-phase) period, $\overline{FA}_5(T_{1,2})$	ms^{-2}	82.3	15.3	5.90	3.3	4	2	—
at (yielding-phase) period, $\overline{FA}_5(T_{2,2})$	ms^{-2}	23.3	3.60	4.32	9.2	18	23	8

Mode-1 response from linear spectra

Effective periods T_b, T_B	s		2.0	2.0	1.45	1.20	1.83	2.83
Effective damping, $\zeta_b; \zeta_B = \zeta_b + \zeta_h$	%		5	20	4.0+20	4.0+21	3.0+38	2.0+45
Spectral acceleration $S_A(T_B, \zeta_B)$	ms^{-2}		1.75	1.33	1.34	1.82	1.21	0.90
Spectral displacement $S_D(T_B, \zeta_B)$	m		0.177	0.120	0.064	0.061	0.076	0.080
Correction factor, $C_F = X_b/S_D(T_B, \zeta_B)$					0.91	0.82	0.88	1.59
Non-linearity factor NL	%				32	33	60	71
Elastic-phase isolation factor:								
$I(K_{b1}) = T_{b1}/T_1(U)$			4	4	3.2	0.6	0.6	3.6

the responses of unisolated and isolated structures, and between those of various isolated structures. Systematic variations in response quantities can be seen as the equivalent viscous damping, the non-linearity factor and the elastic-phase isolation factor are varied.

The first point to note in Figure 2.7 is that the response scales for the unisolated structure of case (i), as emphasised by heavy axis lines, are five times larger than those for all the isolated cases shown in the other parts of the figure. The next general comment is that the force-displacement hysteresis loops have been drawn for cyclic displacements of $\pm 0.4X_b$. This has been done in order to show the relative slopes.

Direct comparisons of various response quantities can be made for the unisolated structure and the four cases (ii), (iii), (v) and (vi) involving the same structure on various isolation systems. Cases (iv) and (vii) involve shorter-period structures on the isolators, so direct comparisons of these with case (i) are not appropriate. The base shears of the isolated systems with the 0.5 s structure are reduced by factors of 4.6 (for the lightly damped linear isolator of case (ii)) to over 10 (for case (vi) with high hysteretic damping). Base displacements, which contribute most of the total displacement at the top of the isolated structures, range from 0.7 to 2.5 times the top displacement of the unisolated structure. Inter-storey deformations in the isolated structures are much reduced from those in the unisolated structures, since they are proportional to the shears. Since large deformations are responsible for some types of damage, the reduction in structural deformation is a beneficial consequence of isolation. First-mode contributions to the top-mass accelerations in the isolated structures are reduced by factors of about 6–14 compared with the values in the unisolated structure. The linear isolation systems show marked reductions in the higher-frequency responses as well, but the second-mode responses for the systems with the greatest non-linearities are only slightly reduced from those in the unisolated structure. These effects are most evident in the top-floor response spectra.

Figure 2.7 shows several important characteristics of the response of isolated structures in general. In isolated systems, increased damping reduces the first-mode responses, but generally increases the ratio of higher-mode to first-mode responses, particularly where the damping results from non-linearity. The elastic-phase isolation factor $I(K_{b1})$ has a marked effect on higher-mode responses, which increase strongly as $I(K_{b1})$ reduces from about 1.0 towards zero. The reason for the strong influence of $I(K_{b1})$ on higher-mode responses is discussed in Section 4.3.4. The effects of these parameters are demonstrated by considering each of the isolated cases in turn.

The lightly damped linear isolation system of case (ii) reduces the base shear by a factor of 4.6 from the unisolated value, but requires an isolator displacement of 180 mm. The response is concentrated almost entirely in the first mode, as shown by the comparison of the first-mode, total acceleration and shear distributions, and by the top-floor spectra. The differences between the first-mode and total distributions arise largely from the difference between the free-free first-mode shape which

was used in the sweeping procedure and the actual first-mode shape with base stiffness K_b . The maximum second-mode acceleration calculated by sweeping with the second free-free mode shape is only about 1/6 that found by sweeping with the first free-free mode shape.

By increasing the base viscous damping from $\zeta_b = 5\%$ to 20% of critical, as in case (iii), the maximum base displacement is reduced from 180 mm to 124 mm, with a smaller percentage reduction in the base shear. The mode-2 acceleration more than doubles, showing the effects of increased base impedance from the increased base damping and modal coupling from the non-classical nature of the true damped modes. The first-mode response still dominates, however. The floor-response spectra reflect the reduction in first-mode response, but show increases in the second- and third-mode responses compared with case (ii).

Case (iv) has an effective base damping similar to case (iii), but with the main contribution coming from hysteretic damping. All first-mode response quantities and those dominated by the first-mode contribution, including the base shear and the base displacement, are reduced from the values for the linear isolation systems. The non-linearity of this system is only moderate (0.32), and there is a high elastic-phase isolation factor of 3.2, but the second-mode response is much more evident than for the linear isolation systems, particularly in the floor-response spectrum.

Case (v) has the same degree of non-linearity as the previous case, but a much reduced elastic-phase isolation factor of 0.6. The low elastic-phase isolation factor has produced a much increased second-mode acceleration response, which is 50% greater than the first-mode response on the top floor. The distribution of maximum accelerations is much different from the uniform distribution obtained for a structure with a large linear isolation factor. The accelerations are much increased from the first-mode values near the top and near the base, while the shear distribution shows a marked bulge away from the triangular first-mode distribution at mid-height. Strong high-frequency components are evident in the top-floor acceleration response spectrum, with prominent peaks corresponding to the second and third post-yield isolated periods.

Case (vi) is an exaggerated version of case (v). The post-yield isolator period has been increased to 3.0 s, giving a high non-linearity factor as well as a low elastic-phase isolation factor, both conditions contributing to strong higher-mode response. The nearly plastic behaviour of the isolator in its yielding phase produces a more than 40% reduction in the base shear from case (v), at the expense of a 33% increase in the base displacement. The maximum second-mode acceleration response at the top floor is 2.5 times the first-mode response, being the highest value of this ratio for any of the seven cases. The acceleration at the peak of the top-floor response spectrum at the second-mode post-yield period has the greatest value of any of the isolated cases, almost identical to the second-mode value in the unisolated structure, which, however, occurs at a shorter period.

Case (vii) demonstrates that high elastic-phase isolation can much reduce the relative contribution of the higher modes for highly non-linear systems. The non-linearity factor of 0.71 is the highest of any of the cases, but the second-mode

response is less than 40% that of cases (v) and (vi), which have poor elastic-phase isolation. The high non-linearity has reduced the base shear to 70% of that of case (iv). The mode-2 acceleration response has been reduced by 13% from that of case (iv), but its ratio with respect to mode 1 has increased from 0.85 to 1.25.

Maximum base shears and displacements of isolated structures are dominated by first-mode responses. Maximum first-mode responses of bilinear hysteretic isolation systems can in turn be approximated by the maximum responses of equivalent linear systems, as discussed earlier in this chapter and in Section 4.3.3. The final section of Table 2.1 demonstrates the degree of validity of the equivalent linearisation approach. It gives effective dampings and periods calculated for the equivalent linearisation of the bilinear isolators, using Equation (2.11b) for T_B and Equations (2.11c) to (2.13) for ζ_B . The response spectrum accelerations and displacements for these values of period and damping are listed. The spectral values for the base displacements give reasonable approximations to the actual values, with correction factors C_F of approximately unity, except for case (vii), the case with the nearly plastic post-yield stiffness, for which the correction factor is 1.6. However, the spectral accelerations $S_A(T_B, \zeta_B)$ provide much poorer estimates of either the first-mode or overall base-mass acceleration \ddot{X}_b . Much improved estimates of the base shear S_b can be obtained from $K_B X_b$, which has a smaller relative error than the estimate of X_b from $S_D(T_B, \zeta_B)$. This is the procedure we recommend when using the equivalent linearisation approach (Section 2.2, Section 4.3.3 and Section 5.1).

2.6 GUIDE TO ASSIST THE SELECTION OF ISOLATION SYSTEMS

The examples summarised in Figure 2.7 and Table 2.1 show the effects of various ranges of isolation system parameters. In particular, the effects of varying the base damping, the non-linearity factor and elastic-phase isolation factor have been demonstrated. Table 2.2 generalises the results found for these examples, and for other cases studied in Chapter 4, and presents them in a more qualitative way, providing guidance to the sets of parameter values appropriate for particular purposes and giving examples of practical isolation systems which can provide the desired parameter values.

In Table 2.2, we consider classes of systems, rather than examples with specific parameter values. The examples (i) to (vii) considered in Figure 2.7 and Table 2.1 fit into the corresponding categories in Table 2.2. However, the qualitative descriptions of the nature of various response quantities show minor deviations from those which would be obtained solely by consideration of these examples. Use has been made of results of other cases considered in Chapter 4 or reported in the literature in order to generalise the results from the specific ones given above.

Thus, class (vi) has been extended to include rectangular hysteresis loops ($K_{b1} = \infty$, $K_{b2} = 0$), while the example of case (vi) has 'high' and 'low' values of these stiffnesses respectively. The response characteristics of simple sliding-friction

systems included by this generalisation are similar to those of the example of case (vi). The ways in which the various cases of Table 2.1 have been generalised to the classes of Table 2.2 are discussed below.

Class (i) represents unisolated linear structures with periods up to about 1 s and damping up to about 10%. This class is provided only for purposes of comparison. Most short- to moderate-period unisolated structures will be designed to respond non-linearly, so their acceleration- and force-related responses may be considerably less than those of the linear elastic cases considered here. Isolation still provides benefits in that non-linear response in such unisolated structures requires ductile behaviour of the structural members, with the considerable energy dissipation within the structure itself often associated with significant damage.

Class (ii) represents lightly damped, linear isolation systems, with the isolator damping less than 10%. Only systems providing a high degree of isolation are considered, with an isolation factor $T_b/T_1(U)$ of at least 2 and a period T_b of at least 1.5 s for El Centro-type earthquakes. The response of such systems is almost purely in the first mode, with very little higher-frequency response, so they virtually eliminate high-frequency attack on contents of the structure. This type of isolation can be readily obtained with laminated-rubber bearings, with the low isolator damping provided by the inherent damping of the rubber. Higher-damping rubbers may be necessary to achieve the 10% damping end of the range without the provision of additional damping devices. The higher-damping rubbers may not behave as linear isolators since they are often amplitude-dependent and history-dependent. Various mechanical spring systems with viscous dampers fall into this category.

Class (iii) corresponds to linear isolation with heavier viscous damping, ranging between about 10% and 25% of critical. Increased damping reduces the isolator displacement and base shear, but generally at the expense of increased high-frequency response. The high-frequency response results from increased isolator impedance at higher frequencies. These systems still provide a high degree of protection for subsystems and contents vulnerable to motions of a few Hz or greater, but with reduced isolator displacements compared with more lightly damped systems.

We consider class (iv), bilinear hysteretic systems with good elastic-phase isolation ($T_{b1}/T_1(U) > 2$) and moderate non-linearity (corresponding to equivalent viscous base damping of 20–30% of critical), as a reference class. For many applications, this represents a reasonable design compromise to achieve low base shears and low isolator displacements together with low to moderate floor-response spectra. This type of isolation can often be provided by lead-rubber bearings.


Class (v) represents bilinear isolators with poor elastic-phase isolation ($T_{b1}/T_1(U) < 1$) and relatively short post-yield periods (~ 1.5 s). The relatively high stiffnesses of these isolation systems produce very low isolator displacements, but strong high-frequency motions and stronger base shears than the reference bilinear-hysteretic isolator class.

Class (vi) is similar in many respects to class (v), but with a long post-yield period ($T_{b2} > \sim 3$ s), which gives nearly elasto-plastic characteristics and thus high

Table 2.2 Guide to the behaviour of isolation systems, showing seven classes corresponding broadly to the cases in Figure 2.7

	Unisolated	Linear		
Shear force-displacement loop:	(Elastic)			
	(i)	(ii)	(iii)	
Description:	<ul style="list-style-type: none"> unisolated elastic structure 	<ul style="list-style-type: none"> linear isolation, low viscous damping 	<ul style="list-style-type: none"> linear isolation, high viscous damping 	
Structural deformation:	high	low	low	
Isolator displacement:		high	moderate	
Accelerations of structure:	high	low	low	
Shears	Base shear:	high	moderate	moderate/low
	Bulge factor:	low	low	low
Top-floor acceleration spectra	Period (0.1-1)s:	<ul style="list-style-type: none"> very high (mode-1) high (higher modes) 	low/very low	low
	Period > 1s:	low	moderate/high	low/moderate
Major advantages:		<ul style="list-style-type: none"> low short-period attack on contents 	<ul style="list-style-type: none"> low short-period attack on contents moderate isolator displacements 	<ul style="list-style-type: none"> simple uniform acceleration responses controlled by isolator properties, insensitive to structural irregularities
Major disadvantages:		<ul style="list-style-type: none"> high isolator displacement susceptible to wind possible resonance at long periods 	<ul style="list-style-type: none"> moderate isolator displacements susceptible to wind external dampers required 	
Examples:		<ul style="list-style-type: none"> laminated rubber bearing flexible piles and viscous damper helical spring and viscous damper 	<ul style="list-style-type: none"> laminated rubber bearing with additional viscous dampers 	

Table 2.2 (continued)

Isolated			
		Bilinear	
			
(iv)	(v)	(vi)	(vii)
<ul style="list-style-type: none"> moderate nonlinearity high elastic-phase isolation 	<ul style="list-style-type: none"> moderate nonlinearity low elastic-phase isolation 	<ul style="list-style-type: none"> high nonlinearity low elastic-phase isolation 	<ul style="list-style-type: none"> high nonlinearity high elastic-phase isolation
low	low	low	low
low	low	low	moderate/high
low	moderate	moderate	moderate
low	moderate	low	very low
low	high	very high	moderate
moderate	moderate/high	high/very high	low/moderate
low/moderate	low	low	low/moderate
<ul style="list-style-type: none"> low seismic forces, isolator displacements and base shears low/moderate attack on contents isolator 'locks' during wind 	<ul style="list-style-type: none"> low isolator displacements isolator 'locks' during wind 	<ul style="list-style-type: none"> low isolator displacements isolator 'locks' during wind 	<ul style="list-style-type: none"> very low base shears, insensitive to strength of seismic excitation low/moderate attack on contents isolator 'locks' during wind
<ul style="list-style-type: none"> some short-period attack on contents 	<ul style="list-style-type: none"> moderate/high attack on contents 	<ul style="list-style-type: none"> high/very high attack on contents 	<ul style="list-style-type: none"> moderate/high isolator displacements, especially for severe earthquakes
<ul style="list-style-type: none"> lead-rubber isolator laminated rubber bearing plus steel dampers 		<ul style="list-style-type: none"> simple friction-sliding system 	<ul style="list-style-type: none"> flexible piles with flexibly anchored lead extrusion damper

hysteretic damping and a high non-linearity factor. Rigid-plastic systems, such as given by simple sliding friction without any resilience, are extreme examples of this class. Low base shears can be achieved because of the low post-yield stiffness and high hysteretic damping, but at the expense of strong high-frequency response. Even this advantage is lost with high yield levels. This class of bilinear isolator is not appropriate when protection of subsystems or contents vulnerable to attack at frequencies less than 1 Hz is important, but some systems in this class can provide low base shears and moderate isolation-level displacements very cheaply. Displacements can become very large in greater than anticipated earthquake ground motions.

Class (vi) consists of non-linear hysteretic isolation systems with a high degree of elastic-phase isolation ($T_{b1}/T_1(U) > 3$) and a long post-yield period ($T_{b2} \gg 3$ s), producing high hysteretic damping. The low post-yield stiffness means that the base shear is largely controlled by the yield force, is insensitive to the strength of the earthquake, and can be very low. The high degree of elastic-phase isolation largely overcomes the problem of strong high-frequency response usually associated with high non-linearity factors. Systems of this type are particularly useful for obtaining low base shears in very strong earthquakes when provision can be made for large isolator displacements. One application of this class of system was the long flexible pile system used in the Wellington Central Police Station (Section 6.2.6), with the elasto-plastic hysteretic damping characteristics provided by lead-extrusion energy dissipators mounted on resilient supports.

As indicated by the preceding descriptions of the isolator systems and the discussion of the response characteristics of the various examples in the last section, the selection of isolation systems involves 'trade-offs' between a number of factors. Decreased base shears can often be achieved at the cost of increased base displacements and/or stronger high-frequency accelerations. High-frequency accelerations affect the distribution of forces in the structure and produce stronger floor-response spectra. If strong high-frequency responses are unimportant, acceptable base shears and displacements may be achieved by relatively crude but cheap isolation systems, such as those involving simple sliding. In some cases, limitations on acceptable base displacements and shears and the range of available or economically acceptable isolation systems may mean that strong high-frequency accelerations are unavoidable, but these may be acceptable in some applications. Some systems may be required to provide control over base shears in ground motions more severe than those expected, requiring nearly elasto-plastic isolator characteristics and provision for large base displacements.

The selection of appropriate isolation systems for a particular application depends on which response quantities are most critical to the design. These usually can be specified in terms of one or more of the following factors:

- (i) base shear
- (ii) base displacement
- (iii) high-frequency (i.e. greater than about 2 Hz) floor-response spectral accelerations

- (iv) control of base shears or displacements in greater than design-level earthquake ground motions
- (v) cost.

Isolation systems are easily subdivided on the basis of those for which high-frequency (> 2 Hz) responses can be ignored and those where they make significant contributions to the acceleration distributions and floor spectra. Floor spectral accelerations are important when the protection of low-strength high-frequency subsystems or contents is an important design criterion. In well isolated linear systems, high-frequency components, which correspond to higher-mode contributions, can generally be ignored although they become more significant as the base damping increases (Figure 2.7, cases (ii) and (iii)). In non-linear systems, there will generally be moderate to strong high-frequency components when there is a low elastic-phase isolation factor of less than about 1.5. This generally eliminates systems with rigid-sliding type characteristics when strong high-frequency response is to be avoided. For a given elastic-phase isolation factor, high-frequency effects generally increase with the non-linearity factor (see Figure 4.12). These considerations suggest that the selection of isolation systems for the protection of high-frequency subsystems is limited to linear systems, or non-linear systems with high elastic-phase isolation factors and moderate non-linearity factors (i.e. corresponding to cases (ii), (iii) or (iv) in Figure 2.7). Some systems with high non-linearity factors but also with high elastic-phase isolation factors may also produce an acceptably low high-frequency response. For example, case (vii) in Figure 2.7 with a high non-linearity factor has a similar top-floor response spectrum to case (iv) for which the non-linearity factor is moderate, and has a spectrum not much stronger than that of the linearly isolated case (iii) which has high viscous damping. The linear systems usually give better performance strictly in terms of high-frequency floor-response spectral accelerations, but the introduction of non-linearity can reduce the base shear and isolator displacement, which may give a better overall performance when the structure, subsystems and contents are considered together.

For situations where a need for small floor-response spectral accelerations is not a major design criterion, the range of acceptable non-linear isolation systems is likely to be much greater. The main performance criteria are then usually related to base shear and base displacement. Both these quantities depend primarily on the first-mode response. Except for nearly elasto-plastic systems, the base shear decreases as Q_y/W increases from zero, passes through a minimum value at an optimal yield force, and then increases as Q_y/W continues to increase (Figure 4.5(d)). Thus the base shear of most linear isolation systems can be reduced by selecting a non-linear isolation system with $T_{b2} = T_b$ of the linear system and an appropriate yield force ratio and elastic-phase period. For a given yield force, the base shear generally decreases as T_{b2} increases (Figure 4.5(d)), i.e. the system becomes more elasto-plastic in character. This is illustrated by the examples in Figure 2.7. This is generally at the expense of greater base displacement, as for case (vii), or strong high-frequency response when the elastic-phase isolation is poor, as in case (vi).

When base shear and base displacements are the controlling design criteria, systems with rigid-plastic type characteristics, such as simple pure friction systems, which are not appropriate when the protection of high-frequency subsystems or contents is a concern, may give cheap, effective solutions provided the coefficient of friction remains less than the maximum acceptable base shear. However, some centring force is usually a desirable isolator characteristic. For protection against greater than design-level excitations, systems with a nearly plastic yielding-phase characteristic have the advantage that the base shear is only weakly dependent on the strength of excitation, but the disadvantage that their isolator displacements may become excessive. A system similar to our reference case characterised by moderate non-linearity and good elastic-phase isolation is often a good design compromise when minimisation of high-frequency floor-response spectral accelerations is not an overriding design criterion.

3 *Isolator Devices and Systems*

3.1 ISOLATOR COMPONENTS AND ISOLATOR PARAMETERS

3.1.1 Introduction

The successful seismic isolation of a particular structure is strongly dependent on the appropriate choice of the isolator devices, or system, used to provide adequate horizontal flexibility with at least minimal centring forces and appropriate damping. It is also necessary to provide an adequate seismic gap which can accommodate all intended isolator displacements. It may be necessary to provide buffers to limit the isolator displacements during extreme earthquakes, although an incorrectly selected buffer may negate important advantages of seismic isolation.

The primary function of an isolation system is to support a structure while providing a high degree of horizontal flexibility. This gives the overall structure a long effective period and hence low maxima for its earthquake-generated accelerations and inertia forces, in general accordance with Figure 2.1(b). However, with low damping, maximum isolator displacements X_b may reach 500 mm or more during severe earthquakes, as shown by Figure 2.1(c). High isolator damping usually reduces these displacements to between 100 and 150 mm. High damping may also reduce the costs of isolation since the displacements must be accommodated by the isolator components and the seismic gap, and also by flexible connections for external services such as water, sewage, gas and electricity. Another benefit of high isolator damping is a further substantial reduction in structural inertia forces. Also, in crowded areas there is the possibility of structures colliding with each other.

Since the expected life of an isolated structure will typically range from 30 to 80 or more years, the isolation system should remain operational for such lifetimes, and its maintenance problems should preferably be no greater than those of the associated structure. This will usually call for relatively simple, well designed and thoroughly tested isolator devices. The primary force-limiting function of an isolator may be called on for only one, or a few, brief periods of operation during the life of the structure: for example, one 15-s episode in 50 years. However, at these times the isolator must operate successfully despite all environmental hazards, including those tending to corrode metal surfaces, cause deterioration of elastomers, or change the physical properties of component materials. In addition to the very infrequent seismic loads, isolators will often be subject to smaller but relatively

frequent wind loads which they must resist without serious deterioration. Diurnal temperature changes will result in displacements which need to be accommodated by the isolation system without the build-up of excessive forces. Finally, since isolator devices which satisfy the above criteria will usually be intended to reduce the overall structural cost, the components must be sufficiently simple to allow supply and installation at moderate cost.

3.1.2 Combination of isolator components to form different isolation systems

The design and performance of various isolator components is described in this chapter. Emphasis is placed on components which were developed in our laboratory, namely steel dampers, lead-extrusion dampers and the lead-rubber bearing. The elastomeric bearing is also described since its properties underlie those of the lead-rubber bearing isolation system. Some description is also given of other isolator components.

The discussion and results presented in Chapters 1 and 2, particularly in Figure 2.7, Tables 2.1 and 2.2 and the associated text, form a context in which to analyse the properties of real isolator components and real isolation systems. The isolation systems considered provide horizontal flexibility and damping and support the weight of the isolated structure. In the simplest case a linear isolation system is produced by using components with linear flexibility and linear damping. In other cases the isolation system may be non-linear. A special case of non-linearity, the bilinear system, occurs when the shear-force/displacement loop is a parallelogram, as shown in Figure 2.3 and discussed in the associated text. Different seismic responses result from linear, bilinear and other non-linear isolation systems.

In the simplest case, a system which has both a linear flexibility component and a linear damping component can be modelled in terms of the differential equation (2.1), i.e.

$$m\ddot{u} + c\dot{u} + ku = -m\ddot{u}_g$$

where the flexibility is the inverse of the stiffness constant 'k' and the velocity damping is described by a constant 'c'. Figure 2.2 and the associated text define this kind of system and show the elliptical velocity-damped shear-force/displacement hysteresis loop which results.

However, the components may not be linear. The most common source of non-linearity in a component is amplitude dependence. For example, in the typical bilinear isolation system the stiffness is amplitude dependent, changing from K_{b1} to K_{b2} at the yield displacement. The damping in this case is also non-linear because the hysteretic contribution to the damping, which usually dominates, depends on the area of the hysteresis loop and therefore also depends on the maximum amplitude X_b .

Table 3.1 analyses the flexibility and damping of some common isolator components, examining each to see if it is linear or non-linear. The analysis is somewhat

idealised and oversimplified, since material properties can vary. Also, it is worthwhile checking to see if a particular system is rate- or history-dependent. For example, types of high-damping rubber depend both on the amplitude and on the number of cycles which the sample has undergone.

Table 3.1 Flexibility and damping of common isolator components

Property	Linear	Non-linear
Restoring Force (providing spring constant and flexibility)	<ul style="list-style-type: none"> • Laminated-rubber bearing • Flexible piles or columns • Springs • Rollers between curved surfaces (gravity) 	<ul style="list-style-type: none"> • High-damping rubber bearing • Lead-rubber bearing • Buffers • Stepping (gravity)
Damping	<ul style="list-style-type: none"> • Laminated-rubber bearing • Viscous damper 	<ul style="list-style-type: none"> • High-damping rubber bearing • Lead-rubber bearing • Lead-extrusion damper • Steel dampers • Friction (e.g. PTFE)

As seen in Table 3.1, the laminated-rubber (elastomeric) bearing is the only single-unit isolation system, among those considered, which has both linear restoring force and linear damping. In the commercially used form, this comprises layers of rubber vulcanised to steel plates. Considerable experience exists for the design and use of the elastomeric bearing, since its initial major application was to accommodate thermal expansion in bridges and it was only later adopted as a solution to seismic isolation problems. However, for seismic isolation, this system has the disadvantage that the maximum achievable damping is very low, approximately 5% of critical. Attempts to overcome this disadvantage by increasing the inherent damping of the rubber have not yet produced an ideal system with linear stiffness and linear damping.

Flexible piles or columns provide a simple, effective linear restoring force but dampers need to be added to control the displacements during earthquakes and on other occasions. If the dampers are linear, e.g. viscous dampers, then a linear system results. Viscous dampers are excellent candidates for linear dampers, but may be difficult to obtain at the required size, may be strongly temperature-dependent and may require maintenance, given that the required lifetime may be 30 to 80 years.

Springs with the required stiffness are likely to be difficult to produce, but do provide a linear restoring force. The German GERB system (Hüffmann, 1985) achieves this and is mainly intended for industrial plant such as large silos. Rollers or spheres between curved (parabolic) surfaces can provide linear restoring forces.

Since they have 'line' or 'point' contact it is difficult to provide for high loads. Again, damping will usually need to be added in practice and linear damping will produce a linear system.

Gravity in the form of a 'stepping' behaviour (see, for example the Rangitikei viaduct, Chapter 6) can provide an excellent non-linear restoring force. Such systems need additional damping for effective isolation. The resultant isolation systems are non-linear.

High-capacity hysteretic dampers may be based on the plastic deformation of solids, usually lead or steel. The damper must ensure adequate plastic deformation of the metal when actuated by large earthquakes. It must be detailed to avoid excessive strain concentrations; for example these may cause premature fatigue failure of a steel damper at a weld. Excessive plastic cycling of steel dampers, for example by wind gusts, must be avoided since this gives progressive fatigue deterioration.

Steel damping devices, often in the form of bending beams of various cross-sections, have a high initial stiffness and are effective dampers but care must be taken in their manufacture to ensure a satisfactory lifetime. They are strongly amplitude-dependent. When combined with components to provide flexibility, they can result in bilinear or non-linear isolation systems. Elasto-plastic steel dampers have been used in New Zealand and other countries, including Italy, where they have been used for the seismic isolation of many bridges (see Chapter 6).

The lead-extrusion damper behaves as a plastic device operating at a constant force with very little rate or amplitude dependence at earthquake frequencies. It creeps at low loads (see Figure 3.10), enabling thermal expansion to be accommodated. When combined with a linear component for flexible support, e.g. flexible piles, then a bilinear system can result, such as that used in the Wellington Central Police Station (see Chapter 6).

The lead-rubber bearing, which comprises an elastomeric bearing with a central lead plug, gives structural support, horizontal flexibility, damping and a centring force in a single easily installed unit. It has high initial stiffness, followed by a lower stiffness after yielding of the lead, and is for many situations the most appropriate isolation system. The hysteretic damping of this device is via the plastic deformation of the lead. The device is non-linear but can be well described as bilinear, i.e. it has a parallelogram-shaped hysteresis loop as shown in Figure 2.3 and discussed in the associated text.

Friction devices behave in a similar way to the extrusion damper; they are simple but may require maintenance. Changes may occur in the friction coefficient due to aging, environmental attack, temperature variation or wear during use. A further problem is that of 'stick-slip', where after a long time under a vertical load the device requires a very large force to initiate slipping. A dramatic example of a system isolated by this means is the Buddha at Kamakura: a stainless steel plate was welded to the base of the statue and it was rested on a polished granite base without anchoring.

3.2 PLASTICITY OF METALS

The damping devices which have been found to be most economic and suitable for use in isolators are usually those which rely on the plastic deformation of metals. To understand the behaviour of these devices and to gain some knowledge of their limitations it is necessary to examine the mechanisms enabling plastic deformation to occur.

Figure 3.1(a) shows the stress-strain curve for a metal in simple tension. Initially the stress σ is proportional to the strain ϵ , and the constant of proportionality is the Young's modulus E . This elastic region of the stress-strain curve is reproduced on loading and unloading and has the equation of state

$$\sigma = E\epsilon \quad (3.1a)$$

so that the slope of the (σ - ϵ) graph is E .

The corresponding relationship between shear stress τ and engineering strain γ (where γ is twice the tensor strain) is given by

$$\tau = G\gamma \quad (3.1b)$$

where G =shear modulus.

If the strain is continually increased, it reaches a value (the yield point B in Figure 3.1(a)) at which the material yields plastically. The yield point is of particular importance in the design of isolator components. It has the coordinates (ϵ_y, σ_y), (γ_y, τ_y) and (X_y, Q_y) on the stress-strain, shear-stress-strain and force-displacement curves respectively.

Further increase in the stress results in a 'plastic-region' curve which is nearly horizontal, in the case of lead, or which rises moderately in the case of mild steel. If the stress is reduced to zero from a very large value of strain, then the curve follows the line CD in Figure 3.1(a). On unloading, the metal no longer returns to its initial state but has a 'set', i.e. an added plastic deformation. The unloading curve has the same gradient as that in the elastic region, namely the Young's modulus or shear modulus (Van Vlack, 1985).

It should be noted that the area ABCE in Figure 3.1(a) represents input work while the area DCE represents elastic energy stored in the metal at point C and released on unloading to point D. The difference area ABCD represents the hysteretic energy absorbed in the metal. In the case of lead, the absorbed energy is rapidly converted into heat, while in the case of mild steel it is dominantly converted to heat, but a small fraction is absorbed during the changes of state associated with work hardening and fatigue.

Since metal-hysteresis dampers involve cyclic plastic deformation of the metal components, it is appropriate to consider the stress-strain relationship for a metal cycled plastically in various strain ranges, as shown in Figure 3.1(b) for a metal with the features typical of mild steel. Included in Figure 3.1(b) is the initial stress-strain curve of Figure 3.1(a). Notice the increasing stress levels with increasing strain range, and the lower yield levels during plastic cycling. With lead,

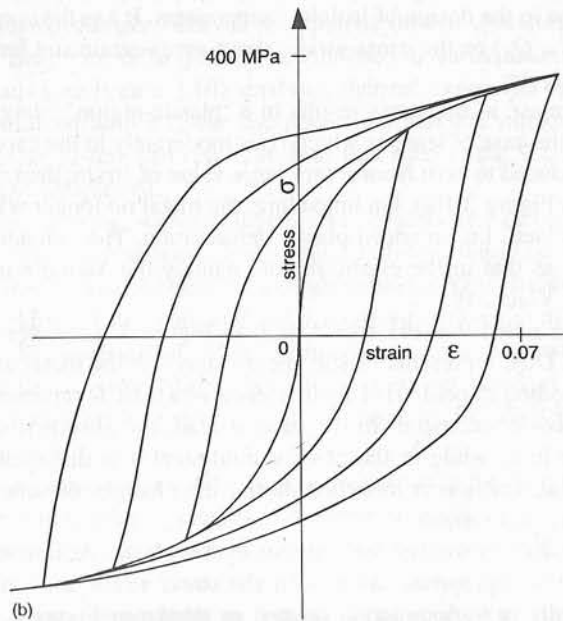
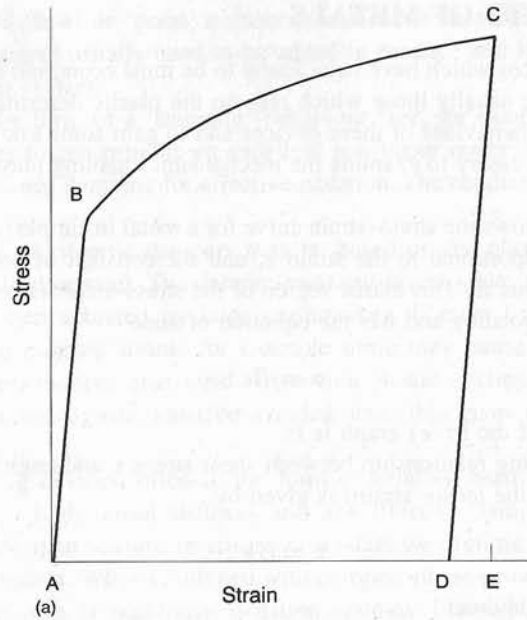


Figure 3.1 (a) Stress-strain curves for a typical metal which changes from elastic to plastic behaviour at the yield point (B). (b) Stress-strain curves for a typical mild steel under cyclic loading

the hysteretic loops are almost elastic-plastic, i.e. an elastic portion is followed by yield at a constant stress (zero slope in the plastic region). Typical operating strains are much greater than the yield strain, the loop tops are almost level, and the loop height is not significantly influenced by strain range.

To understand the behaviour of a metal as it is plastically deformed, it is necessary to look at it on an atomic scale. Before the 1930s, the plastic deformation of a metal was not understood, and theoretical calculations predicted yield stresses and strains very different from those observed in practice. It was calculated that a perfect crystal, with its atoms in well defined positions, should have a shearing yield stress τ_y of the order of 10^{10} Pa, and should break in a brittle fashion, like a piece of chalk, at a shear strain γ_y of the order of 0.1. In practice, metal single crystals start to yield at a stress of 10^6 to 10^7 Pa (a strain of 10^{-4} to 10^{-3}) and continue to yield plastically up to strains of 0.01 to 0.1 or more. The weakness of real metal crystals could in part be attributed to minute cracks within the crystal, but the model failed in that it did not indicate how the crystal could be deformed plastically (van Vlack, 1985; Read, 1953; Cottrell, 1961). The dislocation model was then devised and overcame these difficulties. Since its inception the dislocation model has been extremely successful in explaining the strength, deformability and related properties of metal single crystals and polycrystals.

The plastic deformation in a crystalline solid occurs by planes of atoms sliding over one another like cards in a pack. In a dislocation-free solid it would be necessary for this slip to occur uniformly in one movement, with all the bonds between atoms on one slip plane stretching equally, and finally breaking at the same instant, where the bond density is of the order of 10^{16} bonds cm^{-2} . In most crystals, however, this slip, or deformation, is not uniform over the whole slip plane but is concentrated at dislocations. Figure 3.2(a) is a schematic drawing of the simplest of many types of dislocation, namely an edge dislocation with the solid

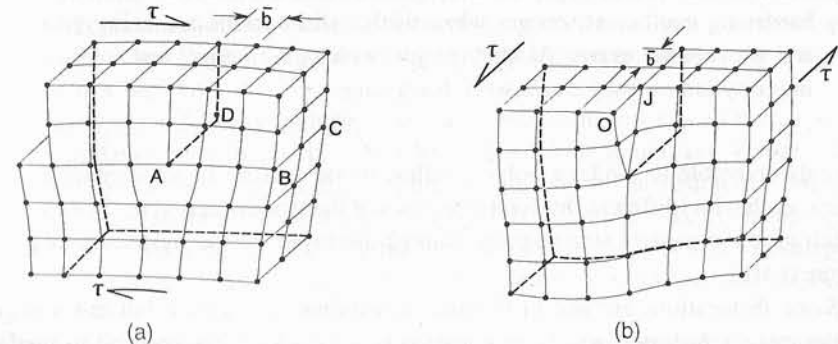


Figure 3.2 Atomic arrangements corresponding to (a) an edge dislocation, (b) a screw dislocation. Here b is the Burgers vector, a measure of the local distortion, and AD is the dislocation line

spheres representing atoms. The edge dislocation itself is along the line AD and it is in the region of this line that most of the crystal distortion occurs. Under the application of the shear stress this dislocation line will move across the slip plane ADCB, allowing the crystal to deform plastically. The bonds which must be broken as the dislocation moves have a concentration of 10^8 cm^{-1} , and are concentrated at the dislocation core, thus enabling the dislocation to move under a relatively low shear stress. As the dislocation moves from the left-hand edge of the crystal (Figure 3.2(a)) it leaves a step in the crystal surface, which is finally transmitted to the right-hand side. Figure 3.2(b) shows the other major type of dislocation, namely a simple screw dislocation, which may also transmit plastic deformation by moving across the crystal.

The dislocations in crystals may be observed using electron microscopy, while the ends of dislocations are readily seen with the optical microscope after the surface of the crystal has been suitably etched. Typical dislocation densities are 10^8 dislocations cm^{-2} in a deformed metal and about 10^5 dislocations cm^{-2} in an annealed metal, namely one which has been heated and cooled slowly to produce softening. Dislocations are held immobile at points where a number of them meet, and also at points where impurity atoms are clustered.

The three main regions of a typical stress-strain curve are interpreted on the dislocation model as follows:

- (1) Initial elastic behaviour is due to the motion of atoms in their respective potential wells; existing dislocations are able to bend a little, causing microplasticity.
- (2) A sharp reduction in gradient at the yield stress is due to the movement of dislocations.
- (3) An extended plastic region, whose gradient is the plastic modulus or strain-hardening coefficient, occurs when further dislocations are being generated and proceed to move. As they tangle with one another, and interact with impurity atoms, they cause work hardening.

It is also possible to model a polycrystalline metal as a set of interconnected domains, each with (different) hysteretic features of the type conferred by dislocations, which give the general stress-strain features displayed by the hysteresis loops of Figure 3.1(b).

Since dislocations are not in thermal equilibrium in a metal, but are a result of the metal's history, there is no equation of state which can be used to predict accurately the stress-strain behaviour of the metal. However, the behaviour of a metal may be approximately predicted in particular situations, if the history and deformation are reasonably well characterised.

3.3 STEEL HYSTERETIC DAMPERS

3.3.1 Introduction

General

By the late 1960s a number of damping mechanisms and devices were being used to increase the seismic resistance of a range of structures. At that time the logical approach to developing high-capacity dampers for structures was to utilise the plastic deformation of steel beams. During that decade the plastic deformation of steel structural beams had been increasingly used to provide damping and flexibility for aseismic steel beam-and-column (frame) buildings. The cyclic ductile capacity of structural members was limited by material properties, local buckling and the effects of welding (Popov, 1966).

Early steel-beam dampers developed in the Engineering Seismology Section of the Physics and Engineering Laboratory, DSIR, were given a much greater fatigue resistance than typical steel structural members by adopting suitable steels and beam shapes, and attachments with welds remote from regions of plastic deformation. Descriptions of the principal steel-beam dampers developed are given by Kelly *et al.* (1972); Skinner *et al.* (1974 and 1975); Tyler and Skinner (1977); Tyler (1978); Cousins *et al.* (1991). The principal developers of the three main classes of steel-beam dampers which emerged from the Physics and Engineering Laboratory programme which started in 1968 were Kelly: twisting-beam dampers (Type E); Tyler: tapered-beam dampers (Type T); and Skinner and Heine: uniform-moment dampers (Type U).

The earliest bridge structure provided with seismic isolation in New Zealand was a bridge at Motu, rebuilt in 1973 (McKay *et al.* 1990). The superstructure was provided with seismic isolation to protect the existing slab-wall reinforced concrete piers, which had only moderate strength to resist seismic forces. Isolator flexibility was provided by sliding bearings. Hysteretic damping was provided by plastic deformations near the bases of vertical cantilevers, in the form of structural-type steel columns. Seismic isolation systems using steel-beam dampers developed at the Physics and Engineering Laboratory, in New Zealand structures, are outlined or listed in Chapter 6.

An early New Zealand application of steel-beam dampers was in the stepping seismic isolation system for the tall piers of the South Rangitikei Viaduct. The seismic responses of the proposed stepping bridge, with the inclusion of hysteretic dampers, were studied by Beck and Skinner (1972, 1974). Steel twisting-beam dampers were selected for the isolation system and prototypes were developed. Construction of the bridge commenced in 1974 and it was opened in 1981 (Cormack, 1988).

Structures with steel tapered-slab dampers in their isolation systems included a stepping chimney in Christchurch (Sharpe and Skinner, 1983) and Union House in Auckland, isolated by mounting on flexible piles, (Boardman *et al.* 1983), while conically tapered steel dampers were used in the isolation systems for the Capacitor

Banks at Haywards (Chapter 6). Uniform-moment steel dampers were used in the superstructure isolation system for the Cromwell Bridge (Park and Blakeley, 1979).

Steel-beam dampers have also been adopted and developed, and used to provide hysteretic damping for seismic isolation in other countries, as outlined in Chapter 6. In Italy they have been used extensively in seismic isolation systems for bridge superstructures. In Japan steel dampers have been used in the seismic isolation systems of a range of structures.

Features of steel hysteretic dampers

Steel was initially chosen as the damper material since it is commonly used in structures and should therefore pose no very unusual design, construction or maintenance problems, apart from possible fatigue failure at welds and stress concentrations. Moreover, it was hoped that the development of these dampers would throw additional light on the performance of steel in ductile aseismic structures.

The performance of steel-beam hysteretic dampers during earthquakes is closely related to the performance of high-ductility steel-frame structures. However, the dampers are designed to have a much higher fatigue resistance and to operate at higher levels of plastic strain. This is achieved by using high-ductility mild steels, by using damper forms with nominally equal strain ranges over each plastic-beam cross-section, by using plastic beams of compact section (usually rectangular or circular), and by detailing the connections between the plastic beams and the loading members so as to limit stress concentrations, particularly at welds.

In this section, the results of many years of experience with different shapes and designs of steel damper are summarised in terms of a 'scaling' procedure, which generalises many different findings and also makes it possible to arrive at initial parameters for the design of steel-beam dampers with the desired properties. However, it must be noted that the following discussion is based on a large number of tests on many models and a few full-scale dampers, using in the main one kind of steel (BS4360/43A) after stress relieving. Other steels and heat treatments are expected to give similar, but not necessarily identical, results, particularly for the life of the damper. The procedures suggested here, particularly for 'scaling', are approximations which are included in order to enable a designer to obtain starting parameters for a given design. In practice, the full-scale device should be tested.

For a given strain range, the load-displacement loop changes only moderately with repeated cycling, with a moderate reduction in damping capacity, until the yielding beams are near the end of their low-cycle fatigue life. The damper loop parameters and their fatigue life can be estimated adequately, on the basis of cyclic tests on damper prototypes or on small-scale models.

Since steel-beam dampers have a strictly limited low-cycle fatigue life, controlled by fatigue-life curves of the type shown in Figure 3.6, it is necessary to design the dampers so as to limit the cyclic strain ranges during earthquakes, and to ensure that there exists a capacity to resist several design-level earthquakes as well as at least one extreme-level earthquake. For a typical well designed isolator

and for El Centro-type earthquakes, this might call for a nominal maximum strain range of $\pm 3\%$ during design earthquakes and $\pm 5\%$ during extreme earthquakes. Again, to avoid premature failure the isolator installation should ensure that wind loads do not impose more than a few tens of cycles of plastic deformation on damper beams during the design life of the isolated structure. The fatigue life of well designed steel-beam dampers is discussed further in Section 3.3.5.

3.3.2 Types of steel damper

While steel beams may be subject to shape instability during cyclic deformations into the plastic range, each of the damper geometries described below is stable for a very wide range of member proportions.

The three types of steel hysteretic damper to be discussed are shown in Figure 3.3:

- (i) A 'uniform'-moment bending-beam damper with transverse loading arms, sloped at an angle as shown in Figure 3.3(a) (Type-U damper).
- (ii) A tapered-cantilever bending-beam damper (Type-T damper). The apex of the tapered slab is at the loading level, while the apex of the tapered cone is substantially above the loading level. The circular-section cantilevered beam in Figure 3.3(b) may be loaded in any direction perpendicular to the beam axis. Figure 3.3(c) shows the load-displacement curves for this cantilever damper, as used in retrofitting the capacitor banks at Haywards Power Station with seismic isolation (see Chapter 6).
- (iii) A torsional-beam damper with transverse loading arms (Type-E damper). Figure 3.3(d) shows the Type-E damper used in the South Rangitikei Viaduct (see Chapter 6).

Note, as shown in Figures 3.3(a) and 3.3(d), that the welds are placed at low-stress regions of the damper. The cross-section of the beam may be circular, square or rectangular, denoted by the subscripts 'c', 's' or 'r' respectively. Thus the beams shown in Figures 3(a), 3(b) and 3(d) are of Types U_c , T_c and E_r respectively.

Dampers with improved features for particular applications may be based on combinations of the three basic types. A considerable range of further types of steel-beam damper has been described in the literature. For example, two compact dampers have been introduced in Japan. One uses a short hollow steel cantilever instead of the solid steel core of the Type-T damper. This bell damper is compact and has good force-displacement features (Kobori *et al.*, 1988). A second steel-beam damper has a set of beams in the form of vertical axis helices which provide for large yielding displacements in any horizontal direction. It has little height and can therefore be installed between horizontal surfaces with a small vertical clearance (Takayama *et al.* 1988). In Italy, sets of conical Type-T

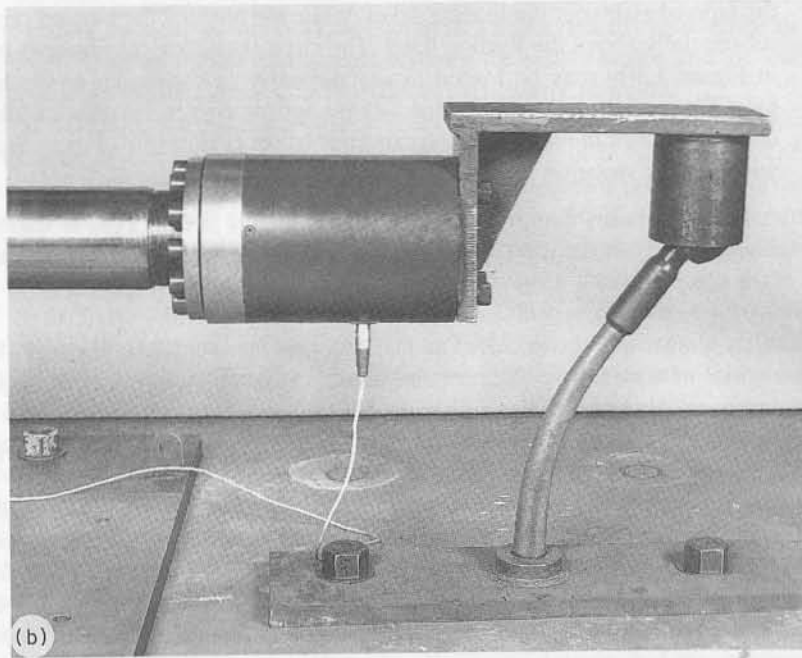
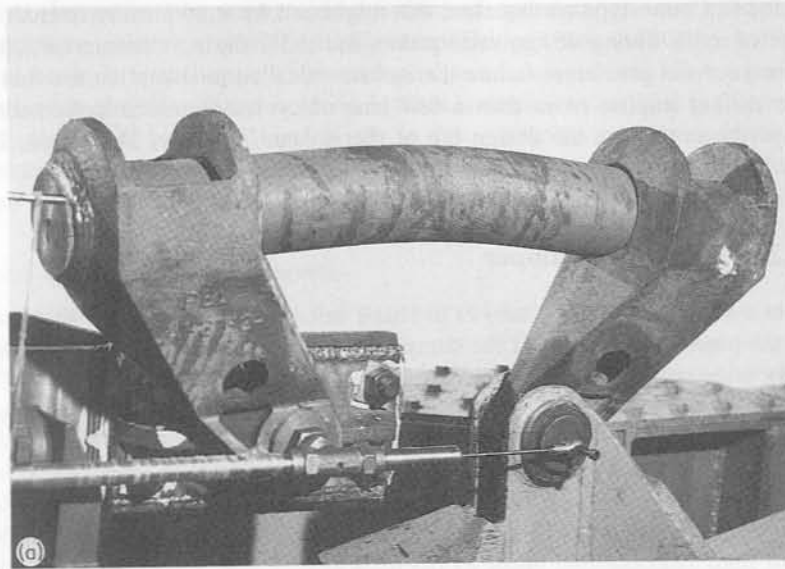
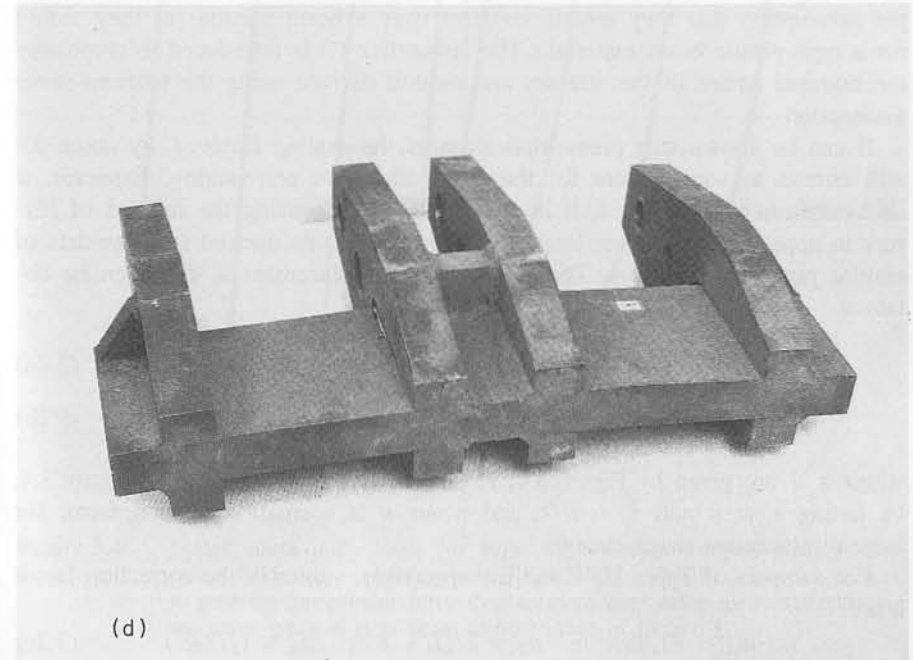
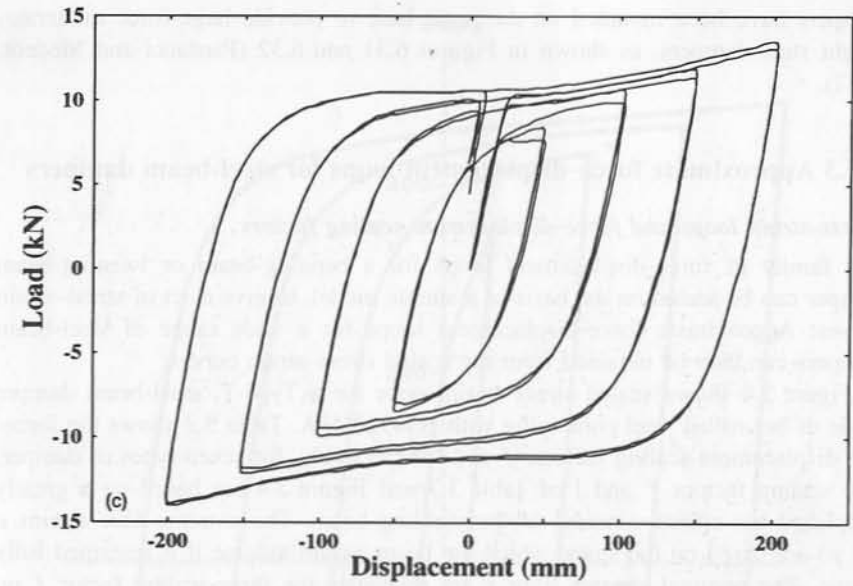


Figure 3.3 (a) Full-scale steel 'Type-U' bending-beam damper prototype (100 kN, ± 50 mm). Shaft diameter 100 mm. Note position of welds in low-stress region. (b) Steel cantilever 'Type-T' damper (10 kN, ± 200 mm), as retrofitted in order to isolate the capacitor banks at Haywards Power Station (see Chapter 6). Shaft diameter 50 mm. (From Cousins *et al.* 1991.)



(d)

(c) Load-displacement loops for steel cantilever damper shown in Figure 3.3(b). (d) Steel torsional-beam 'Type-E' damper with transverse loading arms (450 kN, ± 50 mm), as used in South Rangitikei Viaduct with stepping piers (see Chapter 6). Rectangular section 200 mm \times 60 mm. Note position of welds in low-stress region

dampers have been mounted on the same base to provide large-force moderate-height steel dampers, as shown in Figures 6.31 and 6.32 (Parducci and Medeot, 1987).

3.3.3 Approximate force–displacement loops for steel-beam dampers

Stress–strain loops and force–displacement scaling factors

The family of force–displacement loops for a bending-beam or twisting-beam damper can be scaled on the basis of a simple model, to give a set of stress–strain curves. Approximate force–displacement loops for a wide range of steel-beam dampers can then be obtained from the scaled stress–strain curves.

Figure 3.4 shows scaled stress–strain loops for a Type- T_r steel-beam damper made of hot-rolled steel complying with BS4360/43A. Table 3.2 shows the force- and displacement-scaling factors, f and l respectively, for seven types of damper. The scaling factors f and l of Table 3.2 and Figure 3.4 are based on a greatly simplified but effective model of the yielding beam. The extreme-fibre strains ϵ (or γ) are based on the shape which the beam would assume if it remained fully elastic. The nominal stresses $\hat{\sigma}$ or $\hat{\tau}$ are related to the force-scaling factor f on the assumption that they remain constant over a beam section (as they would for a rigid-plastic beam material.) The circumflex ($\hat{\cdot}$) is introduced to emphasise the nominal nature of the stresses and moduli derived using the uniform-stress assumption.

It can be shown that premultiplication of the scaling factor f by about 0.6 will correct to some extent for the approximation's non-validity. However, if such refinement is required, it is preferable to scale using the method of 'Errors in approximate damper loops' and 'Damper loops derived from models of similar proportions' below. The force F and displacement X can then be obtained

$$X \approx l\epsilon \quad (\text{or } l\gamma) \quad (3.2a)$$

$$F \approx f\hat{\sigma}(1 + aX^2), \quad (\text{or } f\hat{\tau}(1 + aX^2)) \quad (3.2b)$$

where ϵ , $\hat{\sigma}$ are given by Figure 3.4, γ , $\hat{\tau}$ are given approximately by Figure 3.4, by letting $\epsilon = \gamma$ and $\hat{\tau} \approx \hat{\sigma}/2$, and where a is a small correction factor for large-displacement shape changes.

For dampers of Types U, T and E respectively, values of the correction factor a are:

$$a_U \approx -1/(8R^2); \quad a_T \approx 2/(L + R)^2; \quad a_E \approx 1/(2R^2) \quad (3.2c)$$

where R and L are defined in Table 3.2.

Figure 3.3(c) is an example showing the effect of a positive a value on the loop shapes of Figure 3.1(b). The positive a_T and a_E values of Equation (3.2c) cause an increase in the slope of the force–displacement loop for large yield displacements

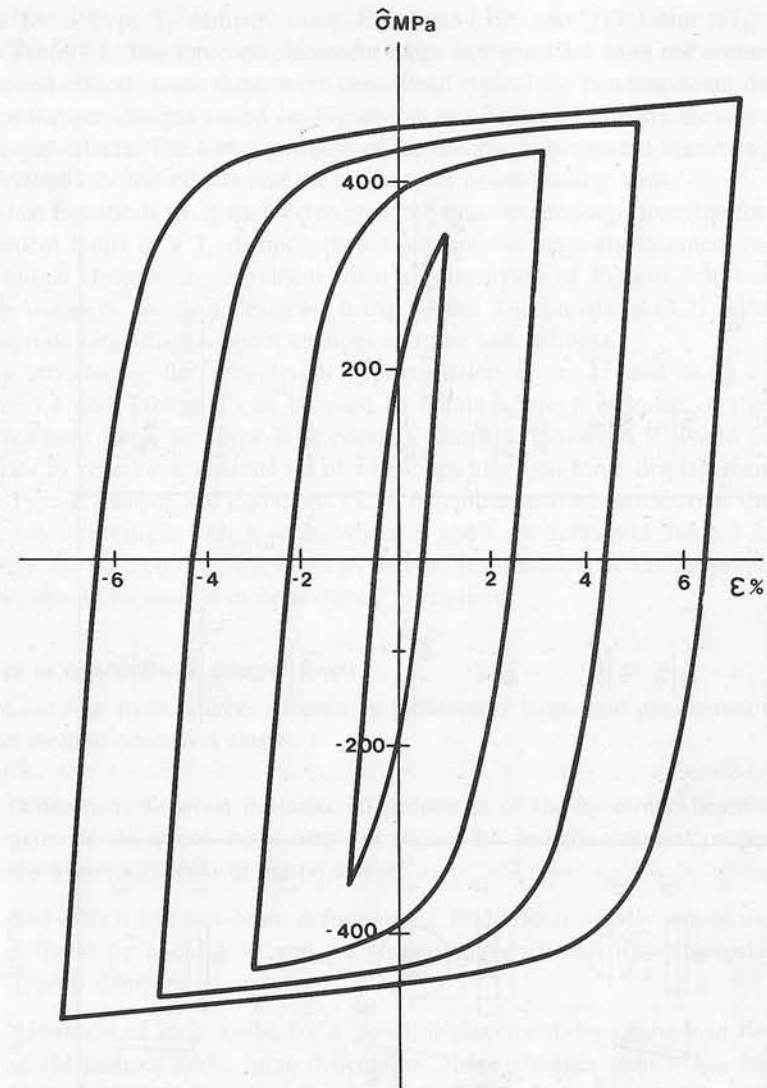


Figure 3.4 Scaled stress–strain loops for Type- T_r steel-beam damper, made of hot-rolled mild steel complying with BS4360/43A. This diagram can be used to generate approximate force–displacement loops using the scale factors for the seven types of steel-beam damper given in Table 3.1

of Type-T and Type-E dampers, in accordance with Equation (3.2b). Similarly, the negative a_U value causes a reduction in the loop slope for large yield displacements of Type-U dampers.

The stress–strain loops of Figure 3.4 were derived from force–displacement

Table 3.2 Scaling factors for steel-beam dampers

Damper	Type	Force Factors f	Displacement Factors l
	U _i U _c	$\frac{Bt^2}{4R}$ $\frac{d^3}{6R}$	$\frac{2LR}{t}$ $\frac{2LR}{d}$
	T _i T _c	$\frac{Bt^2}{4L}$ $\frac{(d + d_r)^3}{24(L + R)}$	$\frac{L^2 - R^2}{t}$ $\frac{8}{3} \frac{(L^2 - R^2)(d^2 + dd_r + d_r^2)}{(d + d_r)^3}$
	E _s	$\frac{2B^3}{3R}$	$1.48 \frac{LR}{B}$
	E _i E _c	$\frac{t^2(3B - t)}{3R}$ $\frac{\pi d^3}{6R}$	$1.1 \frac{(B^2 + t^2) LR}{(B + 0.6t)Bt}$ $\frac{2LR}{d}$

NOTES
 × $d_r = d (R/L)^{1/3}$, $R \geq L/3$
 † $B \geq 2t$

loops for a Type-T_r damper, using Equations (3.2) and $f(T_r)$ and $l(T_r)$ values from Table 3.2. The force–displacement loops in Figure 3.4 were not corrected for beam-end effects, since these were considered typical for bending-beam dampers. Hence damper designs based on Figure 3.4 and Table 3.2 already include typical beam-end effects. The initial stiffness of the damper is somewhat uncertain, owing to variations in end-effects and the stiffness of beam-loading arms.

When Equations (3.2) are used to generate stress–strain loops from the force–displacement loops of a T_r damper, they eliminate the large-displacement increases in nominal stresses, as is evident from a comparison of Figures 3.3(c) and 3.4. When dampers are then designed using Figure 3.4, Equations (3.2) reintroduce appropriate large-displacement changes in force and stiffness.

By introducing the very rough approximation $\hat{\sigma} \approx 2\hat{\tau}$ and using $\epsilon = \gamma$, Figure 3.4 and Table 3.2 can be used to obtain a rough estimate of the force–displacement loops for Type-E (torsional) dampers. However, it would be more accurate to generate a separate set of $\hat{\tau}$ – γ loops based on force–displacement loops for a Type-E damper and Equations (3.2). A representative beam section should be used, say a rectangle with $B = 2t$, where B and t are defined in Table 3.2. Alternatively, the method of ‘Damper loops derived from models of similar proportions’ below, should be used if more accuracy is required.

Errors in approximate damper loops

There are four main sources of error in the damper loops and parameters derived by the method described above.

- (1) Differences between the material properties of the hysteretic beam used to generate the stress–strain loops of Figure 3.4 and the material properties of the hysteretic beam in the prototype.
- (2) End-effects and non-beam deformations. End-effects usually reduce the initial stiffness by about 50% and are particularly important for rectangular-beam Type-E dampers.
- (3) Alteration of loop loads, for a given displacement, by changes in the shape of the damper under large deflections. Shape changes reduce K_{b2} for Type-U dampers and increase K_{b2} for Type-T and Type-E dampers. First-order corrections have been derived for the load changes due to damper shape changes. These have been used to remove large-deflection effects from the loops in Figure 3.4.
- (4) Small changes in the damper loops caused by secondary forces. For example, the Type-E damper is deformed by bending as well as by twisting forces. These effects have been small or moderate for all the damper proportions tested.

The inelastic interaction of primary and secondary beam strains results in a

gradual progressive cycle-by-cycle change in beam shape. The beam of a Type-U damper deforms progressively away from a line through the loading pins. The beams of a Type-E damper deform progressively towards the axis of the loading pin. These effects were not serious in any of the dampers tested. The method given below gives a more accurate procedure for generating force-displacement loops for steel-beam dampers.

Damper loops derived from models of similar proportions

A scale-model method partially eliminates the four sources of error given above. In this method, force-displacement loops are derived for an experimental model, or damper of proportions similar but not identical to those of the prototype, and made of the same material. The scaling is then done in terms of the force- and displacement-scaling factors, f and l , given in Table 3.2.

If subscripts p and e are used for the 'prototype' and the 'experimental model' respectively, then, neglecting the correction factors involving a of Equation (3.2c),

$$F_p/F_e = f_p/f_e \quad (3.3a)$$

$$X_p/X_e = l_p/l_e \quad (3.3b)$$

For example, for a Type- U_c damper, Table 3.2 gives

$$X_p/X_e = (L_p R_p d_e)/(L_e R_e d_p).$$

Section 3.3.4 describes how the stiffness ratios and yield-point ratios can also be obtained.

3.3.4 Bilinear approximation to force-displacement loops

Method of obtaining bilinear approximation

For design purposes, the curved force-displacement loops (such as shown, for example in Figure 3.3(c)) are usually approximated by bilinear hysteresis loops with an initial stiffness K_{b1} , a yielded stiffness K_{b2} and a yield force Q_y . The method adopted here for selecting a bilinear approximation to a hysteresis loop is shown in Figure 3.5. The curved loop $A'B'ABA'$ is symmetric about the centre O , and the coordinates of the vertices A and A' are the maximum displacements $\pm X_b$ and the maximum force $\pm S_b$. The initial stiffness K_{b1} is approximated by the slope of the parallel lines AB , $A'B'$, where B and B' are the loop intercepts on the X -axis. The yield stiffness K_{b2} is approximated by the slope of the parallel lines AC , $A'C'$, where CC' is the line through O with slope K_{b1} . X_y and Q_y , the coordinates of point C , are the yield displacement and the yield force respectively for the bilinear approximation to the curved hysteresis loop. The stress-strain loops of Figure 3.4 can also be approximated by bilinear loops with an initial modulus \hat{E}_1 (or \hat{G}_1), a yielded modulus \hat{E}_2 (or \hat{G}_2) and a yield stress $\hat{\sigma}_y$ (or $\hat{\tau}_y$).

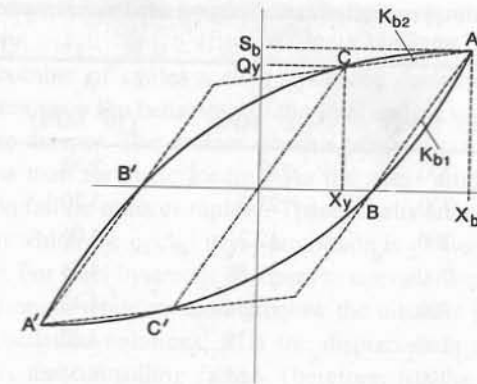


Figure 3.5 The method adopted for selecting a bilinear approximation to a curved hysteresis loop

The bilinear loop parameters change rapidly with the maximum strain amplitude ϵ_m at low strains, but more slowly at larger strains. In practice, these parameter changes do not introduce large errors to seismic designs based on bilinear loops, since seismic responses are dominated by relatively large strains, with slowly varying parameters. With fixed values of K_{b1} , K_{b2} and Q_y , the bilinear loops nest on a two-slope generating curve with a fixed starting point.

Bilinear damper parameters from the bilinear parameters of stress-strain loops

Bilinear approximations to the stress-strain loops of Figure 3.4 have been used to generate the moduli and the yield stresses and strains listed in Table 3.3. These moduli and stresses may be scaled by the factors f and l of Table 3.2 to give the bilinear stiffness and yield parameters for particular dampers, as follows:

$$K_{b1} \approx (f/l)\hat{E}_1 \quad (3.4a)$$

$$K_{b2} \approx (f/l)\hat{E}_2 + aQ_yX_m(1 + \epsilon_y/\epsilon_m) \quad (3.4b)$$

$$Q_y \approx f\hat{\sigma}_y \quad (3.4c)$$

where

$$X_m = l\epsilon_m$$

where ϵ_m is the maximum amplitude of cyclic strain and a , the large-deflection correction factor, is defined in Equation (3.2). For a (torsional) Type-E damper, \hat{E}_1 , \hat{E}_2 and $\hat{\sigma}_y$ of Table 3.3 and Equations (3.4) are replaced by \hat{G}_1 , \hat{G}_2 and $\hat{\tau}_y$ which are, very approximately, half as large.

Table 3.3 Approximated moduli, stresses and strains, up to a strain amplitude ϵ_m of 7%

ϵ_m (%)	\hat{E}_1 (10^2 MPa)	\hat{E}_2 (10^2 MPa)	$\hat{\sigma}_y$ (10^2 MPa)	$\hat{\epsilon}_y$ (%)
1	700	122	2.70	0.36
2	700	25.6	3.70	0.55
3	700	12.2	4.06	0.59
4	700	7.58	4.24	0.61
5	700	5.34	4.42	0.63
6	700	4.79	4.52	0.65
7	700	4.65	4.58	0.66

Stiffness and yield parameters from models of similar proportions

The modelling procedure described in 'Damper loops derived from models of similar proportions', above, can be used to give the parameters of a proposed damper. Again, subscripts p and e refer to the 'prototype' and 'experimental' dampers respectively, and f and l values are obtained from Table 3.2.

If the correction factor involving a is neglected, then Equations (3.4) give

$$K_{b1}(p)/K_{b1}(e) \approx K_{b2}(p)/K_{b2}(e) \approx (f_p l_e)/(f_e l_p) \quad (3.5a)$$

and

$$Q_y(p)/Q_y(e) \approx f_p/f_e. \quad (3.5b)$$

For the Type- U_c damper, for example, Table 3.2 gives either stiffness ratio of the form

$$K_{b1}(p)/K_{b1}(e) \approx (d_p^4 R_c^2 L_e) / (d_e^4 R_p^2 L_p)$$

and

$$Q_y(p)/Q_y(e) \approx (d_p^3 R_e) / (d_e^3 R_p).$$

The above approach is equivalent to generating a loop or loops of the type shown in Figure 3.4, based on an approximate model of a proposed damper, and then using values from Tables 3.2 without end corrections or large-deflection corrections, to find the parameters of the proposed damper.

3.3.5 Fatigue life of steel-beam dampers

While the load-deflection parameters of a steel-beam damper may be achieved readily using the above design parameters, some sophistication is required in design detailing and in manufacturing techniques which will assure a maximum in the potential fatigue life. The potential fatigue life may be estimated from cyclic tests

on simple specimens and from the nominal maximum cyclic strains as derived from simple beam theory.

The 'life', or number of cycles a steel hysteretic damper can be expected to survive, is dependent upon the behaviour of the steel under cyclic loading as well as on the design of the damper. The stresses which a material can survive under cyclic loading are far less than for static loading. As the stress amplitude increases, the number of cycles to failure reduces rapidly. These results are normally summarised in 'S-N' curves, in which the cyclic *stress* amplitude is plotted against the number of cycles to failure. For steel hysteretic dampers to operate, the stress level needs to exceed the yield strength while remaining below the ultimate strength. Fortunately for most seismic isolation solutions, it is the displacement amplitude, and thus the strain, which is the controlling factor. Therefore, for the problem of seismic isolation the important curve is the *strain* amplitude versus the number of cycles to failure (Figure 3.6). Note the logarithmic scale on the abscissa.

By contrast, the lead devices do not fatigue readily at normal operating temperatures, because the melting point of lead is so low. During and after deformation, the deformed lead undergoes the interrelated processes of recovery, recrystallisation and grain growth. This behaviour is similar to that which occurs for steel above about 400°C.

When assessing low-cycle fatigue capacity, the cyclic displacements of an earthquake may be characterised by various strain ranges, say 2 cycles at $\pm 5\%$ strain, 6 cycles of $\pm 4\%$ strain and 12 cycles at $\pm 3\%$ strain, as is commonly done when as-

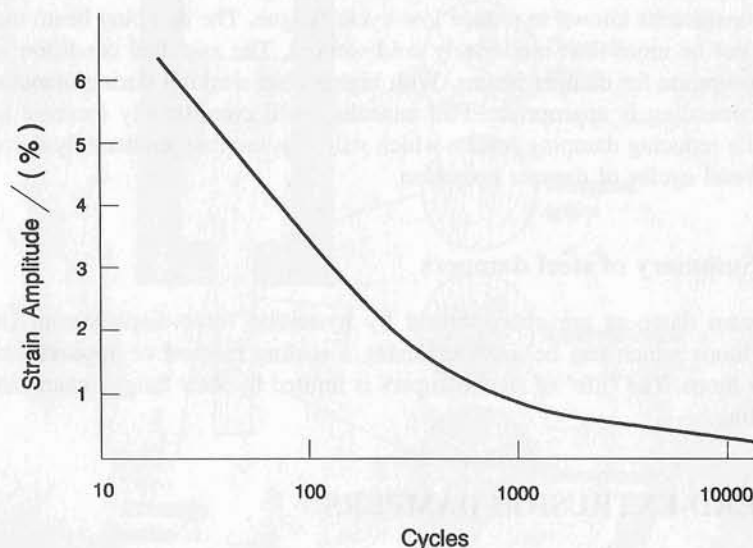


Figure 3.6 Fatigue-life curve for a steel-beam damper. (The strain amplitude versus the number of cycles to failure.) (Based on Tyler, 1978.)

sessing the fatigue capacity of ductile reinforced-concrete structural members. The total fatigue capacity of a well designed steel-beam damper, for any fixed strain range, may be estimated from Figure 3.6. A rough approximation to the reduction in fatigue resistance caused by given earthquake displacements may be obtained as follows. When a strain range of $\pm x\%$ gives a damper fatigue life of n_x cycles, as indicated by Figure 3.6, assume that m cycles consume m/n_x of the total fatigue capacity of the damper. Hence the above earthquake displacement consumes $2/45 + 6/77 + 12/108 = 0.23$ of the total damper fatigue capacity, and the damper is estimated to just survive the cyclic deflections of four such earthquakes. As suggested by this example, the fatigue capacity of damper-beam materials may be compared effectively on the basis of the cyclic fatigue capacity of simple standard specimens subject to a single nominal strain range, say $\pm 5\%$.

The beam and its end fixings must be detailed to avoid severe stress concentrations at locations of high plastic strain. In particular, yielding-beam welds should be confined to lower-strain locations. Again it is appropriate to adopt a damper geometry which gives a decrease in the nominal plastic strain towards the ends of the yielding beams. Large-deformation effects give this end-strain reduction for Type-U dampers with prismatic yielding beams. It also occurs for Type-T_c dampers, with circular cones loaded at the level given at the bottom of Table 3.2. For some dampers, such as Type-T_r, it is appropriate to use curved transitions between yielding and non-yielding parts of the beam.

Rises in the plastic-beam temperature, during design-earthquakes or extreme earthquakes, should cause little change in the damper parameters or in the damper fatigue resistance. The plastic-deformation damper beam should be of mild steel, for example BS4360/43A. It may be an advantage to select for low levels of those constituents known to reduce low-cycle fatigue. The damping beam material should not be more than moderately cold-worked. The as-rolled condition is usually appropriate for damper beams. With higher cold-working during manufacture, partial annealing is appropriate. Full annealing will considerably increase fatigue life while reducing damping forces, which will then increase moderately during the first several cycles of damper operation.

3.3.6 Summary of steel dampers

Steel-beam dampers are characterised by hysteretic force-displacement (stress-strain) loops which can be analysed using a scaling method or approximated by bilinear loops. The 'life' of steel dampers is limited by their fatigue characteristics on cycling.

3.4 LEAD-EXTRUSION DAMPERS

3.4.1 General

Another type of damper utilising the hysteretic energy dissipation properties of

metals is the Lead-Extrusion Damper, sometimes abbreviated to LED, which was developed at PEL (DSIR) (the Physics and Engineering Laboratory of the NZ Department of Scientific and Industrial Research). The cyclic extrusion damper was invented in April 1971 by W H Robinson, immediately after he'd had a morning-tea discussion with R I Skinner on the problems associated with the use of steel in devices to absorb the energy of motion of a structure during an earthquake. The process of extrusion consists of forcing or extruding a material through a hole or orifice, thereby changing its shape (Figure 3.7). The process is an old one. Possibly the first design of an extrusion press was that of Joseph Bramah who in 1797 was granted a patent for a press 'for making pipes of lead or other soft metals of all dimensions and of any given length without joints', (Pearson, 1944).

A lower bound for the extrusion pressure p may be derived from the yield stress σ_y of the material under simple axial load, following Johnson and Mellor (1975). Simple extrusion involves a reduction in the cross-sectional area of a solid prism from A_1 to A_2 by plastic deformation, with an increase in length corresponding

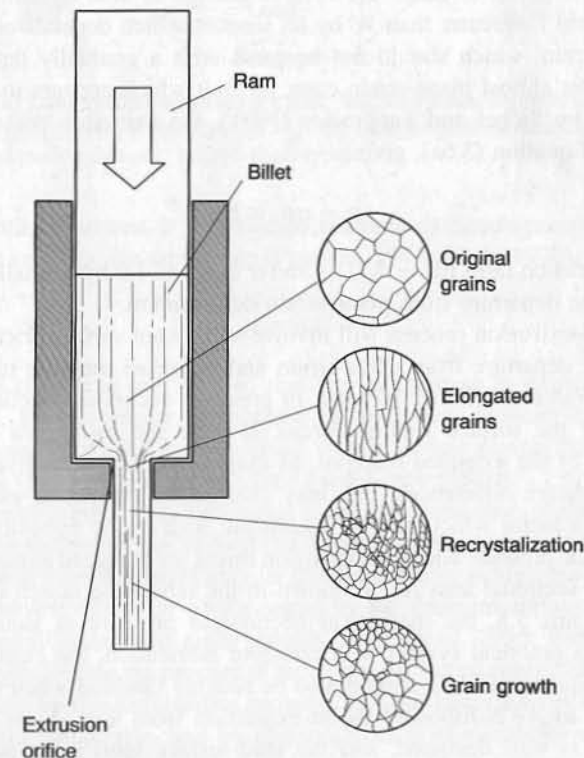


Figure 3.7 A representation of the extrusion of a metal, showing the changes in microstructure. (From Robinson, 1976.)

to little volume change. The process may be idealised as the frictionless extrusion of an incompressible elastic-plastic solid which has a constant yield stress σ_y . The minimum work W , required to change the section from A_1 to A_2 , or the equal minimum work to change the section from A_2 to A_1 , arises when A_1 and A_2 have the same shape and when the deformation involves plane strain. Such plane strain occurs when sections that are plane prior to deformation remain plane throughout the deformation process. The work W of plane-strain deformation can be derived by considering a prism of section A_2 which is compressed between frictionless parallel anvils to form a prism of section A_1 . The yield force increases with the increasing sectional area to give the work W as

$$W = A_1 L_1 \sigma_y \ln(A_1/A_2) \quad (3.6a)$$

where L_1 is the length when the prism area is A_1 . Indeed, Equation (3.6a) can be used as a basis for the experimental determination of the simple-strain yield stress σ_y for lead, since a suitably lubricated lead cylinder, compressed between smooth anvils, deforms in almost true plane strain.

The work required to cause the reverse change in area by simple frictionless extrusion would be greater than W by an amount which depends on the departure from plane-strain, which should not be great with a gradually tapered extrusion orifice. For this almost plane-strain case, a result which appears to have been put forward first by Siebel and Fangmeier (1931), the extrusion pressure p follows simply from Equation (3.6a), giving

$$p = \alpha \sigma_y \ln \underline{ER} \quad (3.6b)$$

where the extrusion ratio $\underline{ER} = A_1/A_2$ and α exceeds 1.0 by a small amount which arises from the departure from plane-strain deformation.

A practical extrusion process will involve significant surface friction which will give a further departure from plane-strain and hence an increase in α beyond the zero-friction value. A further increase in pressure occurs in reaction to the axial component of the surface friction forces. If there are significant changes in σ_y over sections of the extruded material, as may well arise when hysteretic heating causes temperature differences, this may change the pattern of extrusion strains substantially, a factor which may be significant with cyclic extrusion.

When a back-pressure and a re-expansion throat are included to return a lead plug to its original sectional area A_1 , as shown in the schematic sketch of an extrusion damper in Figure 3.8, the theoretical frictionless pressure of Equation (3.6b) is doubled. For a practical system with effective lubrication, the extrusion pressure, as given by Equation (3.6b), should also be roughly doubled when the contraction from area A_1 to A_2 is followed by an expansion from area A_2 to A_1 . When the throat profile is well designed, and the lead-surface lubrication is effective, the pressure should be given approximately by

$$p = \beta_1 \sigma_y \ln(A_1/A_2) + p_0 \quad (3.7a)$$

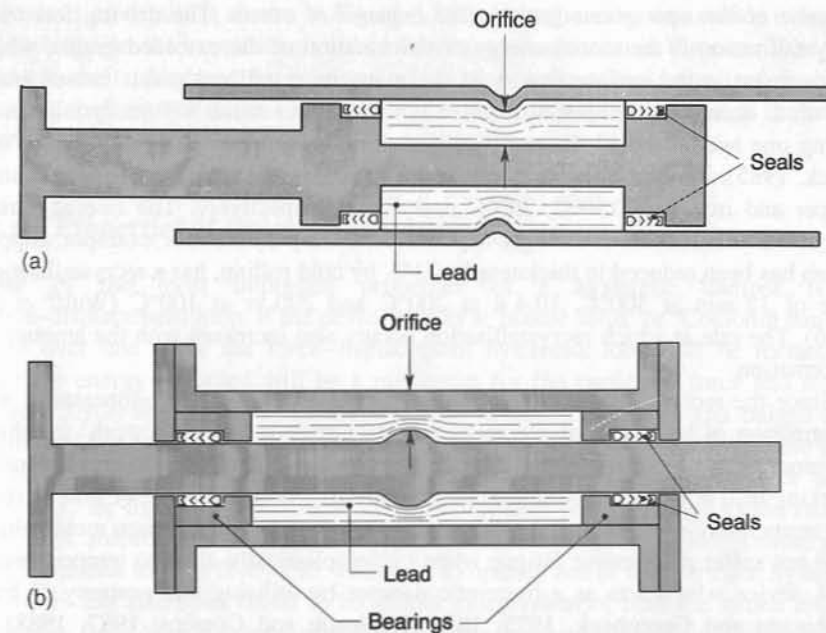


Figure 3.8 (a) Longitudinal section of cyclic lead-extrusion damper: constricted-tube type. (From Robinson, 1976.) (b) Longitudinal section of cyclic lead-extrusion damper: bulged-shaft type

Another result of interest is the relation between extrusion pressure p and the speed of extrusion v , or the strain rate (Pearson, 1944; Pugh, 1970). This is found to be

$$p = av^b \quad (3.7b)$$

where $b = 0.12$ for lead at 17°C , so that for an increase in extrusion speed by a factor of 10, it is necessary to increase the extrusion pressure by 36%. More complete discussions of the behaviour of metals during plastic deformation are found in Nadai (1950), Mendelsson (1968) and Schey (1970).

Deformation of a polycrystalline metal results in elongation of the grains and a large increase in the number of defects (such as dislocations and vacancies) in each grain. After some time the metal may, if the temperature is high enough, return to a state free from the effects of plastic strain by the three interrelated processes of recovery, recrystallisation and grain growth (Wulff *et al.* 1956; Birchenall, 1959; Jones *et al.* 1969). During the process of recovery, the stored energy of the deformed grains is reduced by the dislocations moving, to form lower energy configurations such as subgrain boundaries, and by the annihilation of vacancies at internal and external surfaces.

Recrystallisation occurs when small, new, undeformed grains nucleate among the deformed grains and then grow at their expense. Further grain growth occurs

as some of the new grains grow at the expense of others. The driving force for recrystallisation is the stored energy of deformation of the extruded grains, while the decrease in the surface energy of the many recrystallised grains causes grain growth to occur. The temperature which is sufficient to cause 50% recrystallisation during one hour is called the recrystallisation temperature (Wulff *et al.* 1956; Van Vlack, 1985). For lead this temperature is well below 20°C, while for aluminium, copper and iron it is 150°C, 200°C and 450°C respectively. The rate at which recrystallisation occurs is strongly dependent on temperature. For example, copper which has been reduced in thickness by 71%, by cold rolling, has a recrystallisation time of 12 min at 300°C, 10.4 d at 200°C and 290 yr at 100°C (Wulff *et al.* 1956). The rate at which recrystallisation occurs also increases with the amount of deformation.

Since the recrystallisation temperature of lead is below room temperature, any deformation of lead at or above room temperature is in fact 'hot work' in which the processes of recovery, recrystallisation and grain growth occur simultaneously. Working lead at room temperature is equivalent to working a piece of iron or steel at a temperature of more than 400°C. Indeed, lead is the only common metal which need not suffer progressive fatigue when cycled plastically at room temperature.

A device which acts as a hysteretic damper by utilising this property of lead (Robinson and Greenbank, 1975, 1976; Robinson and Cousins, 1987, 1988) is shown in Figure 3.8(a). It consists of a thick-walled tube co-axial with a shaft which carries two pistons. There is constriction on the tube between the pistons, and the space between the pistons is filled with lead. The lead is separated from the tube by a thin layer of lubricant kept in place by hydraulic seals around the pistons. The central shaft extends beyond one end of the tube. During operation, axial loads are applied with one attachment point at the protruding end of the central shaft and the other at the far end of the tube. The hysteretic damper is fixed between a point on the structure and a point on the earth, which move relative to one another during an earthquake. As the attachment points move to and fro, the pistons move along the tube and the captive lead is forced to extrude back and forth through the orifice formed by the constriction in the tube.

Since extrusion is a process of plastic deformation, work is done and very little energy is stored elastically, as the lead is forced through the orifice during structural deformation. Thus during an earthquake such a device, by absorbing energy, limits the build-up of destructive oscillations in a typical structure. The successful operation of this hysteretic damper depends on the use of a material, in this case lead, which recovers and recrystallises rapidly at the operating temperature, so that the force required to extrude it is practically the same on each successive cycle. If the extruded material had a recrystallisation temperature much above the operating temperature, it would work-harden and be subject to low-cycle fatigue. Moreover, such materials typically have much higher stresses, which would present very severe problems for containment, piston sealing and lubrication in a cyclic extrusion device.

A hysteretic damper which operates on this same principle but has different

construction details is shown in Figure 3.8(b). Here the extrusion orifice is formed by a bulge on the central shaft rather than by a constriction in the outer tube. The central shaft is located by bearings which also serve to hold the lead in place. As the shaft moves relative to the tube, the lead must extrude through the orifice formed by the bulge and the tube.

3.4.2 Properties of the extrusion damper

One of the most important properties of a hysteretic damper is its force-displacement loop. If the device acts as a 'plastic solid' or 'Coulomb damper' then over one cycle the force-displacement hysteresis loop will be rectangular and the energy absorbed will be a maximum for the particular force and stroke. Figure 3.9(a) shows hysteresis loops typical of constricted-tube and bulged-shaft dampers. For both types, the force rises almost immediately on loading while there is no detectable recoverable elasticity on unloading. Note the plastic force is the force Q_y for the extrusion damper. The performance factor, defined as the ratio of the work absorbed by the damper to that contained by the rectangle circumscribing the hysteresis loop, is 0.90–0.95. The force to operate one of the extrusion hysteretic dampers has also been found to be almost independent of both the stroke and the position from which displacement starts. The hysteresis loops in Figure 3.9(b), which show the behaviour of the same damper at an interval of 10 years (1976 and 1986), confirm the stability of the extrusion dampers (Robinson and Cousins, 1987, 1988).

The extrusion force is rate-dependent, as can be understood on the dislocation model by considering the speeds of dislocation motion and grain boundary sliding. To examine the rate dependence of the extrusion force for the extrusion energy absorbers, a number of them were tested at speeds ranging from 3×10^{-10} to 1 m s^{-1} .

The experimental results for the rate dependence of the energy absorbers are shown in Figure 3.10, in which the ordinate is the 'load ratio' relating the force to that which will cause the damper to yield at a speed of 1 ms^{-1} . The damper's performance has two different characteristics, with the change occurring at a speed of 10^{-4} m s^{-1} . Below this speed, the exponential equation (3.7b) is valid with $b = 0.14$. Hence if the rate of cycling is increased by a factor of ten, the load increases by 38%, or the rate must be increased 140 times for the load to be doubled. Above a speed of 10^{-4} m s^{-1} , $b = 0.03$. In this case a 7% increase in load increases the rate by a factor of 10, while a 40% increase in the load requires the rate to be increased 10^5 times. The value of 0.14 for b , for rates below 10^{-4} m s^{-1} , agrees well with the figure of 0.13 obtained by Pearson (1944) for lead at 17°C. Loads which cause creep may also be compared with the load at an earthquake-like speed of 10^{-1} m s^{-1} . At a load ratio $F/F(10^{-1} \text{ m s}^{-1}) = 0.2$, the creep rate becomes $\sim 10 \text{ mm per yr}$. The results above 10^{-4} m s^{-1} indicate that at these speeds the extrusion energy absorbers are nearly rate-independent; for example, at a rate of $\sim 10^2 \text{ m s}^{-1}$ the extrusion force is expected to be 1.15 times that for an earthquake-like speed of 10^{-1} m s^{-1} . Above a rate of $2 \times 10^{-2} \text{ m s}^{-1}$,

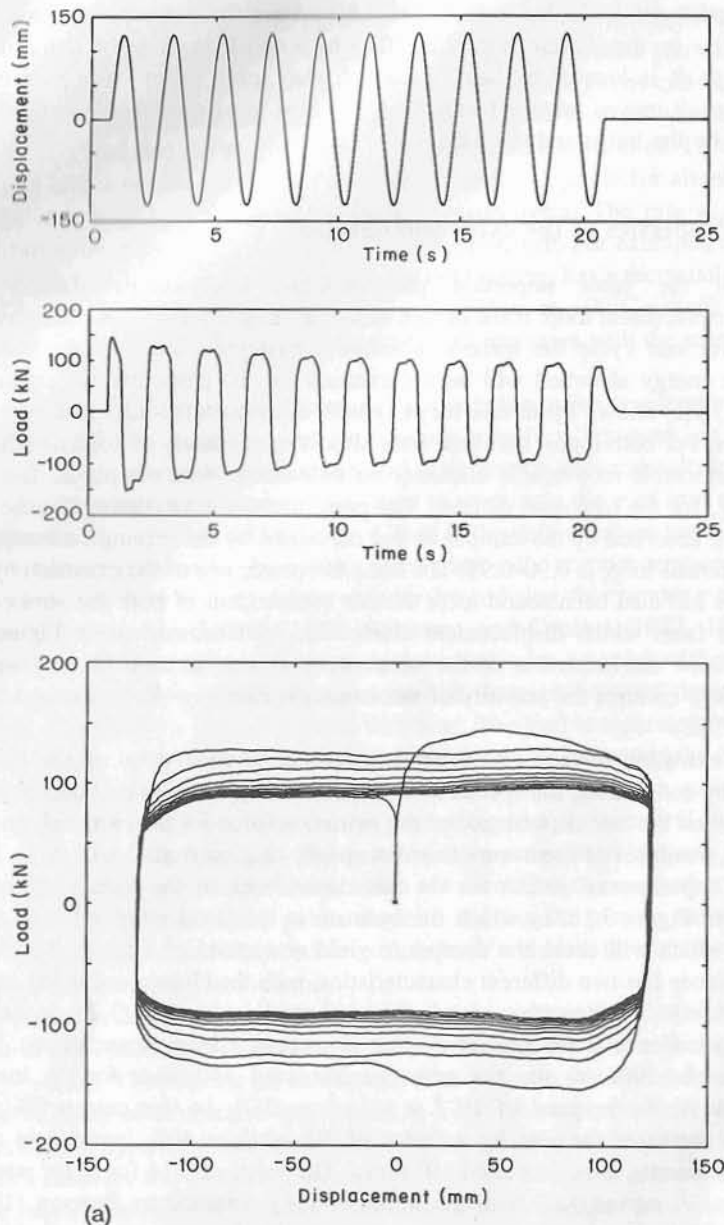


Figure 3.9 (a) Typical load-displacement hysteresis loops for lead-extrusion dampers. (b) Comparison of hysteresis loops obtained for a constricted-tube lead-extrusion damper tested in 1976 (solid line) and again in 1986 (dashed line). (From Robinson and Cousins, 1987.)

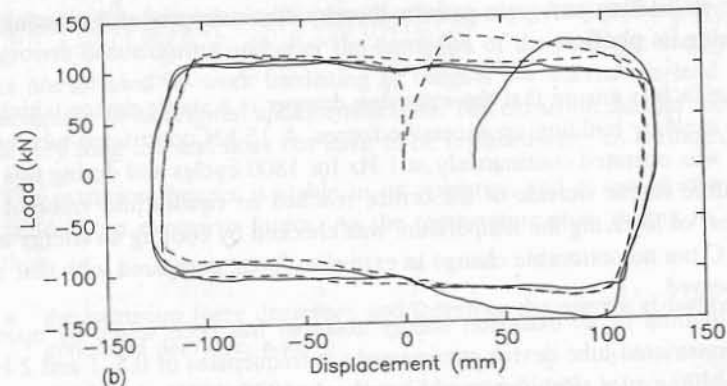


Figure 3.9 (continued)

tests on large energy-absorbing devices become difficult because of the large power required. For example, for a 200 kN hysteretic damper operating at 1 Hz with a total stroke of 250 mm, a power of 100 kW must be supplied.

The effect of temperature on the extrusion energy absorber is complex, in that an increase in temperature, due either to ambient changes or to the absorption of energy during an earthquake, has a twofold effect:

- As the temperature increases the extrusion force decreases.
- The higher the temperature, the more rapidly the lead will undergo recovery,

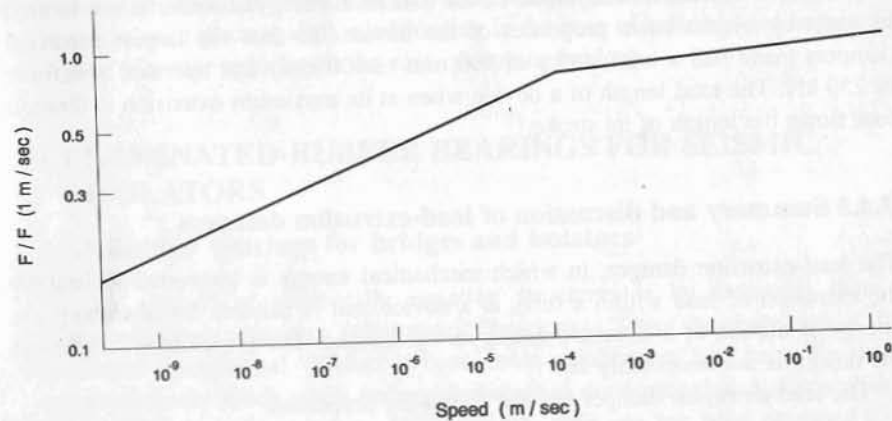


Figure 3.10 Rate dependence of lead-extrusion hysteretic damper. The force is compared with that corresponding to a speed of 1 m s⁻¹, and this load ratio is plotted as a function of speed

recrystallisation and grain growth, thereby eliminating work hardening and regaining its plasticity.

These factors ensure that the extrusion damper is a stable device which cannot destroy itself by building up excessive forces. A 15 kN constricted-tube extrusion damper was operated continuously at 1 Hz for 1800 cycles and during this test the temperature on the outside of the orifice reached an equilibrium value of 210°C. The effect of lowering the temperature was checked by cooling an energy absorber to -20°C but no noticeable change in extrusion force, compared with that at 25°C, was observed.

The lifetime of an extrusion energy absorber has been tested by operating a 15 kN constricted-tube device continuously at frequencies of 0.5, 1 and 2 Hz for a total of 3400 cycles (Robinson and Greenbank, 1975, 1976). After this test, which provided conditions far more severe than those to be expected in service (during an earthquake the device would be expected to undergo ~ 10 cycles), the extrusion energy absorber was found to operate as initially at $1.7 \times 10^{-3} \text{ m s}^{-1}$. This result is not surprising since 'hot-worked' lead is forever recovering its original mechanical properties. Therefore the extrusion damper should be able to cope with a very large number of earthquakes.

The maximum energy an extrusion damper can absorb in a short time is limited by the heat capacity of the lead and the surrounding steel. To increase the temperature of lead from 20°C to its melting point of 327°C, but without melting it, requires $3.8 \times 10^4 \text{ J kg}^{-1}$ of lead. The surrounding steel raises the heat capacity of the device by a factor of ~ 4 so that the total energy capacity of the extrusion device is $\sim 1.6 \times 10^5 \text{ J kg}^{-1}$ (total weight).

An extrusion damper with a 30 mm outside diameter had an extrusion force of ~ 15 kN while a device with a 150 mm outside diameter required a force of ~ 150 kN to operate it. The stroke of the extrusion energy absorber is not limited in any way by the basic properties of the device. To date the largest extrusion dampers made had a total stroke of 800 mm ($\pm 400 \text{ mm}$) and operated at a force of 250 kN. The total length of a device when at its maximum extension is three to four times the length of its stroke.

3.4.3 Summary and discussion of lead-extrusion dampers

The lead-extrusion damper, in which mechanical energy is converted to heat by the extrusion of lead within a tube, is a device that is suitable for absorbing the energy of motion of a structure during an earthquake. The principle is simple but the design is not necessarily so.

The lead-extrusion damper has the following properties.

- (1) It is almost a pure 'Coulomb damper' in that its force-displacement hysteresis loop is nearly rectangular and is practically rate-independent at earthquake-like frequencies.

- (2) Because the interrelated processes of recovery, recrystallisation and grain growth occur during and after the extrusion of the lead, the energy absorber is not affected by work hardening or fatigue, but instead the lead is forever returning to its original undeformed state. The extrusion damper therefore has a very long life and does not have to be replaced after an earthquake.
- (3) The extrusion damper is stable in its operation and cannot destroy itself by building up excessive forces. As the temperature rises during its operation, then
 - the extrusion force decreases and therefore the energy absorbed and heat generated decrease, and
 - the higher the temperature, the more rapidly the lead will recover and recrystallise, thereby regaining its plasticity.
- (4) The length of stroke of the extrusion energy absorber is limited only by the problem of buckling of the shaft during compression. The dimensions of a 150 kN energy absorber with a stroke of $\pm 200 \text{ mm}$ are:

Outside diameter	~ 150 mm
Total length	~ 1.5 m
Total mass	~ 100 kg.

These dimensions ensure simple installation in many isolator applications. The lead-extrusion damper has, to date, been used in New Zealand in three bridges and to provide damping for one ten-storey building mounted on flexible piles (see Chapter 6). It has also been installed in the walls to increase the damping of two buildings in Japan. In addition to providing damping, the extrusion damper 'locks' the structure in place against wind loading in the case of buildings, and against the braking of motor vehicles in the case of sloping bridges.

3.5 LAMINATED-RUBBER BEARINGS FOR SEISMIC ISOLATORS

3.5.1 Rubber bearings for bridges and isolators

Another method of seismically isolating structures is by mounting them on laminated-rubber bearings (elastomeric bearings). These bearings are a fully developed commercial product whose main application has been for bridge superstructures, which often undergo substantial dimensional and shape changes due to changes in temperature. More recently their use has been extended to the seismic isolation of buildings and other structures (Chapter 6).

These bearings are designed to support large weights while providing only small resistance to large horizontal displacements, and to moderate tilts, of the upper

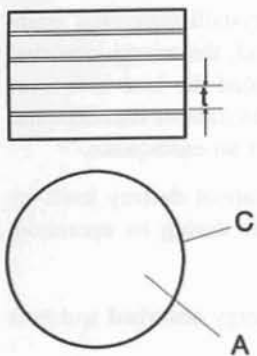


Figure 3.11 Sketch of laminated elastomeric bearing, of area A and circumference C , in which rubber layers, of thickness t , are bonded to thin steel plates

surfaces of the bearings. A typical bridge bearing consists of a stack of horizontal rubber layers vulcanised to interleaved steel plates, as shown schematically in Figure 3.11 for a cylindrical bearing. For a given bearing area and rubber composition, the load capacity is increased by reducing the thickness of each rubber layer, while the resistance to horizontal and tilting movements is reduced by increasing the total height of the rubber.

Rubber bearings, of the types used for bridges, can be dimensioned to provide the support capacity and the horizontal flexibility required for seismic isolation mounts. Of particular importance is the ratio of bearing weight capacity to horizontal flexibility, which determines the maximum achievable value for the rigid-structure period T_b . Of equal importance is the maximum acceptable horizontal displacement X_b , which is set either by the allowable rubber strain or by the allowable offset between the plan areas of the top and bottom of the bearing. Rubber bearings also provide adequate isolator centring forces during large seismic displacements.

Rubber bearings have a considerable range of applications in seismic isolators, as described later in this chapter. In their basic form, rubber bearings may be used to provide support, horizontal flexibility and centring forces. Isolator damping may then be increased by separate components. Alternatively, lead plugs may be inserted in rubber bearings to add high hysteretic damping to the features of the basic bearings, as described in Section 3.6. Again, rubber bearings may be surmounted by horizontal slides which provide increased horizontal flexibility and frictional damping. Additional isolation roles for rubber bearings include tilting supports for rocking structures and elastic components in displacement-limiting buffers.

The detailed design and the manufacture of rubber bearings call for technical sophistication. However, the approximate features of rubber bearings may be derived using simple, well known approaches, as described below. An understanding of the factors influencing the features of elastomeric bearings is useful when developing isolation systems, and may assist during preliminary design studies.

3.5.2 Rubber bearing, weight capacity W_{\max}

The principal features of rubber bearings can be seen from the behaviour of a thin rubber disc, with rigid plates bonded (vulcanised) to its plane surfaces, when subjected to normal (axial) and to parallel (or shearing) loads. The relationship between the load W and the maximum engineering shear strain γ in the disc has been derived by Gent and Lindley (1959) as outlined below in modified form. (Following Borg (1962), $\gamma = \gamma_{xz} = \partial w/\partial x + \partial u/\partial z = 2\eta_{xz}$ where η_{xz} is the tensor shear strain.)

When the rubber is assumed incompressible, a vertical compressive strain ϵ_z causes the rubber to bulge by an amount proportional to its distance from the centre of the disc. When the bulge profile at any radius r is approximated by a parabola, constant rubber volume gives the maximum shear strain γ_{xz} as:

$$\gamma_{xz} = 6S\epsilon_z \quad (3.8a)$$

where the vertical strain $\epsilon_z = \Delta t/t$, the thickness of the rubber layers is denoted by t , and the shape factor $S = (\text{loaded area})/(\text{force-free area})$. For example, for a circular disc of unstrained diameter D and thickness t , $S = D/4t$.

The rubber shear forces cause a pressure gradient within the disc which is proportional to the distance from the centre. This gives a parabolic pressure distribution, as shown in Figure 3.12. The maximum pressure p_0 is given by:

$$p_0 = 2GS\gamma_{xz} \quad (3.8b)$$

where $G =$ shear modulus of rubber.

The corresponding load W may be obtained by summing the pressure over a disc area A to give:

$$W = AGS\gamma_{xz} \quad (3.8c)$$

Now consider a basic rubber bearing consisting of n equal rubber layers of any compact shape. Also let the top of the bearing be displaced by X_b to give an over-

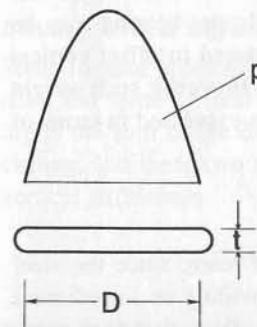


Figure 3.12 Sketch of circular layer of rubber, diameter D , thickness t , and of the parabolic pressure distribution p

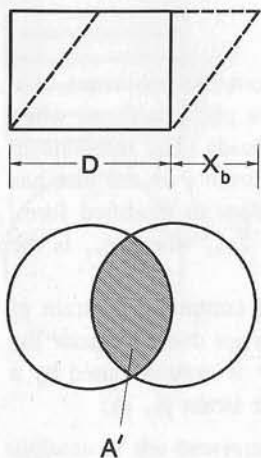


Figure 3.13 Sketch of rubber cylinder of diameter D , with a shear displacement X_b and overlap A'

lap area A' between the top and bottom of the bearing, as shown in Figure 3.13. Then experiment and analysis show that Equation (3.8c) may be generalised approximately as follows:

$$W_{\max} = A'GS\gamma_W \tag{3.8d}$$

where

W_{\max} = allowable weight

γ_W = allowable shear strain due to weight

A' = overlap of bearing top and bottom.

The use of A' in Equation (3.8d) is a somewhat arbitrary simplification and is probably conservative.

3.5.3 Rubber-bearing isolation: stiffness, period and damping

If an isolator consists of a set of equal rubber bearings, each supporting an equal weight, then the isolator period can be calculated directly from the weight and stiffness for a single bearing. In practice the average weight per bearing may be reduced because the weight on some bearings has been reduced to offset vertical seismic loads, or for structural or architectural convenience. However, such weight reductions are neglected here and the isolator parameters are expressed in terms of those for a single bearing.

Bearing horizontal stiffness K_b

A rubber bearing may be approximated as a vertical shear beam, since the steel laminations severely inhibit flexural deformations while providing no impediment to shear deformations. The approximate horizontal stiffness K_b is therefore given

by

$$K_b \cong GA/h \tag{3.9}$$

where

A = rubber layer area

h = total rubber height.

There will be some reduction in bearing height with large displacements, partly due to flexural beam action and partly due to increased compression of the reduced overlap area A' . The resulting inverted pendulum action, under structural weight, reduces the horizontal stiffness K_b and in extreme cases might cause serious reductions in the centring forces. However, the inverted pendulum forces are reduced by increasing the layer shape factor S , and these forces are unlikely to be serious for S values in the range from 10 to 20, a range appropriate for isolator mounts.

Bearing period T_b

The bearing weight capacity, W_{\max} , from Equation (3.8d), and the horizontal stiffness, K_b , from Equation (3.9), can be combined to give the bearing and isolator period T_b , when the bearing is supporting its maximum weight, as

$$T_b = 2\pi(Sh\gamma_W A'/Ag)^{1/2} \tag{3.10}$$

where γ_W is the allowable shear strain due to the weight W .

For example let $S = 16$, $h = 0.15$ m, $A'/A = 0.6$, and $\gamma_{W,\max} = 0.2\Delta L/L$, where the breaking tensile strain $\Delta L/L = 5$, (typically 4.5–7.0). Then $T_b = 2.4$ s.

Bearing damping ζ_b

Energy losses in the deforming rubber layers provide damping which is predominantly velocity-dependent. Typical bridge bearings provide bearing and isolator damping factors in the range from 5% to 10% of critical. However, acceptable bearing rubbers have been manufactured which increase the bearing and isolator damping to about 15%, and development aimed at higher damping values continues.

Bearing vertical stiffness K_z

Some isolator applications of rubber bearings are influenced by their vertical stiffness, and some by their related bending stiffness. The vertical deflection of a bearing is the sum of the deflections due to rubber shear strain and to rubber volume change, and these two respective stiffnesses are added in series. Thus the overall vertical stiffness is

$$K_z = K_z(\gamma)K_z(V)/[K_z(\gamma) + K_z(V)] \tag{3.11a}$$

where $K_z(\gamma)$, the vertical stiffness of the bearing without volume change, is given

by Equations (3.8a) and (3.8c) as

$$K_z(\gamma) = 6GS^2A/h \quad (3.11b)$$

and where $K_z(V)$, the vertical stiffness due to volume change without shear strain, is simply

$$K_z(V) = \kappa A/h \quad (3.11c)$$

where κ = rubber compression modulus. Thus

$$K_z = 6GS^2A\kappa/(6GS^2 + \kappa)h. \quad (3.11d)$$

Equations (3.11) show that a small shape factor S gives a moderate vertical stiffness which is controlled by shear strain, while a sufficiently large value of S gives a very high vertical stiffness which is controlled by volume change. For a typical bridge-bearing rubber, with $G = 1$ MPa and $\kappa = 2000$ MPa, shear strain and volume change make equal contributions to vertical stiffness when $S \approx 18$. The above discussion neglects the usually small reduction in $K_z(\gamma)$ which occurs, due to a pressure redistribution in the layers, when rubber compressibility is introduced. When the S value is high, rubber compressibility reduces considerably the bearing vertical stiffness and the related bending stiffness. However, rubber compressibility causes little change in the other bearing parameters described.

3.5.4 Allowable seismic displacement X_b

Displacement limited by seismic shear strain γ_S

When the rubber shear strain γ_W , due to the vertical load W , is below its maximum allowable value there is a reserve shear strain capacity, say γ_S , to accommodate a horizontal displacement X_b , which is given by

$$X_b = h\gamma_S \quad (3.12)$$

where γ_S = allowable shear strain due to horizontal seismic displacement. If this displacement is inadequate it may be increased by increasing the rubber height h . In addition, or alternatively, γ_S may be increased if the strain due to weight γ_W is reduced.

Displacement limited by overlap factor A'/A

For an isolator bearing, a lower limit to the overlap factor A'/A is set by the reducing weight capacity, Equation (3.8d), and sometimes by the increasing end moments. Typical lower limits for the overlap factor may be 0.8 for a sustained horizontal displacement and 0.6 for design-earthquake displacements. Where possible, such overlap limits should be based on laboratory tests and field experience. The relationship between the overlap factor A'/A , the bearing displacement X_b and

the bearing dimensions depends somewhat on the shape of the horizontal section of the bearing.

For a cylindrical bearing with rubber discs of area A and diameter D

$$A'/A = 1 - (2/\pi)(\theta + \sin\theta \cos\theta) \quad (3.13a)$$

where $\sin\theta = X_b/D$. Hence for moderate values of X_b/D

$$X_b \approx 0.8D(1 - A'/A). \quad (3.13b)$$

Similarly, for a rectangular bearing

$$A'/A \approx 1 - X_b(B)/B - X_b(C)/C \quad (3.13c)$$

where $X_b(B)$ and $X_b(C)$ are the bearing displacements parallel to the sides of lengths B and C respectively. Hence, for displacements parallel to side B ,

$$X_b(B) \approx B(1 - A'/A). \quad (3.13d)$$

When the displacement X_b may be in any direction, a more appropriate displacement limit is

$$X_b \approx 0.8B(1 - A'/A) \quad (3.13e)$$

where B is the shorter side of the bearing. From equations (3.13b) and (3.13e) it is seen that, for a seismic overlap factor $A'/A = 0.6$, the allowable values of X_b are $D/3$ and $B/3$ respectively.

When the weight per bearing is low, the bearing diameter D or side B may be too short to accommodate the required seismic displacement X_b . If the discrepancy is not great it might be met by increasing the bearing area A and/or by reducing the design-earthquake displacement X_b . The bearing area may be increased, without changing the bearing stiffness ratio K_b/W , if there is a compensating reduction in the rubber shear modulus G and/or an increase in the rubber height h , as required by Equation (3.9). Again, the bearing area may be increased if it is possible to design the isolator with fewer bearings and hence with a greater weight W per bearing. Alternatively, the design-earthquake displacement X_b may be reduced by increasing the effective isolator damping.

If the weight per bearing is so low that the allowable displacement falls well short of the design-earthquake displacement, then the allowable displacement may be increased as required, by segmenting the bearing and introducing stabilising plates, as described below.

Segmented bearing for a low weight/displacement ratio W/X_b

When a rubber bearing supports a small weight W it has a small area A , and hence its displacement capacity, as given by Equation (3.13b) or (3.13e), is also small.

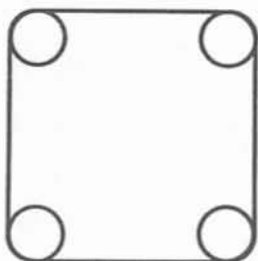
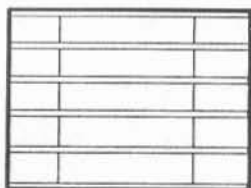


Figure 3.14 Segmented bearing formed by rubber segments placed at the corners of common stabilising plates, illustrated by six stabilising plates and 20 (multilayer) segments

Such a simple bearing may be replaced by an equivalent segmented bearing, as shown in Figure 3.14, which increases the displacement capacity.

Consider the replacement of a simple bearing by an equivalent segmented bearing in which sets of four segments are located near the corners of rectangular stabilisation platforms or plates, as shown in Figure 3.14. If all the linear dimensions (including the thickness) of the segment rubber layers are half those of the simple bearing layers, and if the number of layers is increased so that the rubber height is unaltered, then both bearings have the same values for the rubber area A and the rubber height h , and the same shape factor S , resulting in the same load capacity and the same horizontal stiffness K_b . For a given rubber and operating conditions, a shape factor which is suitable for a non-segmented bearing is also suitable for the equivalent segmented bearing. Typically each of the cylindrical segments shown in Figure 3.14 will be multilayer, to give the small layer thickness required without the use of more stabilising plates than are necessary to retain the overlap factor required for overall bearing stability.

When, as here, the segments have half the horizontal dimensions of the corresponding non-segmented bearing, and there are n segments in each vertical stack (e.g. $n = 5$ in Figure 3.14), then a required overlap factor is retained with an increased allowable displacement given by

$$X_b(n) = nX_b(1)/2 \quad (3.14)$$

where

$X_b(1)$ = allowable displacement for the corresponding non-segmented bearing.

3.5.5 Allowable maximum rubber strains

Allowable shear strains γ_w and γ_s

The allowable rubber shear strains for various loads and displacements are important factors in the performance of rubber bearings, as discussed above. When bearings are used as isolation mounts for compact structures, they must withstand the combined rubber shear strains due to structural weight and seismic displacements. When bearings isolate bridge superstructures, some provision must be made for additional shear strains due to traffic loads and thermal displacements. In addition to their seismic design, rubber bearing mounts must be checked for their capacity to withstand the more sustained non-seismic loads and displacements.

The damaging effect of a given rubber strain increases with its total duration and with the number of times it is reduced or reversed. In particular, rubber strains due to frequent and fluctuating traffic loads are found to be more severe than a corresponding steady strain applied for the life of a bearing. On the other hand, laboratory tests show that the cyclic strains due to seismic displacements are much less severe than corresponding long-duration steady strains, evidently because they involve so few cycles and have such a short duration.

The sustainable steady shear strain in a rubber bearing is sometimes given as (Bridge Engineering Standards, 1976)

$$\gamma_w = 0.2 \epsilon_t \quad (3.15)$$

where ϵ_t = short-duration failure strain in simple tension. Experiments suggest that corresponding factors for shear strain during earthquakes are 0.4 or more for design-earthquakes and say 0.7 for extreme earthquakes.

Allowable negative pressure

Under the combined action of uplift forces and end moments, the rubber within isolator bearings may be subjected to large negative pressures. Consider a rubber bearing subject to an uplift force of $-W_{max}$. From Equation (3.8) it is found that this gives a small increase in bearing height of $\Delta h = h\gamma_w/(6S)$, and a large central negative pressure of $p_o = -2GS\gamma_w$. For a typical bridge bearing, with $G = 1$ MPa, $h = 0.15$ m, $S = 10$, and $-\gamma_w = -1.0$, it follows that $\Delta h = 2.5$ mm and $p_o = -20$ MPa. Negative pressures may also arise from bearing end moments, which are generated by relative displacement and tilting of the ends of a bearing. These end moments cause local increases and decreases of the pressure within the bearing discs. A large negative pressure evidently causes a set of small cavities within the bearing rubber, which grow progressively during sustained and cyclic negative pressures. The cavities cause a large reduction in axial stiffness, which may be regarded as resulting from a reduction in the effective shape factor S , but there is little reduction in the horizontal shear stiffness.

Figures 3.15(a) and (b) show a vulcanised laminated-rubber bearing before and during vertical loading, while Figure 3.15(c) is a stress-strain plot showing both

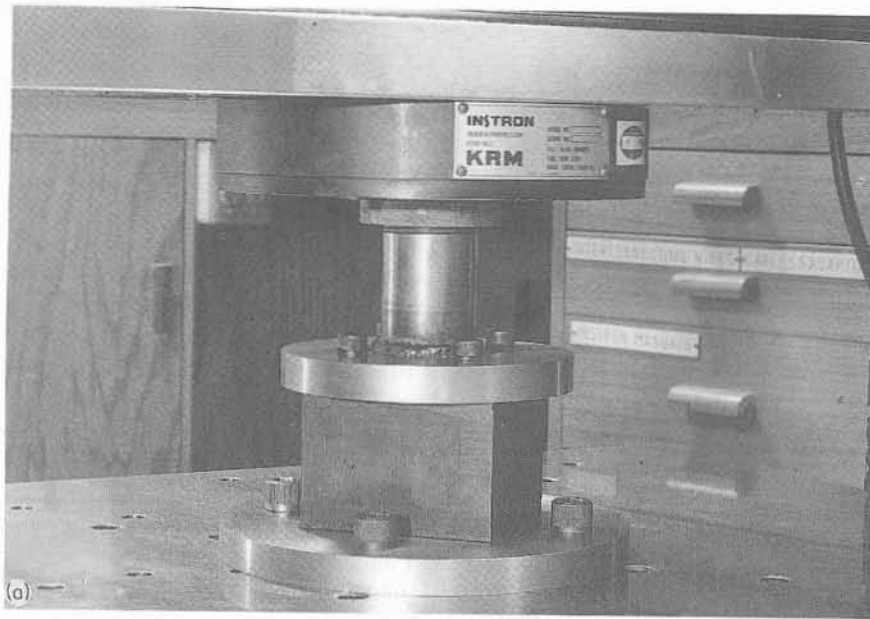


Figure 3.15 (a) Vulcanised laminated-rubber bearing before loading. (b) Vulcanised laminated-rubber bearing under vertical tension. (c) Stress-strain curve for the vulcanised laminated-rubber bearing under both compression and tension. (From Tyler, 1991.)

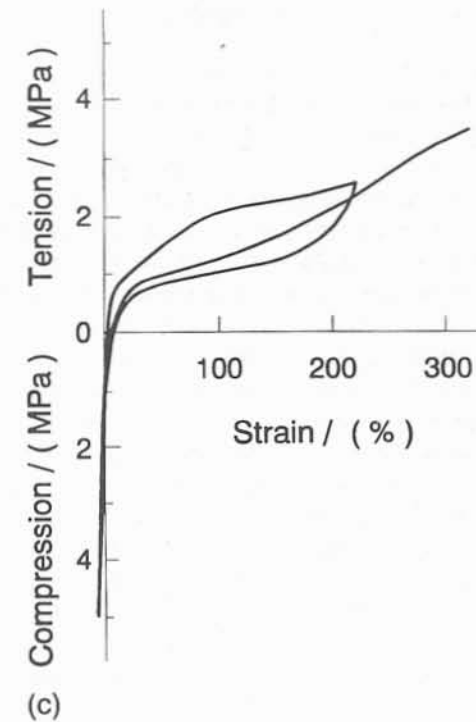


Figure 3.15 (continued)

compression and tension. This bearing failed in the rubber at a tensile strain of 350%, although small internal cracks were most probably formed before this strain was reached.

It is normal practice to design bridge bearing installations so that negative pressures do not occur in the rubber under the combined action of non-seismic loads and motions. It is also appropriate to design isolated structures so that non-seismic actions do not cause negative pressures. However, when seismic actions cause negative pressures in isolator mounts, their duration and frequency are so low that considerable negative pressures might be tolerated (Tyler, 1991). In general, an isolator design should be adopted which avoids very high negative pressures during seismic action. In the particular case of high uplift forces under the corner columns of two-way frame structures, high negative pressures in corner rubber bearings may be avoided by attaching the bearing tops to the bottom beams of the frames designed to allow corner uplift as described, for example, by Huckelbridge (1977).

3.5.6 Other factors in rubber bearing design

In practice the application of laminated-rubber bearings to seismic isolation calls for sophisticated design and specialised manufacturing technology. The rubber must be formulated for long-term stability and resistance to environmental factors, particularly deterioration due to ozone and ultraviolet light. The bonds (vulcanising) between the rubber and the interleaved metal plates must resist the large and varying operating stresses. Bearings must be provided with end and side rubber cover to inhibit corrosion of the metal plates and to remove rubber-surface deterioration from regions of high operating strains. The rubber cover and additional surface materials may be used to increase fire resistance. Interleaved steel plates must have adequate strength to resist rubber shear forces. However, some plate bending may reduce the build-up of rubber tension when large displacements give high end moments. Bearing end-plates must provide for dowels or for other means of preventing end slip under high shear forces. Such shear connections must operate despite end moments, and in some cases when uplift occurs.

The effect of a fire on the performance of rubber elastomeric bearings and lead-rubber bearings has been checked by Miyazaki (1991) in Japan, by heating the outside of bearings to greater than 800°C for more than 100 min while the bearings are under a vertical load. After this heating the rubber elastomeric bearings and the lead-rubber bearings performed in a satisfactory way without any appreciable change in their force-displacement loops or load bearing capacities.

3.5.7 Summary of laminated-rubber bearings

Laminated-rubber bearings are already in use in bridges, in order to accommodate thermal expansion. Their modification for the seismic isolation of buildings and bridges is a fairly simple engineering concept, but in practice it requires sophisticated design and specialised manufacturing technology.

3.6 LEAD-RUBBER BEARINGS

3.6.1 Introduction

Laminated-rubber bearings are able to supply the required displacements for seismic isolation. By combining these with a lead-plug insert which provides hysteretic energy dissipation, the damping required for a successful seismic isolation system can be incorporated in a single compact component. Thus one device is able to support the structure vertically, to provide the horizontal flexibility together with the restoring force, and to provide the required hysteretic damping.

The lead-rubber bearing was invented in April 1975 by W H Robinson, then working at PEL, DSIR, when he saw a rubber elastomeric bearing while trying,

with little success, to get a cylindrical lead shear damper to operate at large strains. The steel plates in the elastomeric bearing were immediately seen to present a solution to the problem of how to control the shape of the lead during large plastic deformation. A glued elastomeric bearing was drilled out to take a lead plug, as shown in Figure 3.16, and was tested immediately, and the results forwarded to the New Zealand Ministry of Works and Development (MWD). In the next few months, the MWD redesigned the isolators for the William Clayton Building (see Chapter 6), replacing the planned design (elastomeric bearings plus steel dampers) with lead-rubber bearings, which were substantially less costly to install, and they provided a 650 mm diameter elastomeric bearing for testing with a range of lead plugs. At the same time the Bridge Section of the MWD designed the Toe Toe and Waitokupuna bridges to take lead-rubber bearings. Thus, during a very short and exciting time, lead-rubber bearings were invented, tested and used in practical applications.

Before describing the lead-rubber bearing in detail, it is worthwhile considering the reasons for choosing lead as the material for the insert in the isolators. The major reason is that the lead yields in shear at the relatively low stress of ~ 10 MPa, and behaves approximately as an elastic-plastic solid. Thus a reasonably sized insert of ~ 100 mm in diameter is required to produce the necessary plastic damping forces of ~ 100 kN for a typical 2 MN rubber bearing. Lead is also chosen because, as noted above for the lead-extrusion damper, it is 'hot-worked' when plastically deformed at ambient temperature, and the mechanical properties of the lead are being continuously restored by the simultaneous interrelated processes of recovery, recrystallisation and grain growth (Wulff *et al.* 1956; Birchenall, 1959 and Van Vlack, 1985). In fact, deforming lead plastically at 20°C is equivalent to deforming iron or steel plastically at a temperature greater than 400°C. Therefore, lead has good fatigue properties during cycling at plastic strains (Robinson and Greenbank, 1975, 1976). Another advantage of lead is that it is used in batteries, and so it is readily available at the high purity of 99.9% required for its mechanical properties to be predictable.

An elastomeric bearing, as described in Section 3.5, is readily converted into a lead-rubber bearing by placing a lead plug down its centre, Figure 3.16. The hole for the lead plug can be machined through the bearing after manufacture or, if numbers permit, the hole can be made in the steel plates and rubber sheets before they are joined together. The lead is then cast directly into the hole or machined into a plug before being pressed into the hole. For both methods of placing the lead, it is imperative that the lead plug is a tight fit in the hole and that it locks with the steel plates and extrudes a little into the layers of rubber. To ensure that this occurs, it is recommended that the lead plug volume be 1% greater than the hole volume, enabling the lead plug to be firmly pressed into the hole. Thus, when the elastomeric bearing is deformed horizontally, the lead insert is forced by the interlocking steel plates to deform in shear throughout its whole volume.

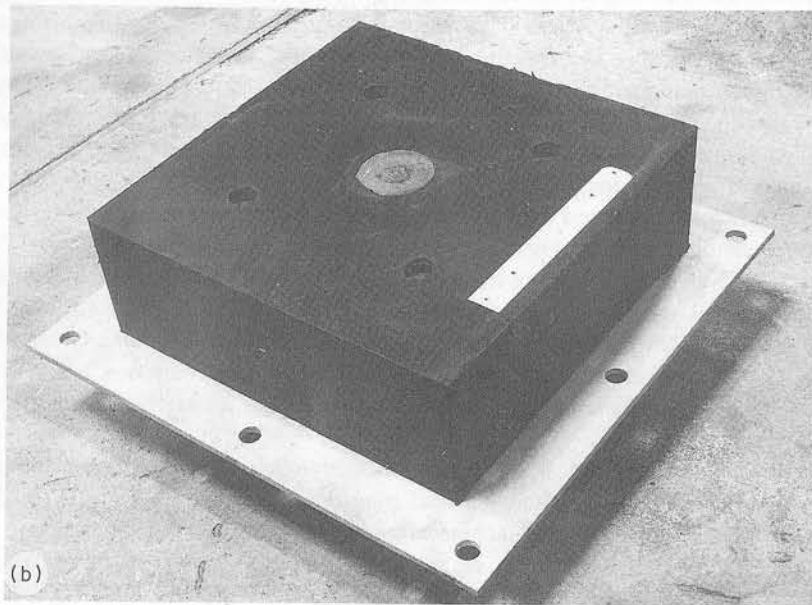
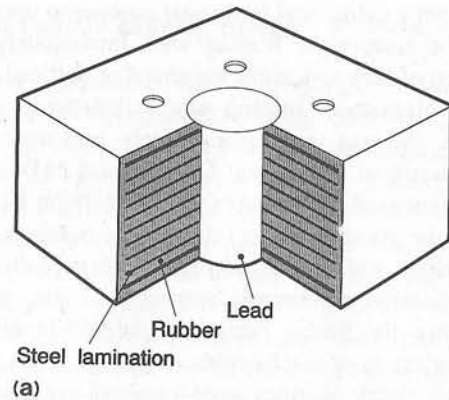


Figure 3.16

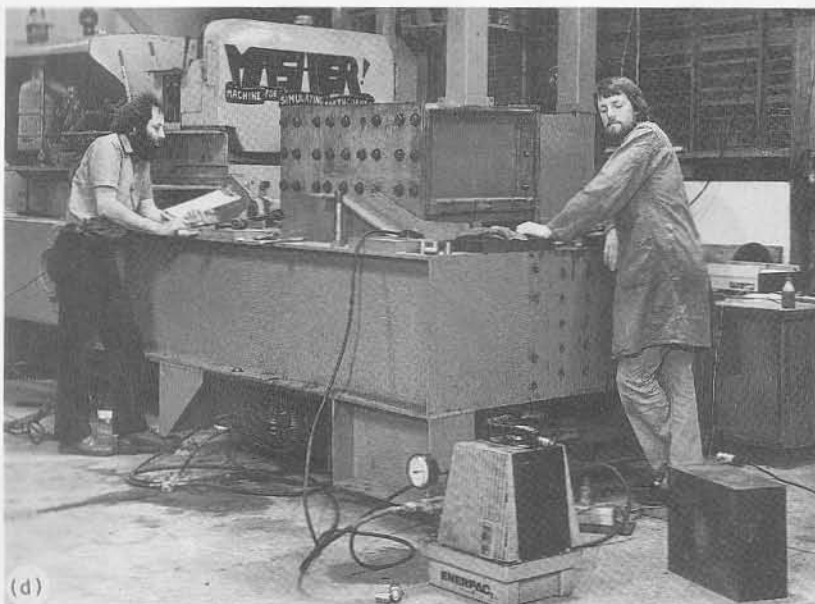
(a) Lead-rubber bearing which consists of a lead plug inserted into a vulcanised laminated-rubber bearing. The form shown here is suitable for applications where there is no applied tension. (b) Lead-rubber bearing for William Clayton Building (see Chapter 6). Note the 300 mm rule placed on the bearing. Load capacity 3 MN, stroke ± 100 mm. (c) Lead-rubber bearing under static test. (d) Lead-rubber bearing for William Clayton Building under dynamic test (1979). The motive force was supplied from the drive of a converted caterpillar tractor: vertical load up to 4 MN, frequency 0.9 Hz, maximum power 100 kW, maximum shear force 400 kN, stroke ± 90 mm.



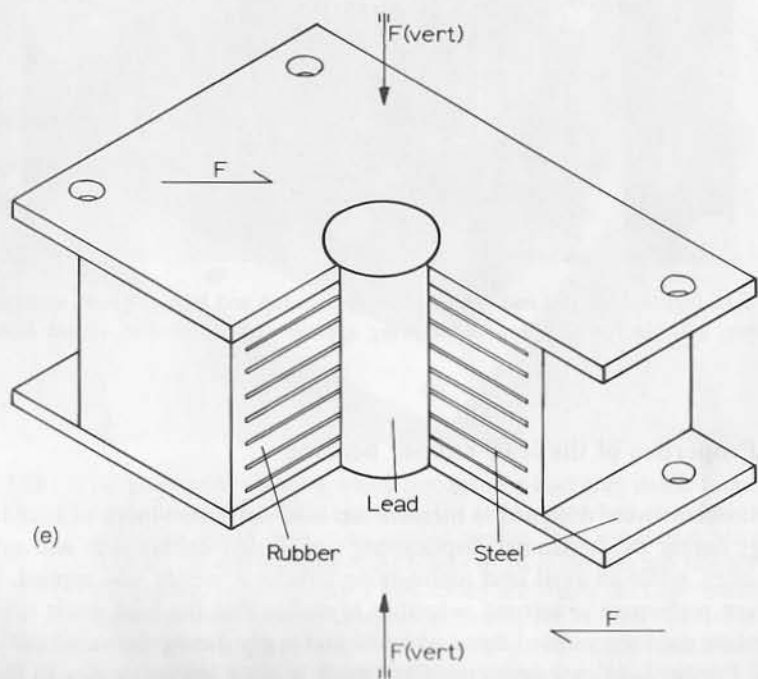
Figure 3.16 (continued) (e) Lead-rubber bearing with top and bottom plates vulcanised to the rubber, suitable for applications requiring applied vertical tension. (From Robinson, 1982.)

3.6.2 Properties of the lead-rubber bearing

Test procedures were designed to measure the load-deflection loops of lead-rubber bearings during the horizontal displacements of design earthquakes and extreme earthquakes, while an axial load representing structural weight was applied. These tests were performed at seismic velocities to ensure that the lead strain rates and temperature rises represented those which would apply during the simulated earthquakes. Further load measurements were made at very low velocities to find the reactions to structural dimension changes arising from daily temperature cycling,



(d)



(e)

Figure 3.16 (continued)

as well as the reactions to the even slower motions associated with the decay of residual isolator displacements after an earthquake (Robinson and Tucker, 1977, 1981; Robinson, 1982).

The force-displacement hysteresis loop of an elastomeric bearing without a lead plug is shown as the dotted curve in Figure 3.17. This loop, which is for a bearing 650 mm in diameter, is mainly elastic with a rubber shear stiffness, $K_b(r) = 1.75 \text{ MN m}^{-1}$ and a small amount of hysteresis. Also in the figure is the loop for the same bearing when it contains a lead insert with a diameter of 170 mm. The dashed lines are at the slope of 1.75 MN m^{-1} and are a good approximation to the post-yield stiffness. In this case the lead is behaving as a plastic solid which adds $\sim 235 \text{ kN}$ to the elastic force required to shear the bearing. Another factor of interest is the initial elastic part of the force-displacement curve for small forces.

Thus a reasonable description of the hysteresis loop is a bilinear solid with an initial elastic stiffness of K_{b1} followed by a post yield stiffness of K_{b2} where

$$K_{b1} \sim 10K_b(r) \tag{3.16a}$$

$$K_{b2} \approx K_b(r) \tag{3.16b}$$

where $K_b(r)$ is given by Equation (3.9).

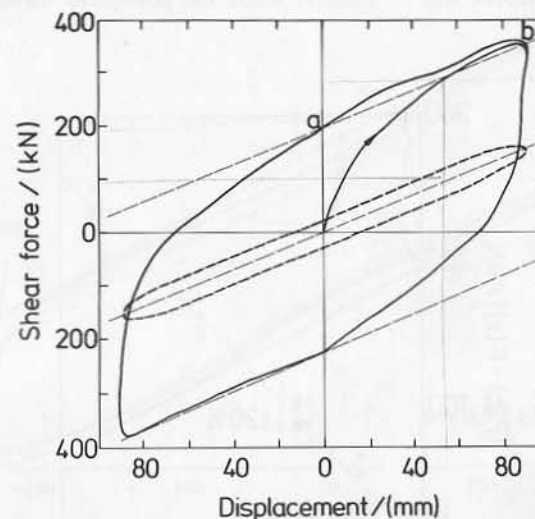


Figure 3.17 Dynamic force-displacement hysteretic loop, for a 650 mm diameter bearing, obtained using equipment shown in Figure 3.16(d), with vertical compression force $F(\text{vert}) = 3.15 \text{ MN}$, frequency 0.9 Hz, stroke $\pm 90 \text{ mm}$. The dashed curve is for the bearing without a lead plug. The solid line is for a lead plug of 170 mm diameter. The slope of the dashed line is $K_b(r)$. (From Robinson, 1982.)

Dependence on the diameter of the lead insert

The horizontal force, F , required to cause the bearing to be horizontally sheared can be considered as two forces acting in parallel, the first due to the rubber elasticity and the second due to the plasticity of the lead. The rubber elasticity results in a force which is proportional to the displacement while the plasticity requires a force which is independent of displacement. Thus to a very good approximation

$$F = \tau(\text{Pb})A(\text{Pb}) + K_b(r)X \quad (3.17)$$

where the shear stress at which the lead yields $\tau(\text{Pb}) = 10.5 \text{ MPa}$, $A(\text{Pb})$ is the cross-sectional area of the lead, $K_b(r)$ is the stiffness of the rubber in a horizontal plane, and X is the displacement of the top of the bearing with respect to its base. This fact is illustrated in Figure 3.18 where the maximum shearing force, minus the force due to the elastic stiffness of the rubber, is plotted against the cross-sectional area of the lead insert. The slope of this line is the yield stress of lead, 10.5 MPa (Robinson, 1982). Note Q_y of a hysteretic damper is given approximately by $\tau(\text{Pb})A(\text{Pb})$.

Figure 3.19 contains the force-displacement hysteresis loops for two recent examples, namely the lead-rubber bearings for the seismic isolation of (a) the William Clayton Building and (b) the Wellington Press Building. For both of these examples the initial stiffness $K_{b1} \sim 10K_b(r)$ while the post-yield stiffness is approximately $K_b(r)$.

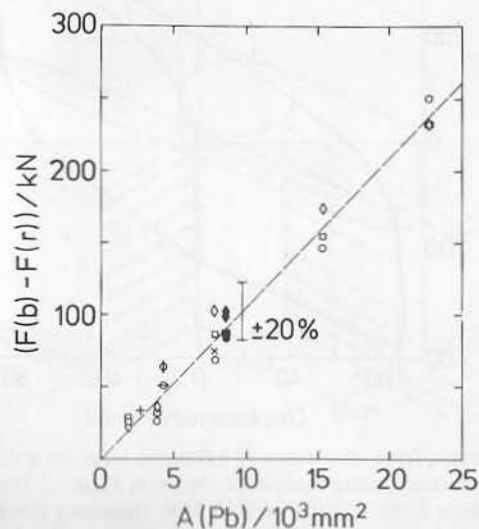


Figure 3.18 Force due to the lead, $F(b) - F(r)$, as a function of the cross-sectional area of the lead insert. (From Robinson, 1982.)

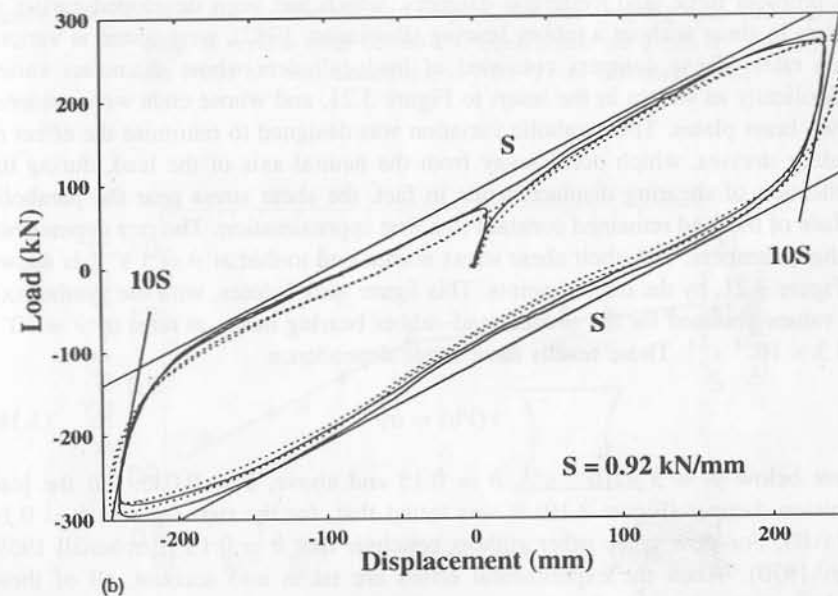
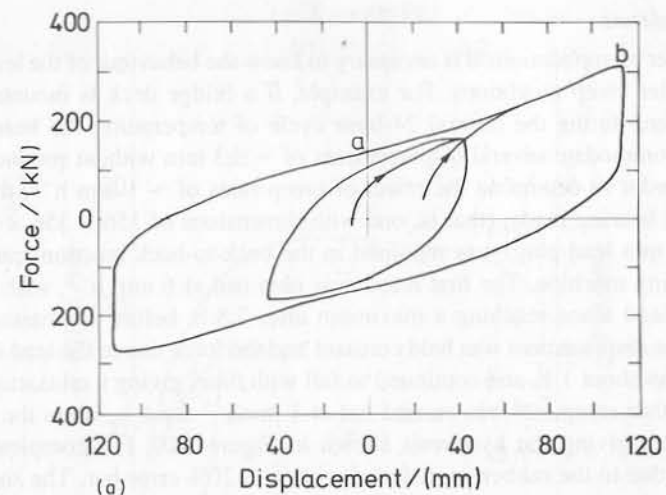


Figure 3.19 (a) Force-displacement hysteresis loops for a lead-rubber bearing used in the William Clayton Building, at 45 and 110 mm strokes, with a vertical force of 3.15 MN at 0.9 Hz . (From Robinson, 1982.) (b) Force-displacement curves for the bearings used in the Wellington Press Building (see Chapter 6). (From Robinson and Cousins, 1987, 1988.)

Rate dependence

For a number of applications it is necessary to know the behaviour of the lead-rubber bearing under creep conditions. For example, if a bridge deck is mounted on the bearings then, during the normal 24-hour cycle of temperature, the bearings will have to accommodate several displacements of $\sim \pm 3$ mm without producing large forces. In order to determine the effect of creep rates of ~ 1 mm h^{-1} , the second lead-rubber bearing made, (that is, one with dimensions of $356 \times 356 \times 140$ mm³ with a 100 mm lead plug) was mounted in the back-to-back reaction frame in the Instron testing machine. The first result was obtained at 6 mm h^{-1} , with the force due to the lead alone reaching a maximum after 2.5 h, before decreasing slowly. After 6 h the displacement was held constant and the force due to the lead decreased to one half in about 1 h, and continued to fall with time, giving a relaxation time of 1–2 h. Another creep test was carried out at 1 mm h^{-1} for 6 h, when the direction was reversed, giving the hysteresis shown in Figure 3.20. For completeness the force $F(r)$, due to the rubber, is included with its $\pm 20\%$ error bar. The shear stress in the lead plug reached a maximum of 3.2 MPa, which is $\sim 30\%$ of the stress of 10.5 MPa for the dynamic tests. The force due to the rubber is great enough to drive the deformed lead, and the structure, back to its original position.

Because of the large errors caused by $F(r)$, it was not possible to determine accurately the rate-dependence of the lead in the lead-rubber bearing. To overcome this problem three lead hysteretic dampers, which had been developed earlier to operate in shear without a rubber bearing (Robinson, 1982), were tested at various strain rates. These dampers consisted of lead cylinders whose diameters varied parabolically as shown in the insert to Figure 3.21, and whose ends were soldered to two brass plates. The parabolic variation was designed to minimise the effect of bending stresses, which occur away from the neutral axis of the lead, during the application of shearing displacements: in fact, the shear stress near the parabolic surface of the lead remained constant to a first approximation. The rate dependence of these dampers, with their shear stress normalised to that at $\dot{\gamma} = 1$ s⁻¹, is shown in Figure 3.21, by the circled points. This figure also denotes, with the symbol (x), the values obtained for the second lead-rubber bearing made, at rates of $\dot{\gamma} = 10^{-5}$ and 3×10^{-1} s⁻¹. These results have a rate dependence

$$\tau(\text{Pb}) = a\dot{\gamma}^b \quad (3.18)$$

where below $\dot{\gamma} = 3 \times 10^{-4}$ s⁻¹, $b = 0.15$ and above, $b = 0.035$. For the lead extrusion damper (Figure 3.10) it was found that, for the two regions, $b = 0.14$ and 0.03. For slow creep other authors conclude that $b = 0.13$ (Birchenall 1959, Pugh 1970). When the experimental errors are taken into account, all of these results are in reasonable agreement.

These results indicate that the lead-rubber bearing has little rate-dependence at strain rates of 3×10^{-4} – 10 s⁻¹, which includes typical earthquake frequencies of 10^{-1} – 1 s⁻¹. For this range of strain rates, an increase in rate by a factor of 10 causes an increase in force of only 8%. Below strain rates of 3×10^{-4} s⁻¹, the

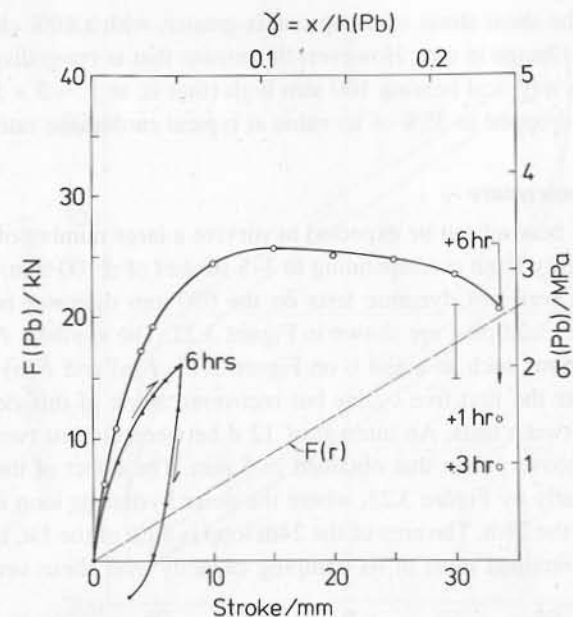


Figure 3.20 Force due to lead during creep of 356 mm² bearing with 100 mm lead plug, at vertical force of 400 kN. Open points are 6 mm h^{-1} , filled points are 1 mm h^{-1} and dashed line is $F(r)$. (From Robinson, 1982.)

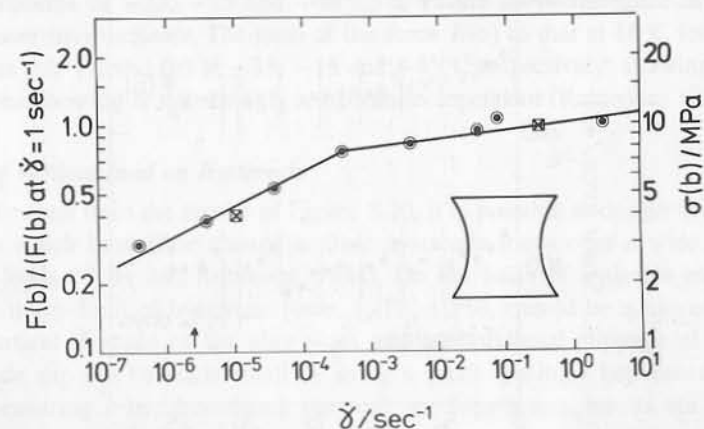


Figure 3.21 Rate dependence of lead cylinders of parabolic section (see insert) in shear, as indicated by the circled points. The crosses indicate the rate dependence of the lead plug in a lead-rubber bearing. (From Robinson, 1982.)

dependence of the shear stress on creep rate is greater, with a 40% change in force for each decade change in rate. However, this means that at creep displacements of $\sim 1 \text{ mm h}^{-1}$ for a typical bearing 100 mm high (that is, at $\dot{\gamma} \sim 3 \times 10^{-6} \text{ s}^{-1}$), the shear stress has dropped to 35% of its value at typical earthquake rates, $\dot{\gamma} \sim 1 \text{ s}^{-1}$.

Fatigue and temperature

The lead-rubber bearing can be expected to survive a large number of earthquakes, each with an energy input corresponding to 3–5 strokes of $\pm 100 \text{ mm}$. For example, the results for a series of dynamic tests on the 650 mm diameter bearing with a 140 mm diameter lead plug are shown in Figure 3.22. The symbols $F(a)$ and $F(b)$ correspond to points such as a and b on Figure 3.17. $F(a)$ and $F(b)$ decreased by 10 and 25% over the first five cycles but recovered some of this decrease in the 5 min breaks between tests. An interval of 12 d between the last two tests did not give a greater recovery than that obtained in 5 min. The effect of the 24 cycles is shown more clearly by Figure 3.23, where the outer hysteresis loop is the 1st, and the inner loop is the 24th. The area of the 24th loop is 80% of the 1st, indicating that the bearing has retained most of its damping capacity over these seven simulated earthquakes.

As a further check on the fatigue performance, the 356 mm bearing was dynamically tested at a shear strain of 0.5 for a total of 215 cycles in a two-day period. This bearing was also subject to 11 000 strokes at $\pm 3 \text{ mm}$ (0.9 Hz), to demonstrate that it could withstand the daily cycles of thermal expansion which occur in a bridge deck over a period of 30 years. It performed satisfactorily.

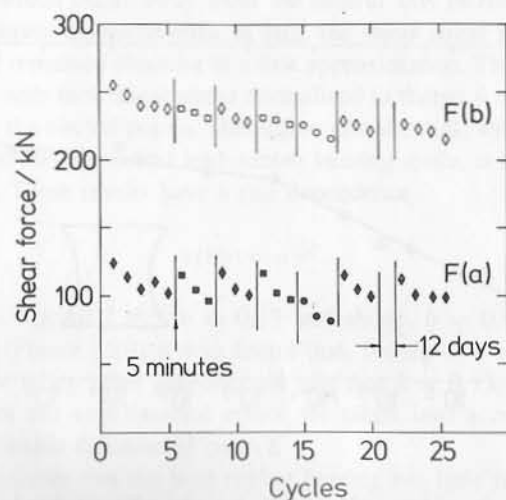


Figure 3.22 Dynamic tests on lead-rubber bearing over seven simulated earthquakes. (From Robinson, 1982.)

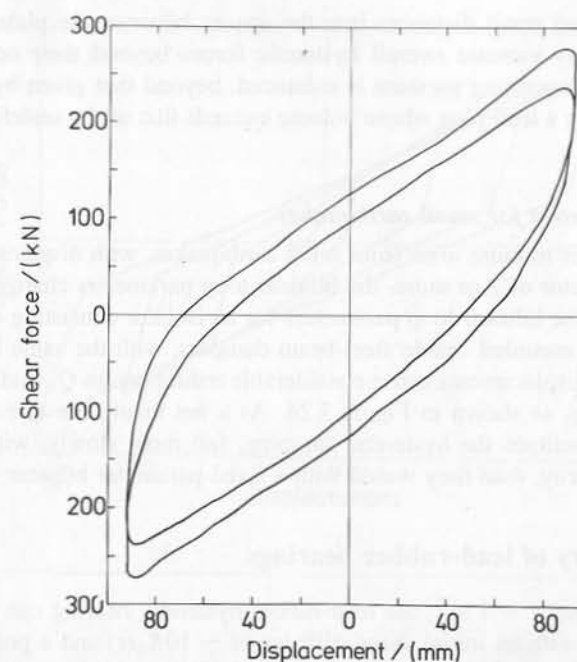


Figure 3.23 1st and 24th hysteresis loops for lead-rubber bearing shown in Figure 3.22. The outer loop is the 1st and the inner loop is the 24th. (From Robinson, 1982.)

The 356 mm bearing was also studied with dynamic tests ($\gamma \sim 0.5$, 0.9 Hz) at temperatures of -35 , -15 and $+45^\circ\text{C}$, to ensure its performance in extreme temperature environments. The ratio of the force $F(b)$ to that at 18°C for the first cycle was 1.4, 1.2 and 0.9 at -35 , -15 and $+45^\circ\text{C}$ respectively, showing that the lead-rubber bearing is not strongly temperature-dependent (Robinson, 1982).

Effect of vertical load on hysteresis

As can be seen from the results of Figure 3.20, it is possible to design lead-rubber bearings which have little change in their hysteresis loops over a wide range of vertical loads (Tyler and Robinson, 1984). On the basis of a simple model, the nominal upper limit of hysteretic force, $\tau_y(P_b)A(P_b)$, should be achieved if there is no vertical slippage of the plug sides and no horizontal slippage of the plug ends. Side slip can be made small by using a small spacing t between the plates and by ensuring a large confining pressure p_o . Satisfactory results are achieved with a spacing t less than $d/10$, and with a pressure p_o , as given approximately by equation (3.8b) when S is greater than 10. The effect of end slip can be made small by using a lead plug with an adequate height-to-diameter ratio h/d , say not less than 1.5. Complicating factors include the hysteretic forces due to the lead

which is extruded small distances into the spaces between the plates, additional forces which may increase overall hysteretic forces beyond their nominal upper limit. Again the confining pressure is enhanced, beyond that given by the vertical load, by inserting a lead plug whose volume exceeds that of the undeformed cavity in the bearing.

Bilinear parameters for small earthquakes

When the isolator motions arise from small earthquakes, with displacement spectra reduced by a factor of 2 or more, the bilinear loop parameters change in the same general way as the bilinear loop parameters for an isolator consisting of laminated-rubber bearings mounted beside steel-beam dampers, with the same beneficial results. Reduced displacements cause considerable reductions in Q_y and considerable increases in K_{b2} , as shown in Figure 3.24. As a net result, the effective (secant) period, and sometimes the hysteretic damping, fall more slowly, with decreasing earthquake severity, than they would with a fixed-parameter bilinear loop.

3.6.3 Summary of lead-rubber bearings

For strain rates of $\dot{\gamma} \sim 1 \text{ s}^{-1}$, the lead-rubber hysteretic bearing can be treated as a bilinear solid with an initial shear stiffness of $\sim 10K_b(r)$ and a post-yield shear stiffness of $K_b(r)$. The yield force of the lead insert can be readily determined from the yield stress of the lead in the bearing, i.e. $\tau_y(\text{Pb}) \sim 10.5 \text{ MPa}$. Thus the maximum shear force for a given displacement is the sum of the elastic force of the elastomeric bearing and the plastic force required to deform the lead. The actual post-yield stiffness is likely to vary by up to $\pm 40\%$ from $K_b(r)$ but will probably be within $\pm 20\%$ of this value. The initial elastic stiffness has only been estimated from the experimental results and may in fact be in the range of $9K_b(r)$ to $16K_b(r)$. The prediction for the maximum force, $F(b)$, is more accurate and has instead an uncertainty of $\pm 20\%$ which is the same as expected for the uncertainty in the shear stiffness of manufactured elastomeric bearings. The actual area of the hysteresis loop formed by this bilinear model is approximately 20% greater than the area of the measured hysteresis loop.

The lead-rubber hysteretic bearing provides an economic solution to the problem of seismically isolating structures, in that the one unit incorporates the three functions of vertical support and horizontal flexibility (via the rubber) and hysteretic damping (by the plastic deformation of the lead). Further discussion on lead-rubber bearings is contained in Robinson and Cousins (1987, 1988); Skinner *et al.* (1980); Skinner *et al.* (1991) and Cousins *et al.* (1991).

3.7 FURTHER ISOLATOR COMPONENTS AND SYSTEMS

A wide range of further isolator components, to provide flexibility and/or damping, have been used or proposed. Some of these isolator components are based on material properties, particularly those which provide flexibility and hysteretic

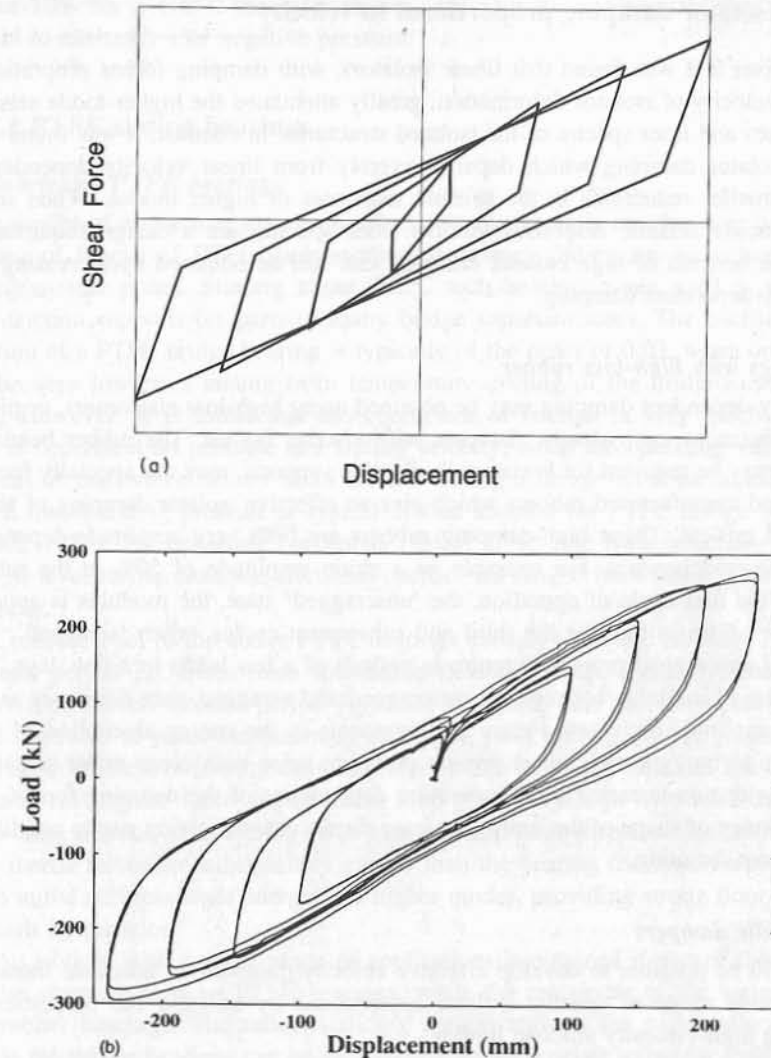


Figure 3.24 (a) Difference in bilinear loop parameters corresponding to small and large displacements. (b) Load-displacement loops for various strokes of lead-rubber bearing used in Press Hall, Petone (see Chapter 6). (From Robinson and Cousins, 1987, 1988.)

damping forces, as in the cases described above. A second class of isolator component depends on sliding supports and on frictional damping forces. A third class depends on geometrical factors such as rocking with uplift, or rolling surfaces, or pendulum action under gravity forces. Representative examples from each class of isolator component are described briefly below.

3.7.1 Isolator damping proportional to velocity

In Chapter 2 it was found that linear isolators, with damping forces proportional to the velocity of isolator deformation, greatly attenuated the higher-mode seismic responses and floor spectra of the isolated structures. In contrast, it was found that high isolator damping which departs severely from linear velocity dependence, gives smaller reductions in the seismic responses of higher modes. When small higher-mode seismic responses, or low floor spectra, are a design requirement then the benefits of high isolator damping can still be obtained by increasing the velocity-dependent damping.

Bearings with high-loss rubber

Velocity-dependent damping may be obtained using high-loss elastomers, or pitch-like substances, or hydraulic dampers with viscous liquids. The rubber bearings, which may be required for horizontally flexible supports, may use specially formulated and manufactured rubbers which give an effective isolator damping of about 15% of critical. These high-damping rubbers are both very amplitude-dependent and history-dependent. For example, at a strain amplitude of 50% in the rubber during the first cycle of operation, the 'unscragged' state, the modulus is approximately 1.5 times that for the third and subsequent cycles, when 'scragged'. The original unscragged properties return in periods of a few hours to a few days. The reduction of modulus between the unscragged and scragged state decreases as the strain amplitude increases. Future improvements in the energy absorption of rubbers are to be expected, but at present problems arise with creep under sustained loads, with non-linearity and temperature dependence of the damping forces, and with change of shape of the bearing at large displacements, giving rise to amplitude dependent damping.

Hydraulic dampers

It should be possible to develop effective velocity dampers, of adequate linearity, for a wide range of seismic isolator applications by utilising the properties of existing high-viscosity silicone liquids.

In principle, the development of a velocity-dependent silicone fluid-based hydraulic damper is straightforward. A double-acting piston might be used to drive the silicone fluid cyclically through a parallel set of tubular orifices, designed to give high fluid shears and hence the required velocity-damping forces. By using a sufficient working volume of silicone fluid to limit the temperature rise to 40°C during a design-level earthquake, the corresponding reduction in damper force is limited to about 25%. For comparison, the thermal capacity per unit volume for silicone fluid is comparable to that for lead, or about 40% of that for iron.

The development of practical linear hydraulic dampers is complicated by a number of factors including the increase in silicone fluid volume with temperature,

about 10% for a 100°C temperature rise, and also the tendency of the silicone liquid to cavitate under negative pressure.

3.7.2 PTFE sliding bearings

Unlubricated PTFE bearings

The weight of a structure may be supported on horizontally moving bearings consisting of blocks of PTFE (polytetrafluoroethylene) sliding on plane horizontal stainless-steel plates. Starting about 1965, such bearings were used to provide low-friction supports for parts of many bridge superstructures. The coefficient of friction of a PTFE bridge bearing is typically of the order of 0.03, when operating at the very low rates arising from temperature cycling of the bridge superstructure. However, it is found that the coefficient of friction is very much higher, and is dependent on pressure and sliding velocity, when the operating velocity is typical of that which occurs in an isolator during a design-level earthquake, and when the operating pressure is typical of that adopted for PTFE bridge bearings (Tyler, 1977). For operating conditions typical of seismic isolator actions during design-level earthquakes, the frictional coefficients ranged from about 0.10 to 0.15 or more.

Consider a set of the above PTFE bearings used as a seismic isolator. The first isolator period T_{b1} arises from foundation flexibility only, and is typically very short. The second isolator period T_{b2} tends to infinity and therefore provides no centring force to resist displacement drift. The yield ratio Q_y/W is given by the bearing coefficient of friction and is therefore rather large and variable. The approximately rectangular force-displacement loop gives very high hysteretic damping. However, absence of a centring force may result in large displacement drift if seismic inertia forces are substantially greater than the bearing frictional forces. Also, high initial stiffness leads energy into higher modes, providing strong floor spectra of high frequencies.

An isolator with a wider range of applications is obtained if part of the weight of the structure rests on PTFE bearings, while the remainder of the weight rests on rubber bearings. The reduced sliding weight reduces the yield ratio Q_y/W , while the rubber bearings can be used to give an appropriate value for the centring force, as indicated by the second isolator period T_{b2} , which should usually be in the range between 2.0–4.0 s. Problems arising from a very short first period T_{b1} may be removed by mounting the PTFE bearings on rubber bearings, as described below.

Lubricated PTFE bearings

Lubricated PTFE bearings have quite small coefficients of friction, usually less than 0.02 (Tyler, 1977), for the pressures and velocities which they would encounter as seismic isolator mounts. When an isolator has low-friction load-support bearings, then components which provide centring and damping forces need not support any

weight. For example, approximately linear centring and damping forces could be provided by blocks of high-loss elastomer, for which creep is not a problem without sustained loads. If higher linear damping is required, hydraulic dampers could be added. However, since almost every isolator application is tolerant of at least a moderate degree of non-linearity, it should usually be possible to provide some of the centring and damping forces by non-linear components, such as weight-supporting lead-rubber bearings.

For high reliability, lubricated PTFE bearings should be serviced regularly. However, for high-technology applications, for example nuclear power plant isolation, maintenance should not present a serious problem.

3.7.3 PTFE bearings mounted on rubber bearings

In Chapter 2 it was found that a bilinear isolator with a short first period T_{b1} results in relatively large higher-mode seismic accelerations and floor spectra. In Chapter 4 it is shown that these higher-mode seismic responses may be substantially reduced by increasing the first bilinear period T_{b1} to exceed the first period of the unisolated structure $T_1(U)$.

A compound isolator component developed in France (Plichon et al, 1980) consisted of a sliding bearing mounted on top of a rubber bearing. Initially the bearings were made of lead-bronze blocks sliding on stainless steel, while later designs replaced the lead-bronze blocks by PTFE blocks. The flexibility of the laminated-rubber components of the compound bearing can be chosen to give a first bilinear period T_{b1} which exceeds $T_1(U)$, the first structural period. As in the previous section, the second bilinear period T_{b2} may be limited to a value which prevents excessive displacement drift by supporting part of the structural weight directly on rubber bearings. This also reduces the value of Q_y/W for the isolator.

3.7.4 Tall slender structures rocking with uplift

The seismic design loads and deformations of tall slender structures are normally associated with high overturning moments at the base level. If the narrow base of such a structure is allowed to rock with uplift, then the base moment is limited to that required to produce uplift against the restraining forces due to gravity. This base moment limitation will usually reduce substantially the seismic loads and deformations throughout the structure.

The feet of a stepping structure are supported by pads which allow some rotation of the weight-supporting feet, while the overall structure rocks with uplift of other feet. Laminated-rubber or lead slabs have been used to allow this rotation. These feet pads also accommodate small irregularities and slope mismatches between the feet and the supporting foundations. The stepping feet move in vertical guides

which prevent 'walking', which would give horizontal or rotational displacements of the base of the structure.

Rocking with stepping is particularly effective in reducing the seismic loads and deformations of top-heavy slender structures such as tower-supported water tanks (where the tanks should be slender or contain baffles to prevent large long-period sloshing forces during major earthquakes). Another top-heavy structure is a bridge with tall slender piers. The piers may be permitted to rock in a direction transverse to the axis of the superstructure, providing the superstructure can accommodate the resulting deformations. The seismic responses of a slender rocking structure are related in some ways to the responses of a structure with an approximately rigid-plastic, horizontally deforming isolator, but there are also major differences.

For mode-1 seismic responses a rigid rocking structure may be assumed, with forces and displacements expressed as horizontal actions at the height of the centre of gravity. The cyclic force-displacement curve is then almost vertical for all forces below the uplift force (which corresponds to Q_y with bilinear hysteresis) and almost horizontal for all displacements during uplift. The force-displacement curve is essentially bilinear elastic. An effective period may be derived using the secant stiffness for maximum seismic displacement. The effective damping will arise from any energy losses during structural and foundation deformations together with the contribution of any added dampers. The effective period and damping may then be used to relate the maximum seismic displacement to the earthquake displacement spectra, as in the case of any other non-linear isolator.

Since stepping isolation is a very non-linear constraint, and since the equivalent first isolator period T_b is substantially less than the first period of the unisolated structure, the maximum seismic acceleration responses of the higher isolated modes are expected to be relatively large. With stepping, the higher-mode periods and shapes may be derived by assuming a zero base moment instead of the zero base shear force assumed when the isolator acts horizontally.

With rocking isolation there is always a substantial centring force, which is given by the uplift force. This centring force ensures that there is little drift displacement to add to the spectral displacement. The substantial centring force and the high first stiffness of the rocking isolator also ensure that there is very little residual displacement after an earthquake, even when substantial hysteretic dampers have been introduced.

An early application of rocking with uplift, to increase the seismic resistance of a tall slender structure, is contained in a design study by Savage (1939). The 105 m piers of the proposed Pit River road-rail bridge were designed with their bases free to rock with uplift under severe along-stream seismic loads. A New Zealand railway bridge at Mangaweka, over the Rangitikei River, with 69 m piers, was designed and built with the pier feet free to uplift during severe along-stream seismic loads (see Chapter 6). A tall rocking chimney structure, built at Christchurch, New Zealand, is described by Sharpe and Skinner (1983).

3.7.5 Further components for isolator flexibility

Tall columns and free piles

Horizontal flexibility can be provided by tall first-storey columns or by free-standing piles. Such flexible columns must have adequate length to avoid Euler instability under combined gravity earthquake loads, while providing adequate horizontal flexibility. With tall columns, the end moments may be severe despite relatively low horizontal shears.

With deep free-standing piles it is usually convenient to provide dampers and stops or buffers at the pile tops since it is usually practical to anchor them at this level. This approach has been used in Union House, Auckland, which uses steel cantilever dampers, and the Wellington Central Police Station, which uses lead-extrusion dampers (see Chapter 6). If tall columns are used to isolate a tower block it would be possible to anchor dampers to a surrounding high-stiffness, high-strength mezzanine structure.

In both the above cases where isolation was provided by tall free-standing piles, the tall piles were required to support the structure on a high-strength soil which underlay a low-strength soil layer. The tall piles were made free-standing by surrounding them with clearance tubes. Basement boxes, supported on shorter piles and embedded in the surface layer, were used to provide anchors for the hysteretic dampers and the buffers.

Hanging links and cables

It is possible to provide horizontal flexibility by supporting a structure with hanging hinged links or with hanging flexible cables (Newmark and Rosenblueth, 1971). Effective pendulum lengths of 1.0 and 2.25 m would give isolator periods of 2.0 and 3.0 s respectively. The necessary overlap of the supports and the structure can certainly be provided but in most cases this would be somewhat inconvenient and probably expensive, particularly for the longer links required for the longer isolator periods. When isolation is required for a relatively small item within a structure it would sometimes be appropriate to suspend it from anchors at a higher structural level.

Rollers, balls and rockers

An object can be supported on rollers or balls, between hardened steel surfaces, to provide a very low resistance to horizontal displacement. Again the object may be supported on rockers with rolling contact on plane or curved upper and lower surfaces, with the curvatures of the four contacting surfaces chosen to give a gravity centring action.

While simple in principle, the use of hard rolling surfaces to provide horizontally flexible isolator supports presents practical problems. These may include load sharing between the rolling components and the low load capacity of rolling units, particularly when only parts of the contacting surfaces are worked during the intervals

between substantial earthquakes. It is therefore likely that rolling supports will normally be restricted to the isolation of special components of low or moderate weight.

3.7.6 Buffers to reduce the maximum isolator displacement

Isolator maximum displacement

Isolators are normally designed to accommodate a travel greater than that which would occur during design earthquakes. However, during extreme low-probability earthquakes there is a possibility that the base of the structure will arrive at the end of the isolator design displacement when the structure still has considerable kinetic energy. If a stiff structure encounters a rigid base stop with considerable kinetic energy the ductility demand on the structure may be high, and may even substantially exceed the structure's design deformation capacity. The use of a resilient or energy-absorbing buffer can considerably increase the acceptable base impact velocity.

There are two components of shear strain when the base of a structure impacts a stiff buffer. One is a transient shear pulse which travels up the structure, with attenuation, and is reflected successively at the top and base. This transient shear pulse can be attenuated substantially by having a buffer stiffness which is substantially less than the inter-storey stiffness. The other component is an overall shear deformation, which can be substantially reduced by having a buffer stiffness lower than the overall structural stiffness. This is not practical in all cases.

During a low-probability extreme earthquake it is acceptable to permit much greater damage than is accepted for design-level earthquakes. The principal requirement is to prevent casualties and particularly to avoid the extreme hazard of structural collapse. Typically a seismic gap and buffer system should be designed to ensure that a structure does not collapse for a base displacement which would be from 50% to 100% greater (in the absence of a buffer) than that provided to accommodate design-level earthquakes.

Omnidirectional buffers using rubber in shear

Consider a structure mounted on laminated-rubber bearings which has a maximum horizontal rubber shear strain of 100% under design earthquakes. Under earthquakes of twice this severity the bearings would deform to a strain of approximately 200%, and store four times the elastic energy. Suppose that the earthquake energy is not reduced by the presence of buffers (in fact it is likely to be reduced by 20% or 30%). The energy to be stored or absorbed in the buffers is three times that stored in the bearings on buffer impact. If stiff rubber shear buffers are used they will be required to store almost three times the energy in the bearings. For a shear strain of 3 in the rubber buffers the energy density is nine times that of the bearings and hence the rubber volume required for the buffers is a third of that in the bearings. The stiffness of the buffers may be based on the maximum base shear acceptable for the structure under extreme earthquake conditions.

Omnidirectional buffers using tapered steel beams

Steel-beam buffers can be made omnidirectional in the same way as can rubber buffers. They may be designed to yield at a level which limits the base shear on the structure to an acceptable level. They may be of lower cost but more costly to install than equivalent-capacity rubber buffers. Operationally they are superior because of their yield-limited resistance force and because of the capacity to absorb most of the energy put into them.

Buffer anchors

For many structures it will be difficult to provide buffer anchors of the desired strength. If the buffer anchors deform in a controlled way with an appropriate level of resistance, they may themselves function as buffers and greatly reduce the demands on a buffer device or even remove the need for added buffers.

The basement box which provides stops for base displacement of the Wellington Central Police Station has a level of soil and pile resistance which allows it to provide considerable buffer action. Because the basement box is comparable in mass to a building storey, it is necessary to have a base-to-basement deformable interaction which has lower stiffness than the inter-storey members, to attenuate impact shear pulses. Such a deformable interaction is provided by lead collars around the columns near their tops, which may impact basement stops during extreme earthquakes.

3.7.7 Active and tuned-mass systems for vibration control

As mentioned in Chapter 1, this book deals primarily with passive systems of seismic isolation, active isolation being a fascinating emerging field which has potential on its own and in combination with passive systems. Like many of the passive systems, active systems are useful for both aseismic applications and for the reduction of wind-induced vibration in tall buildings.

Active control systems involve real-time sensing of the structural vibration, computers to calculate the optimum vibration-suppression force, and forces to counteract the resulting motion. The active-mass damper uses the inertial force of added masses as the reaction to the control force, while other systems utilise reaction forces of the structural body of the building itself.

Tuned-mass damper systems involve the matching of frequencies between the building and the tuned-mass damper so that out-of-phase vibration occurs.

There is a move to using hybrid active-passive systems for reducing the vibration induced by wind and earthquake excitation on large bridge towers and high-rise building structures.

A state-of-the-art review of active systems is given by Soong (1988) and other recent references are to be found in the Proceedings of the various conferences referred to in Chapter 1, such as the 9th and 10th World Conferences on Earthquake

Engineering (1988 and 1992 respectively) and the 4th US National Conference on Earthquake Engineering (1990).

A measure of the interest in 'active control and tuned dampers' for the reduction of vibration due to earthquakes and wind, is the fact that this topic was included in a recent conference (SMiRT-11, 1991). As a special scientific event of this conference an exhibition was organised, with presentations by 18 Japanese companies.

The material presented at this exhibition was presented as a special issue by the organisers of the conference. A list at the end of this publication details buildings using vibration-control devices in Japan. The first of these was completed in 1986 and comprises the 125-m tall Chiba Port Tower which uses a tuned-mass damper. In 1987 the Yokohama Marine Tower was completed; this 30-floor observatory uses tuned liquid dampers for vibration control. In 1988 the Sonic City office building was completed, with friction dampers controlling the level of vibration. This has 31 floors above ground and four basement floors and an area of 107 000 m². Sixteen buildings using such systems were complete in 1991, with eight based on tuned-mass dampers.

4 Structures with Seismic Isolation: Responses and Response Mechanisms

4.1 INTRODUCTION

Major aseismic performance features of well isolated structures were introduced and studied in Chapter 2. This chapter is a more systematic study of the seismic responses of isolated structures as the parameters of the structure and the isolation system are varied over wide ranges.

We begin by considering a uniform continuous linear vertical 'shear-beam' structure mounted on a linear isolator. In the case of a well isolated structure, we show that its earthquake response can be approximated by a fundamental-mode response in which the structure moves as a rigid body attached to the isolator, with the overall flexibility of the system very close to the flexibility of the isolator. Higher modes of the structure make only a minor contribution to the response, with the higher modes of the isolated system approximated very closely by the corresponding modes of the structure with free-free boundary conditions, as would be obtained with an isolator of zero stiffness and damping. The period of the fundamental mode is controlled by the ratio between the mass of the overall structure, plus the isolation system, and the stiffness of the isolator, with the participation factor close to unity throughout the structure. The higher-mode periods are close to those of the free-free structural modes, lying between the fixed-base period for the corresponding mode and the next lower mode. Modes higher than the first have near-zero participation factors.

Since the well isolated modal periods and shapes are approximated well by the corresponding free-free periods and shapes, isolated modal features may be expressed as simple perturbations of the features of free-free modes. Such expressions give a simple picture of the modal features with linear isolation, and assist in the initial design of the isolated structure.

Perturbation expressions are derived giving the correction to the free-free periods and participation factors resulting from a non-zero isolator stiffness. Exact expressions are also given for the isolated periods in terms of the structural free-free modal properties and the base stiffness, but these require the solution of transcendental equations. However, the calculation of the isolator stiffness required to obtain

a given isolated fundamental-mode period greater than the period of the fixed-base structure is explicit.

We next consider the introduction of viscous damping into the structure or isolator, which in general leads to non-classical isolated modes. Usually the damping in the unisolated structure is assumed to be classical, but when base damping is introduced, often at most only one mode remains classical, in the sense that the modal deformations are in phase throughout the structure, and the modes become non-orthogonal leading to coupled modal responses. Many practical isolation systems involve higher damping in the isolation system than that inherent in the structure. For linear isolation systems with flexible bases and moderately high viscous damping (i.e. around 15–20% of critical), the fundamental-mode damping is mainly governed by the base damping. The base damping is generally relatively less important for higher modes, and often the damping from the structure dominates beyond the second mode even when the isolator damping makes a large contribution to the first-mode damping. Damping in the isolator can considerably increase the participation factors of the higher modes, although their participation factors usually remain much less than for the first mode. Increasing isolator damping generally decreases the displacement response of the overall system, which is mainly governed by the first-mode response, but increases the importance of the higher-frequency acceleration components. The earthquake attack on contents of the structure may increase significantly with increasing isolator damping because of the enhanced high-frequency response, although remaining less than in an unisolated structure.

The general effects of isolation on structures which are non-uniform in elevation are similar to those on uniform structures. Some specific mass and stiffness distributions with smooth variations can be handled analytically for continuous models, (e.g. Su *et al.* 1989) but discrete mass and stiffness models are usually more convenient for treating non-uniform structures. As with the uniform continuous model, we develop expressions for the mode shapes and periods of isolated structures modelled as discrete masses and springs in terms of perturbations about free-free modes. Again, a technique is given for explicit calculation of the base damping and stiffness required to obtain a desired fundamental-mode frequency and damping.

Seismic isolation systems can greatly reduce the acceleration response of a building, but some systems are capable of giving even greater reductions in the forces which act on contents of the structure, and on secondary vibratory systems such as plant and equipment attached to it. The response of a linear structure well isolated on a linear isolation system is dominated by low-frequency motion at the isolated fundamental-mode frequency, with only minor high-frequency components. Equipment often has high natural frequencies, so its excitation is much reduced in a well isolated structure, while even for equipment tuned to the isolated structure's fundamental frequency, its excitation may remain modest compared with the earthquake ground motion. For subsystems with multiple attachment points, such as services in buildings or piping systems in industrial structures, the near rigid-

body response of the isolated supporting structure eliminates problems caused by differential movements of the support locations.

Perturbation techniques similar to those for the isolated structure are used in our analysis to determine the important dynamic properties of secondary structures in an isolated structure. Response spectrum techniques accounting for the interaction between the primary and secondary structure are used to estimate the earthquake response of the secondary structure.

Many practical isolation systems involve isolators with non-linear stress-strain characteristics. Non-linear isolators provide hysteretic energy dissipation, either through sliding friction systems or through the plastic deformation of metals such as steel or lead in mechanical energy dissipators. It is usually possible to achieve greater and more reliable energy dissipation with non-linear hysteretic isolators than with linear isolators and viscous damping. The non-linearity also allows the structure to be stiff in small-amplitude motions so that displacements under moderate winds and traffic vibrations and the like are minor, while in larger-amplitude motions, such as those resulting from strong earthquake ground motions, the isolator softens to give the large base flexibility required for effective isolation.

For non-linear isolation systems in which the elastic (i.e. low-amplitude) stiffness of the isolator is sufficiently less than that of the structure, the dynamic responses are similar in character to those of a well isolated structure with linear isolation. The energy dissipation is through hysteretic rather than viscous action, but the superstructure responds essentially as a rigid body mounted on the isolator with little high-frequency response from higher modes. As well as depending on the low- and high-amplitude stiffnesses of the isolation system, the response is governed by a parameter describing the yield level of the isolator. Usually there is an optimal value of the yield strength which will minimise the base shear or acceleration response for a given earthquake motion; this optimal strength increases with the severity of the earthquake motion. One-degree-of-freedom response-history analyses which treat the superstructure as a single lumped mass will be reliable if the dynamic characteristics of the system change little with the effective stiffness of the isolator at different amplitudes of motion, as will occur when the structure is moderately well isolated even with the isolator acting in its elastic range. Alternatively, equivalent linearisation techniques can be used to obtain reliable results with either single-mass or multi-mass models under the same conditions: that the effective mode shapes are similar in character for all isolator displacements.

Unfortunately, the analysis and response mechanisms for many practical and effective non-linear isolation systems are more complicated, in that the dynamic characteristics alter considerably as the displacement of the isolator increases. At small isolator displacements, the elastic isolator stiffness may be high, so that the system is not behaving like a structure with effective linear isolation. The displacements will vary significantly through the structure, with the superstructure no longer having rigid-body characteristics. The non-uniform displacements within the structure occur because of the non-rigid-body shape of the fundamental mode and because higher modes will also participate strongly. As the isolator softens, the

rigid-body fundamental-mode characteristics will appear. There will be little further excitation of higher-frequency response until the response reverses direction, but significant high-frequency motion excited in the initial high-stiffness phase of the isolator response may persist. On the reversal of motion, the effective stiffness of the isolator will again be high. Further high-frequency motion may be excited in this phase of the motion until the isolator softens in the reverse direction, both through direct excitation from the ground motion and from non-linear energy transfer mechanisms which occur on the reversal of motion when the effective mode shapes change. High-energy dissipation through hysteretic action, which limits the overall displacement response, requires a high degree of non-linearity (i.e. a large difference between the low-amplitude and high-amplitude stiffnesses of the isolator together with a significant displacement beyond yield). High non-linearity generally leads to strong excitation of high-frequency response, unless the high non-linearity can be obtained while retaining a reasonable degree of isolation in even the elastic response phase of the isolator. Hysteretic isolation systems may be able to achieve a moderate degree of isolation even in the elastic response stage if the superstructure has a short natural period compared with the elastic period of the structure and isolator, but sliding friction systems generally have poor isolation in their non-sliding phases, allowing both direct excitation of high-frequency motion by the ground accelerations and indirect excitation of high frequencies through non-linear transfer mechanisms.

Our analysis of such systems is based on response-history analysis. However, the results can be presented in terms of various important parameters, with the curves for various response parameters changing smoothly enough with the system parameters that the responses can be estimated for a much wider variety of combinations of system parameters than those we calculated explicitly. Also, to illustrate the underlying response mechanisms, we have developed a 'modal sweeping' (or 'modal filtering') technique, which presents the response histories of various systems with bilinear hysteretic isolation in terms of the modal responses of the elastic phase and post-yield phase. In particular, this presentation shows the effect of the non-linear energy transfer mechanisms which occur at yielding and at the reversal of response motion.

The analysis and prediction of the response of secondary systems in structures with non-linear isolation systems is more difficult than for systems with linear isolation, because of the various mechanisms by which the support point motions may obtain high-frequency components. The modal sweeping technique is used again to illustrate the response mechanisms. Generally the responses of secondary systems in structures with non-linear isolation will be less than in non-isolated structures, but some isolation systems relying on frictional dissipation can produce increased response. The secondary system responses may be less than in linearly isolated structures if the hysteretic energy dissipation is sufficient to counteract the high-frequency components induced by the non-linear action, but generally a high degree of linear isolation is more effective for reducing secondary system responses. As with the calculation of structural responses themselves, the response of secondary

systems in structures with non-linear isolation is calculated by detailed response-history analysis, but despite the complicated interacting response mechanisms at play, the results can be crystallised into a few simple graphs in terms of pertinent system parameters, again allowing generalisation to a much broader range of cases than studied explicitly.

It has long been known that seismic isolation can be very effective in the reduction of torsional response in torsionally unbalanced buildings. Many aspects of the torsional response mechanism are similar to those of secondary system response. Similar analytical techniques have been used to demonstrate the advantages of seismic isolation to overcome the problems of the earthquake response of highly torsional structures (see Section 4.5).

4.2 LINEAR STRUCTURES WITH LINEAR ISOLATION

4.2.1 Introduction

As the starting point of our detailed analysis of the earthquake response of seismically isolated structures, we begin by considering a structure modelled as a continuous uniform linear 'shear-beam', mounted at base level on a linear shear spring and viscous damper which represent the isolation system. We present the equations of motion for the earthquake response of this model, and then derive exact expressions for its mode shapes and modal periods. In general, with the presence of damping the isolated modes are non-classical, i.e. their phases depend on their position in the structure.

For a well isolated structure, i.e. one in which the isolated first-mode period is much more than the first-mode period of the unisolated structure, we present perturbation expressions for the modal properties of the isolated structure. Our results are for perturbations of the structure with free-free boundary conditions at the base and top, corresponding to an isolator spring of zero stiffness.

A similar approach is followed for the modal properties of a non-uniform structure represented in terms of mass, stiffness and damping matrices. Perturbation expressions are derived for a well isolated non-uniform structure in a manner analogous to that for the uniform continuous model, in terms of the free-free structure. For this discrete element representation, we also refer to perturbation results developed by others (Tsai and Kelly, 1989) in terms of the modal properties of the fixed-base structure. As the structural properties are often defined in terms of the fixed-base structure, this perturbation allows a direct comparison of the modal features of the isolated and unisolated structures.

As the damped isolated structures have non-classical modes, their earthquake response cannot be found by the simple modal decomposition technique available for classically damped systems. However, their earthquake responses can still be found in terms of decoupled modal responses by using Foss's method (Hurty and Rubinstein, 1964; Tsai and Kelly, 1988). We derive the expression for the displacement response of a non-classically damped mode in terms of a combination of the

displacement and velocity responses of a single-degree-of-freedom oscillator with the modal frequency and damping. The response expressions can be interpreted in terms of the displacement response of such an oscillator, multiplied by a complex participation factor. Isolator damping increases the modulus of the higher-mode participation factors, as well as introducing the phase shifts, throughout the natural modes, that make them non-classical.

Unlike the exact expressions for the mode shapes and complex modal frequencies which require solution of transcendental equations, it is possible, for both the continuous and discrete models, to develop direct expressions for the isolator spring stiffness and damping which are required in order to achieve a desired ratio between the isolated first-mode frequency and the fixed-base frequency (as well as a given first-mode damping). These direct expressions are of practical importance for design. For the continuous case, the isolator stiffness and damping are given by a pair of algebraic expressions, while in the discrete case they are given by entering the iterative Holzer method (Clough and Penzien, 1975) for determining mode shapes and periods with the desired (complex) frequency.

4.2.2 Modal properties of a uniform linear 'shear-beam' on a linear isolator

General modal features

Consider a structure modelled as a continuous uniform linear vertical 'shear-beam' mounted on a linear isolation system consisting of a mass M_b , a linear spring of stiffness K_b and a linear viscous damper of damping coefficient C_b , as shown in Figure 4.1. The shear-beam has a length L , uniform cross-sectional area A , uniform density ρ , constant shear modulus G , and damping coefficients c_m (proportional to the mass distribution from beam elements to the ground) and c_k (in parallel with the shear modulus, and proportional to the stiffness distribution). The equation of motion for the structure, when subjected to a ground acceleration \ddot{u}_g , is

$$\rho A \frac{\partial^2(u + u_g)}{\partial t^2} + c_m A \frac{\partial u}{\partial t} - \frac{\partial^2}{\partial t \partial z} \left(c_k A \frac{\partial u}{\partial z} \right) - \frac{\partial}{\partial z} \left(GA \frac{\partial u}{\partial z} \right) = 0 \quad 0 < z < L. \quad (4.1)$$

Here $u(z, t)$ is the displacement at position z in the structure in the horizontal x direction with respect to the ground at time t , and u_g is the ground displacement.

The equation of motion of the base mass is

$$M_b(\ddot{u}_b + \ddot{u}_g) + \int_0^L \rho A(\ddot{u} + \ddot{u}_g) dz + \int_0^L c_m A \frac{\partial u}{\partial t} dz + C_b \dot{u}_b + K_b u_b = 0 \quad (4.2)$$

where u_b is the base mass displacement with respect to the ground. The integral expression is the base shear of the superstructure. A variation on this representation of the coupling forces between the isolation system and the superstructure has been used by Su *et al.* (1989).

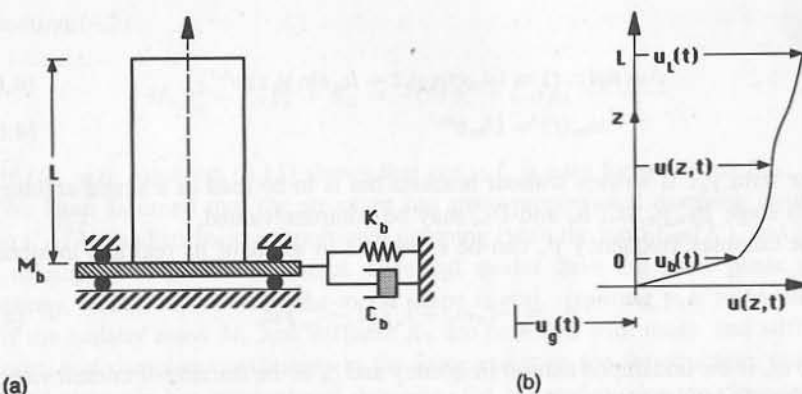


Figure 4.1 (a) Model of a continuous uniform vertical 'shear-beam' structure of height L , on a linear shear isolator whose mass, damping coefficient and stiffness are M_b , C_b and K_b respectively. (b) System coordinates: $u_g(t)$ is the ground displacement, and $u(z, t)$, $u_b(t)$ and $u_L(t)$ are the structural displacements, with respect to the ground, at level z , the base level and the top level respectively

The boundary conditions for the 'shear-beam' are that it has the same displacement as the base mass (the top of the isolator) at $z = 0$, and zero shear at the top ($z = L$):

$$u(0, t) = u_b(t) \quad \frac{\partial u(L, t)}{\partial z} = 0. \quad (4.3)$$

For the continuous uniform shear structure, expressions are simplified by giving its parameters as the overall values:

$$M = \rho AL, \quad C_M = c_m AL, \quad C_K = c_k A/L, \quad K = GA/L.$$

Consider the free vibration case where $\ddot{u}_g = 0$. There are then a pair of coupled differential equations:

$$M\ddot{u}(z, t) + C_M \dot{u}(z, t) - C_K L^2 \frac{\partial^2 \dot{u}(z, t)}{\partial z^2} - KL^2 \frac{\partial^2 u(z, t)}{\partial z^2} = 0 \quad (4.4)$$

and

$$M_b \ddot{u}_b(t) + C_b \dot{u}_b(t) + K_b u_b(t) = -\frac{M}{L} \int_0^L \ddot{u}(z, t) dz - \frac{C_M}{L} \int_0^L \dot{u}(z, t) dz. \quad (4.5)$$

The method of separation of variables produces free-vibration solutions of the

form

$$u_n(z, t) = (a_n \cos \gamma_n z + b_n \sin \gamma_n z) e^{p_n t} \quad (4.6a)$$

$$u_{bn}(t) = U_{bn} e^{p_n t} \quad (4.6b)$$

The term $\gamma_n z$ is written without brackets but is to be read as a single argument. At this stage p_n , γ_n , a_n , b_n and U_{bn} may be complex-valued.

The complex frequency p_n can be expressed in terms of its real and imaginary parts:

$$p_n = -\zeta_n \omega_n + i \sqrt{(1 - \zeta_n^2)} \omega_n \quad (4.7)$$

where ω_n is the undamped natural frequency and ζ_n is the fraction of critical viscous damping. Relationships between a_n , b_n and the wave number γ_n are found from considering the boundary conditions (4.3). From the no-shear condition at the top ($z = L$):

$$-a_n \gamma_n \sin \gamma_n L + b_n \gamma_n \cos \gamma_n L = 0. \quad (4.8a)$$

Again, the term $\gamma_n L$ is written without brackets but is to be read as a single argument. Letting $z = L$ in (4.6a)

$$a_n \cos \gamma_n L + b_n \sin \gamma_n L = U_{Ln} \quad (4.8b)$$

where U_{Ln} is defined by $u_n(L, t) = U_{Ln} e^{p_n t}$.

Provided γ_n is non-zero, that is, there is some structural deformation,

$$a_n = U_{Ln} \cos \gamma_n L, \quad b_n = U_{Ln} \sin \gamma_n L. \quad (4.9)$$

Hence

$$\begin{aligned} u_n(z, t) &= U_{Ln} (\cos \gamma_n L \cos \gamma_n z + \sin \gamma_n L \sin \gamma_n z) e^{p_n t} \\ &= U_{Ln} (\cos [\gamma_n L (1 - z/L)]) \exp(p_n t) \end{aligned} \quad (4.10)$$

Since $u_{bn}(t) = U_{bn} e^{p_n t}$, letting $z = 0$ in (4.10) and applying the boundary condition $u(0, t) = u_b(t)$ gives

$$U_{bn} = U_{Ln} \cos \gamma_n L. \quad (4.11)$$

When $\cos \gamma_n L = 0$, the base displacement is zero, and the structure is unisolated.

The relationship between the complex frequency p_n and the (sometimes complex) wave number γ_n is obtained by substituting (4.10) into (4.4); and requiring a non-zero top displacement U_{Ln} :

$$M p_n^2 + [C_M + C_K (\gamma_n L)^2] p_n + K (\gamma_n L)^2 = 0 \quad (4.12)$$

Provided $U_{bn} \neq 0$, a second relation between p_n and γ_n is obtained by substituting the mode-shape expressions (4.10) and (4.11) into the base mass equation

of motion (4.5)

$$M_b p_n^2 + C_b p_n + K_b = -(M p_n^2 + C_M p_n) \frac{\tan \gamma_n L}{\gamma_n L}. \quad (4.13)$$

If $U_{bn} = 0$, Equation (4.11) shows that $\cos \gamma_n L$ is zero for non-zero U_{Ln} .

We have assumed that the structure has mass-proportional damping (with the ratio C_M/M) and stiffness-proportional damping (with the ratio C_K/K), and hence the unisolated modes are classical. Classical modes have the same phase at all positions, which occurs when the mode shape is real, requiring $\gamma_n L$ to be real.

If the isolator mass M_b and stiffness K_b are provided with mass- and stiffness-proportional damping coefficients in the same ratios as for the structure, then the isolated structure has proportional damping, the isolated modes are classical and γ_n is again real. Hence isolated modes are classical if C_b has the value:

$$C_b = M_b \frac{C_M}{M} + K_b \frac{C_K}{K}. \quad (4.14a)$$

When (4.14a) is substituted in (4.12) and (4.13) it gives Equation (4.14b) below:

$$\tan \gamma_n L = \frac{K_b}{K} \frac{1}{\gamma_n L} - \frac{M_b}{M} \gamma_n L. \quad (4.14b)$$

This equation does not explicitly involve damping terms, gives real values for γ_n , and defines the wave number for classical mode shapes. The modes are also classical if the damping is zero: $C_b = C_M = C_K = 0$. This also satisfies (4.14a) and gives the same real values for $\gamma_n L$ as (4.14b).

When the damping coefficients do not satisfy the constraint given by Equation (4.14a), then $\gamma_n L$ is complex and the mode shapes are non-classical. In particular, it may be desirable to have a much larger C_b value than that which gives classical modes in order to obtain high first-mode damping of the isolated system, and hence reduced structural displacements. Also, an undamped structure supported on a damped isolator gives non-classical modes. Such non-classical mode shapes are generally less convenient to deal with analytically.

For mass-proportional damping (i.e., $C_K = 0$, $C_M \neq 0$), the fraction of critical damping in isolated mode n is given by

$$\zeta_n = 1/2 \frac{C_M}{M \omega_n} = \frac{\omega_{FB1}}{\omega_n} \zeta_{FB1}. \quad (4.15a)$$

This gives high damping in the first mode with respect to the first-mode unisolated (fixed-base) damping, ζ_{FB1} , with the damping decreasing in higher modes in inverse ratio to their isolated frequencies, ω_n . Dampings for the higher modes are greater than the damping for the fixed-base modes of corresponding number, but approach the unisolated values as the mode number increases.

For stiffness-proportional damping (i.e., $C_M = 0$, $C_K \neq 0$)

$$\zeta_n = 1/2 \left(\frac{C_K}{M} \right) \omega_n = \frac{\omega_n}{\omega_{FBn}} \zeta_{FBn}. \quad (4.15b)$$

For the first mode the damping is low with respect to the unisolated value, but it grows for higher modes to approach the damping value for the corresponding unisolated mode.

The actual damping mechanisms in structures are more complicated than the types of viscous damping assumed above. Hysteretic mechanisms are likely to be involved, either from friction between elements of a structure or because of the nature of the material stress-strain characteristics. However, viscous damping gives a mathematically convenient representation of the damping with acceptable accuracy for amplitudes up to the onset of significant yielding in the structure, which often corresponds approximately to the amplitudes at the onset of damaging motions. Usually the distribution of the viscous damping through the structure is assumed to be such that classical mode shapes are obtained, with no coupling between the modes. In addition, the damping is often assumed to be either of the Rayleigh type as assumed above (i.e., the damping distribution is proportional to a linear combination of the mass and stiffness distributions), or such that equal fractions of critical damping are obtained in all modes.

Classical normal modes or no damping

Without damping, $C_M = C_K = C_b = 0$, and also $\zeta_n = 0$. From (4.7), $p_n^2 = -\omega_n^2$. Equations (4.12) and (4.13) become

$$\omega_n = \sqrt{(K/M)} \gamma_n L, \quad (4.16)$$

$$\tan \gamma_n L = \frac{K_b}{K} \frac{1}{\gamma_n L} - \frac{M_b}{M} \gamma_n L. \quad (4.17)$$

This equation is the same as (4.14b) since it also applies with classical damping. The mode shape $u_n(z)$ and frequency ω_n for any degree of isolation, that is for any values of the ratios K_b/K and M_b/M , may be found by solving (4.17) for $\gamma_n L$ and substituting these $\gamma_n L$ values in (4.10) and (4.16).

Before investigating the roots of (4.17) it is worth considering two reference cases. The first is the fixed-base case, in the absence of the isolator. For a fixed-base, $u_n(0, t) = 0$ and (4.11) gives for non-zero U_{Ln}

$$\cos \gamma_n L = 0 \quad (4.18a)$$

i.e.

$$(\gamma_n L)_{FF} = (2n - 1) \frac{\pi}{2} \quad (4.18b)$$

and

$$\begin{aligned} u_{FBn}(z, t) &= U_{Ln} \sin \gamma_n L \sin(\gamma_n z) e^{p_n t} \\ &= (-1)^{n-1} U_{Ln} \sin(\gamma_n z) e^{p_n t}. \end{aligned} \quad (4.19)$$

For the undamped case, (4.16) gives

$$\omega_{FBn} = \sqrt{\frac{K}{M}} (2n - 1) \frac{\pi}{2} \quad (4.20a)$$

$$= (2n - 1) \omega_{FB1}. \quad (4.20b)$$

The second reference case is the free-free case (i.e. $K_b = C_b = M_b = 0$), which corresponds to perfect isolation. The boundary condition at the base of the structure ($z = 0$) corresponds to no shear force, requiring

$$\frac{du_{FFn}(0)}{dz} = 0. \quad (4.21)$$

This leads to the free-free mode shape

$$\begin{aligned} u_{FFn}(z, t) &= U_{Ln} \cos \gamma_n L (\cos \gamma_n z) e^{p_n t} \\ &= (-1)^{n-1} U_{Ln} (\cos \gamma_n z) e^{p_n t} \end{aligned} \quad (4.22)$$

with

$$\sin \gamma_n L = 0 \quad (4.23a)$$

i.e.

$$(\gamma_n L)_{FF} = (n - 1)\pi = (2n - 2) \frac{\pi}{2}. \quad (4.23b)$$

For the undamped case, (4.16) gives

$$\omega_{FFn} = \sqrt{\frac{K}{M}} (n - 1)\pi \quad (4.24a)$$

$$= (2n - 2) \omega_{FB1}. \quad (4.24b)$$

Note that the fixed-base and free-free frequencies interleave. It is also convenient to introduce the frequency

$$\omega_b \equiv \sqrt{(K_b/M)} \quad (4.25)$$

corresponding to a rigid structure of mass M on an isolator of stiffness K_b , and the associated natural period $T_b = 2\pi/\omega_b$. Many of the modal expressions for the isolated system are a function of the isolation ratio

$$I \equiv \omega_{FB1}/\omega_b = T_b/T_{FB1}. \quad (4.26)$$

In places the notation $\omega_1(U)$ and $T_1(U)$ is used for the undamped first-mode frequency and period of the unisolated structure rather than ω_{FB1} and T_{FB1} , where

the subscript 'FB1' denotes 'fixed-base first-mode'. The isolation ratio I varies from 0 for an unisolated system (i.e., a rigid isolator with $T_b = 0$), to infinity for a free-free system where K_b and ω_b are zero. The unisolated first-mode undamped frequency and period are

$$\omega_1(U) = \omega_{FB1} = \sqrt{\frac{K}{M}} \frac{\pi}{2} \tag{4.27a}$$

$$T_1(U) = T_{FB1} = 4\sqrt{\frac{M}{K}} \tag{4.27b}$$

In terms of the parameter I ,

$$\frac{K_b}{K} = \frac{K_b/M}{K/M} = \frac{\pi^2 \omega_b^2}{4 \omega_{FB1}^2} = \frac{\pi^2}{4I^2} \tag{4.28}$$

Here it is seen that ' I ' is a measure of the ratio of isolator flexibility to structural flexibility. ' I ' and ω_b are common parameters in isolated modal features, when expressed as perturbations of free-free modal features.

Return now to a consideration of the roots of Equation (4.17) for the isolated case with no damping, or with classical damping. It is informative to plot the two sides of this equation as functions of $\gamma_n L$ (Figure 4.2). For the case of $M_b = 0$ (the dashed curve), the higher roots $\gamma_n L$ approach but lie above $(n - 1)\pi$, which are the roots for the free-free case. The first root lies in the range $0 < \gamma_1 L < \pi/2$, that is, between the free-free and fixed-base roots.

For a small value of K_b/K , the first root $\gamma_1 L$ will lie near zero. For this case

$$\tan \gamma_1 L \approx \gamma_1 L \tag{4.29a}$$

so from Equation (4.17)

$$\gamma_1 L \approx \sqrt{\frac{K_b}{K}} \tag{4.29b}$$

The natural frequency is given by

$$\omega_1 = \sqrt{\frac{K}{M}} \gamma_1 L \approx \sqrt{\frac{K_b}{M}} \tag{4.30}$$

Higher-order approximations are given by

$$\gamma_1 L \approx \sqrt{\frac{K_b}{K}} \left(1 - \frac{1}{6} \frac{K_b}{K} \right) \tag{4.31a}$$

$$= \frac{\pi}{2I} \left(1 - \frac{\pi^2}{24I^2} \right) \tag{4.31b}$$

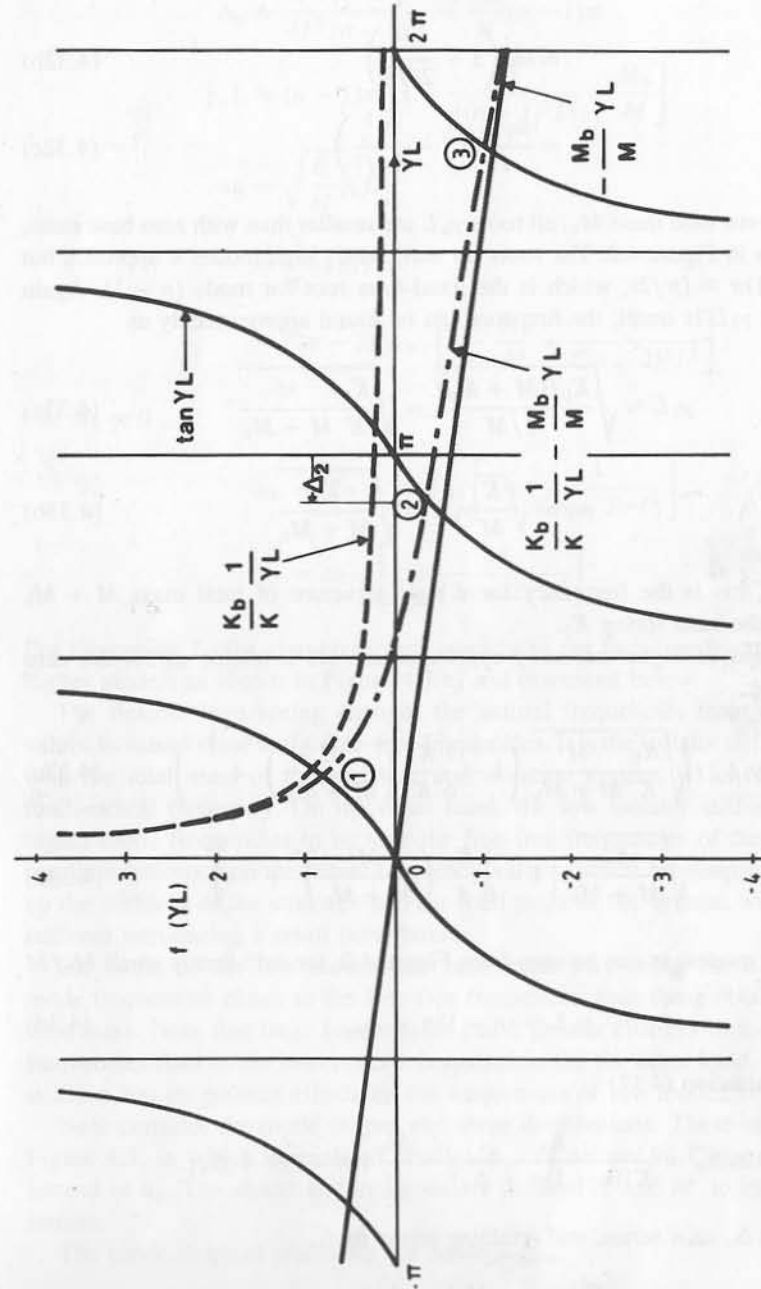


Figure 4.2 Graphical solution of equation (4.17), giving the base-phase parameter $\gamma_n L$ for the first three modes. The solutions are indicated by the circled points 1, 2 and 3 respectively, and are the points of intersection of $\tan(\gamma_n L)$ with the curve for the general case $K_b/K \gamma_n L - M_b \gamma_n L/M$ (shown dash-dotted on the figure); the two components of the general curve are shown as the dashed and solid straight lines respectively. Δ_n is the departure of the base-level phase of mode n from the free-free value $(2n - 2)\pi/2$

$$\omega_1 \approx \sqrt{\frac{K_b}{M}} \left(1 - \frac{1}{6} \frac{K_b}{K}\right) \quad (4.32a)$$

$$= \omega_b \left(1 - \frac{\pi^2}{24I^2}\right) \quad (4.32b)$$

$$= \frac{\omega_{FB1}}{I} \left(1 - \frac{\pi^2}{24I^2}\right). \quad (4.32c)$$

For a non-zero base mass M_b , all roots $\gamma_n L$ are smaller than with zero base mass, as can be seen in Figure 4.2. The roots for sufficiently high modes n approach but exceed $(n-1)\pi - (\pi/2)$, which is the fixed-base root for mode $(n-1)$. Again assuming that $\gamma_1 L$ is small, the first root can be found approximately as

$$\gamma_1 L \approx \sqrt{\frac{K_b/(M+M_b)}{K/M}} = \sqrt{\frac{K_b}{K} \frac{M}{M+M_b}} \quad (4.33a)$$

$$\omega_1 = \sqrt{\frac{K}{M}} \gamma_1 L \approx \sqrt{\frac{K_b}{M+M_b}}. \quad (4.33b)$$

As before, this is the frequency for a rigid structure of total mass $M+M_b$ supported on the base spring K_b .

Similar forms of higher-accuracy approximation are available as for the zero base mass case:

$$\gamma_1 L \approx \sqrt{\frac{K_b}{K} \frac{M}{M+M_b}} \left(1 - \frac{1}{6} \frac{K_b}{K} \left(\frac{M}{M+M_b}\right)^2 + \dots\right) \quad (4.33c)$$

$$\omega_1 \approx \sqrt{\frac{K_b}{M+M_b}} \left(1 - \frac{1}{6} \frac{K_b}{K} \left(\frac{M}{M+M_b}\right)^2 + \dots\right). \quad (4.33d)$$

For the higher modes, as can be seen from Figure 4.2, for sufficiently small M_b/M

$$\gamma_n L \approx (n-1)\pi + \Delta_n. \quad (4.34)$$

Hence from Equation (4.17)

$$\tan \Delta_n = \frac{K_b}{K[(n-1)\pi + \Delta_n]} - \frac{M_b}{M} [(n-1)\pi + \Delta_n].$$

Expanding $\tan \Delta_n$ as a series, and retaining terms to Δ_n

$$\Delta_n \approx \frac{K_b}{K(n-1)\pi} - \frac{M_b(n-1)\pi}{M} \quad (4.35a)$$

i.e.

$$\Delta_n = \frac{\pi^2}{4I^2} \frac{1}{(n-1)\pi} - \frac{M_b}{M} (n-1)\pi \quad (4.35b)$$

$$\gamma_n L \approx (n-1)\pi \left[1 + \frac{1}{4(n-1)^2 I^2} - \frac{M_b}{M}\right] \quad (4.36)$$

$$\omega_n = \sqrt{\frac{K}{M}} \gamma_n L \quad (4.37a)$$

$$= \frac{2}{\pi} \omega_{FB1} \gamma_n L \quad (4.37b)$$

$$\approx (2n-2) \omega_{FB1} \left[1 - \frac{M_b}{M} + \frac{1}{(2n-2)^2 I^2}\right]. \quad (4.37c)$$

For $M_b = 0$

$$\omega_n = (2n-2) \omega_{FB1} \left[1 + \frac{1}{(2n-2)^2 I^2}\right] \quad (4.38a)$$

$$= \omega_{FFn} \left[1 + \frac{1}{(2n-2)^2 I^2}\right]. \quad (4.38b)$$

For increasing I , this converges very quickly to the free-free frequency ω_{FFn} for higher modes, as shown in Figure 4.3(e) and discussed below.

The flexible base spring changes the natural frequencies from the fixed-base values to values close to the free-free frequencies. It is the isolator stiffness, together with the total mass of the structure and isolation system, which determines the fundamental frequency. On the other hand, the low isolator stiffness causes the higher-mode frequencies to be near the free-free frequencies of the structure, but has little influence on the actual frequency values, which are determined primarily by the stiffness of the structure and the total mass of the system, with the isolator stiffness introducing a small perturbation.

For some of the low modes, the base mass may bring the isolated higher-mode frequencies closer to the free-free frequencies than those obtained with zero base mass. Note that large base masses cause greater changes in the higher-mode frequencies than in the lower-mode frequencies. On the other hand, non-zero base stiffness has its greatest effects on the frequencies of low modes.

Next consider the mode shapes and shear distributions. These are presented in Figure 4.3, in which normalised profiles ϕ_n , as defined in Chapter 2, are given instead of u_n . The shears and moments are denoted S' and M' to indicate normalisation.

The mode shape at position z for mode n is

$$u_n(z) = U_{Nn} \cos \gamma_n L \left(1 - \frac{z}{L}\right). \quad (4.39)$$

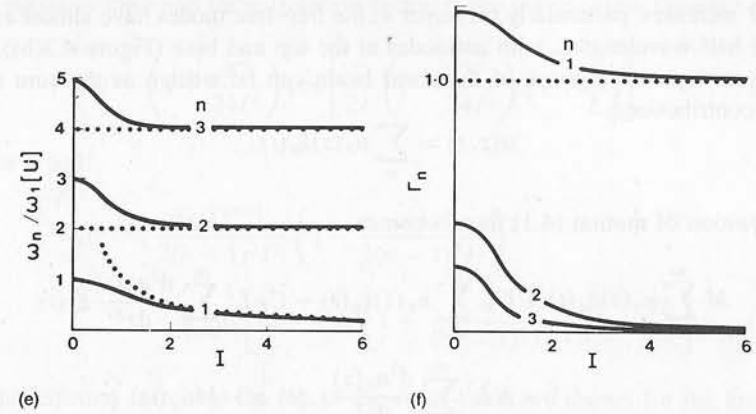
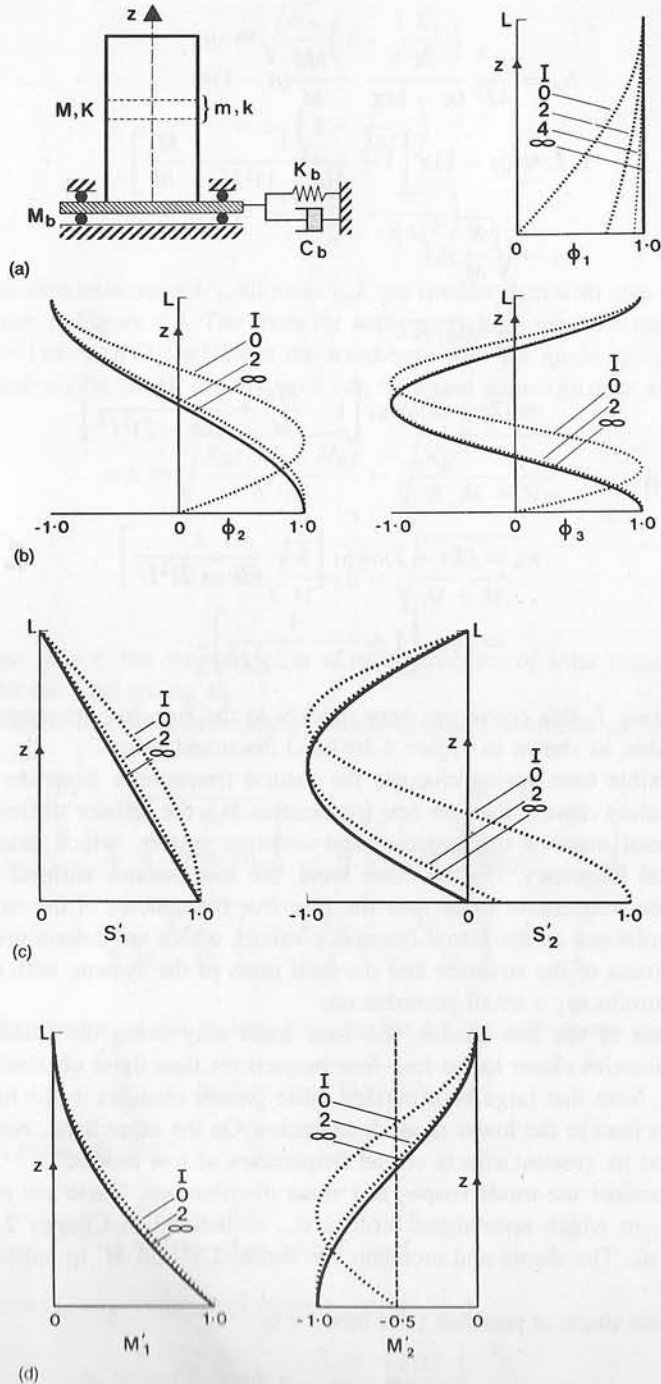


Figure 4.3 (continued)

Here U_{Ln} denotes the n th-mode displacement at the top of the structure. This notation is anticipating the later treatment of discrete systems, where mass N is the top mass of the structure. For the massless base case and small ω_n/ω_{FB1} , i.e. large I :

$$u_1(z) \approx U_{N1} \cos \left[\frac{\pi}{2I} \left(1 - \frac{\pi^2}{24I^2} \right) \left(1 - \frac{z}{L} \right) \right]. \quad (4.40)$$

Also, for higher modes $n > 1$:

$$u_n(z) \approx U_{Nn} \cos \left[(2n - 2) \frac{\pi}{2} \left(1 + \frac{1}{4(n - 1)^2 I^2} \right) \left(1 - \frac{z}{L} \right) \right]. \quad (4.41)$$

The well isolated higher modes have just over $n - 1$ half-wavelengths between $z = 0$ and $z = L$, with antinodes at the top and just above the base, and as I and n increase, quickly converge to the free-free mode shapes

$$u_{FFn}(z) = U_{Nn} \cos \left[(2n - 2) \frac{\pi}{2} \left(1 - \frac{z}{L} \right) \right]. \quad (4.42)$$

Figure 4.3 Modal features of a continuous uniform 'shear-beam' structure with various degrees of linear isolation, given by $I = T_b/T_1(U)$, so that $I = 0$ gives a fixed base (unisolated system) and $I = \infty$ gives a shear-free base (well isolated system). It is seen that, for any degree of isolation greater than 2, the modes have high-isolation modal features. (a) Model defining the parameters of the isolated structure, of height L , and mass m and stiffness k per unit height. (b) Variation with height z of the normalised first, second and third mode shapes ϕ_1 , ϕ_2 and ϕ_3 respectively, for various values of I . (c) Variation with height z of normalised modal shear forces S'_1 and S'_2 , for various values of I . (d) Variation with height z of normalised modal overturning moments M'_1 and M'_2 , for various values of I . (e) Variation of modal frequencies ω_n with degree of isolation I . (f) Variation of top participation factor with I .

As I increases, particularly for larger n , the free-free modes have almost exactly $(n - 1)$ half-wavelengths, with antinodes at the top and base (Figure 4.3(b)).

The earthquake response of the shear beam can be written as the sum of the modal contributions:

$$u(z, t) = \sum_n u_n(z) \xi_n(t).$$

The equation of motion (4.1) then becomes

$$\begin{aligned} M \sum_{n=1}^{\infty} u_n(z) \ddot{\xi}_n(t) + C_M \sum_{n=1}^{\infty} u_n(z) \dot{\xi}_n(t) - C_K L^2 \sum_{n=1}^{\infty} \frac{d^2 u_n(z)}{dz^2} \dot{\xi}_n(t) \\ - K L^2 \sum_{n=1}^{\infty} \frac{d^2 u_n(z)}{dz^2} \xi_n(t) = -M \ddot{u}_g(t). \end{aligned} \quad (4.43)$$

At this stage, we are considering classically damped modes, so using the standard modal decomposition approach (e.g. Clough and Penzien, 1975) and making use of the orthogonality of the normal modes, the equation of motion for the n th mode becomes

$$u_n(z) \ddot{\xi}_n(t) + 2\zeta_n \omega_n u_n(z) \dot{\xi}_n(t) + \omega_n^2 u_n(z) \xi_n(t) = -\Gamma_n(z) \ddot{u}_g(t). \quad (4.44)$$

For an earthquake excitation with a relative displacement response spectrum $S_D(\omega, \zeta)$, the maximum displacement of mode n at position z is given by

$$X_n(z) = \Gamma_n(z) S_D(\omega_n, \zeta_n). \quad (4.45)$$

The frequencies ω_n have been derived earlier. The damping ζ_n is given by

$$2\zeta_n \omega_n = \frac{\int_0^L [C_M + C_K(\gamma_n L)^2] u_n^2(z) dz}{\int_0^L M u_n^2(z) dz} \quad (4.46a)$$

$$\zeta_n = \frac{C_M + C_K(\gamma_n L)^2}{2\omega_n}. \quad (4.46b)$$

The participation factor $\Gamma_n(z)$ is given by

$$\Gamma_n(z) = \frac{\int_0^L M u_n(z) dz}{\int_0^L M u_n^2(z) dz} u_n(z). \quad (4.47)$$

Evaluation of the integrals produces

$$\Gamma_n(z) = \frac{2 \sin \gamma_n L}{\gamma_n L + \sin \gamma_n L \cos \gamma_n L} \cos [\gamma_n L(1 - z/L)] \quad (4.48a)$$

$$= \Gamma_{Nn} \cos [\gamma_n L(1 - z/L)]. \quad (4.48b)$$

For a massless base and large isolation factor I , the participation factors become

$$\Gamma_1(z) \approx \left(1 + \frac{\pi^2}{24I^2}\right) \cos \left[\frac{\pi}{2I} \left(1 - \frac{\pi^2}{24I^2}\right) \left(1 - \frac{z}{L}\right)\right] \quad (4.49a)$$

and for $n > 1$

$$\begin{aligned} \Gamma_n(z) \approx \frac{(-1)^{n-1}}{2(n-1)^2 I^2} \left(1 - \frac{1}{2(n-1)^2 I^2}\right) \\ \times \cos \left[(n-1)\pi \left(1 + \frac{1}{4(n-1)^2 I^2}\right) \left(1 - \frac{z}{L}\right)\right]. \end{aligned} \quad (4.49b)$$

The participation factors at the top of the shear-beam are shown for the first three modes in Figure 4.3(f).

The maximum modal displacements at the top of the shear-beam are given by

$$X_{N1} \approx \left(1 + \frac{\pi^2}{24I^2}\right) S_D(\omega_1, \zeta_1) \quad (4.50a)$$

$$X_{Nn} \approx \frac{1}{2(n-1)^2 I^2} \left(1 - \frac{1}{2(n-1)^2 I^2}\right) S_D(\omega_n, \zeta_n) \quad n > 1. \quad (4.50b)$$

The fundamental mode dominates the displacement response because the first-mode spectral displacement $S_D(\omega_1, \zeta_1)$ is usually much larger than the higher-mode spectral displacements $S_D(\omega_n, \zeta_n)$, and the first-mode participation factor is slightly greater than unity, while the higher-mode participation factors are small.

For an earthquake acceleration response spectrum $S_A(\omega_n, \zeta_n)$, the maximum seismic acceleration at position z in mode n is given by

$$\begin{aligned} \ddot{X}_n(z) &= \Gamma_n(z) S_A(\omega_n, \zeta_n) \\ &= \Gamma_{Nn} \cos [\gamma_n L(1 - z/L)] S_A(\omega_n, \zeta_n). \end{aligned} \quad (4.51)$$

Note that \ddot{X}_n denotes the maximum absolute acceleration, while X_n and \dot{X}_n refer to displacements and velocities relative to the ground. Γ_{Nn} denotes the n th-mode participation factor at the top of the structure, using a similar notation as introduced earlier with U_{Nn} .

The maximum seismic force per unit height, at level z of mode n , is obtained by multiplying the corresponding acceleration by the mass per unit height M/L , to give

$$F_n(z) = -(M/L) \Gamma_{Nn} \cos [\gamma_n L(1 - z/L)] S_A(\omega_n, \zeta_n). \quad (4.52)$$

The corresponding maximum seismic shears and overturning moments at level z of mode n are obtained by successive integration of the maximum seismic forces. This may be done since the modes are classical and therefore all the forces throughout

a given mode are in phase. The integrations give

$$S_n(z) = \int_z^L F_n(z') dz' \\ = [(M/\gamma_n L)] \Gamma_{Nn} \sin[\gamma_n L(1 - z/L)] S_A(\omega_n, \zeta_n) \quad (4.53)$$

$$\underline{OM}_n(z) = \int_z^L S_n(z') dz' \\ = [ML/(\gamma_n L)^2] \Gamma_{Nn} (1 - \cos[\gamma_n L(1 - z/L)]) S_A(\omega_n, \zeta_n). \quad (4.54)$$

For a large isolation factor I , that is for small K_b/K , peak seismic accelerations, forces, shears and overturning moments may be obtained by substituting Γ_{Nn} and $\gamma_n L$ values (from (4.49), (4.33) and (4.36)) into (4.51) to (4.54).

Seismic shears are of particular interest because they are usually a good measure of the seismic loads on a structure. For a massless base and large isolation factor I

$$S_1(z) \approx M \frac{2I}{\pi} \left(1 + \frac{\pi^2}{12I^2}\right) \sin\left[\frac{\pi}{2I} \left(1 - \frac{\pi^2}{24I^2}\right) \left(1 - \frac{z}{L}\right)\right] S_A(\omega_1, \zeta_1) \\ \approx M \left[\left(1 + \frac{\pi^2}{24I^2}\right) \left(1 - \frac{z}{L}\right) - \frac{\pi^2}{24I^2} \left(1 - \frac{z}{L}\right)^3\right] S_A(\omega_1, \zeta_1). \quad (4.55)$$

Thus the first-mode shear distribution is approximately triangular, from zero at the top to the maximum value S_{b1} at the base, as shown in Figure 4.3(c). The first-mode base shear is given by:

$$S_{b1} = S_1(z=0) \approx M \left(1 + O\left(\frac{\pi^4}{I^4}\right)\right) S_A(\omega_1, \zeta_1). \quad (4.56)$$

The higher-mode shears are given by

$$S_n(z) \approx \frac{(-1)^{n-1} M}{2\pi(n-1)^3 I^2} S_A(\omega_n, \zeta_n) \sin\left[(n-1)\pi \left(1 + \frac{1}{4(n-1)^2 I^2}\right) \left(1 - \frac{z}{L}\right)\right] \quad (4.57)$$

This shear distribution has n zeroes, at the top and at spacings of approximately $L/(n-1)$ down the structure. There is a zero just above the base (Figure 4.3(c)). The base shear is

$$S_{bn} \approx \frac{M}{8(n-1)^4 I^4} S_A(\omega_n, \zeta_n). \quad (4.58)$$

The higher-mode base shears are generally much smaller than the first-mode base shear, with their ratios given approximately by

$$S_{bn}/S_{b1} \approx \frac{1}{8(n-1)^4 I^4} \frac{S_A(\omega_n, \zeta_n)}{S_A(\omega_1, \zeta_1)}. \quad (4.59)$$

For the first mode, the base shear is the maximum shear. However, for the higher modes the maximum shear is much larger than the base shear

$$S_{n,\max} \approx \frac{M}{2\pi(n-1)^3 I^2} S_A(\omega_n, \zeta_n) \\ \approx \frac{4}{\pi} (n-1) I^2 S_{bn}. \quad (4.60)$$

The ratio of $S_{n,\max}$ to the first-mode base shear is an important parameter for determining the overall shear distribution in the structure. As shown above, for a well isolated uniform shear-beam structure the first-mode shear distribution is approximately triangular:

$$S_1(z) \approx S_{b1} \left(1 - \frac{z}{L}\right). \quad (4.61)$$

For the other modes, the distribution is approximately an integral number of half-cycle sine waves, with a zero value near the base, with the maxima at various positions up the structure. Obviously, if $S_{n,\max}/S_{b1}$ is not small, the sinusoidal higher-mode shear distributions will modify the overall distribution considerably from the triangular first-mode distribution. The ratio is

$$S_{n,\max}/S_{b1} \approx \frac{1}{2\pi(n-1)^3 I^2} \frac{S_A(\omega_n, \zeta_n)}{S_A(\omega_1, \zeta_1)}. \quad (4.62)$$

This ratio is generally small. Since $S_A(\omega_n, \zeta_n)$ is usually not greater than $I S_A(\omega_1, \zeta_1)$, for $\zeta_1 \approx \zeta_n$, and also since $S_A(\omega_n, \zeta_n)$ is usually not greater than $I^2 S_A(\omega_1, \zeta_1)$, for $\zeta_1 \gg \zeta_n$, therefore,

$$S_{n,\max}/S_{b1} \neq 1/[2\pi(n-1)^3 I], \quad \text{for } \zeta_1 \approx \zeta_n \\ S_{n,\max}/S_{b1} \neq 1/[2\pi(n-1)^3], \quad \text{for } \zeta_1 \gg \zeta_n. \quad (4.63)$$

Hence it is evident that, at most, only mode 2 can significantly increase the seismic shears given by mode 1.

An overall picture given by Figure 4.3 is the extent to which the isolation factor I must be increased in order that the modal features approach their high-isolation values. In Figures 4.3(e) and (f), which show the frequency ratios and top-level participation factors, the high-isolation asymptotes are shown dotted. All the modal features shown approach close to their high-isolation values, or expressions, by the time the isolation factor is increased to 2.0. The greatest, but still moderate, departure is for the mode-1 shape with corresponding departures for mode-1 accelerations and forces. It is shown later that such trends also apply to a wide range of reasonably regular structures.

Base damping C_b , but zero damping in the structure

We now consider the case where there is isolator damping, but no damping in the superstructure i.e. $C_M = C_K = 0$, $C_b \neq 0$. From Equation (4.7), the frequency p_n is defined by

$$p_n = -\zeta_n \omega_n + i\sqrt{1 - \zeta_n^2} \omega_n. \quad (4.64)$$

For C_M and $C_K = 0$, the frequency equation (4.12) gives

$$\frac{K}{M} \gamma_n^2 L^2 = -p_n^2 \quad (4.65a)$$

$$\gamma_n L = \sqrt{\frac{M}{K}} \left(\sqrt{1 - \zeta_n^2} + i\zeta_n \right) \omega_n. \quad (4.65b)$$

Substituting in the frequency equation (4.13) and equating real and imaginary parts leads, after some manipulation, to

$$K_b = M_b \omega_n^2 + \frac{2M}{\pi} \frac{\omega_{FB1} \omega_n}{\sqrt{1 - \zeta_n^2}} \left[\frac{\sin \frac{\sqrt{1 - \zeta_n^2} \omega_n \pi}{\omega_{FB1}}}{\cos \frac{\sqrt{1 - \zeta_n^2} \omega_n \pi}{\omega_{FB1}} + \cosh \frac{\zeta_n \omega_n \pi}{\omega_{FB1}}} \right] \quad (4.66a)$$

$$C_b = 2\zeta_n \omega_n M_b + \frac{2M}{\pi} \omega_{FB1} \left[\frac{\frac{\zeta_n}{\sqrt{1 - \zeta_n^2}} \sin \frac{\sqrt{1 - \zeta_n^2} \omega_n \pi}{\omega_{FB1}} \pi + \sin \frac{\zeta_n \omega_n \pi}{\omega_{FB1}} \pi}{\cos \frac{\sqrt{1 - \zeta_n^2} \omega_n \pi}{\omega_{FB1}} + \cosh \frac{\zeta_n \omega_n \pi}{\omega_{FB1}}} \right] \quad (4.66b)$$

where, as given previously in Equation (4.27a)

$$\omega_{FB1} = \frac{\pi}{2} \sqrt{\frac{K}{M}}.$$

Given a required damping ζ_1 and frequency ω_1 and known unisolated first-mode frequency ω_{FB1} , these lead to explicit expressions for the required base stiffness and base damping for a given base mass. Assuming ω_1/ω_{FB1} is small, and expanding to order $(\omega_1/\omega_{FB1})^2$:

$$K_b = (M + M_b) \omega_1^2 \left[1 + \frac{M}{M + M_b} \frac{\pi^2}{12} \frac{\omega_1^2}{\omega_{FB1}^2} + \dots \right] + O((\omega_1/\omega_{FB1})^3) \quad (4.67a)$$

$$C_b = (M + M_b) 2\zeta_1 \omega_1 \left[1 + \frac{M}{M + M_b} \frac{\pi^2}{6} \frac{\omega_1^2}{\omega_{FB1}^2} + \dots \right] + O((\omega_1/\omega_{FB1})^3). \quad (4.67b)$$

These expressions can be inverted to find ω_1 and ζ_1 in terms of K_b and C_b :

$$\omega_1^2 \approx \frac{K_b}{M + M_b} \left[1 - \frac{M}{M + M_b} \frac{\pi^2}{12} \frac{K_b}{(M + M_b) \omega_{FB1}^2} \right] \quad (4.68a)$$

$$2\zeta_1 \omega_1 \approx \frac{C_b}{M + M_b} \left[1 - \frac{M}{M + M_b} \frac{\pi^2}{6} \frac{K_b}{(M + M_b) \omega_{FB1}^2} \right]. \quad (4.68b)$$

To first order,

$$\omega_1^2 = \frac{K_b}{M + M_b} \equiv \omega_b^2 \quad (4.69a)$$

$$2\zeta_1 \omega_1 = \frac{C_b}{M + M_b} \equiv 2\zeta_b \omega_b. \quad (4.69b)$$

This corresponds to a rigid structure on the base spring and damper. If $M_b = 0$, higher-mode frequencies can be found by substituting:

$$\frac{\sqrt{1 - \zeta_n^2} \omega_n}{\sqrt{K/M}} = (n - 1)\pi + \Delta_n. \quad (4.70)$$

This leads to

$$\Delta_n \approx \frac{K_b}{K} \frac{1 - \zeta_n^2}{2(n - 1)\pi} \left[1 + \cosh \frac{2\zeta_n(n - 1)\pi}{\sqrt{1 - \zeta_n^2}} \right] \quad (4.71a)$$

$$\Delta \omega_n = \frac{\sqrt{K/M}}{\sqrt{1 - \zeta_n^2}} \Delta_n \approx \frac{\sqrt{1 - \zeta_n^2}}{4(n - 1)} \left[1 + \cosh \frac{2\zeta_n(n - 1)\pi}{\sqrt{1 - \zeta_n^2}} \right] \left(\frac{\omega_b}{\omega_{FB1}} \right) \omega_b. \quad (4.71b)$$

Also

$$C_b \approx \frac{2}{\pi} M \omega_{FB1} \tanh \frac{\zeta_n(n - 1)\pi}{\sqrt{1 - \zeta_n^2}}. \quad (4.72)$$

To compare damping in various modes, recall $C_b \approx 2\zeta_1 \omega_1 M$ when $M_b = 0$.

Thus

$$2\zeta_1 \omega_1 M \approx \frac{2}{\pi} M \omega_{FB1} \tanh \frac{\zeta_n(n - 1)\pi}{\sqrt{1 - \zeta_n^2}} \quad (4.73)$$

$$\tanh \frac{\zeta_n(n - 1)\pi}{\sqrt{1 - \zeta_n^2}} \approx \zeta_1 \pi \frac{\omega_1}{\omega_{FB1}}. \quad (4.74)$$

The right-hand side is small, so the leading term of the Taylor series can be used

to expand the left-hand side which must also be small:

$$\zeta_n \approx \zeta_1 \frac{\omega_1}{(n-1)\omega_{FB1}} \approx 2\zeta_1 \frac{\omega_b}{\omega_n} \approx \frac{2\zeta_b \omega_b}{\omega_n}. \quad (4.75)$$

Thus the effectiveness of the base damping in introducing damping to the higher modes is inversely proportional to the frequency of the higher mode. However, if C_b introduces high first-mode damping (e.g. $\sim 20\%$), the second- and third-mode damping from the base damper may still be as high as the internal damping from the structure for those modes. Moreover, as shown later, base damping may have a significant effect on the participation factors of the higher isolated modes, even when it makes only a minor contribution to the overall damping of these modes. Also, the case where there is damping in the structure as well as the isolator, for which the algebra becomes very lengthy for the continuous case, is considered in the following section for discrete-mass structural models.

Now consider the nature of the non-classical mode shapes, which from Equation (4.10) are given by

$$u_n(z) = U_{Nn} \cos\left(\gamma_n L \left(1 - \frac{z}{L}\right)\right). \quad (4.76)$$

This is the same form of expression as for the classical modes, but $\gamma_n L$ is now complex rather than real. U_{Nn} is the n th-mode displacement at the top of the shear beam.

In general, from Equation (4.12)

$$\gamma_n L = \sqrt{\frac{M}{K}} \sqrt{-p_n^2 - \frac{C_M + C_K(\gamma_n L)^2}{M}} p_n \quad (4.77)$$

where p_n is the complex modal frequency as defined in Equation (4.7).

Letting $(C_M + C_K(\gamma_n L)^2)/M = 2\zeta_n' \omega_n$, the expression for $\gamma_n L$ can be rewritten as

$$\gamma_n L = \frac{\pi}{2} \frac{\omega_n}{\omega_{FB1}} \sqrt{1 - 2\zeta_n(\zeta_n - \zeta_n') + i2\sqrt{1 - \zeta_n^2}(\zeta_n - \zeta_n')}. \quad (4.78)$$

Note that $\gamma_n L$ is real when $\zeta_n' = \zeta_n$. The condition for this was derived earlier. We are dealing here with the case where $\zeta_n' = 0$, i.e. no damping in the structure, but damping in the isolator. This simplifies the algebra slightly, but the nature of the modes is similar to the general case. With this simplification

$$\begin{aligned} \gamma_n L &= \frac{\pi}{2} \frac{\omega_n}{\omega_{FB1}} \sqrt{1 - 2\zeta_n^2 + i2\zeta_n \sqrt{1 - \zeta_n^2}} \\ &= \frac{\pi}{2} \frac{\omega_n}{\omega_{FB1}} \exp\left(\frac{i}{2} \tan^{-1} \frac{2\sqrt{1 - \zeta_n^2} \zeta_n}{1 - 2\zeta_n^2}\right) \end{aligned}$$

$$\begin{aligned} &= \frac{\pi}{2} \frac{\omega_n}{\omega_{FB1}} \exp\left(i \tan^{-1} \frac{\zeta_n}{\sqrt{1 - \zeta_n^2}}\right) \\ &= \frac{\pi}{2} \frac{\omega_n}{\omega_{FB1}} \left(\sqrt{1 - \zeta_n^2} + i\zeta_n\right). \end{aligned} \quad (4.79)$$

$\gamma_n L$ is complex, with real and imaginary parts denoted by Re and Im:

$$\begin{aligned} u_n(z) &= U_{Nn} \cos\left\{\text{Re}(\gamma_n L) \left(1 - \frac{z}{L}\right) + \text{Im}(\gamma_n L) \left(1 - \frac{z}{L}\right)\right\} \\ &= U_{Nn} \left[\cos \text{Re}(\gamma_n L) \left(1 - \frac{z}{L}\right) \cosh \text{Im}(\gamma_n L) \left(1 - \frac{z}{L}\right) \right. \\ &\quad \left. - i \sin \text{Re}(\gamma_n L) \left(1 - \frac{z}{L}\right) \sinh \text{Im}(\gamma_n L) \left(1 - \frac{z}{L}\right)\right] \end{aligned} \quad (4.80a)$$

$$\begin{aligned} &= U_{Nn} \sqrt{\cos^2 \text{Re}(\gamma_n L) \left(1 - \frac{z}{L}\right) + \sinh^2 \text{Im}(\gamma_n L) \left(1 - \frac{z}{L}\right)} \\ &\quad \times \exp\left[-i \tan^{-1} \left(\tan \text{Re}(\gamma_n L) \left(1 - \frac{z}{L}\right) \tanh \text{Im}(\gamma_n L) \left(1 - \frac{z}{L}\right)\right)\right] \end{aligned} \quad (4.80b)$$

This compares with the classically damped mode shape

$$u_n(z) = U_{Nn} \cos \frac{\pi}{2} \frac{\omega_n}{\omega_{FB1}} \left(1 - \frac{z}{L}\right). \quad (4.81)$$

When $\text{Im}(\gamma_n L)$ is small, the non-classical mode has a similar variation of displacement modulus along the beam to that of the classical mode, except that it increases slightly from top to bottom. The most noticeable changes are near zeroes of the classical mode shape, with the modulus of the non-classical modes having no zeroes because of the extra $\sinh^2 \text{Im}(\gamma_n L) \left(1 - \frac{z}{L}\right)$ term. Also, the phase θ_n of the mode- n displacements varies down the shear beam, with

$$\tan \theta_n = \tan \text{Re}(\gamma_n L) \left(1 - \frac{z}{L}\right) \tanh \text{Im}(\gamma_n L) \left(1 - \frac{z}{L}\right). \quad (4.82)$$

For the classical system, θ_n is independent of height z , corresponding to $\text{Im}(\gamma_n L) = 0$.

To illustrate the nature of the non-classical modes, Figure 4.4(a) shows the first three mode shapes for the structural and isolator parameters $T_{FB1} = 0.6$ s, $T_b = 2.0$ s, $\zeta_b = 0.3$ and $C_M = C_K = 0$. Hence the isolator is highly damped and the structure is undamped. The solid and dotted lines are the real and imaginary curves respectively and the dashed lines are envelopes for the real and imaginary components of the modal displacements. The envelopes may be defined by their base intercepts, $\pm(1 + \Delta_n')$ and $\pm\alpha_n$ respectively, where $2\alpha_1 = \alpha_n \approx \pi \zeta_b \omega_b / \omega_{FB1} \approx 0.28$ and where $4\Delta_1' \approx \Delta_n' \approx 0.5\alpha_n^2 \approx 0.04$ for this case. Note that $\alpha_n = \text{Im}(\gamma_n L)$.

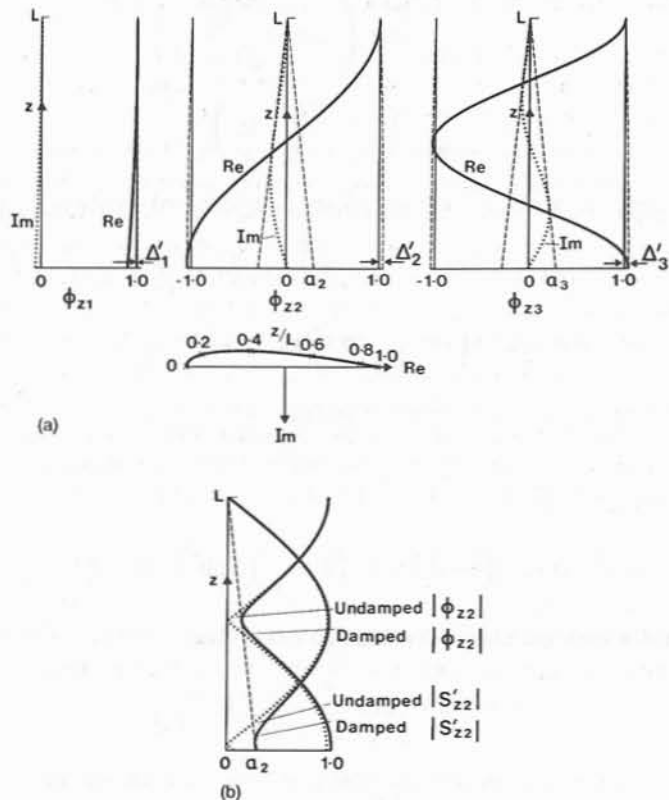


Figure 4.4 Complex mode shapes for the uniform 'shear-beam' structure with a highly-damped linear isolator. (a) The real and imaginary curves, i.e. the solid and dotted lines, are the front and side elevations respectively of the end point of the mode displacement vector ϕ_n at the time when ϕ_{Ln} is real. A plan view for the mode-2 vector is also shown, below the elevations for mode 2. (b) The moduli of the normalised displacements and shears for mode 2, with and without damping. The dotted lines are for $\zeta_b = 0$ and the solid lines are for $\zeta_b = 0.3$

The moduli of normalised displacements and shears for mode 2 are shown in Figure 4.4(b). The solid curves are for the damped isolator, $\zeta_b = 0.3$, and the dotted curves are for an undamped isolator, $\zeta_b = 0$. It is seen that non-classical behaviour has a significant effect on the higher-mode base shear.

The solution of the equations of motion for the forced response, in terms of modal responses, is discussed in a later section. The solution technique shares much in common with that for discrete systems with non-classical damping, so the two solutions are presented together after consideration of the modal properties of discrete models of isolated non-uniform structures.

4.2.3 Non-uniform linear structure on a linear isolator

The results so far in this chapter have been for a structure modelled as a continuous uniform linear 'shear-beam' on a linear isolator. Many structures have non-uniform distributions of mass and stiffness with height. Except for special variations of mass and stiffness, it is generally not possible to obtain closed-form analytical expressions for the mode shapes and frequencies of non-uniform continuous structures. However, if the structures are modelled as systems with discrete masses and springs, i.e. their mass and stiffness distributions are represented in matrix form, it is possible to obtain approximate but accurate expressions for the mode shapes and frequencies of well isolated non-uniform structures in terms of their free-free mode shapes and frequencies. It is also possible to derive expressions in terms of their fixed-base frequencies and mode shapes, for which we give references later.

The equation of motion for a structure modelled as a discrete linear system with viscous damping may be written in terms of the mass, damping and stiffness matrices $[M]$, $[C]$ and $[K]$ as

$$[M]\ddot{u} + [C]\dot{u} + [K]u = -[M]1\ddot{u}_g \tag{4.83}$$

where u is the vector of displacements of the N masses with respect to the ground.

For a well isolated structure, consider a perturbation about the classically damped free-free case. The damping and stiffness matrices may be expressed as:

$$[C] = [C_0] + \begin{bmatrix} 0 & \\ & C_b \end{bmatrix} \tag{4.84a}$$

$$[K] = [K_0] + \begin{bmatrix} 0 & \\ & K_b \end{bmatrix} \tag{4.84b}$$

where the subscript 0 refers to the free-free case and 0 is the $(N - 1) \times (N - 1)$ matrix of zeroes. K_b and C_b are the spring stiffness and damping coefficient of the isolator, respectively.

The eigenvalue problem for the free vibration response of the isolated structure, where $u = u_n e^{p_n t}$, is

$$p_n^2 [M]u_n + p_n [C]u_n + [K]u_n = 0. \tag{4.85}$$

Consider expansion of the complex frequencies and mode shapes of the damped structure on the linear isolator with viscous damping, in terms of perturbations of the free-free undamped cases. The perturbations will be in terms of a power expansion of the parameter ϵ , where ϵ is the ratio of the frequency ω_b of the structure, taken as a rigid mass M_T supported on the isolator spring of stiffness K_b , to the first-mode frequency ω_{FB1} of the unisolated structure. In this expansion scheme, the isolator spring stiffness K_b and isolator damper coefficient C_b are both taken as order ϵ^2 . This implies that the fraction of critical damping ζ_b of the rigid structure on the isolator is of order ϵ , since $C_b = 2\zeta_b \omega_b M_T$, where M_T is the

total mass of the structure and isolator. Normally the fraction of critical damping of the isolator is greater than that of the various modes of the superstructure, so we assume that the modal dampings ζ_{n0} of the free-free structural modes are of order ε^2 . The same orders for the base damping and damping in the structure were assumed by Tsai and Kelly (1988). The damping matrix of the free-free system and its perturbation will then both be of order ε^2 , the same order as the isolator spring stiffness. An alternative assumption, that the damping in the structure is of lower order, so that ζ_{n0} are of order ε , makes little difference to the final results, generally bringing in terms involving the modal damping of the free-free structure at half the (even) orders in which they appear in the expressions we derive below. As will be seen, the damping in the structure is generally of little significance for the isolated system. The particular orders for the damping assumed above lead to simpler algebra in the derivation of the perturbation expressions than the alternative assumption.

There are two technical matters in the perturbation which deserve mention. The first is that the fundamental free-free mode has zero frequency, so the lowest order of the perturbed first-mode frequency is ε , rather than order zero as for the other modal frequencies. The second technical point arises from the first. Since the fundamental free-free mode is a rigid-body mode with no internal deformation in the superstructure and it has zero frequency, the fraction of critical viscous damping is a meaningless concept for this mode. In the modal equations of motion it is multiplied by the zero modal frequency, so there is no loss of generality in taking the modal damping itself as zero. In Tsai and Kelly's work discussed later, where the perturbations were taken about the fixed-base modes for which the first-mode damping is defined, the first-mode damping of the structure has little effect on the isolated properties, so the difficulties of defining the damping for the rigid-body first-mode of the free-free system are of little consequence. The formal expansions for the perturbed complex frequencies and mode-shapes can be written as

$$p_n = p_{n0} + p_{n1} + p_{n2} + p_{n3} + p_{n4} + \dots \quad (4.86a)$$

$$\mathbf{u}_n = \mathbf{u}_{n0} + \sum_m \alpha_{nm} \mathbf{u}_{m0} + \sum_m \beta_{nm} \mathbf{u}_{m0} + \sum_m \gamma_{nm} \mathbf{u}_{m0} + \sum_m \eta_{nm} \mathbf{u}_{m0} + \dots \quad (4.86b)$$

The perturbations are in terms at powers of ε , where

$$\varepsilon = \omega_b / \omega_{FB1}. \quad (4.86c)$$

The mode shapes \mathbf{u}_{n0} are those of the undamped free-free modes. K_b , C_b and $[C]$ are order ε^2 . The first subscript for the frequency and mode shapes indicates the mode number, and the second the order of the expansion. Mode-1 is that with the lowest frequency. Some of the orders of the perturbations turn out to be zero, for example the expansions for the mode-shapes other than the first involve only the even orders. The results are given below:

$$p_1 = i\omega_b - \zeta_b \omega_b - i \frac{\zeta_b^2}{2} \omega_b - \frac{i}{2} M_T \omega_b^3 \sum_{j \neq 1} \frac{u_{bj0}^2}{\mu_{j0} \omega_{j0}^2} + O(\varepsilon^4) \quad (4.87)$$

where $\omega_b^2 = K_b/M_T$, $2\zeta_b \omega_b = C_b/M_T$, u_{bj0} is the base displacement in the free-free mode j , and μ_{j0} is the modal mass of the j th free-free mode defined as

$$\mu_{j0} = \mathbf{u}_{j0}^T [\mathbf{M}] \mathbf{u}_{j0}$$

$$\mathbf{u}_1 = \mathbf{u}_{1,0} - \sum_{j \neq 1} \frac{(K_b + i\omega_b C_b) u_{bj0} u_{b10}}{\mu_{j0} \omega_{j0}^2} \mathbf{u}_{j0} + O(\varepsilon^4) \quad (4.88a)$$

$$p_n = i\omega_{n0} - \zeta_{n0} \omega_{n0} - \frac{C_b u_{bn0}^2}{2\mu_{n0}} + \frac{iK_b u_{bn0}^2}{2\mu_{n0} \omega_{n0}} + O(\varepsilon^4) \quad n \neq 1 \quad (4.88b)$$

$$\mathbf{u}_n = \mathbf{u}_{n0} + (K_b + i\omega_{n0} C_b) u_{bn0} \sum_{j \neq n} \frac{u_{bj0}}{\mu_{j0} (\omega_{n0}^2 - \omega_{j0}^2)} \mathbf{u}_{j0} + O(\varepsilon^4) \quad n \neq 1. \quad (4.88c)$$

Note that the damped n th-mode natural frequency of the free-free system, $\sqrt{1 - \zeta_{n0}^2} \omega_{n0}$, expands to $\omega_{n0} - 1/2 \zeta_{n0}^2 \omega_{n0} \dots$. As ζ_{n0} has been assumed to be $O(\varepsilon^2)$, the second term in this expansion does not appear in the above results, which neglect terms of $O(\varepsilon^4)$.

It is convenient for interpretation to express the complex frequency as

$$p_n = -\zeta_n \omega_n + i\sqrt{1 - \zeta_n^2} \omega_n \quad (4.89a)$$

where ζ_n is the fraction of critical viscous damping and ω_n the undamped natural frequency in isolated mode n . Inverting this expression gives the following relationships for ω_n and ζ_n in terms of the complex frequency p_n :

$$\omega_n = |p_n| \quad (4.89b)$$

$$\zeta_n = \frac{-\text{Re}(p_n)}{|p_n|}. \quad (4.89c)$$

Applying these definitions to the expressions for the complex first-mode frequency given above:

$$\omega_1 = \omega_b \left[1 - 1/2 M_T \omega_b^2 \sum_{j \neq 1} \left(\frac{u_{bj0}^2}{\mu_{j0} \omega_{j0}^2} \right) \right] + O(\varepsilon^4) \quad (4.90a)$$

$$\zeta_1 = \zeta_b \left[1 + 1/2 M_T \omega_b^2 \sum_{j \neq 1} \left(\frac{u_{bj0}^2}{\mu_{j0} \omega_{j0}^2} \right) \right] + O(\varepsilon^5). \quad (4.90b)$$

The corrections to the rigid-structure approximations ω_b and ζ_b for the first-mode natural frequency and damping are both order ε^2 , indicating the high accuracy of the rigid-structure approximation. Note that damping in the structure does not enter into even the correction term for the first isolated mode damping.

Similarly, the higher-mode natural frequencies and dampings are:

$$\omega_n = \omega_{n0} \left[1 + \frac{1}{2} \frac{M_T u_{bn0}^2}{\mu_{n0}} \left(\frac{\omega_b}{\omega_{n0}} \right)^2 \right] + O(\varepsilon^4) \quad n \neq 1 \quad (4.91a)$$

$$\zeta_n = \zeta_{n0} + \zeta_b \frac{M_T u_{bn0}^2}{2\mu_{n0}} \left(\frac{\omega_b}{\omega_{n0}} \right)^2 + O(\varepsilon^4) \quad n \neq 1. \quad (4.91b)$$

Again, the correction term to the free-free frequency is order ε^2 , and becomes smaller for higher modes since it involves the ratio of ω_b to the modal frequency, rather than the first-mode unisolated frequency.

With typical values of $\varepsilon = \omega_b/\omega_{FBI} < 1/3$ and $\omega_b/\omega_{n0} < 1/(6(n-1))$ for practical isolation systems, these expressions show that the approximations

$$\omega_1 \approx \omega_b \quad \zeta_1 \approx \zeta_b \quad (4.92a)$$

$$\omega_n \approx \omega_{n0} \quad \zeta_n \approx \zeta_{n0} \quad n > 1 \quad (4.92b)$$

are in error by a few % at most. Thus, varying the isolator parameters has significant effect on the frequency and damping for the first mode only. The isolation governs the nature of the high modes, in that they are of the free-free type, but the actual frequencies and dampings of the modes higher than the first are determined by the properties of the structure rather than by those of the isolation system.

The nature of the isolated mode shapes is also worthy of investigation. The first isolated mode is real below order ε^3 , which is the lowest order at which damping affects the mode shape, so remains essentially classical, with nearly the same phase throughout the structure and isolation system. The higher-mode shapes become complex and hence non-classical at the lowest perturbation to the free-free mode shapes, which is of order ε^2 .

This different character of the first mode and higher modes with non-classical damping is apparent in the example given earlier for an isolated continuous uniform shear-beam. Figure 4.4 showed that the imaginary component of the mode shape, and the change in the real part of the mode shape from the undamped mode shape, are insignificant for the first mode, and the general character of the first-mode shear distribution is similar for the two cases. The imaginary part of the mode shapes has a greater influence for the higher modes, most importantly in its effect on the base shear.

4.2.4 Base stiffness and damping for required isolated period and damping

A common design problem with base-isolated structures is how to determine the base isolator stiffness and damping required to achieve a target fundamental period and damping for the isolated structure. For a structure which can be modelled as a discrete linear chain system, this problem can be solved exactly and directly by

using the Holzer technique (Clough and Penzien, 1975), an iterative method for determining natural frequencies and mode shapes.

We demonstrate the approach first for a system with classical damping. For such a system, the eigenvalue problem is to find frequencies ω_i and mode-shapes ϕ_i which satisfy

$$[\mathbf{K}]\phi_i = \omega_i^2[\mathbf{M}]\phi_i. \quad (4.93)$$

$[\mathbf{K}]$ is the tridiagonal stiffness matrix and $[\mathbf{M}]$ the diagonal mass matrix for a linear chain system. The Holzer method starts with an arbitrary mode shape value ϕ_{Ni} (often taken as 1) at mass number N at the top of the structure and an assumed value $\omega_i^{(1)}$ for the first iteration for the i th-mode natural frequency. For our problem, the frequency is the required first-mode frequency ω_1 .

In the following, where we are dealing with the first mode, the subscript indicating the mode number is dropped in the mode-shape values, with the remaining mode-shape subscript denoting the position in the structure. M_n denotes the n th mass in the system, from $n = 1$ at the base to $n = N$ at the top, and K_n denotes the stiffness of spring n numbered in the same way.

Consider the equation for the top mass

$$K_N(\phi_N - \phi_{N-1}) = \omega_1^2 M_N \phi_N. \quad (4.94)$$

The only unknown is ϕ_{N-1} , as ϕ_N has been assigned an arbitrary value (the eigenvalue problem is non-unique to the extent of a scaling factor in the mode shapes, so one of the elements of each mode-shape vector can be taken as arbitrary and the other elements defined in terms of it) and the required first-mode frequency is known. The unknown mode-shape value is thus given as

$$\phi_{N-1} = \phi_N - \frac{\omega_1^2 M_N \phi_N}{K_N} \quad (4.95)$$

Stepping down the structure one mass at a time, we come to the equation for general mass n . This can be written directly from the eigenvalue problem as

$$(K_n + K_{n+1})\phi_n - K_{n+1}\phi_{n+1} - K_n\phi_{n-1} = \omega_1^2 M_n \phi_n. \quad (4.96)$$

Alternatively, by summing the equations for masses n to the top mass N , the shear at the level below mass n can be written in terms of the sum of the inertia forces on the masses above it:

$$K_n(\phi_n - \phi_{n-1}) = \sum_{j=n}^N \omega_1^2 M_j \phi_j. \quad (4.97)$$

At this stage, the mode shapes for levels n to N have been determined from the equations for the higher masses, so ϕ_{n-1} is the only unknown. Solving the equation

for mass n gives

$$\phi_{n-1} = \phi_n + \frac{K_{n+1}}{K_n}(\phi_n - \phi_{n+1}) - \frac{\omega_1^2 M_n \phi_n}{K_n} \quad (4.98)$$

or, in the alternative formulation, the equivalent expression

$$\phi_{n-1} = \phi_n - \frac{\omega_1^2}{K_n} \sum_{j=n}^N M_j \phi_j. \quad (4.99)$$

This process continues down to the base mass, $n = 1$, where we have the equation

$$(K_1 + K_2)\phi_1 - K_2\phi_2 - K_1\phi_0 = \omega_1^2 M_1 \phi_1 \quad (4.100)$$

or, in the alternative formulation,

$$K_1(\phi_1 - \phi_0) = \sum_{n=1}^N \omega_1^2 M_j \phi_j. \quad (4.101)$$

For the standard Holzer process for finding natural frequencies and mode shapes, K_1 , K_2 , M_1 , ϕ_1 and ϕ_2 are known. ϕ_0 must be zero from the boundary condition at the base, but unless the process has converged will generally be non-zero, and further iterations are required to find the natural frequency and mode shape.

For our case of finding the required base stiffness of the isolator, the equation for the lowest mass is used in a different way. The stiffness $K_1 = K_b$ is the unknown, with ϕ_0 set equal to zero, satisfying the boundary condition, and all other values are known at this stage of the process. Rewriting the equations gives the alternative, but equivalent, expressions for the base stiffness K_b :

$$K_b = \omega_1^2 M_1 + K_2 \left(\frac{\phi_2}{\phi_1} - 1 \right) \quad (4.102)$$

or

$$K_b = \frac{1}{\phi_1} \sum_{j=1}^N \omega_1^2 M_j \phi_j. \quad (4.103)$$

The fundamental mode shape has been found in the course of the process. With the base stiffness now known, the process can now be repeated in the usual iterative manner to find the frequencies and mode shapes of higher modes, if required.

For the damped case, with a required first-mode natural frequency ω_1 and damping ζ_1 , we start with

$$p_1 = -\zeta_1 \omega_1 + i\sqrt{1 - \zeta_1^2} \omega_1 \quad (4.104)$$

and

$$p_1^2 = (2\zeta_1^2 - 1)\omega_1^2 - i2\zeta_1\sqrt{1 - \zeta_1^2}\omega_1^2. \quad (4.105)$$

Stepping through the masses in similar fashion to before, we obtain the top mass equation

$$(K_N + p_1 C_N)(\phi_N - \phi_{N-1}) + p_1^2 M_N \phi_N = 0 \quad (4.106)$$

which gives the mode-shape value

$$\phi_{N-1} = \phi_N + \frac{p_1^2 M_N \phi_N}{K_N + p_1 C_N}. \quad (4.107)$$

In general, ϕ_{N-1} and other mode-shape values will be complex, unless we happen to have a classically damped situation.

Arriving at the base mass we have the alternative forms of equation

$$p_1^2 M_1 \phi_1 + (K_b + p_1 C_b)\phi_1 + (K_2 + p_1 C_2)(\phi_1 - \phi_2) = 0 \quad (4.108)$$

or

$$p_1^2 \sum_{j=1}^N M_j \phi_j + p_1 C_b \phi_1 + K_b \phi_1 = 0. \quad (4.109)$$

Consideration of real and imaginary parts of these equations will give the required K_b and C_b . As before, the fundamental mode shape has been produced in the course of the process. Again, higher-mode frequencies, dampings and mode shapes can be found in an iterative fashion once the base stiffness and damping have been found, although the process is complicated by the generally complex-valued non-classical mode shapes.

4.2.5 Solution of equations of motion for forced response of isolated structures with non-classical damped modes

Now that we have determined the modal frequencies and mode shapes of the isolated system represented by either a continuous or discrete model, we move on to presenting the solution of the forced vibration problem in terms of modal responses.

For forced response, Foss's method can be used to solve the equations of motion for non-classically damped base-isolated structures in terms of modal responses for both the continuous shear-beam model and the discrete model. We consider first the discrete model, for which Foss's method has been presented for general non-classically damped structures by Hurty and Rubinstein (1964), Igusa *et al.* (1984) and Veletsos and Ventura (1986), and for base-isolated structures by Tsai and Kelly (1988). We then extend the results to the continuous shear-beam, for which they are analogous to the discrete case.

The equation of motion for the discrete case is

$$[\mathbf{M}]\ddot{\mathbf{u}} + [\mathbf{C}]\dot{\mathbf{u}} + [\mathbf{K}]\mathbf{u} = -[\mathbf{M}]\mathbf{1}\ddot{u}_g \quad (4.110)$$

Here $[\mathbf{M}]$, $[\mathbf{C}]$ and $[\mathbf{K}]$ are $N \times N$ matrices, where the system has N masses. Define

$$\mathbf{v} = \begin{pmatrix} \dot{\mathbf{u}} \\ \mathbf{u} \end{pmatrix}. \quad (4.111)$$

Then the equation of motion may be written as

$$[[\mathbf{M}] \ [\mathbf{C}]] \dot{\mathbf{v}} + [[\mathbf{0}] \ [\mathbf{K}]] \mathbf{v} = -[\mathbf{M}]\mathbf{1}\ddot{u}_g. \quad (4.112)$$

By complementing the equations of motion with an identity expression, we obtain

$$\begin{bmatrix} [\mathbf{0}] & [\mathbf{M}] \\ [\mathbf{M}] & [\mathbf{C}] \end{bmatrix} \dot{\mathbf{v}} + \begin{bmatrix} -[\mathbf{M}] & [\mathbf{0}] \\ [\mathbf{0}] & [\mathbf{K}] \end{bmatrix} \mathbf{v} = -\begin{pmatrix} \mathbf{0} \\ [\mathbf{M}]\mathbf{1} \end{pmatrix} \ddot{u}_g. \quad (4.113)$$

Define the $2N \times 2N$ matrices $[\mathbf{A}]$ and $[\mathbf{B}]$:

$$[\mathbf{A}] = \begin{bmatrix} [\mathbf{0}] & [\mathbf{M}] \\ [\mathbf{M}] & [\mathbf{C}] \end{bmatrix} \quad [\mathbf{B}] = \begin{bmatrix} -[\mathbf{M}] & [\mathbf{0}] \\ [\mathbf{0}] & [\mathbf{K}] \end{bmatrix}. \quad (4.114)$$

Then the free vibration case with solutions of the form $\mathbf{v}_n e^{p_n t}$ leads to the eigenvalue problem

$$p_n [\mathbf{A}]\mathbf{v}_n + [\mathbf{B}]\mathbf{v}_n = 0. \quad (4.115)$$

$[\mathbf{A}]$ and $[\mathbf{B}]$ are symmetric real matrices but are not positive definite, so the eigenvalues p_n and eigenvector \mathbf{v}_n occur in complex conjugate pairs.

Also, the following orthogonality conditions apply, for $p_m \neq p_n$ (Hurty and Rubinstein, 1964; Tsai and Kelly, 1988)

$$\begin{aligned} \mathbf{v}_m^T [\mathbf{A}]\mathbf{v}_n &= 0 \\ \mathbf{v}_m^T [\mathbf{B}]\mathbf{v}_n &= 0. \end{aligned} \quad (4.116)$$

For the forced vibration, express the solution as the sum of modal responses

$$\mathbf{v} = \sum_{m=1}^{2N} \xi_m(t) \mathbf{v}_m. \quad (4.117)$$

Then, substituting in the equation of motion and premultiplying by \mathbf{v}_n^T and making use of the orthogonality relation given above, the equations of motion can be

reduced to $2N$ uncoupled modal equations:

$$\dot{\xi}_n(t) - p_n \xi_n(t) = \frac{-\mathbf{v}_n^T \begin{pmatrix} \mathbf{0} \\ [\mathbf{M}]\mathbf{1} \end{pmatrix}}{\mathbf{v}_n^T [\mathbf{A}]\mathbf{v}_n} \ddot{u}_g \quad (4.118)$$

Now

$$\mathbf{v}_n = \begin{pmatrix} p_n \mathbf{u}_n \\ \mathbf{u}_n \end{pmatrix} \quad (4.119)$$

so the above expands to:

$$\begin{aligned} \dot{\xi}_n(t) - p_n \xi_n(t) &= \frac{-\mathbf{u}_n^T [\mathbf{M}]\mathbf{1}}{2p_n \mathbf{u}_n^T [\mathbf{M}]\mathbf{u}_n + \mathbf{u}_n^T [\mathbf{C}]\mathbf{u}_n} \ddot{u}_g \\ &= -N_n \ddot{u}_g \end{aligned} \quad (4.120)$$

Assuming zero initial conditions, the general solution can be written in terms of the Duhamel integral:

$$\xi_n(t) = -N_n \int_0^t e^{p_n(t-\tau)} \ddot{u}_g(\tau) d\tau \quad (4.121)$$

Associated with mode n will be mode n^* , for which \mathbf{u}_{n^*} , p_{n^*} and $\xi_{n^*}(t)$ are the complex conjugates of \mathbf{u}_n , p_n and $\xi_n(t)$.

The solution vector $\mathbf{u}(t)$ is given as

$$\begin{aligned} \mathbf{u}(t) &= \sum_{n=1}^{2N} \xi_n(t) \mathbf{u}_n \\ &= \sum_{n=1}^N (\xi_n(t) \mathbf{u}_n + \xi_{n^*}(t) \mathbf{u}_{n^*}) \\ &= 2 \sum_{n=1}^N \text{Re}(\xi_n(t) \mathbf{u}_n) \end{aligned} \quad (4.122)$$

where the summation is now over one of each complex conjugate pair.

The Duhamel integral can be expanded by writing the complex frequency in terms of its real and imaginary parts:

$$p_n = -\zeta_n \omega_n + i\sqrt{1 - \zeta_n^2} \omega_n \quad (4.123)$$

Then

$$\int_0^t e^{p_n(t-\tau)} \ddot{u}_g(\tau) d\tau = \int_0^t e^{-\zeta_n \omega_n(t-\tau)} \left[\cos \sqrt{1-\zeta_n^2} \omega_n(t-\tau) + i \sin \sqrt{1-\zeta_n^2} \omega_n(t-\tau) \right] \ddot{u}_g(\tau) d\tau \quad (4.124)$$

Here the term $\sqrt{1-\zeta_n^2} \omega_n(t-\tau)$ is to be read as a single argument. This gives:

$$\begin{aligned} \text{Re}[\xi_n(t) \mathbf{u}_n] &= -\text{Re} \left(\frac{\mathbf{u}_n^T [\mathbf{M}] \mathbf{1}}{2p_n \mathbf{u}_n^T [\mathbf{M}] \mathbf{u}_n + \mathbf{u}_n^T [\mathbf{C}] \mathbf{u}_n} \int_0^t e^{-\zeta_n \omega_n(t-\tau)} \right. \\ &\quad \times \left. \left[\cos \sqrt{1-\zeta_n^2} \omega_n(t-\tau) + i \sin \sqrt{1-\zeta_n^2} \omega_n(t-\tau) \right] \ddot{u}_g(\tau) d\tau \right) \\ &= -\text{Re} \left(\frac{\mathbf{u}_n^T [\mathbf{M}] \mathbf{1}}{2p_n \mathbf{u}_n^T [\mathbf{M}] \mathbf{u}_n + \mathbf{u}_n^T [\mathbf{C}] \mathbf{u}_n} \right) \int_0^t e^{-\zeta_n \omega_n(t-\tau)} \\ &\quad \times \left[\cos \sqrt{1-\zeta_n^2} \omega_n(t-\tau) \right] \ddot{u}_g(\tau) d\tau \\ &\quad + \text{Im} \left(\frac{\mathbf{u}_n^T [\mathbf{M}] \mathbf{1}}{2p_n \mathbf{u}_n^T [\mathbf{M}] \mathbf{u}_n + \mathbf{u}_n^T [\mathbf{C}] \mathbf{u}_n} \right) \int_0^t e^{-\zeta_n \omega_n(t-\tau)} \\ &\quad \times \left[\sin \sqrt{1-\zeta_n^2} \omega_n(t-\tau) \right] \ddot{u}_g(\tau) d\tau. \end{aligned} \quad (4.125)$$

To interpret this expression, consider the relative displacement response $Z_n(t)$ of a single-degree-of-freedom oscillator of undamped natural frequency ω_n and damping ζ_n to a ground acceleration $\ddot{u}_g(t)$, governed by the equation

$$\ddot{Z}_n + 2\zeta_n \omega_n \dot{Z}_n + \omega_n^2 Z_n = -\ddot{u}_g(t). \quad (4.126)$$

The solution of this equation for zero initial conditions is

$$Z_n(t) = - \int_0^t e^{-\zeta_n \omega_n(t-\tau)} \frac{1}{\sqrt{1-\zeta_n^2} \omega_n} \sin \left[\sqrt{1-\zeta_n^2} \omega_n(t-\tau) \right] \ddot{u}_g(\tau) d\tau. \quad (4.127)$$

Also, its relative velocity response $\dot{Z}_n(t)$ is given by

$$\begin{aligned} \dot{Z}_n(t) &= - \int_0^t e^{-\zeta_n \omega_n(t-\tau)} \left[\frac{-\zeta_n}{\sqrt{1-\zeta_n^2}} \sin \sqrt{1-\zeta_n^2} \omega_n(t-\tau) \right. \\ &\quad \left. + \cos \sqrt{1-\zeta_n^2} \omega_n(t-\tau) \right] \ddot{u}_g(\tau) d\tau \end{aligned} \quad (4.128)$$

and

$$\dot{Z}_n(t) + \zeta_n \omega_n Z_n(t) = - \int_0^t e^{-\zeta_n \omega_n(t-\tau)} \cos \left[\sqrt{1-\zeta_n^2} \omega_n(t-\tau) \right] \ddot{u}_g(\tau) d\tau. \quad (4.129)$$

Thus

$$\begin{aligned} \mathbf{u}(t) &= \sum_{n=1}^N 2 \text{Re}(\xi_n(t) \mathbf{u}_n) \\ &= \sum_{n=1}^N \left(2 \text{Re} \left(\frac{\mathbf{u}_n^T [\mathbf{M}] \mathbf{1}}{2p_n \mathbf{u}_n^T [\mathbf{M}] \mathbf{u}_n + \mathbf{u}_n^T [\mathbf{C}] \mathbf{u}_n} \right) (\dot{Z}_n(t) + \zeta_n \omega_n Z_n(t)) \right. \\ &\quad \left. - 2 \text{Im} \left(\frac{\mathbf{u}_n^T [\mathbf{M}] \mathbf{1}}{2p_n \mathbf{u}_n^T [\mathbf{M}] \mathbf{u}_n + \mathbf{u}_n^T [\mathbf{C}] \mathbf{u}_n} \right) \sqrt{1-\zeta_n^2} \omega_n Z_n(t) \right). \end{aligned} \quad (4.130)$$

Alternatively, from Equation (4.125) the modal response for the j th component can be written as

$$\begin{aligned} 2 \text{Re}(\xi_n(t) u_{jn}) &= -|i2\sqrt{1-\zeta_n^2} \omega_n| \left| \frac{\mathbf{u}_n^T [\mathbf{M}] \mathbf{1}}{2p_n \mathbf{u}_n^T [\mathbf{M}] \mathbf{u}_n + \mathbf{u}_n^T [\mathbf{C}] \mathbf{u}_n} u_{jn} \right| \\ &\quad \times \left[\int_0^t e^{-\zeta_n \omega_n(t-\tau)} \frac{1}{\sqrt{1-\zeta_n^2} \omega_n} \sin \left(\sqrt{1-\zeta_n^2} \omega_n(t-\tau) - \Psi_{jn} \right) \ddot{u}_g(\tau) d\tau \right] \end{aligned} \quad (4.131a)$$

where

$$\Psi_{jn} = \tan^{-1} \frac{-\text{Re} \left[\frac{\mathbf{u}_n^T [\mathbf{M}] \mathbf{1}}{2p_n \mathbf{u}_n^T [\mathbf{M}] \mathbf{u}_n + \mathbf{u}_n^T [\mathbf{C}] \mathbf{u}_n} u_{jn} \right]}{-\text{Im} \left[\frac{\mathbf{u}_n^T [\mathbf{M}] \mathbf{1}}{2p_n \mathbf{u}_n^T [\mathbf{M}] \mathbf{u}_n + \mathbf{u}_n^T [\mathbf{C}] \mathbf{u}_n} u_{jn} \right]}. \quad (4.131b)$$

Although as written, the phase angle Ψ_{jn} appears in the convolution integral, it is the phase angle of $N_n u_{jn}$, where u_{jn} is the j th component of the vector \mathbf{u}_n . The term $2\sqrt{1-\zeta_n^2} \omega_n N_n u_{jn}$, which equals $2 \text{Im}(p_n) |N_n u_{jn}|$, can be interpreted as

giving the modulus of the j th component of the n th participation factor vector $|\Gamma_{jn}|$ with an associated phase Ψ_{jn}

$$\begin{aligned}\Gamma_{jn} &= i2\sqrt{1 - \zeta_n^2}\omega_n N_n u_{jn} \\ &= |\Gamma_{jn}|e^{i\Psi_{jn}}\end{aligned}\quad (4.132)$$

where Ψ_{jn} is as above.

For a classically damped system, this simplifies to the standard expression. For classical damping, u_n is real, and

$$\begin{aligned}2p_n u_n^T [\mathbf{M}] u_n + u_n^T [\mathbf{C}] u_n &= 2(-\zeta_n \omega_n + i\sqrt{1 - \zeta_n^2} \omega_n) \mu_n + 2\zeta_n \omega_n \mu_n \\ &= i2\sqrt{1 - \zeta_n^2} \omega_n \mu_n\end{aligned}\quad (4.133)$$

where

$$\mu_n = u_n^T [\mathbf{M}] u_n. \quad (4.134)$$

For the classically damped case, the j th component of the n th participation factor vector, Γ_{jn} , is real-valued, given by

$$\begin{aligned}\Gamma_{jn} &= i2\sqrt{1 - \zeta_n^2} \omega_n \frac{u_n^T [\mathbf{M}] \mathbf{1}}{i2\sqrt{1 - \zeta_n^2} \omega_n \mu_n} u_{jn} \\ &= \frac{u_n^T [\mathbf{M}] \mathbf{1}}{u_n^T [\mathbf{M}] u_n} u_{jn}.\end{aligned}\quad (4.135)$$

For the general case, the vector of the moduli of the components of the n th-mode participation factor are

$$|\Gamma_{jn}| = 2 \operatorname{Im}(p_n) \left| \frac{u_n^T [\mathbf{M}] \mathbf{1}}{2p_n u_n^T [\mathbf{M}] u_n + u_n^T [\mathbf{C}] u_n} u_{jn} \right|. \quad (4.136)$$

For well isolated structures, this expression can be evaluated from the frequencies and mode shapes derived from the perturbation analysis. For the first-mode,

$$u_1^T [\mathbf{M}] \mathbf{1} = u_{1,0}^T [\mathbf{M}] \mathbf{1} + O(\varepsilon^4) \quad (4.137)$$

since for $u_{j,0}^T [\mathbf{M}] \mathbf{1} = 0$ for $j \neq 1$ the free-free case. The normalisation used in the perturbation analysis gives

$$\begin{aligned}u_1^T [\mathbf{M}] u_1 &= u_{1,0}^T [\mathbf{M}] u_{1,0} \\ &= \mu_{1,0} \\ &= M_T u_{b1,0}^2.\end{aligned}\quad (4.138)$$

Also

$$\begin{aligned}u_1^T [\mathbf{C}] u_1 &= u_1^T [\mathbf{C}_0] u_1 + u_1^T [\mathbf{O}_{C_b}] u_1 \\ &= 0 + C_b u_{b1,0}^2 + O(\varepsilon^4).\end{aligned}\quad (4.139)$$

This leads to

$$|\Gamma_1| = \mathbf{1} - \sum_{j \neq 1} \frac{K_b u_{bj,0}}{\mu_{j,0} \omega_{j,0}^2} u_{j,0} + O(\varepsilon^4). \quad (4.140)$$

For the higher modes, $n \neq 1$,

$$\begin{aligned}u_n^T [\mathbf{M}] \mathbf{1} &= (K_b + i\omega_{n,0} C_b) u_{bn,0} \frac{u_{b1,0}}{\mu_{1,0} \omega_{n,0}^2} M_T u_{b1,0} + O(\varepsilon^4) \\ &= \left(\left(\frac{\omega_b}{\omega_{n,0}} \right)^2 + i \frac{2\zeta_b \omega_b}{\omega_{n,0}} \right) M_T u_{bn,0} + O(\varepsilon^4).\end{aligned}\quad (4.141)$$

Again from the mode shape normalisation,

$$u_n^T [\mathbf{M}] u_n = \mu_{n,0}. \quad (4.142)$$

Also

$$\begin{aligned}u_n^T ([\mathbf{C}_0] + [\mathbf{O}_{C_b}]) u_n &= u_n^T ([\mathbf{C}_0]) u_n + C_b u_{bn}^2 \\ &= \mu_{n,0} 2\zeta_{n,0} \omega_{n,0} + 2\zeta_b \omega_b M_T u_{bn,0}^2 + O(\varepsilon^4) \\ &= -2\mu_{n,0} \operatorname{Re}(p_n)\end{aligned}\quad (4.143)$$

$$2p_n u_n^T [\mathbf{M}] u_n + u_n^T [\mathbf{C}] u_n = i2\mu_{n,0} \operatorname{Im}(p_n). \quad (4.144)$$

Thus:

$$\begin{aligned}|\Gamma_n| &= \left| \left(\left(\frac{\omega_b}{\omega_{n,0}} \right)^2 + i \frac{2\zeta_b \omega_b}{\omega_{n,0}} \right) \frac{M_T}{\mu_{n,0}} u_{bn,0} \right| |u_n| \\ &= \frac{M_T u_{bn,0}}{\mu_{n,0}} \frac{\omega_b}{\omega_{n,0}} \sqrt{\left(\frac{\omega_b}{\omega_{n,0}} \right)^2 + 4\zeta_b^2} |u_{n,0}| + O(\varepsilon^4).\end{aligned}\quad (4.145)$$

The ratio of moduli of the participation factor components, with and without damping, are

$$\frac{|\Gamma_n(\zeta_b)|}{|\Gamma_n(\zeta_b = 0)|} = \sqrt{1 + 4\zeta_b^2 \left(\frac{\omega_{n,0}}{\omega_b} \right)^2}. \quad (4.146)$$

This gives a ratio of $2\zeta_b(\omega_{n,0}/\omega_b)$ for high modes.

Damping has no effect on the participation factor of the first mode for orders less than ε^6 , in agreement with our earlier interpretation that this mode is essentially real. For the higher modes, the isolator damping enters into the leading term for the participation factor, which is of order ε^2 . As the n th free-free frequency may be considerably greater than the isolator frequency, the participation factors of the higher modes with isolator damping can be considerably greater than their participation factors in the absence of isolator damping. However, even with isolator damping, the participation factor is of the order ε^2 , so is small in absolute terms, much smaller than the isolated fundamental-mode participation factor or the unisolated n th-mode participation factor.

When very small floor spectra are important for design, the small higher-mode participation factors may be further reduced by using an attenuation spring, stiffness K_c , in series with the isolator damper, as shown in Figure 2.2(c). This spring will also cause some reduction in the isolator damping, but this reduction can be kept small, while achieving effective higher-mode attenuation, by using an appropriate value for K_c .

The consequences of adding the stiffness K_c in series with the isolator damper of coefficient C_b can be obtained by considering the mechanical impedance of the isolator components. Since the participation factor ratio of (4.146) is the modulus of the ratio of the isolator impedances with and without damping, it may be expressed as follows:

$$\frac{\Gamma_{Nn}(K_b, C_b)}{\Gamma_{Nn}(K_b)} = \left| 1 + i2\zeta_b \frac{\omega_n}{\omega_b} \right| \quad (4.147a)$$

$$= \left| 1 + i\omega_n \frac{C_b}{K_b} \right| \quad (4.147b)$$

since

$$2\zeta_b = \omega_b C_b / K_b.$$

When K_c is connected in series with C_b their impedances can be used to express the result as a complex damping coefficient:

$$\begin{aligned} C_b(K_c) &= \frac{C_b K_c / i\omega_n}{C_b + K_c / i\omega_n} \\ &= C_b \left(1 + i \frac{\omega_n \omega_b C_b}{\omega_b K_c} \right)^{-1}. \end{aligned} \quad (4.148)$$

Substituting $C_b(K_c)$ in (4.147b), and again noting that $2\zeta_b = \omega_b C_b / K_b$,

$$\frac{|\Gamma_{Nn}(K_b, C_b, K_c)|}{|\Gamma_{Nn}(K_b)|} = \left| 1 + i2\zeta_b \frac{\omega_n}{\omega_b} \left(1 + i \frac{\omega_n \omega_b C_b}{\omega_b K_c} \right)^{-1} \right|. \quad (4.149)$$

Comparing (4.149) with (4.147a) shows that the last factor in (4.149) gives the reduction in the higher-mode participation factor due to the attenuating spring K_c .

The reduction in the mode-1 damping due to K_c is found by noting that the damping of mode 1 is given by half the imaginary part of the impedance ratio, with $\omega_n = \omega_b$. Applied to (4.149) this gives:

$$\begin{aligned} \zeta_b(K_c) &= \zeta_b \operatorname{Re} \left(1 + i \frac{\omega_b C_b}{K_c} \right)^{-1} \\ &= \frac{\zeta_b}{1 + \left(\frac{\omega_b C_b}{K_c} \right)^2}. \end{aligned} \quad (4.150)$$

The reduction in the mode-1 damping can be limited to 20% by choosing a minimum K_c given by $K_c = 2\omega_b C_b$ which gives $\zeta_b(K_c) = 0.8\zeta_b$ from (4.150).

Since mode 2 has the largest higher-mode participation factor, and since K_c is least effective for reducing the participation factor for mode 2, the reduction in participation factor is checked for mode 2. The reduction is increased for increasing ω_2/ω_b . Taking $\omega_2/\omega_b = 6.0$, this gives:

$$\frac{|\Gamma_{Nn}(K_b, C_b)|}{|\Gamma_{Nn}(K_b)|} = |1 + i12\zeta_b| \quad (4.151)$$

and

$$\frac{|\Gamma_{Nn}(K_b, C_b, K_c)|}{|\Gamma_{Nn}(K_b)|} = |1 + 3.6\zeta_b + i1.2\zeta_b|. \quad (4.152)$$

For $\zeta_b = 0.2$ or 0.3 this gives a reduction of about 33% or 50% respectively, due to K_c .

4.2.6 Studies using perturbations about fixed-base modes

Tsai and Kelly (1989) analysed the response of a structure on a linear isolation system, modelled as a base mass and linear base spring and damper, in terms of perturbations about the frequencies and mode-shapes of the fixed-base system. They assumed that the isolated system had classical damping, which in general is not the case even when the superstructure has classical damping. Tsai and Kelly give closed-form expressions for the first-mode isolated periods and mode-shapes. Their general expression for the higher-mode frequencies is iterative, although a closed-form approximation is given for the case where the fixed-base modes are well separated in frequency. Their perturbation approach starts with the mode shapes and frequencies of the N -mass system. A base mass, spring and damper are introduced, giving $N + 1$ modes in all. The unperturbed shape of the extra mode is that of a rigid-body superstructure on the base spring, essentially the same as the first-mode approximation used in our analysis for the undamped case.

Tsai and Kelly (1988) account for the generally non-classical nature of the isolated modes. However, to simplify the perturbation expressions and their derivation,

they consider only the first superstructure mode, giving two modes for the unisolated system. They again represent the structural response in terms of its fixed-base mode-shape. This paper goes on to compare the response of a five-mass isolated structure with the El Centro and Parkfield accelerograms as calculated using the complex non-classical mode approach, and the classical mode approximation. For practical purposes, there is negligible difference in the results of the exact complex mode response and the classical mode approximation. However, they illustrate that the classical mode approximation is not always appropriate by considering the response of equipment in the isolated structure. The non-classical nature of the 'equipment mode' is important, as we discuss in Section 4.4.

4.3 BILINEAR ISOLATION OF LINEAR STRUCTURES

4.3.1 Introduction

The discussion so far has dealt with linear isolation systems. However, as discussed in Section 3.1 and Chapter 6, linear systems comprise only a small proportion of the isolation systems used in practice. Linear systems include laminated-rubber bearings, flexible piles with viscous dampers, etc.

The analysis of non-linear isolation systems is made easier by the fact that almost all of them can be approximated as bilinear systems, namely they can be represented by parallelogram-shaped force-displacement hysteresis loops. For instance, the isolation and damping devices developed at the DSIR can be regarded as bilinear. These include lead-rubber bearings, steel energy dissipators and lead-extrusion dampers. Various systems utilising friction elements, which were compared by Su *et al.* (1989), can also be represented by this type of model, including pure-friction devices such as the sand-layer system used in China (Li, 1984), the resilient-friction base isolator (Mostaghel and Khodaverdian, 1987), the Alexisison system (Ikonomou, 1984), and the Electricité de France (EDF) system (Gueraud *et al.* 1985). The sliding-resilient friction system (Su *et al.* 1989) can be represented by a trilinear loop, but except in extreme motions it is a bilinear device.

Our study of bilinear hysteretic isolation systems begins with a simple one-mass model, with the structure represented as a rigid mass mounted on a combination of springs and a Coulomb damper, to give the required isolator characteristics. Although inadequate for the study of higher-mode effects, this simple model gives a good approximation to the base-shear and displacement responses for an isolated multi-degree-of-freedom structure, and provides a close approximation to the first-mode response of the isolated system.

The base shear and displacement are calculated using time-history analysis for a scaled El Centro accelerogram, for a range of isolator and structural parameters. This provides a basis for the initial design of bilinear isolation systems, as well as providing a standard against which to compare the accuracy of the 'equivalent linearisation' procedure in which the bilinear isolation system is described by 'effective' values of period and damping and then treated as a linear system.

Higher modes of vibration make insignificant contributions to seismic displacements of the isolated structure, but may make substantial contributions to the seismic loads, and dominant contributions to floor spectra for periods less than 1.0 s. A large measure of control of higher-mode contributions can be achieved by an appropriate choice of isolator bilinear parameters, in relation to structural parameters.

The contributions of individual vibrational modes to seismic responses may be calculated accurately using mode-sweeping techniques. Mode sweeping is used to build up a database for the modal responses of a wide range of representative combinations of linear structures with bilinear isolators. These data on modal responses are presented in terms of the isolator and structural parameters, and also in terms of simple derived parameters.

The main isolation and structural parameters are the elastic and post-yield periods T_{b1} and T_{b2} of the isolator, its yield ratio Q_y/W , and the unisolated fundamental-mode period $T_1(U)$ of the structure. The unisolated period $T_1(U)$ corresponds to that of a system for which the isolator is rigid, i.e. K_{b1} and K_{b2} are infinite. The main derived parameters are the effective period (T_B) of the isolator and either its damping (ζ_B) or its non-linearity factor NL . These parameters have all been defined in Chapter 2, in Figure 2.3 and the associated text. The isolation factor I defined above, for linear systems, is extended to the bilinear case, so that the ratios $T_{b1}/T_1(U)$ and $T_{b2}/T_1(U)$ respectively give the isolation factors, $I(K_{b1})$ and $I(K_{b2})$, for the elastic and yielding phases of isolator response.

The presentation in terms of the derived parameters gives a clear picture of the important consequences of bilinear isolation in terms of the trade-off between reductions in base shear and increases in isolator displacements. The simplified presentation also assists during the important preliminary design stage for structures with non-linear isolation, as outlined in Chapter 5. This discussion of bilinear isolation systems, and in particular the analysis of factors controlling higher-mode effects, also forms a basis for the subsequent analysis of the seismic responses of appendages.

4.3.2 Maximum bilinear responses

The 'spectral response' approach has been seen in Chapter 2 to be very useful for linear isolation systems. The maximum seismic responses, for a single mass mounted on a linear isolation system and excited by a given design earthquake, are calculated by time-history analysis, a standard technique in engineering seismology described, for instance, by Newmark and Rosenblueth (1971), Clough and Penzien (1975) and Dowrick (1987). The maximum responses are then tabulated or plotted as functions of the fundamental period T and the fraction of critical viscous damping ζ , as shown in Figure 2.1. A designer wishing to use a given linear isolation system can use these spectra to arrive at suitable values of T and ζ which will give an appropriate 'trade-off' between reduced seismic shear and acceptable seismic displacement.

It is therefore of interest to produce plots of maximum responses of a single rigid mass mounted on a bilinear isolator and excited by a given design earthquake, as a function of the parameters of the bilinear system. Although unable to indicate any higher-mode effects, this model should give good approximations to the first-mode responses, namely the base shear and overall displacement, of a linear structure well isolated on a bilinear isolator.

To be useful for design purposes, the maximum bilinear response thus obtained should present the maximum seismic displacements X_b and accelerations \ddot{X}_b , or equivalent base-shear-to-weight ratio S_b/W , for various values of the bilinear isolator parameters T_{b1} , T_{b2} and Q_y/W or for an equivalent set such as K_{b1} , K_{b2} , Q_y and W . Here Q_y is the yield force of the isolator and W is the weight of the single mass, representing the overall weight of the structure and isolation system. The periods T_{b1} and T_{b2} relate to the elastic and post-yield stiffnesses K_{b1} and K_{b2} respectively. These isolator parameters, together with the velocity-damping parameter ζ_{b2} which is usually of secondary importance compared with the hysteretic damping, have been defined in Chapter 2.

Since a change in earthquake amplitude or period does not simply change the amplitude or period scale of the bilinear responses, as would occur with linear spectra, it is necessary to develop scaling procedures, as discussed in more detail in Section 5.1.3.

Maximum displacement and acceleration bilinear responses are given in Figure 4.5 for the amplitude- and period-scaled accelerations $\ddot{u}_g(t) = P_a \ddot{u}_{ELC}(t/P_p)$, where $\ddot{u}_{ELC}(t)$ are the accelerations for the earthquake, El Centro NS 1940. Note that $\zeta_{b2} = 5\%$ for this figure.

The smoothed maximum response plots of Figure 4.5 are based on values calculated for a single mass mounted on a bilinear isolator, for 72 combinations of isolator parameters, namely the twelve period combinations shown and six yield ratios Q_y/W , namely 1,2,3,5,7 and 10%. For the limit case of a zero yield ratio, the system becomes linear and the maximum acceleration and displacement values are given simply by linear response spectrum values, $S_A(T_{b2}, \zeta_{b2})$ and $S_D(T_{b2}, \zeta_{b2})$, where $\zeta_{b2} = 5\%$.

The maximum bilinear response plots of Figure 4.5 play the same role in the seismic responses of a single-degree-of-freedom bilinear isolator, as that of the linear spectra of Figure 2.1 for a single-degree-of-freedom linear isolator. The single-degree-of-freedom linear displacement spectra and bilinear maximum displacements produce good approximations to the maximum displacements of multi-degree-of-freedom isolated systems, since the first mode dominates the displacement response of isolated structures. The maximum acceleration value multiplied by the total mass is a good approximation to the base shear, which is also dominated by the first-mode response. Higher modes make significant contributions to the acceleration responses away from the base, particularly for highly non-linear isolators.

There are several important features of the single-degree-of-freedom displacement and acceleration diagrams of Figure 4.5.

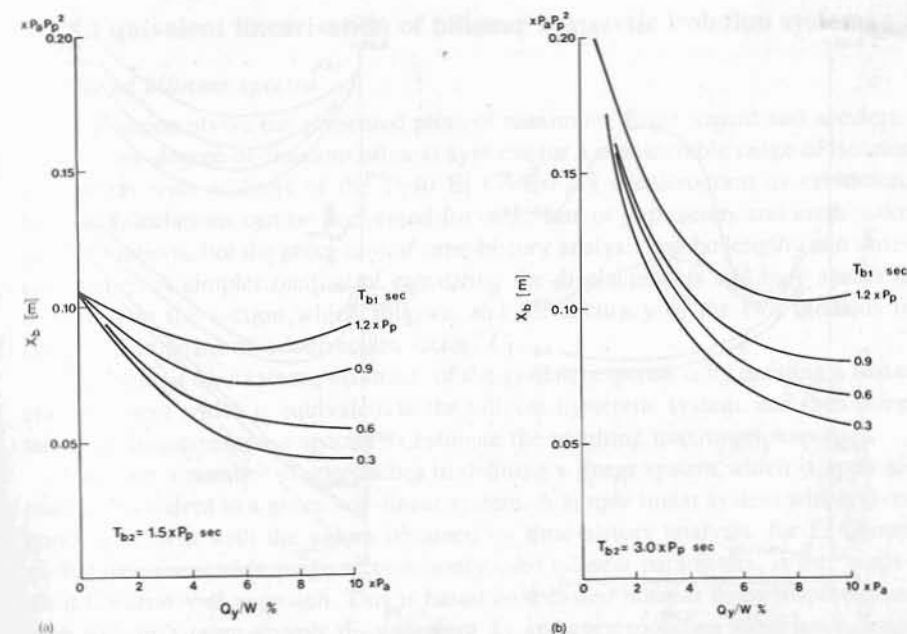


Figure 4.5 Maximum seismic responses of a single mass mounted on a bilinear isolator are shown as functions of the isolator parameters T_{b1} , T_{b2} and Q_y/W . The responses are shown for El Centro NS 1940 with amplitude- and period-scaling factors P_a and P_p respectively, as defined in the text. (a) Maximum displacements X_b for values of $T_{b2} = 1.5 \times P_p$ s and various values of T_{b1} . (b) Maximum displacements X_b for values of $T_{b2} = 3.0 \times P_p$ s and various values of T_{b1} . (c) Maximum displacements X_b for values of $T_{b2} = 6.0 \times P_p$ s and various values of T_{b1} . (d) Maximum accelerations (i.e. base-shear-to-weight ratios) for three values of T_{b2} and various values of T_{b1} .

- (i) For a given T_{b1} , T_{b2} and earthquake scaling factor P_a and P_p , there is an optimal value of Q_y/W for minimum base shear. Base shear is controlled primarily by the fundamental-mode response (Section 4.3.5), so this result holds for multi-degree-of-freedom systems also.
- (ii) For a given T_{b2} , the base shear and displacement decrease as T_{b1} decreases. For multi-degree-of-freedom systems, higher-mode accelerations generally increase as T_{b1} decreases (Section 4.3.6), so care should be taken in reducing T_{b1} to achieve reduced base shear and displacement. Results by Andriano and Carr (1991a, b) for multi-degree-of-freedom systems indicate that base shear and higher-mode accelerations increase as T_{b1} decreases, although the results for the systems we analysed did not show this.
- (iii) For a given Q_y/W , the base shear reduces as T_{b2} increases. However, this is generally at the expense of increased base displacement.
- (iv) The optimal yield level, $(Q_y/W)_{opt}$, for minimum base shear scales directly

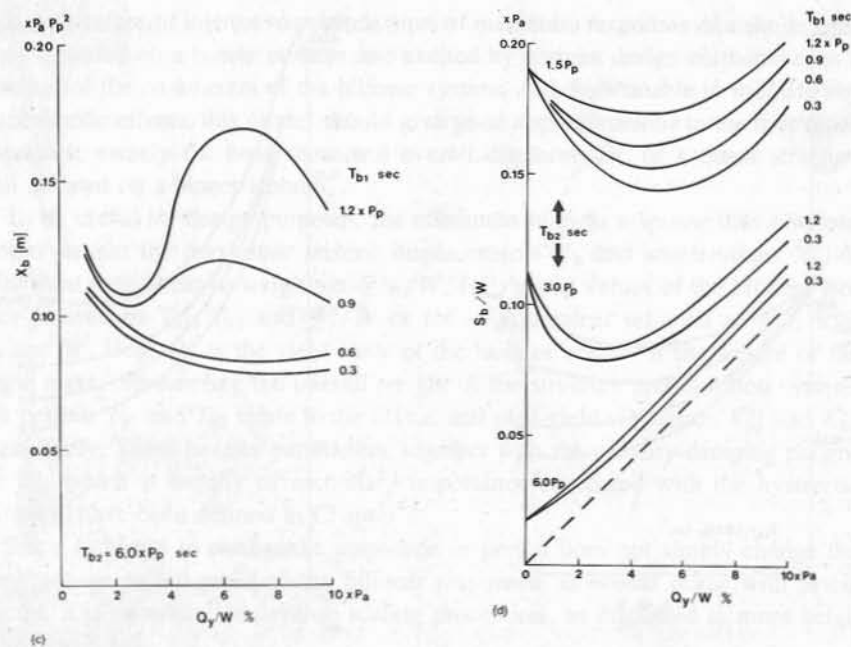


Figure 4.5 (continued)

with the amplitude scaling of the earthquake. Thus if $Q_y = 0.05W$ is optimal for El Centro, $Q_y = 0.10W$ will be optimal for 2 times El Centro motions if all other parameters are held fixed.

- (v) Increasing the yield force parameter Q_y beyond the optimal value for minimising base shear in a given earthquake motion generally produces a moderate increase in the base shear and an increase in higher-mode responses, but a reduction in the base displacement. Decreasing Q_y below the optimal value generally causes a rather rapid increase in base shear as well as increasing the displacement. Taking the yield level larger than the optimal value for the design earthquake scaling provides protection against a more extreme event. Taking Q_y less than the optimal value could place the system in the rapidly increasing branch of the base shear curve obtained for small (Q_y/W) when the earthquake scaling factor P_a is greater than the scaling for the design-level earthquake.

It should be noted that the curves presented in Figure 4.5 represent smoothed trends only and are limited by the 72 choices of isolator and structural parameters.

4.3.3 Equivalent linearisation of bilinear hysteretic isolation systems

Linearised bilinear spectra

The discussion above has presented plots of maximum displacement and acceleration for one-degree-of-freedom bilinear systems for a considerable range of isolator parameters with scalings of the 1940 El Centro NS accelerogram as excitation. Similar calculations can be performed for other sets of parameters and earthquake ground motions, but the procedure of time-history analysis can be lengthy and time-consuming. A simpler method of estimating the displacements and base shears is described in the section which follows, and the accuracy of the two methods is compared in terms of a 'correction factor' C_F .

One method of obtaining estimates of the system response is by defining a linear elastic system which is equivalent to the bilinear hysteretic system, and then using tabulated linear response spectra to estimate the resulting maximum responses.

There are a number of approaches to defining a linear system which is approximately equivalent to a given non-linear system. A simple linear system which gives good agreement with the values obtained by time-history analysis, for El Centro excitations, for a wide range of commonly used bilinear parameters, is the 'equivalent linearisation' approach. This is based on a closed bilinear force-displacement loop with maximum seismic displacement X_b and corresponding shear force S_b , as shown in Figure 2.3 and the associated text. The 'effective' or 'equivalent' period T_B is defined by the system mass M and the secant stiffness $K_B = S_b/X_b$. The 'effective' or 'equivalent' viscous damping ζ_B is obtained by adding the actual viscous damping to ζ_h , the damping associated with the hysteresis loop. A non-linearity factor NL is defined in terms of the hysteresis loop and is proportional to ζ_h . As well as being one of the parameters determining the base shear and displacement, the non-linearity factor is an important parameter governing the ratio of higher-mode to first-mode response, as is shown in Section 4.3.5.

Values of T_B , NL and ζ_h for the scaled El Centro earthquake, as functions of yield level Q_y/W for various combinations of T_{b1} and T_{b2} , are shown in Figures 4.6 and 4.7. For long post-yield periods T_{b2} , the effective bilinear period T_B , as defined from the secant stiffness, drops rapidly from T_{b2} as Q_y/W increases from zero. The equivalent viscous damping factor ζ_h , corresponding to the hysteretic energy dissipation, increases rapidly from zero as Q_y/W increases. For a given yield level, the damping increases rapidly as a function of T_{b2} , and also increases rapidly as T_{b1} is decreased. A small T_{b1} and a large T_{b2} correspond to a hysteresis loop approaching a rigid-plastic loop, which has the greatest ζ_h for a given (X_b , S_b) combination. The theoretical maximum of ζ_h , as defined, is $2/\pi$, i.e. 63%, for a rigid-plastic, i.e. rectangular loop.

Once these 'effective' values of period and damping have been obtained, the seismic responses can be obtained by treating this like any other linear system. The displacement $S_D(T_B, \zeta_B)$ can be obtained from tabulated values of linear spectra.

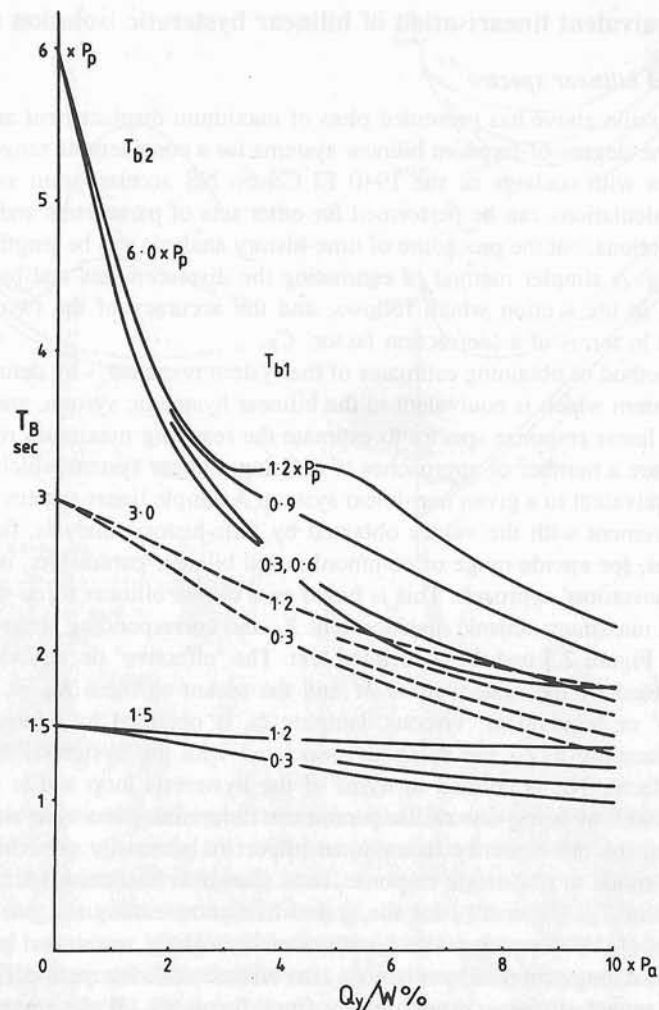


Figure 4.6 Effective period T_B of a bilinear isolator with the parameters T_{b1} , T_{b2} and Q_y/W , for El Centro NS 1940 with amplitude- and period-scaling factors P_a and P_p respectively. Note that T_B is related to K_B , the 'effective' (secant) stiffness of the isolator, by $T_B = 2\pi \sqrt{(M/K_B)}$, where M is the total isolated mass.

The maximum bilinear displacements X_b of Figure 4.5 can now be compared with the equivalent linear spectral displacements $S_D(T_B, \zeta_B)$ obtained from the reference tables for linear isolators with 'equivalent' values T_B and ζ_B . It is convenient to relate them by a simplified correction factor C_F , to give, without scaling (i.e. $P_a = P_p = 1$)

$$X_b(T_{b1}, T_{b2}, Q_y/W, \zeta_{b2}) \approx C_F S_D(T_B, \zeta_B). \quad (4.153)$$

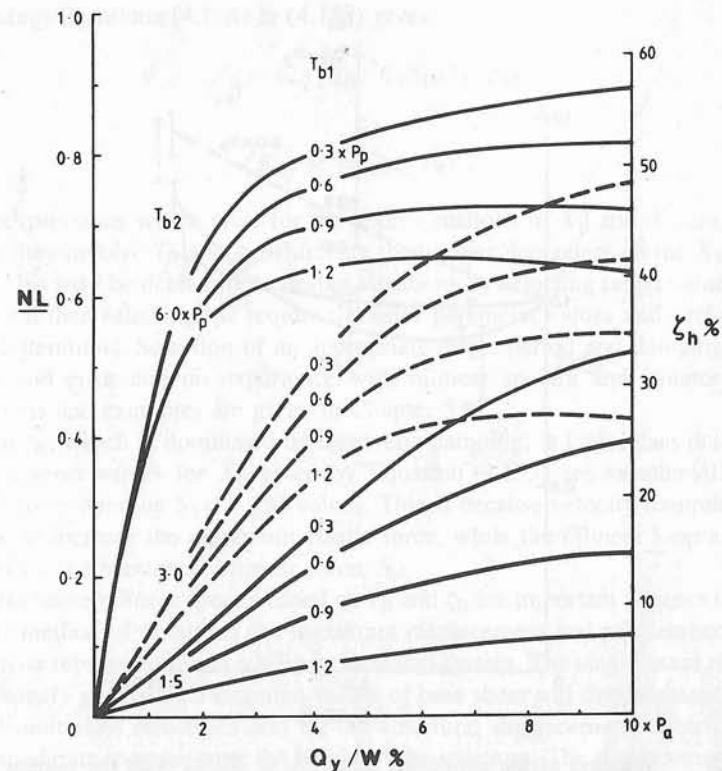


Figure 4.7 Variation, with bilinear isolator parameters T_{b1} , T_{b2} and Q_y/W , of the non-linearity factor NL and the hysteretic damping factor $\zeta_h = (2/\pi) NL$, for El Centro NS 1940 with amplitude- and period-scaling factors P_a and P_p respectively

The C_F values obtained can then be plotted as a function of the isolator parameters to indicate the accuracy of the equivalent linearisation approach. Such plots are important because they indicate the errors involved in using the simpler 'equivalent linearisation' approach rather than the full time-history analysis. As a result the correction factor has been studied for a range of multi-mass systems as well as for the single-mass bilinear isolator. Figure 4.8 shows smoothed plots of the correction factor, based on isolator seismic responses with a stiff five-mass structure (with $T_1(U) = 0.25$ s). The comparison X_b/S_D was also made for a rigid structure and for five-mass structures with $T_1(U) = 0.25, 0.5$ and 0.75 s.

Changes in C_F due to changes in structural period were also examined. For a few cases the changes were considerable and the greatest changes found are indicated by the dotted vertical arrows in Figure 4.8. Results suggested that the noise-like character of the El Centro accelerogram conferred considerable irregularity on the C_F values upon which Figure 4.8 was based.

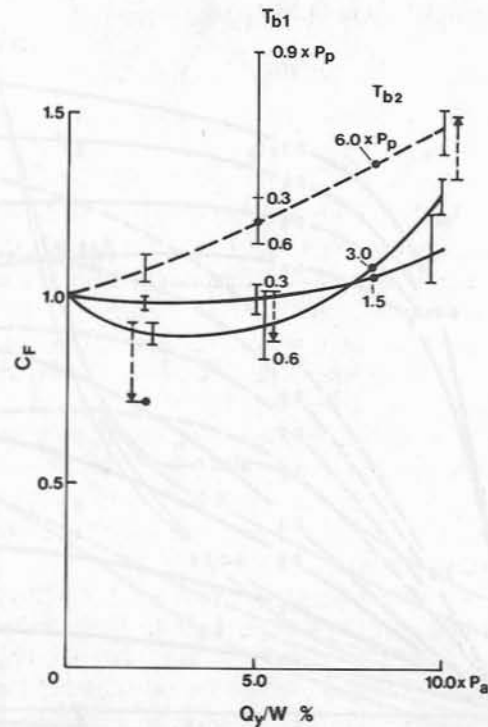


Figure 4.8 Variation of the correction factor $C_F = X_b/S_D$ with the bilinear isolator parameters T_{b1} , T_{b2} and Q_y/W , for El Centro NS 1940 with amplitude- and period-scaling factors P_a and P_p respectively. The two solid lines are for $T_{b2} = 3.0P_p$ and $T_{b2} = 1.5P_p$, while the dashed line is for $T_{b2} = 6.0P_p$. These curves were based on a stiff, rather than a rigid, structure ($T_1(U) = 0.25$ s)

It is seen that C_F is approximately unity, within about 10%, for a wide range of bilinear isolator parameters, but excluding those linked by the dashed line where $T_{b2} = 6 \times P_p$ s. This shows that the equivalent linearisation approach, with effective values of period and damping, is a useful approximation.

Chapter 5 describes how this approach can be used in the preliminary stages of the design of isolated systems. The procedure is to calculate $S_D(T_B, \zeta_B)$ to obtain an estimate of the maximum seismic displacement X_b . The acceleration can then be derived on the assumption that isolator velocity damping ζ_{b2} makes little contribution to the peak isolator force S_b , at least for ζ_{b2} up to 0.15 or so. Hence

$$S_b = K_B X_b. \tag{4.154a}$$

This is the force which accelerates the system mass M and hence

$$\ddot{X}_b = S_b/M. \tag{4.154b}$$

Substituting Equations (4.154) in (4.153) gives

$$\ddot{X}_b \approx (2\pi/T_B)^2 C_F S_D(T_B, \zeta_b) \tag{4.155}$$

since

$$K_B/M = (2\pi/T_B)^2.$$

The expressions which arise for the approximations to X_b and \ddot{X}_b are circular because they involve T_B and ζ_B which are themselves dependent on the X_b and \ddot{X}_b values. This may be dealt with in design situations by selecting target values for T_B and ζ_B and then selecting the required isolator parameter values and performing a series of iterations. Selection of an appropriate target period and damping depend on trial and error and on experience with bilinear spectra and isolator design. Discussions and examples are given in Chapter 5.

When ζ_B , which is dominated by hysteretic damping, is large, then the approximately correct values for \ddot{X}_b given by Equation (4.155) are substantially lower than the corresponding $S_A(T_B, \zeta_B)$ values. This is because velocity-damping forces combine to increase the maximum elastic force, while the bilinear loop area does not increase the maximum bilinear force, S_b .

Approximate bilinear spectra based on T_B and ζ_B are important because they give a simple method of obtaining the maximum displacement and acceleration for the single-mass representation of a bilinear isolation system. The single-mass responses in turn largely govern the maximum values of base shear and displacement for well isolated multimass structures and all the structural displacements which have at most a moderate increase over the height of the structure. The displacement profile is given rather accurately by the static deflections under mass-proportional forces, and with an isolator stiffness of $K_B = S_b/X_b$.

Simplified earthquake spectra

Equations (4.153) and (4.155), and Figure 4.8 for approximate C_F values, express the bilinear displacement and acceleration in terms of earthquake displacement spectra. The analysis can be further simplified and somewhat generalised by using simplified spectra for scaled El Centro-like earthquakes, or other stylised smoothed spectra, as discussed in Chapter 5 and illustrated by Figure 5.1. This results in useful analytical procedures for the design of isolation systems.

4.3.4 Modes of linear structures with bilinear hysteretic isolation

Introduction

The rigid-mass model mounted on a bilinear hysteretic isolation system produces a good approximation to some features of the seismic responses of a structure with bilinear hysteretic isolation. However, for other features of the responses, it is necessary to model the structure as several masses and springs, and then to determine the responses of various of its modes.

For a linear vibrational system, the natural modes of vibration are well-defined. However, for a non-linear system, such as a linear structure mounted on a non-linear isolation system, there are a number of possible ways of defining the modes, but the concept of the response consisting of the combination of a number of modal responses remains a useful one. The various approaches to defining the modes of the non-linear system assist in different ways in interpreting its response and in obtaining estimates of its maximum response.

The alternative ways of defining the modes of a system consisting of a linear structure with bilinear hysteretic isolation depend essentially on the definition adopted for the effective stiffness of the isolation system, the only non-linear element in the overall system. Once this stiffness has been defined, the mass and stiffness matrices of the overall system are defined, and modal properties and responses can be determined using the standard methods.

Three different candidates for the equivalent linear stiffness of the isolator are considered below. (1) adopts the instantaneous tangent values of the bilinear force-displacement relation, K_{b1} during elastic-phase motions and K_{b2} during yielding-phase motions. (2) adopts the yielding-phase stiffness K_{b2} for both elastic-phase and yielding-phase motions. (3) adopts a zero base stiffness for both elastic-phase and yielding-phase motions and hence represents seismic responses in terms of free-free modes.

When setting up the equations of motion for each of the above three cases, (1), (2) or (3), all force terms are retained so that, for any particular case, the sum of the modal responses at any time t is equal to the total response at time t , as given by a time-history analysis.

Before investigating these various possibilities for defining the isolator stiffness, and the modal properties and modal responses which result from these definitions, it is appropriate to review some of the features which make modal analysis of linear systems attractive, and the extent to which they carry over to a modal treatment of non-linear isolation systems. Also, we present a technique for extracting responses of individual modes from the response histories of all masses of an N -degree-of-freedom structure.

The first feature is that the total response $\mathbf{u}(t)$ of an N -mass system can be written as the sum of the modal responses

$$\mathbf{u}(t) = \sum_{i=1}^N \mathbf{u}_i(t) = \sum_{i=1}^N \phi_i \xi_i(t) \quad (4.158)$$

where ϕ_i is the i th mode shape and $\xi_i(t)$ is the i th 'modal coordinate'.

For a classically damped linear system, the response of any natural mode (n) to a ground acceleration $\ddot{u}_g(t)$ can be written in terms of a linear second-order differential equation uncoupled from all the other modes

$$\ddot{\xi}_n(t) + 2\zeta_n\omega_n\dot{\xi}_n(t) + \omega_n^2\xi_n = -\alpha_n\ddot{u}_g(t) \quad (4.159)$$

where ζ_n and ω_n are the modal damping and circular frequency and $\alpha_n =$

$(\phi_n^T[\mathbf{M}]\mathbf{1})/(\phi_n^T[\mathbf{M}]\phi_n)$ is closely related to the mode- n participation factor Γ_n .

In terms of the modal displacement vector $\mathbf{u}_n(t) = \phi_n\xi_n(t)$,

$$\begin{aligned} \ddot{\mathbf{u}}_n(t) + 2\zeta_n\omega_n\dot{\mathbf{u}}_n(t) + \omega_n^2\mathbf{u}_n(t) &= -\alpha_n\phi_n\ddot{u}_g(t) \\ &= -\Gamma_n\ddot{u}_g(t). \end{aligned} \quad (4.160)$$

Usually the participation factors become small for high modes, so only a few modes need be retained in the summation. Thus a set of coupled differential equations of motion involving matrices of dimension $N \times N$ are reduced to a few uncoupled equations for single-degree-of-freedom oscillators for which the solutions are well known.

For a non-linear isolation system, we can define the response as the sum of the responses of a number of modes. However, the modal equations of motion will be coupled, either directly in the equation of motion at any time (t), or through 'initial conditions' at the onset of a particular phase of the response. In general, the participation factors will be smaller for higher modes, but the importance of the higher modes may be much greater than for linear isolation systems, because of non-linear coupling effects feeding energy into them. Such important higher-mode responses are clearly evident in Figure 2.7, cases (v) and (vi).

Sweeping to obtain modal accelerations $\mathbf{a}_n(t)$ from total accelerations $\mathbf{a}(t)$

In order to find the contributions of individual modes to the total seismic responses of a linear structure on a bilinear isolator, it is first necessary to compute the time-history of these modal responses. For this computation it is useful to have an operation which extracts, or sweeps, the responses of individual modes from the time-histories of the overall responses of the system. This may be achieved readily by the technique described below.

A complete set of modes which are orthogonal with respect to the mass matrix is defined. The mode set would normally be the natural modes given by the system masses and stiffnesses, or by simple modifications of the stiffnesses as described later. The system responses are then obtained in terms of responses of this mode set, with the overall responses given by summing the responses of the individual modes. In linear algebra terms, the modes provide a set of 'basis vectors' for the system response. The technique may be used to obtain the exact natural-mode responses for a linear system which is undamped or classically damped. For other linear systems, or non-linear systems, the technique can be used to extract modal responses from the overall responses, when the modes have been defined in terms of a set of vectors which are orthogonal to each other with respect to the mass matrix. Such non-natural modes will be coupled through the stiffness matrix and/or through the damping matrix.

The natural-mode vectors of any general undamped linear structure are linearly independent and are orthogonal with respect to the mass and stiffness distributions, as discussed in Chapter 2. Any vibrational response, for example the absolute accelerations $\mathbf{a}(t)$ of the masses, can therefore be expressed as a linear combination

of modal responses as follows

$$\mathbf{a}(t) = \ddot{\mathbf{u}}(t) + \mathbf{1}\ddot{u}_g(t) = \sum_{n=1}^N (\ddot{\mathbf{u}}_n(t) + \ddot{u}_{gn}(t)). \quad (4.161)$$

The absolute acceleration response $\mathbf{a}(t)$ of the N -mass system is written in terms of the modal relative acceleration responses $\ddot{\mathbf{u}}_n(t)$ and the modal decomposition $\ddot{u}_{gn}(t)$ of the ground acceleration excitation $\ddot{u}_g(t)\mathbf{1}$.

The modal decomposition of the relative acceleration response is given by

$$\ddot{\mathbf{u}}(t) = \sum_{n=1}^N \ddot{\mathbf{u}}_n(t) = \sum_{n=1}^N \phi_n \ddot{\xi}_n(t). \quad (4.162)$$

Pre-multiplying by $\phi_n^T[\mathbf{M}]$ and using the orthogonality of the modes with respect to the mass matrix gives

$$\phi_n^T[\mathbf{M}]\ddot{\mathbf{u}}(t) = \phi_n^T[\mathbf{M}]\phi_n \ddot{\xi}_n(t). \quad (4.163)$$

The modal relative acceleration vector $\ddot{\mathbf{u}}_n(t)$ is given by

$$\begin{aligned} \ddot{\mathbf{u}}_n(t) &= \phi_n \ddot{\xi}_n(t) \\ &= \phi_n \frac{\phi_n^T[\mathbf{M}]\ddot{\mathbf{u}}(t)}{\phi_n^T[\mathbf{M}]\phi_n}. \end{aligned} \quad (4.164)$$

Performing the same operation on the excitation $\mathbf{1}\ddot{u}_g(t)$ leads to

$$\ddot{u}_{gn}(t) = \phi_n \frac{\phi_n^T[\mathbf{M}]\mathbf{1}}{\phi_n^T[\mathbf{M}]\phi_n} \ddot{u}_g(t) \quad (4.165)$$

$$= \Gamma_n \ddot{u}_g(t). \quad (4.166)$$

Similarly, the absolute acceleration of mode n is given by

$$\mathbf{a}_n(t) = \phi_n \frac{\phi_n^T[\mathbf{M}]\mathbf{a}(t)}{\phi_n^T[\mathbf{M}]\phi_n}. \quad (4.167)$$

For interpretation of the modal absolute acceleration, note that

$$\begin{aligned} \mathbf{a}_n(t) &= \ddot{\mathbf{u}}_n(t) + \ddot{u}_{gn}(t) \\ &= \ddot{\mathbf{u}}_n(t) + \Gamma_n \ddot{u}_g(t). \end{aligned} \quad (4.168)$$

Thus the modal absolute acceleration is the modal relative acceleration plus the participation factor vector times the ground acceleration.

For other linear or non-linear systems, the modal responses can be extracted by sweeping the total response vector by $\phi_n^T[\mathbf{M}]$ in the same way, provided that the

mode-shape vectors have been defined such that they are orthogonal with respect to the mass matrix. As for linear systems with classical modes, the total response is the sum of the modal responses. Unlike linear systems with classical modes, the equations governing the individual modal responses will be coupled with the responses of the other modes.

The following sections present the equations governing the modal responses of systems with bilinear hysteretic dampers, with the modes defined in various ways. The modal responses are those which would be obtained by sweeping the response vectors with the appropriate mode-shape vectors.

Equations of motion of a linear chain structure on a bilinear hysteretic isolator

While the following discussion is illustrated by a chain structure for convenience and easy visualisation, it applies to a much wider range of linear structures. The main constraints are that the dynamics are controlled by horizontal motions of the masses in the direction of the ground acceleration, and that the only connection to the ground is through the isolator components. The isolator allows no vertical or tilting motion at its interface with the structure, and provides some resistance to horizontal motion at the interface.

A linear chain structure, of masses m and stiffnesses k , mounted on a bilinear hysteretic isolator, is shown in Figure 4.9. The Coulomb damper is represented as a slider which yields at a force Q , thereby changing the stiffness of the system. An alternative representation has been shown in Figure 1.3(b). As shown in Figure 4.9, C_b is the isolator velocity-damping coefficient. F_b is the isolator force arising from its bilinear resistance to displacement.

The equations of motion are:

$$[\mathbf{M}]\ddot{\mathbf{u}} + [\mathbf{C}]\dot{\mathbf{u}} + [\mathbf{K}]_{\text{FF}}\mathbf{u} + \begin{pmatrix} \mathbf{0} \\ F_b(u_1) \end{pmatrix} = -[\mathbf{M}]\mathbf{1}\ddot{u}_g \quad (4.169)$$

where

$$[\mathbf{C}] = [\mathbf{C}]_{\text{FF}} + \begin{bmatrix} \mathbf{0} \\ C_b \end{bmatrix} \quad (4.170)$$

$[\mathbf{C}]_{\text{FF}}$ and $[\mathbf{K}]_{\text{FF}}$ are the damping and stiffness matrices for the free-free system, i.e. when the base isolator has zero horizontal stiffness and damping coefficient. These were denoted $[\mathbf{C}_0]$ and $[\mathbf{K}_0]$ in the perturbation expressions of Section 4.2 for linear isolation systems. In the elastic phase,

$$\begin{aligned} F_b(u_1) &= (K_{b1} - K_{b2})(u_1 - u_s) + K_{b2} u_1 \\ &= K_{b1} u_1 - (K_{b1} - K_{b2})u_s \end{aligned} \quad (4.171)$$

with u_s remaining zero, and $|(K_{b1} - K_{b2})(u_1 - u_s)| < Q$, where Q is the force across the Coulomb slider at which it yields. Here u_s is the displacement of the

'slider'. In the yielding phase,

$$F_b(u_1) = K_{b2}u_1 + Q \operatorname{sgn}(\dot{u}_1) \quad (4.172)$$

until $\dot{u} = 0$. Also $\dot{u}_s = \dot{u}_1$.

Let us consider next the modal forms of these equations and estimates of the peak modal response quantities for modes defined in terms of the various candidates which have been proposed for the effective base stiffness.

(1) Modes based on instantaneous isolator stiffnesses K_{b1} and K_{b2}

A candidate for the effective stiffness, which can be defined for an isolator with any non-linear force-displacement relation, is the instantaneous tangent stiffness of the force-displacement relation. For a general non-linear relation, this must be redetermined for every instant of the response. However, for bilinear hysteretic isolation, it alternates between two values, K_{b1} and K_{b2} , as defined in Figure 4.9. The mode shapes and frequencies associated with these stiffnesses are effective for the elastic and yielding phases of the response respectively. 'Initial conditions' in terms of the co-ordinates of the new phase need to be determined at changes from the elastic to yielding phase of response, and vice versa.

The stiffness matrices for each of the two phases may be expressed, as for linear isolation, by

$$[\mathbf{K}]_e = [\mathbf{K}]_{FF} + \begin{bmatrix} \mathbf{0} \\ K_{b1} \end{bmatrix} \quad (4.173)$$

$$[\mathbf{K}]_y = [\mathbf{K}]_{FF} + \begin{bmatrix} \mathbf{0} \\ K_{b2} \end{bmatrix} \quad (4.174)$$

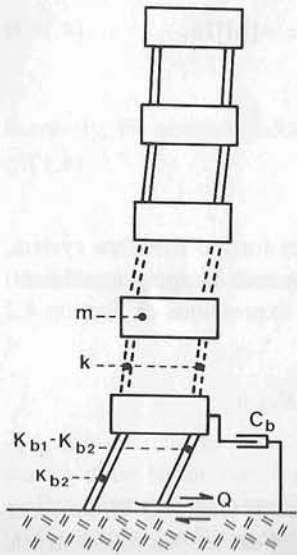


Figure 4.9 Model of a linear chain structure comprising masses m and intermass stiffnesses k , mounted on a bilinear isolator of stiffnesses K_{b1} and K_{b2} , with viscous damping coefficient C_b and Coulomb-damper force Q .

In the elastic phase, F_b is replaced by its residual after $K_{b1}u_1$ has been subtracted

$$F'_e = -(K_{b1} - K_{b2})u_s. \quad (4.175)$$

This has a constant value during any particular elastic phase, since $\dot{u}_s = 0$ during elastic phases, but its value will be different in different elastic phases, since u_s changes during the intervening yielding phases.

In the yielding phase, F_b is replaced by

$$F'_y = Q \operatorname{sgn}(\dot{u}_s). \quad (4.176)$$

This has the same value, apart from its sign, during all yielding phases of response. The natural frequencies and mode shapes are defined by

$$[\mathbf{K}]_e \phi_{e,n} = \omega_{e,n}^2 [\mathbf{M}] \phi_{e,n} \quad (4.177)$$

$$[\mathbf{K}]_y \phi_{y,n} = \omega_{y,n}^2 [\mathbf{M}] \phi_{y,n}. \quad (4.178)$$

Equations (4.177) and (4.178) define a set of normal modes for each response phase. The equations of motion become:

(i) elastic phase

$$\ddot{u}_{e,rn} + \frac{\phi_{e,rn} \phi_{e,n}^T [\mathbf{C}] \sum_i \phi_{e,i} \dot{\xi}_{e,i}}{\phi_{e,n}^T [\mathbf{M}] \phi_{e,n}} + \omega_{e,n}^2 u_{e,rn} + \frac{\phi_{e,rn} \phi_{e,1n} F'_e}{\phi_{e,n}^T [\mathbf{M}] \phi_{e,n}} = -\Gamma_{e,rn} \ddot{u}_g \quad (4.179)$$

(ii) yielding phase

$$\ddot{u}_{y,rn} + \frac{\phi_{y,rn} \phi_{y,n}^T [\mathbf{C}] \sum_i \phi_{y,i} \dot{\xi}_{y,i}}{\phi_{y,n}^T [\mathbf{M}] \phi_{y,n}} + \omega_{y,n}^2 u_{y,rn} + \frac{\phi_{y,rn} \phi_{y,1n} F'_y}{\phi_{y,n}^T [\mathbf{M}] \phi_{y,n}} = -\Gamma_{y,rn} \ddot{u}_g \quad (4.180)$$

where

$$\Gamma_{e,rn} = \frac{\phi_{e,rn} \phi_{e,n}^T [\mathbf{M}] \mathbf{1}}{\phi_{e,n}^T [\mathbf{M}] \phi_{e,n}} \quad (4.181)$$

with y replacing e in a corresponding expression for $\Gamma_{y,rn}$. The modal absolute accelerations at position r , obtained by sweeping with $\phi_{e,n}$ and $\phi_{y,n}$ respectively, are $(\ddot{u}_{e,rn} + \Gamma_{e,rn} \ddot{u}_g)$ and $(\ddot{u}_{y,rn} + \Gamma_{y,rn} \ddot{u}_g)$, as they appear in the above equations.

The damping terms are likely to be coupled between modes, but the coupling terms can generally be neglected. The F'_e and F'_y terms essentially change the

effective excitation, but can be handled without difficulty, as they are constant within a given phase of the response. The participation factors vary between the two phases, making interpretation of modal responses in terms of the response of a single-degree-of-freedom oscillator difficult. Non-linear coupling arises through the initial conditions of the new phase of response at changes from the elastic to the yielding phase and vice versa.

For a change of response phase at time t_c ,

$$\mathbf{u}(t_c) = \sum_i \mathbf{u}_{e,i}(t_c) = \sum_j \mathbf{u}_{y,j}(t_c) \quad (4.182)$$

or

$$\sum_i \phi_{e,i} \xi_{e,i}(t_c) = \sum_j \phi_{y,j} \xi_{y,j}(t_c). \quad (4.183)$$

From the use of orthogonality conditions with respect to the mass matrix

$$\xi_{y,n}(t_c) = \frac{\sum_i \phi_{y,n}^T [\mathbf{M}] \phi_{e,i} \xi_{e,i}(t_c)}{\phi_{y,n}^T [\mathbf{M}] \phi_{y,n}} \quad (4.184)$$

or

$$\mathbf{u}_{y,n}(t_c) = \frac{\sum_i \phi_{y,n}^T [\mathbf{M}] \mathbf{u}_{e,i}(t_c)}{\phi_{y,n}^T [\mathbf{M}] \phi_{y,n}} \phi_{y,n} \quad (4.185)$$

similarly

$$\mathbf{u}_{e,m}(t_c) = \frac{\sum_i \phi_{e,m}^T [\mathbf{M}] \mathbf{u}_{y,i}(t_c)}{\phi_{e,m}^T [\mathbf{M}] \phi_{e,m}} \phi_{e,m}. \quad (4.186)$$

Analogous expressions exist between the modal velocities $\dot{\mathbf{u}}_{y,n}(t_c)$ and $\dot{\mathbf{u}}_{e,m}(t_c)$. These expressions show that a response which is purely in one mode in the elastic phase excites all yielding-phase modes at the change of phase of the response, and similarly a single-mode yielding-phase response induces responses in all elastic modes when the velocity reverses. Examples of the decomposition of elastic-phase modal responses to multiple yielding-phase modal responses are shown in Figure 4.10, discussed later. Through this non-linear modal coupling, the energy of the response is transferred between various frequency bands around the natural frequencies for the two phases of the response.

As indicated by the high-frequency content in the seismic responses of cases (v) and (vi) in Figure 2.7, higher-mode accelerations may play an important role in the design of structures which have bilinear isolators. Equations (4.185) and (4.186), and the corresponding relationships for modal velocities and accelerations, may be used to study the mechanisms by which higher-mode accelerations are excited when the isolator is bilinear. Such studies help in identifying simple parameters,

such as the non-linearity factor and the elastic-phase isolation factor, which play an important role in controlling the severity of higher-mode acceleration responses. These parameter studies then assist the designer in balancing the benefits of moderate higher-mode accelerations against the benefits of other features of the seismic responses, such as low base-level shear forces or moderate overall displacements.

When the isolation factors, $I(K_{b1})$ and $I(K_{b2})$, as defined in Section 4.2, for the elastic-phase and the yielding-phase responses are both large (i.e. $T_{b2}/T_1(U) > T_{b1}/T_1(U) > 2$), then the period and shape of any elastic-phase mode n is close to the period and shape of the corresponding yielding-phase mode n , with each being close to the period and shape of free-free mode n , as indicated by Figure 4.3. The greatest departure from the free-free period and shape is for elastic-phase mode 1, since $I(K_{b1})$ is often substantially less than $I(K_{b2})$ with effective bilinear isolation.

Since all modes have nearly free-free shapes when the isolation factors are large, mode 1 has a participation factor near unity, and all higher modes have small participation factors for both phases of the response, as indicated by Figure 4.3. Hence direct earthquake excitation is largely confined to mode 1 for both response phases.

Since elastic-phase mode n has almost the same shape as yielding-phase mode n , the mode- n accelerations change little at a phase transition, as shown by the acceleration version of Equation (4.186) which gives,

$$\ddot{\mathbf{u}}_{e,n}(t_c) \approx \ddot{\mathbf{u}}_{y,n}(t_c).$$

Again, since the elastic-phase mode m is almost orthogonal (with respect to the mass matrix) to the yielding-phase mode n for $m \neq n$ and vice versa, Equations (4.185) and (4.186) show that there is little transfer of motion between modes of different number at either phase transition. The most significant, but still small, transfers of motion are accelerations from the first mode to the second mode and, to a lesser extent, to the third mode. Hence with small higher-mode participation factors, and small or moderate transfers of motion to higher modes, the higher-mode accelerations resulting either from direct excitation or by transfer of energy at yielding remain moderate. The only other source of excitation is from the F'_y term in Equation (4.180b), which involves the Coulomb damper force Q . This term is usually of order $(1/2)(Q/W)g$ or less, so for small yield ratios Q/W contributes at most small accelerations. Thus when the structure is well isolated in both the elastic and yielding phases of the motion, the higher-mode contributions to seismic loads are moderate and their contributions to floor spectra are not severe.

For any well isolated structure the yielding-phase isolation factor $I(K_{b2})$ is large. When the unisolated first period $T_1(U)$ is small or moderate, the elastic-phase isolation factor $I(K_{b1}) = T_{b1}/T_1(U)$ can also be made large while retaining a value of T_{b1} which is also compatible with bilinear loops which give high hysteretic damping. While the high non-linearity factor which is unavoidable with high hysteretic damping (since $\underline{N}_L = (\pi/2)\zeta_h$) tends to promote higher-mode responses, as discussed in Section 4.3.5 'Higher-mode maximum acceleration responses', these

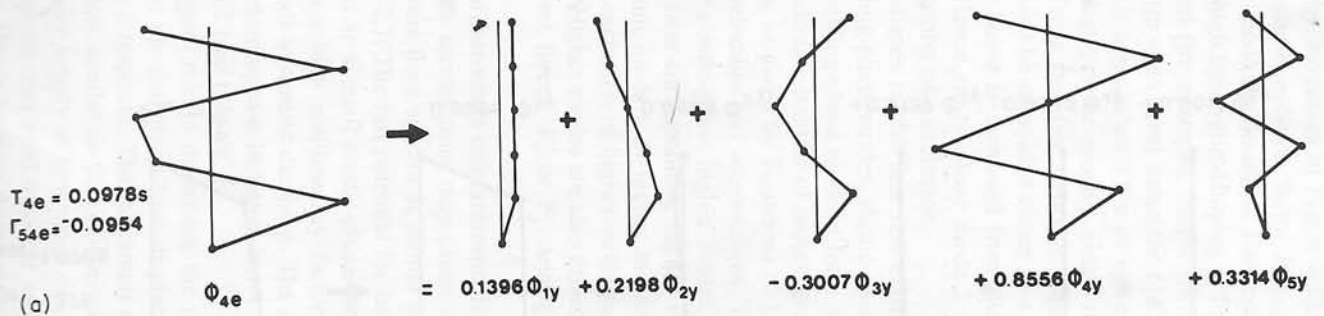
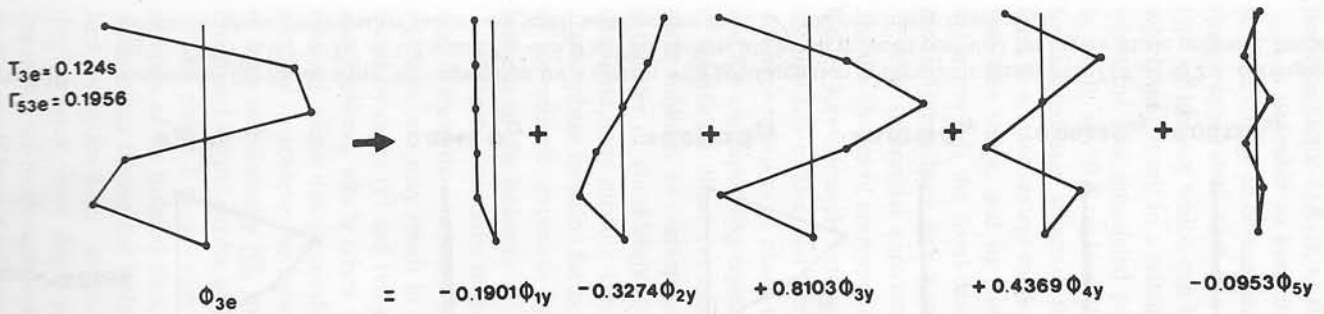
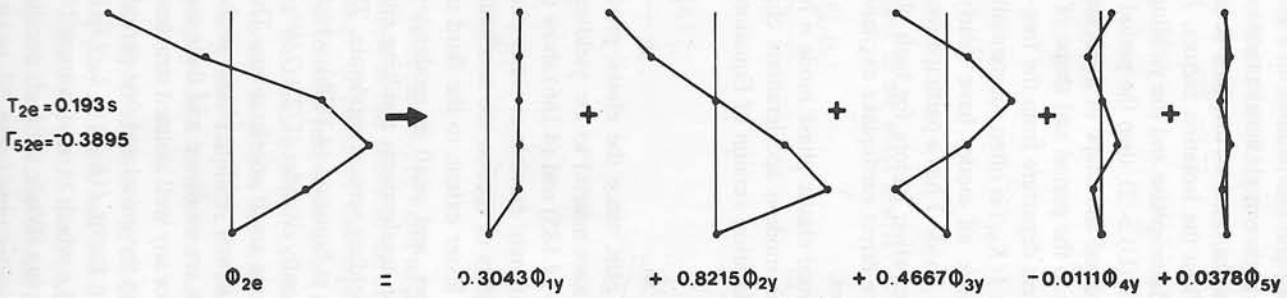
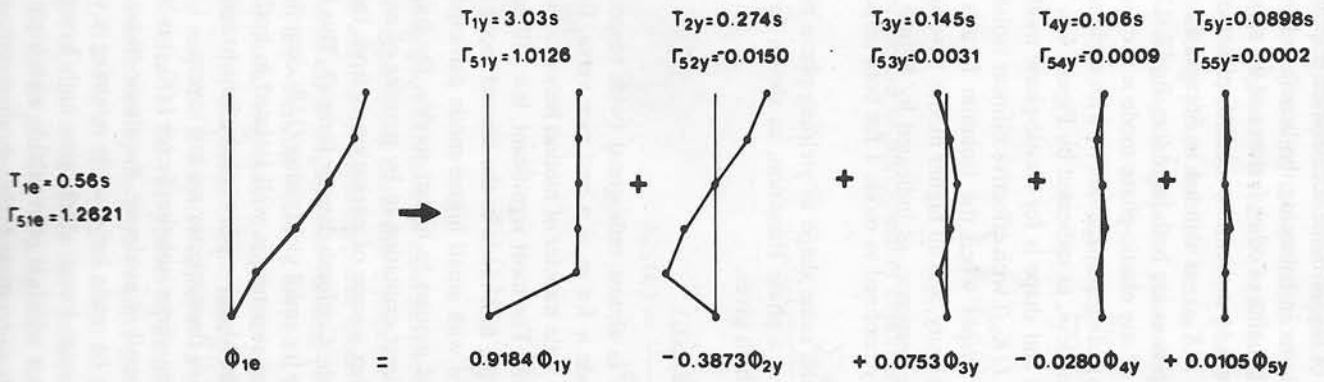


Figure 4.10

The first few elastic mode shapes for a 5-mass uniform structure, and their decomposition in terms of the post-yield modes. Also shown are the periods associated with various modes, and the top-mass participation factors. (a) Mode-shape decomposition for a system with a low elastic-phase isolation factor $I(K_{b1}) = 0.6$, corresponding to $T_1(U) = 0.5$ s, $T_{b1} = 0.3$ s and $T_{b2} = 3.0$ s, which has the potential for relatively strong higher-mode response from both direct excitation of higher modes and non-linear interaction.

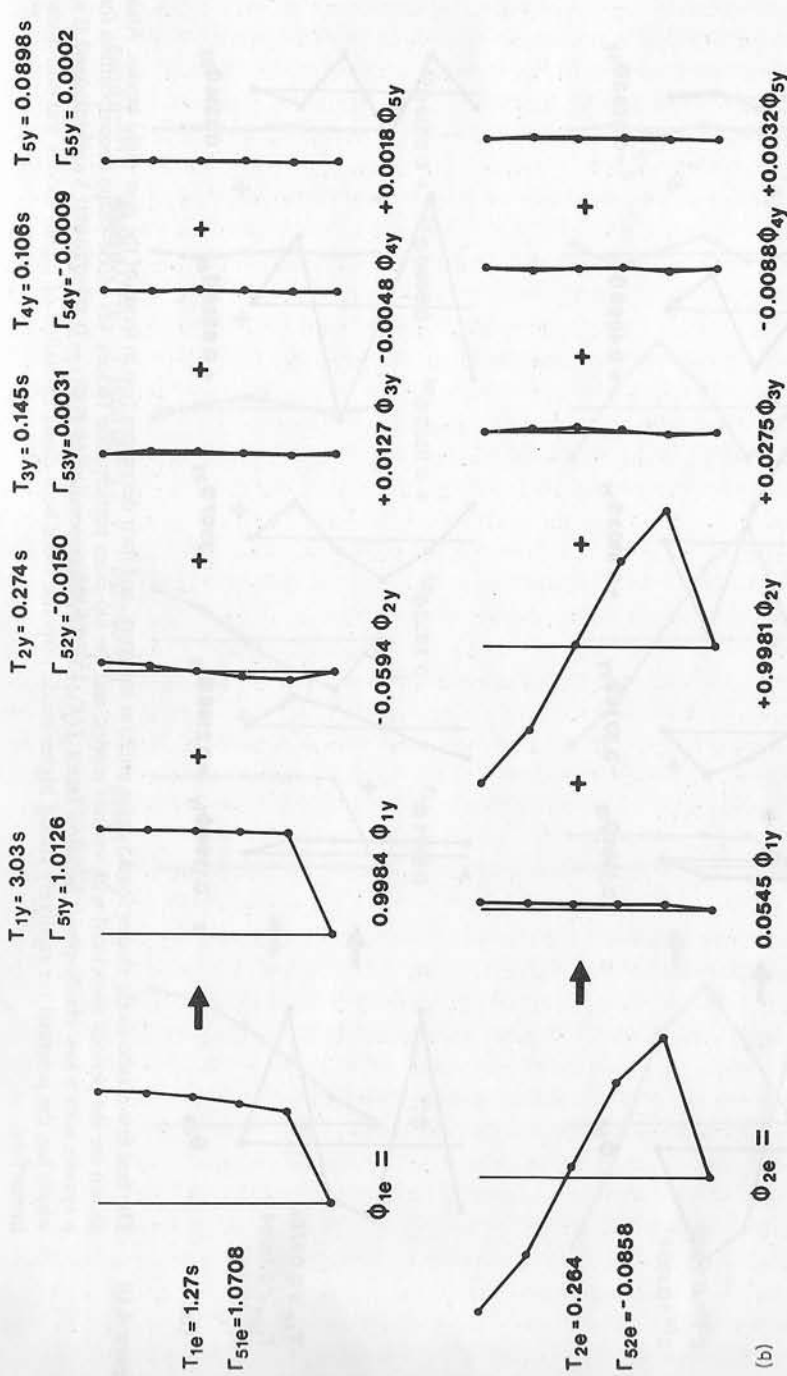


Figure 4.10

(continued) (b) Mode-shape decomposition for a system with good isolation in the elastic phase with $I(K_{b1}) = 2.4$, corresponding to $T_1(U) = 0.5$ s, $T_{b1} = 1.2$ s and $T_{b2} = 3.0$ s. This system has much reduced potential for higher-mode response, because the elastic-phase participation factors are small and because there is little non-linear interaction.

responses are progressively suppressed by increasing values of the elastic-phase isolation factor $I(K_{b1})$, as illustrated by the curves of Figure 4.12.

It is desirable to keep the elastic-phase isolation factor $I(K_{b1}) = T_{b1}/T_1(U)$ relatively large to ensure small higher-mode accelerations. However, there may be design constraints, such as a need for high hysteretic damping or limitations on the type of isolator which can be provided (for example, simple frictional supports), which may result in a relatively low (or even zero) value for $I(K_{b1})$, particularly when the first unisolated period $T_1(U)$ approaches 1.0 s or more. When $I(K_{b1})$ is small, say 0.5 or less, then the elastic-phase mode-1 shape is closer to that for a fixed-base structure than that for a free-free structure. Moreover, mode 2 (and to a lesser extent mode 3) may also be somewhat closer to a fixed-base than free-free shape, and its participation factor is increased from the zero free-free value towards the fixed-base value. Hence elastic-phase mode 2 (and sometimes mode 3) may have significant direct earthquake excitation.

With substantial contrasts in the shapes of the first few elastic-phase modes and the shapes of corresponding yielding-phase modes, elastic-phase mode n is no longer approximately orthogonal to yielding-phase mode m for $n \neq m$, at least for the first few modes, and there is considerable transfer of motion between modes of different numbers at phase transitions, as given by Equations (4.185) and (4.186) and the corresponding equations for velocities and accelerations. The combination of significant direct excitation of the elastic-phase higher modes, the transfer of these motions to corresponding and near-corresponding higher modes, and also a transfer of considerable motion from mode 1 to higher modes at each phase transition, may produce considerable excitation of higher-mode motions when the elastic-phase isolation factor is small. Higher modes are also driven in both phases of the seismic responses by the off-set forces, F'_e or F'_y , arising from the non-linearity of the isolator.

While the increases in the small higher-mode displacements have little design significance; the increased higher-mode accelerations may cause serious increases in loads, and may result in rather severe floor spectra at shorter periods, as illustrated by cases (v) and (vi) of Figure 2.7. The full potential for large higher-mode accelerations, which arises when there is a small elastic-phase isolation factor, is realised when this is combined with a high non-linearity factor which may be adopted to achieve the benefits of high hysteretic damping. The combined effect of high non-linearity NL and a low elastic-phase isolation factor $I(K_{b1})$ is again illustrated by the curves of Figure 4.12 (see below).

The phase-2 modes play the dominant role in describing the peak seismic responses of an isolated structure, since the maximum base displacement and base shear occur during the isolator phase-2 response. The maximum responses of the first mode are likely to occur at a time similar to that of the maximum isolator displacement, since this is made up very largely of first-mode displacement. Maximum higher-mode acceleration responses may tend to occur soon after yielding in the largest base-displacement cycle. This is because their near-zero participation factors result in little direct forcing of the higher modes from ground excitation

during the yielding phase, and so their energy is at a maximum soon after yielding before it is dissipated by viscous damping. This is illustrated by the mode-2 accelerations shown in Figure 4.11, where the strongest response occurs when the modal acceleration next reaches its maximum after yielding.

The higher-mode energy is gradually dissipated during the remainder of the yielding phase, which may occupy several cycles of a higher-mode response because the period of the fundamental mode is much longer than the periods of the higher modes. During the yielding phase, the higher modes respond with essentially damped sinusoidal motions at their damped natural frequencies, with a rate of decay depending on their damping, which is mainly contributed by viscous damping in the superstructure.

The transfer of energy from mode 1 to higher modes during phase transitions, together with the direct excitation of higher-mode accelerations during elastic-phase responses, may result in higher-mode accelerations and forces which are substantially greater than those of mode 1. However, the energy in mode 1 is usually much larger than the energies of higher modes since the square of the modal forces must be weighted by the square of the modal periods if modal energies are to be compared. Hence even if most of the excitation of higher modes is due to energy transfer from the elastic-phase mode 1, this would give little change in the mode-1 energy at a phase transition.

The small influence of higher modes on the responses of mode 1 may be demon-

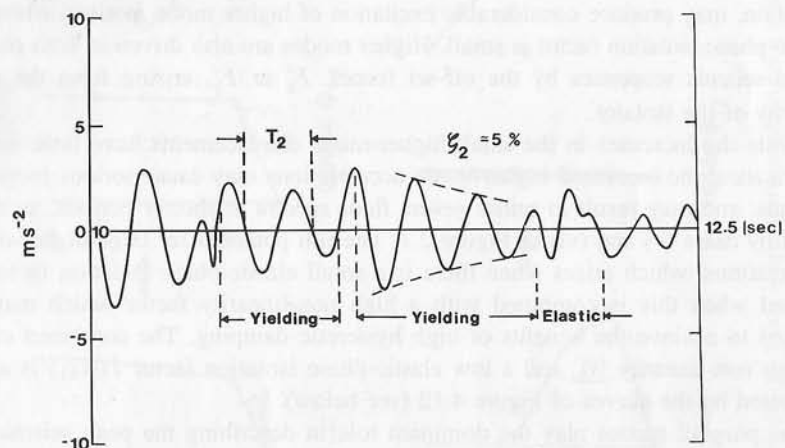


Figure 4.11 Sample time-history of modally swept acceleration response to El Centro NS 1940 for the top of a uniform 3-mass shear structure mounted on a bilinear isolator with parameters given in the text. During the time interval from 10–12.5 s the isolator was in the yielding- and elastic-phases at the times shown. Yielding-phase mode-2 was approximated by sweeping for free-free mode 2. The average logarithmic decrement corresponds to a damping factor of 0.054

strated for a structure and bilinear isolator combination which gives severe higher-mode responses. If the higher modes are suppressed, by modelling the structure as rigid, it is found that there is little change in the mode-1 responses, as can be seen by comparing base shear for corresponding single-mass and multi-mass systems in Tables 2.1 and 4.1.

The equations of motion, (4.179) to (4.181), can be used for response-history analysis, leading to a significant reduction in the amount of computation if the number of modes required is much less than the number of degrees of freedom in the system. The modal approach also throws light on the non-linear response mechanisms which may not be provided as clearly by the step-by-step solution of the matrix equations of motion. It explains some of the features of the response which will be illustrated later by applying modal sweeping to the response-history results.

The transfer of motion between modes at transitions from elastic to yielding-phase responses, as given by Equations (4.185) and (4.186), is illustrated in Figure 4.10 for two contrasting cases. Both cases have a five-mass uniform shear structure with $T_1(U) = 0.5$ s, and an isolator with $T_{b2} = 3.0$ s, so that both have yielding-phase isolation factors $I(K_{b2}) = 6.0$. For case (a), the isolator elastic period $T_{b1} = 0.3$ s, so that the elastic-phase isolation factor $I(K_{b1}) = 0.6$, and hence there is good isolation only in the yielding phase. For case (b), $T_{b1} = 1.2$ s, and hence $I(K_{b1}) = 2.4$ and there is good isolation for both the elastic and yielding phases of the responses.

Figures 4.10(a) and (b) illustrate the first few elastic-phase mode shapes, and represent them in terms of the yielding-phase mode shapes. The figures show to scale the decomposition of the elastic-phase mode shapes (for displacements, velocities and accelerations) to their yielding-phase components. The elastic-phase modes are scaled such that $\phi_{e,n}^T[M]\phi_{e,n}$ are the same for all modes. The relative strengths of the motion in the various elastic-phase modes vary from instant to instant within an earthquake response. The figures also summarise the periods associated with the various modes and their top-mass participation factors. The elastic-phase participation factors provide some indication of whether various modes are likely to be strongly excited.

For the first example, the elastic-phase first-mode decomposition in terms of the yielding modes produces a significant contribution to the second post-yield mode, which is thus excited by the first elastic mode on yielding. On yielding, 15% of the first-mode elastic-phase kinetic energy is transferred to the post-yield second mode. Also, the higher elastic-phase modes have significant participation factors, so are likely to make sizeable contributions to the total elastic-phase response. When significant mode-2 post-yield response is set up by the first-mode elastic response, in most cases mode 2 will be excited directly in the elastic phase also. The second elastic-phase mode produces response in mainly the second and third post-yield modes on yielding, with a lesser proportion of mode-1 response. The third elastic-phase mode, which has a participation factor of 0.2, produces sizeable proportions of mode 3, mode 4 and mode 2 on yielding.

For the second case, with $T_{b1}/T_1(U) = 2.4$, i.e. well isolated even in the elastic phase, the elastic-phase modes are very similar to the corresponding yielding-phase mode. Thus on yielding, very little energy is transferred from elastic-phase modes to higher yielding-phase modes. For both the first and second elastic-phase modes, over 99% of their kinetic energy is transferred to the corresponding post-yield mode on yielding. Only the first and second elastic-phase modes are shown, as the higher modes have insignificant participation factors even in the elastic phase (0.019 for the third mode).

(2) Modes based on post-yield isolator stiffness K_{b2}

In this case the stiffness matrix for both phases of response is the same as $[K]_y$ in the previous section.

$$[K]_y = [K]_{FF} + \begin{bmatrix} 0 & \\ & K_{b2} \end{bmatrix}. \quad (4.187)$$

In the elastic phase, F_b in the equation of motion is replaced by $F'_y(e)$

$$F'_y(e) = (K_{b1} - K_{b2})(u_1 - u_s). \quad (4.188)$$

In the yielding phase, F_b becomes

$$F'_y(y) = Q \operatorname{sgn}(\dot{u}_1). \quad (4.189)$$

The mode shapes and frequencies are defined by

$$[K]_y \phi_{y,n} = \omega_{y,n}^2 [M] \phi_{y,n}. \quad (4.190)$$

The equations of motion become

$$\ddot{u}_{y,tn} + \frac{\phi_{y,tn} \phi_{y,n}^T [C] \sum_i \phi_{y,i} \dot{\xi}_{y,i}}{\phi_{y,n}^T [M] \phi_{y,n}} + \omega_{y,n}^2 u_{y,tn} + \frac{\phi_{y,tn} \phi_{y,1n} F'_y}{\phi_{y,n}^T [M] \phi_{y,n}} = -\Gamma_{y,tn} \ddot{u}_g \quad (4.191)$$

where the appropriate form of F'_y is used for the two phases of the response.

In the elastic phase, the modes defined in this way are coupled through the F'_y term. In the yielding phase, the modes are coupled only through the viscous damping matrix, for which the coupling can usually be neglected, with the F'_y term modifying the excitation but not coupling the modes.

Similar comments apply to this choice of mode shape as were made in the previous section. This selection of base stiffness has been included as a separate case because it leads to the 'natural' modes for the strongest amplitude portion of the response. The maximum modal responses usually occur in the yielding phase

of the response, so the phase-2 mode shapes are more appropriate than the phase-1 mode shapes for interpreting the maximum responses through modal sweeping.

(3) Free-free modes

A further candidate for the appropriate set of mode shapes to represent the response of an isolated structure is the set of free-free modes. These mode shapes deserve consideration because of the low stiffness of the isolation system relative to the structure, at least in the post-yield phase, and by analogy with the free-free modes used in the perturbation analysis of a structure with a linear isolation system which was studied earlier in this chapter (Section 4.2). It turns out that this characterisation of the modes produces a convenient method of representing the first-mode response and the base shear, in terms of a rigid-mass representation of the superstructure on the bilinear isolator, with linear higher modes driven by the base shear.

For the free-free mode-shape representation, the stiffness matrix is $[K]_{FF}$, and the offset force F_b is as defined for the equation of motion in (4.171) and (4.172). It is convenient to add the isolator damping force $C_b \dot{u}_1$ to the isolator offset force F_b .

The mode shapes and frequencies are defined by

$$[K]_{FF} \phi_{FF,n} = \omega_{FF,n}^2 [M] \phi_{FF,n}. \quad (4.192)$$

The equations of motion become

$$\ddot{u}_{FF,rn} + 2\zeta_{FF,n} \omega_{FF,n} \dot{u}_{FF,rn} + \omega_{FF,n}^2 u_{FF,rn} + \frac{\phi_{FF,rn} \phi_{FF,1n} (F_b + C_b \dot{u}_1)}{\phi_{FF,n}^T [M] \phi_{FF,n}} = -\Gamma_{FF,rn} \ddot{u}_g. \quad (4.193)$$

For the fundamental mode $n = 1$, the frequency $\omega_{FF,1} = 0$, the participation factor $\Gamma_{FF,r1} = 1$ and

$$\ddot{u}_{FF,r1} + \ddot{u}_g = -\frac{1}{M_T} (F_b + C_b \dot{u}_1). \quad (4.194)$$

The right-hand side of this equation is simply the negative of the base shear divided by the total mass M_T of the system. This corresponds to the first-mode base acceleration, for the selected mode shapes. This result can be arrived at in another way. The base shear is the sum of the inertia forces over all masses. Summing the inertia forces is the same process as sweeping the inertia forces with the first-mode shape, which consists of unity, at each degree of freedom.

For higher modes ($n > 1$), the participation factors $\Gamma_{FF,rn} = 0$. The equations of motion become

$$\ddot{u}_{FF,rn} + 2\zeta_{FF,n} \omega_{FF,n} \dot{u}_{FF,rn} + \omega_{FF,n}^2 u_{FF,rn} = -\frac{\phi_{FF,rn} \phi_{FF,1n} (F_b + C_b \dot{u}_1)}{\phi_{FF,n}^T [M] \phi_{FF,n}} \quad n > 1. \quad (4.195)$$

Thus the higher-mode responses are excited by accelerations defined by scalings of the base shear divided by the total mass, which we have already shown is the negative of the first-mode absolute acceleration. Thus the fundamental-mode response, defined in terms of the free-free modes, drives the higher-mode responses.

In practice, the first-mode acceleration response will not be known unless the complete response-history of the structure has been calculated. The first-mode response can then be extracted by sweeping with the first free-free mode shape. The maximum values of the first-mode acceleration, the first-mode and total displacements, and the base shear can be estimated accurately by using a one-mass model of the superstructure. However, this model does not produce the higher-frequency content of the response well enough for its base shear to be used as the excitation in Equation (4.195) for calculating the higher-mode responses.

A typical yielding-phase higher-mode acceleration response-history, for a bilinear isolator which gives a small elastic-phase isolation factor, is shown in Figure 4.11. A uniform three-mass isolated shear structure has a bilinear isolator with $T_{b1} = 0.3$ s, $T_{b2} = 1.5$ s, $Q/W = 0.05$ ($Q_y/W = 0.052$), and $\zeta_{b2} = 0.05$. Its unisolated period is $T_1(U) = 0.43$ s and it has free-free modal damping factors of 0.05. Hence $I(K_{b1}) = 0.7$ and $I(K_{b2}) = 3.5$. Also, since $X_b = 0.053$ m and $S_b = 4.30$ N, for $M = 3$ kg, $T_B = 1.21$ s, $\underline{NL} = 0.334$, $\zeta_h = 0.21$, $\zeta_B = \zeta_h + \zeta_{b2} = 0.26$.

Figure 4.11 shows the top acceleration for yielding-phase mode 2 of the three-mass structure. The mode-2 acceleration was computed using Equation (4.164) with ϕ_2 given by the shape of free-free mode 2, which approximates the shape of yielding-phase mode 2. The modal sweeping removed the orthogonal free-free modes 1 and 3. The true modes in the elastic-phase response are far different from the free-free modes, so the net result is a modified top acceleration during elastic-phase responses, and the top acceleration of mode 2 during yielding-phase responses. Yielding-phase mode-2 accelerations have been excited during transitions to the yielding-phase responses. The mode-2 yielding-phase accelerations closely approximate a decaying sinusoidal curve. The average logarithmic decrement corresponds to a damping factor of 0.054, showing that the decay rate is controlled by the structural damping factor, 0.05 in this case. The figure clearly indicates the low excitation given to higher modes during the yielding-phase response.

Since the most severe higher-mode accelerations are approximately sinusoidal, and typically persist for several cycles, they may result in quite severe responses for moderately damped appendages when they are tuned to yielding-phase higher modes, as discussed later.

4.3.5 Higher-mode acceleration responses of linear structures with bilinear isolation

Systematic case studies

In this section we show that higher-mode accelerations may make large contributions to the seismic loads and the floor-acceleration spectra for linear structures

with bilinear isolation. A systematic study was undertaken to establish broad trends for these higher-mode contributions, to clarify the mechanisms involved and to establish guide-lines for preliminary design.

Modal and overall seismic responses to the El Centro NS 1940 earthquake accelerogram were studied for 81 different combinations of structural and isolator parameters. The results are presented in Table 4.1, which shows the maximum responses of three uniform five-mass shear structures, each isolated on 27 different bilinear isolators.

A five-mass uniform shear structure, as shown in Figure 4.9 with $N = 5$, was given one of three 'unisolated' periods

- $T_1(U) = 0.25, 0.5, 0.75$ s.

Each of the major bilinear isolator parameters were given three values:

- $T_{b1} = 0.3, 0.6, 0.9$ s
- $T_{b2} = 1.5, 3.0, 6.0$ s
- $Q_y/W = 0.02, 0.05, 0.10$.

For typical structures with bilinear isolation involving energy dissipation through hysteresis of lead or steel, these parameter values tend to represent low, medium and high values. Responses for some other limiting cases may be evaluated readily. For example, $Q_y/W = 0$ gives a linear isolator, and $T_1(U) = 0$ s gives a rigid structure with seismic responses simply related to the maximum responses of one-mass bilinear systems (Figure 4.5). Designs using other types of bilinear isolation systems may have parameter values well outside these ranges; for example, a sliding isolator may have $T_{b1} = 0$ s, $T_{b2} \approx \infty$ and $Q_y/W \approx 0.2$.

The structure was provided with a set of intermass velocity dampers which gave to each of the 4 higher free-free modes a damping factor of 0.05. The isolator velocity-damping coefficient C_b was chosen to give a yielding-phase isolator damping of $\zeta_{b2} = 0.05$, where $\zeta_{b2} = C_b T_{b2} / (4\pi M)$.

$T_1(U)$ is intended to be representative of the flexibility of the structural component of the overall isolated system, and has been defined as the first-mode period when the isolator stiffness is infinite. The maximum responses presented are the base displacement X_b , the top-mass modal accelerations $\ddot{X}_{5,1}$, $\ddot{X}_{5,2}$, and $\ddot{X}_{5,3}$ and the approximate mid-height shear $S_{av}(3,4)$ given by the average of the shears for springs 3 and 4. The modal responses are defined in terms of the free-free modes. Also shown, at the side of the first set of results, are the base displacements and base accelerations of a rigid structure, $T_1(U) = 0$, mounted on the various isolators.

Higher-mode maximum acceleration responses, $\ddot{X}_{r,n}$, $n > 1$

The maximum acceleration response of the top mass, number 5, was calculated for each mode using the modal sweeping technique (Section 4.3.4) with free-free mode shapes. These free-free mode shapes were only a fair approximation to the mode shapes with an isolator stiffness K_{b2} for the nine cases with $T_{b2} = 1.5$ s and $T_1(U) = 0.75$ s, since $I(K_{b2}) = 2.0$. For the remainder of the 81 cases, $I(K_{b2}) \geq 3$, and hence the free-free mode shapes were quite close to the shapes with an isolator stiffness K_{b2} .

Table 4.1 Maximum responses of uniform 5-mass shear structures isolated on various bilinear isolators when excited by the El Centro NS 1940 accelerogram. $\zeta_b = 0.05$, $\zeta_{FF,n} = 0.05$, $m_r = 1$ kg

(a)		$T_1(U) = 0.25$ s									$T_1(U) = 0$	
No.	T_{b1} (s)	T_{b2} (s)	Q_y/W (%)	X_b (m)	$\ddot{X}_{5,1}$ (m s ⁻²)	$\ddot{X}_{5,2}$ (m s ⁻²)	$\ddot{X}_{5,3}$ (m s ⁻²)	NL	$S_{av}(3, 4)$ (N)	X_b (m)	\ddot{X}_b (m s ⁻²)	
1	0.3	1.5	2	0.079	1.574	0.692	0.448	0.12	4.19	0.079	1.579	
2			5	0.052	1.388	1.929	0.768	0.33	4.79	0.053	1.412	
3			10	0.040	1.653	2.957	0.850	0.54	6.83	0.043	1.717	
4		3.0	2	0.125	0.751	0.820	0.476	0.26	2.17	0.126	0.754	
5			5	0.072	0.810	1.922	0.773	0.59	4.41	0.075	0.822	
6			10	0.051	1.205	2.993	0.985	0.77	7.32	0.056	1.221	
7		6.0	2	0.090	0.296	1.020	0.461	0.66	2.20	0.091	0.298	
8			5	0.087	0.590	1.995	0.704	0.82	4.50	0.078	0.591	
9			10	0.061	1.054	3.139	1.013	0.90	7.81	0.079	1.070	
10	0.6	1.5	2	0.081	1.594	0.478	0.261	0.10	4.14	0.082	1.611	
11			5	0.060	1.468	1.024	0.253	0.27	4.28	0.061	1.492	
12			10	0.053	1.759	1.661	0.466	0.39	5.22	0.053	1.753	
13		3.0	2	0.134	0.784	0.614	0.241	0.24	2.07	0.135	0.787	
14			5	0.081	0.835	1.289	0.308	0.54	3.37	0.087	0.841	
15			10	0.062	1.222	1.833	0.466	0.66	5.57	0.068	1.248	
16		6.0	2	0.096	0.307	0.636	0.304	0.62	1.70	0.100	0.312	
17			5	0.082	0.582	1.450	0.317	0.79	3.69	0.076	0.574	
18			10	0.072	1.058	1.822	0.488	0.80	5.61	0.085	1.072	
19	0.9	1.5	2	0.087	1.664	0.348	0.135	0.07	4.20	0.087	1.663	
20			5	0.071	1.560	0.723	0.138	0.17	4.17	0.072	1.588	
21			10	0.075	1.953	0.780	0.264	0.24	5.48	0.075	1.963	
22		3.0	2	0.145	0.819	0.522	0.118	0.21	0.211	NA	NA	
23			5	0.089	0.840	0.780	0.215	0.47	2.58	0.087	0.834	
24			10	0.079	1.247	0.960	0.254	0.53	3.99	0.080	1.253	
25		6.0	2	0.103	0.313	0.516	0.169	0.59	1.56	0.105	0.315	
26			5	0.127	0.627	0.793	0.200	0.70	2.54	0.122	0.621	
27			10	0.101	1.075	0.947	0.212	0.71	4.18	0.104	1.076	

It was found that in all cases, $\ddot{X}_{5,1}$, the maximum acceleration of mode 1 at level 5, was close to the isolator bilinear spectral accelerations with the structure treated as rigid, with mode-1 accelerations being moderately less when there was a large excitation of higher-mode accelerations. Without energy loss from mode 1, there should be agreement between mode-1 and spectral accelerations,

Table 4.1 (continued)

(b)		$T_1(U) = 0.5$ s								
No.	T_{b1} (s)	T_{b2} (s)	Q_y/W (%)	X_b (m)	$\ddot{X}_{5,1}$ (m s ⁻²)	$\ddot{X}_{5,2}$ (m s ⁻²)	$\ddot{X}_{5,3}$ (m s ⁻²)	NL	$S_{av}(3, 4)$ (N)	
1	0.3	1.5	2	0.074	1.495	0.991	0.839	0.13	4.29	
2			5	0.050	1.363	2.049	1.139	0.34	5.46	
3			10	0.043	1.699	2.810	2.154	0.53	7.05	
4		3.0	2	0.122	0.736	1.136	0.629	0.26	2.38	
5			5	0.067	0.789	2.017	1.313	0.61	4.39	
6			10	0.066	1.265	2.516	2.062	0.75	7.01	
7		6.0	2	0.084	0.296	1.266	0.869	0.66	2.37	
8			5	0.067	0.567	1.908	1.513	0.85	4.18	
9			10	0.075	1.067	2.382	2.068	0.89	7.02	
10	0.6	1.5	2	0.079	1.564	0.880	0.424	0.10	4.42	
11			5	0.059	1.461	1.639	0.961	0.27	4.92	
12			10	0.049	1.683	2.489	0.872	0.40	6.75	
13		3.0	2	0.131	0.767	1.047	0.521	0.24	2.45	
14			5	0.075	0.812	1.653	1.055	0.55	4.06	
15			10	0.055	1.186	2.676	1.202	0.66	6.78	
16		6.0	2	0.099	0.311	1.273	0.418	0.61	2.41	
17			5	0.088	0.589	1.511	1.068	0.79	3.99	
18			10	0.076	1.059	2.696	1.182	0.81	7.04	
19	0.9	1.5	2	0.088	1.676	0.832	0.269	0.07	4.56	
20			5	0.069	1.525	1.460	0.508	0.18	4.53	
21			10	0.070	1.866	1.926	0.518	0.24	6.07	
22		3.0	2	0.142	0.806	0.821	0.441	0.22	2.48	
23			5	0.088	0.841	1.497	0.635	0.47	3.62	
24			10	0.074	1.219	2.253	0.544	0.53	6.00	
25		6.0	2	0.103	0.312	0.759	0.288	0.59	1.68	
26			5	0.133	0.635	1.501	0.691	0.70	3.99	
27			10	0.095	1.068	2.369	0.626	0.71	6.31	

continued overleaf

since sweeping with free-free mode shapes assumes an undeformed or rigid structure for mode 1. The mode-1 accelerations were reduced from the values for the rigid superstructure model, presumably because a major source of higher-mode energy is due to transfer from mode 1 by non-linear mechanisms, as discussed earlier. The transfer, to higher modes, of energy associated with a small reduction in mode-1 accelerations is able to produce relatively large higher-mode accelerations,

Table 4.1 (continued)

(c)									
$T_1(U) = 0.75$ s									
No.	T_{b1} (s)	T_{b2} (s)	Q_y/W (%)	X_b (m)	$\ddot{X}_{5,1}$ (m s ⁻²)	$\ddot{X}_{5,2}$ (m s ⁻²)	$\ddot{X}_{5,3}$ (m s ⁻²)	<u>NL</u>	$S_{av}(3, 4)$ (N)
1	0.3	1.5	2	0.075	1.507	1.201	0.779	0.12	4.38
2			5	0.046	1.291	1.711	1.615	0.36	4.87
3			10	0.037	1.604	2.924	2.221	0.56	7.88
4		3.0	2	0.120	0.727	1.008	0.622	0.27	2.47
5			5	0.055	0.738	1.764	1.514	0.65	4.76
6			10	0.040	1.160	2.929	2.258	0.80	7.75
7		6.0	2	0.089	0.300	1.143	0.752	0.65	2.22
8			5	0.077	0.578	1.787	1.554	0.84	4.77
9			10	0.041	1.036	3.000	2.231	0.90	7.71
10	0.6	1.5	2	0.079	1.554	1.349	0.643	0.10	4.56
11			5	0.053	1.353	1.635	1.054	0.29	4.88
12			10	0.055	1.810	2.290	1.655	0.38	6.88
13		3.0	2	0.127	0.751	0.718	0.521	0.25	2.56
14			5	0.073	0.798	1.717	1.202	0.56	4.44
15			10	0.057	1.203	2.283	1.874	0.66	6.44
16		6.0	2	0.101	0.312	0.819	0.651	0.61	2.30
17			5	0.109	0.609	1.687	1.242	0.77	4.29
18			10	0.064	1.054	2.261	1.872	0.79	6.33
19	0.9	1.5	2	0.085	1.616	1.310	0.376	0.07	4.77
20			5	0.061	1.385	1.763	0.703	0.19	4.74
21			10	0.066	1.806	2.183	0.876	0.24	6.31
22		3.0	2	0.136	0.784	0.655	0.456	0.22	2.59
23			5	0.091	0.853	1.472	0.694	0.47	3.78
24			10	0.081	1.261	2.292	0.835	0.53	6.04
25		6.0	2	0.102	0.315	0.851	0.597	0.58	2.31
26			5	0.146	0.648	1.587	0.687	0.69	4.04
27			10	0.112	1.093	2.049	0.817	0.72	5.83

because higher modes require much smaller energies to achieve a given maximum acceleration. This ensures that although higher-mode responses may be severe, which is important for the overall distribution of shear and floor-response acceleration spectra, the mode-1 response which governs base shear and displacements is little affected by the interaction with higher modes, as observed.

We have found that three factors can be expected to contribute to the sometimes large maximum higher-mode accelerations $\ddot{X}_{5,n}$, for $n > 1$. These are the degree

of isolator non-linearity NL, the level of excitation of mode 1, and the size of the elastic-phase isolation factor $I(K_{b1})$. The first two factors are discussed below, while the role of $I(K_{b1})$ has been described in Section 4.3.4.

Some convenient generalisations follow from the results of the systematic study summarised in Table 4.1 and discussed below. The non-linearity factor NL may be regarded as a simplistic measure of the non-linearity which gives the contrasts between the seismic responses of structures with bilinear and with linear isolation. Other factors, such as the degree of excitation of mode 1, the elastic-phase isolation factor and bilinear loops of extreme shape, may then be regarded as features which modify the consequences of a given degree of non-linearity. Although simplistic in definition, the non-linearity factor gives simple approximate response relationships for a surprisingly large range of system parameters.

In quite general terms, as a result of trends towards equipartition of energy between the modes, a moderate degree of non-linear coupling between a high-energy vibration and other low-energy vibrations should tend to transfer energy to the low-energy vibrations at a rate which increases with the degree of non-linearity.

The maximum mode-1 acceleration $\ddot{X}_{5,1}$ gives some measure of the capacity of mode 1 to contribute to higher-mode accelerations $\ddot{X}_{5,n}$, for $n > 1$. We have found from the range of cases outlined in Table 4.1 that generally the ratios $\ddot{X}_{5,n}/\ddot{X}_{5,1}$ are more simply related to system parameters than is $\ddot{X}_{5,n}$. An exception is when $T_{b2} = 6.0$ s, when the large changes of $\ddot{X}_{5,1}$ with the yield ratio Q_y/W (Figure 4.5) are accompanied by substantially smaller changes in $\ddot{X}_{5,n}$, and the ratio $\ddot{X}_{5,n}/\ddot{X}_{5,1}$ masks the direction of changes in $\ddot{X}_{5,n}$. However, it is still convenient to present maximum higher-mode accelerations as a fraction of the maximum mode-1 acceleration with the same system parameters $T_1(U)$, T_{b1} , T_{b2} and Q_y/W . Moreover, approximate values for $\ddot{X}_{5,1}$ can be obtained from the responses of one-degree-of-freedom systems. As shown by Equation (4.195), the higher-mode responses are driven by the base shear, which is proportional to the first-mode acceleration, so it is physically reasonable that the strength of the first-mode response affects the strength of the higher-mode responses.

The elastic-phase isolation factor $I(K_{b1})$ plays an important role in the excitation of higher modes, as discussed in Section 4.3.4. Small $I(K_{b1})$ values give the contrast between the shapes of elastic-phase and yielding-phase mode 1, which is the basis of the transfer of mode-1 motions to higher-mode motions. A small elastic-phase isolation factor is also associated with increased elastic-phase participation factors of higher modes and hence increases their direct seismic excitation. Such motions are then transferred to yielding-phase modes, mostly to those of the same or similar mode number.

The maximum accelerations for higher modes 2 and 3, namely $\ddot{X}_{5,2}$ and $\ddot{X}_{5,3}$ listed in Table 4.1, have been plotted as fractions of mode-1 accelerations $\ddot{X}_{5,1}$ in Figure 4.12, as functions of the non-linearity factor NL and the elastic-phase isolation factor $I(K_{b1})$. It is seen that for most cases the ratios $\ddot{X}_{5,n}/\ddot{X}_{5,1}$ increase approximately linearly with NL for a given value of $I(K_{b1})$, although there is

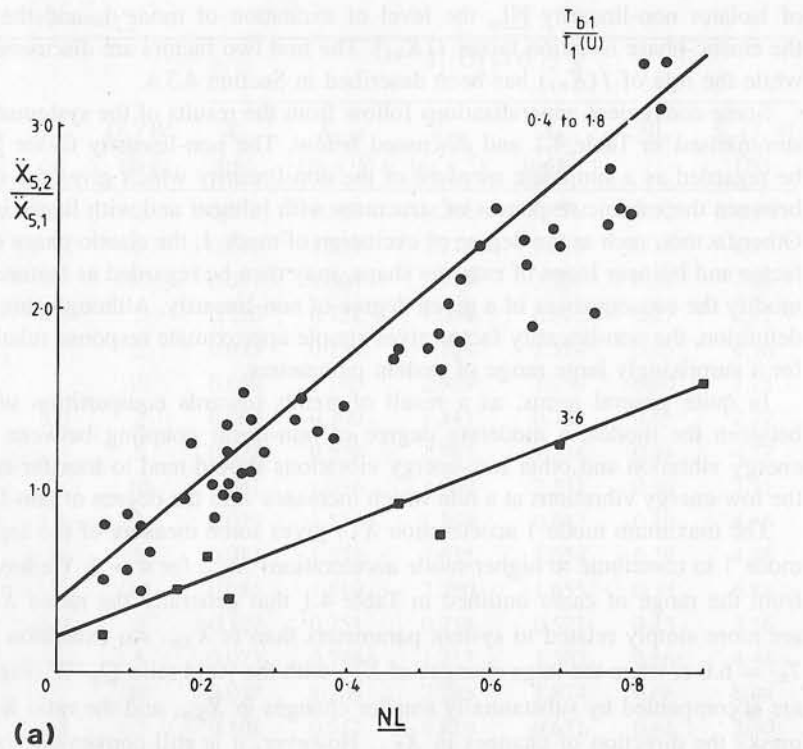


Figure 4.12 Ratios of higher-mode to first-mode acceleration responses to El Centro NS 1940 for 63 of the bilinear isolation systems given in Table 4.1. The top acceleration ratios are plotted against the isolator non-linearity factor NL , and grouped in terms of the elastic-phase isolation factor $T_{b1}/T_1(U)$. For later design-guide purposes, groups of responses are approximated by the near upper envelope lines shown. (a) Second-mode acceleration responses. (b) Second-mode acceleration responses. (c) Third-mode acceleration responses. (d) Third-mode acceleration responses

a fair degree of scatter. Notable exceptions occur when $T_{b2} = 6.0$ s, when the exceptionally small values of $\ddot{X}_{5,1}$ for $Q_y/W = 0.02$ give ratio values well above the linear trend lines. Again the rapid increase in $\ddot{X}_{5,1}$ as Q_y/W is increased from 0.05 to 0.10 tends to give ratio values below the trend line. Some of the more extreme values for $T_{b2} = 6$ s have been excluded from the plots of Figure 4.12, but results for all cases are given in Table 4.1. Hence, where the trend curves are used as a design guide (Figure 5.3(a)), they should not be used to estimate the maximum higher-mode accelerations for the parameter combination of $T_{b2} > 3.0$ s and $Q_y/W < 0.05$. Also, estimates of the higher-mode responses for cases where $Q_y/W = 0.10$ may be quite conservative.

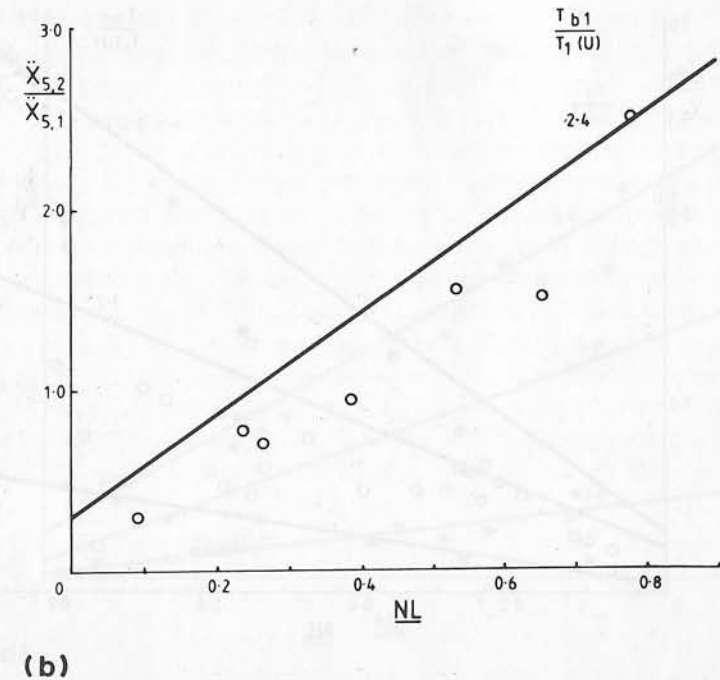


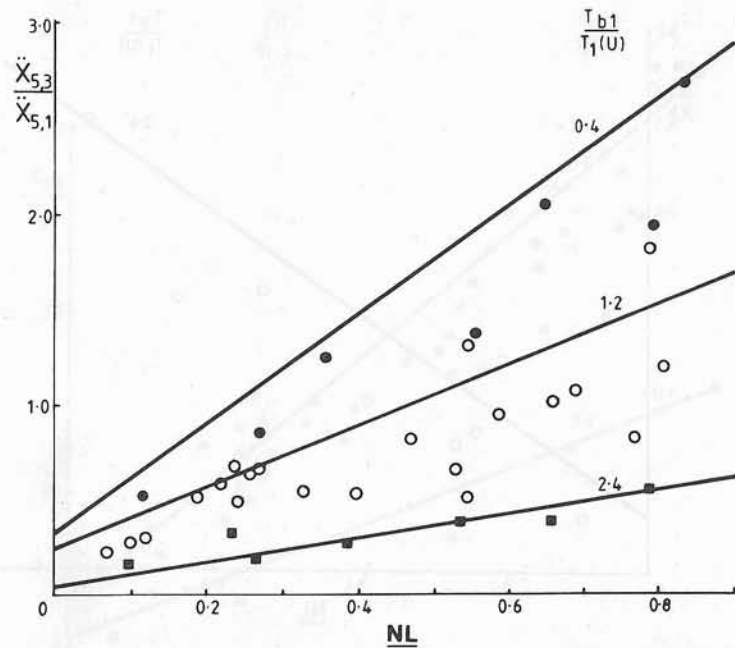
Figure 4.12 (continued)

Distribution of seismic shears

For linear isolation systems with isolation factors $I = T_b/T_1(U)$ of about 2 or greater, the overall seismic response can be approximated very well by the first-mode response, since the higher-mode participation factors are near zero. For a uniform structure, the first-mode shear distribution is approximately triangular, from zero at the top to a maximum value at the base. Also, the base shear can be found approximately by using a simple one-mass model, with the structure represented as a rigid mass supported on the isolator.

For non-linear isolation systems, the base shear can be found approximately from a one-mass rigid structure model, but the shear distribution is generally more complicated than a triangular distribution. We have shown in the previous section that the maximum acceleration responses in the higher modes can be up to several times the maximum first-mode responses, with the ratio of the higher-mode to first-mode responses depending primarily on the isolation ratio in the unyielded phase of the response, i.e. $T_{b1}/T_1(U)$, and the non-linearity factor NL . Thus the contributions of the higher modes to the shears may be significant at various positions in the structure.

For modes defined in terms of the post-yield stiffness K_{b2} of the isolator, the shapes of the shear distributions for all modes are the same as for a linear system

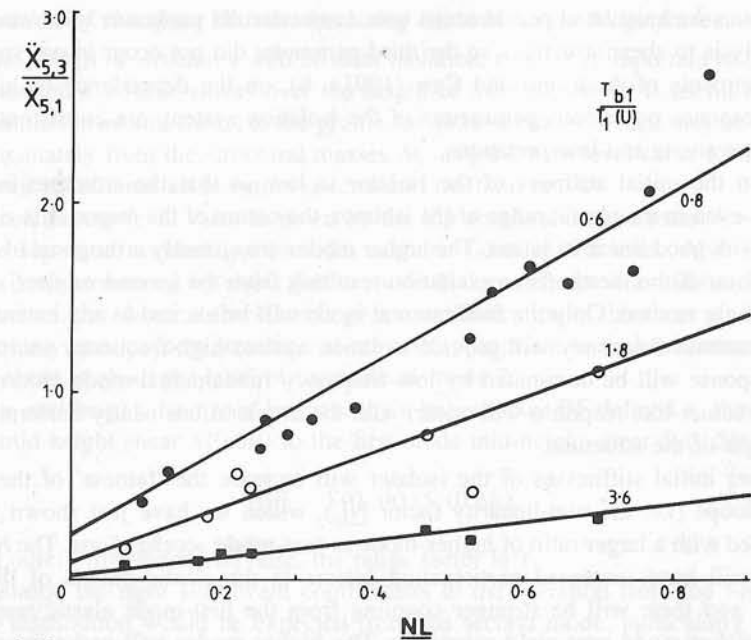


(c)

Figure 4.12 (continued)

with an isolation factor corresponding to $T_{b2}/T_1(U)$. Typical distributions are as plotted for a linear isolation system in Figure 4.3. In common with structures with linear isolation systems, structures with non-linear isolation have shear distributions for modes higher than the first with a zero just above the base, giving higher-mode base shears generally much smaller than the first-mode base shear. Thus the base shears for systems with non-linear isolators are essentially the same as the first-mode shears, as for well isolated linear systems. However, this result arises because of the near-nodal nature of the shear distributions at the base, rather than because the shear distributions in the higher modes are negligible. At positions other than the base, the contributions of the higher modes must usually be taken into account to obtain adequate estimates of the shears.

The contributions of the higher-mode shears will be most important at the antinodes of the higher-mode shear distributions. Since the shear is proportional to an integration of the acceleration or displacement profile from the top of the structure to the point of interest, the antinodes of the modal shear distributions occur at the nodes of the acceleration or displacement modal profiles. For a uniform structure, the second-mode shear distribution has a maximum near mid-height (exactly at mid-height for a free-free system with zero base stiffness). It is thus to be



(d)

Figure 4.12 (continued)

expected that the shear profile for a structure with non-linear isolation, in which higher-mode effects are important, will depart significantly from the triangular distribution expected for a system with a high degree of linear isolation, with a bulge in the shear distribution in the mid-height region of the structure. Such bulged shear distributions are shown for cases (iv) to (vii) of Figure 2.7.

Lee and Medland (1978a, b) pointed out the bulge in the shear distributions for structures on non-linear isolators, recognised that it was caused by higher-mode contributions, and quantified it in terms of a 'bulge defining parameter'. They discussed the relative importance of modes higher than the first in unisolated structures and in structures with bilinear isolation. They also considered the effects of higher modes on the responses of appendages.

Andriono and Carr (1991a, b) recently performed a systematic study of the lateral force distribution in structures with non-linear isolation. They found that the non-linearity factor \underline{NL} (which they described as the hysteresis loop ratio ' R '), the fundamental period of the structure when unisolated, and the amount of frame action in the superstructure were the three factors which have the major influences on the shape of the shear distribution. These results are in line with our own. We have presented the non-linearity factor as being a major parameter governing the higher-mode response, which in turn determines the shape of the shear distribution. We have preferred to use the ratio of the first-mode isolated and unisolated periods

rather than the unisolated period on its own as our second parameter. We restricted our analysis to shear structures so the third parameter did not occur in our studies. The comments of Andriano and Carr (1991a, b), on the dependence of higher-mode response on various parameters of the isolation system, are consistent with our observations and interpretations.

When the initial stiffness of the isolator is low so that the structure is well isolated even in the elastic range of the isolator, the nature of the response is similar to that with good linear isolation. The higher modes are virtually orthogonal to some distribution of the inertia force excitation resulting from the ground motion, so are not strongly excited. Only the fundamental mode will be excited to any extent, and its low natural frequency will provide isolation against high-frequency excitation. The response will be dominated by low-frequency fundamental-mode motions. A rigid-structure-like response will occur, with the accelerations nearly uniform over the height of the structure.

Higher initial stiffnesses of the isolator will increase the 'fatness' of the hysteresis loops (i.e. the non-linearity factor \underline{NL}), which we have just shown to be correlated with a larger ratio of higher-mode to first-mode accelerations. The higher modes will have increased participation factors in the elastic phases of the response, and there will be stronger coupling from the first-mode elastic response to the higher-mode post-yield responses. The higher modes will make important contributions to the response, resulting in a bulged shear distribution.

Increasing the yield strength or decreasing the post-yield stiffness also leads to fatter hysteresis loops with larger non-linearity factors, and hence to stronger higher-mode responses.

As the shapes for the modal shear distributions can be approximated by half-cycle sine-waves, maximum shear envelopes can be estimated if the strength of the individual modal components and appropriate modal combination rules can be established.

The traditional modal combination rule is the square-root-of-sum-of-squares (SRSS) (Der Kiureghian, 1980a, b). This rule is based on uncorrelated modal responses, which are often obtained with well separated modal frequencies. Although structures with non-linear isolation have well separated frequencies, the higher-mode responses may be correlated, in that the post-yield mode shapes are very similar to the free-free mode shapes, and we have shown in Section 4.3.4 that the higher-mode free-free responses are driven by the first-mode acceleration.

The SRSS modal combination method has been tested for the top mass acceleration for the 27 cases with $T_1(U) = 0.5$ s in Table 4.1. It was found that the true peak accelerations exceeded the SRSS values by a factor which increased with both the non-linearity factor \underline{NL} and the yield-ratio Q_y/W , with typical but by no means constant acceleration ratios of 1.13, 1.3 and 1.4 for Q_y/W values of 0.02, 0.05 and 0.10, when \underline{NL} exceeds 0.5. Problems with selecting an appropriate modal combination rule have led to attempts to estimate the shear envelopes by other methods as described below.

Estimation of the shear distribution using the mid-height bulge factor

For the design of structures with bilinear isolation, it is often important to estimate the maximum seismic shears over the height of the structure. It is useful to relate the profile for overall shears to the profile for mode-1 shears, which may be derived approximately from the structural masses M_r and the base level shear for mode 1, as given by bilinear acceleration spectra and the total mass.

Since the top-level shear is given by the top acceleration and mass, knowledge of the top-mass acceleration provides a shear value at this level. Also the base shear is approximated by shear due to mode 1 alone. Hence if a mid-height shear is obtained, the shears at three levels give some indication of the shear profile. (For moderately non-uniform structures it may be appropriate to find the intermediate-level shear at about the level of the node of mode 2.)

The mid-height shear may be given by a bulge factor \underline{BF} defined as the ratio of total mid-height shear $S(0.5h)$ to the first-mode mid-height shear $S_1(0.5h)$.

$$\underline{BF} = S(0.5h)/S_1(0.5h). \quad (4.196)$$

For a purely first-mode response, the bulge factor is 1.

Usually, the most significant contribution to the variation from the first-mode shear distribution would be expected from the second mode, particularly at mid-height where the mode-2 shear distribution has a maximum. The mid-height shear could be estimated from a SRSS combination of the first- and second-mode contributions, but the SRSS approach using all modes appears to give poor results for structures with bilinear isolation. Also, modes higher than the second also contribute.

As a generalisation of the SRSS combination of the first two modes to estimate the shear at mid-height, we have sought a correlation between the bulge factor \underline{BF} and the ratio of the first-mode to second mode top-mass accelerations of the form

$$\underline{BF} = \sqrt{1 + a(\ddot{X}_{N,2}/\ddot{X}_{N,1})^2}. \quad (4.197)$$

The relationship between the mid-height bulge factor \underline{BF} and the ratio of second- to first-mode top acceleration $\ddot{X}_{5,2}/\ddot{X}_{5,1}$ was examined for the 81 case studies of uniform shear structures with bilinear isolation (Table 4.1).

As shown in Figure 4.13, it was found that, when most isolators with $T_{b2} = 6.0$ s were excluded, then Equation (4.197) with $a = 0.85$ gave a good fit for the bulge factors for $T_1(U) = 0.25$ s or 0.75 s. However, it somewhat overestimated the bulge factors for $T_1(U) = 0.5$ s, when the bulge factor was approximated better by taking $a = 0.6$.

For cases with $T_{b2} = 6.0$ s, a number of mid-height bulge factors were considerably less than given by Equation (4.197), while some were moderately greater (when $Q_y/W = 0.02$). This approach is therefore qualitative only, but useful in many cases.

For the 81 cases the bulge factors were calculated in two ways. First the bulge factors were calculated at the exact mid-height, that is with half of the mass-3 forces

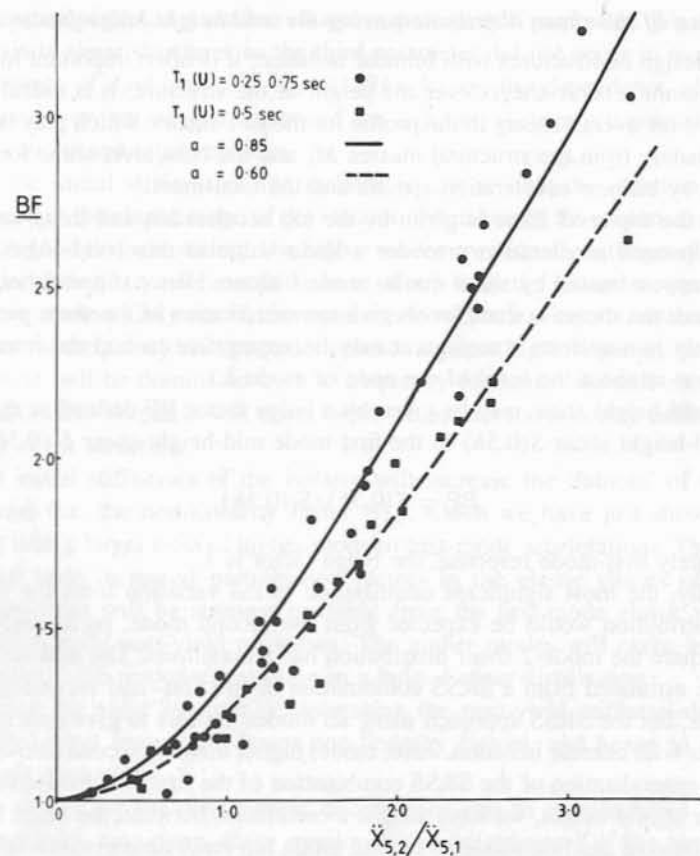


Figure 4.13 Mid-height shear bulge factor \underline{BF} as a function of the top-level acceleration ratio $\ddot{X}_{5,2}/\ddot{X}_{5,1}$ for 63 of the bilinear isolation systems shown in Table 4.1, together with the relationship $\underline{BF} = \sqrt{1 + a(\ddot{X}_{5,2}/\ddot{X}_{5,1})^2}$ and the best-fit values of 'a'

included in the shear values. Since modal shears were based on free-free values, modes 3 and 5 had shear nodes at the mid-height and therefore did not contribute to the computed mid-height bulge factor. Secondly, the mid-height bulge factors were computed using the mean of the shears just above and below mass 3. This is denoted $S_{av}(3, 4)$ in Table 4.1. This approach has some contribution from all five modes. The two approaches gave much the same relationship between the mid-height bulge factors and the top accelerations as expressed by Equation (4.197). The second approach using average near-mid-height shears showed somewhat less scatter from the trend lines given by Equation (4.197).

This approach of estimating the overall shear distribution in terms of the mid-height bulge factor, with the top and base shear already known, has been used in the preliminary design procedure presented in Chapter 5.

Estimation of the shear distribution in terms of exponent p and non-linearity factor \underline{NL}

Use, in design, of the method based on the mid-height bulge factor requires an estimate of $\ddot{X}_{N,2}/\ddot{X}_{N,1}$ from the non-linearity factor \underline{NL} and the elastic-phase isolation factor $I(K_{b1}) = T_{b1}/T_1(U)$, and then the use of an equation of the form (4.197) to obtain \underline{BF} in terms of $\ddot{X}_{N,2}/\ddot{X}_{N,1}$.

Andriono and Carr (1991a) give an approach for obtaining the shear distribution directly from the non-linearity factor \underline{NL} (which they call the hysteretic shape ratio 'R') and the unisolated period $T_1(U)$. They quantified the shear distribution in terms of an exponent p describing a power-law variation of acceleration with height in the structure. They enveloped the equivalent lateral force distribution by a distribution given by

$$F_i = V \frac{W_i h_i^p}{\sum W_i h_i^p} \quad (4.198a)$$

where F_i is the inertia force at level i , V is the base shear, W_i the floor weight and h_i the height of the floor from the base.

For a constant acceleration distribution, corresponding to a structure with a high degree of linear isolation, $p = 0$. With non-linear isolation, the accelerations usually increase towards the top of the structure, corresponding to a positive value of p . The exponent p was found to be highly correlated with the hysteretic shape ratio R (non-linearity factor) for a given unisolated first-mode period. Regression analyses were performed to obtain p as a linear function of R

$$p = A + BR. \quad (4.198b)$$

This expression was usually fitted with a high correlation coefficient. For a given value of R , the exponent p was found to be larger for greater values of $T_1(U)$, in line with the general conclusion that higher-mode effects are more important when the structure is more flexible with respect to the isolation system. The correlations were found to be earthquake dependent (Andriono and Carr, 1991a, Figure 14). The approach is used as part of a design procedure recommended by Andriono and Carr (1991b), to find the overall shear distribution once the base shear and displacement have been estimated.

4.4 SEISMIC RESPONSES OF LOW-MASS SECONDARY STRUCTURES

4.4.1 Introduction

Importance of secondary-structure seismic responses

Many structures contain subsystems, or secondary structures, which are essential for their design functions; in some cases the main role of a structure is to protect the systems which it contains. These secondary systems can pose significant

seismic design problems, in that they may suffer much more severe seismic attack when mounted (above ground level) in a structure than they would experience if mounted on the ground. Greatly increased responses can occur when a secondary system has a natural frequency tuned to a natural frequency of the primary system, so that it is excited by a nearly sinusoidal support motion to which it responds resonantly. On the other hand, those secondary structures which are within appropriately isolated primary structures may experience much lower seismic attack than they would if ground mounted, because the support motions have both their amplitudes reduced and their dominant frequencies much lower than the natural frequencies of the secondary systems. Some types of seismic isolation system can reduce the earthquake response of secondary structures by an even greater factor than that by which they reduce the response of the primary supporting structure. For some important systems which are seismically vulnerable, installation within an appropriately isolated structure may be the only really effective means of providing protection from seismic attack.

Features of secondary-structure seismic responses

The general features of the seismic responses of a secondary structure may be outlined as follows. A secondary structure with very low mass compared with that of its supporting structure responds to the accelerations of its supporting floor in the same way that the structure itself responds to the seismic accelerations of the ground. However, floor accelerations differ in severity and character from the typical noise-like ground accelerations which generate them. For first-mode structural periods up to about 1.0 s, floor accelerations are typically more severe and of longer duration than ground accelerations. Also, floor accelerations are more periodic, being concentrated within frequency bands centred on the frequencies of prominent structural modes. As a result, the seismic attack on secondary structures is frequency selective, with more severe attacks on those secondary structures that have a frequency close to that of a prominent primary mode.

The traditional approach to determining the maximum response of secondary systems with a single attachment point is through floor-response spectra calculated by neglecting any interaction between the primary and secondary structure, as discussed in Section 2.1. These spectra provide a convenient summary of the frequency characteristics of the support-point motion, and such spectra are compared for different isolation systems in Section 4.4.5, but the neglected interaction effects can be important even when the ratio of the mass of the secondary system to that of the primary structure is low.

Three important factors which determine the responses of secondary structures to floor accelerations have been highlighted (Igusa and Der Kiureghian, 1985a). These factors are tuning, interaction and non-classical composite modes. When a secondary mode has its frequency tuned to a primary-mode frequency, its responses to the accelerations of that primary mode are much more severe than the primary-mode motions of its support. For increasing ratios of the effective mass

of a secondary mode to that of the primary structure, the tuned responses of the secondary system are reduced by interaction between the tuned primary and secondary modes. Finally, when the damping of a primary mode is different from the damping of a tuned secondary mode, the pair of natural modes, given by the composite action of the primary and secondary 'modes', are non-classical. These non-classical mode shapes influence the extent to which a secondary mass reduces a tuned secondary-mode response. In its simplest form, a secondary structure supported by a primary structure can be modelled as a two-mass structural system with a very small mass ratio, as shown in Figure 4.14. For small mass ratios, it is convenient to express seismic responses, to a good approximation, in terms of the independent modal features which the primary and secondary structures would have if they were separately mounted on the ground. These independent modal features are given in Figure 4.14 for the simple two-mass system.

The main features of the seismic responses of a secondary structure are most easily derived and understood in terms of the responses of this simple two-mass system. The above factors of tuning, interaction and non-classical mode shapes are included in the derivation of the two-mass responses, for which the results are given below.

The effects of a significant mass-ratio on a secondary-mode response may be provided for by using the mass ratio as one of the parameters in the floor spectra defined by the seismic responses of a two-mass primary and secondary structure. The floor spectra for a particular design earthquake may be found by computing the peak accelerations of the secondary mass when the two-mass system responds to the earthquake accelerogram. Alternatively, floor spectra may be related to ground spectra by factors which are derived using a statistically defined approximation to the accelerogram, as described below, or by modal combination rules which account for closely tuned, non-classical, interacting modes.

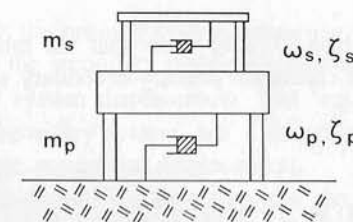


Figure 4.14 Model defining the parameters of a linear 2-mass primary-secondary system. The frequency and damping parameters apply when the systems are mounted separately on rigid ground

4.4.2 Seismic responses of two-degree-of-freedom secondary and primary structural systems

Problems with tuned secondary-structure modes

For a near-tuned secondary structure with a very low mass ratio it is not satisfactory to derive the maximum responses of the secondary structure using a square-root-sum-of-squares (SRSS) combination of the response spectrum values for the modes, as described in Section 2.4.4. Each of the two modes includes both secondary and primary mass motions. For a tuned secondary structure the mode shapes become extreme, with the secondary mass displacements very much greater than the primary mass displacements. The correlation between the appendage-mass responses for the two modes approaches -1 . Moreover, these extreme mode shapes are generally non-classical.

A response spectrum approach can be restored by deriving floor spectra based on a two-degree-of-freedom, '2DOF', model of the mode and the near-tuned appendage. For particular earthquake accelerograms, time-history analysis may be used to find the responses of the 2DOF model as described by Penzien and Chopra (1965) and Skinner *et al.* (1965). Such 2DOF spectra are difficult to apply in practice. For a given earthquake, they have five parameters, including the mass ratio. They call for time-history analysis for each design earthquake, since they cannot be derived from individual or average earthquake response spectra. These difficulties may be avoided by using an approach based on statistically-defined earthquake accelerations (Igusa and Der Kiureghian, 1985a) as described below.

General modal features of 2-mass primary-secondary systems

The peak responses of a secondary-structure mode, to the seismic motions of a primary-structure mode, follow simply from the seismic responses of an equivalent 2DOF system, as shown in Figure 4.14, with a secondary mass m_s of frequency ω_s and damping ζ_s mounted on a primary mass m_p of frequency ω_p and damping ζ_p . The peak responses of the 1-mass secondary structure or appendage, as a function of ω_s and ζ_s , are given by the floor spectra of the one-mass primary structure.

Igusa and Der Kiureghian (1985a) show that the modal shapes, frequencies and damping ratios of the combined primary-secondary system can be expressed as

$$\omega_i = \omega_a \left\{ 1 \pm 1/2 \operatorname{sgn}(\beta) \operatorname{Re} \sqrt{\gamma + \left[i \left(\frac{\omega_p}{\omega_a} \zeta_p - \frac{\omega_s}{\omega_a} \zeta_s \right) + \beta \right]^2} \right\} \quad (4.199)$$

$$\zeta_i = \frac{\omega_a}{2\omega_i} \left\{ \frac{\omega_p}{\omega_a} \zeta_p + \frac{\omega_s}{\omega_a} \zeta_s \pm \operatorname{sgn}(\beta) \operatorname{Im} \sqrt{\gamma + \left[i \left(\frac{\omega_p}{\omega_a} \zeta_p - \frac{\omega_s}{\omega_a} \zeta_s \right) + \beta \right]^2} \right\} \quad (4.200)$$

$$\phi_1 = \left\{ \begin{array}{l} -\frac{\omega_a^2}{\omega_s^2} \beta - i \frac{\omega_p}{\omega_s} \delta_d - \operatorname{sgn}(\beta) \sqrt{\gamma + \left(i \frac{\omega_p}{\omega_s} \delta_d + \frac{\omega_a^2}{\omega_s^2} \beta \right)^2} \\ 1 \end{array} \right\} \quad (4.201a)$$

$$\phi_2 = \left\{ \begin{array}{l} -\frac{\omega_a^2}{\omega_s^2} \beta - i \delta_d + \operatorname{sgn}(\beta) \sqrt{\gamma + \left(i \delta_d + \frac{\omega_a^2}{\omega_s^2} \beta \right)^2} \\ 1 \end{array} \right\} \quad (4.201b)$$

where $\beta = (\omega_p - \omega_s)/\omega_a$ is the tuning parameter, $\gamma = m_s/m_p$ is the interaction parameter and $\delta_d = (\zeta_p - (\omega_p/\omega_s)\zeta_s) \omega_p/\omega_s$ is the non-classical damping parameter with average frequency

$$\omega_a = \frac{\omega_p + \omega_s}{2}$$

average damping

$$\zeta_a = \frac{\zeta_p + \zeta_s}{2}$$

and damping difference

$$\zeta_d = \zeta_p - \zeta_s.$$

The first and second elements of the mode-shape vectors correspond to the primary and secondary degrees of freedom respectively. ϕ_1 is related to the primary structure, (the 'structural' mode shape), and ϕ_2 is the secondary structure, or 'equipment', mode shape.

When the secondary system is detuned from the primary system, i.e. where there is a large separation between their natural frequencies so that β is large compared with the mass ratio γ and dampings ζ_p and ζ_s , the frequencies and damping ratios of the two modes of the combined system are essentially those of the individual systems. Both modes of the combined system are also (almost) real, i.e. the overall system is (almost) classically damped.

Detuned modes

The detuned mode with the primary system frequency (the 'structural mode') has a mode shape in which the secondary system displacement is a factor of $\omega_s^2/(\omega_s^2 - \omega_p^2)$ times the primary system displacement. The 'equipment mode', which has the frequency of the secondary system, has a structural displacement a factor of $\gamma\omega_s^2/(\omega_p^2 - \omega_s^2)$ times the equipment displacement.

The amount of excitation of the structure and the equipment in each of the detuned modes is proportional to the participation-factor vector. The nature of these vectors depends on whether the secondary system is stiff with respect to the primary system ($\omega_s \gg \omega_p$) or whether it is flexible ($\omega_s \ll \omega_p$). The mode shapes produce the participation factors summarised below, where the structural degree of freedom is the first element of each vector.

Table 4.2 Approximate participation factors for detuned primary-secondary systems

	Primary (Structural) mode $\omega_1 \approx \omega_p, \zeta_1 \approx \zeta_p$	Secondary (Equipment) mode $\omega_2 \approx \omega_s, \zeta_2 \approx \zeta_s$
$\omega_s \gg \omega_p$	$\Gamma_1 \approx \begin{pmatrix} 1 \\ 1 + \frac{\omega_p^2}{\omega_s^2} \end{pmatrix}$	$\Gamma_2 \approx \begin{pmatrix} \frac{\gamma \omega_p^2}{\omega_s^2} \\ -\frac{\omega_p^2}{\omega_s^2} \end{pmatrix}$
$\omega_s \ll \omega_p$	$\Gamma_1 \approx \begin{pmatrix} 1 \\ -\frac{\omega_s^2}{\omega_p^2} \end{pmatrix}$	$\Gamma_2 \approx \begin{pmatrix} \frac{\gamma \omega_s^2}{\omega_p^2} \\ 1 + \frac{\omega_s^2}{\omega_p^2} \end{pmatrix}$

As seen in Table 4.2, for a stiff secondary system detuned from the primary system $\omega_s \gg \omega_p$. In the structural mode the secondary system moves virtually with its support point, with a participation factor of slightly greater than unity, while the equipment mode has low participation factors for both the primary and secondary system masses. For a flexible secondary system ($\omega_s \ll \omega_p$), the structural mode involves little displacement of the equipment with respect to the ground, with the structure having a participation factor of unity, while the equipment mode involves little displacement of the structure, with the equipment having a participation factor near unity, i.e. the structure and equipment respond directly to the ground motion with their own natural frequencies and dampings. For detuned systems, none of the participation factors substantially exceeds unity, and some are considerably less than this. As the mode shapes are (almost) real for these detuned systems, and their natural frequencies are well separated, their responses can be calculated by standard response spectrum methods with SRSS combination of modal responses. The nature of the results differs, depending on whether the frequency of the secondary system is much greater or much smaller than that of the primary structure.

For the relatively 'stiff' appendage, with $\omega_s \gg \omega_p$, using the above expressions for the participation factors leads to the following SRSS expression (Der Kiureghian, 1980) for the peak acceleration response of the secondary system mounted on the primary system:

$$\begin{aligned} \ddot{X}_{ps} &= \sqrt{\left(1 + \frac{\omega_p^2}{\omega_s^2}\right)^2 S_A^2(\omega_p, \zeta_p) + \left(\frac{\omega_p}{\omega_s}\right)^4 S_A^2(\omega_s, \zeta_s)} \\ &\approx S_A(\omega_p, \zeta_p) \left[1 + \frac{\omega_p^2}{\omega_s^2} + \frac{1}{2} \left(\frac{\omega_p}{\omega_s}\right)^4 \left(1 + \frac{S_A^2(\omega_s, \zeta_s)}{S_A^2(\omega_p, \zeta_p)}\right)\right]. \end{aligned} \quad (4.202)$$

In this case, the equipment responds rigidly with the structure, so has essentially

the same response as its support point. Damping in the equipment has little effect on its absolute acceleration response. The ratio of the structure-mounted equipment response to its response if ground mounted is approximately $S_A(\omega_p, \zeta_p)/S_A(\omega_s, \zeta_s)$. This is the usual situation for equipment mounted in seismically isolated structures. As $\omega_p \ll \omega_s$ and usually $\zeta_p \gg \zeta_s$, the equipment response can be significantly less than when it is ground mounted. If the equipment was tuned to the first mode of the unisolated structure, its response would have been much stronger than its ground-mounted response.

For a flexible appendage, $\omega_s \ll \omega_p$

$$\begin{aligned} \ddot{X}_{ps} &= \sqrt{\left(\frac{\omega_s}{\omega_p}\right)^4 S_A^2(\omega_p, \zeta_p) + \left(1 + \frac{\omega_s^2}{\omega_p^2}\right)^2 S_A^2(\omega_s, \zeta_s)} \\ &\approx S_A(\omega_s, \zeta_s) \left[1 + \frac{\omega_s^2}{\omega_p^2} + \frac{1}{2} \left(\frac{\omega_s}{\omega_p}\right)^4 \frac{S_A^2(\omega_p, \zeta_p)}{S_A^2(\omega_s, \zeta_s)}\right]. \end{aligned} \quad (4.203)$$

The maximum absolute acceleration response is essentially the same as that of the ground-mounted equipment. The effect on flexible equipment of introducing isolation to the structure would be to move from the case of $\omega_s \ll \omega_p$ for the unisolated structure to $\omega_s = \omega_p$ for the isolated structure. As has been shown in a discussion of perfectly tuned systems (Skinner and McVerry, 1992), the equipment tuned to the isolated structure would have two to three times its ground-mounted response, so also two to three times its response in an unisolated structure. However, for an isolated structure, ω_s is small and hence $S_A(\omega_s, \zeta_s)$ is generally small in absolute terms. The floor-response spectra of Figure 2.7 show the reduction in appendage responses in isolated structures compared with those in an unisolated structure.

Features of tuned modes

For well tuned primary and secondary systems, in which the tuning parameter $\beta = (\omega_p - \omega_s)/\omega_a$ is sufficiently small, the nature of the response is considerably different. The complex frequencies of the two modes of the system are located close to, and symmetrically about, the average complex frequency of the primary and secondary systems.

For small mass ratios γ , the complex frequencies of the two modes are close to those of the primary and secondary systems, diverging from these values for larger γ . For small γ , the equipment mode involves little structural motion.

For perfectly tuned systems, in which $\beta = 0$, the nature of the complex frequencies depends on the relative size of the mass ratio γ and the square of the damping difference ζ_d^2 . For $\beta = 0$ and $\zeta_d^2 < \gamma$, the two modes have equal damping ratios ζ_a but different natural frequencies. For $\beta = 0$ and $\zeta_d^2 > \gamma$, the frequencies are both equal to ω_a but the damping ratios are different, and there is a 90° phase difference between the motions of the equipment and the structure in both modes.

The imaginary components of the mode shapes for tuned systems are significant unless the damping difference ζ_d is zero, which is the only case where the mode shapes are real-valued, corresponding to classical damping. If the damping ratios of the primary and secondary systems are equal, the damping for the two combined modes takes the same value.

To illustrate the potential for high amplification with a tuned secondary system, consider the participation factors when ζ_d is zero. For this case the tuned mode shapes are $(\alpha_i, 1)^T$ where $\alpha_i = -\beta \mp \sqrt{\gamma + \beta^2}$. The participation factor vectors are

$$\Gamma_i = \frac{\alpha_i + \gamma}{\alpha_i^2 + \gamma} \begin{pmatrix} \alpha_i \\ 1 \end{pmatrix}. \quad (4.204)$$

For the completely tuned case, $\beta = 0$, $\alpha_i = \mp \sqrt{\gamma}$ and the participation factors are

$$\begin{aligned} \Gamma_i &= \frac{\gamma \mp \sqrt{\gamma}}{2\gamma} \begin{pmatrix} \mp \sqrt{\gamma} \\ 1 \end{pmatrix} = \frac{1}{2} \begin{pmatrix} 1 \mp \sqrt{\gamma} \\ \mp \frac{1}{\sqrt{\gamma}} + 1 \end{pmatrix} \\ &\approx \frac{1}{2} \begin{pmatrix} 1 \\ \mp \frac{1}{\sqrt{\gamma}} \end{pmatrix}. \end{aligned} \quad (4.205)$$

For low mass ratios γ , the equipment participation factor is very high in both modes and of almost equal amplitudes but opposite signs.

The effect of the degree of tuning on the participation factors can also be investigated for $\zeta_d = 0$ as the mass ratio γ goes to zero. The structural-mode participation factor vector is $(1, -1/(2\beta))^T$ while that for the equipment mode is $(0, 1 + 1/(2\beta))^T$. For small β , but $\beta^2 \gg \gamma$, the equipment participation factor is again high but of almost equal amplitude and opposite sign in the two modes.

For equal damping $\zeta_p = \zeta_s$ so that $\zeta_d = 0$, and for very small γ and β , there is a large measure of cancellation between the secondary-mass responses of the two modes. As shown below, the response for the combined modes is limited by the damping in the system, for β and γ sufficiently small. Moreover, if the parameters are $\beta = \gamma = 0$ with the dampings $\zeta_p = \zeta_s = 0$ also, the peak response is still limited, usually at a very high value, by the duration of the excitation.

The nearly tuned systems have close modal frequencies and, except for the case $\zeta_d = 0$, have non-classical modes. Hence their responses cannot be calculated by the standard response-spectrum methods.

4.4.3 Seismic response of a multimode secondary structure on a multimode primary structure

Parameters of multi-mode primary-secondary systems

Igusa and Der Kiureghian (1985b) extended the analysis of two-degree-of-freedom

equipment-structure systems to a secondary system with m degrees of freedom, mounted with multiple support points on a primary system with n degrees of freedom. The combined system has four key parameters linking the characteristics of mode i of the primary system and mode j of the secondary system. Three of these are analogues of the two-degree-of-freedom system parameters:

Tuning parameters:

$$\beta_{ij} = \frac{\omega_{pi} - \omega_{sj}}{\omega_{a,ij}}. \quad (4.206a)$$

Interaction parameter:

$$\gamma_{ij} = \alpha_{ij}^2 \frac{\mu_{sj}}{\mu_{pi}}. \quad (4.206b)$$

Non-classical damping parameter:

$$\delta_{ij} = \left(\zeta_{pi} - \frac{\omega_{pi}}{\omega_{sj}} \zeta_{sj} \right) \frac{\omega_{pi}}{\omega_{sj}}, \quad (4.206c)$$

where $\omega_{a,ij} = (\omega_{pi} + \omega_{sj})/2$ is the average frequency of the primary and secondary modes. Here ω denotes frequency, ζ damping, the subscripts p and s refer to the primary and secondary system respectively, and i and j refer to the modes. μ_{sj} and μ_{pi} are the modal masses $\phi_{sj}^T [M_s] \phi_{sj}$ and $\phi_{pi}^T [M_p] \phi_{pi}$ where ϕ_{sj} and ϕ_{pi} are the mode shape vectors for the secondary and primary systems on their own.

The fourth key parameter α_{ij} is a spatial coupling parameter between the two subsystems. For the case where there is a single support point at degree-of-freedom c of the primary system, referred to as the coupling point, the coupling parameter α_{ij}^c between the i th primary mode and j th secondary mode is given by

$$\alpha_{ij}^c = \frac{\phi_{sj}^T [M_s] r}{\phi_{sj}^T [M_s] \phi_{sj}} \phi_{pci} = \Gamma_{sj} \phi_{pci}. \quad (4.207a)$$

Here r is the influence vector, a vector of unity for a simple chain primary or secondary structure.

When the secondary system is a single mass oscillator, this further simplifies to

$$\alpha_{ij}^c = \phi_{pci}. \quad (4.207b)$$

For the multi-mass secondary system with a single support point, the interaction parameter becomes

$$\gamma_{ij} = \Gamma_{sj}^2 \phi_{pci}^2 \frac{\mu_{sj}}{\mu_{pi}}. \quad (4.208)$$

The product $\mu_{sj} \Gamma_{sj}^2 = \frac{(\phi_{sj}^T [M_s] r)^2}{\phi_{sj}^T [M_s] \phi_{sj}}$ is the 'effective modal mass' (Clough and Penzien, 1975) of mode j of the secondary system. The appropriate mass

of the primary system for calculating the interaction coefficient is $\mu_{pi}/\phi_{pci}^2 = \phi_{pi}^T [\mathbf{M}_p] \phi_{pi} / \phi_{pci}^2$, which is dependent on the coupling point c . Both effective masses are independent of the normalisation of the mode shape.

The criterion for a primary mode i and a secondary mode j to be considered tuned is analogous to that for the two-degree-of-freedom system. The modes are modified by tuning if

$$\beta_{ij}^2 < \frac{\zeta_{a,ij}^2}{e} \left(4 + \frac{\gamma_{ij}}{\zeta_{sj}\zeta_{pi}} \right) \quad (4.209a)$$

where e is the acceptable relative error in the secondary system mean-square response from the detuned approximation

$$\frac{E(x_s^2) \text{ (detuned)} - E(x_s^2)}{E(x_s^2)} < e. \quad (4.209b)$$

Here $\zeta_{a,ij}$ is the average damping $(\zeta_{pi} + \zeta_{sj})/2$.

Igusa and Der Kiureghian (1985b) consider several categories of tuning. When one primary mode is tuned to one secondary mode, this pair of modes is defined as singly tuned. There may be several pairs of singly tuned modes. When there is a cluster of several primary and secondary modes with closely spaced frequencies so that they are tuned to each other, the situation is referred to as multiply tuned modes. Finally, primary modes which are not tuned to secondary modes, and secondary modes which are not tuned to primary modes, are called detuned. In general a combined primary-secondary system may consist of a combination of several pairs of singly tuned modes and several clusters of multiply tuned modes, with the remainder of the modes detuned.

Modal features of primary-secondary systems

Expressions are given by Igusa and Der Kiureghian (1985b) for the mode shapes, frequencies and dampings of detuned primary and secondary modes, and for singly tuned modes, with a low-order eigenvalue problem formulated to determine the properties of multiply tuned modes.

The results for the detuned and singly tuned cases are summarised below. Parameters of mode k of the overall system are denoted by an asterisk superscript and a k subscript. Parameters of the primary system and secondary system modes have a subscript p or s before the mode or position subscript. The superscript c denoting the coupling point is dropped in α_{ij} . The $n + m$ modes are numbered with the first n corresponding to structural modes and the remaining m to secondary modes. In the mode shape vector, the first n elements correspond to primary system degrees of freedom and the second m to secondary system degrees of freedom.

- Mode corresponding to detuned primary mode k :

$$\omega_k^* = \omega_{pk} \quad (4.210a)$$

$$\zeta_k^* = \zeta_{pk} \quad (4.210b)$$

$$\phi_k^* = \begin{pmatrix} \phi_{pk} \\ \sum_{j=1}^m \frac{\alpha_{kj}\omega_{sj}^2}{\omega_{sj}^2 - \omega_{pk}^2} \phi_{sj} \end{pmatrix}. \quad (4.210c)$$

For a single support location this becomes

$$\phi_k^* = \begin{pmatrix} \phi_{pk} \\ \left(\sum_{j=1}^m \frac{\omega_{sj}^2}{\omega_{sj}^2 - \omega_{pk}^2} \Gamma_{sj} \phi_{sj} \right) \phi_{pck} \end{pmatrix}. \quad (4.210d)$$

This compares with the two-mass expression

$$\phi_p^* = \begin{pmatrix} 1 \\ \frac{\omega_s^2}{\omega_s^2 - \omega_p^2} \end{pmatrix}. \quad (4.211)$$

The mode shape is real, so its participation factor can be found by the standard means. Dropping terms of order γ_{kj} , the participation factor for the mode corresponding to the detuned primary mode k is

$$\frac{\phi_k^{*T} [\mathbf{M}] \mathbf{1}}{\phi_k^{*T} [\mathbf{M}] \phi_k^*} \phi_k^* = \begin{pmatrix} \Gamma_{pk} \phi_{pk} \\ \Gamma_{pk} \phi_{pck} \sum_{j=1}^m \frac{\omega_{sj}^2}{\omega_{sj}^2 - \omega_{pk}^2} \Gamma_{sj} \phi_{sj} \end{pmatrix}. \quad (4.212)$$

The corresponding expression from the analysis of the two-degree-of-freedom system is

$$\Gamma_p = \begin{pmatrix} 1 \\ \frac{\omega_s^2}{\omega_s^2 - \omega_p^2} \end{pmatrix}. \quad (4.213)$$

Thus the responses of structural degrees of freedom in mode k of the combined system are identical to those in the primary system alone, and equal to the structural response of the two-degree-of-freedom system multiplied by the effective participation factor of structural mode k at the point of interest.

The effective participation factors of degrees-of-freedom corresponding to the secondary system in a mode corresponding to a detuned primary mode contain contributions from all secondary modes. The natural frequency and damping are those of the primary system mode.

For the secondary system participation factors, the weighting factor $\Gamma_{pk} \phi_{pck}$ falls rapidly with increasing mode number k for typical unisolated chain-type primary structures. With effective structural isolation $\Gamma_{p1} \phi_{pc1} \approx 1.0$, while values for $k > 1$ are quite small.

• Mode corresponding to detuned secondary mode l :

$$\omega_{n+l}^* = \omega_{sl} \quad \zeta_{n+l}^* = \zeta_{sl} \quad (4.214a, b)$$

$$\phi_{n+l}^* = \left(\begin{array}{c} \sum_{i=1}^n \frac{\gamma_{il}}{\alpha_{il}} \frac{\omega_{sl}^2}{\omega_{pi}^2 - \omega_{sl}^2} \phi_{pi} \\ \phi_{sl} \end{array} \right). \quad (4.214c)$$

For a single support location, this becomes

$$\phi_{n+l}^* = \left(\begin{array}{c} \sum_{i=1}^n \frac{\gamma_{il} \omega_{sl}^2}{\omega_{pi}^2 - \omega_{sl}^2} \frac{\phi_{pi}}{\Gamma_{sl} \phi_{pci}} \\ \phi_{sl} \end{array} \right). \quad (4.214d)$$

This mode shape is real-valued, so the participation factor takes the conventional form for a classical mode given above

$$\Gamma_{n+l} = \frac{\phi_{n+l}^{*T} [M] r}{\phi_{n+l}^{*T} [M] \phi_{n+l}^*} \phi_{n+l}^* \quad (4.215)$$

Evaluating Γ_{n+l} to lowest order produces (Skinner and McVerry, 1992)

$$\Gamma_{n+l} = \sum_{i=1}^n \frac{\omega_{pi}^2}{\omega_{pi}^2 - \omega_{sl}^2} \Gamma_{pi} \phi_{pci} \left(\begin{array}{c} \sum_{i=1}^n \frac{\gamma_{il} \omega_{sl}^2}{\omega_{pi}^2 - \omega_{sl}^2} \frac{\phi_{pi}}{\phi_{pci}} \\ \Gamma_{sl} \phi_{sl} \end{array} \right). \quad (4.216)$$

In the case of one primary and one secondary mode, this simplifies to the two-degree-of-freedom expression

$$\Gamma_s = \left(\begin{array}{c} \frac{\gamma \omega_s^2 \omega_p^2}{(\omega_p^2 - \omega_s^2)^2} \\ \frac{\omega_p^2}{\omega_p^2 - \omega_s^2} \end{array} \right). \quad (4.217)$$

The participation factors for the structural degrees of freedom for the detuned secondary modes are small, of order γ_{il} . The participation factors for the secondary system degrees of freedom may be of order 1. They differ by a factor of

$$\left(\sum_{i=1}^n \frac{\omega_{pi}^2}{\omega_{pi}^2 - \omega_{sl}^2} \Gamma_{pi} \phi_{pci} \right)$$

from their ground-mounted values, which is small if ω_{sl} is large, but may be of order unity if ω_{sl} lies in the range of the low modal frequencies of the primary system or is less than the fundamental mode frequency of the primary system.

The effective participation factor of primary mode i at the connection point c , $\Gamma_{pi} \phi_{pci}$, falls rapidly with increasing mode number i for typical unisolated chain structures. Again with effective isolation the factor is approximately 1.0 for $i = 1$ and is small for $i > 1$. Hence with effective isolation only the first term of the summation may be required.

• Modes corresponding to a singly tuned primary-secondary mode pair: We next consider modes corresponding to the singly tuned modes, mode k in the primary system and mode l in the secondary system.

The criterion for tuning of a pair of primary system and secondary system modes has been given earlier. The frequencies, dampings and shapes of the two modes $r = k$ and $r = n + l$ of the combined system, corresponding to the tuned modes, are

$$\omega_r^* = \omega_{a,kl} \left\{ 1 \pm 1/2 \operatorname{sgn}(\beta_{kl}) \operatorname{Re} \sqrt{\gamma_{kl} + \left[i \left(\frac{\omega_{pk}}{\omega_{a,kl}} \zeta_{pk} - \frac{\omega_{sl}}{\omega_{a,kl}} \zeta_{sl} \right) + \beta_{kl} \right]^2} \right\} \quad (4.218a)$$

$$\zeta_r^* = 1/2 \left\{ \frac{\omega_{pk}}{\omega_{a,kl}} \zeta_{pk} + \frac{\omega_{sl}}{\omega_{a,kl}} \zeta_{sl} \pm \operatorname{sgn}(\beta_{kl}) \times \operatorname{Im} \sqrt{\gamma_{kl} + \left[i \left(\frac{\omega_{pk}}{\omega_{a,kl}} \zeta_{pk} - \frac{\omega_{sl}}{\omega_{a,kl}} \zeta_{sl} \right) + \beta_{kl} \right]^2} \right\} \quad (4.218b)$$

$$\phi_r^* = \left\{ \begin{array}{c} \sum_{i \neq k}^n \frac{\gamma_{il}}{\alpha_{il}} \frac{\omega_{sl}^2}{\omega_{pi}^2 - \omega_{sl}^2} \phi_{pi} + a_{r,kl}^{(0)} \phi_{pk} \\ \sum_{j \neq l}^m a_{r,kl}^{(0)} \frac{\alpha_{kj} \omega_{sj}^2}{\omega_{sj}^2 - \omega_{pk}^2} \phi_{sj} + \phi_{sl} \end{array} \right\} \quad (4.218c)$$

with

$$a_{k,kl}^{(0)} = -\frac{1}{\alpha_{kl}} \left[\frac{\omega_{a,kl}^2}{\omega_{sl}^2} \beta_{kl} + i \frac{\omega_{pk}}{\omega_{sl}} \delta_{kl} + \operatorname{sgn}(\beta_{kl}) \sqrt{\gamma_{kl} + \left(i \frac{\omega_{pk}}{\omega_{sl}} \delta_{kl} + \frac{\omega_{a,kl}^2}{\omega_{sl}^2} \beta_{kl} \right)^2} \right] \quad (4.218d)$$

$$a_{n+l,kl}^{(0)} = -\frac{1}{\alpha_{kl}} \left[\frac{\omega_{a,kl}^2}{\omega_{sl}^2} \beta_{kl} + i \delta_{kl} - \operatorname{sgn}(\beta_{kl}) \sqrt{\gamma_{kl} + \left(i \delta_{kl} + \frac{\omega_{a,kl}^2}{\omega_{sl}^2} \beta_{kl} \right)^2} \right] \quad (4.218e)$$

The tuned modes are in general complex-valued if the non-classical damping parameter is non-zero.

For complex-valued mode shapes, the standard participation factor expression for a classical mode is replaced by generalised participation factors as given by Igusa and Der Kiureghian (1985a). For the case of exact tuning, i.e. $\omega_{pk} = \omega_{sl}$ so $\beta_{kl} = 0$, it can be shown that the effective participation-factor vector for secondary system degrees of freedom is the equipment participation factor in the two-degree-of-freedom system times $\Gamma_{pk}\phi_{pck}\Gamma_{sl}\phi_{sl}$. For the primary system degrees of freedom, the effective participation factor vector is the two-degree-of-freedom structural participation-factor times $\Gamma_{pk}\phi_{pk}$. These results should be good approximations for near-tuned cases as well. For a base-isolated structure, the product $\Gamma_{pk}\phi_{pck}$ is approximately unity for the first mode and nearly zero for higher modes.

Combination of modal responses

The detuned modes are well separated in frequency and real-valued, so the combination of their peak modal responses can be treated by the standard SRSS approach (Der Kiureghian, 1980).

Pairs of singly tuned modes are both very closely spaced in frequency and in general complex-valued. Igusa and Der Kiureghian (1985) give a modal-combination rule for calculating their contribution to the overall peak response, but it is a rather complicated expression. We take a different but similar approach which gives a simpler, although more approximate result.

Consider first the nearly-tuned two-mass system. Analytically it is convenient to express a peak seismic response of the structure, and a peak response of the appendage, either mounted on the structure or mounted on the ground, as the product of the root-mean-square, RMS, value of the response and a 'peak factor' P , which is defined to be the ratio of the peak response to the RMS response. Hence for peak displacement responses,

$$X = P \cdot X(\text{RMS}). \quad (4.219)$$

For a ground-based 1DOF oscillator, with frequency ω and damping ζ , $X(\omega, \zeta)$ is the displacement spectrum value $S_D(\omega, \zeta)$ for the ground motion.

The peak seismic responses of the secondary structure can be derived from the ratios of RMS seismic responses and of peak factors, using Equation (4.219):

$$X_{ps} = [X_{ps}(\text{RMS})/X_s(\text{RMS})][P_{ps}/P_s]X_s \quad (4.220)$$

where

X_{ps} , $X_{ps}(\text{RMS})$, P_{ps} = peak response, RMS response, and peak factor for the secondary structure when mounted on the primary structure,
 X_s , $X_s(\text{RMS})$, P_s = peak response, RMS response, and peak factor for the secondary structure when mounted on the ground.

A common assumption is to neglect the effects of the ratio of the peak factors, a conservative assumption in that this ratio generally lies between about 0.75 and 1.0

(Skinner and McVerry, 1992). As a second assumption, take the RMS ratio in the first bracket to be the same as for the white-noise case. Then, from Equation (36) of Igusa and Der Kiureghian (1985a),

$$X_{ps} = \frac{1}{\sqrt{8\zeta_p\zeta_a}\sqrt{1 + \beta^2/(4\zeta_a^2) + \gamma/(4\zeta_s\zeta_p)}} \left(\frac{\omega_s}{\omega_a}\right)^{3/2} X_s \\ \approx \frac{1 - 3\beta/4}{\sqrt{8\zeta_p\zeta_a}\sqrt{1 + \beta^2/(4\zeta_a^2) + \gamma/(4\zeta_s\zeta_p)}} S_D(\omega_s, \zeta_s). \quad (4.221)$$

It is implicit in this assumption that response-spectrum values for frequencies in the vicinity of the near-tuned primary and secondary frequencies ω_s and ω_p scale in the same way with frequency, and particularly with damping, as the RMS response of a ground-mounted oscillator to white noise, i.e.

$$X(\text{RMS}) = [\pi G_0/(4\zeta\omega^3)]^{1/2} \quad (4.222)$$

where G_0 is the white-noise power density spectrum, and hence

$$S_D(\omega, \zeta) \propto \frac{1}{\sqrt{\zeta\omega^3}}. \quad (4.223)$$

Generalising to the multi-mass case involves replacing the parameters by their multi-mass analogues, and multiplying by the appropriate component of the participation factor product $\Gamma_{pk}\phi_{pck}\Gamma_{sl}\phi_{sl}$ for the point of interest. The expression for combining the modal responses to find the maximum relative displacement response $d_{\max,r}$ at point r of the secondary system then becomes

$$(d_{\max,r})^2 = \sum_{i \text{ detuned}} \Gamma_{\text{eff},r,i}^2 S_D^2(\omega_i, \zeta_i) + \sum_{k,l \text{ tuned pairs}} (\Gamma_{pk}\phi_{pck}\Gamma_{sl}\phi_{srl})^2 \\ \times \frac{\omega_{sl}^3 S_D^2(\omega_{sl}, \zeta_{sl})}{8\zeta_{pk}\zeta_{a,kl} [1 + \beta_{kl}^2/(4\zeta_{a,kl}^2) + \gamma_{kl}/(4\zeta_{sl}\zeta_{pk})] \omega_{a,kl}^3}. \quad (4.224)$$

The effective participation factors $\Gamma_{\text{eff},r,i}$ at point r in the secondary system of detuned mode i can be obtained from Equation (4.212) for detuned primary modes and Equation (4.216) for detuned secondary modes. For the tuned-mode term, the expression gives the combined contribution of the two contributing modes so is evaluated only once for each contributing pair.

Similar modal combination expressions can be written for velocity or acceleration responses, although strictly the tuned-mode expressions vary for different response quantities. It is expected that using the displacement form of expression, with S_D replaced by S_V or S_A for the relative velocity or absolute accelerations, should be of comparable accuracy to other approximations used in the derivation.

When the tuned modes are high-frequency modes of the system, the contributions from the lower-frequency detuned modes may be a significant portion of the

total response. Note that the above expression assumes that the primary system modes are well separated, and also that the secondary system modes are well separated. Also, the expressions have been developed for the individual subsystems being classically damped.

4.4.4 Response of secondary systems in structures with linear isolation

The analysis of combined primary-secondary systems given so far does not apply exactly to structures with linear isolation, as the isolated primary system has non-classical modes. Kelly and Tsai (1985) and Tsai and Kelly (1988, 1989) have performed three analyses of equipment in base-isolated structures. In each case they have restricted their attention to equipment with a single mode. In the first analysis (Kelly and Tsai, 1985) they consider the base-isolated structure represented by two modes, the rigid-body-like isolator mode and the first superstructure mode, assuming classical damping with the equipment represented by a single spring-damper-mass system. In the second analysis (Tsai and Kelly, 1988) they again consider a two-mode representation of the base-isolated structure, this time with non-classical damping. In the third analysis (Tsai and Kelly, 1989) they consider a multi-mode representation of the base-isolated structure, but revert to classical damping.

The results we have derived for a classically damped primary structure with an attached secondary system can be applied directly to a base-isolated structure if the non-classical nature of the primary system mode-shapes is neglected. This is a reasonable approximation in that the structural motion of a well isolated structure is dominated by the first mode. From the results of Section 4.2.3, the two leading terms in the perturbation expression for the fundamental mode shape of a well isolated structure are real, with the effects of damping first appearing at order $(\omega_b/\omega_{FB1})^3$, an order higher than the effect of the base-isolation spring. Higher modes, for which the effect on the mode shape of the isolator damping appears at $O(\omega_b/\omega_{FB1})^2$, the same order as the effect of the isolator spring, have small participation factors, of order $(\omega_b/\omega_{n0})^2$, while the fundamental mode has a participation factor of order 1. Even when the superstructure deformation with respect to the isolator is considered, the first mode is still dominant. Its superstructure deformation is $O(\omega_b/\omega_{FB1})^2$, while the superstructure deformation of the higher modes is $O(\omega_b/\omega_{n0})^2$, where ω_b is the bearing frequency $\sqrt{(K_b/M_T)}$, ω_{FB1} is the first-mode frequency of the fixed-base structure, and ω_{n0} is the n th-mode free-free frequency of the free-free superstructure, with $\omega_{n0} = (2n - 2)\omega_{FB1}$ for a uniform structure. Thus the higher-mode contributions to the superstructure deformation are of order $(\omega_{FB1}/\omega_{n0})^2$ times the first-mode superstructure deformation, which is of order $1/(2n - 2)^2$.

These features of the mode shapes and participation factors of a linear structure with a linear isolation system mean that the first-mode approximation to the superstructure deformation retains the essential features of the response.

Consider first the case of an N -mass superstructure mounted on an isolation

system consisting of a mass, spring and damper, so the primary system has $(N + 1)$ degrees of freedom, with non-classical damping effects of the primary structure neglected. The equipment is modelled as a single-degree-of-freedom oscillator of mass m_e , frequency ω_e and damping ζ_e and is attached at degree of freedom c of the superstructure, giving an $(N + 2)$ degree-of-freedom system. For equipment detuned from all the isolated modes, the maximum absolute acceleration of the equipment is given as

$$\ddot{X}_e = \left\{ \sum_{i=1}^{N+1} \left[\frac{\Gamma_{pi} \phi_{pci}}{1 - \left(\frac{\omega_{pi}}{\omega_e}\right)^2} S_A(\omega_{pi}, \zeta_{pi}) \right]^2 + \left[\sum_{i=1}^{N+1} \frac{\Gamma_{pi} \phi_{pci}}{1 - \left(\frac{\omega_e}{\omega_{pi}}\right)^2} S_A(\omega_e, \zeta_e) \right]^2 \right\}^{1/2} \quad (4.225)$$

Here Γ_{pi} , ϕ_{pci} , ω_{pi} and ζ_{pi} refer to the parameters of the isolated modes of the primary system, with non-classical mode shape effects neglected, not to the modal parameters of the unisolated structure. The first series of terms corresponds to the detuned structure modes, while the second term corresponds to the detuned equipment mode, which has contributions from all the structure modes.

For the equipment tuned to isolated mode k of the structure, the result given earlier simplifies in the case of a single-mass appendage to

$$\ddot{X}_e \approx \left\{ \sum_{i=1, i \neq k}^{N+1} \left[\frac{\Gamma_{pi} \phi_{pci}}{1 - \left(\frac{\omega_{pi}}{\omega_e}\right)^2} S_A(\omega_{pi}, \zeta_{pi}) \right]^2 + \left[\frac{\Gamma_{pk} \phi_{pck} \omega_e^{3/2}}{\omega_a^{3/2} \sqrt{8\zeta_{pk} \zeta_a} [1 + \beta_k^2 / (4\zeta_a^2) + \gamma_k / (4\zeta_e \zeta_{pk})]} S_A(\omega_e, \zeta_e) \right]^2 \right\}^{1/2} \quad (4.226)$$

where $\omega_a = (\omega_{pk} + \omega_e)/2$ and $\zeta_a = (\zeta_{pk} + \zeta_e)/2$.

For the case of detuned equipment, the first term dominates the first bracket summation, because the first-mode participation factor is much greater than for other modes. In the second bracket, even this term can be neglected assuming $\omega_e \gg \omega_b$, so for the detuned case

$$\ddot{X}_e \approx \Gamma_{p1} \phi_{p1} S_A(\omega_{p1}, \zeta_{p1}).$$

For the tuned case, the tuned-mode expression will dominate when the term under the square-root sign is of the same order as $\Gamma_{pk} \phi_{pck}$ or less. For tuning with the first mode, $\Gamma_{pk} \phi_{pck}$ is of order 1, so the tuned mode will dominate. Except for long-period items like sloshing water tanks, or equipment with very flexible mounts, the equipment is unlikely to be tuned to the first mode of an isolated

structure. For higher-mode tuning, $\Gamma_{pk}\phi_{pck}$ is of order $(\omega_b/\omega_{n0})^2$ while the term under the square-root sign at least equals its value of $\sqrt{4\zeta_{pk}(\zeta_{pk} + \zeta_e)}$ obtained when $\gamma_k = 0$ and $\beta_k = 0$, which is of order ζ_{pk} . Often this is greater than $(\omega_b/\omega_{k0})^2$, so the tuned mode does not dominate. The maximum response of a 'high frequency' ($\omega_e \sim O(\omega_{FB1})$ or greater) appendage in an isolated structure will be of the same order as the maximum response of the isolated structure, rather than the structure response amplified by a factor of $O(1/\sqrt{\gamma})$ which may be very large.

Tsai and Kelly (1989) give an example of a very lightweight piece of equipment attached to a base-isolated structure with a first-mode period of 2 s and damping of 10%, and higher-mode and equipment damping of 1%. The first-mode response dominates except when the equipment is tuned to the second mode, when both terms are of similar size. Generally, similar results for somewhat different dampings are given by cases (ii) and (iii) of Figure 2.7.

This analysis showed that the response of 'high-frequency' equipment (i.e. natural frequency of order ω_{FB1} or greater) in a base-isolated structure was strongly dependent on the first two modes, at most, of the isolated structure. Tsai and Kelly (1988) used a simple representation of the base-isolated structure to consider the effects of non-classical damping. They represented the superstructure deformation by its first mode only, so the isolator-structure-equipment system became represented by a three-mode model. They chose the equipment frequency so that it was nearly tuned to the second mode of the isolated structure. The results discussed above showed that this is the only case when the equipment response is likely to be dominated by a mode other than the first isolated mode.

It was found that the deformation of the equipment relative to the floor involved terms corresponding to the classical-mode terms with slightly different natural frequencies and dampings, plus two additional terms arising from the imaginary parts of the eigenvector, which do not occur in the classical-mode method. One of these terms is of $O(1)$, so the equipment response calculated from the classical-mode approximation may be completely different from that given by the more exact complex mode method. For the particular example considered, the true response was about double that given by the classical-mode method. This ratio is also given by Equation (48) of Igusa and Der Kiureghian (1985a) for a two-mass system for very small γ and a maximum value for δ^2 , i.e. ζ_p^2 or ζ_s^2 , where ζ_s or ζ_p are zero respectively.

Chalhoub (1988) and Chalhoub and Kelly (1990) considered the earthquake response of cylindrical water tanks in base-isolated structures, with an experimental shake-table study supported by a theoretical treatment. The sloshing frequency of tanks of fluid may be close to the frequency of the fundamental mode which generally dominates the response of isolated structures. The natural frequencies of most other equipment are unlikely to be tuned to the low fundamental frequency of an isolated structure.

Pressures on the walls of tanks containing fluids consist of an impulsive component and a convective component. The impulsive pressure results from the acceleration of the container wall against the fluid. The convective component results

from waves causing changes in the free-surface elevation of the fluid. The results showed that low-frequency sloshing could be of larger amplitude in a tank mounted on an isolated structure, but the slight increase in convective pressure was much more than offset by the decrease in the impulsive pressure because of the reduced accelerations in the isolated structure. Thus even for sloshing water tanks, where isolation could be perceived as introducing problems, isolation has real advantages in reducing the accelerations on contents of a structure. The only serious concern is the possibility of spillage from open tanks with insufficient freeboard.

In summary, the earthquake response of equipment in structures with linear isolation is not susceptible to the strong amplification of the ground acceleration which may occur for equipment mounted in fixed-base structures. Even for the worst case where the equipment is tuned to the frequency of the lowest superstructure mode of the isolated system, the amplitude of the acceleration response of the equipment is only of the same order as its response when mounted on the ground. For accurate calculation of the expected response of equipment in an isolated structure, it is necessary to account for the non-classical nature of the equipment-structure modes since the classical mode method may grossly underestimate the true responses.

4.4.5 Response of secondary systems in linear structures with non-linear isolation

Introduction

The previous section has treated the response of secondary systems in linear structures with linear isolation by using an analytical response spectrum approach which accounts for interaction between the primary and secondary systems and the non-classical nature of the combined primary-secondary modes when there is near tuning between modes of the two systems. The approach relied on the synthesis of the modal properties of the combined system, and the development of appropriate modal combination rules (Skinner and McVerry, 1992) derived from random vibrations theory, based on the results of Igusa and Der Kiureghian (1985a, b).

Systems with non-linear isolation are much less amenable to such an approach, although Igusa (1990) has extended it to two-degree-of-freedom primary-secondary systems with moderate non-linearities. However, the single-mass representation of the structure in this simple model eliminates the non-linear interaction effects which feed energy between the different modes of the primary system, which we have shown in Section 4.3 to be very important for structures with non-linear isolation. Also, the assumption of moderate non-linearity inherent in the perturbation approach used in the analysis may be violated for a base-isolation system.

The results in this section for appendage response in non-linear primary structures have been derived in two ways. First, standard floor-response spectra derived by ourselves and Fan and Ahmadi (1990) and Fourier spectra of the floor motions obtained experimentally by Kelly and Tsai (1985) are used to indicate the frequency bands in which energy is available in the floor motions to drive appendages. This approach neglects interaction effects, which are important in linear

systems for the response of lightly damped appendages tuned to lightly damped modes of the primary system. An important result of Igusa's exploratory study of non-linear primary-secondary systems is that interaction is less important than for linear primary-secondary systems. This is presumably because hysteretic energy dissipation in the non-linear system gives a high value of equivalent viscous damping, in which situation interaction is not a significant factor for linear systems. However, this result needs to be treated with caution for appendages tuned to the higher modes of the non-linearly isolated structure. High viscous damping at the base was shown in Section 4.2 to produce high first-mode damping in the base-isolated system, but small to moderate damping in the higher modes. If hysteretic base damping makes a similar small contribution to the damping in the higher modes, then lightly damped appendages tuned to a higher mode of the non-linear isolation system give the situation of lightly damped primary and secondary system modes, for which interaction may be important. The amount of damping in the higher non-linear modes is difficult to assess, in that the energy dissipation mechanisms are competing with energy transfer through non-linear interaction. However, the results shown in Figure 4.11 indicate that higher-mode energy dissipation within the yielding phases of a system with bilinear isolation is small, although there may be significant higher-mode accelerations imparted from the non-yielding phases of the response.

The second approach considers response histories calculated for one-mass appendages attached to multi-mass isolated structures. Fan and Ahmadi (1992) calculated response histories to derive exact floor-response spectra including the effects of interaction for appendages on a structure supported by various isolation systems. Fan and Ahmadi compared the appendage responses for an unisolated structure and for a linear isolation system with those for bilinear isolation systems with either a rigid pre-yield phase or perfectly plastic post-yield phase or both. The responses of these types of bilinear isolators contain strong high-frequency components, as they involve a low isolation ratio $I(K_{b1})$ in the pre-yield phase or a high non-linearity factor. We performed a less extensive study which was restricted to appendages which were perfectly tuned in the post-yield phase of the response to either the second or third mode, but with spring elements active in both response phases for the bilinear isolators.

Floor-response spectra

The traditional approach to evaluating lightweight appendage response is through floor-response spectra, in which the support-point excitation of the appendage is assumed to be unmodified by the presence of the appendage. 'Floor-response spectra' calculated from the support-point motion in the absence of the oscillator are shown in Figure 2.7 for the top floor of a structure supported by a variety of base-isolation systems. Similar results have been calculated by Fan and Ahmadi (1990).

The systems considered in Figure 2.7 are tabulated in Table 2.1 and comprise a ground-mounted four-mass structure with $T_1(U) = 0.5$ s; and a similar structure (in some cases with $T_1(U) = 0.25$ s) mounted on non-zero-mass base isolation

systems. Two of these systems are linear and four are non-linear (bilinear) as detailed in Table 2.1 and the associated text. The north-south component of the 1940 El Centro accelerogram was used as the earthquake ground motion. The floor response spectrum was calculated for an appendage with 2% damping subjected to the top-mass motion in each case, and compared with the corresponding spectrum for appendage responses to the first-mode contribution to the floor motion. The first-mode motion was obtained by sweeping with the free-free first-mode shape for the isolated systems, and with the exact first-mode shape for the ground-mounted structure.

The discussion of the characteristics of isolation systems in Sections 4.2 and 4.3 indicates that relatively little higher-mode response should be expected for the linearly isolated structures and for cases (iv) and (vii) which have a high degree of isolation in the elastic phase (see Table 2.1). Cases (v) and (vi) with stiff isolators in the elastic phase are likely to produce significant higher-mode responses. The floor-response spectra obtained confirm these expectations, as shown in Figure 2.7.

The ground-mounted structure has peaks in its floor-response spectrum corresponding to the first-, second- and third-mode periods, with the first-mode peak the strongest. All peaks show a much stronger response of the appendage than it would experience if ground-mounted.

The lightly damped linear isolation system has a strong first-mode peak, although much reduced in acceleration from the strongest peak of the unisolated system, and small second- and third-mode peaks. The first-mode peak occurs at a period close to T_b , while the second-mode peak is at about $T_1(U)/2$, as expected for the second mode of this well isolated structure. The floor-response spectrum differs little from that for the first-mode floor motion alone, as obtained by sweeping the overall response by the first free-free mode shape.

The more heavily damped linear isolator led to a reduced first-mode appendage response, but a slightly stronger second- and third-mode appendage response compared with that for the lightly damped isolator. The increased higher-mode response is presumably related to the higher effective participation factor arising from the non-classical mode shape and increased base impedance for the more highly damped isolator, as discussed in Section 4.2.

As anticipated, the bilinear isolation systems with stiff elastic phases, i.e. low $I(K_{b1})$, produced floor-response spectra showing strong short-period excitation of appendages. The strongest of these peaks is of smaller amplitude than the first-mode peak of the unisolated structure. However, the higher-mode peaks have amplitudes similar to those for the higher modes of the unisolated structure. The higher-mode peaks are considerably stronger than the first-mode peak. The periods of the higher-mode peaks correspond to the natural periods in the post-yield phase, which are close to the free-free periods for the higher modes.

The floor-response spectrum for cases (iv) and (vii) is similar at low frequencies to that for the linear isolator with high damping. However, there is a significant peak at the second-mode frequency for case (vii), which has an isolator with a virtually elasto-plastic force-displacement characteristic, and hence a high non-

linearity factor. This is consistent with the considerable strength of the second-mode response for this system, as predicted by the plot of second-mode to first-mode response as a function of non-linearity factor (Figure 4.12).

Floor-response spectra for 2% damped appendages mounted on the top storey of structures with various types of isolation systems were also produced by Fan and Ahmadi (1990). The results were summarised in their Figure 5, reproduced here as Figure 4.15. Fan and Ahmadi considered a uniform three-mass structure with a fundamental period of 0.3 s mounted on a fourth mass of the same value supported by the non-linear springs and viscous damper of the isolation system. They gave results for five types of isolation system, as well as the unisolated structure. The systems considered were a linear isolation system with 2 s natural period and 8% critical damping, taken as a representation of laminated-rubber bearings, and four non-linear systems containing frictional sliding elements. Two of these isolators had rigid characteristics in the non-sliding phase.

Fan and Ahmadi found that, for excitation by the El Centro 1940 north-south component, the base isolation systems which they considered eliminated the resonance peak of about 10g in the floor-response spectrum which occurred for the unisolated structure at its fundamental period. The amplitudes of the floor-response

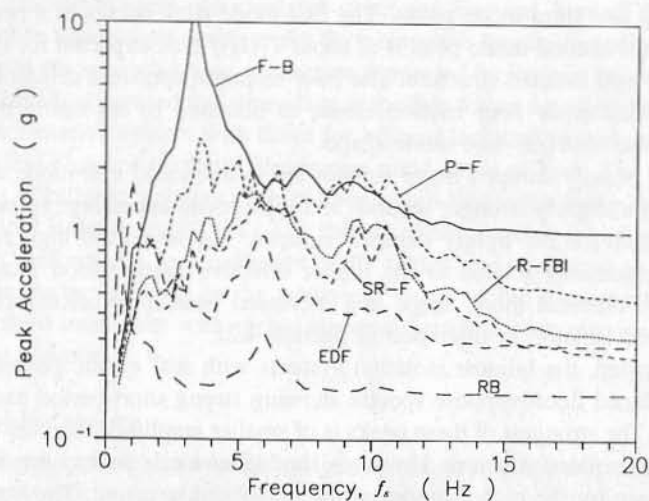


Figure 4.15 Floor-response acceleration spectra with various isolation systems, at the top of a uniform three-mass structure with a fundamental period of 0.3 s and a damping factor of 0.02, for El Centro 1940 NS (from Figure 5 of Fan and Ahmadi, 1990). Systems shown are fixed-base (F-B), pure friction (P-F), resilient friction (R-FBI), sliding resilient friction (SR-F), Electricité de France (EDF) and laminated-rubber bearing (RB). Note the high-frequency content in the response of the PF, R-FBI and SR-F systems which have rigid non-sliding phases

spectra at the fundamental period of the unisolated structure were generally reduced by a factor of 10 or more for the various isolation systems, except for the pure friction (i.e. rigid/perfectly plastic) system with a coefficient of friction of 0.2 which had a series of peaks of about 2g amplitude. The linear rubber bearing system, with 2 s period and 8% damping, produced a peak of about 1.8g at its natural period, but its amplitude over the rest of the spectrum was about 0.15–0.3g, the lowest for the various isolation systems considered. The spectrum for the rubber bearing isolator was smooth with only a few peaks, corresponding to the modes of the isolated system. The second peak was at about 6 Hz, about twice the natural frequency of the ground-mounted structure as expected for the second isolated mode. The spectra for the other systems generally fell between those for the rubber-bearing system and the pure friction system. The spectra were very irregular for those systems with stick-slip frictional sliding characteristics, particularly where the isolator was rigid in the non-sliding phase. The 'EDF' system, with elastic-perfectly plastic characteristics, had a spectral shape similar to that of the rubber-bearing system, although with larger amplitudes, with a well defined second-mode peak. This system is similar in response characteristics to our case (vii), with reasonable isolation in even the elastic phase of the response but a high non-linearity factor because of its elasto-plastic character.

Fan and Ahmadi (1990) showed further differences in the nature of the various isolation systems by comparing the floor-response spectra at various levels in the structure. Their Figure 6 and some additional material are given as Figure 4.16.

For the linear rubber-bearing isolation system (Figure 4.16b), the spectra were virtually identical for all floors except for frequencies in the vicinity of the small second-mode peak, where the appendage response was strongest at the level immediately above the isolator and at the top of the structure. This is consistent with a rigid-body-type fundamental mode contributing most of the response, with a small contribution from the second mode which is characterised by antinodes of virtually equal amplitude at the top and immediately above the isolators, with a node at mid-height.

The 'EDF' system, an elasto-plastic system with a coefficient of friction of 0.2 and a 1 s period in the non-sliding phase, showed an essentially rigid-body first-mode response (Figure 4.16(e)), with the differences between the mid-height response and those at the top and base of the structure more accentuated by relatively stronger second-mode response than in the rubber-bearing system.

The resilient-friction system (R-FBI), where the isolator is rigid in the non-sliding phase but has spring resilience during sliding, showed evidence in the floor-response spectra from the various levels of at least the first three modes participating in the response (Figure 4.16(d)). The acceleration response in the third mode, at about 10 Hz, was strongest in the mid-height region.

Fan and Ahmadi also considered the response of the isolation systems to excitation by the 1971 Pacoima Dam S16E and 1985 Mexico City SCT east-west records. The Pacoima Dam component had a very strong peak ground acceleration of 1.17g, and produced an extreme resonance (about 50g) in the top-floor-response

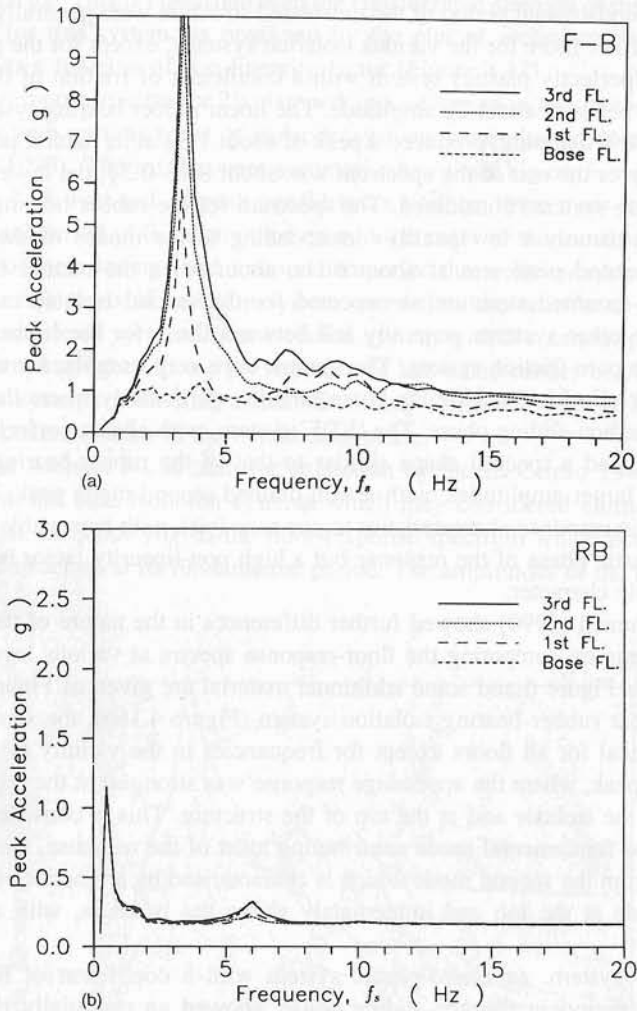


Figure 4.16 Floor-response spectra with various isolation systems at the floor levels of the structure considered by Fan and Ahmadi (Figure 6 of Fan and Ahmadi, 1990, and personal communication, 1992). Note the second-mode response at approximately 6 Hz and the third-mode response at approximately 10 Hz for the isolated structure. (a) Fixed base system. (b) Laminated-rubber bearing. (c) Pure friction system. (d) Resilient friction system. (e) Electricité de France system

spectrum of the unisolated structure. The SCT record had only a moderate peak ground acceleration ($0.17g$), but was characterised by strong frequency content in the 0.45–0.5 Hz band, which may be important for some types of isolation system, particularly the linear rubber bearing system when the natural period is 2 s.

As with the El Centro excitation, all of the isolation systems considered com-

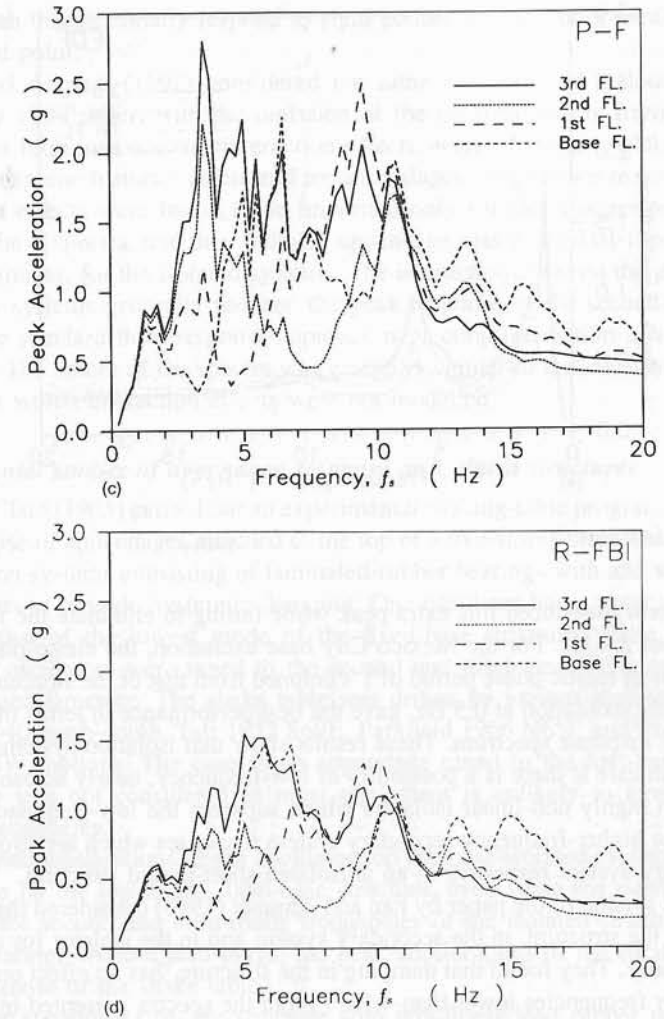


Figure 4.16 (continued)

pletely eliminated the resonant peak of the unisolated structure at 3.33 Hz in the Pacoima response, with maximum amplitudes of the floor-response spectra 10 to 25 times lower than for the unisolated structure. For the Mexico City excitation, the rubber bearing system, with 2.0 s period, showed the expected resonance at about 0.5 Hz, reaching an amplitude of about $10g$ compared with about $1.7g$ for the unisolated structure. At greater frequencies, the floor-response spectrum was almost flat. The three isolation systems with rigid non-sliding phases, that is the pure friction, resilient friction and sliding resilient friction isolators, showed strong second-mode peaks under the low-frequency, near-sinusoidal Mexico City excitation. The pure-

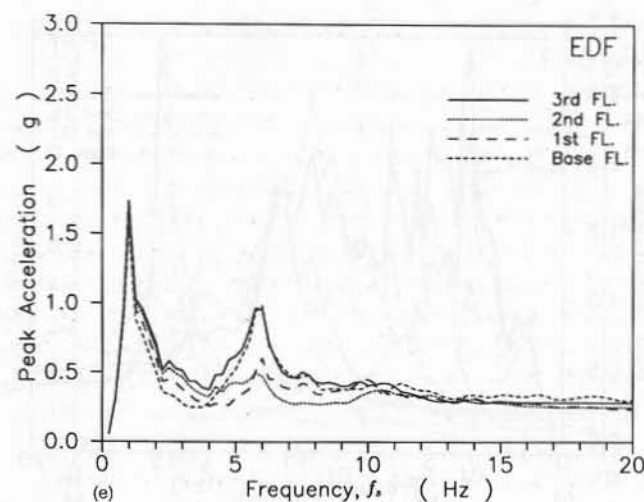


Figure 4.16 (continued)

friction system introduced this extra peak while failing to eliminate the fixed-base peak at about 3.3 Hz. For the Mexico City base excitation, the elasto-plastic EDF system, with an elastic phase period of 1 s detuned from that of the structure at 0.3 s and that of the excitation at 0.5 Hz, gave the best performance in terms of the floor acceleration response spectrum. These results show that isolation systems must be selected with care if there is a possibility of low-frequency, nearly sinusoidal excitation. Even highly non-linear isolators which suppress the low-frequency motion may produce higher-frequency secondary system responses which are stronger than the secondary system responses in an unisolated short-period structure.

The final section of the paper by Fan and Ahmadi (1990) considered the effect of damping in the structure, in the secondary system and in the isolator for a resilient friction isolator. They found that damping in the structure 'has no effect on the floor spectrum for frequencies lower than 4 Hz'. From the spectra presented in Figure 8 of their paper, we interpret this result as showing that damping in the structure has little effect on the first-mode response of an isolated structure and increasingly greater effect on the higher modes. This is consistent with our analysis of linear isolation systems, for which the isolator contributes most of the damping in the first mode, while the damping in the structure becomes progressively more important at higher frequencies.

Increased damping in the secondary system significantly reduces its response for secondary-system frequencies less than 15 Hz, but has little effect for higher-frequency appendages. We interpret this as showing that damping in the appendage has significant effect in the frequency range of the modes of the isolated structure. In the example considered, 15 Hz is a higher frequency than the natural frequency of any of the modes of the isolated structure, so appendages with frequencies

greater than this essentially respond as rigid bodies with the same motion as their attachment point.

Fan and Ahmadi (1992) considered the same structure and isolation systems as in their 1990 paper, with the omission of the resilient sliding friction system. This paper took into account interaction effects, with maximum values extracted from the response histories calculated for appendages with various mass ratios. The interaction effects were found to be important only for the stronger peaks of the floor-response spectra, and then only for appendage masses of 0.01 times the floor mass, or greater, for the isolated systems. The interaction between the primary and secondary systems generally reduced the peak response of the secondary system, so that the standard floor-response approach neglecting interaction is usually conservative. The nature of the spectra was generally similar to that of those discussed above, for which interaction effects were not modelled.

Experimental studies of appendage response on isolated structures

Kelly and Tsai (1985) carried out an experimental shaking-table programme to study the response of appendages attached to the top of a five-storey steel frame mounted on isolation systems consisting of laminated-rubber bearings with and without lead plug inserts to provide hysteretic damping. One oscillator had a natural frequency close to that of the lowest mode of the fixed-base structure, while the second and third oscillators were tuned to the second and third-mode frequencies of the base-isolated structure. The shake table was driven by various scalings of the El Centro 1940 north-south, Taft 1952 S69E, Parkfield 1966 N65E and Pacoima Dam 1971 S14W motions. The case of an appendage tuned to the first-mode isolated frequency was not considered as most equipment is unlikely to have such low natural frequencies.

The peak accelerations of the oscillators on the base-isolated systems were less than those on the top of the fixed-base structure, even when the oscillators were tuned to the second and third-mode frequencies of the isolated structure. For the rubber bearings without lead plugs, the peak accelerations of the oscillators were less than those of the shake table.

For the appendages on the structure with non-linear lead-rubber isolators, the magnification, defined as the ratio of the peak oscillator acceleration to the peak shake-table acceleration, reduced as the earthquake scalings increased. This demonstrated that the non-linear nature of the lead-rubber isolator system provides more isolation as the intensity of the earthquake excitation increases.

The reduction factors for the peak oscillator accelerations on the isolated structures with respect to those on the unisolated structure were large for the rubber bearings with no lead plug, typically around 15–20 for the first-mode oscillator and usually 10–15 for the higher-frequency oscillators. The factors were much less for the oscillators on the lead-rubber isolator system, ranging from 1.4–4.9. Greater reductions would have been possible by reducing the yield forces of the lead-rubber isolators by reducing the size of the lead plugs, but the lead plugs are effective mainly for reducing the isolator displacements rather than reducing the accelera-

tion response of oscillators tuned to the higher-mode frequencies of the yielded isolator-structure system. These experimental results show the same trends as our calculated floor-response spectra shown in Figure 2.7. The calculated spectra are for systems with bilinear hysteretic loops, while the loops for the experimental system were likely to have been curved. Fourier spectra of the measured floor motions showed much stronger high-frequency content with the lead-rubber isolators than with the linear isolation system obtained with the rubber bearings alone.

Another experimental study of the response of contents in base-isolated structures was that by Chalhoub (1988) and Chalhoub and Kelly (1990), which considered containers of fluids with sloshing frequencies similar to the first-mode frequency of the isolated system, a situation where it might be thought that isolation would increase the response. However, as discussed earlier, the reduction in the impulsive forces through isolation was much greater than the increase in the convective forces from sloshing, leading to much reduced dynamic forces in the tank compared with those when the tank is installed in an unisolated structure.

4.5 TORSIONALLY UNBALANCED STRUCTURES

4.5.1 Introduction

A structure is torsionally unbalanced when its centre of stiffness is offset from its centre of mass. Some structures are inherently torsionally unbalanced, due to an asymmetric floor plan (probably dictated by the needs of the building), an asymmetric layout of the structural members, or the location of stair-wells and lift-shafts, etc. With nominally balanced structures, accidental torsional unbalance can arise due to material inhomogeneities; distribution of live loads; inhomogeneous structural stiffening around cladding, windows etc; or failure of structural members. Again, when an isolated structure is nominally balanced, allowance must be made for inevitable accidental unbalance. Design codes therefore call for a minimum eccentricity in calculations, typically 10% of the length of the structure perpendicular to the direction of loading.

When a transverse mode is coupled to a rotational mode by moderate static torsional unbalance, there is a dynamic amplification of the torsional component of seismic responses if certain conditions are met. The main conditions are: close modal frequencies, sufficiently large torsional unbalance and sufficiently low modal dampings.

The principal effects of torsional unbalance on the seismic responses of linear structures have received considerable attention (Newmark and Rosenbluth, 1971). The treatment of modal features which is closest to that given in this section is presented in papers by Skinner *et al.* (1965) and Penzien (1969). These papers give combined seismic responses of close-frequency torsional modes, based on time-history analysis of responses to earthquake accelerations. Combined responses are treated more systematically by Penzien, who proposes special response spectra for close-frequency mode pairs. The need for these special spectra has been largely

removed by the introduction of the more convenient CQC rules for modal combination (Der Kiureghian, 1980a, b; Wilson *et al.* 1981). The CQC treatment is used in the present discussion.

The approach used here is an analytical treatment of the modal features and seismic responses of a 2DOF structure whose centre of stiffness (C.S.) is offset from its centre of mass (C.G.). This applies to linear structures with or without linear isolation. Secondly, there is consideration of a torsionally unbalanced structure with bilinear isolation. The seismic responses of a torsionally unbalanced structure, with and without bilinear isolation, have been evaluated by Lee (1980) using response-history analysis. This shows the clear-cut reduction in torsional (and other) responses that can be achieved by mounting the (single-storey, asymmetric) structure on a bilinear isolator. As with linear isolation, the bilinear isolation system was found to be most effective if mounted with its centre of stiffness below the centre of mass of the structure.

4.5.2 Seismic responses of linear 2DOF structures with torsional unbalance

Modal features

The modal features of 2DOF structures with torsional unbalance are given in detail by Skinner *et al.* (1965). The present treatment emphasises cases with moderate unbalance and with close translational and rotational frequencies.

The quantitative effects of torsional unbalance may be well illustrated with a simple two-degree-of-freedom, 2DOF, model, as shown in Figure 4.17(a), in which a torsionally unbalanced structure is oriented along the x -axis and translation in the y -direction, and/or torsion in the horizontal ($x - y$) plane, occur in response to excitation in the y -direction. Here the circled dot and cross refer to the centre of mass (C.G.) and centre of stiffness (C.S.) of the structure respectively. The structure is assumed balanced for excitation in the x -direction.

Figure 4.17(b) shows a simplified plan view of a model with two equal masses $M/2$ (equal weights $W/2$), which retains the same C.G. and angular momentum as the original structure of Figure 4.19(a). The masses are separated by $\pm r$ from the C.G. Torsional unbalance is given by offsetting the centre of stiffness (C.S.) by $r\delta$ from the C.G. The supporting 'springs' of stiffness $K/2$ are taken as equidistant from the C.S., with a radius of torsional stiffness which is $(1 + \Delta)$ times the radius of inertia r . The masses are displaced by Y_a and Y_b respectively during the mode-1 rotation shown, and the springs are displaced by Y_c and Y_d .

If both $\delta = 0$ and $\Delta = 0$ then the system has equal translational and torsional frequencies but it is degenerate and no unique natural mode shapes are defined. Close frequencies and moderate unbalance are achieved by giving Δ and δ , respectively, small fractional values. For small values of Δ and δ the modal features may be expressed approximately as perturbations of the features of the equal-frequency, balanced modes, as discussed below.

The model in Figure 4.17 may be interpreted as representing a one-storey uniso-

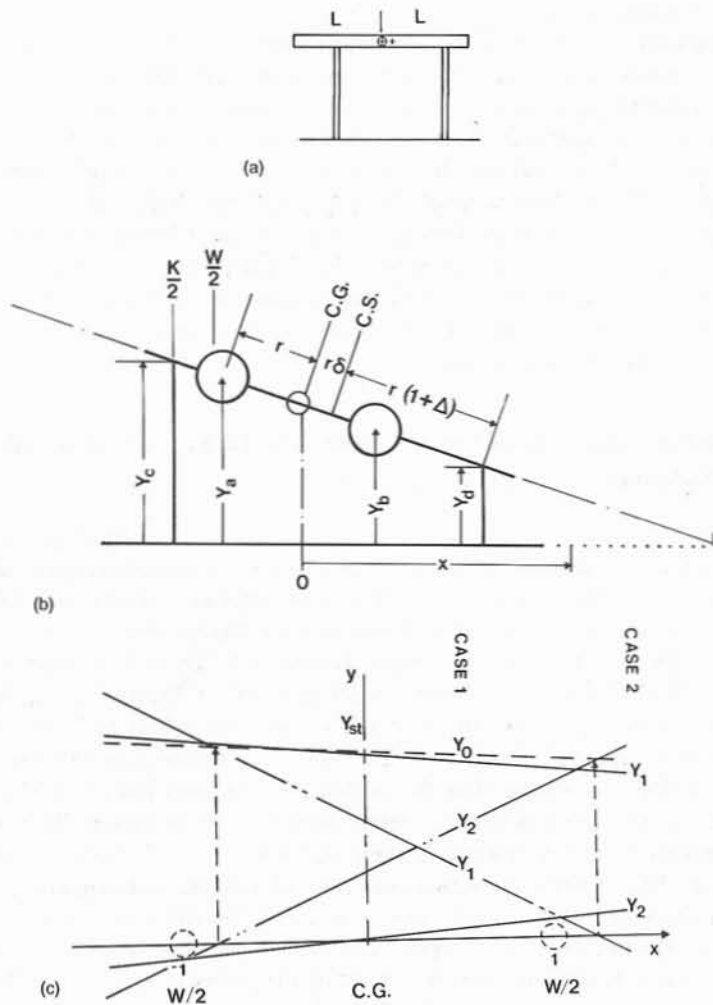


Figure 4.17 Modal features of two-degree-of-freedom (2DOF) structures with close frequencies and moderate torsional unbalance. (a) Elevation of a model of a torsionally unbalanced 2DOF structure. (b) Plan view defining the structural parameters and the coordinate system. (c) Modal deflection when a small unbalance is dominant, case 1, (broken line) and when a small frequency separation is dominant, case 2 (solid line). (d) The modal participation factors $\Gamma_1(x)$ and $\Gamma_2(x)$, and a combined-response participation factor $\Gamma_{1c2}(x)$, as derived in the text, are shown for case 1

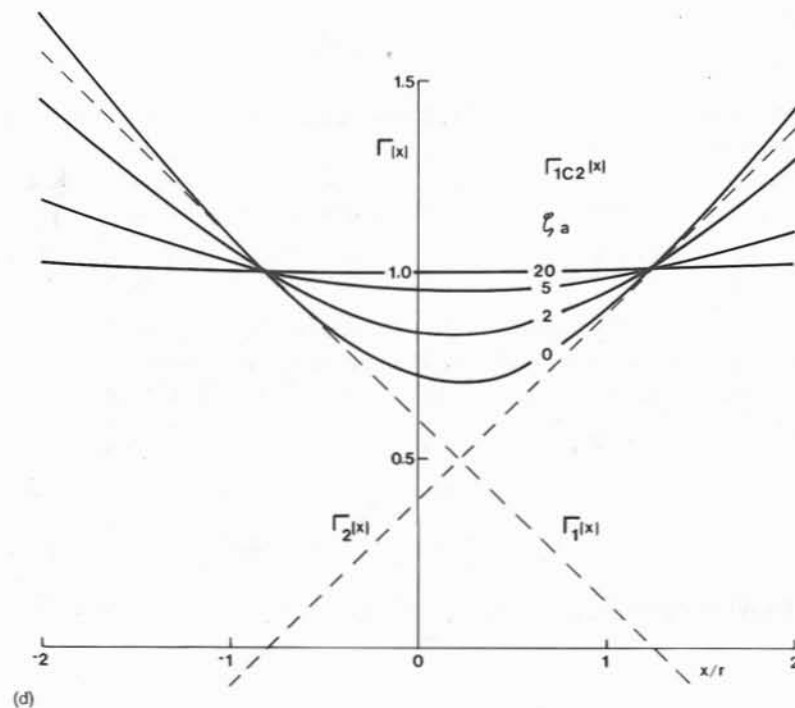


Figure 4.17 (continued)

lated structure with a shear stiffness K , or as a model of a structure with linear isolation, with $K = K_b$, and with the structure approximated as rigid. The shapes of the two normal modes and their natural periods may be obtained by equating translational forces and by taking moments about a node such as that on the right of Figure 4.17(b), for free vibrations at frequency ω in the absence of external forces. Thus

$$\text{from forces: } \frac{W}{2g} \omega^2 (Y_a + Y_b) = \frac{K}{2} (Y_c + Y_d) \quad (4.227a)$$

and

$$\text{from moments: } \frac{W}{2g} \omega^2 (Y_a^2 + Y_b^2) = \frac{K}{2} (Y_c^2 + Y_d^2). \quad (4.227b)$$

Geometrical relationships may now be used to express the displacements Y in terms of distances to the node; eliminating ω gives

$$x^2 - 2r \frac{\delta}{\delta} x - r^2 = 0 \quad (4.228a)$$

where

$$\varepsilon = \Delta + (\Delta^2 + \delta^2)/2 \quad (4.228b)$$

so that $\varepsilon \approx \Delta$ for small Δ and δ . The positions of the two nodes, which define the two mode shapes, are then

$$\text{Mode 1 : } x_1 = (r/\delta)[\sqrt{(\varepsilon^2 + \delta^2)} + \varepsilon] \quad (4.229a)$$

$$\text{Mode 2 : } x_2 = -(r/\delta)[\sqrt{(\varepsilon^2 + \delta^2)} - \varepsilon]. \quad (4.229b)$$

Note that $x_1 x_2 = -r^2$, which shows that the nodes of the two modes lie on opposite sides of the C.G., one within and one beyond the radius of inertia.

The natural (circular) frequencies can be obtained from Equations (4.227a) and (4.229) which give:

$$\omega_1^2 = gK/W [1 + \varepsilon - \sqrt{(\varepsilon^2 + \delta^2)}] \quad (4.230a)$$

$$\omega_2^2 = gK/W [1 + \varepsilon + \sqrt{(\varepsilon^2 + \delta^2)}]. \quad (4.230b)$$

It is useful to define the term in the above square root separately, as the variable β :

$$\beta = \sqrt{(\varepsilon^2 + \delta^2)}. \quad (4.231)$$

Note that β is a measure of the relative separation of the modal frequencies, as

$$\beta \approx (\omega_2 - \omega_1)/\omega_a$$

where the average frequency

$$\omega_a = (\omega_1 + \omega_2)/2.$$

The mode shapes $y = \phi(x)$ are defined conveniently by the locations x_1 and x_2 of their nodes, (Equations 4.229) and are scaled to give unit displacement at $x = 0$. Hence

$$\phi_1(x) = 1 - x/x_1 \quad (4.232a)$$

and

$$\phi_2(x) = 1 - x/x_2. \quad (4.232b)$$

Modal participation factors

From the mode shapes and mass distribution, the participation factors are given by

$$\Gamma_1(x) = (1/2)[1 + \varepsilon/\beta - (\delta/\beta)(x/r)] \quad (4.233a)$$

$$\Gamma_2(x) = (1/2)[1 - \varepsilon/\beta + (\delta/\beta)(x/r)]. \quad (4.233b)$$

The above modal features may be illustrated by the modal displacements for an acceleration of $-g$ along the y -axis, as shown for two cases by the plan view in Figure 4.17(c). For case 1, $\Delta = 0.01$ and $\delta = 0.05$, the unbalance parameter δ exceeds the frequency separation parameter Δ , and both modes contain large (and opposite) rotational components. Modal displacements Y_1 and Y_2 are given by broken lines, while the dotted line shows the static deflection for this case. For case 2, $\Delta = 0.05$ and $\delta = 0.01$, the frequency separation parameter Δ exceeds the unbalance parameter δ , and both modes contain small (and opposite) rotational components. Mode 1 is dominantly translational and mode 2 is dominantly torsional, and small, as shown by the modal displacements Y_1 and Y_2 given by solid lines.

In case 2 there is little axial-mode interaction. In case 1 strong axial-mode interaction is caused by the small unbalance δ of the translational mode, with little suppression by the even smaller frequency separation term Δ .

Peak combined responses of modes 1 and 2

The peak seismic displacements of modes 1 and 2 may be obtained using the participation factors of Equation (4.233) and the response spectrum values for the modal periods and dampings. For close modal frequencies, as considered here, it may be assumed that

$$S_{D,1} \approx S_{D,2} \approx S_D(\omega_a, \zeta_a)$$

where ω_a, ζ_a are the average values for the modal frequencies and dampings. The modal responses may be combined using the CQC approach (Der Kiureghian, 1980a, b) to give the peak seismic response at x as:

$$Y(x) = \sqrt{\Gamma_1^2(x) + 2\rho_{1,2}\Gamma_1(x)\Gamma_2(x) + \Gamma_2^2(x)} S_D(\omega_a, \zeta_a). \quad (4.234a)$$

On substituting for the participation factors $\Gamma_1(x)$ and $\Gamma_2(x)$, this becomes

$$\begin{aligned} Y &= (1/\sqrt{2})\sqrt{[(1 + R^2) + \rho_{1,2}(1 - R^2)]} S_D(\omega_a, \zeta_a) \\ &= \Gamma_{1c2}(x) S_D \end{aligned} \quad (4.234b)$$

where

$$R = \varepsilon/\beta - (\delta/\beta)(x/r). \quad (4.234c)$$

From Der Kiureghian (1980a, b) it can be shown, for the close modal frequencies considered here, that the correlation coefficient $\rho_{1,2}$ may be approximated by

$$\rho_{1,2} \approx 1/[1 + (\beta/2\zeta_a)^2]. \quad (4.234d)$$

The coefficient of S_D in Equation (4.234b) may be regarded as the participation factor $\Gamma_{1c2}(x)$ of the combined modes 1 and 2.

The participation factors of the combined modes reflect the features of the participation factors of the individual modes. When $\delta \ll \Delta$ (case 2) then $\beta \approx \varepsilon$ and Equation (4.234) gives

$$\Gamma_{1c2}(x) \approx 1.0. \quad (4.235a)$$

Alternatively if there is strong interaction, (case 1) given by $\Delta \ll \delta$ then $\varepsilon \ll \beta$, and

$$\Gamma_{1c2}(x) \approx \sqrt{[1 + (1/2)(x^2/r^2 - 1)/(4\zeta_a^2/\delta^2 + 1)]}. \quad (4.235b)$$

If there is a high correlation $\rho_{1,2} \approx 1.0$, given by $4\zeta_a^2 \gg \delta^2$, which may readily occur, then the combined participation factor is again approximately unity.

The greatest dynamic amplification is given when strong interaction occurs, as for Equation (4.235b), and at the same time there is a low correlation between modal responses, given by $4\zeta_a^2 \ll \delta^2$; which is however a relatively extreme case. The upper limit of the combined participation factor, for this case where $\Delta \ll \delta$ and $\rho_{1,2} \ll 1.0$ is then given as:

$$\Gamma_{1c2}(x) \approx \sqrt{[1 + 1/2(x^2/r^2 - 1)]}. \quad (4.235c)$$

Example of individual and combined participation factors

Figure (4.17d) shows examples of individual and combined participation factors, as given by Equations (4.233) and (4.235). To give strong axial-mode interaction, the frequency separation Δ was made smaller than the torsional unbalance δ , with $\Delta = 0.01$ and $\delta = 0.05$, as in case (1). The damping was taken as $\zeta_a = 0, 0.02, 0.05, 0.20$, which give the correlation coefficient the values $\rho_{1,2} = 0, 0.38, 0.79, 0.98$, respectively.

The dotted lines in Figure 4.17(d) give the individual participation factors $\Gamma_1(x)$ and $\Gamma_2(x)$ for modes 1 and 2, while the full lines give the corresponding values for the combined participation factors $\Gamma_{1c2}(x)$ for various average modal dampings ζ_a , and hence for various correlations between modal responses. The figure shows that the combined participation factor is greater than unity whenever the values of $\Gamma_1(x)$ and $\Gamma_2(x)$ have opposite signs. This combined-response participation factor illustrates the ability of modal damping to largely suppress the effects of small, but dominant, torsional unbalance.

The above features of the combined modal responses may be summarised as follows. When a translational mode is coupled to a rotational mode, then sufficiently close modal frequencies give strong modal interactions. If strong modal interaction occurs when there is also a low correlation between modal responses, given by sufficiently low modal dampings, then there is a dynamic amplification of the combined seismic responses in those regions of the structure which have normal mode responses of opposite sign.

High dynamic amplification of torsional unbalance requires

$$\zeta_a < \beta < \delta.$$

Therefore an increase in the torsional unbalance δ allows dynamic amplification to occur with a greater frequency separation β and then also with greater modal damping ζ_a . Conversely dynamic amplification can be suppressed by a sufficient increase in the frequency separation and/or in the modal damping.

4.5.3 Seismic responses of structures with linear isolation and torsional unbalance

Using the above 2DOF model, seismic isolation may be used to reduce the torsional unbalance δ to a small value. This can be achieved by an appropriate placement of the isolator springs. The isolator may also provide large damping in the pair of modes. The seismic isolation reduces the responses of the first pair of modes, and the small unbalance and high damping limit the torsional components of these modes to their static values by suppressing dynamic amplification of torsional responses.

Consider a torsionally unbalanced three-dimensional structure with its C.G. directly above the centre of stiffness, C.S., of its linear isolator. The first triplet of isolated modes is given by a system which is almost torsionally balanced since the modal motions involve little structural deformation, and with no structural deformation the system would have exact torsional balance. Next consider a moderate offset between vertical axes through the structural C.G. and through the isolator centre of stiffness, which will normally occur despite a nominally zero offset. Torques will then be introduced by seismic forces perpendicular to this offset. Since the torsional and translational frequencies of the first isolated modes may be quite close, a moderate torsional unbalance of the isolator (corresponding to δ) may be sufficient to overcome the inhibiting effect of the small frequency separations, as discussed above. The mode shapes are now the 3DOF equivalent to case 1 in Figure 4.17(c), with each natural mode containing a large component of each of the three axial modes, for unbalance along both horizontal axes. With sufficiently low isolator damping, such a system of modes results in large dynamic amplification of rotational motions, as shown for its 2DOF counterpart by Equation (4.235b), and illustrated for a particular case by Figure 4.17(d). However, the equation and figure indicate that an isolator damping ζ_a which is equal to the unbalance offset, expressed as a fraction of the radius of inertia of the structure, is largely sufficient to suppress dynamic amplification of torsional unbalance for the first triplet of isolated modes.

The second triplet of isolated modes, arising from the second modes for the three axes, may again have close frequencies for a regular shear-like structure. If the torsional unbalance of these structure-dominated axial modes is relatively high, and structural damping is moderate, there may well be dynamic amplification of the torsional unbalance for this second triplet of isolated modes. This may give comparable responses for the rotational and translational components of the second triplet of isolated modes. These add little to the displacements and loads of the first triplet of isolated modes, where our cases (ii) and (iii) of Figure 2.7 give some

indication of the consequences of combining the translational components of the first and second modes.

4.5.4 Seismic responses of structures with bilinear isolation and torsional unbalance

The consequences of torsional unbalance, for a simple linear structure supported on a bilinear isolator, were investigated by Lee (1980) using seismic response-history analysis. Lee modelled a square building by a single storey with corner masses, columns and bilinear isolator components. The C.G. was at the centre of the building. When the building or the isolator was torsionally unbalanced, these shifts in their centre of stiffness had equal components along the x - and y -axes. Since all springs and masses were at the same distance from the centre of the structural model, the radii of inertia and stiffness were equal and, when torsionally balanced, the frequencies of the translational and torsional modes were equal, corresponding to $\Delta = 0$ for the two-dimensional model of Figure 4.17.

The bilinear isolator parameters were $T_{b1} = 0.9$ s, $T_{b2} = 2.0$ s and $Q_y/W = 0.05$. These parameters were close to the isolator parameters for our case (iv) in Figure 2.7. Lee's seismic responses gave isolator displacements moderately larger than for our case (iv) (as a consequence of exciting the isolated structure by both components of the El Centro 1940 earthquake simultaneously) and the equivalent period and damping for Lee's isolator were close to our values, namely 1.45 s and 24%. Lee's model included a set of small masses at the interface between the isolator and the structure which appear to have caused little change in the character of the seismic responses of the isolated structure.

Initially the structure was given eccentricities typical of code prescriptions for accidental unbalance, with $e_x = e_y = 0.1 b$, where b is the length of the sides of the structure. This corresponds to an unbalance factor $\delta = 0.2$ along a diagonal of the structure. The structure was given periods from 0.1 to 1.2 s and responses were obtained for simultaneous excitation by the El Centro 1940 accelerograms, with the N-S component along the x -axis and the E-W component along the y -axis.

Without isolation, the x -axis and y -axis responses were approximately those which would have resulted from the 5% damped spectra of the N-S and E-W accelerograms respectively (with a balanced structure). The torque, at various structural periods, corresponded to column forces which equalled or exceeded the column forces for x -axis responses. Hence, all three components of the structural responses were high and the torques corresponded to a considerable dynamic amplification of the torsional unbalance.

With a balanced bilinear isolator all three components of the response were greatly reduced, with the x - and y -axis forces close to the value given by the acceleration of 1.08 m s^{-2} for our case (iv) in Figure 2.7. The torques were reduced to give corresponding column forces which were a small fraction of the small x - and y -axial forces. Hence the balanced isolator was very effective in suppressing torsional responses to the structural unbalance.

Lee also investigated the effects of isolator unbalance. The resulting torques were essentially those given by the static unbalance, without dynamic amplification. This was the result to be expected for an unbalanced system with high equivalent viscous damping.

It appears that all the results reported by Lee have the general trends which would be given by replacing the bilinear isolator by a linear isolator with the effective period and damping based on maximum loop displacements, as described in Section 4.3, and approximated above by comparison with our similar balanced system (case (iv)).

When a multi-storey structure is mounted on a bilinear isolator, with structural and isolator parameters corresponding to cases (v) and (vi) of Figure 2.7, then the second triplet of isolated modes will be more severely excited, and they may make significant contributions to the 'static' unbalance responses given by the highly damped first triplet of isolated modes. Such higher-mode torsional responses will have the greatest design significance for structures with high-value, seismically vulnerable contents.

4.6 SUMMARY

The main results in this chapter are summarised here. The seismic responses of isolation systems can be regarded as falling into two categories. The first category comprises first-mode responses, or responses which are dominated by first-mode contributions; examples are the maximum base shears and isolator displacements. The second category comprises higher-mode quantities, or responses which are strongly affected by higher-mode responses; examples are the distribution of accelerations and shears in the structure, and the floor-response spectra for frequencies greater than about 2 Hz.

A high degree of linear isolation markedly reduces both first- and higher-mode responses within the structure itself compared with those in the unisolated structure. 'Floor spectra', which govern the earthquake forces on the contents of the structure, are correspondingly reduced at short periods. These large reductions in the accelerations, loads and deformations in the structure are obtained at the expense of large displacements across the isolators.

The acceleration reductions result from a lengthening of the fundamental period of the structure so that it lies outside the range of periods of the dominant peaks of the acceleration spectra of most earthquakes. For linear isolation systems, the higher-mode excitations are suppressed because the mode shapes are nearly orthogonal to the distribution of inertia forces imposed by the ground motions. The base shear is determined almost entirely by the first-mode response, because the shapes of the higher modes mean that the higher-mode inertia forces almost cancel when summed across the various masses, as well as the higher-mode participation factors being nearly zero. The displacements are also controlled by the first mode, because of the low participation factors of the higher modes and their much shorter periods compared with the first mode.

In the first isolated mode, the structure responds almost as a rigid body, with the fundamental period determined by the overall mass and the stiffness of the isolator. The first-mode damping is determined largely by the damping in the isolator because of the low deformations in the structure. The low base-stiffness produces free-free type higher modes, with the periods of the higher modes a function mainly of the stiffness of the structure rather than that of the isolator.

Because of the rigid-body nature of the first mode and its dominance in the overall response, the base shear and isolator displacement can be estimated accurately by a one-mass model, with the stiffness and damping corresponding to those of the isolator.

The degree of linear isolation depends on the isolation factor $I = T_b/T_1(U)$, namely the ratio between the period T_b of the isolator and the fundamental period $T_1(U)$ of the unisolated structure. The isolated mode shapes and higher-mode periods are very close to the free-free values for $I > 2$.

The isolator displacements can be reduced by increasing the energy dissipation in the isolator. This can be achieved either through viscous damping, in which the isolation system remains linear, or through non-linear hysteretic damping from yielding of metals or frictional sliding mechanisms.

Providing a high viscous damping in the base, such as about 20% of critical, produces non-classical mode shapes. The base impedance may increase significantly from that due to the isolator stiffness alone, and the higher modes are no longer orthogonal to the inertia force excitation. Both these effects may lead to substantially increased higher-mode effects. The higher-mode contributions are important in producing deviations from the mass-proportional force distribution of the first mode, and in increasing the floor-response spectra at higher frequencies.

Non-linear hysteretic energy dissipation in the isolator can lead to response characteristics significantly different from those for high degrees of linear isolation. The significant features of non-linear isolation can be modelled by bilinear hysteretic isolation. The different character of the response of non-linear isolation systems is related to the excitation of higher modes. The first-mode response, which governs the maximum base shear and the isolator displacement, can be closely approximated by that of a one-mass model, as for linear isolation.

The similarity between the first-mode responses of linear, viscously damped and bilinear-hysteretic isolation systems makes it useful to define an 'effective' or 'equivalent linear' period and damping for the bilinear system. This period and damping can then be used in a 'response spectrum' approach as for linear systems. The maximum base shear and isolator displacement of the non-linear isolation system when subjected to an earthquake ground motion can be obtained from linear response spectra. The accuracy of this approach can be estimated by comparing these values with the maximum displacements and accelerations of single-mass models on bilinear isolators, calculated from response-history analyses and presented in Figure 4.5. The approach is sufficiently accurate that it is useful as the basis for the preliminary design procedure recommended in Chapter 5.

The high-frequency ($> \sim 2$ Hz) responses of bilinear-hysteretic isolation sys-

tems can be understood in terms of their modal character. The seismic responses of a linear structure with a bilinear isolator are controlled by two sets of natural modes and the interactions between them. The elastic-phase set of modes is that given with an isolator stiffness K_{b1} . The yielded-phase modes are those resulting from an isolator stiffness K_{b2} . The yield-level ratio plays an important role in determining the level of first-mode response, and in the degree of excitation of the higher modes of the yielded-mode set. Interaction between the elastic-phase and yielded-phase modes is strongly dependent on the elastic phase isolation factor $I(K_{b1})$.

Since the maximum seismic responses typically occur during the yielded phase of the isolator, the distributions of maximum modal responses within the structure are given by yielded-phase mode shapes. These mode shapes are the same as for a linear isolation system with an isolation factor $I(K_{b1})$. However, the amplitudes of the higher-mode responses may be considerably greater than for the linear system because of the various non-linear excitation mechanisms besides direct excitation by ground motion during the yielding isolator phase. As for linear isolation systems, the higher-mode forces again almost cancel when summed over the structure, and the low frequency of the fundamental mode in the yielded phase means that it dominates the displacement response. Unlike the case of effective linear isolation systems, higher modes may make important contributions to the overall acceleration and shear distributions, and to the floor-response spectra for non-linear isolation systems.

The elastic-phase isolation factor $I(K_{b1})$ and the non-linearity factor NL , for which the yield ratio is an essential parameter, combine to play an important role in the strengths of the yielded-phase higher-mode responses. A low value of $I(K_{b1})$ combined with a large non-linearity factor is correlated with a high ratio of higher-mode to first-mode acceleration response. Poor elastic-phase isolation allows strong excitation of the higher modes directly by the ground motion in this phase of the response. In addition, a low value of $I(K_{b1})$ produces a strong contrast between the shapes of the elastic-phase and yielding-phase modes of the same number, resulting in significant coupling between elastic-phase and yielding-phase modes of different numbers. In more general non-linear systems with curvilinear rather than bilinear force-displacement characteristics, this coupling process occurs continuously as the effective mode shapes change with the amplitude of the motion, rather than at the discrete times associated with the changes in response phases as in the bilinear model. A large non-linearity factor is often required as the equivalent viscous damping from hysteresis is proportional to NL , and high damping is required to reduce isolator displacements. Idealised simple-friction sliding systems have no isolation in their locked phase and have the maximum possible non-linearity factor of 1 because of their rigid-plastic force-displacement loop, so usually have strong higher-mode responses. On the other hand, by designing isolation systems with hysteretic mechanisms which provide considerable isolation in their elastic phase, it is possible to achieve the desired property of high damping to limit the first-mode responses without inducing strong high-frequency responses which will attack subsystems and contents of the structure.

Strong higher-mode responses produce an overall shear distribution which is 'bulged' in comparison with the first-mode distribution, producing substantially increased values in the top half of a structure in particular. Strong higher-mode responses also make important, and often dominant, contributions to floor spectra, which determine the seismic forces on the contents of the structure.

The installation of seismic isolation is shown to reduce the effects of torsional unbalance, particularly if the centre of stiffness of the isolating system is beneath the centre of mass of the structure.

In summary, structures with a high degree of linear isolation and low isolator damping have much reduced acceleration responses and floor spectra compared to those of unisolated structures in El Centro type earthquakes, but may require large isolator displacements. Lightly damped linear isolation produces mainly first-mode response, which is characterised by nearly uniform, rigid-body-like motion in the structure which is insensitive to irregularities in the structure. The isolator displacements may be reduced by introducing high viscous damping or hysteretic damping in the isolator, but this generally increases the higher-mode responses which may be important for the overall shear distributions and floor spectra. Rigid-plastic isolator characteristics give particularly bad high-mode effects. Non-linear systems with good isolation in the elastic phase retain the desirable feature of first-mode dominated response as for linear isolation, producing both low forces throughout the structure and moderate isolator displacements.

5 *A Basis for the Design of Seismically Isolated Structures*

5.1 GENERAL APPROACH TO THE DESIGN OF STRUCTURES WITH SEISMIC ISOLATION

5.1.1 Introduction

Design approaches for seismically isolated buildings and bridges are presented in this chapter, together with a numerical example and some comments on design codes and guidelines. The procedures follow from the features of seismically isolated structures and the properties of the isolating devices, as discussed in Chapters 2, 3 and 4. The preliminary aseismic design of an isolated structure calls for approximate estimates of seismic loads, deformations and floor-acceleration spectra (which indicate levels of appendage loads) when the structure is subject to design earthquake accelerations. The procedure for structures with bilinear hysteretic isolation is similar to that recommended by Andriono and Carr (1991b), for a wide range of earthquake excitations and for a range of structures with bilinear isolation (Andriono and Carr, 1991a).

These initial estimates of seismic responses allow an assessment to be made of the effectiveness of seismic isolation for the particular structure and site. The estimates also allow initial decisions to be made on structural form and isolator parameters, and a tentative assignment of member sizes. These preliminary design choices form the basis of the second design stage, which calls for further optimisation of the aseismic design based on more accurate evaluations of seismic responses, and for a more detailed design of the structure and isolator.

It is emphasised that the procedures outlined in this chapter are intended as a design guide only, namely as a means of enabling the designer to arrive at suitable starting values for system parameters, which will then be refined in further computation and dynamic analysis.

As discussed in Chapter 4, when a structure and isolator can be treated as linear, then seismic responses may be evaluated approximately by the general modal procedures used for non-isolated linear structures, namely using modal periods, dampings and participation factors, together with design-earthquake spectra. With linear isolation, the response is dominated by a simple first mode. Higher-mode displacements are usually insignificant. First-mode loads can be combined with the small higher-mode contributions to give the overall structural response.

Even moderate isolator non-linearity tends to increase the higher-mode accelerations and hence to increase the floor spectra. Therefore when low appendage responses, and hence low floor spectra, are an important design consideration, a more detailed analysis may be required to evaluate the floor spectra, even when non-linear isolator effects are only moderate.

When the effects of isolator non-linearity are large, or when an irregular structure with a linear isolator has seismic responses which are complicated by close modal periods or greatly non-classical mode shapes, then the evaluation of the modal participation factors and the definition of rules for combining modal responses become more difficult. It is then usual to compute the seismic responses of the structure directly, using step-by-step evaluation of the responses of a model of the structure to the time history of design-earthquake accelerations. However, a modal approach may be retained for the more complicated linear structures by adopting the analytical approaches presented by Hurty and Rubinstein (1964), Wilson *et al.* (1981) and Der Kiureghian (1980).

Even when structural response evaluations call for detailed time-history analysis, an understanding of the importance of various structural and isolator features is increased by also computing the contributions of individual isolated modes. This increased understanding assists in selecting the structural and isolator modifications required to improve aseismic performance. When it is difficult to compute the response contributions of significant modes directly, these individual mode responses may be derived from the time-history responses by using the mode-sweeping technique which has been described in Chapter 4 and used to derive many of the results presented in Chapters 2 and 4.

5.1.2 The seismic isolation option

Principal features given by isolation

Seismic isolation below all or part of a structure provides flexibility and usually damping, which generally reduce the severity of earthquake attacks. Chapters 2 and 4 demonstrated the principal reductions in attack which isolation can confer on structures and their contents. These chapters also showed the isolator deformations and structural displacements which must be accepted in order to achieve the reductions in seismic attack. Three central features emerged:

- (1) Isolators may give large reductions in the seismic loads and deformations for those structures, with short periods and low dampings, which are most prone to suffer severe seismic attack if unisolated.
- (2) Selected isolators may give very large reductions in the seismic loads on secondary structures and on the contents of appropriate structures.
- (3) An isolator which is effective in reducing seismic attacks on a structure must have features which result in relatively large isolator displacements. The total structural displacements are then a little larger than the displacements of the supporting isolator, since they are moderately increased by structural deformation.

Seismic isolation may be used to give additional benefits:

- (1) Isolation gives a large increase in the first-mode period and substantial increases in higher-mode periods and this may sometimes be used to reduce severe seismic responses of secondary structures if the severity is caused by approximate tuning to the period of an unisolated structural mode, particularly unisolated mode 1.
- (2) Isolated bridge superstructures may lead to more integrated and balanced structures with a better distribution of seismic loads between vulnerable support substructures.
- (3) Hysteretic isolators may be used to confer ductility on otherwise brittle structures, thus enabling them to resist seismic loads. If the structure has high stiffness and low damping, effective ductility can be introduced without large increases in structural deformations.

Factors favouring seismic isolation

At the initial design stage, it is necessary to consider whether the addition of seismic isolation will prove to be a cost-effective means of providing appropriate levels of seismic resistance for a structure and its significant secondary structures and contents. However, the final decision to use seismic isolation must be made on a case-by-case basis. The introduction of seismic isolation may be beneficial when several of the following conditions apply to a proposed structure, when unisolated:

- (1) The unisolated structure is subject to severe seismic attack due to high seismicity at its site, and due to its responsiveness to design-earthquake accelerations. Dominant structural modes, that is modes with high participation factors, have moderate damping together with periods within the high-value range of acceleration spectra, and therefore high seismic responses may occur.
- (2) Earthquake motions likely to occur at the site have relatively short-period accelerograms, typically with dominant periods not greater than those for the El Centro 1940 record. When the seismic attack has short periods, less isolator flexibility is required for a given reduction in the spectral acceleration values for isolated mode 1, which usually dominate the seismic attack. Both the reduced flexibility, and the consequent smaller isolator deformations, should generally reduce the costs of the isolator components and the cost of providing for structural displacements. Dominant seismic spectral periods are generally reduced by smaller site flexibility, particularly as occurs at rock sites. Moderate epicentral distance and earthquake magnitude, and the absence of large movements on nearby faults, may also tend to give short-period spectra.

The fact that earthquake motion dominated by short-period content favours the adoption of seismic isolation does not rule out its use where 'fault-fling' type motions with long-period displacements are expected. The large displacement demands imposed by fault-fling components may be more readily

- accommodated by isolated structures with provision for large isolator displacements than by conventional structures.
- (3) Primary or important secondary structures are particularly vulnerable to seismic attack. This includes primary or secondary structures with moderate strength and a low capacity for inelastic deformation, that is, with low ductility. Vulnerability of secondary structures may be increased by near-resonance with dominant unisolated structural modes.
 - (4) Structural foundations are weak and have low ductility. This may present severe problems since such foundations are usually difficult to inspect, and to repair if damaged.
 - (5) Seismic loads and deformations are increased in parts of the unisolated structure by an irregular structural form. Such forms include severe set-backs, irregular floor profiles such as an L-shape, and mass and stiffness distributions which give torsional unbalance. Unbalanced foundation stiffness may also cause torsional vibrations of a structure.
 - (6) Seismic deformations of the unisolated structure make it difficult to protect non-structural components.
 - (7) The structure requires little modification to accommodate an isolation system. Such structures include bridges with superstructures which already have provisions for substantial length and shape changes. They may also include structures already isolated from ground-transmitted non-seismic vibrations, such as those generated by railway traffic. Buildings with three-dimensional beam-column frames may have a distribution of columns which gives appropriate locations for isolator mounts. Buildings which have deep slender piles to gain support from a high-strength subsurface layer may be given horizontally flexible mounts by making the piles free-standing within clearance sleeves.
 - (8) Reliable isolator components, which provide the required isolator features, are available at an acceptable cost.

5.1.3 Design earthquakes

In principle, design earthquakes for seismically isolated structures should be selected on the same general basis as design earthquakes for an unisolated structure at the same site. In practice, design motions for isolated structures tend to place greater emphasis on excitation with strong long-period content than is usual for conventional structures. In particular, accelerograms with long-duration 'fault-fling' components are often considered for base-isolated structures located near faults. Appropriate return periods for 'design-level' and extreme or 'maximum credible' motions are selected on a similar basis to those for unisolated structures, taking into account the seismicity of the region and the importance and risk factors for the structure.

For many sites with high seismicity, and ground of moderate flexibility and high strength, amplitude-scaled El Centro-like accelerograms and spectra may be used

for seismic design; other conditions such as near-fault location or highly flexible soil give different accelerograms and spectra. In some cases the significant features of the accelerograms and spectra can be approximately matched by scaling the amplitudes and periods of the El Centro NS 1940 accelerogram $\ddot{u}_g(t)$ by the multipliers P_a and P_p respectively, to give the scaled El Centro accelerogram $P_a \ddot{u}_g(t/P_p)$. The period scale factor increases the spectral periods and the duration of the accelerogram by the multiplier P_p . For linear structures with bilinear isolators, the seismic responses to scaled El Centro accelerograms can be obtained from the responses to the El Centro accelerogram by weighting the structural and isolator parameters and response quantities by appropriate factors involving P_a and P_p , as presented in Chapter 4 and included in the seismic response summaries below.

A factor which may influence the character of the earthquake motions at a site is the proximity to the causative fault, and the nature of the faulting action. A large movement on a nearby fault is thought to increase the amplitude of long-period ground accelerations through the presence of a 'fault-fling' pulse, which is important for isolator displacements. The Uniform Building Code (UBC)(1989) commonly used in the USA calls for increases of 20% and 50% in design displacements of isolators when an active fault is within 10 km and 5 km of the site respectively, compared with those in the absence of an active fault.

Response spectra for some typical design earthquakes are discussed in Chapter 2, where it is shown that the acceleration response spectra are dominated by periods in the range 0.1–1 s while displacement spectra are dominated by much longer periods. With seismic isolation it is usually found that a number of important design features, such as the isolator-level displacements and shears, are dominated by displacement spectral values for periods in the range from 1.0 s to 3.0 s, and frequently within the range from 1.5 s to 3.0 s, as illustrated in Figure 2.1. For this period range, the spectra of El Centro-like earthquakes may be approximated by very simple trend curves.

Figure 5.1(a) shows simplified linear acceleration, velocity and displacement response spectra for the scaled El Centro earthquake. The long-period 'enhanced' option, shown dotted, makes some provision for greater long-period spectral values which may be appropriate for some sites or for earthquakes with magnitudes greater than the M_S 7.0 value of the 1940 Imperial Valley earthquake which produced the El Centro accelerogram.

To denote that these are simplified spectra, the symbols are underlined in the figure and text below.

Figure 5.1(a) is based on a simple model in which, for a given spectral damping ζ , the El Centro NS 1940 velocity spectrum $S_V(T, \zeta)$ is approximated by a curve $\underline{S}_V(T, \zeta)$ which is proportional to period from 0.25 s to 0.5 s, is independent of period from 0.5 s to 3.0 s, and is inversely proportional to period from 3.0 s to 4.5 s. The model also adopts a simple relationship between the acceleration, velocity and displacement spectra given by

$$a_1 T \underline{S}_A(T, \zeta) = \underline{S}_V(T, \zeta) = (a_2/T) \underline{S}_D(T, \zeta) \quad (5.1)$$

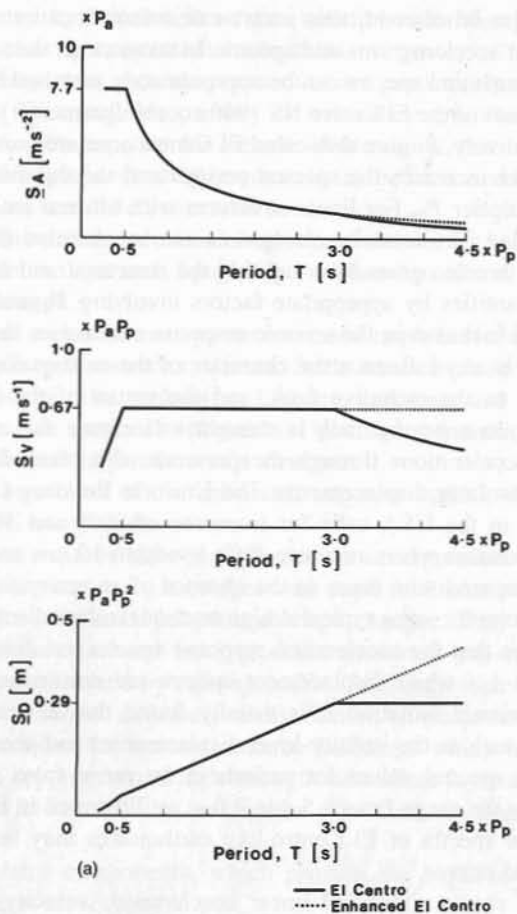


Figure 5.1 Simplified linear response spectra. (a) Smoothed and simplified approximations to the 5% damped linear response spectra \underline{S}_A , \underline{S}_V and \underline{S}_D , for the scaled El Centro NS 1940 design earthquake (solid lines). The spectra with 'long-period enhancement' are also shown (dotted lines). (b) Multipliers C_A , C_V and C_D which can be used to derive simplified scaled El Centro spectra with other damping-factor values, from the 5% damped curves in Figure 5.1(a). (c) Simplified El Centro displacement spectra with long-period enhancement (dashed lines) for damping factors of 5, 10 and 20%, multiplied by a factor of 0.9 (see text) and compared with the average spectra for eight earthquake components (solid lines)

where $a_1(\zeta)$ and $a_2(\zeta)$ are constant for a given damping factor ζ . This approach gives relationships between the acceleration, velocity and displacement spectra similar to, but not the same as, the commonly used pseudo-acceleration spectra ωS_V and pseudo-displacement spectra S_V/ω for which a_1 and a_2 are $1/2\pi$ and 2π respectively for all dampings.

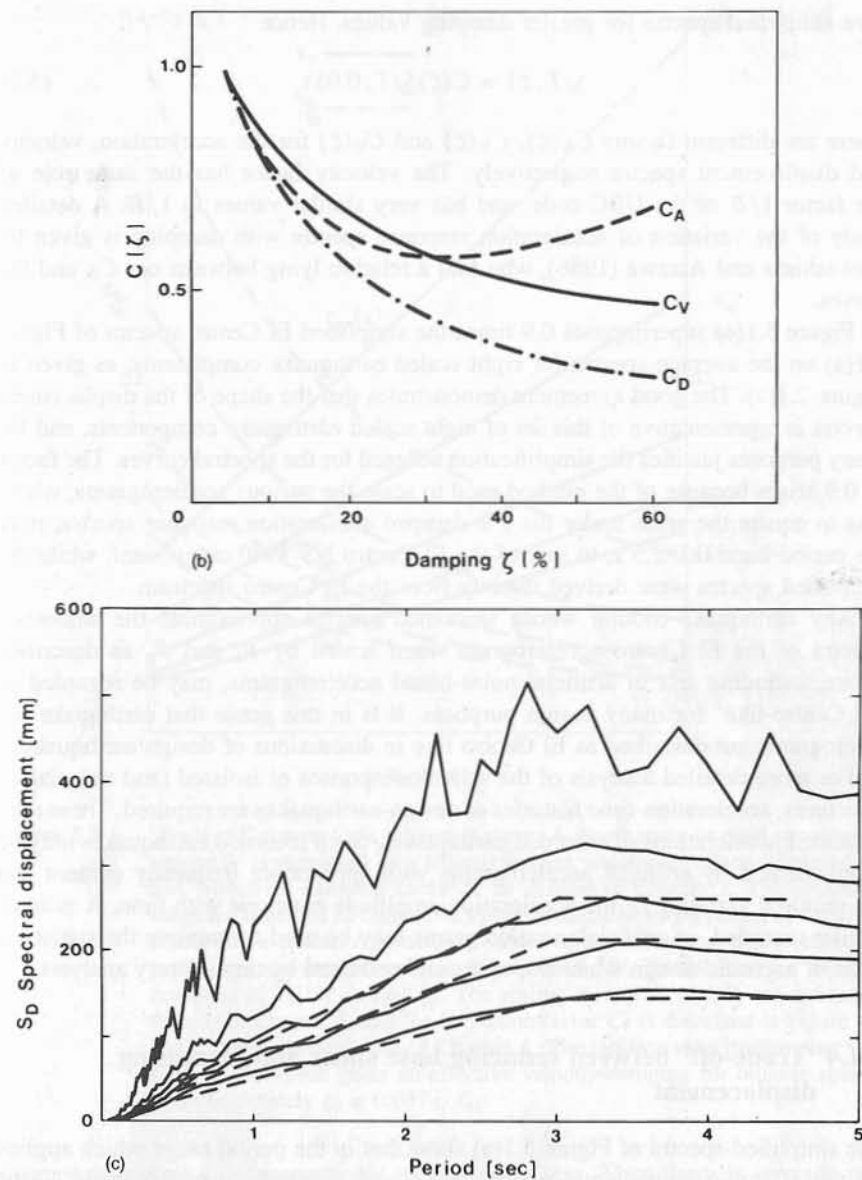


Figure 5.1 (continued)

The vertical scales of the curve shapes of Figure 5.1(a) were adjusted to give best fits to the corresponding 5% damped spectra for El Centro NS 1940. The curves of Figure 5.1(a) show the simplified spectra $\underline{S}(T, 0.05)$ for a spectral damping factor $\zeta = 0.05$. The curves of Figure 5.1(b) give the scale multipliers $C(\zeta)$ required to

give simplified spectra for greater damping values. Hence

$$\underline{S}(T, \zeta) = C(\zeta)\underline{S}(T, 0.05). \quad (5.2)$$

There are different factors $C_A(\zeta)$, $C_V(\zeta)$ and $C_D(\zeta)$ for the acceleration, velocity and displacement spectra respectively. The velocity factor has the same role as the factor $1/B$ of the UBC code, and has very similar values to $1/B$. A detailed study of the variation of acceleration response spectra with damping is given by Kawashima and Aizawa (1986), who find a relation lying between our C_A and C_V curves.

Figure 5.1(c) superimposes 0.9 times the simplified El Centro spectra of Figure 5.1(a) on the average spectra for eight scaled earthquake components, as given in Figure 2.1(c). The good agreement demonstrates that the shape of the displacement spectra is representative of this set of eight scaled earthquake components, and for many purposes justifies the simplification adopted for the spectral curves. The factor of 0.9 arises because of the method used to scale the various accelerograms, which was to equate the areas under the 2% damped acceleration response spectra, over the period band 0.1–2.5 s, to that of the El Centro NS 1940 component, while the simplified spectra were derived directly from the El Centro spectrum.

Any earthquake motion whose smoothed spectra approximate the smoothed spectra of the El Centro accelerogram when scaled by P_a and P_p as described above, including sets of artificial noise-based accelerograms, may be regarded as 'El Centro-like' for many design purposes. It is in this sense that earthquake accelerograms are described as El Centro like in discussions of design earthquakes.

For more detailed analysis of the seismic responses of isolated (and unisolated) structures, acceleration-time histories of design-earthquakes are required. These may be scaled accelerations of recorded earthquakes. Such recorded earthquakes may be supplemented by artificial accelerograms with appropriate frequency content and the required variation of the acceleration amplitude envelope with time. A suite of similar recorded, or artificial, accelerograms may be used to improve the statistical basis of aseismic design when responses are evaluated by time-history analysis.

5.1.4 'Trade-off' between reducing base shear and increasing displacement

The simplified spectra of Figure 5.1(a) show that in the period range which applies for the effective fundamental period of isolated structures, namely about 1 s or greater, increasing the period reduces the spectral acceleration for a given damping while increasing the spectral displacement. Considering the $C_A(\zeta)$ and $C_D(\zeta)$ curves of Figure 5.1(b), it can be seen that increasing the damping, from 5% of critical, reduces the spectral displacement for a given period, while the acceleration decreases until 25–30% damping and then increases with a further increase in damping. For a single-degree-of-freedom system, or a linear system in which the base shear is dominated by the fundamental mode as for isolated structures, the

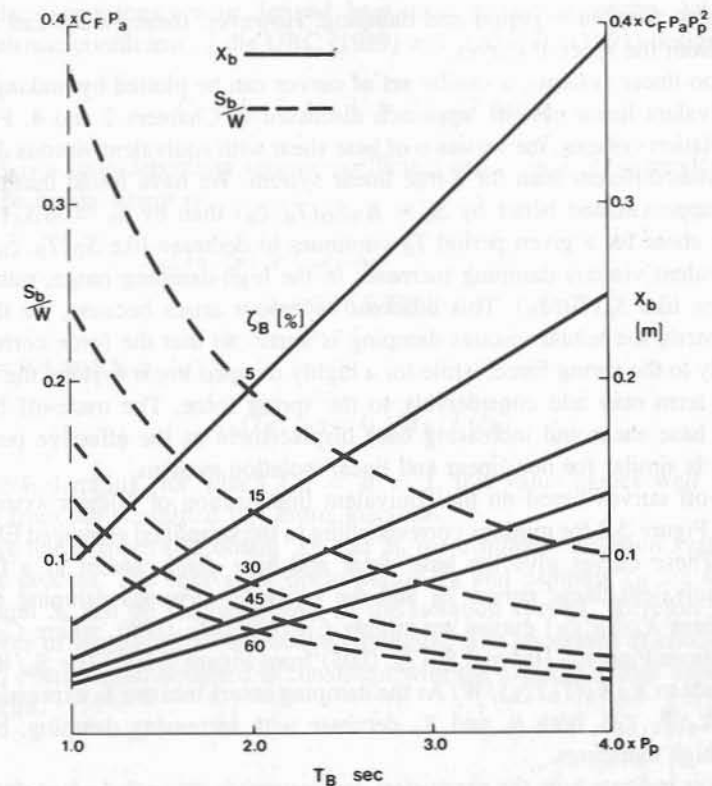


Figure 5.2 'Trade-off' curves for a bilinear isolator. A single mass or rigid structure of weight W is supported by a bilinear isolator which has 'effective' period T_B and 'effective' damping factor ζ_B as defined in Chapter 2. The system is subjected to scaled El Centro NS 1940, enhanced to a long period of 4.0 s, the conservative option. Approximate values of the maximum displacement X_b (solid line) and maximum shear force ratio S_b/W (dashed line) are given as functions of T_B for various ζ_B . The scaling factors P_a and P_p are defined in the text in Chapter 5, and the correction factor C_F is discussed in Figure 4.8 and in the associated text in Chapter 4. The isolator velocity-damping was $\zeta_{b2} = 0.05$, which gives an effective velocity-damping for bilinear spectra of approximately $\zeta_b = 0.05T_B/T_{b2}$

spectral acceleration is proportional to the base shear. Thus there is a 'trade-off' between reducing base shear and increasing displacement as the fundamental-mode period is increased, and also to a lesser extent as the damping is increased beyond about 30% of critical.

For linear isolation systems these trade-offs can be emphasised by plotting on a single diagram the spectral displacements $S_D(T_b, \zeta_b) \approx X_b(T_b, \zeta_b)$ and the normalised spectral acceleration $S_A(T_b, \zeta_b)/g \approx S_b/W$, as a function of T_b for various dampings ζ_b , where it is assumed that T_b and ζ_b are close approximations to the

true isolated first-mode period and damping. However, these values can be read directly from the spectral curves.

For non-linear systems, a similar set of curves can be plotted by making use of the 'equivalent linear system' approach discussed in Chapters 2 and 4. For non-linear isolation systems, the variation of base shear with equivalent viscous damping is somewhat different than for a true linear system. We have found that the base shear is approximated better by $S_b \approx K_B S_D(T_B, \zeta_B)$ than by $S_b \approx M S_A(T_B, \zeta_B)$. The base shear for a given period T_B continues to decrease like $S_D(T_B, \zeta_B)$ when the equivalent viscous damping increases in the high-damping range, rather than to increase like $S_A(T_B, \zeta_B)$. This different behaviour arises because, for the non-linear system, the actual viscous damping is small, so that the force corresponds essentially to the spring force, while for a highly damped linear system, the viscous damping term may add considerably to the spring force. The trade-off between reducing base shear and increasing base displacement as the effective period T_B increases is similar for non-linear and linear isolation systems.

Trade-off curves based on the equivalent linearisation of bilinear systems are shown in Figure 5.2 for motions corresponding to the simplified enhanced El Centro spectra. These curves give the base shear and base displacement as a function of the equivalent linear period T_B and the equivalent viscous damping ζ_B . The displacement $X_b(T_B, \zeta_B)$ curves are simply $C_D(\zeta_B) \underline{S}_D(T_B, 0.05)$, where $C_D(\zeta_B)$ is obtained from Figure 5.1(b) and $\underline{S}_D(T_B, 0.05)$ from Figure 5.1(a). The S_b/W curve corresponds to $K_B X_b(T_B, \zeta_B)/W$. As the damping enters into the S_b expression only through $X_b(T_B, \zeta_B)$, both S_b and X_b decrease with increasing damping, both for low and high dampings.

The axes indicate how the parameters and responses are scaled when the design motion is scaled from the smoothed El Centro spectrum by an amplitude factor P_a and a period factor P_p . The correction factor C_F , corresponding to Figure 4.8, is also included; for most cases C_F is close to unity.

For the particular displacement spectrum shown in Figure 5.1(a)

$$\underline{S}_D(T_B, 0.05) = 0.29(T_B/3) \quad (\text{m}). \quad (5.3)$$

Thus the curves of Figure 5.2 correspond to

$$\begin{aligned} X_b(T_B, \zeta_B) &= C_F P_a P_p^2 0.29(T_B/3 P_p) C_D(\zeta_B) \quad (\text{m}) \\ &= 0.097 C_F P_a P_p T_B C_D(\zeta_B) \quad (\text{m}) \end{aligned} \quad (5.4a)$$

and

$$\begin{aligned} S_b(T_B, \zeta_B)/W &= \omega_B^2 X_b(T_B, \zeta_B)/g \\ &\approx 0.39 C_F P_a P_p C_D(\zeta_B)/T_B \end{aligned} \quad (5.4b)$$

where $\omega_B = 2\pi/T_B$ is the effective frequency, given by $\sqrt{(K_B g/W)}$.

Similar expressions can be derived from other simplified spectra. An example is the seismic coefficient of the UBC (1989) and AASHTO (1991) design specifications:

$$C_s = S_b(T, \zeta)/W = A S_i/(T B(\zeta)) \quad (5.5)$$

where A is a zone-dependent seismic coefficient and S_i is a site-dependent coefficient. The displacement is

$$\begin{aligned} X_b(T_B, \zeta_B) &= C_s g / \omega_B^2 \\ &= 0.25 A S_i T_B / B(\zeta_B) \quad (\text{m}). \end{aligned} \quad (5.6)$$

For $A = 0.4$ and $S_i = 1$,

$$X_b(T_B, \zeta_B) = 0.10 T_B / B(\zeta_B). \quad (5.7)$$

For 5% damping, for which $C_D = B = 1$, this value agrees well with that derived from our simplified El Centro spectrum.

Using linear spectra to obtain X_b and S_b for a bilinear isolation system is an iterative process. The equivalent linear period T_B and damping ζ_B are dependent on X_b and S_b and on the parameters of the isolation system. Therefore, in using the curves of Figure 5.2 or the above equations, it is necessary to check that the (X_b, S_b) combination obtained is consistent with the (T_B, ζ_B) values used to enter the spectra.

5.1.5 Higher-mode effects

Displacement and base shear are related mainly to first-mode responses, and can therefore be predicted well by the response of single-degree-of-freedom systems. However, the distribution of shears in the structure is also dependent on the higher-mode responses.

In Chapter 4, it was shown that the ratio of higher-mode to first-mode responses was strongly correlated with the elastic-phase isolation factor $I(K_{b1}) = T_{b1}/T_1(U)$ and the non-linearity factor \underline{NL} . The results given in Figure 4.12 for 63 of the bilinear isolation systems given in Table 4.1 are generalised to an N -mass structure and simplified in Figure 5.3(a). This figure shows the ratio of the n th-mode acceleration response at the top of the structure (mass N) to the corresponding first-mode acceleration, for modes $n = 2$ (solid lines) and $n = 3$ (dashed lines), as a function of \underline{NL} for various ranges of elastic-phase isolation factors. As discussed in Chapter 4, the results were derived for uniform 5-mass isolated shear-structures subjected to the N-S component of El Centro 1940. However, they should apply reasonably well for nearly uniform shear-structures with any number of masses (storeys) with $N \geq 4$. Figure 5.3(a) does not represent the responses of systems with nearly elasto-plastic characteristics, i.e. very large values of T_{b2} , such as the cases of Table 4.1 with $T_{b2} = 6$ s.

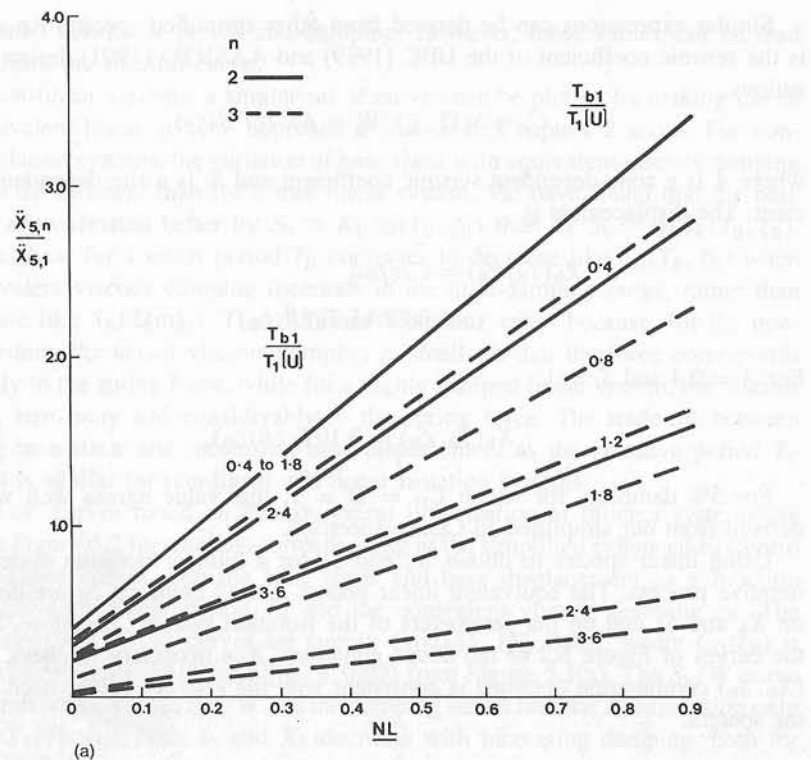


Figure 5.3 Features of higher-mode responses of a standard uniform 5-mass shear structure with bilinear isolation, subject to El Centro NS 1940. (a) Trend lines derived from Figure 4.12, showing ratios of peak modal accelerations at the top of the structure, for 63 of the bilinear isolation systems given in Table 4.1. Parameters for the trend lines are the non-linearity factor \underline{NL} and the elastic-phase isolation factor $T_{b1}/T_1(U)$. (b) Variation of the total seismic shear (solid line) and the first-mode shear (dashed line), illustrated for a case with substantial higher-mode accelerations. The value of the ratio $S_r/S_{r,1}$ halfway up the structure is defined as the ‘mid-height shear bulge factor’ \underline{BF}

Figure 5.3(a) demonstrates that bilinear isolators give strong higher-mode acceleration and load responses when the non-linearity \underline{NL} is high, and when the elastic-phase isolation factor is low. If such higher-mode responses are undesirable then these two parameters should be chosen suitably, as discussed in Chapters 2 and 4.

Figure 5.3(b) illustrates typical ratios of total (solid line) and mode-1 (dashed line) seismic shear forces using a uniform shear-beam structure mounted on a bilinear isolator. The ratio of these shears at any height z_r is defined as the shear bulge factor $\underline{BF}_r = S_r/S_{r,1}$. The mid-height shear bulge factor \underline{BF}

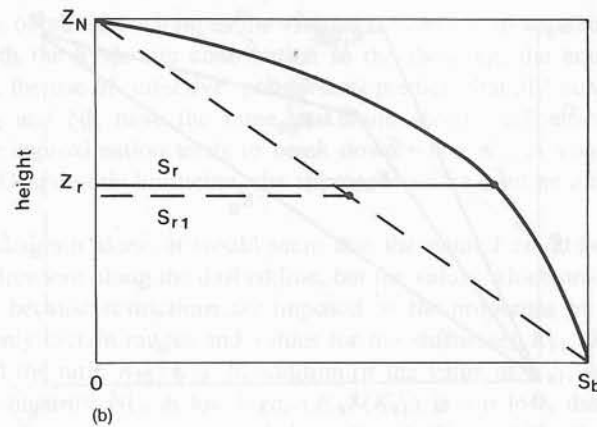


Figure 5.3 (continued)

Figure 4.13 and the associated text to be given approximately by

$$\underline{BF} \approx (1 + a(\ddot{X}_{N,2}/\ddot{X}_{N,1})^2)^{1/2} \tag{5.8}$$

where $a \sim 0.85$ for $T_1(U) = 0.25$ s, 0.75 s, and $a \sim 0.6$ for $T_1(U) = 0.5$ s. The shear at positions other than mid-height can be estimated by adding a half-sine-wave variation to the triangular first-mode distribution.

Strong higher-mode responses also produce strong floor-response spectra in the range of higher-mode frequencies, as shown in the examples of Figure 2.7. Higher-mode responses can generally be reduced by increasing $I(K_{b1})$, which has little effect on first-mode responses, or by reducing \underline{NL} , which generally increases base shears and displacements. Typically, reduced higher-mode responses are obtained at the expense of increased base displacement.

5.1.6 The locus of yield-points for a given \underline{NL} and K_B , for a bilinear isolator

Geometrical construction

A method of determining combinations of K_{b1} , K_{b2} and Q_y which will produce a bilinear isolator with a given non-linearity factor \underline{NL} and effective stiffness K_B , is illustrated in Figure 5.4(a).

The non-linearity factor \underline{NL} was defined in Figure 2.3(c) to be equal to the ratio between two perpendiculars standing on the common diagonal of the shear-force/displacement hysteresis loop and the circumscribed axis-parallel rectangle with vertices $(+X_b, +S_b)$ and $(-X_b, -S_b)$. For the bilinear case, the non-linearity factor \underline{NL} is also the ratio between the area of the hysteresis loop and that of the rectangle.

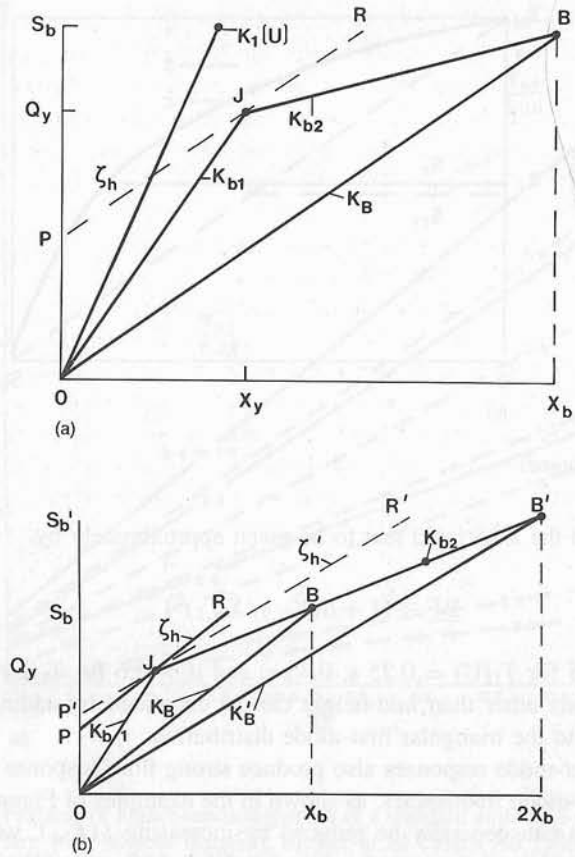


Figure 5.4 (a) Detail of part of the bilinear hysteresis loop shown in Figure 2.3, showing the initial and yielded stiffnesses K_{b1} and K_{b2} , the effective (secant) stiffness $K_B = S_b/X_b$, the yield-point J , and a line PR of gradient K_B through J which is the locus of yield-points which give the same non-linearity factor $NL = OP/S_b$. (b) Extension of Figure 5.4(a), in which the primed variables show how doubling the cyclic displacement X_b of a bilinear isolator affects its 'effective' stiffness K_B and non-linearity NL , and hence the effective period T_B and damping factor ζ_b

Simple geometry, using similar triangles, results in the formula $NL = Q_y/S_b - X_y/X_b$. Further geometrical construction results in another useful result, namely $NL = OP/S_b$, where the point P is obtained by drawing a line of slope $K_B = S_b/X_b$ through the yield-point, i.e. parallel to the diagonal linking the origin and the point (X_b, S_b) . This line is shown dashed in Figure 5.4(a). The yield-point is indicated J on the diagram.

The dashed line PR is thus the locus of yield-points J which give the same non-linearity. By moving J along the line, systems with different K_{b1} , K_{b2} and

Q_y/W can be obtained. As long as the viscous component of the damping is small compared with the hysteretic contribution to the damping, the equivalent linear approach (i.e. the use of 'effective' parameters) predicts that all such systems with the same K_B and NL have the same maximum seismic responses X_b and S_b . However, the approximation tends to break down when K_{b1} is very large or K_{b2} is near zero. Despite this limitation, the approach can be used as a framework for design.

From the diagram alone, it would seem that the point J could be moved with considerable freedom along the dashed line, but the values which are obtained may be unsuitable because restrictions are imposed by the properties of real isolators, which have only certain ranges and values for the stiffnesses K_{b1} , K_{b2} , the yield-point Q_y , and the ratio K_{b1}/K_{b2} . In addition, if the value of K_{b1} , in combination with the non-linearity NL , is too high, i.e. $1/(K_{b1})$ is too low, then undesirable higher-mode effects may be produced. In some situations, there may be ways of designing the isolation system so that desired values of K_{b1} and K_{b2} can be obtained. For instance, a combination of laminated-rubber bearings and lead-rubber bearings has been used in some buildings (see Chapter 6) which gives more freedom in the achievable combination of parameters K_{b1} , K_{b2} , and Q_y than is given by lead-rubber bearings alone.

A numerical example

A numerical example is given here which illustrates the 'yield-point-locus' concept. It is assumed that $T_1(U)$ is less than 1 s, so that seismic isolation, by means of period shifting, is appropriate. A typical value chosen is $T_1(U) = 0.6$ s. A value chosen for the effective period is then $T_B \approx 1.5$ s, with high effective damping i.e. $\zeta_B \approx 0.25$. The target peak base displacement is $X_b = 0.071$ m and the base shear $S_b = 0.127W$, where W is the total weight above the isolator interface. Reference to Figure 5.2 shows that these values are consistent with each other.

Appropriate isolator parameter values are now selected by using Figure 5.4(a). At this stage a value for the viscous damping ζ_b must be chosen, for example choose $\zeta_b = 0.05$. Then $\zeta_h = 0.2$ is required to give the total effective damping $\zeta_B = 0.25$. Since the non-linearity and effective damping factor are related by $NL = (\pi/2)\zeta_h$, this gives $NL = 0.31$. Hence OP in Figure 5.4(a) is given by:

$$OP = NL S_b \approx S_b/3.$$

Fixing P locates the line PJR in Figure 5.4(a), since it is parallel to OB . If the bilinear parameters could be chosen freely to satisfy $T_B = 1.5$ and $\zeta_h = 0.2$, then the point J could lie at any position along PR . This is satisfied, for example, when J is near the mid-point of PR . Let $PJ=JR$, giving

$$Q_y = 0.645 S_b = 0.083W.$$

Also

$$K_{b1} = 1.92K_B \text{ and } K_{b2} = 0.52K_B.$$

Also, since K_B , with the rigid-structure mass, gives $T_B = 1.5$ s, it follows that

$$T_{b1} = 1.08 \text{ s} \quad T_{b2} = 2.1 \text{ s}.$$

These parameters now give an elastic-phase isolation factor $T_{b1}/T_1(U) \approx 1.8$ while the non-linearity $NL = 0.31$.

This situation can now be compared with that shown in case (iv) in Figure 2.7, and discussed in the associated text, in order to assess the higher-mode responses. The non-linearity factors are the same but the present example has an elastic-phase isolation factor only slightly more than half that of case (iv), because of the different unisolated periods. As a result, case (iv) has reasonably low higher-mode responses and acceptably low floor spectra, but the case being studied here still has significant higher-mode effects. This can be seen by estimating the mode-2 to mode-1 acceleration ratio from Figure 5.3(a). It is seen that this ratio has a value of approximately 1.4 which can be substituted in equation (5.8) to give a mid-height shear-bulge factor BF of 1.5, a value considerably more than for case (iv). If this degree of higher-mode response is unsuitable, or if the real parameters of the isolators under consideration are unable to satisfy the values of K_{b1} , K_{b2} and/or Q_y/W required by the analysis above, then iteration must be performed to achieve more useful parameters.

If it is assumed that the bilinear parameters K_{b1} , K_{b2} and Q_y remain unaltered when the base displacement is increased from X_b to $2X_b$, then revised values of the effective isolator period and damping, T'_B and ζ'_B , can be found readily, as illustrated by Figure 5.4(b), which is an extension of Figure 5.4(a).

It is assumed above that the bilinear parameters remain unaltered when the peak displacement increases from X_b to $2X_b$. This may not be strictly true. As indicated by Figure 3.24 in Chapter 3, there tends to be some change in K_{b1} and K_{b2} with increasing X_b , giving a small increase in T'_B . There is probably a small increase in ζ'_B also.

5.2 DESIGN PROCEDURES

5.2.1 Selection of linear or non-linear isolation system

An early decision in the design of a seismically isolated structure is to determine whether a linear or non-linear isolation system is required. The selection will be governed partly by the nature of the design criteria. As discussed in the summary of Chapter 4, non-linear isolation systems can usually produce lower values of first-mode-dominated response quantities, such as base shears and displacements, while linear systems are particularly effective at suppressing higher-frequency responses. This is an important factor when the protection of contents or subsystems of the structure is a critical design criterion.

When the protection of high-frequency subsystems is a major concern, linear isolation systems, or non-linear systems with high elastic-phase isolation factors

and moderate non-linearity factors, are likely to provide effective solutions. Some systems with high non-linearity factors but also with high elastic-phase isolation may also provide acceptably low high-frequency response. Systems with rigid-sliding type characteristics are generally unsuitable for these types of applications. Figure 5.3(a) provides guidance to the relative strength of higher-mode response as a function of the elastic-phase isolation factor and the non-linearity factor.

Where high-frequency responses do not pose a major design problem, there is likely to be a much wider range of acceptable non-linear isolation systems. The main performance criteria are then usually related to base shear and base displacement, for which the trade-off curves of Figure 5.2 are relevant. Increased effective period usually reduces base shear, but increases displacements, as shown by the trade-off curves. Increased effective damping, or non-linearity factor, usually reduces both base shear and displacement, at the expense of stronger higher-mode responses. Systems with nearly elasto-plastic characteristics may appear attractive, but usually some centring force is a desirable isolator characteristic.

These characteristics provide initial guidance to the type of isolation system required. In some cases, it may be necessary to perform trial calculations for both linear and non-linear systems. In many cases other factors, such as the range of isolation systems for which local suppliers or design expertise are available, may determine the selection.

5.2.2 Design equations for linear isolation systems

Standard modal analysis procedures can be used to estimate the design responses of linear isolation systems. Initial estimates of displacements and base shears can be obtained from a simplified one-mass model because of the low participation factors of higher modes. Linear isolation systems with high damping in the isolator have non-classical modes, but usually the classical-mode approximation gives conservative estimates of the response of the structure itself. The non-classical nature of the modes may need to be taken into account when considering the response of nearly tuned subsystems, as the classical mode approach can considerably underestimate the response of subsystems.

A summary of the major equations relevant to the design of structures with linear isolators is given below.

(1) As a first approximation, the fundamental mode period and damping of a system with a high degree of linear isolation can be obtained by treating the structure as rigid. Then

$$T_1(I) \approx T_b = 2\pi(M/K_b)^{1/2} \quad (5.9a)$$

$$\zeta_1(I) \approx \zeta_b = C_b/(2(MK_b)^{1/2}). \quad (5.9b)$$

The isolator has stiffness K_b and damping coefficient C_b , and supports a total mass M .

The maximum base displacement X_b and base shear S_b can be approximated from

$$X_b \approx S_D(T_b, \zeta_b) \quad (5.10a)$$

$$\begin{aligned} S_b &= M\ddot{X}_b \\ &= MS_A(T_b, \zeta_b). \end{aligned} \quad (5.10b)$$

(2) More accurate modal responses can be obtained by obtaining the actual modal frequencies and dampings, together with the participation factors. These can be obtained by solving the standard eigenvalue problem

$$[\mathbf{K}]\phi_i = \omega_i^2[\mathbf{M}]\phi_i \quad (5.11)$$

where $[\mathbf{K}]$ and $[\mathbf{M}]$ are the stiffness and mass matrices of the isolated system, and ω_i and ϕ_i are the modal frequency and mode shape for mode i .

Chapter 4 provides perturbation expressions for the frequencies and dampings in terms of the free-free modal expressions (equations (4.90) and (4.91)). The modal dampings can be obtained from

$$2\zeta_i\omega_i = \phi_i^T[\mathbf{C}]\phi_i/\phi_i^T[\mathbf{M}]\phi_i. \quad (5.12)$$

In general, damping produces coupling between the modes unless

$$\phi_i^T[\mathbf{C}]\phi_j = 0 \quad i \neq j. \quad (5.13)$$

These coupling terms are ignored in the classical mode approach.

The participation factor of mode i at position r is given by

$$\Gamma_{ri} = \frac{\phi_i^T[\mathbf{M}]\mathbf{1}}{\phi_i^T[\mathbf{M}]\phi_i} \phi_{ri}. \quad (5.14)$$

The maximum modal displacement and acceleration of mode i at position r are given by

$$X_{ri} = \Gamma_{ri}S_D(T_i, \zeta_i) \quad (5.15a)$$

$$\ddot{X}_{ri} = \Gamma_{ri}S_A(T_i, \zeta_i). \quad (5.15b)$$

Again, perturbation expressions for Γ_{ri} are available from Chapter 4. As a first approximation $\Gamma_{r1} \approx 1.0$ and $\Gamma_{ri} \approx 0$, $i \neq 1$.

(3) The maximum responses of subsystems can be estimated using a modal response spectrum approach. For single-degree-of-freedom subsystems, the relevant modal combination rules are given by Equation (4.225) when the subsystem mode

is detuned from all the modes of the isolated structure:

$$\ddot{X}_e = \left\{ \sum_{i=1}^{N+1} \left[\frac{\Gamma_{ri}\phi_{rci}}{1 - \left(\frac{\omega_{ri}}{\omega_e}\right)^2} S_A(\omega_{ri}, \zeta_{ri}) \right]^2 + \left[\sum_{i=1}^{N+1} \frac{\Gamma_{ri}\phi_{rci}}{1 - \left(\frac{\omega_e}{\omega_{ri}}\right)^2} S_A(\omega_e, \zeta_e) \right]^2 \right\}^{1/2}. \quad (5.16)$$

This equation applies to a system with $N+2$ degrees of freedom comprising an N -mass structure mounted on an isolator represented by a base mass and spring, with another degree of freedom contributed by the appendage.

The more complicated expression of Equation (4.226) is required when the subsystem is tuned to mode k of the isolated structure:

$$\begin{aligned} \ddot{X}_e \approx & \left\{ \sum_{\substack{i=1 \\ i \neq k}}^{N+1} \left[\frac{\Gamma_{ri}\phi_{rci}}{1 - \left(\frac{\omega_{ri}}{\omega_e}\right)^2} S_A(\omega_{ri}, \zeta_{ri}) \right]^2 \right. \\ & \left. + \left[\frac{\Gamma_{rk}\phi_{rck}\omega_e^{3/2}}{\omega_a^{3/2} \sqrt{8\zeta_{rk}\zeta_a[1 + \beta_k^2/(4\zeta_a^2) + \gamma_k/(4\zeta_e\zeta_{rk})]}} S_A(\omega_e, \zeta_e) \right]^2 \right\}^{1/2}. \end{aligned} \quad (5.17)$$

The tuned expression accounts for interaction between the structure and subsystem, and also takes into account the generally non-classical nature of the mode shapes of the combined isolated structure and subsystem.

For multi-mass subsystems, the general form of expression is given by Equation (4.224), where the participation factors $\Gamma_{\text{eff},r,i}$ for the detuned isolated modes have similar forms to the expressions given in (4.225). When there is multiple tuning of a subsystem mode to several modes of the isolated structure, or of several subsystem modes to an isolated structure mode, a more complicated approach is required, as indicated by Igusa and Der Kiureghian (1985b).

(4) It is usually advisable to perform response-history analysis for a variety of accelerograms relevant to the specified earthquake ground motions in order to check the detailed design of the isolated structure.

5.2.3 Design procedure for bilinear isolation systems

It is assumed that design-earthquake motions are available in terms of displacement response spectra, e.g. EERL Reports (1972-5). Often design motions are specified in terms of 5% damped acceleration response spectra. These may be converted to

the required form by using

$$S_D(T, \zeta) = \frac{T^2}{4\pi^2} C_D(\zeta) S_A(T, 0.05). \quad (5.18)$$

The damping-dependent coefficients $C_D(\zeta)$ may be obtained from Section 5.1.3, or may be available as part of the specification of the earthquake ground motion.

Design criteria will usually involve acceptable base shears and displacements, and perhaps allowable shears at other levels of the structure and acceptable floor response spectra. The estimation of the seismic response for a structure with bilinear hysteretic isolation may proceed as follows.

Step 1 Select a trial isolation system. For design to a scaled El Centro type motion, the curves of Figure 4.5, which give base shear and base displacement as a function of Q_y/W for various T_{b1} and T_{b2} , provide guidance as to the possible combinations of parameters which produce responses meeting the design criteria.

Some types of isolators have restrictions on the achievable ratios of strength to stiffness, Q_y/K_{b1} and Q_y/K_{b2} , or ratios of pre-yield to post-yield stiffnesses K_{b1}/K_{b2} , which may limit the possible combinations of parameters Q_y/W , T_{b1} and T_{b2} .

The responses tend to be more sensitive to variations in Q_y/W and T_{b2} than to variations of T_{b1} , so it is usually sensible to select Q_y/W and T_{b2} ahead of T_{b1} .

It is often advisable to select Q_y/W as, or greater than, the value $(Q_y/W)_{opt}$ which gives minimum base shear for the design-level earthquake motions. This lessens the chances of $Q_y/P_a W$ falling in the range of rapidly increasing displacements and shears as P_a increases above that for the design-level motion.

Step 2 Take a trial value of the base displacement X_b for the specified earthquake motion. Figures 4.5(a)–(c) provide guidance to likely displacement responses for El Centro type motions. Calculate S_b , T_B and ζ_B from the hysteresis loop which is drawn for the chosen values of K_{b1} , K_{b2} , Q_y/W and X_b .

Obtain the isolator force S_b from the hysteresis loop, the period T_B from the secant stiffness, and the equivalent damping ζ_B from the area of the hysteresis loop and the contribution from the actual viscous damping.

The relationships between X_b , S_b , T_B and ζ_B are as follows. For an assumed X_b , the bilinear loop gives the base shear S_b as

$$\begin{aligned} S_b &= Q_y + K_{b2}(X_b - X_y) \\ &= Q_y \left(1 - \frac{K_{b2}}{K_{b1}} \right) + K_{b2} X_b \end{aligned} \quad (5.19)$$

and hence

$$S_b/W = \left(\frac{Q_y}{W} \right) \left(1 - \frac{T_{b1}^2}{T_{b2}^2} \right) + \frac{4\pi^2 X_b}{g T_{b2}^2}.$$

The effective stiffness is the secant stiffness

$$K_B = S_b/X_b. \quad (5.20)$$

The equivalent linear period based on this stiffness is

$$\begin{aligned} T_B &= 2\pi/\sqrt{K_B/M} \\ &= 2\pi/\sqrt{(S_b/W)g/X_b} \\ &= T_{b2} \left(1 + \frac{g(T_{b2}^2 - T_{b1}^2)}{4\pi^2 X_b} \frac{Q_y}{W} \right)^{-1/2} \end{aligned} \quad (5.21)$$

The equivalent viscous damping corresponding to the hysteretic damping is ζ_h , where

$$\begin{aligned} \zeta_h &= \frac{2}{\pi} \left(\frac{Q_y}{S_b} - \frac{X_y}{X_b} \right) \\ &= \frac{2}{\pi} \frac{Q_y/W}{S_b/W} \left(1 - \frac{T_{b1}^2}{T_B^2} \right). \end{aligned} \quad (5.22)$$

To obtain the total damping ζ_B , the viscous damping ζ_v must be added. Sometimes ζ_v is added as a fraction of critical damping which is assumed not to change as T_B changes. More correctly, ζ_v should be associated with a particular viscous damper coefficient C_b , which gives a fraction ζ_{b2} of critical viscous damping at period T_{b2} . The corresponding fraction of critical viscous damping at period T_B is $(T_B/T_{b2})\zeta_{b2}$. This definition gives

$$\zeta_B = \zeta_h + \frac{T_B}{T_{b2}} \zeta_{b2}. \quad (5.23)$$

For the bilinear hysteretic system, the non-linearity factor NL , which is an important parameter governing higher-mode response is simply related to ζ_h :

$$NL = \frac{\pi}{2} \zeta_h. \quad (5.24)$$

Step 3 Use the earthquake displacement spectrum to find $S_D(T_B, \zeta_B)$, which is assumed to correspond to X_b , and hence estimate S_b from the hysteresis loop. Note that this approximation assumes that the structural flexibility and damping has little effect on the first-mode period and damping, as the structure is regarded as rigid to obtain T_B and ζ_B . Andriano and Carr (1991b) include the effect of structural flexibility in their procedure which is otherwise similar to that given here.

If the simplified enhanced El Centro spectrum is used, these responses may be read from the trade-off curves of Figure 5.2, or taken from Equations (5.4a) and (5.4b). For other spectra, the equivalent expressions developed as indicated at the end of Section 5.1.4 can be used.

Step 4 Check whether the base displacement and base shear of step 3 agree with the assumed displacement and corresponding base shear of step 2. If satisfactory convergence has not occurred, further iteration is required. New values of T_B and ζ_B can be calculated using the latest values of X_b and S_b . Faster convergence may be obtained by taking a new X_b with double the change from the previous iteration, and returning to step 2 with this value.

Step 5 Check the final estimates of X_b and S_b with the design criteria. If the values are not acceptable, or it is felt that improved values may be possible, select a new trial isolation system. Generally, lengthening the periods, particularly T_{b2} , reduces shears but increases displacements. Increased equivalent damping, which results from loops closer to rigid-plastic and yield levels closer to $(Q_y/W)_{opt}$, usually reduces base shears and displacements. Re-enter the procedure at step 2.

Step 6 An isolation system has now been found for which the isolator displacement and base shear, predicted by the equivalent linearisation procedure and the earthquake spectra, are acceptable. Now check that the higher-mode responses are also acceptable, using the procedure discussed in Section 5.1.5.

Calculate the elastic-phase isolation factor

$$I(K_{b1}) = T_{b1}/T_1(U) \quad (5.25)$$

where $T_1(U)$ is the first-mode period of the unisolated structure.

Also obtain the non-linearity factor,

$$NL = (\pi/2) \zeta_h \quad (5.26)$$

where ζ_h is as given in step 2.

Use these parameters and the curves of Figure 5.3(a) to estimate the ratios between the second- and third-mode top-mass accelerations and the first-mode top-mass acceleration.

From the second-mode to first-mode ratio $\ddot{X}_{N,2}/\ddot{X}_{N,1}$, estimate the mid-height shear bulge factor \underline{BF} , as in Equation (5.8) above.

The shear at mid-height is obtained from the bulge-factor

$$\begin{aligned} S(0.5h) &\approx \underline{BF} S_1(0.5h) \\ &\approx \underline{BF} \frac{1}{2} S_b. \end{aligned} \quad (5.27)$$

An approximate overall shear profile can be sketched by adding a sinusoidal variation to the first-mode triangular profile, from zero at the top to S_b at the base, which passes through $S(0.5h)$ at mid-height.

If the higher-mode effects are unacceptably large, they can usually be reduced by increasing the elastic-phase isolation factor $T_{b1}/T_1(U)$. This can be achieved by stiffening the structure to obtain a shorter unisolated period $T_1(U)$, or by reducing the isolator elastic-phase stiffness K_{b1} .

The equivalent linear system approach suggests that if the yield force Q_y and the stiffnesses K_{b1} and K_{b2} can be varied in such a way that the yield-point still lies on the same ζ_h locus, then the maximum base shear and base displacement should be unaltered, as discussed in Section 5.1.6. Thus, in theory, the higher-mode responses can be modified without affecting the first-mode response, by adjusting the yield-point along a constant ζ_h locus, and adjusting K_{b2} to retain the same secant stiffness K_B .

As discussed in step 1, there may be physical limitations on the achievable combination of parameters for a particular type of isolation system, so it may not be possible to use this approach to adjust the higher-mode responses without affecting the first-mode response. Also, the equivalent linearisation approach is an approximation, so some changes may occur in the first-mode response on moving along the constant ζ_h locus. If it is necessary for physical reasons to move off the ζ_h locus to achieve acceptable higher-mode responses, the iteration will need to be re-entered at step 2.

Step 7 Repeat the calculations for any other required earthquake motions. Often two levels of earthquake spectra are specified, such as 'design-level' and 'extreme-level', or 'operating-basis' and 'maximum credible' motions. It is necessary to check the relevant design criteria for the various levels of specified motions.

Step 8 Perform response-history analysis for a number of appropriate accelerograms to confirm the results obtained with the spectral approach for the equivalent linear system. For non-linear isolation systems, such analysis is required to obtain reliable estimates of floor spectra. The results may indicate that further adjustments to the isolation system are required.

5.3 TWO EXAMPLES OF THE APPLICATION OF THE DESIGN PROCEDURE

5.3.1 Isolation of capacitor banks

This example of a seismic isolation design procedure is based on the retrofitted isolation of capacitor banks at the Haywards substation described in Chapter 6. The isolation system was designed to withstand very strong earthquake motions, more than twice El Centro amplitudes. The choice of isolator and damping components for one of the several types of capacitor bank is described here.

The example illustrates the selection of a trial isolation system, the iteration procedure required to estimate the base shear and displacement corresponding to the specified earthquake spectrum, modifications of the trial isolation system to obtain responses within the design specification, and an illustration of the variation of effective period and damping with amplitude, performed by estimating the responses for a less severe spectrum.

The design motions were specified in terms of a 5% damped acceleration spectrum given by $0.84g/T$ for periods greater than 1 s. This is a scaling of the simplified smoothed El Centro spectrum of Figure 5.1(a) by multiplication by a

factor of 2.15. The variation of response with damping was assumed to be given by the curves of Figure 5.1(b).

Several types of capacitor banks were involved, with masses between 20×10^3 kg and 34×10^3 kg when the retrofitted support frames were included. The light vertical loads were insufficient for the lead-rubber bearings available at the time, so a combination was selected of segmented rubber-steel-laminated bearings, to provide horizontal flexibility, with steel conical taper-beam dampers.

Allowable base shears for the filter banks considered in this example were 0.32 W , with the rubber bearings able to accommodate 200 mm displacement. Bearing periods of approximately 1.5–2 s could be achieved readily.

Previous work and the base-shear versus yield-force diagram of Figure 4.5(d) suggested that the optimum yield ratio Q_y/W for minimum base shear in earthquake motions corresponding approximately to the El Centro accelerogram is around 0.04–0.05, for $T_{b2} \sim 1.5$ –2.0 s. For the scaling factor of 2.15 associated with the specified earthquake spectrum, the optimum value of Q_y/W increased to about 0.08–0.12. Taking a target value of Q_y/W of 0.10, the required total yield forces for the dampers for the various filter banks were approximately 16–40 kN. It was decided to consider the option of two or three taper-beam dampers with yield forces of approximately 10 kN.

Experience showed that conical tapered-beam dampers with a taper along 2/3 of their length were reliable. The design equations are (Tyler, 1978)

$$L = 5.270\sqrt{Dx}$$

$$Q_d = 11.067\sqrt{D^5/x}$$

where x (mm) is the design displacement corresponding to a strain of ± 0.03 which gives a full-displacement plastic fatigue life of 80–100 cycles, D (mm) is the base diameter, and L (mm) is the total length. The force Q_d (kN) corresponds to the zero-displacement point on the bounding hysteresis loop, which is somewhat less than the yield force of the bilinear loop.

With x taken as 200 mm and Q_d as 10 kN, these equations produced damper dimensions of $D = 44$ mm and $L = 494$ mm. These values were rounded to $D = 45$ mm and $L = 500$ mm, which gave $x = 200$ mm and $Q_d = 10.6$ kN. Tests of these dampers produced elastic and post-yield stiffness $K_e = 560$ kN/m and $K_y = 14$ kN/m, rather lower values than predicted by the expressions in Tyler's paper (Tyler, 1978).

The filter banks considered in this example had a mass M of 34×10^3 kg. The elastic- and yielded-phase periods from the combination of two or three steel dampers was denoted T_{es} and T_{ys} . Rubber bearings with combined periods $T_r = 1.5$ s or 2 s were considered in parallel with the dampers. The period of the unisolated capacitor banks was $T_1(U) = 0.11$ s, so the capacitor bank flexibilities could be ignored in the calculations. The elastic-phase and yielded-phase

periods T_{b1} and T_{b2} of the overall system are given by

$$\frac{1}{T_{b1}^2} = \frac{1}{T_r^2} + \frac{1}{T_{es}^2}$$

and

$$\frac{1}{T_{b2}^2} = \frac{1}{T_r^2} + \frac{1}{T_{ys}^2}$$

The yield-force ratio Q_y/W of the combined rubber-bearing and steel-beam isolation system is given by

$$Q_y/W = \frac{T_{b2}^2}{T_{b2}^2 - T_{b1}^2} \frac{nQ_d}{W}$$

where Q_y , T_{b1} , T_{b2} and $W = Mg$ correspond to the overall system, Q_d is the force for an individual damper, and n is the number of dampers.

Various periods and yield-force ratios relevant to this example are summarised below.

	$T_r = 1.5$ s		$T_r = 2.0$ s	
	$n = 2$	$n = 3$	$n = 2$	$n = 3$
T_{es} (s)	1.09	0.89	1.09	0.89
T_{ys} (s)	6.91	5.64	6.91	5.64
T_{b1} (s)	0.88	0.77	0.96	0.82
T_{b2} (s)	1.47	1.45	1.92	1.89
Q_y/W	0.0995	0.1330	0.0851	0.1178

The iterative calculation of the responses of the various systems can now begin. As given previously

$$S_A(T, 0.05) = \left(\frac{0.84}{T}\right)g.$$

The corresponding displacement spectra are

$$S_D(T, \zeta) = \frac{0.84gTC_D(\zeta)}{4\pi^2} \quad (\text{mm})$$

$$= 209TC_D(\zeta) \quad (\text{mm}).$$

Consider first 1.5 s bearings with two steel dampers. Take a trial displacement

$X_b = 200$ mm. From Equation (5.19),

$$S_b/W = \frac{Q_y}{W} \left(1 - \frac{T_{b1}^2}{T_{b2}^2} \right) + \frac{4\pi X_b}{g T_{b2}^2}$$

$$= 0.414.$$

From (5.21)

$$T_B = 2\pi \sqrt{\frac{X_b}{(S_b/W)g}}$$

$$= 1.395 \text{ s.}$$

Ignore any viscous damping, which for this example is very low (~ 0.01) because of the inherently light damping of the capacitor banks and the segmented rubber bearings. Then from Equation (5.22)

$$\zeta_B = \frac{2(Q_y/W)}{\pi(S_b/W)} \left(1 - \frac{T_{b1}^2}{T_B^2} \right)$$

$$= 0.0922.$$

From Figure 5.1(b), $C_D(0.0922) = 0.79$, so that

$$S_D(1.395 \text{ s}, 0.0922) = 209 \times 0.79 \times 1.395 \text{ mm}$$

$$= 230 \text{ mm}$$

and

$$\Delta X_b = S_D(T_B, \zeta_B) - X_b$$

$$= 30 \text{ mm.}$$

For the second iteration, double this value of ΔX_b to obtain the estimate of X_b . The iteration procedure produces

$$X_b = 260 \text{ mm}, S_b/W = 0.548, T_B = 1.382 \text{ s},$$

$$\zeta_B = 0.069, C_D(0.069) = 0.9, S_D = 259.6 \text{ mm.}$$

Thus convergence has been obtained.

Both the base shear and isolator displacement are too large with this isolation system. Increased damping can reduce both responses, so consider three dampers rather than two. Again, take $X_b = 200$ mm for the first trial. The iteration sequence produces

$$X_b = 200 \text{ mm}, S_b/W = 0.452, T_B = 1.33 \text{ s}, \zeta_B = 0.125,$$

$$C_D(\zeta_B) = 0.7, S_D(1.33 \text{ s}, 0.125) = 194 \text{ mm} \quad \Delta X_b = -6 \text{ mm.}$$

Try a new iteration beginning with double this displacement discrepancy. Then

$$X_b = 188 \text{ mm}, S_b/W = 0.429, T_B = 1.33 \text{ s}, \zeta_B = 0.132,$$

$$C_D(0.132) = 0.675, S_D(1.33 \text{ s}, 0.132) = 187 \text{ mm.}$$

For practical purposes, this iteration has converged. The displacement is acceptable, but the base shear is too large.

Consider another trial isolation system with longer-period bearings, $T_r = 2.0$ s, which will reduce shears but increase displacements. Again, assume $X_b = 200$ mm. The iteration sequence produces

$$X_b = 200 \text{ mm}, S_b/W = 0.322, T_B = 1.58 \text{ s}, \zeta_B = 0.171,$$

$$C_D(0.171) = 0.605, S_D(1.58 \text{ s}, 0.171) = 199 \text{ mm} \quad S_b/W = 0.320.$$

Convergence has occurred in one iteration, with the base shear and isolator displacement just within their allowable limits. The elastic-phase isolation factor $T_{b1}/T_1(U) = 7.5$, which is very high, and the non-linearity factor $\underline{NL} = 0.27$ is low, so higher-mode effects should be small. It can be seen that in this example, T_B remains unchanged between iterations for the same isolation system. This is not a general feature of the iteration procedure, but rather of the particular parameter values of this example.

Finally, to illustrate the dependence of the effective period and effective damping on earthquake size, we calculate the response to the simplified El Centro spectrum with $P_a = 1$, i.e. the spectral displacement is given by $S_D(T_B, \zeta_B) = 97 C_D(\zeta_B) T_B$ (mm).

Take $X_b = 100$ mm for the first iteration, as the strength of the earthquake has been approximately halved. Working through the iteration produces

$$X_b = 100 \text{ mm}, S_b/W = 0.2083, T_B = 1.390 \text{ s}, \zeta_B = 0.2348,$$

$$C_D(0.2348) = 0.51,$$

while

$$S_D(1.390 \text{ s}, 0.2348) = 97 \times 0.51 \times 1.390 \text{ mm} = 68.8 \text{ mm.}$$

Doubling the change in X_b appears likely to give a new estimate far too low, so continue with $X_b = 68.8$ mm.

Continuing the iterations, working down a column and then across for the next iteration:

X_b (mm)	68.8	60.1	57.8	57.2
S_b/W	0.1732	0.1634	0.1608	0.1601
T_B (s)	1.265	1.217	1.203	1.199
ζ_B	0.251	0.251	0.250	0.250
$C_D(\zeta_B)$	0.49	0.49	0.49	0.49
$S_D(T_B, \zeta_B)$ (mm)	60.1	57.8	57.2	57.0

The result has converged to an estimated displacement of 57 mm for the smoothed El Centro spectrum, with a base shear $S_b/W = 0.16$. The effective period is

$T_B = 1.20$ s, with an effective damping of 25% of critical. The effective period is shorter for the reduced design motion, but the damping has increased from the value of 17% for the larger motion. The effective period must reduce as the amplitude of motion decreases, but the effective damping may increase or decrease.

Approximately halving the design motion has halved the base shear, but the displacement has reduced to less than 30% that for the stronger excitation. Often it is the displacement rather than the base shear that scales approximately linearly with earthquake size. Note that in this example the value of the effective damping converged quickly, while the effective period changed between iterations, unlike the calculations for the response of the same system to the stronger excitation, where the effective period converged immediately and the damping varied between iterations.

5.3.2 Design of seismic isolation for a hypothetical eight-storey shear building

Design brief for hypothetical building

A hypothetical building of the type which might benefit from seismic isolation is proposed for illustrative purposes. The building is supposed to have eight storeys and a variety of intended uses, which impose architectural and structural design constraints. The intended occupancy for storeys 2 to 7 is professional, including medical, legal and specialist consultants, with the main emphasis on medical and related services; speciality shops are to be provided in the first storey and dining facilities in the eighth storey. To enhance these facilities, large display windows are proposed on two sides of storey 1 and large picture windows on three sides of storey 8. Extensive double-glazing for storeys 2 to 7 will take advantage of the excellent views from two sides of the building, above storey 3. Verandahs on the two public-access sides of storey 1 will enhance displays, provide rain shelter, and protect those using exits.

Required building facilities include a sprinkler system with a large supply of drinkable emergency water, and a stand-by diesel-electric plant for extensive emergency lighting, a sprinkler pump, and low-speed operation of one lift. Essential natural ventilation must be available in the event of failure of the air conditioning system. A tank buried below an adjoining car park will provide emergency storage for building wastes in the event of earthquake damage to nearby sewers.

The functional requirements, including potential changes in occupier needs and the architectural need for maximum access to exterior windows, call for a relatively flexible structural form, namely a reinforced-concrete space frame. The building design adopted is therefore a regular eight-storey reinforced-concrete frame with 28 columns, namely six bays by three bays with bay lengths of 6 m and storey heights of 3.5 m, with a set of lifts and a stairway in the second and fifth bays along the building length.

A check on equipment items for the intended occupiers indicates that they can be given some protection from earthquakes by simple devices, for example by

suitable fixing or the use of resilient stops for equipment on anti-vibration mounts. Similarly, local detailing can to some extent protect building plant, including lift counterweight operation, the stand-by power plant, the emergency water supply and other essential facilities. However, without isolation of the structure, direct seismic loads do pose some threat to this equipment and it would be difficult to avoid excessive damage to glazing, and interior damage which would also pose some threat to the high-cost facilities and equipment.

The diversity of use gives an uncertain level of fire risk during earthquakes and at other times. The costs of the non-structural features are comparatively high, as would be the cost of an interruption to availability of services. Moreover, the loss of the medical facilities would remove a valuable contribution to Civil Defence activities during the immediate post-earthquake period.

A value for the unisolated first period using an appropriate empirical rule is calculated as $T_1(U) \approx 0.08 \times \text{number of storeys} \approx 0.64$ s, which is in the range of periods associated with the strongest acceleration responses in typical accelerograms of the El Centro type.

The option of seismic isolation of the building is therefore investigated as a means of limiting the structural deformations to the low values required. Moreover, the resulting low loads and ductility demands would reduce structural costs. Seismic isolation has also been shown (Section 4.5) to reduce seismic responses due to torsional unbalance.

Design earthquake

The hypothetical building is supposed to be situated in an area where it is appropriate to select a design-level earthquake, for a return period of 150 years, with the severity and character of the 1940 El Centro NS earthquake motion without scaling; hence $P_a = P_p = 1$. For the extreme earthquake, with a return period of 500 years, acceleration amplitudes are doubled but frequencies are not altered, giving the scaling factors $P_a = 2.0$ and $P_p = 1.0$.

It is further assumed that a major active fault passes within 1 km of the building site, with an estimated return period for rupture of about 500 years. To provide for increased demand on isolator displacement due to movement of such a fault, allowance is made for a maximum displacement 50% greater than that given by the extreme earthquake with $P_a = 2.0$. This agrees with the provisions of the Uniform Building Code (1991) (see Section 5.5).

Hence, if X_b is the isolator displacement for the design-level earthquake, the extreme earthquake displacement is approximately $2X_b$. A displacement allowance of $3X_b$ includes possible effects of movement on the nearby fault.

Preliminary design calculations

The choice of isolation system is based on considerations such as discussed in Tables 2.1 and 2.2, in Figure 2.7 and in the associated text. A bilinear isolation system such as presented in case (iv) of Figure 2.7 is chosen, with lead-rubber

bearings, or a combination of these with laminated rubber bearings, in mind as a possible isolation system. This kind of isolation system has been shown to give a good combination of seismic responses, together with the advantage that the structure is locked in place during wind and small earthquakes.

Approximate loads for interior, side and corner columns are estimated as 300, 250 and 200 t. For standardisation, and as additional provision for vertical seismic loads, bearings under corner columns are given the same load capacity as those under side columns, giving a minimum bearing load of 250 t.

Preliminary design calculations are carried out according to the design procedures described above (Section 5.2), choosing realistic initial parameters from the known properties of the intended isolation system and the known acceptable seismic displacement. Iteration procedures such as described in the example above are carried out until convergence is obtained. If the 'trade-off' between base displacement and the resulting base shear is unsatisfactory then the isolator parameters are adjusted and the iteration procedure is repeated until a satisfactory 'trade-off' is obtained. This gives tentative values for the isolator parameters.

These parameters may now be used to estimate the general effects of higher modes on the distribution of shears over the height of the building, in accordance with Section 5.2. Hence the shear distribution is indicated by combining the values in Figure 5.3(a) with Equation (5.8). The general level of floor spectra may be obtained by interpolation between cases given in Figure 2.7 and Table 2.1. This interpolation can be either on the basis of isolator parameters or on the basis of modal acceleration ratios as given by Figure 5.3(a).

Since none of the contents of the building are particularly vulnerable to seismic attack, a certain degree of higher-mode response is tolerable. If the floor-acceleration spectra for a given set of isolation parameters are too high, iteration can be repeated with different values of the elastic-phase isolation factor $I(K_{b1})$ and/or non-linearity factor N_L ; the 'yield-point locus' method described above (Section 5.1.6) may be useful in choosing new values for these parameters.

Once preliminary isolator parameters have been obtained, a time-history analysis should be performed for the detailed design. A nine-mass one-dimensional model of the type shown in Figure 2.4 is adequate for dynamic analysis. Floor masses and inter-storey stiffnesses are estimated as for the dynamic analysis of non-isolated structures. A time-history dynamic analysis based on the average of five statistical approximations to the design earthquake gives peak accelerations and peak shears at each floor level. Also, floor accelerations at four mass levels, say 0, 3, 6, 9, should be adequate for checking floor spectral values.

Stops and resilient buffers

The greatest uncertainty in the major responses of most isolated structures is the maximum low-probability seismic displacement which will be demanded of the isolators. As a result isolators are usually given considerable reserve capacity for displacements beyond even extreme design values, and structures usually have a considerable reserve capacity for resisting increased seismic loads. Some al-

lowance is therefore made for the possibility that unusually large displacements may occur.

Maximum use of reserve displacement and load capacities will usually call for the use of resilient buffers to limit base-level displacements. These should be provided where it is economically practical. Increased buffer resilience will usually increase the effectiveness, but also the costs of these buffers. As a very approximate guide to limiting impulsive loads on a building, the effective flexibility of the buffer should not be less than that of the first two storeys of the building. For dynamic analysis of structural responses the buffer may be modelled as a third elastic slope K_{b3} which extends from the vertices of the bilinear displacement loops.

Stops or resilient buffers have been provided for seismically isolated New Zealand buildings. The William Clayton Building in Wellington has been provided with stops at ± 0.15 m. The Police Station building, also in Wellington, has been provided with resilient buffers for displacements of about ± 0.35 m.

Other considerations

A number of other considerations need to be taken into account when detailing a seismically isolated building:

- The seismic gap.
It is necessary to make provision for clearances around the structure. Drainage and exclusion of water and rubbish from the isolator region are also necessary. Water exclusion barriers and other cover-plates should not provide stiff or strong bridges across the seismic gap.
- Services.
It is necessary to detail connections for external services such as water, gas, sewerage, power, signal lines and pedestrian and equipment access, to accommodate the seismic motions and to ensure that the services and their connections do not interfere with the operation of the isolation system. Flexible couplings may be appropriate in some cases.
- Anchors.
Floor-acceleration spectra can be used when designing anchors for equipment and facilities within the structure, and buffers for equipment which is flexibly mounted. Baffles or subdivisions may need to be included in the emergency water supply tank, to prevent excessive wave action under mode-1 accelerations.
- Inspection procedures.
Construction groups and inspectors should be clearly instructed on the intended purpose of all structural features which have been introduced because seismic isolation has been used. Appropriate long-term inspection, maintenance and emergency procedures for the building are also recommended.
- Recording instrumentation.
It is recommended that the installation of seismic-acceleration and isolator-displacement recorders should be considered so that the community of seis-

mic isolation engineers can build up good records of the performance of isolation systems during actual earthquakes.

- Fire protection.

Further detailing related to the isolation system includes provision of fire resistance for the mounts. Under suitable conditions flexible fire-resistant blankets may be adequate.

- Inspection.

There should be reasonable access for inspection of the isolation system, and if necessary for the replacement of isolation components. In practice there may be a need for very occasional replacement of a component of the isolation system for testing.

- Variations on the original design.

Particular attention should be paid to the possibility that minor design changes or later modifications of the structure, or its surroundings, may prevent the full intended operation of the isolation system. In particular the 'seismic gap' must remain secure. Some protection can be given by appropriate detailing of the interface of the exterior of the structure with adjoining unisolated features. This is an educational issue which should become less severe as seismic isolation becomes more common.

5.4 ASEISMIC DESIGN OF BRIDGES WITH SUPERSTRUCTURE ISOLATION

5.4.1 Seismic features with superstructure isolation

The seismic design of a bridge structure must satisfy many conditions, including some which are particular to its site. This section concentrates on factors common to the design of many bridges. For many simple bridges, it has been found that seismic isolation of the superstructure gives improved seismic resistance, often at a reduced cost, while also providing effectively for thermal expansion of the superstructure.

The aim when seismically isolating bridge superstructures is usually to protect the piers and their foundations, and sometimes to protect the abutments also. There is less frequent need for isolation to protect the superstructure because bridge superstructures are inherently strong as a result of being designed for vehicle loads.

The superstructure isolation systems are designed to reduce the overall seismic loads, and to distribute them better in relation to the strengths of the piers and abutments and their foundations. Longitudinal seismic displacements are held to moderate values to reduce the problems of supporting traffic across seismic gaps in the deck, and also to reduce isolator-component problems, and structural problems arising from large displacements.

Superstructure isolation systems are designed, as far as is practical, to provide moderate flexibility and high damping, torsional balance and an appropriate distribution of seismic loads between the superstructure supports. In cases where a

long superstructure has high transverse flexibility, an attempt should be made to equalise the transverse stiffnesses of the superstructure supports.

With superstructure isolation, the piers and abutments are not isolated from the ground motions. Piers then tend to respond to seismic excitation as independent structures with some top constraint. When a pier is relatively tall and heavy these responses may make a substantial contribution to the seismic loads on the pier and its foundations.

Attention is given here to commonly occurring simple bridge structures, with moderate span lengths and pier heights. Discussions assume that the superstructures are straight and level. The number of bridge spans is typically between 3 and 5. Such bridge structures, with rather short piers, are shown in Figures 6.22 and 6.31(a), while a wider range of simple bridge structures is illustrated by Blakeley (1979). Much of the following discussion would also apply when a superstructure, continuous over about 5–7 spans, is a separate section of a longer bridge structure.

The overall form of bridges may be complicated to provide for sloping or curved decks, as shown in Figures 6.3 and 6.1. For longer-span bridges, intermediate girder support is often provided by steep arches, while for very long spans intermediate support is provided by tower-supported cable stays or catenary cables. Emi *et al.* (1987) and Katayama *et al.* (1987) show that cable stays and catenary cables allow a high degree of longitudinal flexibility for superstructure motions. Moreover, the intersections of cable support towers and the carriage-way girder provide convenient locations for longitudinal dampers.

When bridge piers are quite high it may sometimes be appropriate to adopt overall isolation of the bridge structure, by allowing a moment-limiting stepping action near the pier bases. Such isolation was adopted for the South Rangitikei viaduct described in Chapter 6.

When soil stiffnesses, and hence also seismic motions, differ across a building site the consequences are reduced by tying the tops of the foundations together. However, for long bridges, where soil stiffness variations may well be more extreme, such foundation interconnections are not practical.

The cost of providing seismic isolation is often relatively low for bridges because little structural modification is required. In unisolated bridges many of the interfaces between the superstructure and the supports must be designed for the installation of horizontally flexible bearings, to accommodate longitudinal movements between the superstructure and most of the supports, caused mainly by thermal expansion. Indeed, since many unisolated bridges are compatible with flexible superstructure bearings, it is often practical and relatively inexpensive to retrofit their superstructures with seismic isolation (Park *et al.* 1991).

5.4.2 Seismic responses modified by superstructure isolation

Factors to consider with superstructure isolation

The systems considered here for bridge superstructure isolation introduce isola-

tor components which provide increased horizontal flexibility and damping at the interfaces between a continuous superstructure and its supporting piers and abutments. The bridge piers, abutments and, if necessary, the superstructure, are given protection by designing the isolation system to give reduced seismic loads, and a better distribution of the reduced loads between the superstructure supports. The seismic loads are reduced by increasing the overall flexibility and damping of the superstructure supports. The load distributions are improved by relating support stiffnesses to substructure strengths.

With isolation for transverse seismic responses, overall seismic loads may also be reduced by adjusting transverse stiffnesses to give improved torsional balance. Moreover, high transverse damping suppresses the dynamic magnification of the torsional unbalance, as discussed in Chapter 4. Finally, when the isolated section of superstructure is long and slender in plan view, seismic loads may sometimes be reduced by adjusting the transverse stiffnesses of supports to be approximately equal.

Seismic gaps in the deck at the ends of a section of superstructure should be kept as small as is practical in order to simplify the problem of supporting traffic crossing the gaps. Seismic gap lengths are reduced by designing the longitudinal isolation system to limit superstructure displacements. When the overall support system for the superstructure has moderate flexibility and high damping for longitudinal responses, there may be a large reduction in seismic loads, but only moderate displacements of the superstructure. Seismic gaps must also provide for any pre-earthquake reductions in the gaps, which may arise from temperature changes in the superstructure and from ground creep.

Reduced seismic displacements have additional benefits. Isolator components with moderate displacements are less expensive, and lower costs are also associated with their installation. Moreover, moderate superstructure displacements reduce the structural costs of providing for relative displacements.

The ideal values for the stiffness and damping of various supports, which satisfy particular design requirements considered above, will sometimes be in conflict. Moreover, further limitations arise from the range of features available from existing practical isolator components, particularly with regard to simultaneously satisfying both longitudinal and transverse requirements. However, consideration of the effects of isolation on various seismic responses should assist in selecting isolator components which give a reasonable trade-off between various seismic design requirements.

Superstructure isolation may be used to reduce or eliminate deformations of substructures beyond their elastic range during design-level earthquakes. It is particularly important to avoid severe post-elastic deformations at locations which are difficult to inspect or repair, such as partly submerged piers and their foundations.

Parameters of superstructure isolators

With superstructure isolation, the isolator component parameters combine with the parameters of the substructures on which they are mounted to give a set of composite isolator parameters at each support, and these sets of support parameters

combine to give the parameters for the overall superstructure isolation system. These isolator parameters may be expressed as effective stiffnesses, periods and dampings for individual superstructure supports, and for the overall support system.

Figure 5.5 shows a pier of stiffness K_p and effective top mass M_p which supports an isolator component of stiffness K_b and an associated superstructure mass M . For the usual case, when the pier mass is much smaller than the superstructure mass, the pier mass may be neglected when evaluating approximate seismic responses of the superstructure. In this case the spring forces of the pier and isolator component may be combined statically to give the composite spring force for the support. Moreover, the pier mass makes no significant contribution to mode 1, as shown in Figure 5.5. Figure 5.5 also shows a second or 'pier' mode, which has little displacement of the superstructure mass, for the usual case when the superstructure mass is much greater than the effective mass of the pier.

Hence the parameters of linear and bilinear isolator components combine with the horizontal elastic stiffnesses, at the tops of piers and abutments, to give individual and overall support stiffnesses and dampings as described below.

We define the cyclic displacements of a pier (or abutment) and of the superstructure, at a support location, as X_p and X'_b respectively. Corresponding deformations of the interface isolator components are X_b . Hence $X'_b = X_p + X_b$.

When a linear, or bilinear, isolator is placed on a non-rigid pier or abutment support, of horizontal stiffness K_p , the composite isolator stiffness, say K'_b , is less than the isolator component stiffness K_b , as given by

$$K'_b = K_b / (1 + K_b / K_p) \quad (5.28)$$

with corresponding expressions for the reduced bilinear stiffnesses K'_{b1} , K'_{b2} and K'_B . Primes are used for the parameters of composite isolators. The bilinear yield value Q_y is not changed by K_p .

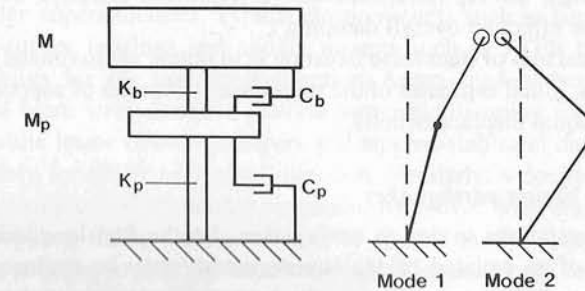


Figure 5.5 Two-mass model of an isolated bridge superstructure of mass M supported by a pier of top mass $M_p \ll M$. The stiffnesses of the isolator component and pier are K_b and K_p respectively, and the damping coefficients are C_b and C_p respectively. The two modes of vibration shown apply when angular momentum effects may be neglected

With bilinear isolation, the relationships between the cyclic displacements, X'_b and X_b , and the corresponding hysteretic dampings ζ'_h and ζ_h may be obtained by comparing the force-displacement loops, as given by K'_{b1} and K'_{b2} (Equation (5.28)) and Q_y , with the corresponding loop for a rigid support ($K_p = \infty$), and the smaller displacement X_b .

This gives

$$X'_b = X_b(1 + K_{b2}/K_p) + Q_y(1 - K_{b2}/K_{b1})/K_p \quad (5.29)$$

and

$$\zeta'_h = \zeta_h X_b / X'_b \quad (5.30)$$

For a given value of X'_b , the isolator component deformation X_b , as given by Equation (5.29), becomes progressively smaller as K_p is reduced. In some cases the reduction in X_b will cause an increase in K_B and ζ_h . However, in all cases, the values for the composite isolator, K'_B and ζ'_h , are reduced by reducing K_p .

When all the superstructure supports have the same longitudinal displacement X'_b (or the same transverse displacements Y'_b), the effective overall stiffness K' is obtained by summing all the support stiffnesses K'_b and K'_B , as given by Equation (5.28). The effective period T' is then given by substituting K' in Equation (5.21).

A comparison between the force-displacement loops for individual supports and the corresponding loop for the overall support system (all with a displacement X'_b), gives the overall hysteretic damping as a weighted sum of the support dampings ζ'_h . When added to an estimated velocity damping ζ_b , this gives the effective overall damping ζ' as

$$\zeta' = \sum_i \zeta'_{hi} K_{Bi} / K' + \zeta_b \quad (5.31)$$

Since reductions in K_p at individual supports reduce their stiffnesses and hysteretic dampings, the K_p reductions also increase the effective overall period T' and reduce the effective overall damping ζ' .

Since a usual aim of transverse isolation is to obtain approximately equal support displacements, initial estimates of the transverse stiffnesses of supports may usually be based on equal displacements Y'_b .

Responses to design earthquakes

The seismic responses to design earthquakes, for the first longitudinal and transverse modes of an isolated bridge superstructure, may be evaluated by trial and error in essentially the same way as the base responses are evaluated for an isolated building. A trial superstructure displacement X'_b (or Y'_b) is selected and an effective period T' and damping ζ' is derived, using Equations (5.22), (5.23), and (5.28)–(5.31). The design-earthquake displacement spectrum value, for this period and damping, gives the first resultant displacement. Further trial values for the dis-

placement lead to agreement between trial and resultant displacements and hence to an approximate value for the design-earthquake displacement of the superstructure.

When a substructure is sufficiently flexible it greatly reduces the hysteretic damping of the isolator component which it supports, as indicated in Equation (5.30).

For bridges of moderate length, bilinear isolator damping may well be confined to the usually stiffer and stronger abutments. When bilinear damping is introduced at pier supports it may be confined to acting in the transverse direction, for which the pier is usually stiffer and stronger, as in the case of the King Edward Street Overpass, Dunedin, New Zealand (McKay *et al.* 1990).

As with building isolation, bilinear isolators at superstructure supports may provide little damping of higher modes. However, elastic analysis indicates that velocity-damping at the pier supports may provide effective damping of longitudinal and transverse pier modes, and hence a substantial reduction in their seismic responses. Again, transverse velocity damping at all superstructure supports may provide effective damping and reduced seismic responses for higher transverse modes. In contrast, isolator velocity-damping (viscous damping) is not so effective in damping higher building modes.

If a superstructure-isolated bridge is very simple, with approximate torsional balance, little superstructure flexure, and little loading of piers by direct seismic excitation, then a design procedure based on a spectral approach, as discussed above in general terms, should give reasonable approximations to seismic responses.

For isolated bridges with less simple features, the final seismic design should be based on a time-history analysis of the responses to design earthquakes, using a sufficiently detailed bridge model. Such an analysis should give the effects of the main features of the bridge model, such as superstructure flexure, irregular substructure stiffnesses, and non-linear mechanisms which excite higher modes.

5.4.3 Discussion

Some of the isolator components described in Chapter 3 have particular relevance to isolated bridge superstructures. Typical elastic mounts such as laminated-rubber bearings, lead-rubber bearings and sliding mounts such as PTFE bearings, have the same flexibility for any horizontal direction. Again, lead-rubber bearings and vertical conical-beam steel dampers provide hysteretic damping for any horizontal direction, while lead-extrusion dampers and tapered-slab steel dampers may be applied separately for either horizontal direction. Similarly, velocity dampers can be designed for single-axis or biaxial operation. Moreover with elastic or sliding bearings at a support, sliding constraints can be applied to allow, say, only longitudinal bearing motion, so that the superstructure is isolated only for longitudinal motions.

Hysteretic dampers based on lead have relatively low creep resistance while providing high damping forces during rapid seismic movements. This feature is often important for bridge applications. For example, lead-based dampers may be located on both abutments of a bridge so that the abutments share equally in the

hysteretic damping forces. However, the dampers have relatively low resistance to slow length changes arising from superstructure temperature changes and ground creep. Moreover, if the dampers are biaxial, as in the case of lead-rubber bearings, the transverse damping forces are torsionally balanced, provided the abutments have comparable or high transverse stiffnesses.

Examples of superstructure isolation systems in New Zealand which include longitudinal dampers to protect tall slab-wall piers founded in moderate-strength ground, are the Bannockburn bridge and the Cromwell bridge, in Central Otago (McKay *et al.* 1990). These bridges have partly submerged piers about 33 m high. The Bannockburn bridge has both abutments founded on ground of moderate strength. Each abutment is provided with three longitudinal lead-extrusion dampers, and hence they share the seismically induced damping forces. Moreover, inspection of the dampers indicates that the lower-force creep displacements, arising from slow changes in superstructure length and in abutment spacing, are shared by the dampers at each abutment. In the case of the Cromwell bridge, one abutment has moderate strength, while the other abutment is founded on rock and is considerably stronger. For this bridge, a set of 6 Type-U flexural steel-beam dampers, for longitudinal operation, was provided at the rock-based abutment.

When detailing a bridge with a seismically isolated superstructure, care should be taken to give as much continuity as possible. Buffers and links should be provided to limit the maximum relative displacements between the superstructure and its supports, and between sections of the superstructure if it is not continuous over its whole length. With such precautions some damage may occur in the event of an extreme earthquake, but there should be no danger of collapse.

Care must be taken in detailing road surface links across isolation seismic gaps. These must be designed to minimise the likelihood of the seismic gap becoming blocked and exerting forces which may seriously degrade the aseismic performance of the isolation system. As with isolated buildings, bridge builders must be clearly instructed regarding the aims and requirements of the isolation system, and bridge controllers must be clearly instructed as to the maintenance which is required to ensure that the seismic isolation system may operate as intended.

5.5 GUIDELINES AND CODES FOR THE DESIGN OF SEISMICALLY ISOLATED BUILDINGS AND BRIDGES

Since the early 1970s a number of guidelines and later codes have been written to assist and control the design of structures utilising seismic isolation. These are illustrated here by a number of examples from New Zealand and the United States, first regarding buildings and then bridges.

Seismically isolated public buildings in New Zealand have been designed by the Ministry of Works and Development (MWD) on the basis of special studies, consultation with other groups working in this field, and developing in-house guidelines. A review of the use of flexible mountings and damping devices, to provide seismic isolation for a wide range of bridges (Blakeley, 1979), identifies a range

of factors requiring attention during design. A recent design procedure for isolated buildings (Andriono and Carr, 1991a) gives distributed shears and the resulting displacements, with design earthquakes represented by their response spectrum accelerations S_A . The design approach, described in a companion paper by the same authors (Andriono and Carr, 1991b), utilises effective periods and dampings, earthquake spectra and an isolator non-linearity factor, and has a general similarity to the approaches described in Chapter 4, and is simplified and summarised here.

In 1991 the USA Uniform Building Code (UBC) adopted, as an Appendix-Division III, a set of regulations 'Earthquake Regulations for Seismic-isolated Structures'. These requirements were developed from earlier versions, e.g. 'Tentative Seismic Isolation Design Requirements', September 1986, which was circulated by a Base Isolation Sub-committee on behalf of the Structural Engineers Association of Northern California.

The UBC regulations for the design of seismically isolated structures are closely related to their regulations for the seismic design of non-isolated structures. The requirements particular to isolated structures can be related to material covered in this book.

General control of the design is related to a simple static design procedure which is used to find reliable maximum values for the isolator displacements and shear forces, for a maximum credible earthquake based on the seismic zone and soil classification. The isolator displacement is increased by a factor of up to 1.5 for a site near an active fault. The isolator displacements, including torsional effects, must be accommodated by the seismic gap, and the isolator must remain stable, but may be somewhat overloaded, at the maximum displacement.

Isolator displacements are made proportional to the effective isolator period as in Figure 5.2(a). The displacement reduction factor $1/B$ for effective damping, as given in the UBC requirements, is proportional to the C_V values given in Figure 5.1(b), and is therefore more conservative for large damping values than the linear spectral values given by the reduction factor C_D (Figure 5.1(b)). This use of relatively higher displacements at higher damping values is equivalent to increasing our C_F values for large non-linearity factors (which are proportional to the hysteretic damping ζ_h).

The UBC requirements for the load capacity of the foundations and structure are somewhat less conservative than those for the isolator. The base shear force is distributed over the structure in proportion to its masses, as given by a constant acceleration over the structure, i.e. as given by a well isolated first mode.

When the features of the design earthquake, the structure, and the isolation system satisfy a rather strict set of constraints, then the final design may be based on the above static evaluation of displacements and loads. The constraints may be interpreted as follows, in terms of factors discussed in this book:

- The design earthquake is El Centro-like, since the constraints require zones of high seismicity, soils of high strength and stiffness, and no active fault nearby.

- The mode-1 response is almost rectangular, since the constraints require an isolation factor greater than 3.0.
- Higher-mode accelerations of bilinear isolation systems are small or moderate, since the constraints require a damping factor not greater than 0.2, and hence a non-linearity factor not greater than 0.3, which will lead to small higher-mode response in conjunction with other constraints which appear to ensure a relatively high elastic-phase isolation factor (see discussion related to Figure 2.7).

These conditions for static design also limit the number of storeys, the overall height, and the degree of structural irregularity.

The code requires dynamic analysis for seismically isolated structures not complying with the specified strict conditions, and may be used for any structure. The dynamic responses may be obtained using either response spectra or time-history analysis. On the basis of the displacements and loads given by dynamic analysis, the displacements may be reduced by a small amount and the loads reduced by a somewhat larger amount from the values given by the static design procedure.

The Office of Statewide Health Planning and Development has issued a guideline, 'An Acceptable Procedure for the Design and Review of California Hospital Buildings Using Base Isolation' (April 1989). This guideline gives somewhat stricter procedures for isolated hospital buildings, which are designed in most respects in accordance with the UBC regulations. The current status of design codes is discussed by Mayes (1992).

The guide specifications for isolated bridge structures generally parallel the corresponding provisions for isolated buildings, including related static and dynamic design procedures. However, there are a number of design requirements particular to bridges. These include the substantial non-seismic lateral displacements and loads to which the bridge may be subjected. Particular attention is given to the stability and the lateral load capacity of commonly used laminated-rubber bearings which may have large total displacements, due to combined seismic and non-seismic causes, but limited areas due to moderate unit loads. Features which are particular to isolated bridges have been discussed above.

Designs for seismically isolated New Zealand bridges were generally undertaken or reviewed by the MWD. Research and development work for the seismic design of New Zealand bridges, non-isolated and isolated, has been strongly supported by the National Roads Board with important results published in Road Research Unit (RRU) Bulletins and in various papers and reports. For example, RRU Bulletins 41 to 44 review work undertaken from 1975 to 1978 (RRU, 1979).

An approach to the seismic isolation of the superstructures of simple bridges was outlined by Blakeley (1979a), supported by charts giving maximum seismic responses of simple bridge models for a range of earthquake accelerations. The bridge models had two equal piers and two equal abutments, each remaining elastic during earthquake. The continuous superstructure was uniform and the middle span was 40% longer than the end spans. Small pier masses and a small ground flexibility were included. Superstructure deformations and angular momenta were neglected.

Horizontally flexible isolators were included between the bridge superstructure and its four supports. The charts gave the maximum superstructure displacement responses and the maximum shear loads on each support for a wide range of isolator parameters for each of three general isolation systems. The first isolation system had linear isolators at each support, while the second and third had bilinear isolators at the abutment tops and at the pier tops respectively.

The responses of the simple bridge model above may also be obtained using the approaches to isolated structure responses given in our Chapters 4 and 5. With elastic piers and abutments in the above bridge model, the first isolation system gives the rigid superstructure a flexible linear support, while the second and third isolation systems give the superstructure a support system which is bilinear for horizontal displacements. Combined with the superstructure mass these linear and bilinear supports give periods corresponding to T_b and to T_{b1} and T_{b2} , as defined in Chapter 2. With estimated viscous damping ζ_b , the maximum seismic responses of the linear bridge systems are given by the linear displacement and acceleration response spectra of design earthquakes. For the scaled El Centro NS 1940 earthquake, the maximum responses of the bridge systems with bilinear isolation are given by the 'spectra' of Figure 4.5, or the approximate spectra of Figure 5.2. The overall isolation-interface shear forces may then be distributed among the supports by applying the maximum superstructure displacement to the force-displacement relationship for each support.

The parameter-study results given by Blakeley have been extended and refined progressively by a number of researchers in the Department of Civil Engineering, University of Canterbury, Christchurch, New Zealand. Published results include Kwai (1986), Moss *et al.* (1986) and Turkington, *et al.* (1987). These studies include more detailed models of a wider range of bridge structures, a wider range of isolator parameters, and a wider range of design earthquakes, some of which give different ground motions at the locations of different supports. These studies, and related studies in other countries which are involved in the seismic isolation of bridge structures, are leading to more effective and sometimes simpler design procedures and guidelines.

As shown by Blakeley (1987), isolator components designed to provide high mode-1 damping must be located on supports which are not more flexible than the associated isolator components, in order to achieve high damping. Hence the high axial damping for the Bolton Street and Aurora Terrace overbridges in Wellington (see Chapter 6) is provided by abutment-mounted lead-extrusion dampers, and for the Cromwell bridge by abutment-mounted steel-beam dampers, since each of these bridges has stiff high-strength abutments and axially flexible, relatively low-strength piers.

In the USA, 'Guide Specifications for Seismic Design of Highway Bridges', which parallel the UBC regulations for the design of isolated building structures, were adopted by AASHTO in 1991. A commercially developed procedure for the design of bridges with superstructures seismically isolated by lead-rubber bearings, is available in the USA (Mayes, 1990-92; Mayes *et al.* 1992).

A procedure for the design of Japanese highway bridges with seismically isolated superstructures, referred to as the Menshin design method, is outlined by Matsuo and Hara (1991).

Guidelines for the seismic isolation of bridges have also been produced recently in Italy (Parducci, 1992).

6 Applications of Seismic Isolation

6.1 INTRODUCTION

This chapter presents details of seismically isolated buildings, bridges and other structures all over the world. We should like to thank our colleagues worldwide for their help in enabling us to compile this information, for checking relevant material in draft form, and for supplying photographs and tables.

In this book we have attempted to be objective. This has been aided by the fact that, up to 30 June 1992 when this manuscript was completed, we and our organisation, the DSIR, have had no financial involvement in the patents, design, manufacture and marketing of seismic isolation systems. From this objective point of view, it has been a challenge to decide which of the many worthy applications of seismic isolation to include in this chapter.

Since beginning our studies of seismic isolation, some 25 years ago (1967), we have been in more or less continuous contact with our colleagues in Japan, the United States of America, and more recently Italy. We are thus well aware of the situation in New Zealand and in these countries and the emphasis of this chapter is placed on applications of seismic isolation in these locations. However, as discussed by Buckle and Mayes (1990), seismic isolation has also been applied in many other countries, as summarised in Table 6.1.

This table, together with Tables 6.2 to 6.8, gives an indication of the criteria for choosing the seismic isolation option, namely the likelihood of a seismic event occurring, multiplied by the intensity of the anticipated event, multiplied by the value or the hazard of the structure and/or contents. In the text we have discussed seismic applications under three broad headings, namely, buildings, bridges and 'delicate' or 'hazardous' structures.

An issue of prime importance is the performance of seismically isolated structures in severe earthquakes, but none of the structures discussed below has been subjected to such a test. Of the buildings and bridges seismically isolated in New Zealand to date, only one, the Te Teko bridge over the Rangitaiki River, has undergone the effects of a large earthquake. This was the Edgecumbe earthquake in March 1987, Richter magnitude 6.3, MM9, epicentre 9 km north of the bridge. A strong-motion accelerograph located 11 km south of the bridge recorded a peak horizontal ground acceleration of 0.33g. This bridge 'provides an example of good

Table 6.1 Applications of Seismic Isolation world-wide (after Buckle and Mayes, 1990)

Country	Constructed facilities
Canada	Coal shiploader, Prince Rupert, BC
Chile	Ore shiploader, Guacolda
China	2 houses (1975); weigh station (1980); 4-storey dormitory, Beijing (1981)
England	Nuclear fuel processing plant
France	4 houses (1977-82) 3-storey school, Lambesc (1978) Nuclear waste storage facility (1982) 2 nuclear power plants, Cruas and Le Pelliren
Greece	2 office buildings, Athens
Iceland	5 bridges
Iran/Iraq	Nuclear power plant, Karun River 12-storey building (1968)
Italy	See text and Table 6.8
Japan	See text and Tables 6.4 and 6.5
Mexico	4-storey school (Mexico City)
New Zealand	See text and Tables 6.2 and 6.3
Rumania	Apartment
USSR	3 buildings, Sevastopol 3-storey building
South Africa	Nuclear power plant
USA	See text and Tables 6.6 and 6.7
Yugoslavia	3-storey school, Skopje (1969)

performance of modern earthquake resistance technology, i.e. base isolation using lead-rubber bearings' (Dowrick, 1987). However, one of the standard elastomeric bearings elsewhere on the bridge was not properly restrained against sliding, and was thrown out of position, so that it ceased supporting the deck (Skinner and Chapman, 1987). The behaviour of the bridge was, therefore, not perfect.

In order that seismic isolation be effective, it must be stressed that it is the responsibility of all the people concerned in the design, manufacture and use of a seismically isolated structure, to ensure that the system is maintained operative, and particularly that the seismic gap is protected. As mentioned in Chapter 1, this space must be uncluttered by waste material, and it must be respected during subsequent building alterations. The seismic gap must remain free at all times, so that the structure can move by the required amount during the 15 or so seconds of a major earthquake, which can occur at any unpredictable time in the life of the structure.

This is obviously an educational problem, which is currently severe because seismic isolation is a relatively new technology. New owners/operators are likely, through ignorance, to abuse the seismic gap and thereby render the seismic isolation system inoperative. It is suggested that permanent notices or plaques be situated at or near the gap, that the state and relevance of the seismic isolation be stressed in the 'ownership papers', and that engineers and building inspectors take particular notice of the need for security of the gap.

6.2 STRUCTURES ISOLATED IN NEW ZEALAND

6.2.1 Introduction

In New Zealand, seismic isolation has been achieved by a variety of means: transverse rocking action with controlled base uplift, horizontally flexible elastomeric bearings, and flexible sleeved-pile foundations. Damping has been provided through hysteretic energy dissipation arising from the plastic deformation of steel or lead in a variety of devices such as steel bending-beam and torsional-beam dampers, elastomeric bearings with and without lead plugs, and lead-extrusion dampers (see Chapter 3).

The New Zealand approach to seismic isolation incorporates energy dissipation in the isolation system, in order to reduce the displacements required across the isolating supports, to further reduce seismic loads, and to safeguard against unexpectedly strong low-frequency content in the earthquake motion. Combined yield-level forces of the hysteretic energy dissipators range from about 3-15% of the structure's weight, with a typical value of about 5%. Displacement demands across the isolators range from about 100-150 mm for motions of El Centro type and severity, to about 400 mm for the Pacoima Dam record. Structural response can often be limited to the elastic range in the design-level earthquake, with limited ductility requirements during extreme earthquake conditions. Substantial cost savings of up to 10% of the structure's cost, together with an expected improvement in the seismic performance of the structure, have resulted from the adoption of the isolation approach. Some New Zealand applications are discussed by McKay *et al.* (1990).

Bridges and structures which have been built in New Zealand are discussed in this section. Table 6.2 shows the variety of techniques used in the seismic isolation of buildings, of which the William Clayton Building in Wellington, started in 1978 and completed in 1981, was the first in the world to incorporate lead-rubber bearings. This and other buildings are discussed in the text. Current work in progress is the design of a retrofitted seismic isolation system for the New Zealand Parliament Buildings (Poole and Clendon, 1991).

Table 6.3 shows that lead-rubber bearing isolation is the technique favoured in bridges. The particular applicability of lead-rubber bearings for bridge isolation arises from the fact that elastomeric bearings, made of laminated steel and rubber as described in Chapter 3, are already an accepted technology for the accommodation

Table 6.2 Seismically isolated buildings in New Zealand

Building	Height/ Storeys	Total Floor Area (m ²)	Isolation System	Date Completed
William Clayton Building, Wellington	4 storeys 17 m	17000	Lead-rubber bearings	1981
Union House, Auckland	12 storeys 49 m	7400	Flexible piles and steel dampers	1983
Wellington Central Police Station	10 storeys	11000	Flexible piles and lead extrusion dampers	1990
Press Hall, Press House, Petone	4 levels 14 m	950	Lead-rubber bearings	1991
Parliament House, Wellington	5 storeys 19.5 m	26500	Retrofit of elastomeric and lead-rubber bearings	Original building 1921; retrofit proposed
Parliament Library, Wellington	5 storeys 16 m	6500	Retrofit of elastomeric and lead-rubber bearings	Original 1883/1899; retrofit proposed

of thermal expansion in bridges. Isolation can then be added at a small additional cost by the removal of further constraints, by provision for larger displacements, and by the incorporation of suitable lead plugs to provide high levels of hysteretic damping.

6.2.2 Road bridges

Since 1973, forty-eight road bridges and one rail bridge in New Zealand have been seismically isolated, see Table 6.3. Four examples of seismic upgrading by the retrofitting of isolation systems are included in this list.

By far the most common form of isolation system for bridges uses lead-rubber bearings, usually installed between the bridge superstructure and the supporting piers and abutments. The lead-rubber bearing combines the functions of isolation and energy dissipation in a single compact unit, while also supporting the weight of the superstructure and providing an elastic restoring force. The lead plug in the

Table 6.3 Seismically isolated bridges in New Zealand

	Bridge Name	Superstructure Type	Length (m)	Isolation System	Date Built
1	Motu	Steel Truss	170	Steel UBs in flexure	1973
2	South Rangitikei viaduct	PSC Box	315	Steel torsion bar/ rocking piers	1974
3	Bolton Street	Steel I Beam	71	Lead extrusion	1974
4	Aurora Terrace	Steel I Beam	61	Lead extrusion	1974
5	Toetoe	Steel Truss	72	Lead rubber	1978
6	King Edward Street	PSC Box	52	Steel Cantilever	1979
7	Cromwell	Steel Truss	272	Steel flexural beam	1979
8	Clyde	PSC U-Beam	57	Lead-rubber	1981
9	Waiotukupuna	Steel Truss	44	Lead-rubber	1981
10	Ohaaki	PSC U-Beam	83	Lead-rubber	1981
11	Maungatapu	PSC Slab	46	Lead-rubber	1981
12	Scamperdown	Steel Box	85	Lead-rubber	1982
13	Gulliver	Steel Truss	36	Lead-rubber	1983
14	Donne	Steel Truss	36	Lead-rubber	1983
15	Whangaparoa	PSC I-Beam	125	Lead-rubber	1983
16	Karakatuwhero	PSC I-Beam	105	Lead-rubber	1983
17	Devils Creek	PSC U-Beam	26	Lead-rubber	1983
18	Upper Aorere	Steel Truss	64	Lead-rubber	1983
19	Rangitaiki (Te Teko)	PSC U-Beam	103	Lead-rubber	1983
20	Ngaparika	Steel Truss	76	Lead-rubber	1983
21-24	Hikuwai No. 1-4 (retrofit)	Steel Plate Girder	74-92	Lead-rubber	1983-4
25	Oreti	PSC I-Beam	220	Lead-rubber	1984
26	Rapids	PSC I & U-Beam	68	Lead-rubber	1984
27	Tamaki	PSC I-Beam	40	Lead-rubber	1985
28	Deep Gorge	Steel Truss	72	Lead-rubber	1984
29	Twin Tunnels	PSC I-Beam	90	Lead-rubber	1985
30	Tarawera	PSC I-Beam	63	Lead-rubber	1985
31	Moonshine	PSC U-Beam	168	Lead-rubber	1985
32	Makarika No. 2 (retrofit)	Steel Plate Girder	47	Steel Cantilever	1985
33	Makatote (retrofit)	Steel Plate Girder	87	Lead-rubber	1986
34,35	Kopuaroa No. 1 & 4 (retrofit)	Steel Plate Girder	25 & 55	Steel Cantilever	1986-7

continued overleaf

Table 6.3 (continued)

	Bridge Name	Superstructure Type	Length (m)	Isolation System	Date Built
36,37	Glen Motorway & Railway	PSC T-Beam	60	Lead-rubber	1987
38	Grafton No. 4	PSC T-Beam	50	Lead-rubber	1987
39	Grafton No. 5	PSC I-Beam	80	Lead-rubber	1987
40	Northern Wairoa	PSC I-Beam	492	Lead-rubber	1987
41	Ruamahanga at Te Ore Ore	PSC U-Beam	116	Lead-rubber	1987
42	Maitai (Nelson)	PSC I-Beam	93	Lead-rubber	1987
43	Bannockburn	Steel Truss	147	Lead-rubber & Lead extrusion	1988
44	Hairini	PSC Slab	62	Lead-rubber	
45	Limeworks	Steel Truss	72	Lead-rubber	1989
46	Waingawa	PSC U-Beam	135	Lead-rubber	1990
47	Mangaone	Steel Truss	52	Lead-rubber	1990
48	Porirua State Highway	PSC T-Beam	38	Lead-rubber	1992
49	Porirua Stream	PSC U-Beam	84	Lead-rubber	1992

Key: PSC = prestressed concrete.
UB = U-beam.

centre of the elastomeric bearing is subjected to a shear deformation under horizontal loading, providing considerable energy dissipation when it yields under severe earthquake loading. The lead-rubber bearing provides an extremely economic solution for seismically isolating bridges.

Many unisolated New Zealand bridges use elastomeric bearings between superstructures and their supports, to accommodate thermal movements. Little modification to standard structural forms has been necessary in order to incorporate the lead plug to produce seismic isolation bearings, apart from the removal of some constraints and provision of a seismic gap to accommodate the increased superstructure displacements which may occur under seismic loading. As well as providing energy dissipation during large movements, the lead plug also stiffens the bearing under slow lateral forces up to its yield point, reducing the displacements under wind and traffic loading (Robinson, 1982).

Further information on the seismic isolation of road bridges in New Zealand, including case studies and design procedures, is given by Blakeley (1979), Billings and Kirkcaldie (1985), and Turkington (1987).

The first bridge to be seismically isolated in New Zealand was the Motu Bridge, built in 1973. The lightweight replacement superstructure was a 170 m steel truss supported by the existing reinforced-concrete slab-wall piers. The superstructure

was isolated using sliding bearings with the damping provided by vertical-cantilever structural-type steel columns. An example of the use of lead-rubber bearings in bridges is illustrated in Figures 6.1 and 6.2, which show the Moonshine Bridge, a 168 m prestressed-concrete, curving bridge on a motorway in Upper Hutt.

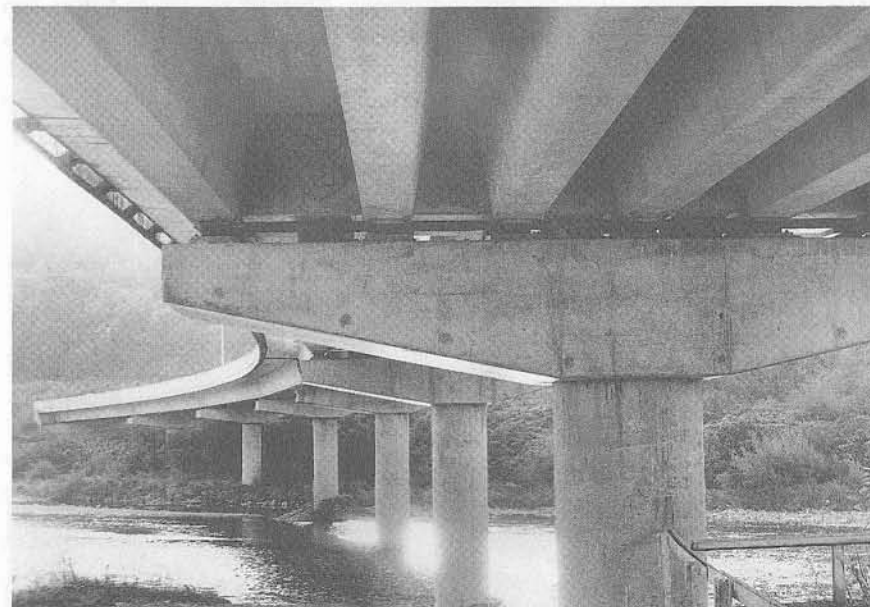


Figure 6.1 Moonshine Bridge, Upper Hutt, New Zealand

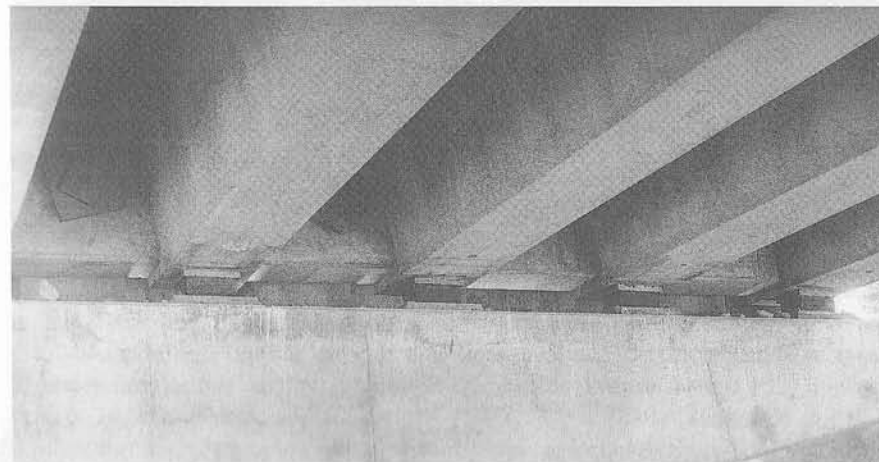


Figure 6.2 Moonshine Bridge, Upper Hutt, showing lead-rubber bearing under the beams, and restraining stops

Figure 6.3 shows a bridge over the Wellington Motorway which is fitted with lead-extrusion dampers at the lower abutment. It is one of a pair of sloping bridges which were seismically isolated by being mounted on glide bearings, the restoring force being provided by steel columns. The advantage of the extrusion dampers is that they lock the bridge in place during the braking of vehicles travelling downhill, yet at earthquake loads allow the bridge to move. Thermal expansion forces can be released by the creep of the extrusion dampers. After a large earthquake it is expected that the bridges will no longer have the seismic gaps ideally positioned. If necessary the bridges can then be jacked to the ideal position or allowed to creep back with the flexible columns providing the restoring force.



Figure 6.3 Aurora Terrace overbridge, Wellington City

6.2.3 South Rangitikei Viaduct with stepping isolation

The South Rangitikei Viaduct, which was opened in 1981, is an example of isolation through controlled base-uplift in a transverse rocking action. The bridge is 70 m tall, with six spans of prestressed concrete hollow-box girder, and an overall length of 315 m (Cormack, 1988).

Figure 6.4 shows the stepping isolation schematically, and Figures 6.5 and 6.6 are photographs of the bridge under construction, and of the first train to use it.

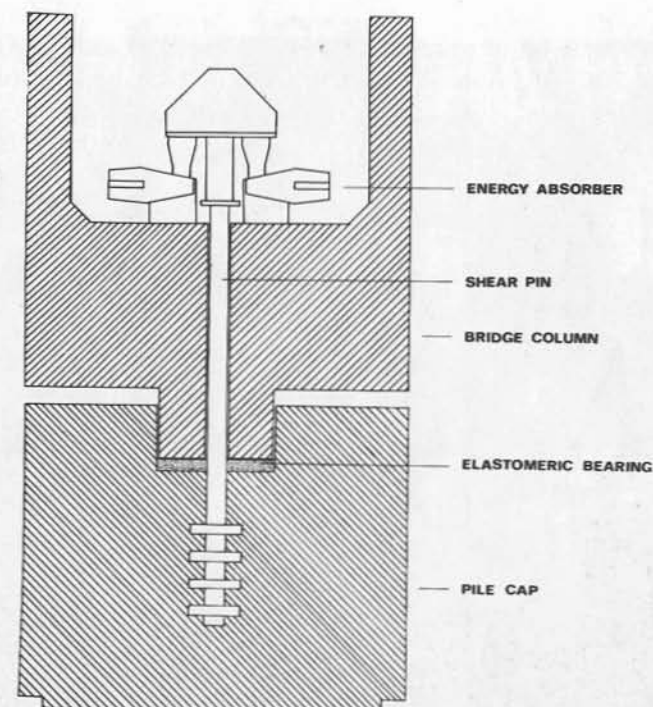


Figure 6.4 Schematic of base of stepping pier, South Rangitikei Viaduct

The stresses which can be transmitted into the slender reinforced-concrete H-shaped piers under earthquake loading are limited by allowing them to rock sideways, with uplift at the base alternating between the two legs of each pier. The extent of stepping, and the associated lateral movement of the bridge deck, are limited by energy dissipation provided by the hysteretic working of torsionally yielding steel-beam devices connected between the bottom of the stepping pier legs and the caps of the high-stiffness supporting piles. (The Type-E steel damper used is shown in Figure 3.3.)

The stepping action reduces the maximum tension calculated in the tallest piers, for the 1940 El Centro NS record, to about one-quarter that experienced when the legs are fixed at the base; unlike the fixed-base case there is little increase in base-level loads for stronger seismic excitations. The dampers reduce the displacements to about one-half those in the undamped case, and reduce the number of large displacements to less than one-quarter. The maximum displacement at the deck level for the damped stepping bridge is about 50% greater than for the fixed-leg bridge (Beck and Skinner, 1974).

The 24 energy dissipators operate at a nominal force of 450 kN with a design stroke of 80 mm. The maximum uplift of the legs is limited to 125 mm by stops.

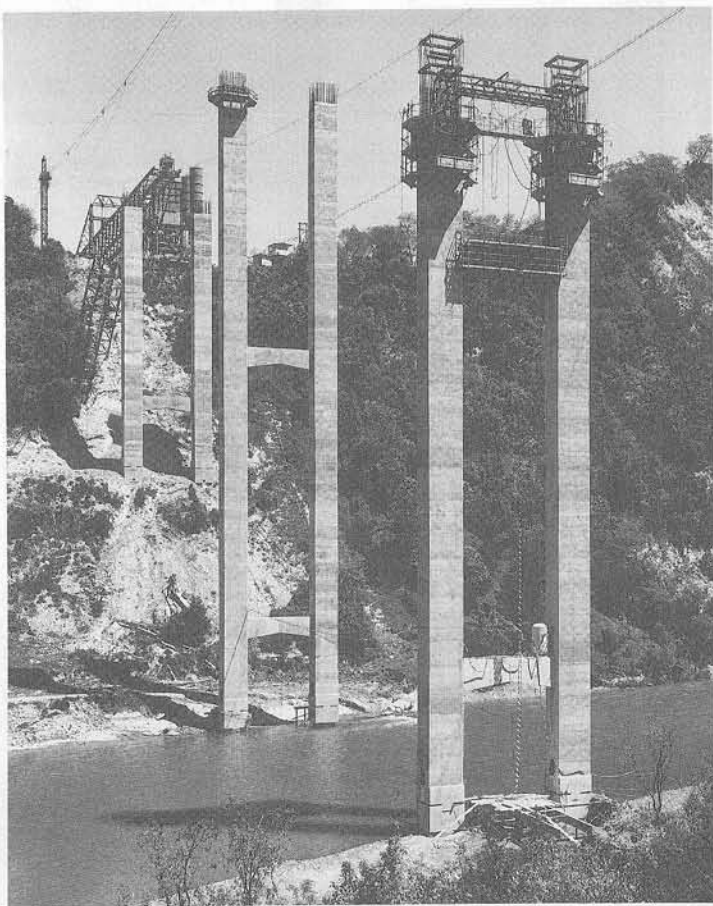


Figure 6.5 South Rangitikei Viaduct during construction

The weight of the bridge at rest is not carried by the dampers, but is transmitted to the foundations through thin laminated-rubber bearings whose primary functions are to allow rotation of each unlifted pier foot, and to distribute loads at the pier-pile-cap interfaces.

The stepping action is very effective in reducing seismic loads on this bridge because its centre of gravity is high, so that the non-isolated design was strongly dominated by overturning moments at the pier feet. The hysteretic damping during stepping is quite effective because the estimated self-damping of the stepping mechanism is quite low, due to the relatively rigid pile caps. A chimney structure at the Christchurch Airport was also provided with a stepping base. The resultant cost saving was about 7% (Sharpe and Skinner, 1983).



Figure 6.6 Inaugural train on South Rangitikei Viaduct

6.2.4 William Clayton Building

The William Clayton Building in Wellington, started in 1978 by the New Zealand Ministry of Works and Development and completed in 1981, was the first building in the world to be seismically isolated on lead-rubber bearings. (See Chapter 3)

Details of a lead-rubber bearing for this building are shown in Figure 6.7. The 80 bearings are located under each of the columns of the four-storey reinforced concrete frame building, which is 13 bays long by 5 bays wide with plan dimensions of 97 m \times 40 m. Each bearing carries a vertical load of 1 to 2 MN and is capable of taking a horizontal displacement of ± 200 mm. Detailed descriptions of the building have been given by Meggett (1978) and Skinner (1982). It is shown, during construction and after completion, in Figures 6.8 and 6.9.

The pioneering nature of the building and its proximity to the active Wellington fault dictated that a conservative design approach be taken. The design earthquake was taken as 1.5 El Centro NS 1940, for which the calculated maximum dynamic base shear was 0.20 times the total building weight W , and this was selected as the design static base shear force. The artificial A1 record, which is intended to represent near-fault motion in a magnitude-8 earthquake, was considered as the

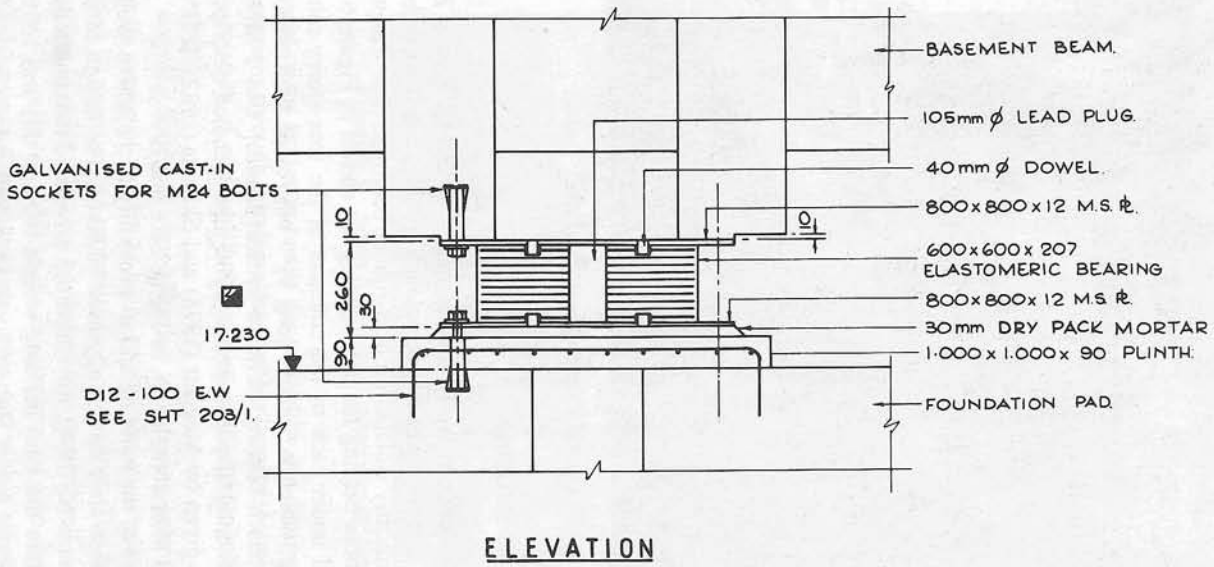


Figure 6.7 Diagram showing detail of lead-rubber bearing, William Clayton Building, Wellington

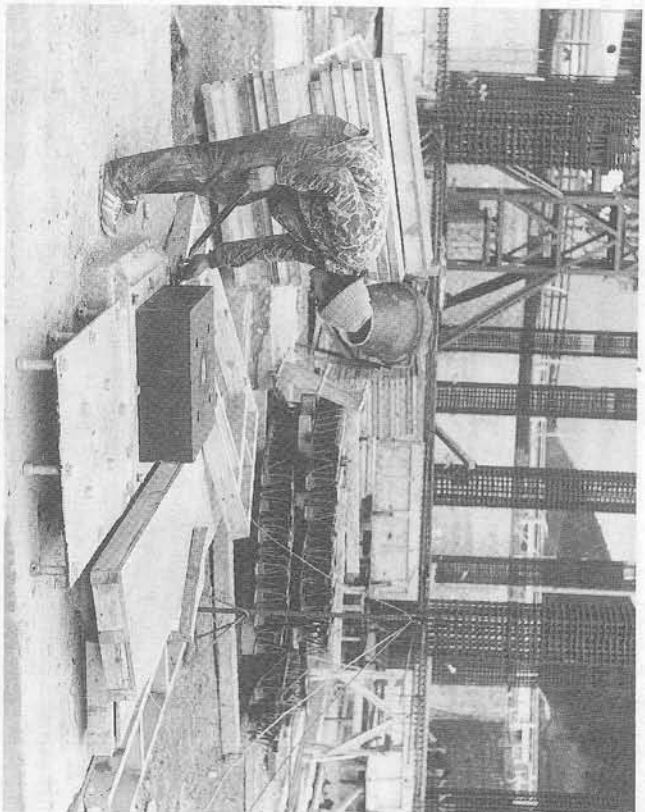


Figure 6.8 William Clayton Building during construction; note lead-rubber bearing

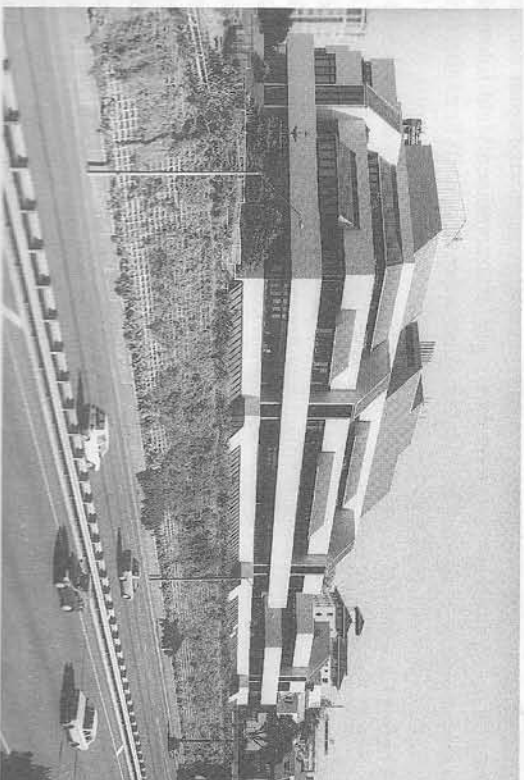


Figure 6.9 William Clayton Building completed and occupied

'maximum credible' motion, producing a calculated maximum base shear of $0.26W$. Even though the calculated response of the seismically isolated structure was essentially elastic for the design-earthquake motions, a capacity design procedure was used, as required for a design with high ductility.

The bearing size and lead diameter were chosen after careful dynamic analysis. Meggett (1978) discussed this design in detail and found that accelerations, inter-storey drifts and maximum base shear forces were approximately halved by the introduction of the seismically isolated system. He concluded that reasonable values for the shear stiffness of the elastomeric bearing and lead-yield stiffness were

$$K_b(r)/W = 1-2 \text{ m}^{-1} \quad (6.1)$$

giving

$$T_{b2} = 2.0-1.4 \text{ s} \quad (6.2)$$

and

$$Q_y/W \approx 0.04-0.09 \quad (6.3)$$

while in fact the bearings were measured with $K_b(r)/W = 1.1 \text{ m}^{-1}$ and $Q_y = 0.07W$ for 1.5 El Centro.

Horizontal clearances of 150 mm were provided before the base slab impacts on retaining walls. This corresponds to the maximum bearing displacement calculated for the A1 record, with 105 mm calculated for 1.5 El Centro. Water, gas and sewerage pipes, external stairways and sliding gratings over the seismic gap were detailed to accommodate the 150 mm isolator displacement.

Thus the lead-rubber bearings lengthened the period of the structure from 0.3 s for the frame structure alone, to 0.8 s for the isolated structure with the lead plugs unyielded, and 2.0 s in the fully yielded state (i.e. calculated from the structural mass and post-yield stiffness of the bearings). The combined yield force of all the bearings and lead plugs was calculated to be approximately 7% of the structure's 'dead plus seismic live' load.

The maximum base shear for the isolated structure calculated for 1.5 El Centro was $0.20W$, which is half the value of $0.38W$ for the unisolated structure. Only the roof beam yielded for the isolated structure with a rotational ductility of less than 2 and no hinge reversal. For both 1.5 El Centro and the A1 record, the maximum inter-storey drifts for the isolated structure were about 10 mm, about 0.002 times the storey height, and were uniform over the structure's height. For the unisolated structure, the inter-storey drifts increased up the height of the building, reaching a maximum of 52 mm. The markedly reduced inter-storey drifts should minimise the secondary damage in the isolated structure, and they greatly simplified the detailing for partitions and glazing.

As a first attempt at seismic isolation of a building with lead-rubber bearings, the design of the William Clayton Building was very much a learning experience. The design was conservative, and if it was repeated now, it is probable that more advantages would be taken of potential economies offered by the isolation

approach to seismic design. Nevertheless, the design analysis demonstrated the improved seismic performance which can be achieved through isolation of appropriate structures. Moreover, in the light of subsequent tests on lead-rubber bearings, the extreme-earthquake capacity could in principle be extended substantially simply by increasing the base-slab clearance to 200 or 250 mm.

6.2.5 Union House

The 12-storey Union House (Boardman *et al.* 1983), completed in 1983, achieves isolator flexibility by using flexible piles within clearance sleeves. It is situated in Auckland alongside Waitemata Harbour. Poor near-surface soil conditions, consisting of natural marine silts and land reclaimed by pumping in hydraulic fill, led to the adoption of long end-bearing piles, sunk about 2.5 m into the underlying sandstone at a depth of about 10-13 m below street level, to carry the weight of the structure. Although Auckland is in a region of only moderate seismic activity, there is concern that it could be affected by large earthquakes, up to magnitude 8.5, centred 200 km or more away in the Bay of Plenty and East Cape regions near the subduction-zone boundary between the Pacific and Indo-Australian plates. Such earthquakes could cause strong shaking in the flexible soils at the site.

Isolation was achieved by making the piles laterally flexible with moment-resisting pins at each end. The piles were surrounded by clearance steel jackets allowing ± 150 mm relative movement, thus separating the building from the potentially troublesome earthquake motions of the upper soil layers and making provision for the large base displacements necessary for isolation. An effective isolation system was completed by installing steel tapered-cantilever dampers at the top of the piles at ground level to provide energy dissipation and deflection control. The structure was stiffened and strengthened using external steel cross-bracing (see Figure 6.10). The increased stiffness improved the seismic responses, giving reduced inter-storey displacements, a reduced shear-force bulge at mid-height and reduced floor spectra. Moreover, the cross-bracing provided the required lateral strength at low cost. The reduced structure ductility was adequate with the well damped isolator. The dampers are connected between the top of the piles supporting the superstructure and the otherwise structurally separated basement and ground-floor structure, which is supported directly by the upper soil layers.

As Auckland is a region where earthquakes of only moderate magnitude are expected, the seismic design specifications for Union House are less severe than for many other seismically isolated structures. The maximum dissipator deflections in the 'maximum credible' El Centro motion were 150 mm, with 60 mm in the design earthquake. The effective period of the isolated structure was about 2 s. Maximum inter-storey deflections were typically 10 mm for the maximum credible earthquake and 5 mm for the design earthquake.

Union House is an example of the economical use of seismic isolation in an area of moderate seismicity. An appropriate structural form was chosen to take advantage of the reductions of seismic force, ductility demands and structural de-

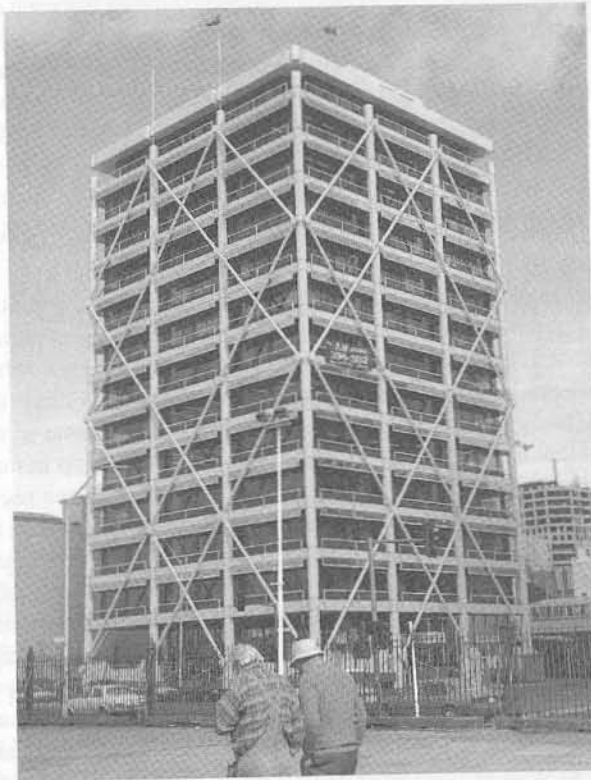


Figure 6.10 Union House, Auckland City; note the external diagonal bracing

formations offered by the seismic isolation option. The inherently stiff cross-braced frame is well suited to the needs for a stiff superstructure in the seismically isolated approach. Isolation in turn makes the cross-bracing feasible, because low ductility demands are placed on the main structure. However, if very low floor spectra are required, it may be necessary to use more linear velocity dampers. An important factor in the design of such isolation systems is the need for an appropriate allowance for the displacement of the pile-sleeve tops with respect to the fixed ends of the piles.

Other structural forms were investigated during the preliminary design stages, including two-way concrete frames, peripheral concrete frames, and a cantilever shear core. The cross-braced isolated structure allowed an open and light structural façade, and a maximum use of precast elements. The seismically isolated option produced an estimated cost saving of nearly 7% in the total construction cost of NZ\$6.6 million (in 1983), including a saving in construction time of three months.

6.2.6 Wellington Central Police Station

The new Wellington Central Police Station (Charleston *et al.*, 1987), completed in 1991, is similar in concept to Union House. The 10-storey tower block is supported on long piles founded 15 m below ground in weathered greywacke rock. The near-surface soil layer consists of marine sediments and fill of dubious quality.

Again the piles are enclosed in oversize casings, with clearances which allow considerable displacements relative to the ground. Energy dissipation is provided by lead-extrusion dampers (Robinson and Greenbank, 1976), connected between the top of the piles and a structurally separate embedded basement (see Figure 6.11). A cross-braced reinforced-concrete frame provides a stiff superstructure (see Figure 6.12). The flexible piles and lead-extrusion dampers provide an almost elastic-plastic force-displacement characteristic for the isolation system, which controls the forces imposed on the main structure.

The seismic design specifications for the Wellington Central Police Station are considerably more severe than those for Union House in Auckland. The Police Station has an essential Civil Defence role and is therefore required to be in operation after a major earthquake. The New Zealand Loadings Code requires a risk factor $R = 1.6$ for essential facilities. The site is a few hundred metres from the major active Wellington fault, and less than 20 km from several other major fault systems.

Functional requirements dictated that the lateral load-resisting structure should be on the perimeter of the building. Three structural options were considered: a cross-braced frame, a moment-resisting frame or a seismically isolated cross-braced

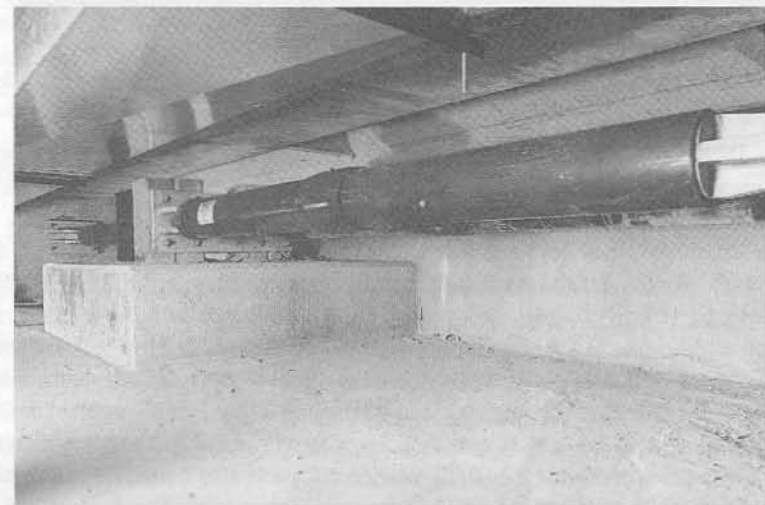


Figure 6.11 Lead-extrusion damper in basement of Wellington Central Police Station



Figure 6.12 Wellington Central Police Station; note the external diagonal bracing

frame. This last option looked attractive from the outset because the foundation conditions required piling, but the perimeter moment-resisting frame was also considered at length.

The structure is required to respond elastically for seismic motions with a 450-year return period, corresponding to a 1.4 times scaling of the 1940 El Centro accelerogram. The building must remain fully functional and suffer only minor non-structural damage for these motions. This is assured by the low inter-storey deflections of approximately 10 mm. Using an isolation system with a nearly elastic-plastic force-deflection characteristic, and a low yield level of 0.035 of the building seismic weight, it was found that there was only a modest increase in maximum frame forces for the 1000-year return period motions, corresponding to 1.7 El Centro NS 1940 or the 1971 Pacoima Dam record. The increase in force was almost accommodated by the increase from dependable to probable strengths

appropriate to the design and ultimate load conditions respectively. It is possible that some yielding will occur under the 1000-year return period motions, but the ductility demand will be low and specific ductile detailing was considered unnecessary. The Pacoima Dam record poses a severe test for a seismic isolation system because it contains a strong long-period pulse, thought to be a 'fault-fling' component, as well as high maximum accelerations. The Pacoima record imposes severe ductility demands on many conventional structures.

The degree of isolation required to obtain elastic structural response with these very severe earthquake motions requires provision for a large relative displacement between the top of the piles and the ground. A clearance of 375 mm was provided between the 800 mm diameter piles and their casings, to give a reasonable margin above the maximum calculated displacements; 355 mm was calculated for one of the 450-year return period accelerograms. Consideration was also given to even larger motions, when moderately deformable column stops might contact the basement structure which has been designed to absorb excess seismic energy in a controlled manner in this situation.

The large displacement demands on the isolation system and the almost elastic-plastic response required from the energy dissipators led to the choice of lead-extrusion dampers rather than steel devices as used in Union House. In total, 24 lead-extrusion dampers each with a yield force of 250 kN and stroke of ± 400 mm were required. This was a considerable scaling-up of previous versions of this type of damper used in several New Zealand bridges: the bridge dampers had a yield level of 150 kN and a stroke of ± 200 mm. The new model damper was tested extensively to ensure the required performance.

The seismically isolated option was estimated to produce a saving of 10% in structural cost over the moment-resisting frame option. In addition, the seismically isolated structure will have a considerably enhanced earthquake resistance. Moreover, the repair costs after a major earthquake should be low. Importantly, the seismically isolated structure should be fully operational after a major earthquake.

6.3 STRUCTURES ISOLATED IN JAPAN

6.3.1 Introduction

The first seismically isolated structure to be completed in Japan was the Yachiyodai Residential Dwelling, a two-storey building, completed in 1982. This building is mounted on six laminated-rubber bearings and relies on the friction of a precast concrete panel for the damping. Since 1985, more than 50 buildings have been authorised, of 1 to 14 storeys in height. They range from dwellings to tower blocks, with floor areas from 114 m² to 38 000 m². Details of buildings seismically isolated in Japan are given in Table 6.4 (Shimoda 1989-1992; Saruta, 1991, 1992; Seki, 1991, 1992). Various seismic isolation and damping systems have been used, often in hybrid combinations, as indicated in Table 6.4 and its footnote. The most popular

Table 6.4 Seismically isolated buildings in Japan

Type	Building Name	Storey	Total Floor Area (m ²)	Isolation System	Licence Date
Dwelling	Yachiyodai	2	114	EB+F	1982
Institute	Research Lab	4	1330	EB+S	1985
Institute	High-Tech Research Lab	5	1623	EB+S	1986
Laboratory	Oiles Tech. Centre	5	4765	LRB+E	1986
Dormitory	Tikuyu-Ryo	3	1530	EB+V	1986
Institute	Acoustic Lab	2	656	EB+S	1986
Museum	Elizabeth Sanders (re-design)	2	293	EB+S	1986
Test Model	Tohoku University	3	208	EB	1986
Apartment	Apt. Hukumiya	4	681	EB+S	1986
Office	Sibuya Simizu Building	5+B1	3385	EB+S	1987
Institute	Research Lab No. 6	3	306	LRB	1987
Institute	Tsukuba Muki-Zaiken	1	616	EB+S	1987
Office	Tsuchiura branch	4	636	LRB	1987
Institute	Lab. J building	4	1173	SL+R	1987
Apartment	Kousinzuka	3	476	EB+S	1987
Office	Toranomon Building	8	3373	EB+S	1987
Apartment	Itoh Mansion	10	3583	LRB	1988
Dormitory	Itinoe Dormitory	3	770	EB+S	1988
Institute	Clean Room Lab	2	405	EB+V	1988
Rest house	Atagawa Hoyojo	1	140	SL+S	1988
Apartment	Ogawa Mansion	4	1186	HDR	1988
Office	Asano Building	7	3255	LRB	1988
Store	Kusuda Building	4+B1	1047	HDR	1988
Dwelling	Ichikawa residence	2	297	EB	1988
Computer	Computer Centre	6	10032	HDR	1988
Office	Sagamihara Centre	3	255	HDR	1988
Clinic	Gerontology Res. Lab.	2+B1	1615	EB+S	1988
Dwelling	M-300 Hoyosyo	2	309	LRB	1989
Apartment	Harvest Hills	6	2065	EB+S	1989
Institute	Acoustic Lab	2	656	EB+S	1989
Office	Toshin Building	9+B1	7573	EB+S	1989
Laboratory	Dwell. Test Lab	3	680	EB+S	1989
Office	MSB-21 Ootuka	12+B	5962	LRB	1989
Institute	Wind Laboratory	3	555	HDR	1989

Table 6.4 (continued)

Type	Building Name	Storey	Total Floor Area (m ²)	Isolation System	Licence Date
Office	CP Fukuzumi	5	4406	EB+F	1989
Apartment	Employees Buildings	4	652	LRB+HDR	1989
Office	Toho-Gas Centre	3	1799	SL+RS	1989
Dormitory	Tudanuma Dormitory	2	202	EB+S	1989
Dwelling	M-300 Yamada's	2	214	LRB	1989
Apartment	Koganei-Apartment	3	714	LRB+EB	1989
Computer	Operation Centre	2	10463	LRB	1989
Factory	Urawa-Kogyo	5	1525	HDR	1989
Office	Kanritou	3	955	EB+V	1990
Computer	Noukyou Centre	3	5423	LRB	1990
Office	C-1 Building	7+B1	37846	LRB	1990
Office	Keisan Kenkyusyo	3	627	EB+V	1990
Office	Kasiwa Kojo	4	2186	HDR	1990
Institute	Acoustic Laboratory	2	908	EB+F	1990
Dormitory	Yamato-ryo	8	1921	EB+S	1990
Dormitory	Kawaguchi-ryo	4	659	LRB	1990
Computer	Dounen Computer Centre	4	3310	EB+LD	1991
Laboratory	Andou Tech. Centre	3	545	LRB	1991
Dormitory	Toyo Rubber Shibamata-ryo	7	3520	EB+S+oil	1991
Office	Aoki Tech. Centre	4+B1	4400	LRB	1991
Dormitory	Dai Nippon Daboku Ichigaya-ryo	4	1186	EB+LD	1991
Apartment	Domani-Musashino	3	742	EB+S	1991

Key:

- EB = elastomeric bearing
- LRB = lead-rubber bearing
- HDR = high damping rubber bearing
- SL = sliding system (PTFE)
- S = steel damper
- V = viscous damper
- F = friction damper
- RS = rubber spring
- LD = lead damper
- B1, B2 = basements

Table 6.5 Seismically isolated bridges in Japan

Bridge name	Site	Super-structure Type	Bridge Length (m)	Isolation System	Completion (Scheduled)
On-netoh Oh-hashii Bridge	Hokkaido	4-span continuous steel girder	102	RB(12) LRB(18)	1991
Nagaki-gawa Bridge	Akita	3-span Continuous steel girder	99	LRB(20)	1991
Maruki Bridge	Iwate	3-span Continuous PC Girder	122	LRB(8)	1991
Miyagawa Bridge	Shizuoka	3-span Continuous steel girder	104	LRB(10)	1991
Metropolitan Highway Bridge No. 12	Tokyo	6-span Continuous PC slab	138	LRB(10)	1991
Hokuso Line Viaduct (Railway)	Chiba	2-span Continuous steel girder	80	LRB(8)	1990
Kanko Bridge	Tochigi	6-span Continuous PC girder	296	LRB(10)	1991
Matsuno-hama Bridge	Osaka	4-span Continuous steel girder	211	LRB(12)	1991
Uehara Bridge	Aichi	2-span Continuous steel girder	65	LRB(18)	1991
Shirasuji Viaduct (Railway)	Chiba	2-span Continuous steel girder	76	RB(4) LRB(4)	1993 (scheduled)
Trans-Tokyo Bay Highway Bridge	Tokyo Bay	10-span Continuous steel girder	800	LRB(18)	1994 (scheduled)
Karasu-yama No. 1 Bridge	Tochigi	6-span Continuous PC girder	245	High-damping rubber (14)	1992 (scheduled)

Key:

EB = elastomeric bearing

LRB = lead-rubber bearing

HDR = high damping rubber bearing

SL = sliding system (PTFE)

S = steel damper

V = viscous damper

F = friction damper

RS = rubber spring

LD = lead damper

B1,B2 = basements

isolation systems for buildings are laminated-rubber for the isolation, with either steel or lead providing the damping.

The first seismically isolated bridge in Japan was completed in 1990 and is mounted on lead-rubber bearings. Details of some bridges seismically isolated in Japan are given in Table 6.5 (Shimoda 1989-1992; Seki, 1991, 1992; Saruta, 1991, 1992). Except for one mounted on a high-damping rubber bearing, all of these use lead-rubber bearings.

6.3.2 The C-1 Building, Fuchu City, Tokyo

This, currently (1992) the largest seismically isolated building in the world, has a total area of more than 45 000 m², of which the isolated parts (higher building) have an area of 37 846 m², a height of 41 m and a weight of 62 800 t. It will be used as a computer centre: seismic isolation was chosen to protect the equipment.

The building will consist of a seven-floor superstructure, a penthouse and a one-floor basement, with the composite structure being formed of steel and steel-reinforced concrete. It is mounted on 68 lead-rubber bearings for seismic isolation. The bearings are between 1.1 and 1.5 m in diameter, with lead plugs from 180 to 200 mm in diameter (Nakagawa and Kawamura, 1991). Each bearing is surrounded by 10 mm of rubber to protect it from attack by ozone and fire damage.

At small displacements the natural period for the isolated building is expected to be about 1.4 s, while at large displacements, about 300 mm, the period is about 3 s. This should give an adequate frequency shift for an earthquake of the kind expected at the site. The maximum base shear force at the isolators due to wind is not expected to exceed 45% of the yield shear force of the bearings, so the building should not move appreciably during strong winds.

6.3.3 The High-Tech R&D Centre, Obayashi Corporation

This reinforced-concrete structure, five storeys high, was completed in August 1986 (Teramura *et al.*, 1988). It is equipped with a seismic isolation system consisting of 14 laminated-rubber bearings, with an axial dead load of 200 t, as well as 96 steel bar dampers, of diameter 32 mm. It also has friction dampers as subdampers for experimental purposes. The laminated-rubber bearings give the seismically isolated structure a horizontal natural period of 3 s (see Figures 6.13 and 6.14).

Seismic isolation has allowed a reduction of design strength and permits a large span structure with smaller columns and beams, which in turn provides open space. Key equipment, including a supercomputer, is installed on the top floor. During the 1989 Ibaraki earthquake, the building clearly demonstrated the effectiveness of seismic isolation, with a ten-fold reduction in roof acceleration.

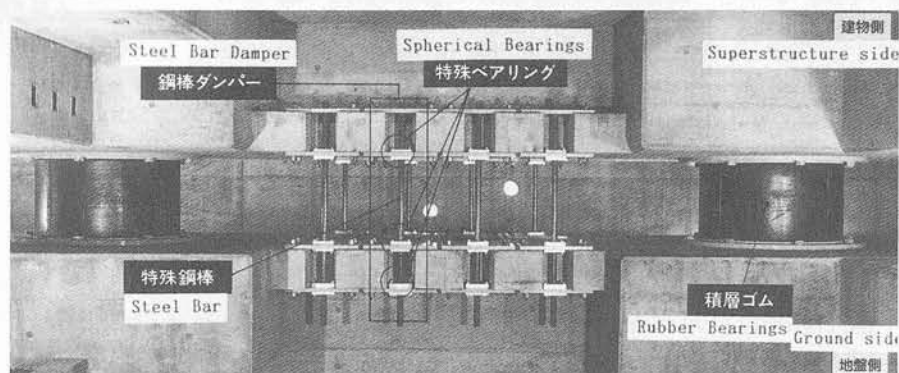


Figure 6.13 Isolation system used in the Obayashi High-tech R & D Centre, Tokyo (photograph courtesy Obayashi Corporation)

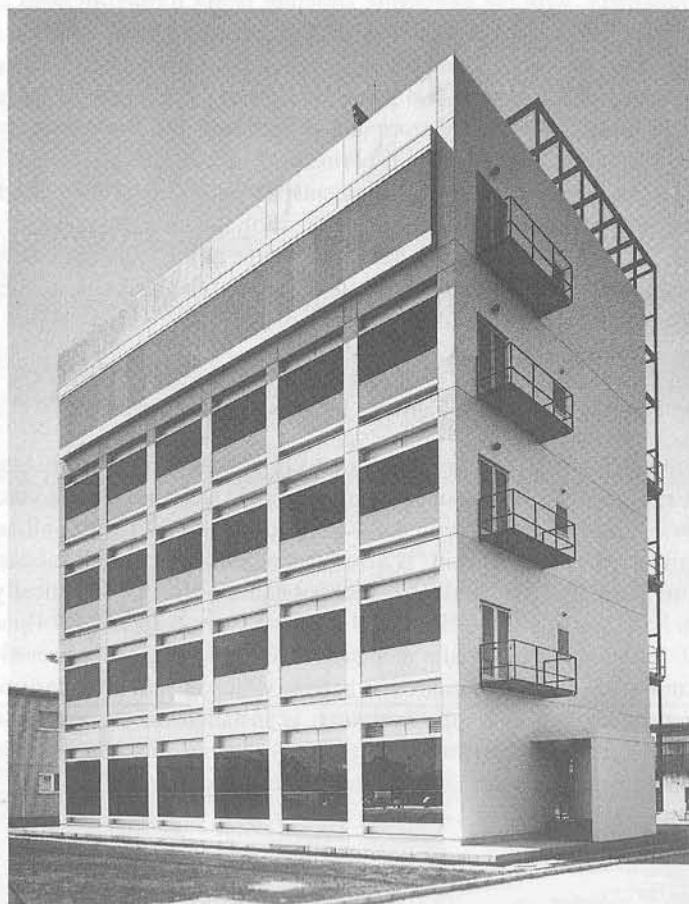


Figure 6.14 Obayashi High-tech R & D Centre (photograph courtesy Obayashi Corpo-

6.3.4 Comparison of three buildings with different seismic isolation systems

A comparative study has been carried out (Kaneko *et al.*, 1990) on the effectiveness and dynamic characteristics of four types of base isolation system, namely: laminated-rubber bearing with oil damper system; high-damping rubber bearing system; lead-rubber bearings; and laminated-rubber bearings with a steel damper system. The study was carried out by earthquake response observations of full-sized structures, as well as by numerical analyses. The three buildings studied were the test building at Tohoku University in Sendai, northern Japan, Tsuchiura Office building northeast of Tokyo and the Toranomon building in Tokyo.

The test building at Tohoku University was seismically isolated in order to be used experimentally in studies of performance; for comparison, an identical building on the same campus was 'conventional', i.e. it had not been isolated. Both buildings are 3-storey reinforced concrete structures 6 m × 10 m in plan. In the first stage of the investigation, the isolated building was fitted with 6 laminated-rubber bearings and 12 viscous dampers (oil) (see Figures 6.15 and 6.16), and earthquake observation was conducted for a year. After that, the devices were changed to high-damping rubber bearings, and observations continued. The natural frequencies and damping ratios of each building were obtained by forced vibration tests. The damping ratios of the isolated building with viscous dampers were about 15% and those with high-damping rubber about 12%, which are respectively about 10 times and 8 times larger than those of the unisolated building.

The Tsuchiura office building of Shimizu Corporation is a four-storey reinforced-concrete structure 12.5 m × 12.5 m in plan. It is isolated by lead-rubber bearings and the damping ratios were found to be anisotropic, being 9.9% and 12.7% along two orthogonal directions.

The Toranomon building is eight-storey steel-framed reinforced concrete with an irregular shape and large eccentricity. The isolation devices have been arranged to reduce the eccentricity for earthquake loading. The building is supported by bearing piles on the Tokyo gravel layer, about 22 m below the surface. The isolation devices consist of 12 laminated-rubber bearings and 25 steel dampers, each consisting of 24 steel bars (see Figure 6.17). Eight oil dampers (four for each direction) are also installed for small vibration amplitudes.

Accelerograms of the largest earthquake motions in the records of each building can be summarised as follows. In the two systems studied on the test building at Tohoku University, the maximum accelerations at the roof of the isolated building were about one-third of those on the unisolated building. For the lead-rubber bearing system at Tsuchiura, the maximum acceleration at the roof was about 0.6 times that at the base. The response of the Toranomon building could not be clearly evaluated because only small-amplitude earthquakes occurred and the steel damper system was still in the elastic region. Torsional responses were small in all four isolated structures.

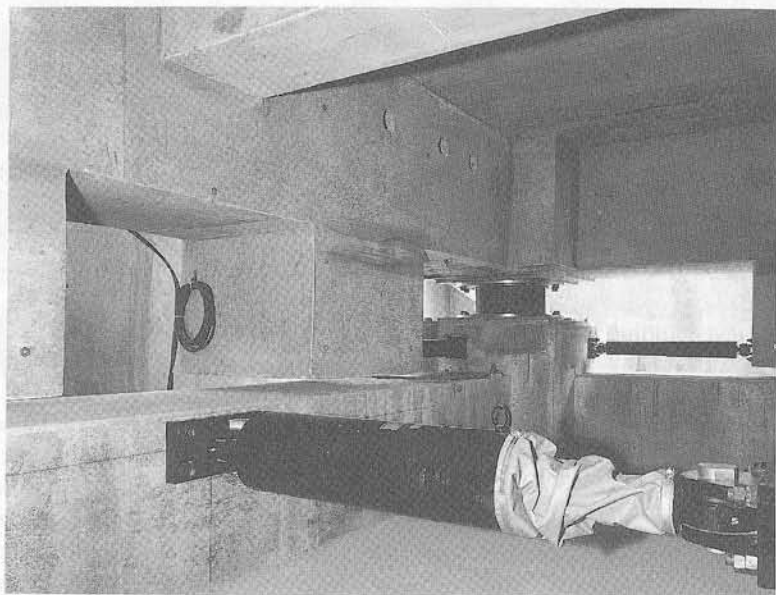


Figure 6.15 Oil dampers and laminated-rubber bearings in Test Building at Tohoku University, Sendai (photograph courtesy Shimizu Corporation)



Figure 6.16 Test Buildings at Tohoku University. On the left is the conventional building, and on the right is the seismically isolated building (photograph courtesy Shimizu Corporation)

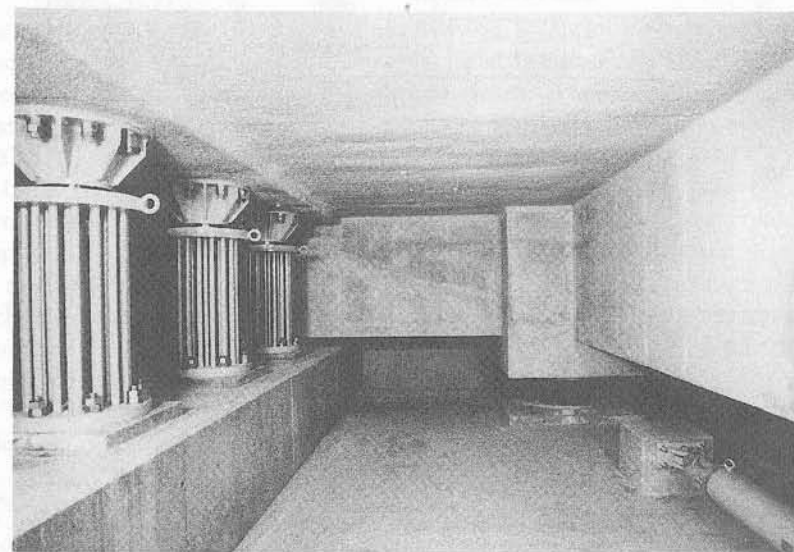


Figure 6.17 High-damping rubber bearing, steel dampers and oil damper in basement of Bridgestone Toranomon Building, Tokyo (photograph courtesy Shimizu Corporation)

6.3.5 Oiles Technical Centre Building

The Technical Centre Building of the Oiles Corporation (Shimoda *et al.* 1991) received special authorisation from the Ministry of Construction, based on the provisions under Article 38 of the Building Standards Law of Japan, since it was the first building in Japan to be equipped with lead-rubber bearings for seismic isolation, and it was completed in February 1987. It is a 5-storey structure of reinforced concrete, with a total floor area of approximately 4800 m² and a total weight of 7500 t (see Figures 6.18 and 6.19).

Tests were carried out to verify the reliability of the base-isolated building under an earthquake. The tests consisted of free vibration tests, forced vibration tests and microtremor observations. The appropriateness and accuracy of the method were also verified.

The results of dynamic analysis showed that the response acceleration of each floor of the building was reduced to about 0.2g even during strong earthquakes (0.3–0.5g) at an input of 50 cm s⁻¹. The maximum response acceleration was reduced to between 0.2 and 0.3g even under a velocity of 0.75 m s⁻¹. The building remained elastic since the shearing force for each storey was shown to be less than the yielding force, while the maximum response displacement was 370 mm.

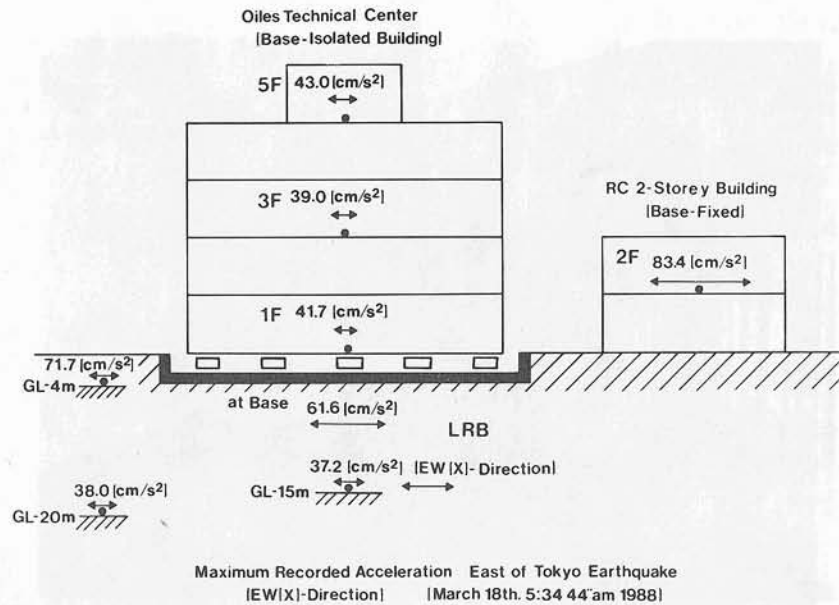


Figure 6.18 Diagram of Oiles Technical Centre showing seismic accelerations as measured on 18/03/88 (courtesy Oiles Corporation)



Figure 6.19 Oiles Technical Centre, Tokyo (photograph courtesy Oiles Corporation)

6.3.6 Miyagawa Bridge

The Miyagawa Bridge, across the Keta River in Shizuoka prefecture, is the first seismically isolated bridge constructed in Japan (Matsuo and Hara, 1991). The three-span continuous bridge with steel plate girders of length 110 m, is in an area where the ground is stiff, and it is mounted on lead-rubber bearings (see Figures 6.20–6.22).

In the traverse direction the bridge superstructure is restrained, allowing movements in the longitudinal direction of ± 150 mm before restraints at the abutments stop further displacement. The lead-rubber bearings were chosen and distributed so that 38% and 12% of the total inertia force was allocated to each pier and each abutment, respectively. The fundamental period of the unisolated bridge was computed as 0.3 s, while the isolated design has a natural period of 0.8 s for small amplitude vibrations, and 1.2 s for larger.

The system used for the design for seismic isolation is known in Japan as the 'Menshin design method' (Matsuo and Hara, 1991).

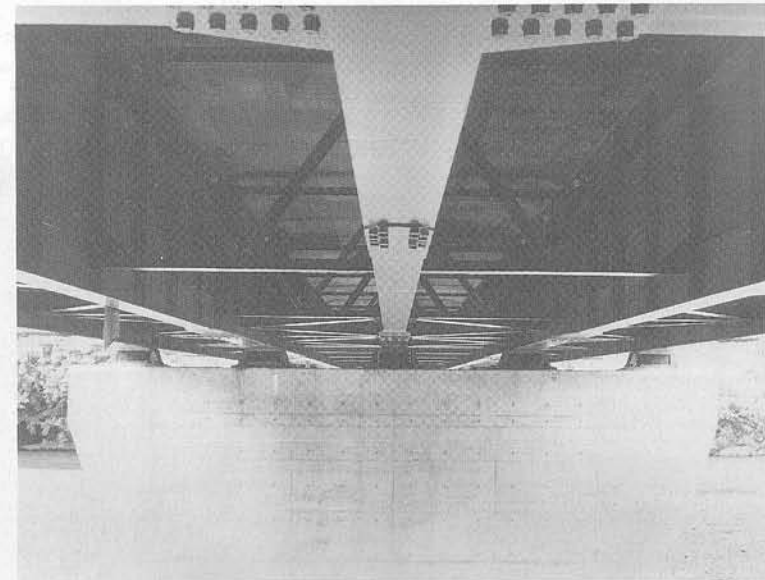


Figure 6.20 Miyagawa Bridge, Shizuoka Prefecture, showing bridge deck, isolation system and piers (photograph courtesy Oiles Corporation)

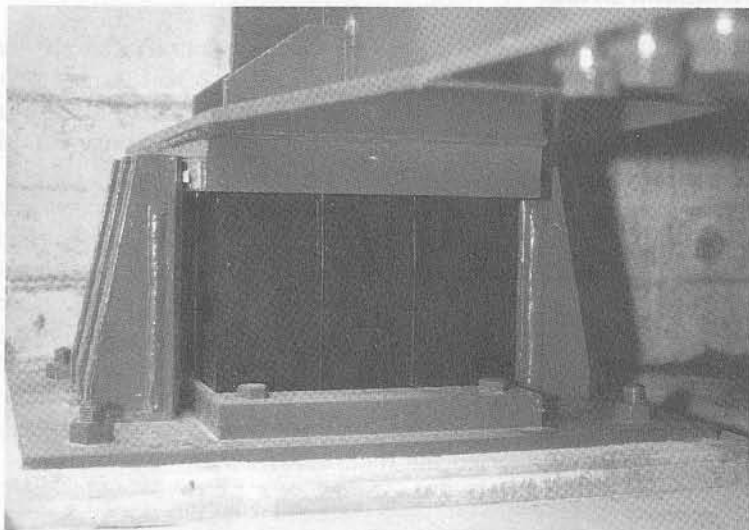


Figure 6.21 Lead-rubber bearing in Miyagawa Bridge showing transverse restraints (photograph courtesy Oiles Corporation)



Figure 6.22 Miyagawa Bridge, Shizuoka Prefecture, Japan (photograph courtesy Oiles Corporation)

6.4 STRUCTURES ISOLATED IN THE USA

6.4.1 Introduction

The first use of seismic isolation in the USA occurred during 1979, when circuit breakers were mounted on 7% damped elastomeric bearings. Since that time a number of bridges and buildings have been built or retrofitted with seismic isolation. The Foothill Communities Law and Justice Centre, on elastomeric bearings, was the first new building in the USA to be mounted on seismic isolation. Tables 6.6 and 6.7 show buildings and bridges which have been seismically isolated in the USA (Mayes, 1990–1992).

Table 6.6 Seismically isolated buildings in the United States

Building	Height/ Storeys	Floor Area (m ²)	Isolation System	Date
Foothill Communities Law and Justice Centre	4	17 000	10% damped elastomeric bearings	1985/6
Salt Lake City and County Building (Retrofit)	5	16 000	Rubber and Lead-rubber bearings	1987/8
Salt Lake City Manufacturing Facility (Evans and Sutherland Building)	4	9 300	Lead-rubber bearings	1987/88
USC University Hospital	8	33 000	Rubber and Lead-rubber bearings	1989
Fire Command and Control Facility	2	3 000	10% damped elastomeric bearings	1989
Rockwell Building (Retrofit)	8	28 000	Lead-rubber bearings	1989
Kaiser Computer Center	2	10 900	Lead-rubber bearings	1991
Mackay School of Mines (Retrofit)	3	4 700	10% damped elastomeric bearings plus PTFE	1991
Hawley Apartments (Retrofit)	4	1 900	Friction-pendulum/slider	1991
Channing House Retirement Home (Retrofit)	11	19 600	Lead-rubber bearings	1991
Long Beach VA Hospital (Retrofit)	12	33 000	Lead-rubber bearings	1991

Table 6.7 Seismically isolated bridges in the United States

Bridge	Superstructure type	Bridge Length (m)	Isolation System	Completion Date
• Sierra Point Bridge, California (US101) (Retrofit)	Longitudinal steel plate girders	190	LRB	1984/5
• Santa Ana River Bridge, California (Retrofit)	Steel trusses	310	LRB	1986/7
• Main Yard Vehicle Access Bridge, California (Retrofit)	Steel plate girders	80	LRB	1987
• Eel River Bridge, California (US101) (Retrofit)	Steel through truss simple spans	185	LRB	1987
• All American Canal Bridge, California (Retrofit)	Continuous steel plate girders	125	LRB	1988
• Sexton Creek Bridge, Illinois	Continuous steel plate girders	120	LRB	1990
• Toll Plaza Road Bridge, Pennsylvania	Simple span steel plate girder	55	LRB	1990
• Lacey V. Murrow Bridge West Approach, Washington (Retrofit)	Continuous concrete box girders	340	LRB	1991
• Cache River Bridge, Illinois (Retrofit)	Continuous steel plate girders	85	LRB	1991
• Route 161 Over Dutch Hollow Road, Illinois	Steel plate girder	110	LRB	1991
• West Street Overpass, New York (Retrofit)	Steel beam	50	LRB	1991
• US 40 Wabash River Bridge, Indiana	Continuous steel plate girders	270	LRB	1991
• Metrolink Light Rail, St Louis, (7 dual bridges)	Concrete box girder	65–280	LRB	1991
• Pequannock River Bridge, New Jersey	Steel plate girders	260	LRB	1991
• Blackstone River Bridge, Rhode Island	Steel plate girders	305	LRB	1992
• Bridges, B764 E & W, Nevada (Retrofit)	Steel plate girders	135	LRB	1992
• Squamscott River Bridge, New Hampshire	Steel plate girders	270	LRB	1992
• Olympic Blvd Separation, California	Steel plate girders	210	LRB	1992
• Carlson Blvd Bridge, California	Concrete box girder	45	LRB	1992
• Clackamas Connector, Oregon	Concrete box girder	305	LRB	1992
• Cedar River Bridge, Washington	Steel plate girders	160	LRB	1992

Key:

LRB = Lead-rubber bearings

6.4.2 Foothill Communities Law and Justice Centre, San Bernardino, California

This building, the first in the USA to be seismically isolated, in 1986, is mainly of steel-frame construction with the basement level consisting of concrete shear walls. It is a four-storey building with a total floor area of about 17 000 m² mounted on 96 'high damping' rubber bearings (see Figures 6.23 and 6.24) (Way, 1992). The 'high damping' of 10–15% is obtained by increasing the amount of carbon black in the rubber. Before the plans were finalised, estimates were made of the accelerations and displacements of the structure when isolated and unisolated. For an unisolated building with a structural damping of 5%, it was estimated that the resonant period would be 1.1 s, the base shear 0.8g and the rooftop would undergo accelerations and displacements of 1.6g and 300 mm respectively.

For the isolated case with a conservative value of 8% for the damping, the acceleration above the bearings was estimated to be 0.35g, while at the rooftop the acceleration was estimated at 0.4g with a displacement of 380 mm. The resonant period had a value of 2 s.

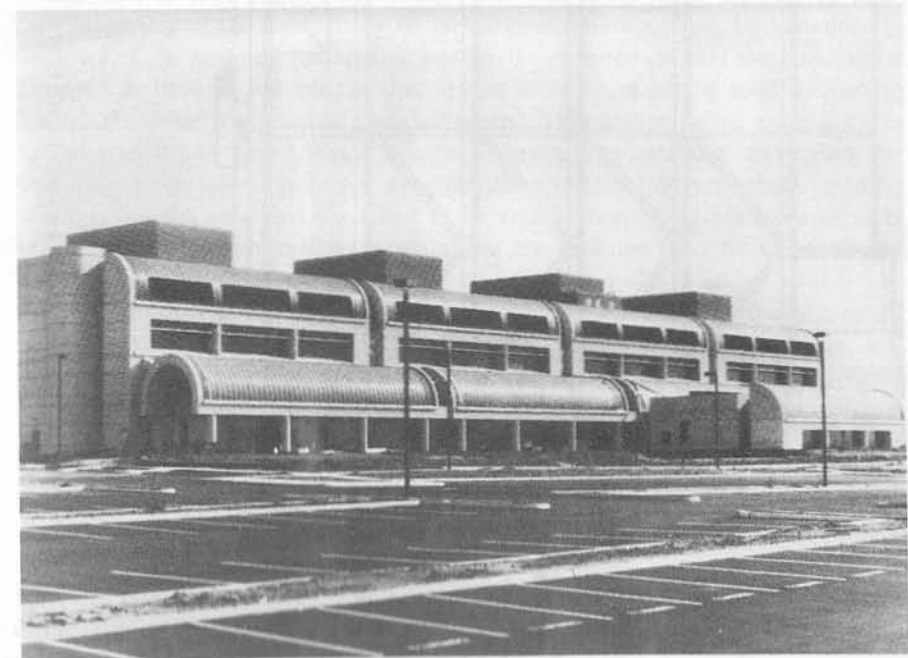


Figure 6.23 Foothill Communities Law and Justice Centre (photograph courtesy Base Isolation Consultants, Incorporated)

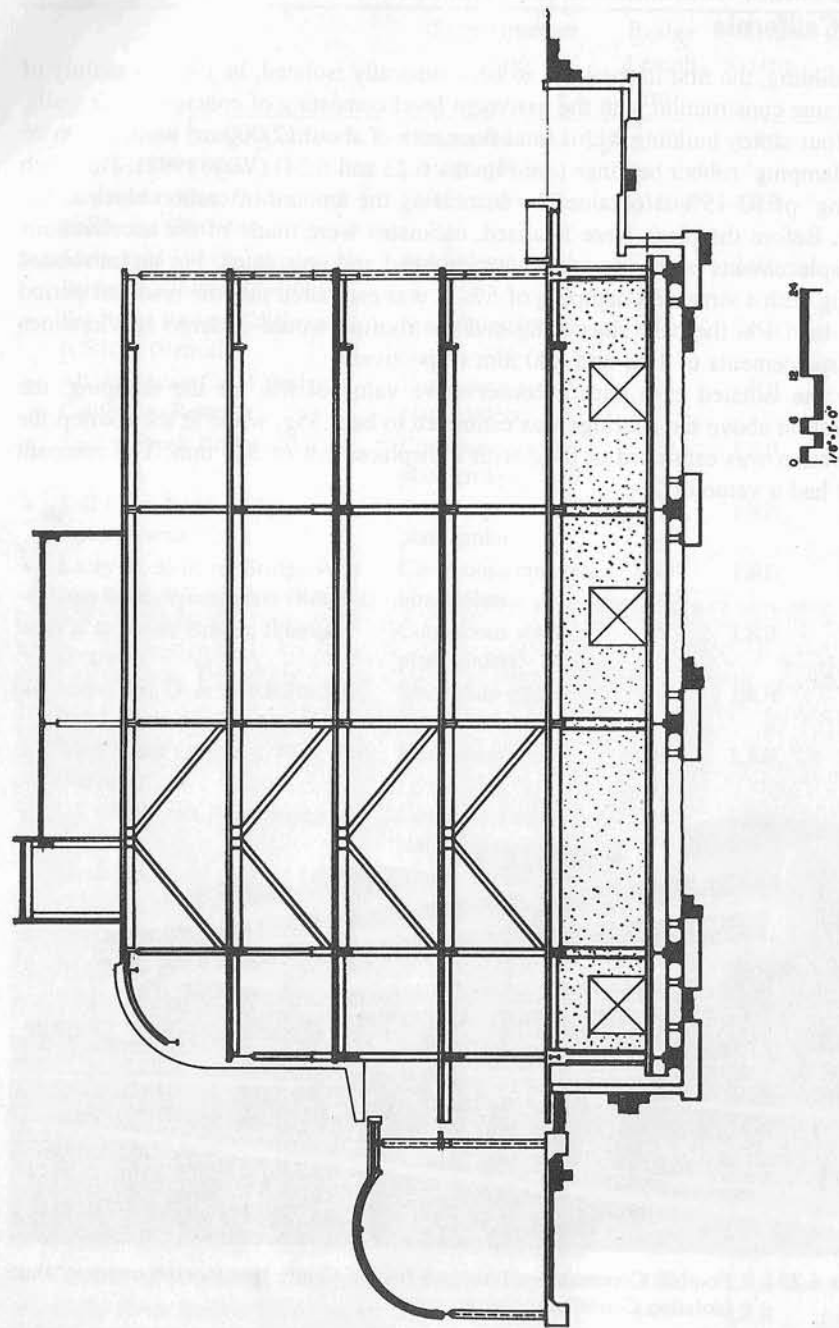


Figure 6.24

End elevation of Foothill Communities Law and Justice Centre, San Bernardino, California (courtesy Base Isolation Consultants, Incorporated)

6.4.3 Salt Lake City and County Building: retrofit

The Salt Lake City and County Building is a historic building, a massive five-storey unreinforced masonry and stone structure with a 76 m high central clocktower, which was completed in 1894. It is highly susceptible to earthquake damage, being 3 km from the Wasatch fault. It was retrofitted with seismic isolation, using a combination of lead-rubber bearings and elastomeric bearings (Bailey and Allen, 1989)

Figure 6.25 shows the façade of the building.

The retrofitting project began with an analysis of possible seismic isolation systems, each of these to be carried out in conjunction with other structural changes such as a steel space truss within the clocktower, various plywood diaphragms, and anchorage of seismic hazards, such as chimneys, statues, gargoyles and balustrades, around the exterior of the building.

The option of seismic isolation by means of a combination of elastomeric bearings and lead-rubber bearings at the base of the building was chosen because it would be least disruptive to the interior of the building; other options required considerable demolition. Calculations indicated that this system would be adequate to withstand the design earthquake.

The task of retrofitting was complex, and was made more difficult by inaccurate detailing of the foundations on the original building plans, by variations in the level of the building foundation, and by the requirement that the building be damaged as little as possible, so that impact tools could not be used for cutting through the stone. The original plan had placed 500 isolators below existing foundations, but it was found that a massive concrete mat extended underneath the four main tower piers. Isolators were therefore installed on top of the existing footings, but the new first floor had to be raised 36 cm, and hundreds of slots had to be cut through existing walls above the footings in order to install the isolators.

A major concern of the construction engineers was that an earthquake might occur during retrofit, when part of the building was isolated and part not, and when some walls had been removed. It was suggested (Bailey and Allen, 1989) that, in future, isolator locking mechanisms be employed during isolator installation in areas of high seismicity.

A total of 443 isolators was used. All isolators were of the same size, approximately 43 cm square by 38 cm tall, to cut down on fabrication costs and to simplify installation. Not all the isolators had lead plugs, since computer analyses had indicated unacceptably high tower shear for certain earthquake records. The isolators with lead plugs, approximately half of the total, were located around the perimeter of the building to give high damping for rotational vibrations, and hence cut down on torsional response.

A retaining wall was constructed round the building's exterior to ensure a 400 mm seismic gap, this including a large safety factor as computer analysis



Figure 6.25 Salt Lake City and County Building, Utah; an historic building retrofitted with seismic isolation (photograph courtesy Dynamic Isolation Systems, Incorporated)

had predicted only 12 cm lateral displacement of the building during the design earthquake. A bumper restraint system was also installed as a back-up safety device.

The project clearly demonstrated the feasibility of retrofitted isolation for a building of this kind, where:

- short periods result in high seismic forces
- the ratio of horizontal strength to weight is low
- ductility is low
- the risk of seismic collapse or cost of seismic repairs is unacceptable
- preservation has high cultural value
- the need to preserve exteriors and interiors limits scope for increasing strength and ductility
- it is practical to modify for inclusion of isolators
- the structural form and proportions do not give uplift for isolator-attenuated seismic forces
- adequate clearances for isolator and structure may be provided
- a practical isolation system gives an adequate reduction in seismic loads and deformations.

6.4.4 USC University Hospital, Los Angeles

This is an eight-storey, 35 000 m², steel-braced frame structure, with an asymmetric floor plan, scheduled for occupation in 1991 (Asher *et al.* 1990). It is a 275-bed teaching hospital, and is the first seismically isolated hospital in the world. The owner had been made aware of the potential benefits of seismic isolation and requested that it be considered as an alternative during the schematic design phase.

As no consensus document for isolation design procedures existed, the structural engineer submitted proposed criteria for approval by the California Office of the State Architect. Issues addressed by the criteria were: seismic input; design force levels and essentially elastic behaviour; design displacement limits; and specific analysis requirements. The scope of the analysis was set by the approved criteria and extensive computation followed.

The seismic isolation solution arrived at is shown schematically in Figure 6.26, namely a combination of lead-rubber bearings at the exterior braced-frame columns, and elastomeric bearings at the interior vertical load-bearing columns. The completed hospital is seen in Figure 6.27.

The design displacement arrived at was about 260 mm, a value in good accordance with those obtained by seismic isolation engineers in similar projects. All

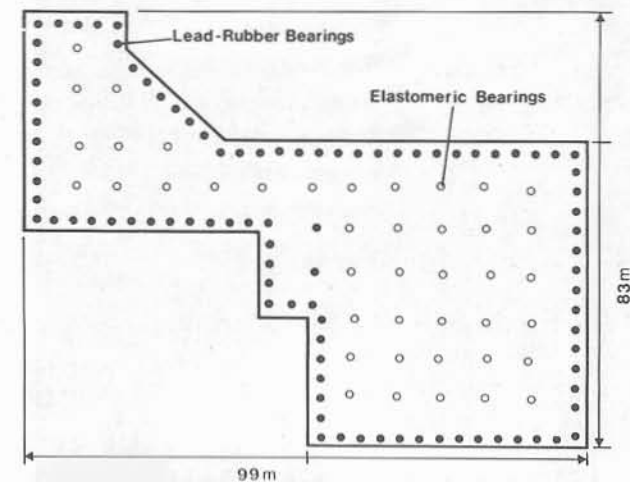


Figure 6.26 Plan of USC Hospital, Los Angeles, showing positions of lead-rubber bearings and elastomeric bearings (courtesy Dynamic Isolation Systems, Incorporated)

joints were detailed to allow a seismic gap 75 mm larger than the design displacement.

Provision was made for inspection and replacement of the bearings if necessary. This is currently common practice throughout the world, although in the future, as experience with elastomeric bearings is gained, it will probably be found that these bearings do not need replacement during the life of a building.

It was concluded (Asher *et al.* 1990) that, although the analysis procedures for a seismically isolated structure are more complex than for a conventional fixed-base structure, the actual design problems are no more complex than for an ordinary building.



Figure 6.27 Completed USC Hospital, Los Angeles, California (photograph courtesy Dynamic Isolation Systems, Incorporated)

6.4.5 Sierra Point Overhead Bridge, San Francisco

The Sierra Point Bridge was the first bridge in North America to be retrofitted using seismic isolation (Mayes, 1992). Originally built in 1956, it is 200 m long and 40 m wide on slight horizontal curvature (see Figure 6.28). Dynamic analysis indicated the bridge would sustain damage during a large design earthquake with horizontal acceleration of 0.6g. The solution was to seismically isolate the bridge by replacing the existing steel spherical pin type bearings with lead-rubber bearings.

It was calculated that, in an earthquake of magnitude Richter 8.3 on the San Andreas Fault, 7 km from the site, these bearings would lengthen the natural period of vibration of the structure so as to produce a six-fold reduction in real elastic forces to a level within the elastic capacity of the columns. Restraint bars were added to prevent the stringers from falling off their connections to the transverse girders. All work was done with no interruption of traffic on or under the bridge.

The bridge is expected to remain in service during and immediately after the design event. (It did not receive a good test in the 1989 Loma Prieta earthquake, since the maximum ground acceleration was 0.09g.)



Figure 6.28 Sierra Point Overhead Bridge, San Francisco, seismically isolated by retrofitting with lead-rubber bearings (photograph courtesy Dynamic Isolation Systems, Incorporated)

6.4.6 Sexton Creek Bridge, Illinois

This structure, carrying Illinois Route 3 over Sexton Creek near the town of Gale in Alexander County, is the first new bridge in North America to be seismically isolated (1988). It was designed by the Illinois Department of Transportation Office of Bridges and Structures. It is a three-span continuous composite steel plate girder superstructure on slightly curved alignment, supported on wall piers and seat-type abutments. There are five 1.4 m deep girders in the 13 m wide cross-section, and the spans are 40–50–40 m. The piers and abutments are founded on piled footings (see Figure 6.29) (Mayes, 1990–92).

Feasibility studies were conducted, leading to alternative solutions. The solution selected achieved the objective of reducing the seismic and non-seismic loads on the piers as much as possible, because of the poor foundation conditions. Seismic criteria for Sexton Creek included an acceleration coefficient of $0.2g$ and a Soil Profile Type III, in accordance with the AASHTO Guide Specifications for Seismic Design of Highway Bridges. The scheme chosen distributed the seismic load demands to the abutments using twenty lead-rubber bearings, with twenty elastomeric bearings at the piers ('Force Control Bearings').

Seismic and wind forces at the piers were minimised through adjustments in bearing stiffness at the piers and abutments. The real elastic base shear was reduced to $0.13W$.



Figure 6.29 Sexton Creek Bridge, Illinois, fitted with lead-rubber bearings (photograph courtesy Dynamic Isolation Systems, Incorporated)

6.5 STRUCTURES ISOLATED IN ITALY

6.5.1 Introduction

The concept of seismic isolation, with an emphasis on energy absorption, has been enthusiastically applied to bridges in Italy, but there are far fewer examples of seismically isolated buildings.

The earliest records of bridges built in Italy go back two thousand years or more. A wooden bridge is described in Caesar's Gallic Wars, Book 4, but bridges spanning powerful rivers were usually built with stone piers and wooden superstructures, such as the Flavian Rhine bridge at Moguntiacum, or Trajan's Danube bridge, some 1120 m long (Cary, 1949). The modern technology of seismic isolation has been incorporated into the Italian bridge-building tradition since 1974, as shown in Table 6.8 (Parducci, 1992), in which details are given of over 150 bridges seismically isolated in Italy. A wide variety of isolating systems has been used, as seen in Table 6.8, although the earliest applications were designed without modern isolation criteria and certainly without official guidelines. A preliminary design guideline was published by Autostrade Company in 1991. Generally, elastic-plastic systems based on flexural deformations of steel elements of various shapes ('EP' in Table 6.8) were chosen. One such device is seen in Figure 6.30, while a device used in the Mortaiolo Bridge is described in detail below. Table 6.8 shows that, even when two-way bridges are regarded as single structures, over 100 km of bridge in Italy has been seismically isolated in some way.

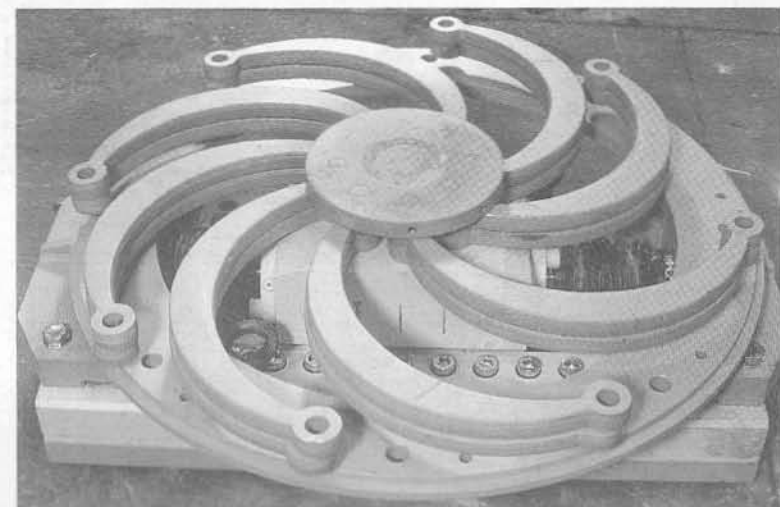


Figure 6.30 An elastic-plastic device used in the seismic isolation of bridges in Italy (photograph courtesy A Parducci)

Table 6.8 Bridges seismically isolated in Italy

No. of Bridges	Name/Location	Range of Lengths (m)	Total Length (m)	Superstructure Type	Isolating System	Date Completed
1	Somplago, Udine-Tarvisio		1240	Precast segments	EL (neoprene disc)	1974
5	Tiberina E45		1700		OL	1974
16	Udine-Tarvisio	240-900	7900	Box girder	Long: elastom. sleeves Transv: elastom. discs	1981-1986
3	Udine-Tarvisio	400-830	1600	Box girder	Long: EP dampers Transv: elastom. discs	1983
1	Cellino, Road SS251		580	Concrete beams	EL (neoprene)	1983
3	Udine-Tarvisio	480-900	2100	Steel girder	OL	1983-1986
1	Sesia, Trafori Highway		2100		OL	1984
1	Bruscata, Greco		70	Steel truss	EL	1984
1	Pontebba, Udine-Tarvisio		960	Box girder	EL (elastomer)	1984
2	Milano-Napoli	350-780	1100	Box girder	EP (steel)	1985
12	*Napoli-Bari	70-720	5700	PCB boxed, piers or framed RC columns	Long: EP devices on abutments or on each span. Transv: EP on pier	1985-1988
1	Slizza 3, Udine-Travisio		160	Steel girders	EL	1985
1	Vallone, railway		240	Steel girders	EL	1985
1	Rivoli Bianchi, Udine-Tarvisio		1000	Concrete beams	Pneumatic dampers	1985
2	Salerno-Reggio	600	1400	Concrete beams	OL	1988
3	Fiano-San Cesareo	300-1200	1850	Concrete beams	RB + metal-shock	1986-1987
5	Fiano-San Cesareo	120-700	1400	Box girders	RB + metal-shock	1986-1987
6	Fiano-San Cesareo	100-650	1600	Box girders/concrete beams	EL (rubber discs)	1986-1987

continued overleaf

APPLICATIONS OF SEISMIC ISOLATION

Table 6.8 (continued)

No. of Bridges	Name/Location	Range of Lengths (m)	Total Length (m)	Superstructure Type	Isolating System	Date Completed
2	Fiano-San Cesareo	300-700	1000	PCB	Visco-elastic shock absorber	1986-1987
3	*Napoli-Bari	130-200	500	PCB	LRB (long and transv)	1986
2	Milano-Napoli		170	Concrete beams	LRB	1986
2	Salerno-Reggio	350-900	1200	PCB	OL	1987
1	Sizzine, Trafori Highway		1800	PCB	OL	1987
1	Aqua Marcia, Milano-Napoli		325	Box girders	Long: EP Transv: EL dampers	1987
4	Monte Vesuvio		6000	PCB	EL dampers with mechanical dissipators	1987-1990
12	Roma-Firenze railway	200-2700	12400	Box girders	OL	1987-1989
1	Lontrano, Salerno-Reggio		550	Box girders	OL	1988
1	Tagliamento, Pontebbana		1000	PCB	Visco-elastic	1988
6	Roma-L'Aquila-Teramo	128-450	1800	Box girders	EL (rubber + metal shock)	1988
1	Calore, Caserta (railway)		100	PCB	EL dampers + mechanical dissipators	1988
1	Granola, railway overpass		120	Concrete slab	Bearings + EL buffers	1988
2	Viaducts, San Mango	600, 640	1200	Steel girders	OL	1988-1990
1	Morignano, A14 highway		450	PCB	EP dampers	1989
1	*Lenze-Pezze, Napoli-Bari		300	PCB	EP dampers	1989
2	Vittorio Veneto -Pian di Vedoia	210-2100	2300	PCB	Long: Visco-elastic Trans: EP	1989
1	Pont Suaz, Aosta		240	PCB	EP shock absorber	1989
1	Flumicello, Bologna-Firenze		300	PCB	OL	1989
1	Temperino, Roma-L'Aquila		830	PCB	EP dampers	1989
1	S.Onofrio, Salerno-Reggio		450	PCB	OL	1989

6.5 STRUCTURES ISOLATED IN ITALY

323

3	Roma-L'Aquila	230-1300	1800	Box girders	OL + RB	1989
1	*D'Antico, Napoli-Bari		250	Composite deck	EP	1989
1	Viadotto, Targia-Siracusa		23	Concrete beams	EP	1989
3	Napoli-Bari (retrofitted)	160-390	720	PCB	EP	1989-1990
1	*3rd Line, Roma-Napoli		580	Concrete beams	LRB	1990
7	*Milano-Napoli	100-200	1000	PCB	EP	1990-1991
1	Santa Barbara, railway overpass		120	Concrete slab	EP	1990
1	Tora, Firenze-Pisa-Livorno		5000	Steel girders	EP multidirectional	1990
3	Roma-L'Aquila	230-500	1200	Box girders	Pneudynamic + RB	1990-1991
2	Salerno-Reggio	190, 390	600	Concrete beams	OL	1990
1	Railway Rocca Avellino		400	Concrete beams	OL	1990
1	SS 206, Firenze-Pisa-Livorno		2500	Steel girders	EP	1990
1	Tiasca, Trafori highway		1610	PCB	Elastic buffers	1990
1	Vesuvio, SS 269		1860	PCB	Elastic buffers	1990
3	Messina-Palermo	900	900	Prestressed concrete box girder	EP (long)	1990
1	Mortaiolo, Livorno-Civitavecchio		9600	Prestressed concrete slabs	EP with shock absorbers	1990-1992
1	S Antonio, Bretella		700	Prestressed concrete	EP with shock absorbers	1991
2	Salerno-Reggio	350, 500	850	PCB	EP	1991
2	PN-Conigliano	500, 800	1300	Prestressed concrete	EP	1991
1	Minuto, Fondo Valle Sele		1000	PCB	OL	1991
3	Roma-L'Aquila-Teramo	200-300	700	Box girders	OL	1991-1992
1	Poggio Iberna, Livorno-Civitavecchia		2500	PCB	OL	1991-1992
3	Livorno-Cecina	600-1800	2800	PCB	EP, EP + RB	1991-1992

continued overleaf

Table 6.8 Continued

No. of Bridges	Name/Location	Range of Lengths (m)	Total Length (m)	Superstructure Type	Isolating System	Date Completed
1	*Rumeano, Via Salaria		340	PCB	EP	Retrofit designed
1	Viadotto No 2, Tangenziale Potenza		240	PCB	EP	1990
1	Angusta, Siracusa		450	Boxed RC beams	EL	1990
7	*Salerno-R Calabria	100-500	1800	PCB with connecting slabs	EP	Retrofit designed
1	Fragneto		870	Steel box girder with RC slabs	EP devices on piers, with ST long. Highest piers connected	Designed
1	Ponte Nelle Alpi, Via Veneto-Pian di Vedoia		310	Steel box girder with RC slabs	Long: EP with ST Transv: EP on all piers	Designed

Key:
 EP = Elastic-plastic behaviour
 EL = Elastic
 OL = Oleodynamic system (EP equivalent)
 SL = Sliding support
 ST = Shock transmitter system associated with SL
 RB = Rubber bearings
 LRB = Lead-rubber bearings
 RC = Reinforced concrete
 PCB = Prestressed concrete beams

Notes:
 Where bridges are two-way, they have been regarded as a single bridge in estimating the length.
 The total length of isolated bridges is thus greater than 100 km.

Of the more recent bridges (1985-1992), typical design values of the parameters are:

- Yield/weight ratio: 5-28%, with a representative value of 10%.
- Maximum seismic displacement: ± 30 to ± 150 mm, with a representative value of ± 60 mm.
- Peak ground acceleration: 0.15-0.40 g, with a representative value of 0.25 g.

Known retrofits are indicated with an asterisk (*)

6.5.2 Seismically isolated buildings

To date, only a few seismically isolated housing constructions have been designed or built in Italy (Parducci, 1992). These are detailed below. Vulcanised rubber-steel multi-layer pads are the seismic isolation system used.

- (i) SIP Regional Administration Centre, Ancona.
Five 7-storey seismically isolated buildings.
Elastomeric bearings had diameter 600 mm, height 190 mm.
Type 'A': Isolated mass = 7.0×10^6 kg, 61 isolators
Type 'B': Isolated mass = 3.7×10^6 kg, 36 isolators
Horizontal stiffness = $114,65 \text{ MN m}^{-1}$
Natural periods = 1.5, 1.6 s
Design viscous damping = 0.06 (experimental ≈ 0.12)
Maximum response spectrum acceleration = 0.5g
Maximum design displacement = 145 mm
A full scale test was carried out on a Type-'A' building; imposed displacements were up to 107 mm, before instant release.
- (ii) Nuovo Nucleo Arruolamento Volontari, Ancona.
Isolated mass = 0.5×10^6 kg
Natural period = 1.6 s
Equivalent damping = 10%
Maximum ground acceleration = 0.5g ('single shock' quake)
Maximum design displacement = 85 mm
- (iii) Centro Medico Legale Della Marina Militare, Augusta (designed).
Isolated mass = 0.2×10^6 kg
Natural period = 2.0 s
Equivalent damping = 10%
Maximum ground acceleration = 0.25g
Maximum design displacement = 180 mm
- (iv) Buildings Della Marina Militare, Augusta (designed).
Isolated mass = 0.4×10^6 kg
Natural period = 2.0 s
Equivalent damping = 13%
Maximum ground acceleration = 0.25g
Maximum design displacement = 180 mm

6.5.3 The Mortaiolo Bridge

The Mortaiolo Bridge, a major two-way bridge in the Livorno-Cecina section of the Livorno-Civitavecchia highway, was completed in 1992. The bridge crosses the large plain composed of deep soft clay stratifications lying near Livorno, in a region of seismic risk.

The bridge is 9.6 km long, with typical spans of 45 m (see Figure 6.31(a)), made of prestressed reinforced-concrete slab, with elastic-plastic devices on all the piers, shock-transmitter systems in the longitudinal direction, and a designed peak ground acceleration of 0.25g. The elastic stiffness of the isolating device, in a typical section, is 135 MN m^{-1} , the yield/weight ratio is 0.11 and the maximum seismic displacement of the isolating system is $\pm 80 \text{ mm}$ (Parducci and Mezzi, 1991; Parducci, 1992).

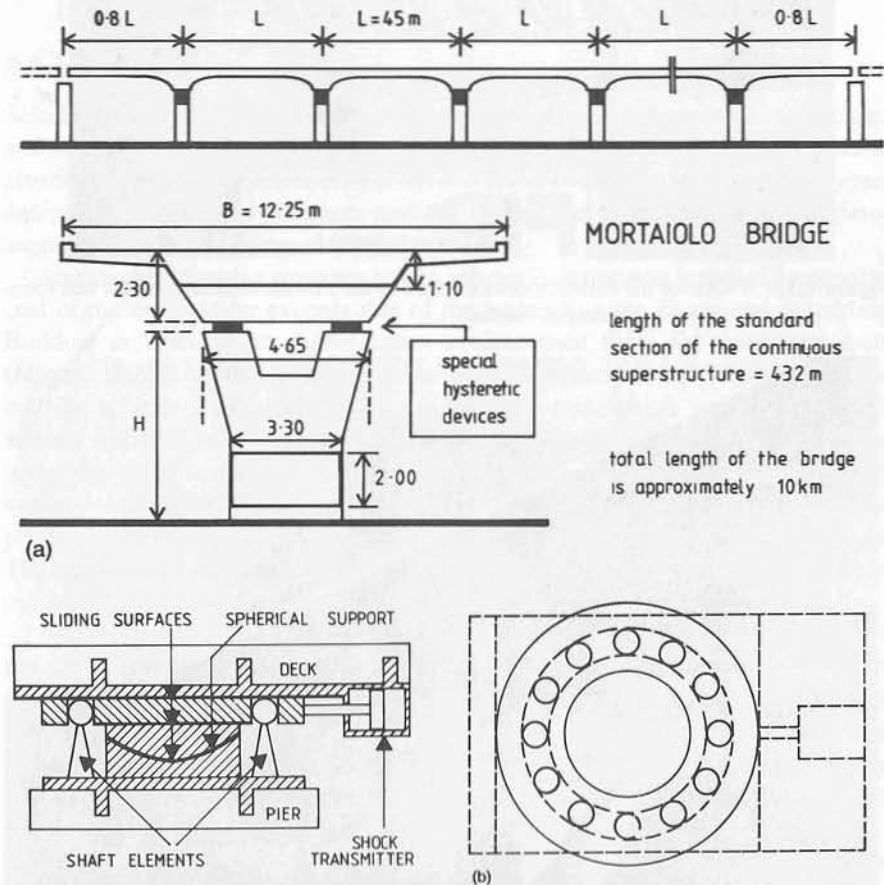


Figure 6.31 (a) A schematic diagram of Mortaiolo Bridge. (b) A schematic diagram of one of the isolation devices used in the Mortaiolo Bridge (courtesy A Parducci)

Two equivalent isolating systems, manufactured by Italian firms, have been utilised in the bridge. Although they are based on different mechanical systems, they respond in the same elastic-plastic way. In both the devices the dissipat-

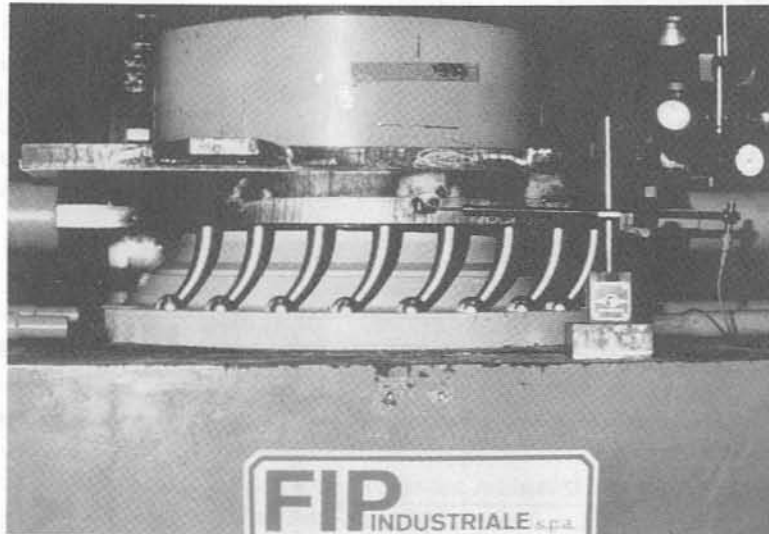


Figure 6.32 One of the isolation devices used in the Mortaiolo Bridge, under test (photograph courtesy A Parducci)



Figure 6.33 Mortaiolo Bridge near completion (photograph courtesy A Parducci)

ing behaviour is based on the hysteretic flexural deformations of steel elements. Figure 6.31(b) illustrates the principle of operation of one of these devices. Provision for relative tilting between the piers and superstructure is provided by a spherical bearing. Damping is provided elasto-plastically by the deflection of numerous steel cantilevers arranged in a ring. A shock transmitter, a highly viscous device based on an oil-piston system, is in series with the isolator. The device is shown under test in Figure 6.32.

Figure 6.33 shows the Mortaiolo Bridge when nearly completed; further details are given by Parducci and Mezzi (1991), who also show that the real incremental cost of the isolating systems was only 4.8% of the bridge cost.

6.6 ISOLATION OF DELICATE OR POTENTIALLY HAZARDOUS STRUCTURES OR SUBSTRUCTURES

6.6.1 Introduction

Seismic problems arise with lightweight, delicate or potentially hazardous structures and substructures, such as life-support equipment in hospitals; important works of artistic or religious significance, e.g. the big statue of Buddha at Kamakura, Japan; equipment sensitive to vibration; and the radioactive components and associated support systems of nuclear reactors.

An example of such a structure, where seismic isolation was installed because the cost of the contents far exceeds that of the building, is the Evans and Sutherland Building in Utah, which manufactures computerised flight simulator equipment (Mayes, 1992). Another example is the Mark II detector for the Stanford Linear collider at Stanford University, Palo Alto, California, which was provided with seismic isolation in 1987 (Mayes, 1992). Four lead-rubber bearings were installed under the detector, also supporting the 1500 t mass of the collider. The isolation system was designed to reduce seismic forces by a factor of 10 and provide seismic protection of this sensitive and expensive equipment at less than 0.4% of its cost. The detector was not damaged during the 1989 Loma Prieta earthquake (Richter magnitude 7.1).

Approximately bilinear isolators, which usually provide most of the mode-1 damping, have been found to be practical and convenient for the large-scale isolation of buildings and bridges as such. However, when an aseismic design is critically controlled by the responses of relatively lightweight substructures it is often appropriate to restrict the isolators to moderate or low levels of non-linearity. For such isolators it will sometimes be appropriate to provide a substantial part of the mode-1 damping by approximately linear velocity dampers.

These restrictions would not preclude the use of moderate levels of bilinear damping by means of metal yielding or by low sliding-friction forces. For example, the weight of an isolated structure might be carried on lubricated PTFE bearings. However, to minimise resonant-appendage effects during relatively fre-

quent moderate earthquakes, such PTFE bearings should be supported by flexible mounts, as in the laminated-rubber/lead-bronze bearings pioneered by Jolivet and Richli (1977). Further isolator components should include flexible elastic components to provide centring forces, and sometimes substantial velocity damping. Both the latter components reduce the maximum extreme-earthquake base movements for which provision must be made.

Nuclear power plants contain critical lightweight substructures essential for their safe operation and shut-down, including control rods, fuel rods and essential piping. These can be given a high level of protection by appropriate seismic isolation systems, designed to give low levels of seismic response for higher vibrational modes of major parts of the power plants. Further serious seismic problems arise with fast-breeder reactors in which critical components are given low strength by measures designed to give high rates of heat transfer. For some breeder-reactor designs it may be desirable to attenuate vertical as well as horizontal seismic forces. In this case it may be practical to provide horizontal attenuation for the overall plant and vertical attenuation for the reaction vessel only. Since the dominant vertical earthquake accelerations have considerably shorter periods than the associated horizontal accelerations, displacements associated with vertical attenuation should be much smaller than those for horizontal attenuation.

Early papers on nuclear power plant isolation, (Skinner *et al.* 1976a, 1976b), concentrated on the protection of the overall power plant structure but did not treat the problems with lightweight substructures, which arise from the seismic responses of higher modes of structural vibration. Structural protection may now be achieved with simpler alternative isolator components; for example the use of lead-rubber bearings may remove the need for installing steel-beam dampers.

6.6.2 Seismically isolated nuclear power stations

Seismic isolation of nuclear structures is seen as a way to simplify design, to facilitate standardisation, to enhance safety margins and possibly to reduce cost (Tajirian *et al.*, 1990). For example, it has been demonstrated that the weight of a pool-type fast-breeder reactor can be reduced by half if horizontal isolation is used. An exhibition at a recent conference (SMiRT-11, 1991) had an emphasis on seismic isolation for nuclear structures.

By 1990 it was reported (Tajirian *et al.*, 1990) that six large pressurised water reactor units had been installed, with seismic isolation, in France and South Africa and that several advanced nuclear concepts in the USA, Japan and Europe had also incorporated this approach.

The design concepts for seismic isolation of two liquid-metal reactors, with the acronyms PRISM and SAFR, have been carried out in the USA. For the PRISM design, horizontal protection, for the reactor module only, is provided by 20 high-damping elastomeric bearings, while the SAFR design is unique in providing vertical as well as horizontal isolation, by using bearings which are flexible, both hor-

izontally and vertically. The entire SAFR building is supported on 100 isolators. The seismic design basis for both plants is expected to cover over 80% of potential nuclear sites in the USA, and options for higher seismic zones have also been investigated.

6.6.3 Protection of capacitor banks, Haywards, New Zealand

The AC Filter Capacitor Banks at the Haywards HVDC Converter Station in the Hutt Valley, New Zealand were built in 1965. Their earthquake resistance was increased in 1988 to the current seismic design requirement using a base-isolation method employing rubber bearings and hysteretic steel dampers (Pham, 1991) (see Figures 6.34 and 6.35). Design considerations for one of the structures have been discussed in Chapter 5.

Owing to the light mass involved, lead-rubber bearings were found to be inappropriate and specially designed segmented rubber bearings were used. These bearings have rubber layers bonded alternatively with steel plates in the conventional manner. However the rubber layers are not continuous but divided into four discs of 110 mm diameter each, as shown in Figure 3.14. This is to reduce the rubber shear area, while maintaining stability, and hence reduce the shear stiffness sufficiently to shift the natural periods of the relatively light AC Filter Capacitor Banks from 0.2–0.5 s to 1.8 s.

Dynamic shaking tests were done on 1 t bearings and static shear tests were done on 5 t bearings of this design. Test results have indicated that the bearings met the design specifications. To limit the displacements during large earthquakes and provide lateral restraints during minor earthquakes and for wind loads, hysteretic steel dampers were provided (see Figure 3.3(b)).

Even with the base isolation, it was found that the insulators supporting the capacitor stack would not have adequate seismic strength. To reduce the bending moment at the support insulators, the stacks are split into two halves, thus effectively reducing the bending moment at the support insulators by a factor of two.

The specifications are as follows.

AC Filter Capacitor Banks: a total of 18 banks of three different types with individual masses varying from 20 000 kg to 32 000 kg. The heights of the banks vary from 6.6 m to 9.6 m.

Rubber Bearings: each bank has four to six bearings rated at 5000 kg each. Each bearing has 19 layers with a total height of 254 mm and a plan dimension of 400 × 400 mm. The shear stiffness is rated at 0.06 kN mm⁻¹.

Dampers: each bank is provided with two circular tapered-steel dampers with a base diameter of 45 mm, a height of 500 mm and was designed for a yield force Q_y of 10.6 kN.

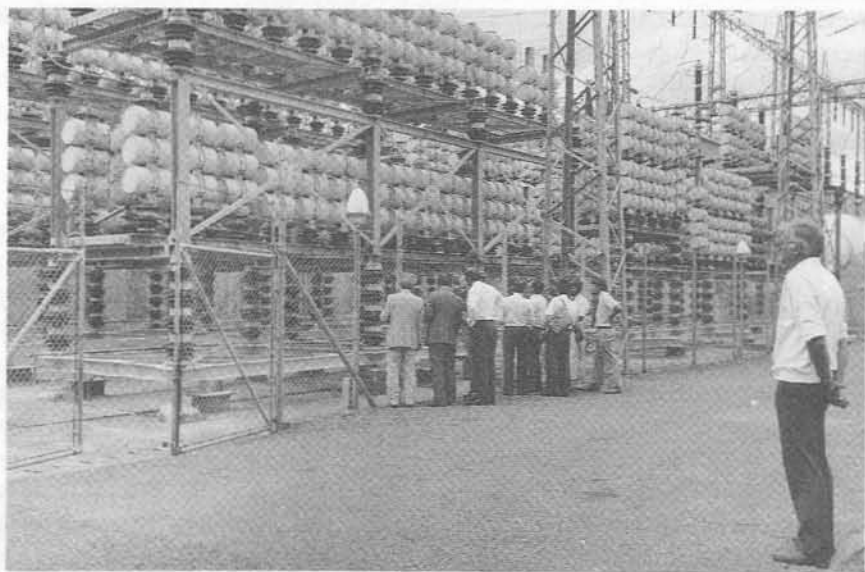


Figure 6.34 Capacitor banks at Haywards HVDC converter station in the Hutt Valley, New Zealand, seismically isolated by retrofitting with segmented rubber bearings and steel dampers (photograph courtesy of R.T. Hefford)

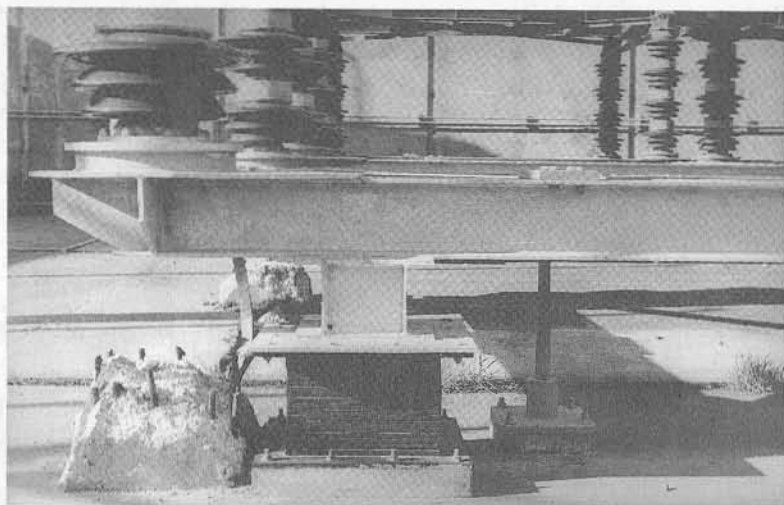


Figure 6.35 Detail of retrofitted seismic isolation system for Haywards, as seen on the left of Figure 6.30. Note the low-stiffness elastomeric bearing, the steel cantilever damper and the original concrete support

6.6.4 Seismic isolation of a printing press in Wellington, New Zealand

In 1988 Wellington Newspapers Ltd approached the DSIR seeking advice on earthquake protection for a proposed new printing press establishment to be built in the Wellington region at Petone (Dowrick *et al.*, 1991). The need for special protection of brittle cast-iron press machines had been demonstrated by the vulnerability of paper-printing machines in the 1987 Edgecumbe earthquake. The site for this project was chosen because of its ready access to rail and road transport, but turned out to be traversed by the Wellington fault.

To give the printing presses maximum protection from earthquakes, the building required a seismic isolation system, and in addition the building had to be as stiff as possible up to the top of the presses to limit the horizontal deflections of the presses in all directions. The originally proposed concrete walls were therefore extended in height and length around the ends of the press hall, and the mezzanine floor was stiffened. Creating enough horizontal stiffness in the direction lateral to the presses at the top platform level proved to be particularly difficult because visibility required for operations necessitated the use of a horizontal steel truss at this level (rather than using an opaque concrete slab). It was not practicable to create a truss with the optimum desired stiffness, but a workable solution was found (see Figure 6.36).

The dynamic analyses were carried out using a computer program for analysing seismically isolated structures incorporating the non-linear behaviour of the special isolating and damping system introduced below the ground floor. From the results of the first trial analysis, it was found that the horizontal accelerations applied to the isolated structure, due to the very strong shaking caused by a rupture on the Wellington fault, would be in the range approximately 0.4–0.6g. It would have been both expensive and physically very difficult to give a high level of protection to the press against damaging deflections under such accelerations, particularly at the upper platform level. An additional disadvantage arose from the fact that it was not feasible operationally to apply any lateral restraint to the press at a level midway between the top platform and the mezzanine floor.

It was found practicable to provide protection against earthquake-generated accelerations, transmitted through the structure, of about 0.3g at the top of the press and 0.25g at the lower levels. The specially designed building housing the press was mounted on lead-rubber bearings 460 mm thick. This reduced the estimated loads and deflections on the press by a factor of 8–10 compared with the non-isolated case (see Figures 6.37 and 6.38). As a result, the press should suffer only modest damage in earthquake shaking somewhat stronger than that required by the New Zealand earthquake code for the design of buildings.

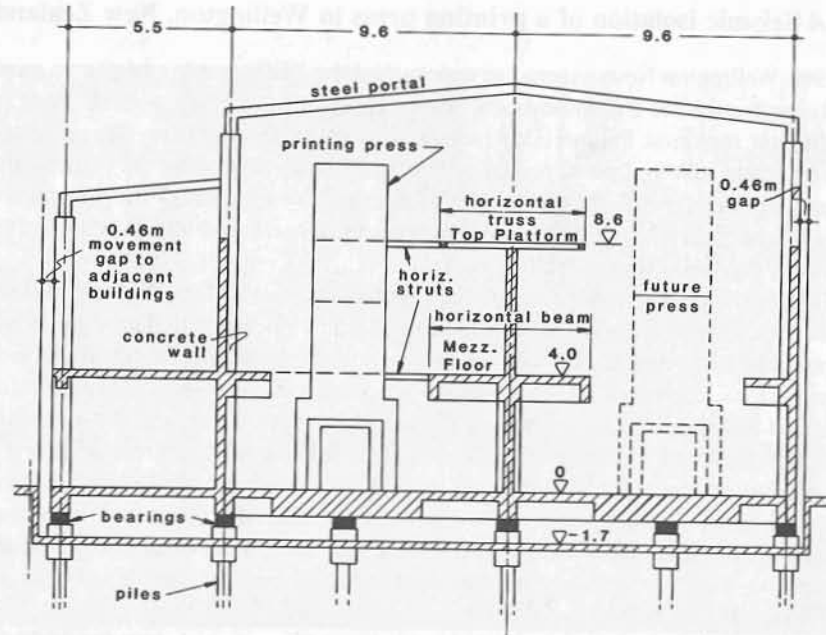


Figure 6.36 End elevation of Press Hall for Wellington Newspapers, Petone

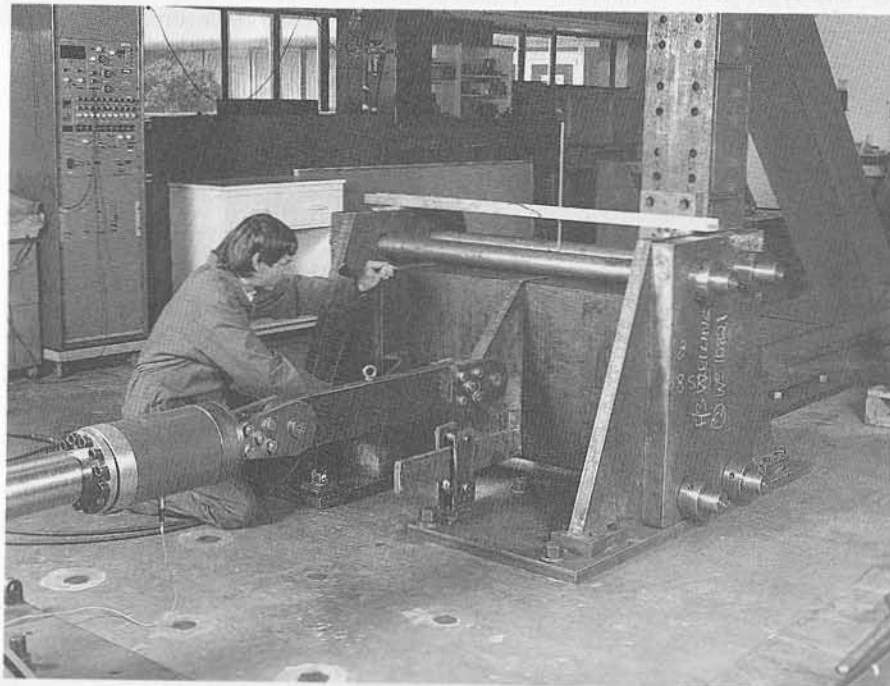


Figure 6.37 Lead-rubber bearings for Press Hall under test

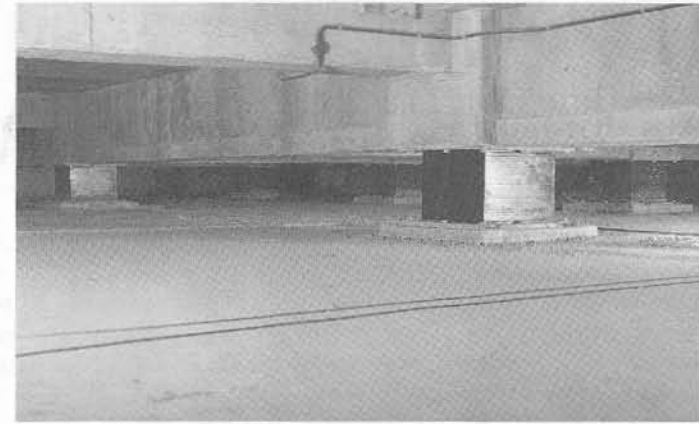


Figure 6.38 Lead-rubber bearings in place in Press Hall

6.7 NOTE ADDED IN PROOF (JANUARY 1993)

During the six months since the manuscript of this book was submitted, applications of seismic isolation in New Zealand, Japan, the USA and Italy have continued to progress at a significant rate.

- **New Zealand** Parliament House in Wellington, a building of importance for New Zealand, built in 1921, is at present being retrofitted with seismic isolation using a lead-rubber bearing system. The new New Zealand National Museum, to be built on the waterfront in Wellington, will be seismically isolated, probably using a similar system.
- **Japan** In addition to the bridges listed in Table 6.5, at least ten further new bridges in Japan are to be seismically isolated, most of these using a lead-rubber bearing system. The new Post Office Building in Tokyo is to be seismically isolated using a lead-rubber system and will be twice the area of the C-1 Building, currently the largest seismically isolated building in the world.
- **USA** A large number of bridges are being retrofitted with the lead-rubber bearings while many buildings, including hospitals, are scheduled for seismic isolation.
- **Italy** A number of new buildings with seismic isolation are 'on the drawing-board', with many of these being hospitals or other buildings needed in civil emergency. New bridges continue to be constructed with seismic isolation.

An emerging trend in the development of seismic isolation is the use of systems which incorporate the benefits of many different isolator components, for instance lead-rubber bearings together with (high-damping) rubber bearings and/or together with steel or viscous dampers. Such combinations confer the maximum benefit of each component to the system as a whole.

References

This list of references has been grouped according to chapter, since it is not a complete bibliography of the concept of seismic isolation, but is largely intended as an extension of specific topics discussed in the text.

CHAPTER 1

- T.L. Anderson, Ed. (1990), 'Theme issue: seismic isolation', *Earthquake Spectra*, EERI, **6**, no. 2, 438 pp.
- I. Buckle and R. Mayes (1990) 'These issue: seismic isolation', *Earthquake Spectra*, EERI, **6**, no. 2, 161-201.
- R.W. Clough and J. Penzien (1975), *Dynamics of Structures*, McGraw-Hill, USA.
- D.J. Dowrick (1987), *Earthquake Resistant Design, for Engineers and Architects*, 2nd Edition, John Wiley and Sons, Chichester, England.
- International Meeting on Base-isolation and Passive Energy Dissipation*, Universita' degli Studi di Perugia, Assisi, June 8, 1989.
- J.M. Kelly (1986), 'Aseismic base isolation: review and bibliography', *Soil Dyn. Earthq. Eng.*, **5**, no. 3, 202-216.
- D.M. Lee and I.C. Medland (1978), 'Base isolation - an historical development, and the influence of higher mode responses', *Bull. NZ. Nat. Soc. Earthq. Eng.*, **11**, no. 4, 219-233.
- Proceedings of the First US-Japan Workshop on Seismic Retrofit of Bridges*, December, 1990, Public Works Research Institute, Tsukuba Science City, Japan, 441 pages.
- Proceedings of the Fourth US National Conference on Earthquake Engineering*, Palm Springs, CA, 1990, Earthquake Engineering Research Institute, CA, USA.
- Proceedings of International Workshop on Recent Developments in Base-isolation Techniques for Buildings*, Architectural Institute of Japan, Tokyo, 27-30 April, 1992, 335 pages.
- Proceedings of the Ninth World Conference on Earthquake Engineering*, Tokyo, 1988, 9WCEE organising committee, Japan Association for Earthquake Disaster Prevention, Tokyo, Japan, Vols V and VIII.
- Proceedings of the Tenth World Conference on Earthquake Engineering*, Madrid, Spain, 1992, A.A. Balkema, Rotterdam, Vol. IV.
- Proceedings of the Pacific Conference on Earthquake Engineering*, Auckland, NZ

- 1991, NZ Nat. Soc. Earthq. Eng. 3 vols.
Proceedings of New Zealand-Japan Workshop on Base Isolation of Highway Bridges, 1987, Technology Research Center for National Land Development, Japan, 183 pages.
- R.I. Skinner and G.H. McVerry (1975), 'Base isolation for Increased Earthquake Resistance', *Bull. NZ. Nat. Soc. Earthq. Eng.*, **8**, no. 2.
- SMiRT-11, 'Seismic isolation and response control for nuclear and non-nuclear structures', *Structural Mechanics in Reactor Technology* August 18-23, 1991, Tokyo.

CHAPTER 2

- R.W. Clough and J. Penzien (1975), *Dynamics of Structures*, McGraw-Hill, USA.
- Earthquake Engineering Research Laboratory (EERL) Reports (1972-5), e.g. 'Volume III - Response Spectra, Parts A to Y', California Institute of Technology, Pasadena, California, Occasional Reports from EERL 72-80 to EERL 75-83.
- F.-G. Fan and G. Ahmadi (1990), 'Floor response spectra for base-isolated multistorey structures', *Earthq. Eng. Struct. Dyn.*, **19**, no. 3, 377-388.
- F.-G. Fan and G. Ahmadi (1992), 'Seismic responses of secondary systems in base-isolated structures', *Earthq. Eng. Struct. Dyn.*, **14**, no. 1, 35-48.
- der Kiureghian, A. (1980), 'A response-spectrum method for random vibrations', *Earthq. Eng. Res. Center, College of Eng., University of California, Berkeley, Report no. UCB/EERC-80/15*, 31 pages.
- N. Mostaghel and M. Khodaverdian (1987), 'Dynamics of resilient-friction base isolation (R-FBI)', *Int. J. Earthq. Eng. Struct. Dyn.*, **15**, 379-90.
- N.M. Newmark and E. Rosenblueth (1971), *Fundamentals of Earthquake Engineering*, Prentice-Hall, New Jersey.
- R.I. Skinner (1964), 'Earthquake-generated forces and movements in tall buildings', *Bull. 166, NZ Department of Scientific and Industrial Research*.
- E.L. Wilson, A. Der Kiureghian and E.P. Bayo (1981), 'A replacement for the SRSS method in seismic analysis', Short Communications, *Int. J. Earthq. Eng. Struct. Dyn.*, **9**, 187-94.

CHAPTER 3

- J.L. Beck and R.I. Skinner (1974), 'The seismic response of a reinforced concrete bridge pier designed to step', *Int. J. Earthq. Engng. Struct. Dyn.*, **2**, 343-358.
- J.L. Beck and R.I. Skinner (1972), 'The seismic response of a proposed railway viaduct', *Tech. Rpt. No. 369, Physics and Engineering Laboratory, DSIR, NZ*.
- C.E. Birchenall (1959), *Physical Metallurgy*, McGraw-Hill, London.
- P.R. Boardman, B.J. Wood and A.J. Carr (1983), 'Union House - a cross-braced structure with energy dissipators', *Bull. NZ Nat. Soc. Earthq. Eng.*, **16**, no. 2, 83-97.

- S.F. Borg (1962), *Fundamentals of Engineering Elasticity*, van Nostrand, Princeton N.J., p 40.
- L.G. Cormack (1988), 'The design and construction of the major bridges on the Mangaweka rail deviation', *Trans. IPENZ*, **15**, I/CE, March 1988, 16-23.
- A.H. Cottrell (1961), *Dislocations and Plastic Flow in Crystals*, Clarendon Press, Oxford.
- W.J. Cousins, W.H. Robinson and G.H. McVerry (1991), 'Recent developments in devices for seismic isolation', *Proc. Pacific Conference on Earthquake Engineering*, Auckland 20-23 November, New Zealand National Society for Earthquake Engineering, Volume 2, 221-232.
- Bridge Engineering Standards (1976), *Technical Memorandum (Bridges), No. BE 1/76*, 'Design Requirements for Elastomeric Bridge Bearings', Bridge Engineering (Design Standards) Division BES, Department of the Environment, London.
- A.N. Gent and P.B. Lindley (1959), 'The compression of bonded rubber blocks', *Proc. Inst. Mech. Engrs.*, **173**, 111-122.
- A.A. Huckelbridge (1977), 'Earthquake simulation tests for nine-storey steel frame with columns allowed to uplift', *Earthq. Eng. Res. Center, College of Eng., University of California, Berkeley, Report no. UCB/EERG-77/23*, 181 pages.
- G.K. Hüffmann (1985), 'Full base isolation for earthquake protection by helical springs and visco-dampers', *Nucl. Eng. Design*, **84**, 331-8.
- J.J. Jones, C.M. Sellars and W.J. McG. Tegard (1969), 'Strength and structure under hot-working conditions', *Met. Rev.*, **130**, 1-24.
- J.M. Kelly, R.I. Skinner and A.J. Heine (1972), 'Mechanisms of energy absorption in special devices for use in earthquake resistant structures', *Bull. NZ Nat. Soc. for Earthq. Eng.*, **5**, no. 3, 63-88.
- T. Kobori, T. Yamada, Y. Takenaka, Y. Maeda and I. Nishimura (1988), 'Effect of dynamic tuned connector on reduction of seismic response - application to adjacent office buildings', *Proc. 9th World Conf. on Earthq. Eng.*, Tokyo-Kyoto, Vol. V, 773-778.
- G.R. McKay, H.E. Chapman and D.K. Kirkcaldie (1990), 'Seismic isolation: New Zealand applications', *Earthquake Spectra*, **6**, no. 2, 203-222.
- A. Mendelsson (1968), *Plasticity: Theory and Application*, MacMillan, New York.
- Mitsuo Miyazaki (1991), Sumitomo Construction Co. Ltd, Japan, personal communication.
- A. Nadai (1950), *Theory of Flow and Fracture of Solids*, McGraw-Hill, New York.
- N.M. Newmark and E. Rosenblueth (1971), *Fundamentals of Earthquake Engineering*, Prentice-Hall, New Jersey.
- A. Pardini and R. Medeot (1987), 'Special dissipating devices for reducing the seismic response of structures', *Pacific Conference on Earthq. Eng.*, New Zealand, August 1987, Vol. 2, 329-340.
- R. Park and R.W.G. Blakeley (1979), 'Seismic design of bridges', *Road Research Unit, National Roads Board, New Zealand, Bull.* **43**, 101-105.
- C.E. Pearson (1944), *The Extrusion of Metals*, John Wiley and Sons, New York.
- C. Plichon, R. Gueraud, M. Richli and J.F. Casagrande (1980), 'Protection of

- nuclear power plants against seisms', *Nuclear Technology*, **49**, 295-306.
- E.P. Popov (1966), 'Low cycle fatigue of steel beam to column connections', *Proc. International Symposium on the Effects of Repeated Loadings of Materials and Structures*, Vol. VI, RILEM = Inst. Ing., Mexico.
- H.L.I.D. Pugh (1970), 'Hydrostatic extrusion' in *Mechanical Behaviour of Materials under Pressure* (Ed. H. L. I. D. Pugh), Applied Science, London.
- W.T. Read (1953), *Dislocations in Crystals*, McGraw-Hill, New York.
- W.H. Robinson (1982), 'Lead-rubber hysteretic bearings suitable for protecting structures during earthquakes', *Earthquake Eng. and Str. Dyn.*, **10**, 593-604.
- W.H. Robinson and W.J. Cousins (1987), 'Recent developments in lead dampers for base isolation', *Proc. Pacific Conference on Earthquake Engineering*, 5-8 August 1987, Wairakei, New Zealand National Society for Earthquake Engineering, Volume 2, 279-284.
- W.H. Robinson and W.J. Cousins (1988), 'Lead dampers for base isolation', *Proc. 9th World Conference on Earthquake Engineering*, Tokyo and Kyoto, Japan, August 2-9, Vol 8, 427-432.
- W.H. Robinson and L.R. Greenbank (1976), 'An extrusion energy absorber suitable for the protection of structures during an earthquake', *Earthquake Eng. and Str. Dyn.* **4**, 251-9.
- W.H. Robinson and L.R. Greenbank (1975), 'Properties of an extrusion energy absorber', *Bull. NZ Nat. Soc. Earthq. Eng.*, **8**, 287-91.
- W.H. Robinson and A. Tucker (1977), 'A lead-rubber shear damper', *Bull. NZ Nat. Soc. Earthq. Eng.*, **10**, 151-3.
- W.H. Robinson and A. Tucker (1981), 'Test results for lead rubber bearings for the Wm Clayton Bldg, Toe Toe and Waiotukupuna Bridges', *Bull. NZ Nat. Soc. Earthq. Eng.*, **14**, 21-33.
- J.L. Savage (1939), 'Earthquake studies for Pit River Bridge', *Civil Engineering*, **9**, no. 8, 470-2.
- J.A. Schey (1970), *Metal Deformation Processes, Friction and Lubrication*, Ed. J.A. Schey, Marcel Dekker, Amsterdam.
- R.D. Sharpe and R.I. Skinner (1983), 'The seismic design of an industrial chimney with rocking base', *Bull. NZ Nat. Soc. for Earthq. Eng.*, **16**, no. 2, 98-106.
- E. Siebel, and E. Fangmeier (1931), 'Researches on power consumption in extrusion and punching of metal', *Mitt. K.-Wilhem-Inst. Eisenforsch.*
- R.I. Skinner, G.N. Bycroft and G.H. McVerry (1976), 'A practical system for isolating nuclear power plants from earthquake attack.' *Nucl. Eng. Design*, **36**, 287-297.
- R.I. Skinner, J.M. Kelly and A.J. Heine (1974), 'Energy absorption devices for earthquake resistant structures', *Proc. 5th World Conf. on Earthq. Eng.*, Rome 1973, Vol. 2, 2924-2933.
- R.I. Skinner, J.M. Kelly and A.J. Heine (1975), 'Hysteretic dampers for earthquake resistant structures', *Int. J. Earthq. Engng. Struct. Dyn.*, **3**, 287-296.
- R.I. Skinner, W.H. Robinson and G.M. McVerry, (1991), 'Seismic isolation in New Zealand', *Nuclear Eng. Design*, **127**, 281-9.

- R.I. Skinner, R. Tyler, A. Heine and W.H. Robinson (1980), 'Hysteretic dampers for the protection of structures from earthquakes', *Bulletin NZ Nat. Soc. for Earthq. Eng.*, **13**, 22-36.
- SMiRT-11, 'Seismic isolation and response control for nuclear and non-nuclear structures', *Structural Mechanics in Reactor Technology*, August 18-23, 1991, Tokyo.
- T.T. Soong (1988), 'Active structural control in civil engineering', *Eng. Struct.*, **10**, 74-82.
- M. Takayama, A. Wada, H. Akiyama and H. Tada (1988), 'Feasibility study on base-isolated building', *Proc. 9th World Conf. on Earthq. Eng.*, Tokyo-Kyoto, Vol. V, 669-674.
- R.G. Tyler (1977), 'Dynamic tests on PTFE sliding layers under earthquake conditions', *Bull. NZ Nat. Soc. Earthq. Eng.*, **10**, no. 3.
- R.G. Tyler (1991), 'Rubber bearings in base-isolated structures—a summary paper', *Bull. NZ Nat. Soc. Earthq. Eng.*, **24**, no. 3, 251-274.
- R.G. Tyler (1978), 'A tenacious base isolation system using round steel bars', *Bull. NZ Nat. Soc. for Earthq. Eng.*, **11**, no. 4, 273-281.
- R.G. Tyler and W.H. Robinson (1984), 'High-strain tests on lead-rubber bearings for earthquake loadings', *Bull. NZ Nat. Soc. Earthq. Eng.*, **17**, 90-105.
- R.G. Tyler and R.I. Skinner (1977), 'Testing of dampers for the base isolation of a proposed 4-storey building against earthquake attack', *Proc. 6th Australasian Conf. on the Mechanics of Structures and Materials*, University of Canterbury, NZ, 376-382.
- L.H. van Vlack (1985), *Elements of Materials Science and Engineering*, Addison-Wesley Publishing Co.
- J. Wulff, J.F. Taylor and A.J. Shaler (1956), *Metallurgy for Engineers*, Wiley, New York.

CHAPTER 4

- T. Andriono and A.J. Carr (1991a), 'Reduction and distribution of lateral seismic inertia forces on base-isolated multistorey structures', *Bull. NZ Nat. Soc. Earthq. Eng.*, **24**, no. 3, 225-237.
- T. Andriono and A.J. Carr (1991b), 'A simplified earthquake resistant design method for base-isolated multistorey structures', *Bull. NZ Nat. Soc. Earthq. Eng.*, **24**, no. 3, 238-250.
- M.S. Chalhoub (1988), 'Response of fluids in cylindrical containers and applications to base isolation', *J. Appl. Mech. Trans. ASME*.
- M.S. Chalhoub and J.M. Kelly (1990), 'Shake table test of cylindrical water tanks in base-isolated structures', *J. Eng. Mech.*, **116**, no. 7, 1451-72.
- R.W. Clough and J. Penzien (1975), *Dynamics of Structures*, McGraw-Hill, USA.
- A. Der Kiureghian (1980a), 'Structural response to stationary excitation', *J. Eng. Mech. Div., ASCE*, **106**, 1195-1213.
- A. Der Kiureghian (1980b), 'A response spectrum method for random vibrations',

- Earthq. Eng. Res. Center, College of Eng., University of California, Berkeley, Report No. UCB/EERC-80/15*, 31 pages.
- A. Der Kiureghian (1981), 'A response spectrum method for random vibration analysis of MDF systems', *Int. J. Earthq. Eng. Struct. Dyn.*, **9**, no. 5, 419-35.
- D.J. Dowrick (1987), *Earthquake Resistant Design for Engineers and Architects*, 2nd edn, John Wiley & Sons, Chichester.
- Earthquake Engineering Research Laboratory (EERL) Reports (1972-5), e.g. 'Volume III - Response Spectra, Parts A to Y', California Institute of Technology, Pasadena, California, Occasional Reports from EERL 72-80 to EERL 75-83.
- F.-G. Fan and G. Ahmadi (1990), 'Floor response spectra for base-isolated multistorey structures', *Eng. Struct.*, **19**, no. 3, 377-388.
- F.-G. Fan and G. Ahmadi (1992), 'Seismic responses of secondary systems in base-isolated structures', *Earthq. Eng. Struct. Dyn.*, **14**, no. 1, 35-48.
- R. Gueraud, J.-P. Noel-Leroux, M. Livolant and A.P. Michalopoulos (1985), 'Seismic isolation using sliding-elastomer bearing pads', *Nucl. Eng. Des.*, **84**, 363-77.
- W.C. Hurty and M.F. Rubinstein (1964), *Dynamics of Structures*, Prentice-Hall, New Jersey.
- T. Igusa (1990), 'Response characteristics of inelastic 2DOF primary-secondary system', *J. Eng. Mech.*, **116**, no. 5, 1160-74.
- T. Igusa and A. Der Kiureghian (1983), 'Dynamics of multiply-tuned and arbitrarily supported secondary systems', *Earthq. Eng. Res. Center, College of Eng., University of California, Berkeley, Report No. UCB/EERC-83/07*, 220 pages.
- T. Igusa and A. Der Kiureghian (1985a), 'Dynamic characterisation of two-degree-of-freedom equipment-structure systems', *J. Eng. Mech.*, **111**, no. 1, 1-19.
- T. Igusa and A. Der Kiureghian (1985b), 'Dynamic response of multiply supported secondary systems', *J. Eng. Mech.*, **111**, no. 1, 20-41.
- T. Igusa, A. Der Kiureghian and J.L. Sackman (1984), 'Modal decomposition method for stationary response of non-classically damped systems', *Int. J. Earthq. Eng. Struct. Dyn.*, **12**, no. 1, 121-136.
- A.S. Ikononou (1984), 'Alexisimon seismic isolation levels for translational and rotational seismic input', *8th World Conf. Earthq. Eng. San Francisco*, Vol. 5, 975-82.
- J.M. Kelly and H.-C. Tsai (1985), 'Seismic response of light internal equipment in base-isolated structures', *Int. J. Earthq. Eng. Struct. Dyn.*, **13**, no. 6, 711-32.
- D.M. Lee (1980), 'Base isolation for torsion reduction in asymmetric structures under earthquake loading', *Earthq. Eng. Struct. Dyn.*, **8**, 349-359.
- D.M. Lee and I.C. Medland (1978a), 'Base isolation - an historical development, and the influence of higher mode responses', *Bull. NZ. Nat. Soc. Earthq. Eng.*, **11**, no. 4, 219-233.
- D.M. Lee and I.C. Medland (1978b), 'Estimation of base-isolated structure responses', *Bull. NZ. Nat. Soc. Earthq. Eng.*, **11**, no. 4, 234-44.

- Li, Li (1984), 'Base isolation measure for aseismic buildings in China', *8th World Conf. Earthq. Eng. San Francisco*, Vol. 6, 791-8.
- N. Mostaghel and M. Khodaverdian (1987), 'Dynamics of resilient-friction base isolation (R-FBI)', *Int. J. Earthq. Eng. Struct. Dyn.*, **15**, 379-90.
- N.M. Newmark and E. Rosenblueth (1971), *Fundamentals of Earthquake Engineering*, Prentice-Hall, New Jersey.
- J. Penzien (1969), 'Earthquake response of irregularly-shaped buildings', *Proc. 4th World Conf. Earthq. Eng.* Vol. II, A-3, 75-89.
- J. Penzien and A.K. Chopra (1965), 'Earthquake response of appendage on a multistorey building', *Proc. 3rd World Conf. Earthq. Eng. New Zealand*, Vol. 2, 471-86.
- R.I. Skinner and G.H. McVerry (1992), *Report on an Introduction to Seismic Isolation*, Internal IGNS Report, Institute of Geological and Nuclear Sciences, Lower Hutt, New Zealand.
- R.I. Skinner, D.W.C. Skilton and D.A. Laws (1965), 'Unbalanced buildings and buildings with light towers, under earthquake forces', *Proc. 3rd World Conf. Earthq. Eng.*, January 1965, Auckland, NZ, Vol. II, 586-602.
- L. Su, G. Ahmadi and I.G. Tadjbakhsh (1989), 'A comparative study of performances of various base-isolation systems: Part I: Shear beam structures', *J. Eng. Mech. Div. ASCE*, **115**, 1976-92.
- H.-C. Tsai and J.M. Kelly (1988), 'Non-classical damping in dynamic analysis of base-isolated structures with internal equipment', *Int. J. Earthq. Eng. Struct. Dyn.*, **16**, no. 1, 29-43.
- H.-C. Tsai and J.M. Kelly (1989), 'Seismic response of the superstructure and attached equipment of a base-isolated building', *Int. J. Earthq. Eng. Struct. Dyn.*, **18**, no. 4, 551-564.
- A.S. Veletsos and C.E. Ventura (1986), 'Modal analysis of non-classically damped linear systems', *Int. J. Earthq. Eng. Struct. Dyn.*, **14**, no. 2, 217-43.
- E.L. Wilson, A. Der Kiureghian and E.P. Bayo (1981), 'A replacement for the SRSS method in seismic analysis', Short Communications, *Int. J. Earthq. Eng. Struct. Dyn.*, **9**, 187-94.

CHAPTER 5

- AASHTO (1991), 'Guide Specifications for Seismic Isolation Design', included in *Standard Specification for Seismic Design of Highway Bridges*, American Association of State Highway and Transportation Officials, Washington.
- An Acceptable Procedure for the Design and Review of California Hospital Buildings using Base Isolation*, California Office of Statewide Health Planning and Development, Building Safety Board, April 1989.
- T. Andriano and A.J. Carr (1991a), 'Reduction and distribution of lateral seismic inertia forces on base-isolated multistorey structures', *Bull. NZ Nat. Soc. Earthq. Eng.*, **24**, no. 3, 225-237.
- T. Andriano and A.J. Carr (1991b), 'A simplified earthquake resistant design

- method for base-isolated multistorey structures', *Bull. NZ Nat. Soc. Earthq. Eng.*, **24**, no. 3, 238-250.
- R.W.G. Blakeley, A.W. Charleson, H.C. Hitchcock, L.M. Meggett, M.J.N. Priestly, R.D. Sharpe and R.I. Skinner (1979), 'Recommendations for the design and construction of base isolated structures', *South Pacific Regional Conference on Earthquake Engineering*, Wellington, NZ.
- R.W.G. Blakeley (1979), 'Parameter studies for (bridge) design', *Road Research Unit, National Roads Board, NZ, Bulletin* **43**, 117-42
- R.W.G. Blakeley (1987), 'Analysis and design of bridges incorporating mechanical energy dissipating devices for earthquake resistance', *Proc. NZ-Japan Workshop on Base Isolation of Highway Bridges*, Technology Research Center for National Land Development, Japan, November 1987.
- N. Cooke, A.J. Carr, P.J. Moss, and T.F. Kwai (1986), 'The influence of non-geometric factors on the seismic behaviour of bridges on isolating bearings', *Bull. NZ Nat. Soc. Earthq. Eng.*, **19**, no. 4, 263-71.
- A. Der Kiureghian (1980), 'A response spectrum method for random vibrations', *Earthq. Eng. Res. Center, College of Eng., University of California, Berkeley, Report No. UCB/EERC- 80/15*, 31 pages.
- Earthquake Engineering Research Laboratory Reports (1972-5), e.g. 'Volume III - Response Spectra, Parts A to Y', *California Institute of Technology, Pasadena, California, Occasional Reports from EERL 72-80 to EERL 75-83*.
- S. Emi, K. Oshima, T. Takeda and H. Nakayama (1987), 'Earthquake resistant design of cable-stayed bridges', *Proc. NZ-Japan Workshop on Base Isolation of Highway Bridges*, Technology Research Center for National Land Development, Japan, November 1987.
- W.C. Hurty and M.F. Rubinstein (1964), *Dynamics of Structures*, Prentice-Hall, New Jersey.
- T. Igusa and A. Der Kiureghian (1985), 'Dynamic response of multiply supported secondary systems', *J. Eng. Mech.*, **111**, no. 1, 20-41.
- T. Katayama, K. Kawashima and Y. Murakami (1987), 'Current design considerations for reducing seismic lateral force of highway bridges in Japan', *Proc. NZ-Japan Workshop on Base Isolation of Highway Bridges*, Technology Research Center for National Land Development, Japan, November 1987.
- K. Kawashima and K. Aizawa (1986), 'Earthquake response spectra taking account of number of response cycles', *Int. J. Earthq. Eng. Struct. Dyn.*, **14**, no. 2, 185-97.
- T.F. Kwai (1986), 'Seismic behaviour of bridges on isolating bearings', *Research Report 86/13*, Department of Civil Engineering, University of Canterbury, Christchurch, NZ, May 1986, 118 pages.
- G.R. McKay, H.E. Chapman and D.K. Kirkcaldie (1990), 'Seismic isolation: New Zealand applications', *Earthquake Spectra*, **6**, no. 2, 203-222.
- Yoshiro Matsuo and Koji Hara (1991), 'Design and construction of Miyagawa Bridge (first Menshin bridge in Japan)', *1st US-Japan Workshop on Earthquake Protective Systems for Bridges*, Buffalo, USA, Sept. 1991.

- R.L. Mayes (1990-92), Dynamic Isolation Systems Incorporated, California, personal communications.
- R.L. Mayes (1992), 'Current status and future needs of US seismic isolation codes', *Proc. Int. Workshop on Recent Developments in Base-isolation Techniques for Buildings, Tokyo, Japan, 27-30 April 1992*, 321-34.
- R.L. Mayes, I.G. Buckle, T.E. Kelly and L.R. Jones (1992), 'AASHTO seismic isolation design requirements for highway bridges', *J. Struct. Eng.*, **118**, no. 1, 284-304.
- P.J. Moss, A.J. Carr, N. Cooke and T.F. Kwai (1986), 'The influence of bridge geometry on the seismic behaviour of bridges on isolating bearings', *Bull. NZ Nat. Soc. Earthq. Eng.*, **19**, no. 4, 255-62.
- A. Pardini (1992), Facoltà di Ingegneria, Istituto di Energetica, Università degli studi di Perugia, personal communications.
- R. Park, H.E. Chapman, L.G. Cormack and P.J. North (1991), 'New Zealand contributions to the International Workshop on the Seismic Design and Retrofitting of Reinforced Concrete Bridges, Bormio, Italy, April 2-5, 1991', *Bull. NZ. Nat. Soc. Earthq. Eng.*, **24**, no. 2, 139-201.
- RRU, *Road Research Unit, National Roads Board, Wellington, NZ, Bulls.* **41-44**, 1979.
- D.H. Turkington (1987), 'Seismic design of bridges on lead-rubber bearings', *Research Report 87/2 Department of Civil Engineering, University of Canterbury, NZ, Feb. 1987*, 172 pages.
- R.G. Tyler (1978), 'Tapered steel energy dissipators for earthquake resistant structures', **11**, no. 4, 282-294.
- Uniform Building Code (UBC)(1991), *Earthquake Regulations for Seismic-isolated Structures*, Chapter 23, Division 3, USA.
- E.L. Wilson, A. Der Kiureghian and E.P. Bayo (1981), 'A replacement for the SRSS method in seismic analysis', *Short Communications, Int. J. Earthq. Eng. Struct. Dyn.*, **9**, 187-94.

CHAPTER 6

- J.W. Asher, D.R. van Volkinburg, R.L. Mayes, T. Kelly, B.I. Sveinsson and S. Hussain (1990), 'Seismic isolation design of the USC University Hospital', *Proc. 4th US Nat. Conf. Earthq. Eng.*, Vol 3, May 1990, 529-538.
- J. Bailey and E. Allen (1989), 'Seismic isolation retrofitting of the Salt Lake City and County building', *Post-SMIRT8 seminar, 1989, paper 14*.
- J.L. Beck and R.I. Skinner (1974), 'Seismic response of a reinforced concrete bridge pier designed to step', *Int. J. Earthq. Engrg. Struct. Dyn.*, **2**, no. 4, 343-358.
- I.J. Billings and D.K. Kirkcaldie (1985), 'Base isolation of bridges in New Zealand'. *Proc. Second Joint US-New Zealand Workshop on Seismic Resist. Highway Bridges ATC-12-1, May 1985*, Applied Technology Council, California, USA.

- R.W.G. Blakeley (1979), 'Analysis and design of bridges incorporating mechanical energy dissipating devices for earthquake resistance'. *Proc. Workshop Earthq. Resist. Highway Bridges ATC-6-1 (Jan 1979)*, Applied Technology Council, California, USA, 314-342.
- P.R. Boardman, B.J. Wood and A.J. Carr (1983), 'Union House - a cross-braced structure with energy dissipators', *Bull. NZ Nat. Soc. Earthq. Eng.*, **16**, no. 2, 83-97.
- I.G. Buckle and R.L. Mayes (1990), 'Seismic isolation: history, application and performance: a world view', *Earthquake Spectra*, **6**, no. 2, 161-201.
- M. Cary, *et al.*, (eds), *The Oxford Classical Dictionary*, Oxford University Press, London, 1949.
- A.W. Charleson, P.D. Wright and R.I. Skinner (1987), 'Wellington Central Police Station: base isolation of an essential facility', *Proc. Pacific Conf. on Earthquake Eng., NZ*, Vol. 2, 377-388.
- L.G. Cormack (1988), 'The design and construction of the major bridges on the Mangaweka rail deviation', *Trans. IPENZ*, **15**, I/CE, March 1988, 16-23.
- D.J. Dowrick (1987), 'Edgcombe earthquake of March 2, 1987', *NZ Engineering*, 7-9.
- D.J. Dowrick, J. Babor, W.J. Cousins and R.I. Skinner (1991), 'Design of a seismically isolated printing press', *Pacific Conf. on Earthq. Eng., NZ*, **3**, 35-44.
- J. Jolivet and M.H. Richli (1977), 'Aseismic foundation system for nuclear power stations', *Proc. SMIRT4, San Francisco 1977*, Paper K.9/2
- M. Kaneko, K. Tamura, K. Maebayashi and M. Saruta (1990), 'Earthquake response characteristics of base-isolated buildings', *Proc. 4th US Nat. Conf. Earthq. Eng.* Vol. 3, May 1990, 569-578.
- G.R. McKay, H.E. Chapman and D.K. Kirkcaldie (1990), 'Seismic isolation: New Zealand applications', *Earthquake Spectra*, **6**, no. 2, 203-222.
- Yoshiro Matsuo and Koji Hara (1991), 'Design and construction of Miyagawa Bridge (first Menshin bridge in Japan)', *1st US-Japan Workshop on Earthquake Protective Systems for Bridges*, Buffalo, USA, Sept. 1991.
- R.L. Mayes (1990 - 1992), Dynamic Isolation Systems Incorporated, California, personal communications.
- L.M. Meggett (1978), 'Analysis and design of a base-isolated reinforced concrete frame building', *Bull. NZ Nat. Soc. for Earthq. Eng.*, **11**, no. 4, 245-254.
- Susumu Nakagawa, Mitsuru Kawamura (1991), 'Aseismic design of C-1 Building, the biggest base-isolated building in the world', *Post SMIRT11 Seminar, Seismic Isolation of Nuclear and Non-nuclear Structures*, Aug. 26-27 1991, Japan.
- A. Parducci and M. Mezzi (1991), 'Seismic isolation of bridges in Italy', *Pacific Conf. on Earthq. Eng., New Zealand 1991*, Vol. 3, 45-56.
- A. Parducci (1992), Facoltà di Ingegneria, Istituto di Energetica, Università degli studi di Perugia, personal communications.
- Tan Pham (1991), AC Power Group Ltd, Wellington, personal communication.
- R.A. Poole and J.E. Clendon (1991), 'NZ Parliament buildings: seismic protection by base isolation' *Pacific Conf. on Earthquake Eng., Auckland, NZ, Nov 1991*, Vol. 3, p 13.

- W.H. Robinson and L.R. Greenbank (1976), 'An extrusion energy absorber suitable for the protection of structures during an earthquake'. *Earthq. Eng. Struct. Dyn.*, Vol. 4, no. 3, 251-259.
- Masaaki Saruta (1991, 1992), Institute of Technology, Shimizu Corporation, Tokyo, personal communications.
- Matsutaro Seki (1991, 1992), Technical Research Institute, Obayashi Corporation, Tokyo, personal communications.
- R.D. Sharpe and R.I. Skinner (1983), 'The seismic design of an industrial chimney with rocking base', *Bull. NZ Nat. Soc. for Earthq. Eng.*, **16**, no. 2, 98-106.
- Ikuo Shimoda (1989 - 1992), Technology Development Division, Oiles Corporation, Tokyo, personal communications.
- Ikuo Shimoda, Seiji Nakano, Yoshikazu Kitagawa and Mitsuo Miyazaki (1991), 'Experimental study on base-isolated building using lead-rubber bearing through vibration tests', *SMIRT11 Conference, Seismic Isolation of Nuclear and Non-nuclear Structures, 1991, Japan*.
- R.I. Skinner (1982), 'Base isolation provides a large building with increased earthquake resistance; development, design and construction', *Int. Conf. Natural Rubber for Earthq. Prot. of Bldgs. and Vibration Isolation, Kuala Lumpur, Malaysia, Feb. 1982*, 82-103.
- R.I. Skinner, G.N. Bycroft and G.H. McVerry (1976a), 'A practical system for isolating nuclear power plants from earthquake attack.' *Nucl. Eng. Des.*, **36**, 287-297.
- R.I. Skinner and H.E. Chapman (1987), 'Edgcombe earthquake reconnaissance report', M.J. Pender and T.W. Robertson eds., *Bull. NZ Nat. Soc. for Earthq. Eng.*, **20**, no. 3, 239-240.
- R.I. Skinner, R.G. Tyler and S.B. Hodder (1976b) 'Isolation of nuclear power plants from earthquake attack.' *Bull. NZ. Nat. Soc. Earthq. Eng.*, **9**, no. 4 199-204.
- SMiRT-11, 'Seismic isolation and response control for nuclear and non-nuclear structures', *Structural Mechanics in Reactor Technology*, August 18-23, 1991, Tokyo.
- Frederick Tajirian, James M. Kelly and Ian D. Aiken (1990), 'Seismic isolation for advanced nuclear power stations', *Earthquake Spectra*, **6**, no. 2, 371-401.
- Akira Teramura, Toshi Kazu Takeda, Tomohiko Tsunoda, Matsutaro Seki, Mitsuru Kageyama, and Arihide Nohata (1988), 'Study on earthquake response characteristics of base-isolated full scale building', *Proc. 9th World Conf. on Earthq. Eng., Aug 1988, Tokyo, Japan*, Vol. V, 693-8.
- D.H. Turkington (1987), 'Seismic design of bridges on lead-rubber bearings', *Research Report 87/2 Department of Civil Engineering, University of Canterbury, NZ, Feb. 1987*, 172 pages.
- Douglas Way (1992), Base Isolation Consultants Incorporated, California, personal communication.

Index

- Active isolation *see* Seismic isolation
- Appendage responses *see* Secondary system responses
- Base displacement *see* Horizontal seismic displacement
- Base isolation *see* Seismic isolation
- Base shear 6(F), 7, 26, 37, 138, 160, 163, 194, 235, 262, 266
 in 7 case studies and 7 classes of isolator 40–54, 42(F), 44(T)
 ratio to weight 42(F), 44(T), 162, 163(F), 294
see also Shear distribution
- Bearings
 elastomeric (rubber or laminated-rubber) 57, 57(T), 85–96, 86(F), 87(F), 88(F), 92(F), 94(F), 220, 220(F), 221, 221(F), 225, 253, 262, 268, 275, 278, 283, 284(T), 290, 299, 300(T), 302(T), 303, 304(F), 305, 311, 311(T), 313, 314(F), 317, 317(F), 320, 322(T), 326, 331
 and modification to form lead-rubber bearing 58, 97, 98(F), 101(F), 284
 high-damping 57, 57(T), 110, 300(T), 302(T), 303, 305, 313, 314(F)
 with lead bronze 330
 lead-rubber (LRB) 57(T), 58, 96–108, 98(F), 101(F), 102(F), 103(F), 105(F), 106(F), 107(F), 109(F), 160, 225, 253, 268, 275, 279, 283, 284, 284(T), 285(T), 286, 287(F), 300(T), 302(T), 303, 305, 307, 308(F), 309(F), 310(F), 311(T), 312(T), 315, 316(F), 317, 317(F), 319, 319(F), 320, 320(F), 322(T), 329, 330, 333, 334(F), 335(F)
 PTFE sliding 111, 112, 275, 330
- Buffers and stops 55, 57(T), 115, 116, 268, 269, 276, 299, 316
- Case studies
 7 linear-chain structures with different isolation 12, 40–48, 44(T)
 and generalisation to 7 classes of isolation system 48–54
 81 linear-chain structures with bilinear isolation 12, 26, 186–199, 188(T), 192(F), 198(F)
 secondary responses of various isolation systems 217–225, 220(F), 222(F)
- Choice of isolation system *see* Guidelines
- Classical *see* Mode
- Combination rules 212–213, 256
 CQC 37, 231
 SRSS 37, 196–199, 204, 212
- Contents *see* Secondary system responses 199, 329
- Correction factor 26, 44(T), 165–169, 168(F), 247(F), 248
- Costs 2, 3, 21, 55, 116, 241, 242, 270, 271, 272, 283, 294, 299, 315, 329, 330
- Coupling parameter *see* Secondary system responses 207
- Damper
 Coulomb 9, 9(F), 24(F), 81, 84, 160, 173, 174(F)
 friction 57(T), 58, 160, 300(T)
 hydraulic 110
 lead extrusion (LED) 57(T), 58, 79(F), 80–85, 82(F), 160, 275, 283, 284(T), 285(T), 288, 288(F), 297, 297(F), 299, 300(T)
 steel (steel beam) 57(T), 58, 63–76, 66(F), 69(F), 73(F), 75(F), 160, 262, 275, 283, 284(T), 285(T), 295, 296(F), 300(T), 303, 304(F), 305, 321, 321(F), 322(T), 327(F), 328(F), 329, 330, 331
 viscous (velocity-damper) 9, 9(F), 23(F),

- Damper (*cont.*)
 57, 57(T), 110, 124, 275, 300(T), 305, 306(F), 322(T)
see also Bearings 3-4
- Damping 4, 5(F), 15, 19(F)
 and energy dissipation 59, 121, 122, 236, 283, 284, 289, 297, 329
 base 120, 140-145, 149-151, 236
 coefficient 16, 22, 23(F), 24(F), 124, 127, 174(F), 255, 273(F)
 classical *see* Mode
 hysteretic 25, 44(T), 58, 128, 165, 236, 259, 274, 275, 290
 mass-proportional 127, 201
 non-classical *see* Mode
 of isolator components 55-58, 57(T)
 stiffness-proportional 127, 220
 viscous 25, 120, 128, 236, 259, 326, 329
- Damping factor (fraction of critical viscous damping) 16, 17, 22, 36, 44(T), 126, 136, 147, 259
 'effective' or 'equivalent' *see* Equivalent linearisation
 hysteretic 25, 44(T), 165, 259
- Damping matrix 29
 free-free 145, 173
- Degree of isolation *see* Isolation factor
- Degree of non-linearity *see* Non-linearity factor
- Design detailing 7, 55, 64, 65, 67(F), 74, 96, 242, 266, 269, 294, 330, 333
- Design displacement *see* Seismic gap
- Design earthquake 4, 20, 164, 242-246, 244(F), 257, 261, 267, 274, 277, 283, 291, 295, 319, 333
- Design guidelines *see* Guidelines
- Devices *see* Bearings; Buffers; Dampers; Gravity devices; Isolators and isolating systems; Piles; Springs
- DSIR xi, xiii, 160, 281, 333
 Physical Sciences xiii, 10
 Physics and Engineering Laboratory xi, xiii, 10, 63, 77
- Duhamel integral 17, 153
- Earthquakes
 artificial 4, 246, 291
 Edgcombe 281, 333
 El Centro 1934 19(F)
 El Centro NS 1940 4, 12, 18, 19(F), 40-48, 42(F), 44(T), 160, 186-199, 220, 222, 234, 249, 283, 289
 scaled El Centro 160, 162, 163(F), 164, 165, 166(F), 167(F), 168(F), 225, 242-246, 244(F), 247(F), 250(F), 261, 298
 Loma Prieta 319, 329
 Mexico City 4, 221
 Olympia 19(F)
 Pacoima Dam 4, 221, 225, 283, 298, 299
 Parkfield 160, 225
 Taft 19(F), 225
- Earthquake spectrum *see* Response spectrum
- Effective period; Effective stiffness; Effective damping factor *see* Equivalent linearisation
- Equation of motion 16, 29, 56, 124, 136, 145, 152-155, 170, 173, 175, 183-185
- Equivalent linearisation 23(F), 24-26, 24(F), 44(T), 48, 121, 160, 165-169, 166(F), 167(F), 168(F), 236, 247(F), 248, 251-254, 252(F), 259, 261-266
- Energy dissipation *see* Damping
- Extreme earthquake event *see* Design earthquake
- Extrusion 77-84, 77(F), 79(F), 82(F), 83(F)
see also Damper, lead-extrusion
- Fatigue 64, 74-76, 75(F), 80, 85, 106
- Flexibility (inverse of stiffness) 4, 5(F), 10
 in 7 structures 40-48, 42(F), 44(T)
 in 7 classes of isolating system 48-54, 50(T)
 in 81 structures on bilinear isolators 186-199, 188(T)
 of common isolator components 55-58, 57(T)
- Floor (response) spectra 12, 18, 27, 34(F), 158, 161, 181, 200, 218-225, 235, 236, 238, 240, 254, 268, 295
 of 7 structures 40-48, 42(F), 44(T)
 of various isolation systems 218-225, 220(F)
see also Secondary system responses
- Force-displacement loop (load versus deflection hysteresis loop) 22-25, 40-54, 44(F), 50(T), 237
 for bridge 274
 for small displacements 108, 109(F)
 of bilinear isolator 9, 9(F), 24(F), 25, 56, 160, 251-254, 252(F)
 of extrusion damper 81, 82(F)

- of lead-rubber bearing 101, 101(F), 102, 103(F)
 of linear isolator 9, 9(F), 22, 23(F)
 of PTFE bearings 111, 112
 of rocking structure 113
 of rubber bearing 94(F), 101, 101(F)
 of typical metal 59
 of steel damper 68-72, 69(F), 73(F)
- Foss's method 123, 151-159
- Frequency (inverse of period) *see* Period complex 126-160, 205
- Frequency equation 126, 127, 131, 145
- Fundamental (first) mode 20, 32(F), 40-48, 42(F), 119, 121, 138, 149-151, 178(F), 182(F), 186, 188(T), 192(F), 198(F), 235, 249, 250(F), 255, 278
- Gravity devices
 stepping and rocking 57(T), 58, 63, 112, 113, 283, 285(T), 288, 289(F), 290(F), 291(F)
 rollers, balls and rockers 57, 57(T), 114
 hanging links and cables 114, 271
- Guidelines 239-280
 and design codes 276-280
 and iterative procedures for design 257-261
 for design of an isolated structure 13, 192(F), 239, 244(F), 247(F), 249, 250(F), 251-254, 252(F)
 for linear isolation systems 255-257
 for bilinear isolation systems 257-261
 for selection of isolation system components 55-58
 for selection of isolation systems 50(T), 48-54
 for torsionally unbalanced structures 226
- Higher modes 12, 20-21, 23(F), 27-28, 40-54, 122-124, 128, 138, 148, 150, 161, 163, 165, 176-184, 178(F), 182(F), 186-199, 188(T), 192(F), 198(F), 235, 236, 237, 239, 249, 250(F), 251, 253, 260, 265, 268, 275, 278
- Higher-mode attenuator 23, 23(F), 158
- Holzer technique 124, 149-151
- Horizontal seismic displacement 4, 19(F), 21, 37, 55, 90-92, 125(F), 134(F), 144(F), 163, 236, 247(F), 256, 258, 262, 266, 283, 291
- of 7 cases and 7 classes of isolators and isolating systems 40-54, 42(F), 44(T), 50(T)
see also Mode-shape; Seismic gap; Peak values of
- Hysteresis loop
 and damping and energy dissipation *see* Damping
 (shear) force versus displacement *see* Force-displacement loop
 (stress versus strain) and (torque versus shear) 59-62, 60(F), 68-72
- Interaction parameter (interaction coefficient) *see* Secondary system responses 203, 207
- Isolation factor (degree of isolation) (isolation ratio) 4, 12, 28, 40-54, 44(T), 128-199, 134(F), 192(F), 219, 236, 237, 249, 250(F), 254, 260, 265, 268
- Isolator force 173, 174
- Isolators and isolation systems 8, 9, 10, 40-54, 42(F), 44(T), 50(T), 55-58, 57(T)
 Alexisimon 160
 bilinear (simple case of non-linear) 9, 9(F), 23-26, 24(F), 40-48, 42(F), 44(T), 55-58, 57(T), 160-199, 163(F), 166(F), 167(F), 168(F), 174(F), 178(F), 182(F), 192(F), 198(F), 251-254, 252(F), 257-261
 damped linear 9, 9(F), 22, 23(F), 40-48, 42(F), 44(T), 55-58, 57(T), 123-160, 125(F), 131(F), 134(F), 144(F), 235, 254-257
 elastoplastic 219, 220(F), 221, 222(F)
 Electricité de France 160, 220(F), 221, 222(F)
 friction 122, 160, 220, 220(F), 222(F), 237
 for seismic protection of capacitor banks 261-266, 331, 332(F), 334(F)
 for a hypothetical building 266-270
 guide to selection *see* Guidelines
 non-linear, in general 22, 55-58, 57(T), 121, 160
 parameters 22-26, 161-169, 163(F), 166(F), 167(F), 168(F), 187, 188(T), 239, 251-254, 258, 268, 272-274
 resilient-friction 160, 220(F), 221, 222(F), 224
 sand-layer 160

- sliding resilient friction 2-42, 160, 220(F), 221, 222(F)
see also Bearings; Dampers; Piles; Gravity devices; Springs
- Italy
 seismic isolation in this country 65, 280, 281, 282(T), 322(T)
 structures seismically isolated 321
 buildings 326
 bridges 321(F), 322(T), 327, 327(F), 328(F)
- Japan
 seismic isolation in this country 1, 65, 85, 96, 280, 281, 282(T), 300(T), 302(T), 307, 309, 330
 structures seismically isolated 329
 buildings 299, 300(T), 303-308, 304(F), 306(F), 307(F), 308(F)
 bridges 299, 302(T), 309-310, 309(F), 310(F)
- Lead extrusion damper (LED) *see* Damper
 Lead-rubber bearing (LRB) *see* Bearing
- Lifetime
 of isolation system 9, 57, 276
 of steel damper 75, 75(F)
 of extrusion damper 84, 85
- Maintenance, inspection, repair 3, 9, 55, 57, 58, 64, 269, 272, 282, 299, 318
- Mass ratio *see* Interaction parameter
- Maximum values of displacement, velocity, acceleration *see* Peak values
- Modal coupling 169-186, 178(F)
- Modal decomposition 39, 136
see also Modal filtering
- Modal filtering (mode sweeping) 12, 40, 122, 161, 171-186, 178(F), 182(F), 187, 219, 240
- Mode
 classical (in phase) 31, 35, 120, 127, 128-139, 149, 150, 156, 255
 free-free 119, 129, 131(F), 134(F), 135, 177, 185, 187, 236, 256
 perturbation to free-free mode 119, 145-148
 fixed-base 127, 128, 132
 perturbation to fixed-base mode 159
 fundamental *see* Fundamental (first) mode
- higher *see* Higher modes
 mode shape (mode profile) 30-33, 32(F), 133, 134(F), 144(F), 149-151, 178(F), 256
 non-classical 120, 127, 140-145, 144(F), 151-160, 200, 236, 240, 255
 of bridge 273, 273(F), 274
 of elastic and yielded phases of bilinear isolator 177-184, 178(F), 237
 of linear structures with bilinear isolation 169-186, 178(F)
 primary-secondary, tuned and detuned 202-214, 204(T)
 secondary systems in structures with linear isolation 214-217
 secondary systems in structures with bilinear isolation 217-225
 torsional 226-235, 228(F)
- Models of structures
 bilinearly isolated system, treated as 'equivalently linear' 165-169
 isolated bridge 273, 273(F), 279
 non-uniform linear structure on linear isolator 145-148
 secondary structure mounted on primary structure 199-226, 201(F)
 single mass on Coulomb damper 160-169
 torsionally unbalanced structure 226-235, 228(F)
 uniform continuous shear beam or linear chain on bilinear isolator 169-199, 174(F)
 uniform continuous shear beam or linear chain on linear isolator 28, 29(F), 31, 119, 123-160, 125(F)
- New Zealand (NZ)
 Ministry of Works and Development (MWD) xii, 10, 97
 seismic isolation in this country 2, 63, 85, 97, 113, 269, 275, 276, 278, 279, 281, 297, 333
 structures seismically isolated 282(T), 284(T), 285(T), 287(F), 288(F), 289(F), 290(F), 291(F), 292(F), 293(F), 296(F), 297(F), 298(F), 331, 332(F), 333, 334(F), 335(F)
 buildings 284(T), 291-299, 292(F), 293(F), 296(F), 297(F), 298(F), 333

- bridges 284-290, 285(T), 287(F), 288(F), 289(F), 290(F), 291(F), 299
 delicate and hazardous structures 331-335, 332(F), 334(F), 335(F)
- Non-classical *see* Mode
- Non-classical damping parameter *see* Secondary system responses 203, 207
- Non-linearity 27, 121, 122, 181
 factor 12, 24(F), 25, 27, 40-54, 42(F), 44(T), 161, 165, 181, 186, 187, 188(T), 192(F), 195, 220, 237, 249, 250(F), 251-254, 252(F), 259, 260, 265, 268
- Non-uniform structure *see* Models of structures
- Overtuning moments 37, 134(F), 138
- Orthogonality conditions 34, 136, 152, 171, 176
- Participation factor 36, 38, 119, 120, 134(F), 136, 156-159, 171, 176, 183, 185, 204(T), 206, 209, 213, 228(F), 230, 232, 256
- Peak values of displacement, velocity and acceleration 26, 36, 40-54, 42(F), 44(T), 137, 162-169, 163(F), 181, 186-199, 188(T), 192(F), 198(F), 236, 237, 247(F), 252, 256
- Performance and/or testing of isolators or systems 5, 10, 64, 66(F), 71, 75(F), 81, 82(F), 83(F), 94(F), 98(F), 101, 101(F), 102(F), 103(F), 105(F), 106(F), 107(F), 109(F), 281, 303, 305, 306(F), 307, 328(F), 329, 331, 334(F)
 shaking-table tests 10, 216, 225
- Period (inverse of frequency)
 'effective' or 'equivalent' *see* Equivalent linearisation
 elastic 161, 177, 187, 188(T), 263
 post-yield 161, 177, 187, 188(T), 263
 natural (fundamental) 4, 16, 28-33, 89, 119, 126, 147, 161, 305, 309, 313, 326
- Period shift 4, 5(F), 7, 15, 55, 236, 294, 295, 303, 309, 313, 319, 331
- Piles (or columns) 57, 57(T), 63, 114, 283, 284(T), 295, 296(F), 297, 297(F), 298(F), 305
- Plasticity 59-62, 60(F), 61(F), 79
 and dislocations 61-62, 61(F), 79, 81
 of steel 64
 of lead 79-81, 97, 104, 105(F)
- Response history analysis (time history analysis) 160, 161-164, 170, 182(F), 183, 186, 240, 257, 261, 268, 275, 278
- Response spectrum 11, 15, 16-20, 19(F), 26, 161-169, 236, 243, 244(F), 256, 275, 278, 326
- Retrofit 2, 271, 283, 284(F), 285(F), 311, 315, 316(F), 319, 319(F)
- Scaling procedures
 for steel-beam dampers 64, 68-74, 69(F), 70(T)
 for earthquakes *see* Earthquakes, scaled El Centro
- Secondary system responses 12, 18, 27, 34(F), 120, 122, 158, 161, 181, 199-226, 235, 238, 239, 240, 254, 268, 295
 of 7 structures 40-48, 42(F), 44(T)
 of various isolation systems 219-225, 220(F), 222(F)
- Seismic displacement *see* Horizontal seismic displacement
- Seismic force 37, 137
- Seismic gap (closely related to design displacement) 2, 4, 55, 115, 243, 269, 270, 272, 276, 277, 282, 286, 288, 295, 299, 309, 318, 322(T), 326
- Seismic isolation
 active *vis-à-vis* passive 2, 116, 117
 rationale, criteria and features 1, 3, 6(F), 4-8, 16, 19(F), 21, 55, 240-242, 281, 316, 317, 329
 reviews 1
- Seismic responses 33-40, 40-54, 161, 239, 271-275, 305
 of isolated bridge 274, 275
 of 7 cases and 7 classes of isolation systems 40-54, 42(F), 44(T), 50(T)
 of 81 linear-chain structures on bilinear isolators 186-199, 192(F), 198(F)
 of torsionally unbalanced structures 226-235, 228(F)
see also Base shear; Shear distribution; Horizontal seismic displacement; Peak values of; Secondary system responses; Torsion

- Site conditions 3, 241, 243, 249, 270, 277, 291, 295, 297, 305, 309, 315, 319, 320, 327, 333
- Shear
- bulge factor 194-199, 198(F), 250, 251(F), 254
 - distribution 37, 40-48, 42(F), 44(T), 93, 133, 138, 143(F), 144(F), 194-199, 198(F), 235, 238, 247(F), 250(F), 254, 256, 260, 268
 - see also* Base shear modulus 59, 73, 74(F)
- Spectral responses (spectral velocity, displacement, acceleration) *see* Response spectrum
- Spring 16, 57, 57(T)
- Stiffness
- between masses of multimass structure 29(F), 149
 - 'effective' or 'secant' (diagonal slope of force-displacement loop) *see* Equivalent linearisation 9(F), 22, 23(F), 24(F), 25, 33, 166(F), 251-254, 252, 252(F), 259
 - 'effective' as defined in three alternate ways 170-186
 - 'effective' for bridge 273, 273(F)
 - of base 140, 148-151
 - of each phase of bilinear isolator 23, 24(F), 237, 262
 - of lead-extrusion damper 82(F)
 - of lead-rubber bearing 101, 101(F), 108
 - of linear isolator 22, 23(F), 255
 - of real isolated structures 294, 326, 327, 331
 - of rubber bearing 88-90, 101(F)
 - of plastically deformed metals *see* Plasticity
 - of steel dampers 72-74, 74(T)
- Stiffness matrix 29
- free-free 145, 173, 185
 - elastic-phase 174
 - yielding-phase 174, 184
- Stroke 66(F), 75, 75(F), 84, 85, 101, 106
- Torsion 7, 13, 15, 123, 226-235, 228(F), 238, 272, 275, 277, 305
- 'Trade-off' between base shear and displacement 8, 161, 246-249, 247(F), 259, 268, 272
- Tuning parameter *see* Secondary system responses 203, 207
- United States of America (USA)
- seismic isolation in this country 1, 243, 276, 277, 281, 282(T), 311(T), 312(T)
 - structures seismically isolated 330
 - buildings 311(T), 313-318, 313(F), 314(F), 316(F), 317(F), 318(F)
 - bridges 312(T), 319, 319(F), 320, 320(F)
- Wave number 126-160, 131(F)
- Wind and traffic loads 8, 22, 50(T), 56, 58, 65, 85, 268, 270, 272, 286, 303, 320, 331
- Worldwide use of seismic isolation xi, 1, 13, 281, 282(T), 330, 335
- Yield
- displacement 24, 24(F), 72, 73(F)
 - force 24, 24(F), 72, 73(F), 161, 262, 283, 331
 - point 24, 24(F), 59-62, 60(F), 72, 73(F), 251-254, 252(F), 261, 268
 - ratio 24, 24(F), 121, 161, 163, 187, 237, 262, 294, 298

An Introduction to Seismic Isolation

R. I. Skinner

W. H. Robinson

New Zealand Institute for Industrial Research and Development

G. H. McVerry

Institute of Geological and Nuclear Sciences Limited, New Zealand

All three authors were formerly affiliated to the
New Zealand Department of Scientific and Industrial Research (DSIR)

This book is the product of twenty five years of collaboration between engineering seismologists and materials scientists working in the field of plasticity.

A synthesis of three parallel approaches to seismic isolation is presented: the development of theoretical concepts, the design and testing of practical devices, and their application in the seismic isolation of real structures. After a definition of the concept of seismic isolation, various isolator components and isolation systems are defined. Much emphasis is given to isolator devices and the response mechanisms. Results of previous developments are applied to practical design situations, including the design of isolation systems for a fragile structure and for a typical building. Finally, a survey of seismic isolation applications in several countries is presented.

JOHN WILEY & SONS

CHICHESTER·NEW YORK·BRISBANE·TORONTO·SINGAPORE

ISBN 0-471-93433-X



9 780471 934332



WILEY

Publishers Since 1807